Electron-Phonon
Interactions and
Phase Transitions

NATO ADVANCED STUDY INSTITUTES SERIES

A series of edited volumes comprising multifaceted studies of contemporary scientific issues by some of the best scientific minds in the world, assembled in cooperation with NATO Scientific Affairs Division.

Series B: Physics

RECENT VOLUMES IN THIS SERIES

Volume 19 – Defects and Their Structure in Nonmetallic Solids
edited by B. Henderson and A. E. Hughes

Volume 20 – Physics of Structurally Disordered Solids
edited by Shashanka S. Mitra

Volume 21 – Superconductor Applications: SQUIDs and Machines
edited by Brian B. Schwartz and Simon Foner

Volume 22 – Nuclear Magnetic Resonance in Solids
edited by Lieven Van Gerven

Volume 23 – Photon Correlation Spectroscopy and Velocimetry
edited by H. Z. Cummins and E. R. Pike

Volume 24 – Electrons in Finite and Infinite Structures
edited by P. Phariseau and L. Scheire

Volume 25 – Chemistry and Physics of One-Dimensional Metals
edited by Heimo J. Keller

Volume 26 – New Developments in Quantum Field Theory and Statistical Mechanics–Cargèse 1976
edited by Maurice Lévy and Pronob Mitter

Volume 27 – Topics in Theoretical and Experimental Gravitation Physics ·
Edited by V. De Sabbata and J. Weber

Volume 28 – Material Characterization Using Ion Beams
Edited by J. P. Thomas and A. Cachard

Volume 29 – Electron–Phonon Interactions and Phase Transitions
Edited by Tormod Riste

The series is published by an international board of publishers in conjunction with NATO Scientific Affairs Division

A	Life Sciences	Plenum Publishing Corporation
B	Physics	New York and London
C	Mathematical and Physical Sciences	D. Reidel Publishing Company Dordrecht and Boston
D	Behavioral and Social Sciences	Sijthoff International Publishing Company Leiden
E	Applied Sciences	Noordhoff International Publishing Leiden

Electron-Phonon Interactions and Phase Transitions

Edited by

Tormod Riste

Institute for Atomic Energy
Kjeller, Norway

PLENUM PRESS • NEW YORK AND LONDON
Published in cooperation with NATO Scientific Affairs Division

PREFACE

    This NATO Advanced Study Institute was the fourth in a series
devoted to the subject of phase transitions and instabilities with
particular attention to structural phase transformations. Beginning
with the first Geilo institute in 1971 we have seen the emphasis
evolve from the simple quasiharmonic soft mode description within
the Landau theory, through the unexpected spectral structure re-
presented by the "central peak" (1973), to such subjects as melting,
turbulence and hydrodynamic instabilities (1975). Sophisticated
theoretical techniques such as scaling laws and renormalization
group theory developed over the same period have brought to this
wide range of subjects a pleasing unity. These institutes have
been instrumental in placing structural transformations clearly in
the mainstream of statistical physics and critical phenomena.

    The present Geilo institute retains some of the counter cul-
tural flavour of the first one by insisting whenever possible upon
peeking under the skirts of even the most successful phenomenology
to catch a glimpse of the underlying microscopic processes. Of
course the soft mode remains a useful concept, but the major em-
phasis of this institute is the microscopic cause of the mode
softening. The discussions given here illustrate that for certain
important classes of solids the cause lies in the electron phonon
interaction. Three major types of structural transitions are
considered. In the case of metals and semimetals, the electron
phonon interaction relies heavily on the topology of the Fermi
surface. In special situations the electronic energy of the con-
duction band can be lowered by a greater amount than the energetic
cost of a lattice distortion, so that lattice distortion will in-
deed occur. As Professor Friedel has emphasized, instabilities
of this type are relatively more likely in band structures of lower
dimensionality because of the less severe requirements for "nesting"
of various portions of Fermi surface. Several of the papers herein
are devoted to the calculation, observation and consequences of
this type of electron phonon interaction.

    One of the most striking manifestations of this interaction is
the so-called "charge density wave" instability, responsible for a
structural transformation to a "$2K_F$" superlattice. Since $2K_F$ is

most often <u>not</u> an integral submultiple of the reciprocal lattice
vector, the unit cell's new structure is not a simple multiple of
the old unit cell. While such "incommensurable" structures have
been long known, (the spin density wave in chromium is perhaps
the most familiar example), their incorporation into the lore of
phase transitions is quite recent and still incomplete. Nor are
"incommensurable" structures confined to cases where mobile
carriers are present. The lectures of Drs. Axe, Di Salvo, Shirane
and Yamada highlight the wealth of anomalous physical properties
associated with incommensurate transitions in both metals and
insulators. Drs. Bak and Luther treat the formal and microscopic
theoretical aspects of these systems. Among the concepts that
they and Professor McMillan discuss are solitons, a subject that
we undoubtedly will hear more about in the future. And Professor
de Wolff presents an important systematic means of classifying the
symmetries of incommensurate transitions.

The second important class of electron-phonon driven struc-
tural transitions is represented by the Jahn Teller systems. The
relationssships among the symmetries of the interacting electronic
and vibrational states and the resulting lattice distortions are
systematized by Professor Thomas. And a variety of experimental
discussion of several examples are detailed in this volume by Drs.
Harley and Kjems. A quantitative description of many singular
properties may be obtained from the "pseudo spin" model of Jahn
Teller systems - as discussed here by Dr. Stinchcombe.

The third major area addressed by this institute concerns
structural phase transitions and high temperature superconductivity.
This subject perhaps epitomizes the meeting inasmuch as structural
transitions in the prototypical A-15's (Nb_3Sn, etc.) have been
addressed from both the band Jahn Teller and the charge density
wave theoretical viewpoint. Professor McMillan's lectures provide
an admirable synthesis of both phenomenological and microscopic
theories for the charge density wave, the superconducting and
structural phase transitions. Dr. Testardi, in his experimental
lectures on the A-15 compounds emphasized the recent striking
effects which defects in unstable lattices have upon limiting the
realizable superconducting T_c.

The lectures of Dr. Romestain called our attention to another
class of transition (the metal insulator) to which he has recently
applied very sophisticated optical techniques. The several seminars
generally provided an excellent complementarity to the subject
areas addressed by the main lecturers. In retrospect two of the
most exciting and stimulating topics addressed in this institute
were the new class of structural transitions represented by "in-
commensurate" super structures and the beginning of progress in
understanding more fully the role of structural transitions in
high T_c superconductors.

As in the past, the atmosphere of the setting provided the opportunity for vigorous intellectual and physical activity, so that the participants departed with the clear impression that ideas had not only been exchanged but that new understanding was generated and the beginnings of some new research directions were established at Geilo.

The programme committee joins the other participants in expressing their sincere thanks to Mr. Eigil Andersen, Mrs. Gerd Jarrett and the staff of the Institutt for atomenergi, Kjeller, Norway for their careful planning and creative assistance, upon which largely rested the success of this conference.

J. D. Axe
J. Feder
P. A. Fleury
A. Luther
T. Riste

June, 1977

CONTENTS

J. FRIEDEL: (invited lecturer)

PHASE TRANSITIONS AND ELECTRON-PHONON COUPLINGS IN PERFECT
CRYSTALS. MODULATED STRUCTURES. AN INTRODUCTION.

J.D. AXE: (invited lecturer)

NEUTRON SCATTERING STUDIES OF ELECTRON-PHONON INTERACTIONS

PHASE CHANGES AND ELECTRON PHONON COUPLINGS IN PERFECT CRYSTALS.

MODULATED STRUCTURES. AN INTRODUCTION.

J. Friedel

Physique des Solides, Université Paris Sud, Orsay

LA du CNRS

The purpose of this introduction is to place the field of this meeting in the general frame work of phase changes and the nature of the interatomic forces involved,then to discuss the possibility of small amplitude phase changes arising in perfect crystals as a weak modulation of the simpler structure. This modulation can be viewed as due to a phonon mode of the simpler structure becoming soft ; and conditions for this to occur through strong electron-phonon coupling are recalled.

I - THE FRAMEWORK

A. Phase changes in perfect crystals

We consider phases in thermal equilibrium, neglecting all problems of nucleation and growth kinetics involved in most phase changes. Each phase is then defined by a free enthalpy

$$F = H - TS,$$

a continuous function of temperature T, pressure p. It might involve also composition ; but we only consider here perfect crystals with fixed composition. $H = U + pV$ is the enthalpy, and variations of the volume V involved in phase changes of condensed phases only introduce small and trivial effects.

A phase change arises for a transition temperature T_t (or a pressure p_t) where two possible phases have the same free enthalpy. The phase change is said of the first or second order, depending on whether the two curves F_A (T or p) and F_B (T or p) cross

with an angle or are tangent at the transition (figure 1a,b). To predict the transition temperature T_t of a phase change, one must
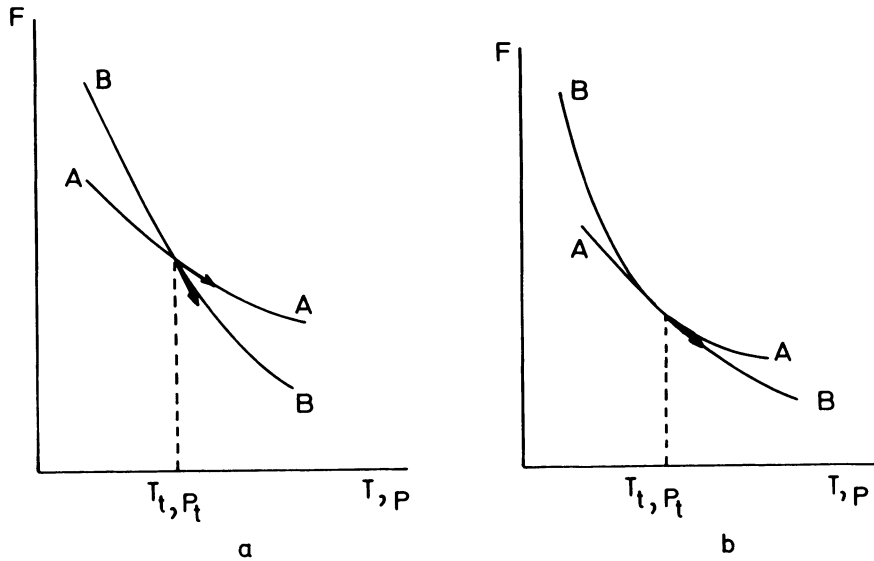
Figure 1 : Phase transitions : a first order ; b second order.

therefore know the difference in enthalpy H and in entropy S bet-ween the two phases, and how they vary with temperature. Only the relative stability of phases at zero degree can be discussed ne-glecting entropy.

In most crystalline phase changes, the difference in internal energy U_B-U_A of the two phases is much less than the latent heat of sublimation, which measures the total stability of the conden-sed phases. Furthemore in most of these changes, large structural changes occur. As a result, only a limited study of the relative stability of typical simple crystal phases has been made in this general case.

In phase changes by crystal structure modulations however, there is a continuous or nearly continuous transition from phase B to phase A ($U_B - U_A \simeq 0$). Some phonon modes of phase B become soft at or near to the transition temperature T_t or pressure p_t.

Such transitions are usually described 'à la Landau', in terms of the amplitude u and the phase ϕ of the soft modes :

$$F_A - F_B = \alpha\ u^2 + \beta\ u^4 + \gamma(grad\ u)^2 + \delta(grad\ \phi)^2 + \ldots$$

This description assumes u and ϕ to be the relevant order parameters. Even when applicable, it is purely formal in that it hides the computation of the coefficients of α, β, γ, δ in terms of the enthalpy and entropy changes as deduced from a microscopic model.

A special case of crystal modulation is that of a <u>uniform</u> distortion.

B. Interatomic forces

Microscopic models require an analysis of the atomic and electronic structure.

One starts from the two usual fundamental approximations:

- The adiabatic approximation (Born Oppenheimer) uncouples the motion of the atoms from that of the electrons around the atoms, assumed at rest.

- The mean field one electron approximation (Hartree) uncouples the relative motions of the electrons. It takes two extreme selfconsistent forms, between which one nowadays believes there is necessarily a first order cooperative transition at low temperature (Mott transition[1]).

1 - Localized valence electrons

Each electron is assumed to be localized on a small building block of the structure - atom or molecule. The structure is then necessarily an insulator.

This is probably a good description of the stable state in <u>rare gases</u> and most <u>ionic solids</u> or <u>molecular solids</u>.

The building blocks are held together by various forces which correspond to successive refinements in the description of the electronic structure :

- Long range <u>Coulomb</u> interactions. These can be between static monopoles (ionic solids, figure 2.a), static dipoles (ferro or antiferroelectrics, figure 2.b,c) or static multipoles (molecular crystals such as Cl_2, figure 2.d) as described in the stable state of the <u>Hartree</u> approximation.

↑ ↓ ↑ ↓ ↑

b

− + − +   − | − | −

a   d

→ → → →

c
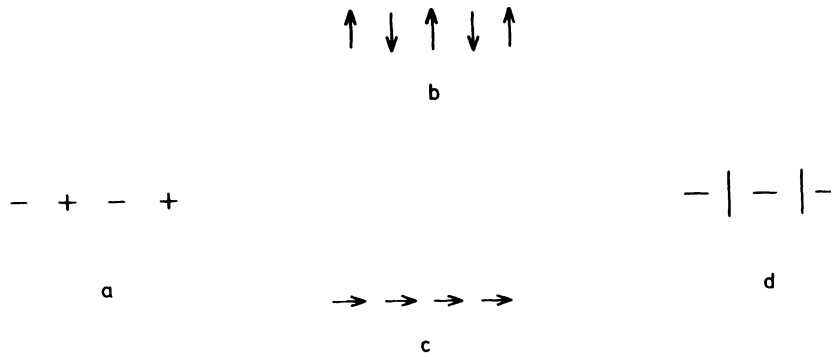
Figure 2 : Three types of Coulomb forces between static mono or
multipoles : a monopoles ; b and c dipoles ; d higher multi-
poles.

- Short range exchange interactions : magnetic couplings
between incompletely filled atomic shells or repulsions between
filled shells ; medium range magnetic couplings by superexchange.
These come in the Hartree Fock scheeme when respectively stable
states or virtually excited states of the Hartree scheeme are
considered.

- Short range dispersion interactions. These arise through
the virtual excitation of Hartree state by long range Coulomb
correlation forces between electrons in different building blocks.
It can be considered as due to interactions between dynamic dipo-
les (Van der Waals and more general dispersion forces).

- H bonds, coming from quantum tunnelling of light nuclei.

It is worth pointing out that static Coulomb forces tend to
aggregate unlike blocks together (+ with −, up dipole parallel to
down dipole in case of figure 2.b, quadrupoles at right angles ...
cf figure 2). Contrary wise, dispersion forces tend to aggregate
like blocks together (figure 3, cf Appendix A).

One can list a number of phase changes with crystal modula-
tions or small crystal distortions:

- Ferroelectric and antiferroelectric transitions, with the
apparition or change of orientation of permanent dipoles.

- Magnetic phases (including cooperative Jahn Teller effects)
if spin-orbit coupling and thus magnetostrictive effects are con-
sidered.

<div align="center">

___ A A A A ____ B B B B___

a

___ B A B A B A B A B A B A B___

b

</div>

Figure 3 : Tendency to aggregation by dispersion forces : a   pre-
ferred to b.

- 'Plastic' phases, where molecules rotate around their center
of gravity.

- Insulator metal transitions (Mott transition) ...

Except in the ferroelectric case, the small lattice modula-
tions are but a shadow of a larger change in ordering of an elec-
tronic or molecular parameter, and fall therefore really outside
the scope of this discussion. The ferro (antiferro) electric cases
themselves are made more difficult to study by the ambivalent na-
ture of the interactions of dipoles (cf figures 2.b,c), by the mo-
re or less covalent nature of interatomic bondings and, in some
cases, by the difficulty of describing correctly the H bonds. Thus
if much experimental work has been done in that field, the theore-
tical analysis remains elementary in many cases. This is especial-
ly true for the displacive ferroelectrics where dipoles are crea-
ted by a small crystal modulation of the non ferromagnetic phase,
and which therefore fall most directly within the field of inte-
rest here.

It is also worth pointing out that, because electrons are
localized, each phonon mode possibly involved in a phase transi-
tion interacts necessarily with all the valence electrons. Cou-
pling of individual electrons with phonons are only involved in
states excited above or near the conductibility gap, thus in exci-
ted conductive electrons or valence holes or in excitons. These
couplings are well known both in polar and non polar crystals. They
change the effective mass of the carriers, can lead to their self-
trapping and to hopping conduction processes. Such processes only

involve strongly excited electronic states of no importance in
phase changes, except near to a Mott transition.

Two examples of modulated structures with short range interactions

The magnetic helical structures provide historically the
first example of modulated structure, with a wave length that can
vary continuously and thus can be incommensurate with the period
of the lattice. Although actually found in metallic structures,
they were first analyzed in terms of short range (magnetic) interactions valid for insulators[2]. It is worth recalling this analysis and point out a direct extension to non magnetic modulations.

a) Helical magnetism

One considers a 3 dimensional lattice made of a stacking of
parallel and identical planes of magnetic atoms. We assume a ferromagnetic coupling between atoms in each plane, and a strong magnetic anisotropy which forces the atomic moments to lie in the
corresponding xy plane. Let S_n be the magnetic moment per atom in
the nth plane. The coupling between atoms of different planes is
limited to interactions between <u>first</u> and <u>second</u> neighbouring planes. The coupling energy U per atom is given by

$$N\ U = \sum_{n=1}^{N} \left[A_1 \sum_{i=\pm 1} S_n\ S_{n+i} + A_2 \sum_{j=\pm 2} S_n\ S_{n+j} \right]$$

If one Fourier analyses the components S_n^x, S_n^y of S_n in the xy
planes (within the first Brillouin zone $0 \leqslant k < K = 2\pi/a$),

$$S_n^x = \sum_k S_k \cos (k\ R_n + \phi_k)$$

$$S_n^y = \sum_k S_k \sin (k\ R_n + \phi_k)$$

with $R_n = na$

one finds

$$U = 2 \sum_k S_k^2\ (A_1 \cos ka)$$

The different Fourier components are thus additive and their energy is phase independent.

At T = OK, $(\sum_k S_k^2)^{1/2}$ = S, length of the magnetic moment.
The minimum energy U is obtained for <u>one</u> mode k, which, depending
on the values of A_1 and A_2, is (figure 4)

F : ferromagnetic (ka = 2m π).
A : antiferromagnetic (ka = (2m+1)π).
H : helical (cos ka = $-A_1/4 A_2$).
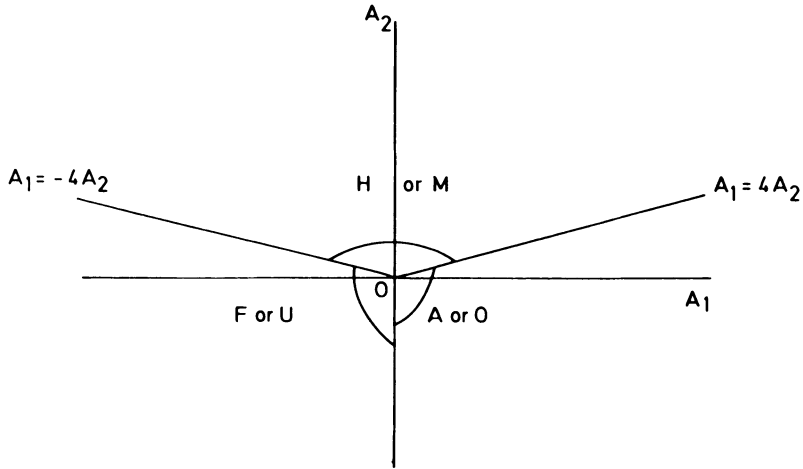
Figure 4 : Magnetic couplings of layered structures with in-
teractions between nearest and second nearest neighbouring planes.
Also elastic distortion of layered structures.

At T ≠ OK, magnetic entropy coupled with excitation of spin
waves introduces terms in S_n for the free energy which reduce the
average atomic spin moment $<S_n>$ and couple the modes k. At high
enough temperatures, it leads $<S_n>$ to disappear.

b) Modulated crystal structures

Let a 3 dimensional layered structure have elastic interac-
tions between first and second neighbouring planes so that the
energy of distortion is expressed in terms of the displacement u_n
of each n plane by

$$N U_M = \sum_{n=1}^{N} \left[A_1 \sum_{i=\pm 1} (u_n - u_{n+i})^2 + A_2 \sum_{j=\pm 2} (u_n - u_{n+j})^2 \right] + O(\delta u_n^{p>2})$$

where $O(\delta u_n^{p>2})$ describes corrective anharmonic terms in relative
displacements $\delta u_n = u_n - u_{n'}$.

Taking

$$u_n = \sum_k u_k \cos(k R_n + \phi_k)$$

leads to the same analysis at OK. Depending on the values of A_1, A_2, the most stable state is (figure 4)

U : undistorted (k = 2 m π)
O : optically distorted (k =(2m+1)π)
M : modulated sinusoïdally (cos ka = - $A_1/4\ A_2$).

The <u>amplitude</u> u_k of the distortion must now be limited at OK by a supplementary factor : it is the role of the anharmonic terms $O(\delta u_n^{P>2})$ in NU_M, which also actually couple somewhat the modes k. At finite temperature, entropy terms must be taken into account, which can make the average $<u_n>$ go to zero.

2 - Delocalized valence electrons

Barring complications such as ionocovalent structures or rare earth metals, which are somewhat on the borderline with the pre-ceeding case, three types of bonding belong to this class :

- covalent structures (figure 5.a), where the atomic struc-ture respects the highly directional conditions for building over-lapping atomic s p^n hybrids. This opens a gap between the valence and conductive band, for interatomic distances d smaller than the critical hybridizing distance d_c. Insulators correspond to equi-librium distances $d_o << d_c$; semiconductors and semimetals to $d_o \lesssim d_c$ or $d_o > d_c$.

- normal metals (figure 5.b), where the atomic structure does not respect covalent sp bonding conditions, but is as closepacked as possible. Near d_o, the lower part of the broad sp band looks like that of a nearly free electron gas.

- transition metals : the broad s band overlaps a narrow d band. The atomic structure is again fairly closepacked.

Because in b, c there is no energy gap near the Fermi level, these structures are necessarily conductors.

Linear combinations of atomic orbitals (i.e. tight binding) are a possible starting point on the two extremes a (sp^n) and c (<u>d</u> s) ; nearly free electrons is more adapted to b. More exact computations require the full panapherlia of muffin tin and computers.

General features of <u>cohesion</u> can again be understood using successive approximations for the electronic structure (cf Appen-dix B).

- In the Hartree approximation, and in a Wigner Seitz approach[3] which uses for computing the energy band the same atomic potential
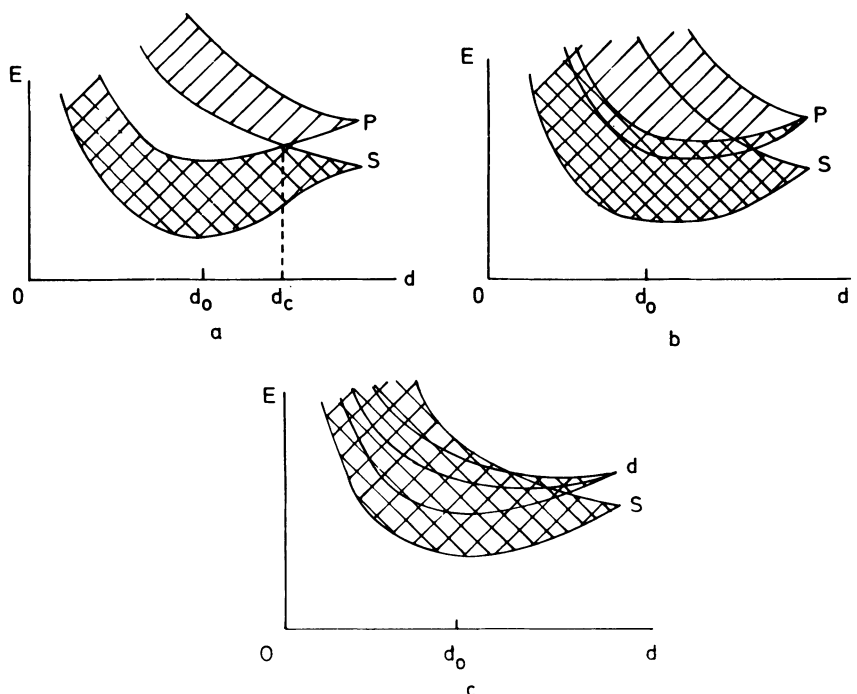
Figure 5 : Schematic band structures : a covalent; b normal metal; c transition metal – Shaded areas : allowed regions; crosshatched areas : regions occupied by valence electrons for a given number of electrons per atom. d interatomic distance.

as seen by an electron in free atoms, cohesion comes from the fact that the broadening of atomic states into bands is essentially symmetrical in energy : for an incompletely filled s, sp or sd shell, the electrons then gain energy by going into the condensed phase ; maximum cohesion occurs for half filled band systems,when the 'bonding' states are full and the 'antibonding' ones empty.

The total band width is related to the frequency of escape of an electron from one atomic orbital, thus both to the strength of the overlap with the orbital on a neighbouring atom and to the number of bonds this orbital takes part in. In covalent structures, bonds are few but very effective (strong overlap, and energy gap lowering the average energy of valence electrons); in metals, cohesion is maximum for maximum number of neighbours : compact and little directional bonding is favoured.

A more refined study in the Hartree scheeme introduces an average electron-electron repulsion which destabilizes somewhat the

condensed phase, especially for normal metals[4][5]. Hartree Fock
and Coulomb corrections are then essential in normal metals to com-
pute the <u>absolute</u> cohesive energy. They also lead to significant
corrections in the middle of transitional series (Appendix C).
They should however play only a reduced role in the latent heats
of phase changes, as they are mostly sensitive to the atomic vo-
lume more than to the crystal structure. This is not quite true
of long range Coulomb corrections, which come in when all the a-
toms do not play equivalent roles in at least one of the phases.

If now crystal modulation is made on one of the structures of
figure 5, it will induce 'virtual excitations' or a 'polarization'
of the valence electrons. There is therefore a strong relation
with the problem of electron-phonon coupling, especially in conduc-
tors.

II - ELECTRON-PHONON COUPLINGS (FOR DELOCALIZED ELECTRONS)

A. Soft Modes at OK. Adiabatic and kinematic approximations

1 - General (crystals)

We consider a time independent real perturbation

$$v = \sum_{q} v_{q} \exp(i q r) + C.C.$$

To first order in (non degenerate) perturbation, each Bloch func-
tion $|n, k\rangle$ becomes

$$|n, k\rangle + \sum_{q} v_{q} \sum_{n'} \frac{|n', k+q+K\rangle\langle n', k+q+K| e^{iqr} |n, k\rangle}{E_{k}^{n} - E_{k+q+K}^{n'}}$$

$$+ \sum_{q} v_{q}^{*} \sum_{n'} \frac{|n', k-q+K\rangle\langle n', k-q+K| e^{-iqr} |n, k\rangle}{E_{k}^{n} - E_{k-q+K}^{n'}}$$

K is a period of the reciprocal lattice K_{RL}. In reduced zone schee-
me, one chooses K such that k and $K' = k \pm q + K$ are in the first
Brillouin zone (figure 6).

If v represents the effect of a (static) phonon mode, q is
restricted to

$$q = q_{o} + K'$$

with $K' \in K_{RL}$.
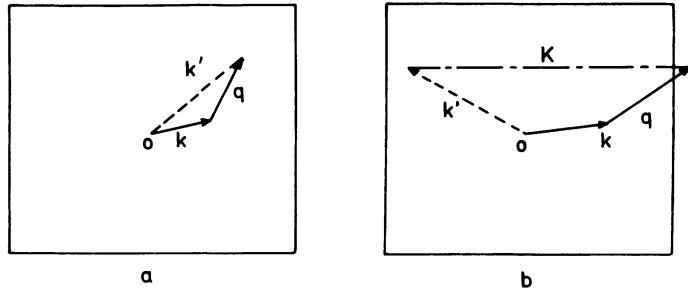
Figure 6 : Convention for $\underset{\sim}{K}$: a   normal (K=0); b   umklapp (K≠0).

To second order in this non degenerate perturbation scheeme, v introduces then an electron $|n,\underset{\sim}{k}>$ phonon $\underset{\sim}{q}_o$ coupling energy

$$\delta E_{\underset{\sim}{k}}^{n}(\underset{\sim}{q}_o)=<n,\underset{\sim}{k}|v|n,\underset{\sim}{k}>+\sum_{\substack{n' \\ \underset{\sim}{K}'}} \frac{|<n,\underset{\sim}{k}|v_{\underset{\sim}{q}_o+\underset{\sim}{K}'}\ e^{i(\underset{\sim}{q}_o+\underset{\sim}{K}')\underset{\sim}{r}}|n',k+\underset{\sim}{q}_o+\underset{\sim}{K}>|^2}{E_{\underset{\sim}{k}}^{n}-E_{k+\underset{\sim}{q}_o+\underset{\sim}{K}}^{n'}}$$

$$+\sum_{\substack{n' \\ \underset{\sim}{K}'}} \frac{|<n,k|v_{\underset{\sim}{q}+\underset{\sim}{K}'}^{*}\ e^{-i(\underset{\sim}{q}_o+\underset{\sim}{K}')\underset{\sim}{r}}|n',\underset{\sim}{k}-\underset{\sim}{q}_o+\underset{\sim}{K}>|^2}{E_{\underset{\sim}{k}}^{n}-E_{k-\underset{\sim}{q}_o+\underset{\sim}{K}}^{n'}} \qquad (1)$$

To this order of perturbations, the various Fourier components $\underset{\sim}{K}'$ introduce in the energy terms that are <u>additive</u> and <u>independent of the phase in v.</u>

The total energy change for the electron is

$$\delta E_{\underset{\sim}{k}}^{n} = \sum_{\underset{\sim}{q}_o occ} \delta E_{\underset{\sim}{k}}^{n}(\underset{\sim}{q}_o) \quad .$$

The total energy change for the phonon is

$$\delta E_{\underset{\sim}{q}_o} = \sum_{n,\underset{\sim}{k}occ} \delta E_{k}^{n}(\underset{\sim}{q}_o) \qquad (2)$$

2 - Energy change for the phonon

   - <u>First order term</u>. It is zero except if $\underset{\sim}{q}_o$ = 0, thus except for a <u>uniform distortion</u>.

Example : if a degenerate strong Van Hove anomaly is lifted
by a uniform shear ε without much change in form (figure 7), and
if the Fermi level falls initially on the anomaly, the distortion
will lower the average (Hartree) energy of the valence electrons
by an amount proportional to the lifting of the energy degeneracy,
itself proportional to v thus to ε. This negative linear term
$\delta E_o = - A\varepsilon$ in the energy must be balanced by an elastic reaction of
the lattice $E_o(\varepsilon) = (1/2)E \varepsilon^2$, associated with the rest of the elec-
tronic and ionic structure :

$$E_o(\varepsilon) + \delta E_o(\varepsilon) = - A\varepsilon + (1/2)E \varepsilon^2$$

This results necessarily in a spontaneous distortion $\varepsilon = \dfrac{A}{E}$, which
can be termed a <u>band Jahn Teller effect</u>.

- <u>Second order term</u>. Terms where $|n,k\rangle$ and $|n',k'\rangle$ are both
occupied cancel out two by two. Only unoccupied $|n' k'\rangle$ states
need thus be considered.

a   b
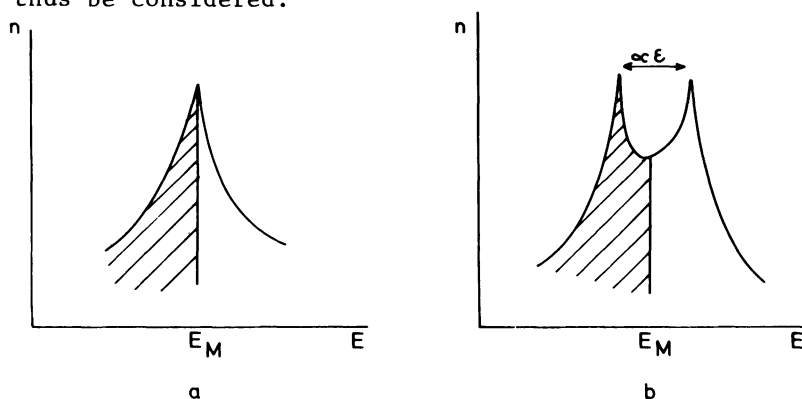
<u>Figure 7</u> : Band Jahn Teller effect : a v = 0 ; b v $\neq$ 0 .

They also provide <u>negative</u> contributions : the second order
electron-phonon coupling necessarily lowers the phonon energy.

In an <u>insulator</u> , the denominator $E_k^n - E_{k'}^{n'}$ is always fini-
te (larger in amplitude than the energy gap between the valence
and conduction band). δE_{q_o} is therefore a correction that varies
continuously with q_o. It remains small everywhere, being of the
second order in the small phonon amplitude. Explicit estimates of
v_q later on will show that the total perturbed energy $E_{q_o} + \delta E_{q_o}$ of
all phonons are then expected to remain positive : the mode softe-
ning due to electron phonon coupling is much too small to become
catastrophic. Crystal modulation is therefore expected <u>not</u> to take
place normally in covalent crystals. This is after all reasonable:
the strongly directional covalent bonds are not expected to lead
normally to several structures of comparable energy and differing

only little from each other.

In conductors, a large contribution is expected for pairs $|n,\underset{\sim}{k}>$, $\overline{|n'\ \underset{\sim}{k'}>}$ of states both near to the Fermi level. With $\underset{\sim}{k'} = \pm \underset{\sim}{q_o} + \underset{\sim}{K}$, such points are near to lines such as L, figure 8.a where the Fermi Surface S_M cuts a surface S'_M obtained by a translation of S_M by $\pm \underset{\sim}{q_o} + \underset{\sim}{K}$. When, for a given direction, $\pm \underset{\sim}{q_o} + \underset{\sim}{K}$ increases in size, L decreases to a point (figure 8.b), then disappears (figure 8.c). One then expects the special contribution from the neighbourhood of L to vary strongly near to the critical values of $\pm \underset{\sim}{q_o} + \underset{\sim}{K}$ such that S_M and S'_M just touch.

a   b   c
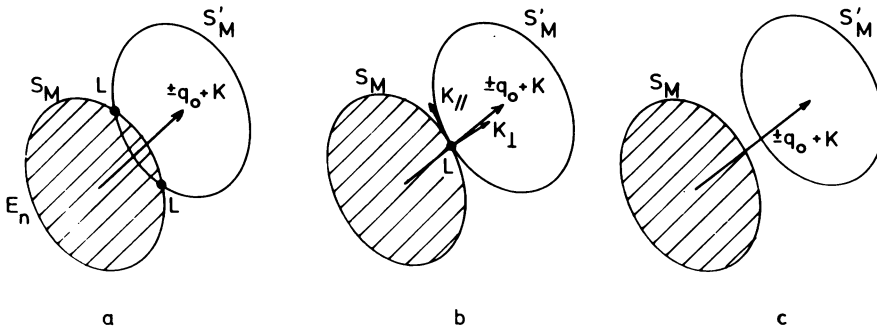
Figure 8 : Critical region L of integration and its variation with $\pm \underset{\sim}{q_o} + \underset{\sim}{K}$, near a critical value of that vector.

Figure 9, 10 describe schematically four general cases in three dimensions.

α . S_M and S'_M touch on a conical point.

β . S_M and S'_M have in common a point and a tangent plane, but different curvatures.

γ . S_M and S'_M have in common a point, a tangent plane and one common curvature.

δ . S_M and S'_M have in common a point and the two principal curvatures.

Case β is the normal three dimensional one. α arises if the Fermi level happens to fall on a Van Hove anomaly, and $\underset{\sim}{q_o}$ is such that S_M and S'_M touch on that point. Cases γ and δ are possible if the Fermi surface has a complex geometry ; they are traditionally called nesting conditions. Inspecting the immediate neighbourhood of L, one sees that the general two dimensional case (where in three dimensions Fermi surfaces are parallel cylinders) corresponds to case γ; the general one dimensional case (in three dimensions, Fermi surfaces are parallel planes) corresponds to case δ.
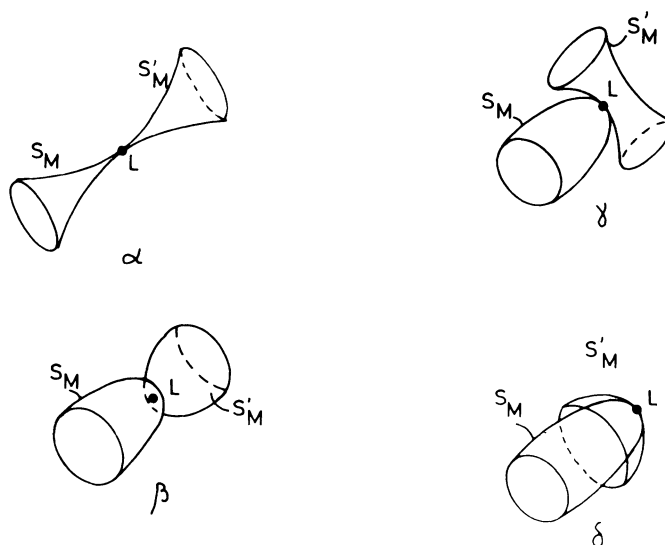
Figure 9 : Four cases of contact between S_M and S'_M.
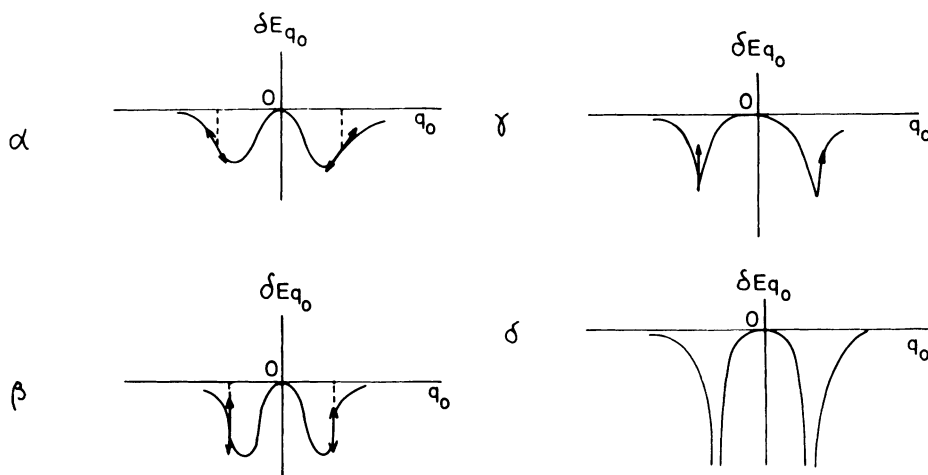
Figure 10 : Corresponding Kohn anomalies.

Figure 10 gives the corresponding behaviour of δE_{q_0} in the immediate neighbourhood of the critical value for q_0 :

α : inflextion point.

β : inflexion point with infinite tangent.

γ : discontinuous change of slope.

δ : negative infinity.

In the 3 dimensional case β for instance, one can choose suitable axes $K_\perp$, $K_{//}$ (figure 8.b) such that E_k^n and $E_{k-q_o+K}^n$ can be developped near L as

$$E_k^n = E_1 = E_M + a\, K_\perp^2 + b\, K_{//}^2$$

$$E_{k-q_o+K}^n = E_2 = E_M - a\, (k_o - K_\perp)^2 + b\, K_{//}^2$$

The integral in (1), (2) can be written

$$\delta Eq_o = \int \frac{f(k)}{E_1 - E_2}\, d_3 k = const + \frac{1}{b}\, k_o \ln |k_o|$$

where k_o measures the distance or the overlap between S_M ans S'_M, figure 8.

Because of the contribution to integration in (1), (2) of the neighbourhood of the Fermi surface, the negative correction in δEq_o is larger in conductors than in (band) insulators. It has furthermore an anomalous behaviour when this contribution disappears : this is the Kohn anomaly predicted initially for nearly free electrons[6] and observed in the phonon dispersion curves of many normal and transition metals.

The discussion below on v_q will show that $v_{q_o} \propto q_o$, thus δEq_o vanishes with q_o and is usually too small to produce soft phonons. The general form of δEq_o pictured figure 10 takes into account the variation in q_o^2 of δEq_o near the origin. This form predicts that soft modes

- should always occur at the critical value of q_o in the 3 dimensional case δ of complete nesting (or in general in one dimension).

- might occur at the critical value of q_o in the 3 dimensional case γ of partial nesting (or in general in two dimensions).

- might occur, for q_o near to the critical value, in the general 3 dimensional case β .

- are unlikely to be associated with a Van Hove anomaly at the Fermi surface (case α).

3 - Classical examples

a) Nearly free electrons in 3 dimensions

The first application of these ideas can be said to date from the 1930's. It refers to the explanation by Jones[7] of the regular succession of crystal phases noticed by Hume Rothery[8] in 'normal' metals and alloys when one varies their electron per atom ratio. In such crystals where the valence electrons are only weakly scattered by the atoms, the scattering by the crystal structure can be Fourier analyzed, and each Fourier component acts on the nearly free electrons as a (static) phonon mode. This mode has a stability that varies rapidly when its wave vector q_o is near to one of the critical values defined figure 8.b, and the whole crystal structure has a stability very sensitive to the electron per atom ratio (or the size of the Fermi sphere) when the critical condition is fullfilled for a maximum number of Fourier components. As the q_o are here reciprocal lattice vectors, it is the same to say that the structure is such that the Fermi sphere touches a maximum number of Brillouin zone boundaries. Figure 11 pictures the behaviour of the contribution of δE_{q_o} to cohesion versus electron per atom ratio in two such structures. It is here the whole atomic
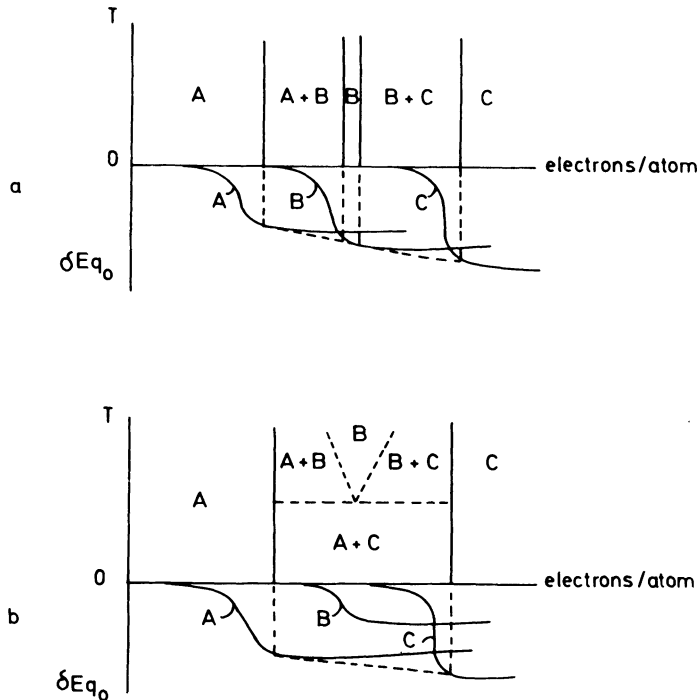
Figure 11 : Two possible cases of Hume Rothery- Jones phases in normal metals and alloys, and the corresponding phases diagrams at OK.

potentials which scatter the electron, and not their displacements from a periodic arrangement. As a result v_{q_o} and δEq_o do <u>not</u> vanish at small values of q_o (for a fixed number of electrons) or at large electron per atom ratio (for fixed q_o and thus crystal structure). As stressed figure 11, the successive Hume Rothery Jones structures met at increasing electron per atom ratio will be actually observed at OK only if their corresponding stabilities are increasing (case a). Even then, one should distinguish two types of conditions for the phase diagram at OK of a solid solution between two elements $M_1 M_2$: the extremal phases (such as A, C figure 11a) should extend to near the critical electron per atom ratio ; and the intermediary phases (B, figure 11.a) should have a narrow range of stability near the corresponding critical electron per atom ratio. One does not expect much change in the phase boundaries with temperature at low temperatures (because the electron entropy is near to that of free electrons in any case) except that the lattice entropy might stabilize at high temperatures[9] a phase such as B, figure 11.b, which is unstable at OK. A famous example is the BCC β phase of Cu Zn alloys.

The same condition of Brillouin zone boundary tangent to the Fermi sphere has been used to explain more complex alloy structures where superstructures modulate a fundamental simple crystal structure[10]. The modulation can either be a concentration modulation, thus producing a special kind of ordering (Au Cu alloys) or a periodic succession of stacking faults (Ag Cd alloys).

b) Narrow d bands in three dimensions

The conditions for soft modes by critical Kohn anomaly can be expressed explicitly for transitional metals in a tight binding (LCAO) description of the d band[11]. They are usually complex, owing to the complexity of the Fermi surface.

c) Narrow d bands in 2 dimensions (planes)

This case was first seriously considered for the layered 3 dimensional structures of <u>transition dichalcogenides</u>[12], where the transition elements build up close packed planes which are separated by rather insulating layers of S, Se or Te. To first order at least, each plane has a two dimensional d band with an electronic structure which can be treated separately (figure 12.a).

d) Narrow bands in one dimension (chains)

This case was first considered theoretically by Peierls[13] and Fröhlich[14] (figure 12.b) : Kohn anomalies appear very clearly in compounds with parallel conducting chains separated by more or less insulating material :
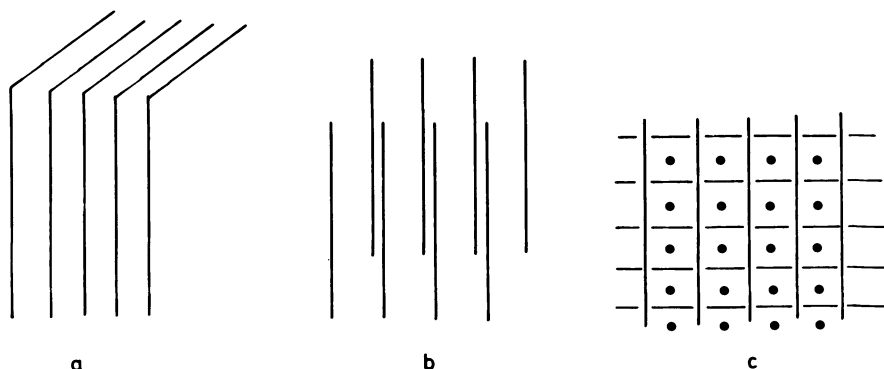
Figure 12 : Three types of two dimensional cases : a parallel
planes ; b parallel chains ; c 3 orthogonal sets of parallel
chains.

- KCP (chains of Pt atoms)[15].

- TTFTCNQ (organic chains)[16].

e) Band Jahn Teller

The first application of Band Jahn Teller effects was made on
A15 transition compounds (V_3 Si, Nb_3 Sn ..), which have three or-
thogonal sets of parallel chains of transition atoms (figure 12.c).
The first studies considered the lifting of degeneracy by shear of
the edges of the d bands of the linear chains, assumed independent
[17]; further studies considered the lifting of degeneracy of in-
termediary peaks possibly connected with the interactions between
the chains[18][19].

NB : In the historical development of these concepts, there is
an intimate relation with metal magnetism. Thus

- ferromagnetism is the analogous of the Band Jahn Teller
effect.
- antiferromagnetism and helical magnetism are modulated
structures.

Conditions for the stability of these magnetic phases were
in all cases expressed in terms of Coulomb and exchange interac-
tions, sometimes before the corresponding conditions for crystal
modulation (Stoner's criterion for ferromagnetism[20], Slater for
antiferromagnetism [21], Lomer for helical and modulated structu-
res[22]). The quantitative differences involved will be discussed
below.

- In all the low dimensional cases, there exist interplane or interchain couplings which actually make the substance a three-dimensional one, at least at low temperature.

B. Discussion of the approximations

1 - The meaning of v

We must define more precisely the meaning of the effective potential v which describes the effect of a phonon on the electrons. We shall show on two extreme simple cases that it is not actually a proper potential. We shall also see that v_q it proportional to q and has necessarily an order of magnitude which makes an instability condition only possible near a Kohn anomaly.

- <u>Nearly free electrons</u> (one atom per unit cell)[23]. If we assume each weak atomic potential $V_i(\underline{r} - \underline{R}_i)$ to be bodily shifted by the phonon <u>without change of form</u>, we have

$$v_q \exp i\, \underline{q}\,\underline{r} = \sum_i \left[V_i(\underline{r} - \underline{R}_i - \underline{u}_i) - V_i(\underline{r} - \underline{R}_i) \right] \approx \sum_i \underline{u}_i \, \nabla_{R_i} \, V_i(\underline{r} - \underline{R}_i)$$

Assuming

$$\underline{u}_i = \underline{u}_{q_o} \exp i\, \underline{q}_o \, \underline{R}_i \qquad\qquad (3)$$

and <u>if V_K is the Fourier transform</u> of $V_i(\underline{r})$,

$$\langle k | v_{q_o} e^{i\underline{q}\underline{r}} | k' \rangle = - i(\underline{q}_o \, \underline{u}_{q_o}) \, V_{q_o} \, \delta(\underline{k}' - \underline{k} + \underline{q}_o).$$

This goes to zero with q_o. For free electrons, there are no umklapp terms, and no coupling of electrons with shear waves.

<u>NB</u> :-The assumption of <u>rigid</u> displacement of V_i will be discussed and somewhat corrected later on.

- V_i is a <u>pseudopotential</u>[24], thus as operator, such that $\langle k | V_i | k' + K \rangle = V_K$ is a function of K = k'-k but also of k. Thus the continuous variation of V_K with k will distort Eq_o, without changing however the mathematical form of the Kohn anomaly ; and the value of V_K appearing near to Kohn anomaly refers specifically to states k and k' near to the Fermi level.

- In the undistorted crystal structure, the Fermi surface is distorted from a sphere by the scattering by the undisplaced pseudopotentials V_i. However in the approximation so far used, these distortions are of second order in V_i. To take them into account in computing δEq_o would introduce correction of higher

order than v_q^{2}. [25]

   - Tight binding (one atomic orbital per unit cell) [25][26].
With the energy of an atomic orbital $|i\rangle$ in a free atom taken as
zero of energy, the tight binding hamiltonian for a non degenera-
te band reads

$$H \simeq \sum_{\substack{i \\ j \text{ near to } i}} \beta_{ij} |i\rangle\langle j|$$

if one neglects the electrostatic crystal field term, an approxi-
mation valid in pure metals.

   In the same spirit as for free electrons, one can assume that
the displacement u_i given by (3) bodily displaces the atoms and
their atomic orbitals $|i\rangle$ without otherwise changing the atomic
potentials and orbitals. With these shifted orbitals $|i'\rangle$, the
change in hamiltonian produced by the displacements u_i reads

$$\delta H \simeq \sum_{\substack{i \\ j \text{ near to } i}} \delta\beta_{ij} |i'\rangle\langle j'|$$

where

$$\delta\beta_{ij} = \beta'_{ij} \ \delta d_{ij} = \beta'_{ij}(u_j - u_i) \cos \theta_{ij} \ .$$

   θ_{ij} is the angle made by $R_j - R_i = d_{ij}$ with the direction
of displacement (figure 13)
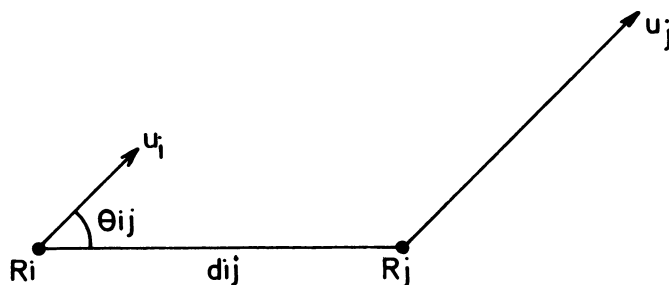
Figure 13 : Definition of θ_{ij}, d_{ij} .

To first order in u, $|i'\rangle$ can be replaced by $|i\rangle$. Hence

$$\langle n, \underset{\sim}{k} | v | n \underset{\sim}{k}' \rangle = \sum_{j \text{ near to } i} \frac{1}{N} e^{i(\underset{\sim}{k}'\underset{\sim}{R}_j - \underset{\sim}{k} \underset{\sim}{R}_i)} \delta\beta_{ij}$$

$$= \sum_{j \text{ near to } i} \beta'_{ij} u_{\underset{\sim}{q}_o} \cos\theta_{ij} \left[1 - \exp(-i\underset{\sim}{q}_o \underset{\sim}{d}_{ij})\right] e^{i\underset{\sim}{k}\underset{\sim}{d}_{ij}}$$

$$\times \delta(\underset{\sim}{k}' - \underset{\sim}{k} + \underset{\sim}{q}_o + \underset{\sim}{K}_{RL}).$$

This goes again to zero with $\underset{\sim}{q}_o$. In general, shear waves are now coupled with electrons. There are umklapp processes. Finally, as for free electrons, this expression is not only a function of $\underset{\sim}{k}' - \underset{\sim}{k} = \underset{\sim}{q}_o + \underset{\sim}{K}_{RL}$, but also a function of $\underset{\sim}{k}$: v is an operator and not a simple potential function. Only near to k = 0 can one neglect this variation.

    – Orders of magnitude for soft modes. Both expressions of v_{q_o} are similar in order of magnitude : $u_{q_o} q_o V_{qo}$, where V_{q_o} is the derivative or the Fourier transform of an electronic energy term.

    In expression (2), the denominator of $\delta E_k^n(q_o)$ is larger than the energy gap g, if one considers an insulator . In that case, the second order correction is

$$\delta E_{q_o} \simeq \chi_{q_o} |v_{q_o}|^2$$

with $\chi_{q_o} = g^{-1}$,

and the mode would be soft only if

$$E_{q_o} + \delta E_{q_o} < 0$$

or

$$\frac{(v_{q_o})^2}{E_{q_o}} > -\frac{1}{\chi_{q_o}} \simeq g$$

with

$$E_{q_o} = \frac{1}{2} M^2 \omega_{q_o}^2 u_{q_o}^2$$

M atomic mass, ω_{q_o} pulsation of the phonon without electron–phonon coupling.

    Hence the condition :

$$\frac{\left| q_o \; V_{q_o} \right|}{\sqrt{g/2}} > M \; \omega_{q_o}$$

As $M \; \omega_{q_o} \gg 1$ atomic unit, and $g \simeq q_o \; V_{q_o} \simeq$ a fraction of atomic unit, this condition cannot usually be fullfilled, except perhaps for very small gap semiconductors ($g \simeq 0$).

The same applies to <u>metals</u>, with $\chi_{q_o}^{-1}$ of the order of the Fermi energy, except near a $\overline{\text{Kohn}}$ anomaly where the soft mode condition can possible be realized.

In conclusion, although v is not exactly a potential, simple estimates applicable respectively to normal or transition metals show that only modes connected with a Kohn anomaly can usually become soft.

2- Self consistency (to first order)

This point has some general interest, and will therefore be developped in some detail.

In the same approximation used so far, a perturbing potential $v(\underset{\sim}{r})$ produces in the valence electrons a local change in electronic density

$$\delta\rho(\underset{\sim}{r}) = \sum_{\underset{\sim}{q}} v_{\underset{\sim}{q}} \sum_{\substack{n,\underset{\sim}{k}_{occ} \\ n'k'_{inocc}}} \frac{\langle n', \underset{\sim}{k} + \underset{\sim}{q} + \underset{\sim}{K} | \; e^{i\underset{\sim}{q}\underset{\sim}{r}} |n,\underset{\sim}{k}\rangle}{E_{\underset{\sim}{k}}^n - E_{\underset{\sim}{k}+\underset{\sim}{q}+\underset{\sim}{K}}^{n'}} u_{\underset{\sim}{k}}^{n*}(\underset{\sim}{r}) \; u_{\underset{\sim}{k}+\underset{\sim}{q}+\underset{\sim}{K}}^{n'}(\underset{\sim}{r}) + C \tag{4}$$

where, as before, C is deduced from the first term by changing $\underset{\sim}{q}$ in $-\underset{\sim}{q}$ and $v_{\underset{\sim}{q}}$ in $v_{\underset{\sim}{q}}^*$

a) Asymptotic perturbation, far away from a localized perturbation v.

For insulators, all terms in (4) are regular. The integrals are obviously dominated by the regions where $E_{\underset{\sim}{k}}^n$ and $E_{\underset{\sim}{k}}^{n'}$ are nearly stationary, i.e. the neighbourhood of Van Hove anomalies. If the perturbation v acts near to the origin, the main contribution for $r \to \infty$ will come from the couple of Van Hove singularities for which $E_{\underset{\sim}{k}}^n - E_{\underset{\sim}{k}}^{n'}$ is a minimum, i.e. the top E_v of the valence band and the bottom E_c of the conduction band, figure 14. A regular
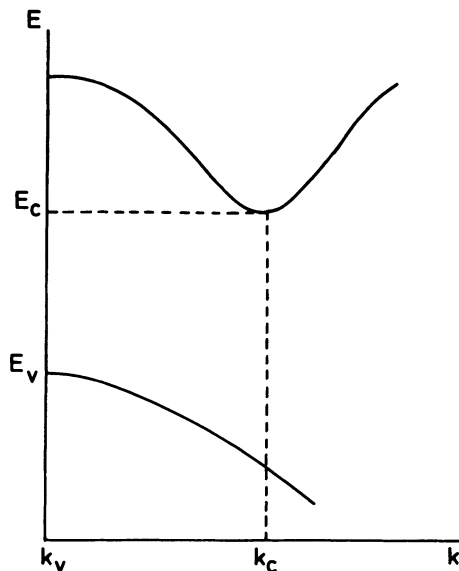
Figure 14 : Energy gap in a band insulator.

development of E_k^n and $E_{k'}^{n'}$ near to the corresponding points $\underset{\sim}{k}_V$, $\underset{\sim}{k}_c$ in the reciprocal space gives easily[27]

$$\delta\rho \underset{r \to \infty}{\to} \sum_{K \in K_{RL}} \text{oscill } (\underset{\sim}{K} \, \underset{\sim}{r}) \text{ oscill } (\underset{\sim}{k}_c - \underset{\sim}{k}_V) \underset{\sim}{r} \, \exp(\frac{-r}{a})$$

where oscill (x) means a sinusoïdal function of x. One can show that

$$a \simeq \frac{2h}{\left[m^*(E_c - E_V) \right]^{1/2}}$$

where the effective mass m^* is itself proportional to $E_c - E_V$. Hence $a \propto (E_c - E_V)^{-1}$.

The interband terms thus give rise to a rapid exponential degrease of $\delta\rho(\underset{\sim}{r})$ outside the perturbed region where $v \neq 0$.

For conductors, the contributions near the Fermi level give one or several further intraband terms[28][29]. The asymptotic behaviour is dominated by the neighbourhood of lines such as L, figure 8. And the main contributions will arise when the phase of the matrix element of exp i $\underset{\sim}{q} \, \underset{\sim}{r}$ is nearly stationary. This requires L to reduce to a point (figure 8.b and 15) where the normal to the Fermi Surface S_M is parallel to $\underset{\sim}{r}$. If there are only
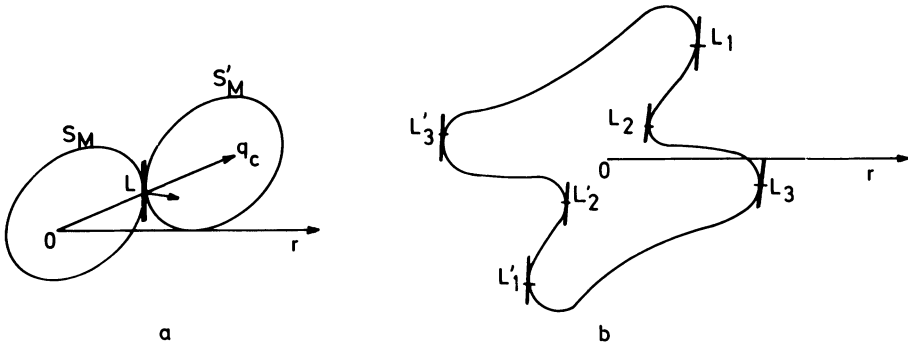
Figure 15 : Value of q dominating the asymptotic behaviour of $\delta\rho(\underset{\sim}{r})$ in a metal : a simple case ; b more complex case.

two such values of q = ± q_c (figure 15.a), an integration near the them gives

$$\delta\rho \underset{r \to \infty}{\to} (\sum_{K \in K_{EL}} \text{oscill } \underset{\sim}{Kr}) \; r^{-n} \; \text{oscill } (\underset{\sim}{q_c} \; \underset{\sim}{r})$$

with   n = 4, 3, 2, 1 depending on whether the contact of S_M and S'_M on L is of the type α, β, γ,δ respectively (figure 9). In more complex cases (figure 15.b), there are interference terms between these various points : q_c = all the possible $L_i \, L_j (L_i = L_1, L_2, L_3, L'_1, L'_2, L'_3)$ (figure 15.b).

b) Screening to an external potential.

Let $v_e(\underset{\sim}{r})$ be an external perturbing potential applied to the system. It will produce a displaced charge $\delta\rho(\underset{\sim}{r})$ which itself produces a supplementary internal screening potential $v_i(\underset{\sim}{r})$, so that the total potential acting on the electrons is

$$v(\underset{\sim}{r}) = v_e(\underset{\sim}{r}) + v_i(\underset{\sim}{r})$$

Poisson's equation gives[*]

$$\Delta v_i(\underset{\sim}{r}) = -4\pi e^2 \delta\rho(\underset{\sim}{r})$$

and $\Delta\rho$ is related to v by equation (4).

Fourier transforms give

---

[*] As usual, v is the potential energy of an electron.

$$v_q = v_{eq} + v_{iq}$$

$$q^2 v_{iq} = 4 \pi e^2 \delta\rho_q$$

$$\delta\rho_q = \sum_{K \in K_{RL}} \chi_q^K v_{q+K}$$

where the general susceptibility χ_q^K which relates charge to potential is a tensor. This set of equations allows in principle to compute the selfconsistent perturbing potential v and perturbed electronic density $\delta\rho$ for a given external potential $v_e(r)$.

Thus, introducing the general dielectric tensor

$$\varepsilon_q^K = \left(\delta(K) - \frac{4\pi e^2}{q^2} \chi_q^K \right)$$

such that

$$\sum_K \varepsilon_q^K v_{q+K} = V_{eq}$$

one obtains

$$\sum_K \varepsilon_q^K \delta\rho_q = \frac{q^2}{4\pi e^2} \sum_K (\delta(K) - \varepsilon_q^K) v_{eq}$$

c) Screening of a phonon wave. Charge density wave.

v_e is now the perturbation potential due to a phonon. The preceeding equations show that each Fourier component v_{eq} of the phonon potential produces a charge density wave[30] with various Fourier components $\delta\rho$, at $q' = q + K_{RL}$. This wave screens the external potential v_e into a total potential v with Fourier components $v_{q'}$. Thus in general the charge density wave has a somewhat complex structure ; and it couples the various Fourier components of the total potential v, so that the dielectric constant ε_q^K is a tensor.

The consequence of this screening on the stability of the phonon will only be discussed in the two extreme cases where these formulae simplify.

– Nearly free electrons. The umklapp terms $K \neq 0$ disappear ; and the susceptibility takes a simple form (figure 16):

$$\chi_q = \frac{q^2(1-\varepsilon_q)}{4\pi} = \sum_{k_{occ}} \frac{1}{E_k - E_{k+q}} \propto - \left[1 + \frac{4k_M^2 - q^2}{4 k_M q} \ln \left| \frac{2k_M + q}{2k_M - q} \right| \right] (<0)$$
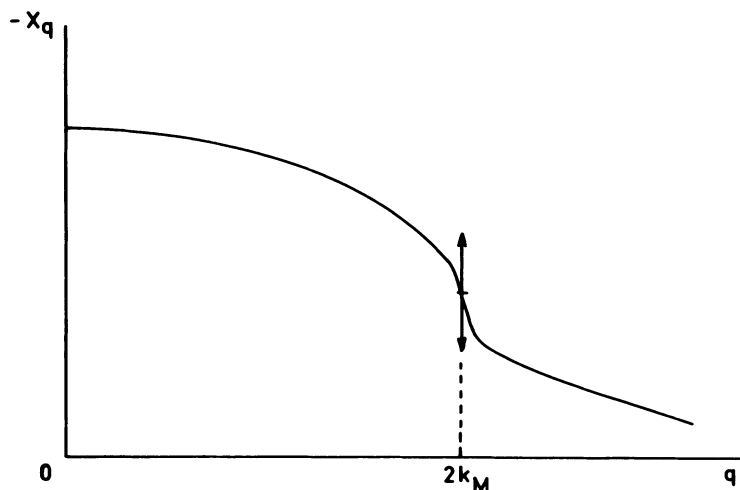
Figure 16:Susceptibility χ_q for free electrons.

In the second order terms in v for δE_{q_0}, equations (1), (2), one must distinguish the contributions of v_e and v_i, and not count twice the Coulomb interactions of $\delta\rho$ with itself. As a result, $|v_q|^2$ should be replaced by $|v_q \, v_{eq}| = \varepsilon_q^{-1}|v_{eq}|^2$. Hence the second order term in δE_q reads[24][31]

$$\delta E_q = \frac{\chi_q}{\varepsilon_q} \, |v_{eq}|^2 = (\frac{1}{\chi_q} - \frac{4\pi \, e^2}{q^2})^{-1} \, |v_{eq}|^2 \; .$$

Thus the Kohn anomaly due to χ_q is reduced but not suppressed by that in ε_q.

The instability condition of the phonon mode becomes

$$\frac{|v_{eq}|^2}{E_q} \quad \frac{1}{\varepsilon_q} > - \frac{1}{\chi_q}$$

The production of a charge density wave coupled with the phonon and screening its potential thus introduces a reduction factor $\frac{1}{\varepsilon_q} < 1$, for $\chi_q < 0$. The charge density wave stiffens the phonon, and thus makes its instability less easy to produce.

Tight binding

 - For half filled bands and elementary alternate structures,

there is no charge density wave coupled with a phonon mode[26].
Alternate structures are such that only closed circuits with an
even number of interatomic jumps between neighbouring sites are
possible (figure 17.a).

a   b
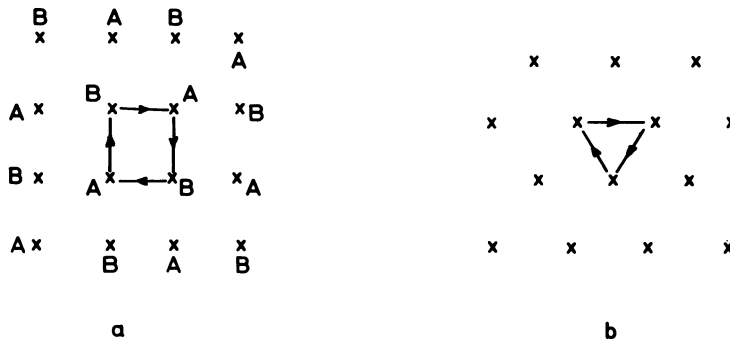
Figure 17 : Two types of crystal structures : a alternate ; b non
alternate.

In such structures, one can define two interpenetrating latti-
ces A,B such that each A site has only B nearest neighbours, and
vice versa. To each electron function

$$|\psi> = \sum_{nA} a_A^n |n,A> + \sum_{mB} a_B^m |m,B>$$

with energy

$$E = \sum_{\substack{nA \\ mB \text{ near } nA}} (\beta_{AB}^{nm} a_A^{n*} a_B^m + \beta_{BA}^{mn} a_B^{m*} a_A^n)$$

there corresponds a function

$$|\psi'> = \sum_{nA} a_A^n |n,A> - \sum_{mB} a_B^m |m,B>$$

with energy $- E$, symmetrical with respect to the middle of the
band ; and these two wave functions give equal electronic densi-
ties ($\sum_n |a_A^n|^2$ or $\sum_m |a_B^m|^2$) on each (A or B) site. Thus, whatever
the distortion and as long as the alternate topology is preserved,
such structures with half filled bands have the same number of
electrons on each site, equal to the number of atomic orbitals
involved.

For less than half filled bands, such structures have an
accumulation of electrons in the compressed regions, where the

transfer integrals β_{ij} are larger in amplitude, thus the band ef-
fectively larger but still symmetrical ; the converse is true
in extended regions ; there should thus be a charge density wave
associated with the phonon, providing a repulsive correction in
the compressed regions and an attractive one in the extended re-
gions (figure 18.a). The converse should hold for more than half
filled bands (figure 18.b), where it is justifiable to talk in
terms of positive holes.
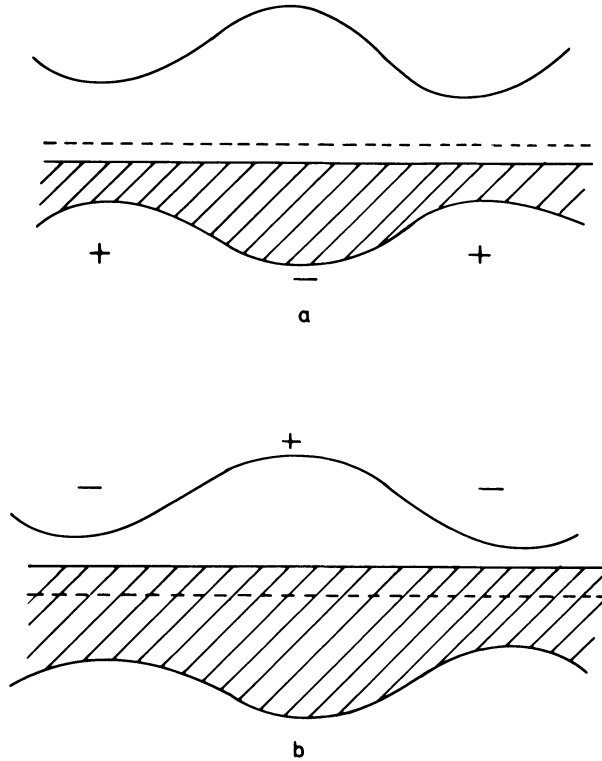
Figure 18 : Longitudinal phonons in alternate structures : a
electrons ; b positive holes.

In non alternate structures, the same distinction between
electrons and holes respectively for nearly empty and nearly
full bands ; but the transition from one type of behaviour to
the other, thus the exact filling for which no charge density wave
is produced, will depend on the type of phonon considered. The
condition for no charge density wave will still occur near the
middle of the band.

- If one considers only the <u>intraatomic</u> contribution to screening due to the charge density wave, this again can but <u>stiffen</u> the phonon[32]. Let U be the average Coulomb interaction between valence electrons on the same site. To a local change $\delta\rho_i$ in electronic density there would correspond a local change δV_i in the atomic potential of site i such that

$$\delta V_i = U \ \delta\rho_i$$

This replaces Poisson's equation in the preceeding analysis. And, in the extreme case of nearly full or nearly empty non degenerate bands, where a simple geometry of the Fermi surface prevents umklapp processes to occur, the unstability condition reads

$$\frac{\left|v_{eq}\right|^2}{E_q} - U > - \frac{1}{\chi_q}$$

The addition of U indeed makes a soft mode less easy to produce.

- One should however also consider <u>interatomic</u> contributions of the screening to the stability of the mode[26]. This Madelung energy can lower the energy of suitable modes. A historical example is the special stability of Kohn anomalies along parallel chains when neighbouring chains are in phase opposition, which was
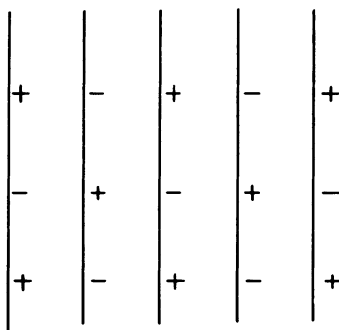
Figure 19 : Coupling in antiphase of Kohn anomalies along parallel chains, stabilized by long range electrostatic interactions.

predicted by Barisic[26] and later observed in linear chain compounds such as KCP[15].

A general study of the tight binding case, combining the intra and interatomic contributions of screening has <u>not</u> been made so far.

It is conceivable that in some cases the overall effect could make
the phonon mode softer. It is however very unlikely, because U is
a large positive quantity. Indeed the electrostatic correction is
most favourable for stabilization if modulation is at wave lengths
such that neighbouring atoms have opposite charges $\pm$ q. The total
electrostatic correction then reads $\frac{1}{2} U_q^2 - \frac{\alpha q^2}{R}$ per atom where R
is the interatomic distance and α the Madelung constant. With
$\alpha/R \simeq 1/4$ Atomic unit, and $U \simeq 1/4$ to $1/2$ At. unit, the correction
is negative but small. Furthermore we have seen that at such wave
lengths, the amplitudes of a charge density wave produced by a
phonon is small.

<center>Conclusion</center>

- The screening changes the strength, but not the nature of
the Kohn anomaly.

It corresponds usually (but not always) to a charge density
wave which is coupled with the phonon ; this usually stiffens the
phonon, thus making soft mode conditions less easy.

- Indeed the production of a charge density wave without a
phonon[30] would require $\delta\rho \neq 0$ for $v_e = 0$, or, according to the
analysis above, the dielectric constant ε_q going to zero. This is
clearly impossible for free electrons, where $\chi_q < 0$, and very unli-
kely in tight binding, except perhaps for modes with short wave
lengths which are but weakly coupled with the phonons. It is thus
unfortunate, to say the least, that the fashion is nowadays to
call a soft phonon mode by the name 'charge density wave' which
actually is the part in the mode that fights against its instabi-
lity!

- The situation would be quite different for a spin density
wave, because there the positive U term is replaced by a negative
term describing intraatomic exchange effects : a spin density wave
can soften into a magnetically modulated stable structure, without
necessarily being coupled with a structural distortion. Coupling
between spin density waves and phonons by spin orbit coupling can
lead indeed to weak but non zero magnetostrictive lattice modula-
tions.

- For nearly free electrons, the second order term in δE_q
can be thought of as due to the modulation by the displacement u
of the pair interactions between the atomic pseudopotentials, each
treated to second order as the interactions of two impurities
in a free electron gas. Taking $\varepsilon_q^{-1} |v_{eq}|^2$ is the same as conside-
ring the interaction of the screened potential of one atom
acting on the maked charge of the other in the pair.

- The (screened) Kohn anomaly can be considered as a resonance between the phonon and the Fermi electrons responsible for the long range oscillations of the screening. It is also an interference effect of the long range oscillating (screened) interatomic forces. Indeed if the Fermi electrons have a long but finite mean free path ℓ, due to say scattering by imperfections, this will dampen exponentially the long range oscillations of the interatomic forces (in $\exp - \frac{r}{\ell}$) and correlatively broaden the Kohn anomaly over a width $\delta k \simeq 2 \pi/\ell$. But it will pratically <u>not</u> change the nature and the stability of the possible soft modes.

3 - Other correlation effects

- Magnetism : exchange effects lead to possible ferromagnetism or soft spin density waves, thus various modulated magnetic structures, which will not be considered here.

- Energy : Coulomb correlations introduce corrections in the energy. As stressed above, they are important for evaluating the absolute value of cohesion, but play only a reduced role in the relative stability of crystal phases (cf Appendix D).

- Damping : electron-electron collisions are only active at finite temperatures. They introduce resistive terms which are usually at most comparable with those due to imperfections (impurities, phonons). In all cases, electron phonon coupling seem to dominate on electron-electron scattering ; this last term can be treated as a fairly small correction, analogous to that just mentioned for scattering by imperfections[33].

4 - Degeneracy of electronic states

- First order terms. If the lattice structure has degenerate Van Hove anomalies at <u>different</u> points k_r, k_s ... in the first Brillouin zone, a phonon mode v_q with $q = k_s - k_r + K_{RL} \neq 0$ can lift their degenerary to first order :

$$\langle n \, k_r \mid v_q \mid n \, k_s \rangle \neq 0$$

This is a natural extension of the effect possibly associated with uniform distortions, and can thus be termed an <u>extended Band Jahn Teller effect</u>.

- Second order terms. The one beam (kinematic) approximation used until now is not valid, strictly speaking, near the lines L, figure 8, where it is used to analyse the Kohn anomaly. In such a region, one Bloch function $|n', k \pm q_0 + K\rangle$ takes an amplitude comparable with $|n,k\rangle$. It is then better to develop the perturbed function $|\psi\rangle$ in these two wave functions, neglecting the contri-

butions of the other Bloch functions $|n'',k''\rangle$, which will be small and regular.
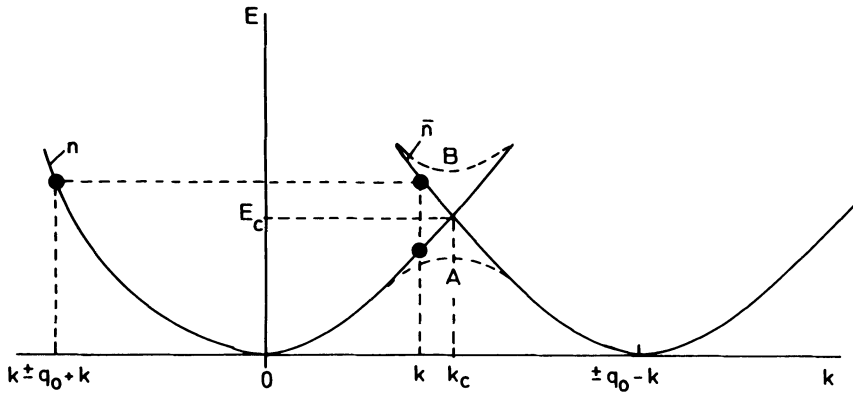
Figure 20 : Two beams approximation (in the case n' = n).

Thus we reduce the hamiltonian

$$H = \sum_{n,k} E_k^n |n,k\rangle\langle n,k| + \sum_{kk'} |n,k\rangle\langle k|v|k'\rangle\langle n'k'|$$

to

$$H = \sum_k \left[E_k^n |n,k\rangle\langle n,k| + E_k^{\bar{n}} |\bar{n},k\rangle\langle \bar{n},k| \right.$$

$$\left. + v_{q_o} |n,k\rangle\langle \bar{n},k| + C.C. \right]$$

where $E_k^{\bar{n}} = E_{k\mp q_o+K}^{n'}$ (figure 20).

The well known solutions of this (nearly) degenerate problem is

$$E_k^n(q_o) \simeq \frac{1}{2} \left[E_k^n + E_k^{\bar{n}} \pm \sqrt{(E_k^n - E_k^{\bar{n}})^2 + 4|v_{q_o}|^2} \right] \tag{5}$$

with

$$|\psi_k\rangle = u_k |n,k\rangle + v_k |\bar{n},k\rangle$$

$$\frac{v_k}{u_k} = \frac{v_{q_o}}{\frac{1}{2}\left[E_k^n - E_k^{\bar{n}} \pm \sqrt{(E_k^n - E_k^{\bar{n}})^2 + 4|v_{q_o}|^2}\right]}$$

where the sign + refers to the upper continuous curve B, the sign — to the lower one A, which replace the crossing point.

This two beams approximation supresses the divergencies in one electron energy $E_k^n(q_o)$, densities of electronic states n(E), and eventually Kohn anomalies which arise in the one beam approximations.

Thus, in three dimensions, figure 21 pictures schematically the differences arising for n(E) and the corresponding (non self consistent) Kohn anomaly for nearly free electrons. The anomaly is split into two successive anomalies, corresponding to the two
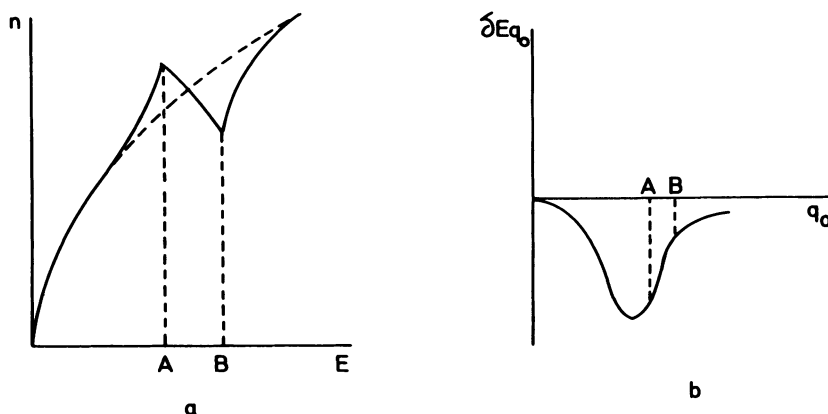
Figure 21 : Three dimensional free electrons scattered by a phonon in the two beams approximation : a density of electronic states ; b Kohn anomaly.

Van Hove anomalies A, B induced by the phonon at the extremities of the energy gap, figure 20. The special stability can thus be viewed as due to the fact that, over a fairly large part of the reciprocal space, the scattering by the phonon lowers the energy of the occupied electronic states and lifts the energy of the empty states. The total effect is clearly less marked than as

computed in the one beam approximation. But it can be shown[34]
that, when developped to second order in v_q, the results for
cohesion of the two beams approximation are identical with those
of the one beam approximation, in the general 3 dimensional case
(cases α, β of figure 9).

In one or two dimensions, no such equivalence exists between
one beam and two beams approximations. This last one systematical-
ly gives less marked Kohn anomalies.

Thus, in one dimension, figure 22 gives the density of sta-
tes and the (non selfconsistent) Kohn anomaly. It is first clear
that there is a total energy gap between A and B, figures 20 and
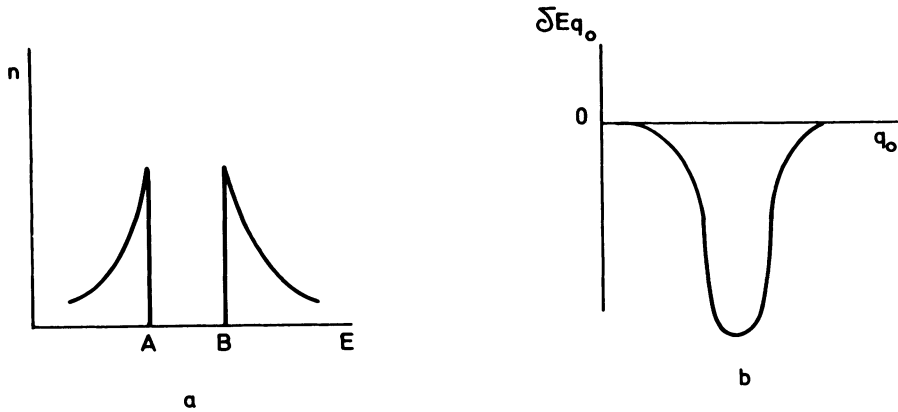
Figure 22 : Effect of a phonon on one dimension electrons : a
density of electronic states ; b Kohn anomaly.

22, so that when the Fermi level falls within that gap, one pro-
duces an insulator, at least as long as the phonon is static.
From equation (5), one deduces, with $n(E) \propto dk/dE''_k(q_o)$,

$$n(E) \simeq \pm \, n_o(E_c) \sqrt{1 + \frac{|v_q|^2}{(E - E_c)^2}} \quad \text{for} \quad E < E_A \text{ or } E > E_B$$

$$= 0 \text{ for} \quad E_A < E < E_B.$$

where $E_c = \frac{1}{2} (E_A + E_B)$ is the center of the energy gap, and $n_o(E)$ is
the electronic density of states in the absence of the phonon
(figure 22.a).

Also

$$\delta E_{q_o} = \frac{1}{\pi} \int_o^{k_M} (E_{\underset{\sim}{k}}^n(q) - E_{\underset{\sim}{k}}^n) dk$$

With

$$\frac{d\,E_{\underset{\sim}{k}}^n}{dk} \simeq -\frac{d\,\bar{E}_{\underset{\sim}{k}}^n}{dk} = \frac{k - k_c}{\pi\,n_o(E_c)}$$

where $n_o(E_c)$ is the unperturbed density of electronic states at energy E_c, this gives

$$\delta E_{q_o} = -\frac{1}{\pi} \int_0^{k_M} \left[\sqrt{\frac{(k - k_c)^2}{\pi^2\,n_o^2(E_c)} + |v_q|^2} - \frac{k - k_c}{\pi\,n_o(E_c)} \right] dk$$

$$= -\frac{|v_q|^2}{2\,\pi^2 n_o(E_c)} \left[\frac{q}{|v_q|}\sqrt{1 + \frac{q^2}{|v_q|^2}} - \text{argsh}\,\frac{q}{|v_q|} - \frac{q^2}{|v_q|^2} \right]_{-k_c}^{k_M - k_c}$$

$$\simeq -\frac{|v_q|^2}{2\,\pi^2 n_o} \left[\ln\frac{2\,k_c}{\pi n_o\,v_q} - \left|\frac{k_M - k_c}{\pi\,n_o\,v_q}\right|^2 + \frac{2}{3}\left|\frac{k_M - k_c}{\pi\,n_o\,v_q}\right|^3 \right.$$

$$\left. + O_4\left|\frac{k_M - k_c}{\pi\,n_o\,v_q}\right| \right]$$

The anomaly is very peaked (because $|v_q| \ll k_c/\pi\,n_o$, which is of the order of the electronic band width). But it remains <u>finite</u>, as soon as v_q is finite (figure 22.b).

It must also be stressed that a proper selfconsistent description in the two beams approximations has not yet been developped. It is however not expected to lead to fundamentally different results.

5 – Anharmonic terms

There are various terms higher than second order in the amplitude of the phonons that must be taken into account.

– Terms in u^n with $n > 2$ must be considered to study the <u>equilibrium amplitude of a soft mode</u>. Such terms should be screened selfconsistently, and this has not been studied completely so far.

– <u>Phonon-phonon couplings</u> arise from such anharmonic terms. This leads to various effects :

   - Strong attenuation of the nearly soft mode, just above the
transition conditions. As a result, such a nearly soft mode with
large amplitude might loose its physical meaning near the tran-
sition.

   - Star of soft modes with equivalent q's : these must be
treated together, and their couplings considered[35][36].

   - Phase modulation and phase locking[37][38]. Only a few re-
marks will be made on this topic, which will be treated fully la-
ter at this Institute.

   Consider   a (sinusoidal) longitudinal mode of distortion
produced in a crystal, with a wave vector q. This will usually
set up a charge density wave which will in turn produce a sinu-
soidal (or nearly sinusoidal) potential with wave vector q. The
lattice will react in turn to this potential : the atomic planes
will tend to avoid the top of the sinusoid and concentrate in
the lower parts.

   - To first order, this reaction can be described by a supple-
mentary sinusoidal distortion which, for nearly free electrons
or holes, will certainly be in antiphase with the intial distor-
tion, as stressed above.

   - If the initial distortion is large, one must however consi-
der the non linear response of the crystal. This is very similar
to the problem of the reaction of a periodic elastic chain of
atoms on a rigid periodic substrate, as a model for epitaxy[39]
[40][41] (fig. 23).

   - The first deviation from linearity can be described as if
the medium was continuous. It will distort the sinusoidal distor-
tion (or introduce harmonics) in such a way that the phase of the
initial simusoid will be modulated. By analogy with a classical
hydrodynamical problem, each period in the modulation has been
called a soliton.

   As the lattice is assimilated to a continuous medium, the
initial sinusoidal distortion could be shifted with respect to
the lattice without change in energy. In fact, one must distin-
guish two cases :

   - q is commensurate with a lattice period. When one shifts
the sinusoidal wave with respect to the lattice, one necessarily
goes through different configurations, such as a, b figure 22,
with different energies. One of them must be more stable than the
others, and the wave must have its phase locked in that position
at OK. The locking is obviously more effective for large amplitude

sinusoids, and for short period sinusoids, with wave lengths small multiples of the crystal period.
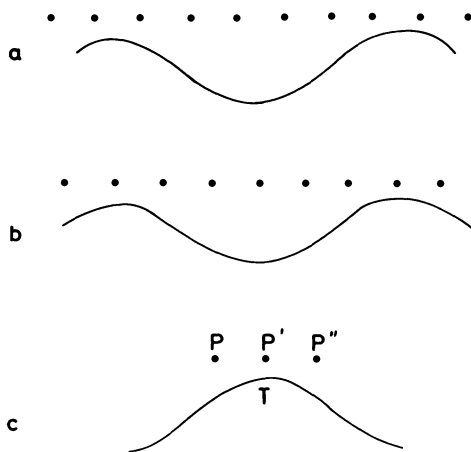
Figure 23: Phase locking. a, b commensurate wave, c uncommensurate wave.

- if q is <u>not</u> commensurate with the lattice, the continuous non linear solution mentioned above leads to atomic planes being distributed all over the top of the sinusoidal potential so that, when the wave is shifted, its energy is <u>not</u> changed : the phase of the distortion wave is not locked ; the wave could in principle be a travelling one, and has thus been called a <u>phason</u>. It is however most probable that it is pinned down by stationary defects or slowed down by anharmonic interactions with normal phonons. But if the amplitude of the initial sinusoidal distortion increases, there will necessarily be a moment when the phase of this uncommensurate wave will also become locked. One is sure this has happened when the negative curvature at the top T of the sinusoidal potential, figure 23.c, becomes larger than the elastic constant that keeps the atomic planes PP'P" more or less equidistant. The plane P' at the top of the sinusoid will then become unstable and be locked on the left or the right of T ; a finite energy will be necessary to move it across T. This is the analogue of the Peierls friction against the 'epitaxial dislocations' whose glide allows the glide of the epitaxial layer. As in epitaxy, and depending on the exact conditions of the problem, the phase locking can lead to <u>commensurate or uncommensurate phase locked structures</u>.

Finally it must be stressed that a selfconsistent description of the phase modulation would require a modulation of the initial sinusoidal screening potential. This is <u>not</u> expected to lead to

new physical effects.

6 – Adiabatic approximation

A travelling phonon has a finite frequency ω_q which should be taken into account in the exact description of the electron-phonon coupling[14].

A phonon now couples strongly electronic states with energies E_k^n and $E_{k'}^{n'}$ differing by $\hbar\omega_q$. But as this is usually much smaller than the electronic energies involved, this only rounds off slightly the central part of the Kohn anomaly, without altering its essential characteristics. The effect is furthermore vanishing in the limit of soft modes, where $\hbar\omega_q$ tends to zero.

The only cases where the adiabatic approximation is not sufficient for the study of Kohn anomalies is when the slow electrons near a Van Hove anomaly are considered[42].

The adiabatic approximation is of course also insufficient to compute the indirect attractive electron-electron coupling responsible for supraconductivity, although once the form of this coupling is obtained, a time independent treatment is sufficient.

7 – Entropy at finite temperature

The discussion has centred so far on OK phase changes, induced for instance by a variation of pressure.

If a crystal modulation is stable at OK, one usually observes it to disappear above a sufficient temperature. This is due to entropy effects, which can be complex.

There are indeed a priori several possibilities and only a study case by case can show which of several possible factors is predominant.

The entropy can arise from electrons excited across the (first or second order) energy gap[21]. It can also be due to phonons. If it is due to phonons, it can be due mainly to the soft mode[33] renormalized by its anharmonic interaction with other phonons[44]; or it can be due to other modes.

In one or two dimensions, critical fluctuations of the soft mode should be dominant at low temperatures[35][36]. They are however usually kept down in that range by three dimensional couplings.

APPENDIX A – SHORT RANGE ORDER DUE TO DISPERSION FORCES

Let A, B be two atoms or molecules interacting at long range by dispersion forces. Let $|0A>$, $|1A>$, $|0B>$, $|1B>$ be the fundamental and main excited states of the two molecules involved in the dispersion forces, with energies E_0^A, E_1^A, E_0^B, E_1^B. The development of the long range Coulomb interaction between A and B gives rise to a pair interaction between electric dipoles on A and B. If A and B have no permanent dipoles, only dipoles induced by mutual polarization interact. Thus if C is the Coulomb correlation term in the hamiltonian describing the pair, its only matrix elements different from zero are $<A_0 B_0 | C | A_1 B_1> = <A_1 B_1 |C| A_0 B_0>$, and it is proportionnal to $u_0 u_1$, with

$$u_i = <i_0 | \chi | i_1>.$$

A perturbation development

$$| \psi> = (|A_0> + \alpha |A_1>)(|B_0> + \beta |B_1>)$$

then gives

$$\begin{vmatrix} E_0^A + E_0^B - E & <A_0 B_0 | C | A_1 B_1> \\ <A_1 B_1| C |A_0 B_0> & E_1^A + E_1^B - E \end{vmatrix} = 0$$

Hence the dispersion interaction

$$w_{AB} = E - E_0^A - E_0^B = \frac{<A_0 B_0 | C | A_1 B_1>^2}{E_1^A + E_1^B - E_0^A - E_0^B} \propto - \frac{u_A^2 u_B^2}{\delta A + \delta B}$$

where $\delta_i = E_1^i - E_0^i > 0$

Considering now three pairs AB, AA, BB <u>at the same relative distance</u>. One can define a <u>short range order energy as</u>

$$\delta w = \frac{1}{2}\left(w_{AA} + w_{BB} - 2w_{AB}\right) \propto \frac{u_A^2 u_B^2}{\delta A + \delta B} - \frac{u_A^4}{2\delta A} - \frac{u_B^4}{2\delta B} \propto - \frac{(u_A - u_B)^2 \delta A \delta B + (u_A \delta B - u_B \delta A)^2}{(\delta A + \delta B)\delta A \delta B} < 0$$

The negative sign of δw for dispersion forces can be constrasted with its positive sign for Coulomb forces between ions, where

$$w_{AB} \propto Z_A Z_B$$

hence $\delta w \propto (Z_A - Z_B)^2 > 0$

A negative sign of δw favours segregation in pure A and B phases ; a positive sign of δw favours ordered compounds (cf figure 3, a and b respectively).

APPENDIX B -- LCAO STUDIES OF THE BAND STRUCTURES OF METALS AND COVALENTS

In the LCAO approximation, the one electron wave functions are analyzed in terms of atomic functions $|i, m>$ (site i, wave function of type m), assumed nearly orthogonal :

$$| \psi > \simeq \sum_{i,m} a_i^m | i, m > ,$$

$$< i, m | j, n > \simeq \delta_{ij} \delta_{mn}$$

With a suitable origin of energies, the hamiltonian reduces to one site and two sites terms :

$$H \simeq \sum_i \Delta_i^{mn} |im> <in| + \sum_{\substack{i,j \text{ near to } i \\ m,n}} \beta_{ij}^{mn} |im><jn|$$

The transfer integrals β allow interatomic jumps. The intraatomic terms Δ come from electrostatic crystal field interactions (for m = n) and from atomic promotion energies if the $|i,m>$ functions are hybrids made with atomic functions of different energies.

1 - H broadens the atomic states into bands without changing the average energy. This can be seen by computing the first moment of the density of states (per unit energy and per atom) in the bands ; using the $|i,m>$ set as a (pseudo) complete set :

$$M_1 = \int n(E) E dE = \text{Trace } H \simeq \frac{1}{N} \sum_{i,m} <i,m| H |i,m> = 0$$
(N atoms)

A rough estimate of the band width can then be deduced from the second moment[45]

$$M_2 = \int n (E) E^2 dE = \text{Trace } H^2 \simeq \frac{1}{N} \sum_{\substack{i,m \\ l,n}} <i,m |H| jn><j,n |H| i,m >$$

$$\simeq \frac{1}{N} \left(\sum_{\substack{i,j \text{ near to } i \\ m,n}} \beta_{ij}^{mn} \beta_{ji}^{nm} + \sum_{\substack{i \\ m,n}} \Delta_{mn}^i \Delta_{nm}^i \right)$$

with usually $|\Delta| << |\beta|$, at least in elementary structures, the effective band width is finally given by an average value of the β_s' multiplied by the square root of the average number of nearest neighbours. Hence large cohesion for strong bands (large β's) or many bonds (large p's).

2 - In sp metals or covalents, the lower limit of the valence band is obtained with pure atomic s states, and coefficients a_i^s of constant sign (minimum number of nodal surfaces). In crystals with one atom per unit cell, the solution is $a_i^s = $ const. and

$$E_{min} = \frac{1}{N} \sum_i \qquad \beta_{ij}^{ss} = p < \beta >$$
$$j \text{ near to } i$$

As $p > p^{1/2}$, this estimate of the band width is larger than the previous one, but of the same order of magnitude.

3 - In sp covalents, the $|im>$ functions can be taken as sp hybrids such that only functions $|in>$ and $|jn>$ pointing along the same covalent bond between two neighbouring sites i, j have a non vanishing (negative) transfer integral β [46]. There are then non vanishing one site terms $\Delta_i^{n \neq m} = \Delta$ associated with the atomic (negative) promotion energy $E_s - E_p$. Thus (figure B.1)

$$H \simeq \beta \sum_{\substack{i, j \text{ near to } i \\ n}} |in><jn| + \Delta \sum_{i, m \neq n} |in><im|$$

Writing $H|\psi> = E|\psi>$ and projecting on $|in>$ gives

$$\Delta \sum_{m \neq n} a_i^m + \beta \quad a_j^n = E a_i^n$$

or

$$\Delta \sum_m a_i^m + \beta \quad a_j^n = (E + \Delta) a_i^n$$
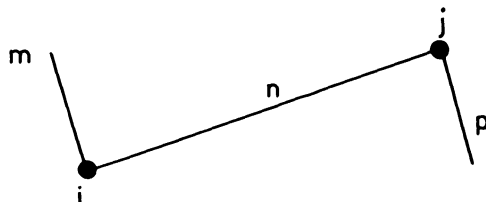
Figure B.1 : Notation of sites and bonds in an sp covalent structure

Similarly

$$\Delta \sum_p a_j^p + \beta \quad a_i^n = (E + \Delta) a_j^n$$

Hence $(E + \Delta) a_i^n = \Delta \sigma_i + \frac{\beta}{E+\Delta} (\Delta \sigma_j + \beta a_i^n)$
and
$$\left((E + \Delta)^2 - \beta^2 - p\Delta(E + \Delta) \right) \sigma_i - \beta \Delta \sum_j \sigma_j = 0 \qquad (B-1)$$

with $\qquad \sigma_i = \sum_m a_i^m$

Equation (B-1) is the LCAO equation for an s band on the same atomic structure, with transfer integral $\beta\Delta$ and energy

$\varepsilon = (E + \Delta)^2 - \beta^2 - p\Delta(E + \Delta)$. General theorems tell us that such an s band has limits ε_1 ε_2 such that

$$- p\ \beta\Delta = \varepsilon_1 \lesssim \varepsilon \lesssim \varepsilon_2 \lesssim + p\beta\Delta$$

The symmetry in energy pointed out in the text shows that ε_2 is equal to $p\beta\Delta$ for alternate structures ; a variational procedure shows that ε_2 is lower than $p\beta\Delta$ for non alternate structures, as defined in the text.

Hence for $\mid \beta \mid > \frac{p}{2} \mid \Delta \mid$,

$\beta + (p - 1)\Delta \lesssim E \lesssim \beta - \Delta$ or $-\beta + (p - 1)\Delta \lesssim E \lesssim - \beta - \Delta$

for $\mid\beta\mid < \frac{p}{2} \mid \Delta \mid$,

$\beta + (p - 1)\Delta \lesssim E \lesssim - \beta + (p - 1)\Delta$ or $+ \beta - \Delta \lesssim E \lesssim - \beta - \Delta$.

Figure B.2 schematizes the results, taking into account an exponential variation of β with the interatomic distance d[47][48].
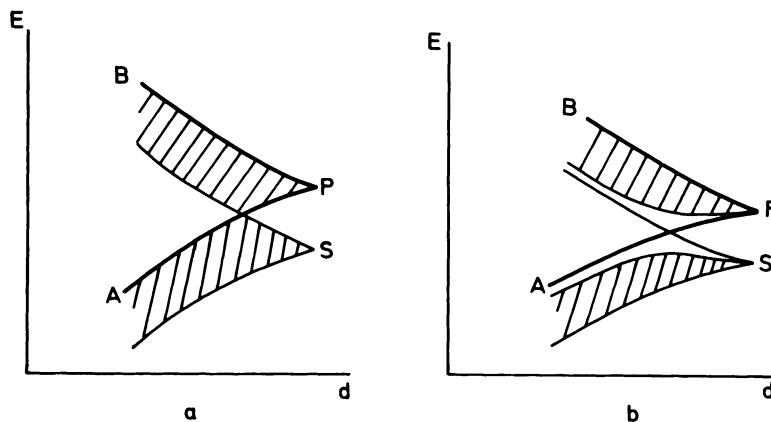
Figure B.2 : Allowed regions of energy for an sp covalent band in the LCAO approximation : a   alternate structures ; b non alternate ones (NB : for sp^n bands with n > 1, the lines pA, pB are allowed pure p states not discussed here).

3 – More exact details about $n(E)$ are necessary to compute the relative stability of different condensed phases. This can be obtained from a study of higher moments[45][49].

$$M_q = \int n(E) \, E^q \, dE$$

and from a development of the Hilbert transform of $n(E)$ as a continuous fraction[50][51][52]

$$\int \frac{n(E')}{E-E'} \, dE' = \cfrac{a_o}{E-a_1 - \cfrac{b_1}{E-a_2 - \cfrac{b_2}{\cdots}}}$$

where the a_i's and b_i's can be expressed in terms of the M_q's, and have an asymptotic behaviour dominated in crystals by the van Hove anomalies of $n(E)$.

APPENDIX C – PHASE STABILITY FOR NEARLY FREE ELECTRONS

Treating the scattering of a free electron gas by the atomic pseudopotentials $v_i(r-R_i)$ as small, the total energy of the valence electrons can be written[53][54]

$$E = E_0 + E_1 + E_2 + O_3(v)$$

The zero order term E_0 is the cohesive energy of a free electron gas in a uniform background of positive charge that neutralizes the system. It is a function of the <u>electron density</u> or of the Fermi wave number k_M. It contains exchange and Coulomb correlations, essential to stabilize this 'jellium'.

The first order term E_1 corresponds to first order (Born) scattering of the free electrons by the pseudopotentials v_i. Each site scatters independently as an impurity, and the Born approximation is only meaningful if screening of each v_i by the valence electrons is included : in E_1, the v_i are 'clothed', the relation with the 'naked' v_i's being, for each Fourier component K

$$v_{iK}^c = v_{iK}^n / \varepsilon_K$$

(ε_K dielectric constant of the free electron gas).

The second order terms E_2 have two different origins :
- double scatterings on single sites.
- successive scatterings on two different sites.

E_1 and the first terms in E_2 are only a function of the <u>nature and density of atoms.</u> Only the second terms in E_2 depend on the relative arrangement of the atoms, i. e. on the atomic structure. They can be written as a sum of central pair interactions E_{ij}

between two atoms i and j, acting as if they were an isolated pair of impurities in a free electron-gas. General theorems tell us that to this lowest order, E_{ij} is the Coulomb interaction of the clothed potential of one atom on the naked charge of the other. Thus, using Poisson's equations[55][56]

$$E_{ij} = \iint v^c_{iK} \; e^{iK(r-R_i)} \; d_3K \; \frac{K'^2 v_{jK'}}{4\pi e^2} \; e^{iK'(r-R_j)} \; d_3K'$$

$$= \int \frac{K^2}{4\pi e^2} \; \frac{v^n_{iK} v^n_{jK}}{\varepsilon_K} \; e^{iK R_{ij}} \; d_3K$$

Owing to the logarithmic anomaly of ε_K for $K \simeq 2k_M$, this is an oscillating function of $2k_M R_{ij}$, with an amplitude decreasing as R_{ij}^{-3} at long range. It is the change in $\sum_{i,j\neq i} E_{ij}$ between different lattice structures which gives rise to the latent heat of phase change. In crystals, the integral reduces to the periods K_{RL} of the reciprocal lattice :

$$\sum_{i,j\neq i} E_{ij} = \sum_{K\in K_{RL}} \frac{K^2}{4\pi e^2} \; \frac{v^n_{iK} v^n_{jk}}{\varepsilon_K}$$

Owing to the logarithmic decrease of ε_K for $K > 2k_M$, this term increases suddenly, for increasing electron per atom ratios, when $2k_M \simeq K_{RL}$, or for the Fermi sphere tangent to Brillouin zone Boundaries.

Third order terms in v would introduce directional forces and possibly finite mean free path effects. They are however difficult to analyze in a convincing way[25].

APPENDIX D - COHESION IN TRANSITIONAL METALS

Considering only the d band and within the LCAO approximation, this can be written as

$$E = E_0 + E_1 + E_2 + \ldots.$$

The zero order terms is the Hartree one electron term when one neglects interactions between valence electrons (or uses the Wigner Seitz approximation referred to in the text)[57] :

$$E_0 = - \int^{E_M} n(E)E \; dE$$

where the zero of energy is taken as the energy of a d state in

the atom. The Fermi level E_M is related to the number z of d electrons per atom :

$$z = \int^{E_M} n(E) \, dE$$

From $dE_0/d_z = -E_n$ and $d^2E_0/d_z^2 = -\dfrac{1}{n(E_n)}$, one deduces that $E_0(z)$ has a single maximum for a half filled band ($E_n = 0$ or, as the first moment of the band is zero, z = 5). Indeed it does not deviate much from the parabola obtained if n(E) was a constant over an energy $-\dfrac{W}{2} < E < \dfrac{W}{2}$ (figures D.1)

$$E_0 \simeq \frac{z(10-z)}{20} W$$

And the (small) deviations with crystal structures are coherent with the succesion FCC, HCP, BCC, HCP, FCC observed in the transitional series[49].

The first order correction originates from the Coulomb and exchange interactions between valence electrons, as computed in the Hartree Fock approximation i. e. for valence electrons randomly distributed over the lattice sites, taking only into account the exclusion principle[58]. If one only considers the average intraatomic terms $U_{nm} = U$ and $J_{n \neq m} = J$, the differences in population of the 10 d orbitals in atoms and in the paramagnetic metals gives[5]

$$E_1 \simeq -\frac{z(10-z)}{20} U - \mu(\mu - 1)\frac{J}{4} - \lambda LS$$

where $\mu = \begin{cases} z & \text{for } z < 5 \\ 10-z & \text{for } z > 5 \end{cases}$
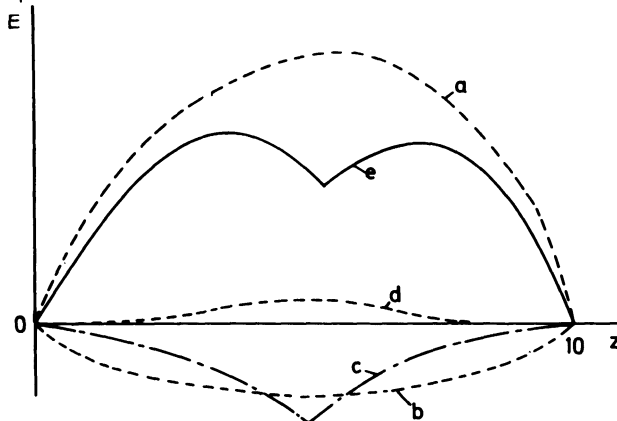
Figure D.1 : Contribution to cohesion in a transitional series : (schematic) : a - E_0 ; b, c : E_1 ; d - E_2 ; e - Total.

The term in U reduces the amplitude of cohesion ; the term in J,
due to the special stability of half filled magnetic d shells,
introduces a secondary minimum in cohesion near the middle of
the transitional series (figure D.1).

The second order contribution E_2 is the first correction
for electron-electron correlations. As U >> J, only the term in
V^2 need be considered. As U induces virtual transitions between
occupied and unoccupied valence states, with number $\frac{z}{10}$ and $1- \frac{z}{10}$
per atomic orbital, an estimate neglecting conservation of momen-
tum in electron-electron collisions gives

$$E_2 \simeq \int_{-\frac{w}{2}}^{E_M} \int_{-\frac{w}{2}}^{E_M} \int_{E_M}^{w/2} \int_{E_M}^{w/2} \frac{Un(E_1)n(E_2)n(E_3)n(E_4)dE_1 dE_2 dE_3 dE_4}{E_1 + E_2 - E_3 - E_4}$$

This is approximately (for rectangular d bands)[5] :

$$E_2 \simeq Z \ A \ \frac{\left(\frac{3}{10}(1 - \frac{3}{10})U\right)^2}{w}$$

The numerical factor A is of the order of 50.

This is a small positive correction, which does not play a
large role in the cohesive energy but explains the secondary mini-
ma observed in the surface tension and the elastic constants, near
the middle of the transition series[59].

Cohesive energies, elastic constants and surface tensions are
coherent with the set of values of the parameters involved as gi-
ven in the following table[5]. As stated in the text, the first
order Coulomb interaction (term in U) decreases cohesion by a term
independent of crystal structure. The second order correlation
correction increases but a little cohesion, by a term somewhat
structure sensitive.

	TABLE I - Values of parameters in eV			
	J	U	w	λ
3d	0.7	(3)	(6)	0.05
4d	0.55	3	9	0.15
5d	0.55	< 3	12	0.40

REFERENCES

(1) Mott N. F., Canad. J. Physics $\underline{34}$, 1356 (1956) ; Phil. Mag. $\underline{6}$, 287 (1961).

(2) Villain J., J. Phys. Chem. Solids $\underline{11}$, 303 (1959) ; Yoshimori A. J. Phys. Soc. Japan $\underline{14}$, 807 (1959)

(3) Wigner E. and Seitz F., Phys. Rev. $\underline{43}$, 804 (1933) ; $\underline{46}$, 509 (1934) ; cf Seitz F., Modern theory of solids Mc Graw Hill New York (1940).

(4) Pines D., Elementary excitations in solids, Benjamin, New York (1963).

(5) Friedel J. and Sayers C. M., J. Physique (1977) under press.

(6) Kohn W., Phys. Rev. Letters $\underline{2}$, 393 (1959).

(7) Jones H. Proc. Roy. Soc. $\underline{144}$, 225 (1934) ; $\underline{147}$, 396 (1934).

(8) Hume Rothery W., J. Inst. Met. $\underline{35}$, 309 (1926) : The structure of metals and alloys, Inst. of Metals Monographs, London(1936).

(9) Friedel J., J. Physique Lettres $\underline{35}$, 159 (1974).

(10) Jehanno G., Thèse Orsay (1965) ; Sato H. and Toth H. S., J. Phys. Chem. Solids $\underline{29}$, 2015 (1968) ; Toth R. S. and Sato H. Acta Met. $\underline{16}$, 413 (1968).

(11) Lomer M., Phase stability in Metals and Alloys (Ed. Rudman P.S.) New York, MacGraw Hill (1966) ; Labbé J., J. Physique $\underline{29}$, 195 (1968) ; cf Friedel J. The Physics of Metals I Electrons (Ed. J. M. Ziman) Cambridge University Press (1969).

(12) Wilson J. A. et al., Adv. Phys. $\underline{24}$, 117 (1975).

(13) Peierls R. E., Quantum theory of solids, Clarendon Press Oxford (1955).

(14) Froehlich H., Proc. Roy. Soc. $\underline{A\ 233}$, 296 (1954).

(15) Comès R., Lambert M. and Zeller H. R., Phys. Stat. Sol.(b) $\underline{58}$ 587 (1973) ; Renker B. et al. Phys. Rev. Lett. $\underline{30}$, 1144 (1973).

(16) Comès R. et al., Phys. Rev. $\underline{B8}$, 571 (1973) ; Phys. Rev. Lett. $\underline{35}$, 1518 (1975).

(17) Labbé J. and Friedel J., J. Physique $\underline{27}$, 153, 303, 708 (1966).

(18) Weger M., J. Phys. Chem. Solids $\underline{31}$, 1621 (1970).

(19) Gor'kov L. P., J. E. T. P. Lett. $\underline{17}$, 379 (1973) ; Soviet Phys. J. E. T. P. $\underline{38}$, 830 (1974).

(20) Stoner E. C. Proc. Roy. Soc. A $\underline{154}$, 656 (1936).

(21) Slater J. C. Phys. Rev. $\underline{82}$, 535 (1951) ; Lidiard A. B. Proc. Roy. Soc. A $\underline{224}$, 161 (1954).

(22) Lomer M., Proc. Phys. Soc. $\underline{80}$, 489 (1962).

(23) Ziman J. M., Principles of the Theory of Solids, Cambridge University Press, 2d edition (1972).

(24) Harrison W. A., Pseudopotentials in the theory of metals, Benjamin New York (1966) ; Heine V. Solid State Physics $\underline{24}$, 1 (1970)

(25) Heine V. and Weaire D., Solid State Phys. $\underline{24}$, 336 (1970)

(26) Barisic S., Sol. State Comm. $\underline{9}$, 1507 (1971) ; Annales de Physique $\underline{7}$, 23 (1972) ; Saub K., Barisic S. and Friedel J., Phys. Lett. $\underline{56A}$, 302 (1976)

(27) Bloembergen N. and Rowland T. J., Acta Met. $\underline{1}$, 731 (1953)

(28) Roth L.M., Thesis Harvard (1957).

(29) Blandin A., Thèse Orsay (1961).

(30) Overhauser A.W., Phys. Rev. 128, 1437 (1962) ; 167, 691 (1968) ; B 3, 3173 (1971).

(31) Blandin A., Alloying behaviour and effects of concentrated Solid Solutions (ed. Massalsky T.B.) Gordon and Breach 1963.

(32) Chan S.K. and Heine V., J. Phys. F 3, 795 (1973).

(33) Barisic S., Fizika 8, 181 (1976) ; Bjelis A., Saub K. and Barisic S., Nuovohin. 23 B1, 102 (1974).

(34) Pick R. and Blandin A., Phys. Kond. Mat. 3, 1 (1964).

(35) Shapiro S.M. et al., Sol. State Comm. 15, 377 (1974).

(36) Garel A.T., Thèse 3ème Cycle Orsay (1976).

(37) Bak P. and Emery V.J., Phys. Rev. Lett. 36, 978 (1976).

(38) Bjelis A. and Barisic S., Phys. Rev. Lett. 37, 1517 (1976).

(39) Frenkel J. and Kontorova T., Phys. Z. Sowjetunion 13, 1 (1938) ; Fiz. Zh. 1, 137 (1939).

(40) Frank F.C. and van der Merwe J.H., Proc. Roy. Soc. A 200,125 (1950).

(41) Ying S.C., Phys. Rev. B 3, 4160 (1971).

(42) Barisic S., Bjelis A. and Saub K., Sol. State Comm. 13, 1119 (1973) ; Horowitz B., Weger M. and Gutfreund H., Phys. Rev. B 9, 1246 (1974).

(43) de Gennes P.G., J. Phys. Rad. 23, 630 (1962).

(44) Lee P. A., Rice T.M. and Anderson P.W., Phys. Rev. Lett. 31, 462 (1973).

(45) Cyrot-Lackmann F., Adv. Phys. 16, 393 (1967).

(46) Leman G., Annales de Physique 18, 1 (1963).

(47) Thorpe M.F. and Weaire D., Phys. Rev. B 4, 3518 (1971).

(48) Friedel J. and Lannoo M., J. Physique 34, 115, 483 (1973).

(49) Ducastelle F., Thèse Orsay (1972) ; cf Ducastelle F. and Cyrot-Lackmann F., J. Phys. Chem. Sol. 131, 1295 (1971) ; 132, 285 (1972).

(50) Gaspard J.P. and Cyrot Lackmann, J. Phys. C. : Sol. St. Phys. 6, 3077 (1973).

(51) Haydock R. et al, J. Phys. C. Sol.St. Phys. 5, 2845 (1972) ; Desjonquères M.C. and Cyrot Lackmann F., J. Phys. F. Metal Physics 5, 1368 (1975).

(52) Hodges C. H., J. Physique Lettres 38, L187 (1977); Pottier N. Thèse Paris (1976).

(53) Blandin A., Phase Stability in Metals and Alloys (Ed. Rudman JS) Mc Graw Hill (1967).

(54) Harrison W.A., Pseudopotentials in the theory of metals, Benjamin, New York (1966).

(55) Corless G.K. and March N., Phil. Mag. 6, 1285 (1961).

(56) Blandin A. and Déplanté J.L., J. Phys. Rad. 23, 609 (1962) ; Blandin A., Déplanté J.L. and Friedel J., J. Phys. Soc. Japan 18, 1; (1963) ; Déplanté J.L., J. Physique 28, 465 (1967).

(57) Friedel J., Physics of Metals I Electrons (Ed. Ziman J.M.) Cambridge University Press (1969).

(58) Friedel J., J. Phys. Rad. 16, 829 (1955).

(59) Friedel J. and Sayers C.M., J. Physique Lettres (1977) under press.

NEUTRON SCATTERING STUDIES OF ELECTRON-PHONON INTERACTIONS

J.D. Axe

Institute Laue-Langevin, Grenoble, France, and

Brookhaven National Laboratory, Upton, N.Y., U.S.A.

This review is an attempt to summarize the areas in which neutron scattering has been used in studying electron-phonon interactions, and to display some of the key results. The examples chosen reflect the interests of the author and represent in no way a complete survey of the subject.

I. PHONON DISPERSION IN METALS

The most obvious and direct way in which electron phonon interaction manifests itself is in the phonon dispersion of metals. When phonon dispersion curves of simple metals are analyzed by Born-von Karman theory typically force constants between fifth nearest or even more distant neighbors are needed.[1,2] Furthermore the magnitude of the successive force constants is often oscillatory,[2,3] reflecting the rather long ranged oscillatory character of electronic screening. Born-von Karman models are both unweildy and unphysical, and it is now generally recognized that it is more satisfactory to formulate models in which conduction electron -phonon interactions are explicitly dealt with.

In the harmonic approximation phonon frequencies and eigenvectors are obtained by diagonalizing a dynamical matrix $\underset{\sim}{D}(\vec{q})$. For our purposes a sufficiently general form is[4]

$$D_{xy}(\vec{q}) = \frac{1}{v} \sum_{G} \{(\vec{G}+\vec{q})_x \phi(\vec{G}+\vec{q})(\vec{G}+\vec{q})_y - \vec{G}_x \phi(\vec{G})\vec{G}_y\} \qquad (1)$$
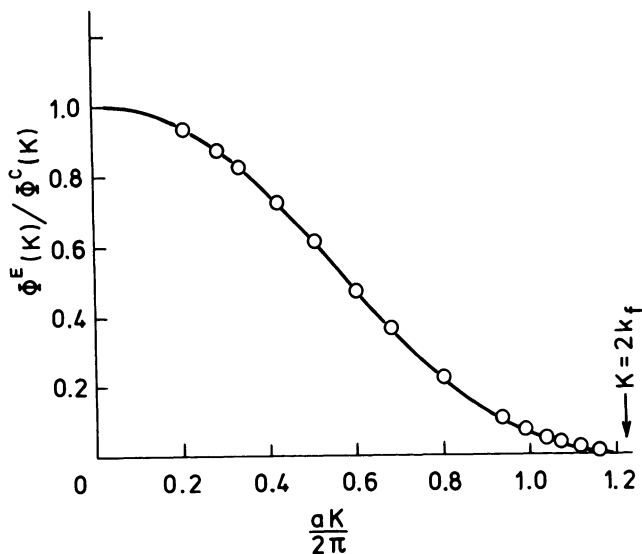
Fig. 1 The effective electron screening potential for sodium
metal. The solid curve is deduced from phonon dispersion measure-
ments (Ref. 5). The crosses represent calculations by Toya (Ref.
6).

where $\phi(\vec{K})$ is the Fourier transform of an appropriate ion pair
potential, v is the volume of a unit cell and the sum is over all
reciprocal vectors $\vec{G}$. For metals it is convenient to write the
potential as the sum of three terms,

$$\phi(\vec{K}) = \phi^C(\vec{K}) + \phi^R(\vec{K}) + \phi^E(\vec{K}) \qquad (2)$$

representing a) Coulomb interactions between ions, b) core repul-
sion of ions and c) ion-electron-ion interactions, respectively.

Figure 1 shows a comparison of the potential for sodium de-
rived by Cochran[5] from experimental phonon dispersion curves,[1]
compared with an early calculation by Toya[6] which attempted to
deal in a fundamental way with the conduction electrons. $\Phi^E(K)$ is
normalized by the coulomb term $\Phi^C(K) = 4\pi e^2/K^2$. Although the agree-
ment is remarkably good, the further comparison of the measured

and calculated dispersion curves, while impressive, was not com-
pletely satisfactory. This is the result of the near cancellation
of the ϕ^C and ϕ^E terms in eq. (2). (ϕ^R is nearly negligible in
sodium.) As a result phonon dispersion in metals generally pro-
vides a very stringent test of our understanding both of electron
-ion potentials and of many body screening effects within the elec-
tron gas itself. It is fair to conclude that much of the stimulus
for developments in pseudopotential theories[7] over the last decade
came with the availability of reliable inelastic neutron scattering
measurements of phonons in metals.[8,9]

The additional comment that must be made concerning Figure 1
is that it is not in general possible to uniquely deduce interionic
potentials from phonon dispersion curves. There are two distinct
difficulties. The first is that both the phonon frequencies and
eigenvectors are needed to reconstruct the dynamical matrix $\underset{\sim}{D}(\vec{q})$.
Although the eigenvectors can in very favorable cases be deduced
from inelastic scattering intensities, in simple structures the
problem is best resolved by measuring along those directions in
reciprocal space where the eigenvectors are fixed by symmetry.
The second problem is that the structure of eq. (1), which in prin-
ciple involves reciprocal lattice vectors G of arbitrarily large
value, is such that no unique value of $\phi(\vec{q})$ can be deduced from a
knowledge of $\underset{\sim}{D}(\vec{q})$. This reflects the fact that in a real space
formulation $\underset{\sim}{D}(\vec{q})$ depends only upon $\partial\phi/\partial r$ and $\partial^2\phi/\partial r^2$ evaluated at
distances of interatomic separation. Cochran was able to derive
$\phi^E(K)$ shown in Figure 1 only by assuming physically plausible con-
straints on its behavior.

II. KOHN SINGULARITIES

Kohn singularities arise because of the abrupt changes in
electronic screening which occur when the phonon wavevector $\vec{q}$,
spans the Fermi surface of a metal.[10] The effect is most simply
discussed in the case where the electron wavefunctions are suf-
ficiently planewave-like over most of the unit cell to allow $\phi^E(K)$
to be approximately factorized in the form

$$\phi^E(K) = -|v(K)|^2\chi^0(K)/\{1 + v_e(K)\chi^0(K)\} \qquad (3)$$

Here $v(K)$ is the effective ion-electron potential and $v_e(K)$ is
the electron coulomb plus exchange potential.[11] $\chi^0(K)$ is the fam-
iliar one electron susceptibility

$$\chi^0(K) = \sum_K \frac{f_k - f_{k+K}}{\varepsilon_{k+K} - \varepsilon_k} \qquad (4)$$

The magnitude of the Kohn singularity depends greatly on how well pieces of Fermi surface separated by the wavevector $\vec{K}$ are matched. For simple ellipsoidal surfaces where the matching is poor $\chi^0(K)$ is regular, but there is a logarithmic singularity in the derivative $\partial\chi^0(K)/\partial K$.[12] Brockhouse, et. al.[13] were the first to find phonon anomalies with these expected properties in a study of lead. Lead is favorable because of the large electron-ion potential, $v(K)$. In most other simple metals the effects are too small to be obvious by direct inspection of the dispersion curves. Nevertheless, Stedman and coworkers, by making very careful measurements ($\sim 0.2\%$ precision) and by examining $\Delta\omega/\Delta q$ have identified a large number of other anomalies in Al[14] and Cu[15] as well as Pb[16]. (It is important to realize that while the first moment of the line shape can be determined with such precision, the lines typically have a width $\sim 5\%$ due to instrumental resolution.) A substantial fraction of the anomalies have been assigned to known features of the Fermi surface with reasonable certainty. Ng and Brockhouse[17] have followed the changes in the size of the Fermi surface that occurs when Pb is alloyed with Tl.

In the event that a substantial portion of the Fermi surface "nests" into a matching portion displaced by a wavevector $\vec{K}$, the singularity in $\chi^0(K)$ becomes stronger. In the limit of perfect nesting there is a logarithmic singularity in $\chi^0(K)$ rather than in $\partial\chi^0/\partial K$.[12] When the nesting is less than mathematically perfect it is still possible to have strong cusp-like singularities in $\chi^0(K)$ itself.[12,15] Such cusps are seen in the phonon dispersion in Cr,[18] Mo,[19] and W,[20] and are believed to result from nesting of electron and hole pockets in the rather complex Fermi surfaces of these materials. A particularly strong example occurs in Cr, as shown in Figure 2. Nb and Nb-Mo alloys also have suspected Kohn anomalies at wavevectors that can be reasonably correlated with a rigid band model of the Fermi surface.[21,22] While it is often possible to find qualitative correlations, it is a common observation that anomalies predicted by simple considerations of Fermi surface topology are in some cases too weak to be observed and in other cases relatively strong. There has been little effort to understand the shape and strength of the anomalies in a quantitative way.[18]

It is a very striking fact that many high T_c superconductors exhibit rather broad anomalous dips in their dispersion relations which are not seen in their neighboring low T_c counterparts.[10] For example, (Figure 3) Nb has such features which are not seen in Mo, and similiar relationships are observed in the V,Cr and Ta,W
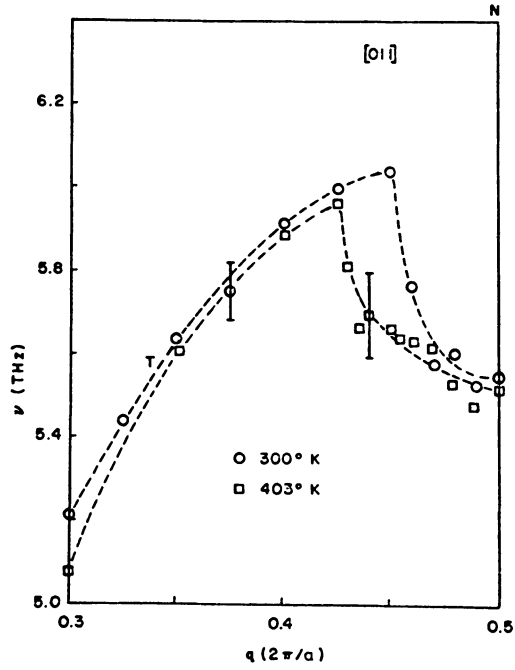
Fig. 2 A portion of the phonon dispersion of chromium near the N
symmetry point at two temperatures. (Ref. 19).
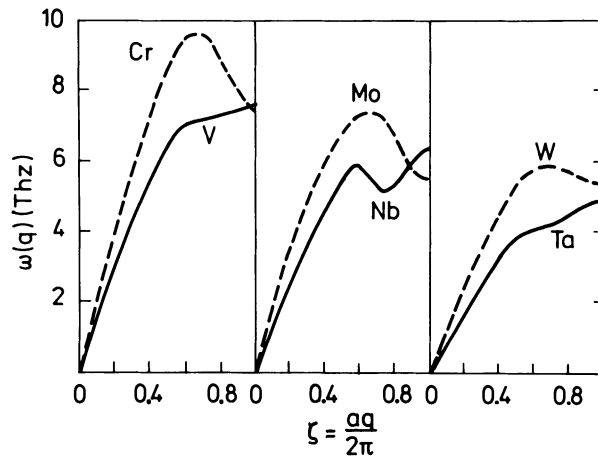
Fig. 3 Longitudinal acoustic phonons in Group V and VI transition
metals. (After ref. 23).

pairs. Similar features have been pointed out by Smith and his coworkers[11] for the transition metal carbides. These features are too broad to be Kohn anomalies and furthermore, as has been shown for the Nb-Mo system, do not scale with the size of the Fermi surface. Sinha and Harmon[12] have proposed a model in which collective charge fluctions within the localized d-states softens the lattice response. They suggest that a large density of d-states at the Fermi surface is required. It is not clear whether the correlation with high T_c superconductivity, which undoubtedly exists, is or is not a causal one.

III. NEUTRON SPECTROSCOPY OF SUPERCONDUCTORS

Thus far we have been concerned with the electronic screening effects of the phonon frequencies. These can be adequately described in the adiabatic approximation. In order to discuss the influence of the electrons on phonon linewidths, it is necessary to consider the damping due to excitation of electron-hole pairs. This is accomplished by replacing the static susceptibility $\chi^0(K)$ in eq. (3) by

$$\chi^0(K,\omega + i\eta) = \sum_k \frac{f_k - f_{k+K}}{\varepsilon_{k+K} - \varepsilon_k + \omega + i\eta} \qquad (5)$$

The electronic damping is introduced via Im $\chi^0(K,\omega)$, and is in most cases small enough to be completely masked by phonon-phonon scattering. In a neutron scattering experiment this in turn is usually masked by instrumental resolution!

Nevertheless in strong coupling superconductors in the vicinity of T_c there are abrupt changes in electronic damping which are sufficiently strong to be studied by neutron scattering.[26,27] This behavior arises because phonons with energy less than that of the temperature-dependent superconducting energy gap, $2\Delta(T)$, are energitically incapable of decaying by excitation of electron-hole quasiparticle pairs.

Although the theory of this effect dates from the early BCS period[28], the effect was first seen in neutron scattering some ten years later in Nb_3Sn.[26] Recently more refined measurements have been performed in Nb.[27] Figure 4 summarises some of these latter measurements. When $2\Delta(T)$ equals the phonon energy, $\hbar\omega_q$, an abrupt change occurs in the linewidth. Certain qualitative features, such as the displacement of the curves to lower temperature with increasing phonon energy, are obvious from the sketch included in
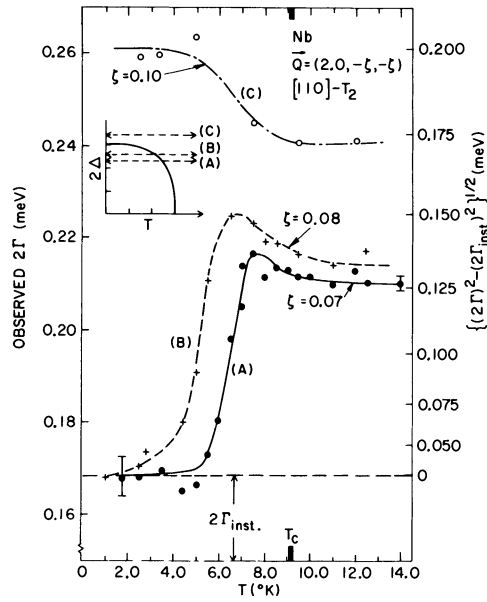
Fig. 4. Temperature dependence of several $[\zeta\zeta 0]T_2$ phonons in Nb, showing the change in width due to the superconducting gap.
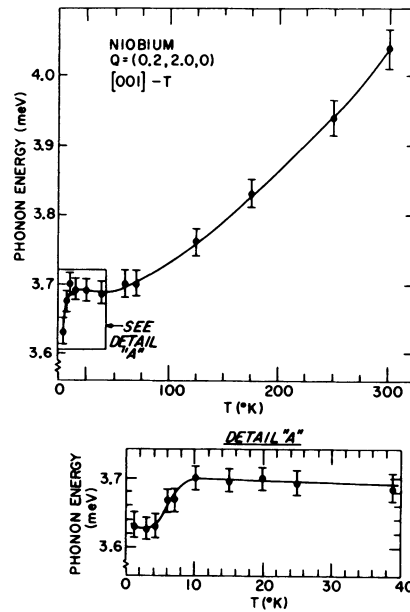
Fig. 5. Temperature dependence of $[00\zeta]T$ phonon frequency in Nb.

the Figure. The rounding of the discontinuity can be partly ac-
counted for by resolution effects. All three sets of data in Fig-
ure 4 show that when $\hbar\omega_q$ slightly exceeds $2\Delta(T)$ the phonon line-
widths are greater than their values far above T_c. This effect,
which is due to an increased density of electron states at the gap
energy, is in qualitative agreement with theory. Since the real
and imaginary parts of $\chi^0(K,\omega)$ are related by Kramers-Kronig re-
lations, we expect[29] and find anomalies in the phonon frequencies
in the vicinity of T_c as well (see Figure 5).

Measurements of this type are of course of interest because
they provide an alternate means for direct determination of the
temperature dependence and anisotropy of the gap energy. In ad-
dition, they measure that part of the phonon linewidth, γ_{ep}, which
is due to electron-phonon interaction. Allen[30] has pointed out that
it is very closely related to quantities of interest in strong
coupling superconductivity by deriving a simple explicit relation
between γ_{ep} and the electron-phonon spectral function $\alpha^2F(\omega)$.

Obviously neutron scattering measurements of this sort are
successful only if the electron-phonon interaction is sufficiently
strong that the quenching of the interaction when $2\Delta(T) \geq \hbar\omega_q$ pro-
duces a measureable effect. Given presently available spectrometer
resolution, the technique is unfortunately restricted to a small
handful of strong coupled superconductors.

IV. MAGNETIC FIELD EFFECTS

In the preceding section we saw how the presence of an energy
gap in the conduction electrons can be manifested in the phonon
spectrum. Another way of introducing energy gaps in the conduction
electrons is by application of an external magnetic field, and
under suitable conditions this too may produce interesting effects
in the phonon spectrum.

When a magnetic field is applied to a metal the energies of
the conduction electrons are quantized into a series of Landau
levels. In momentum space this quantization is represented by the
condensation of the electron energy states into a series of tubes,
each having a constant cross section in a plane perpendicular to
the applied field, $\vec{H}$, as shown in Figure 6. The cross sectional
area of each tube is proportional to $\vec{H}$. The energy of an electron
lying on the n'th tube is

$$\varepsilon_n(k_z) = (n + \tfrac{1}{2})\hbar\omega_c + \frac{\hbar^2 k_z^2}{2m_{||}} \tag{6}$$
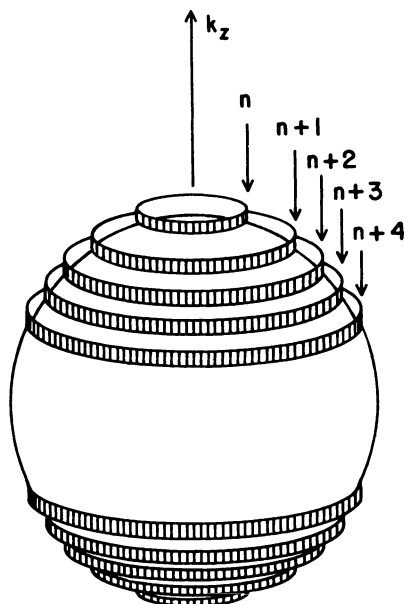
Fig. 6 Free electron Fermi surface and tubes onto which electron states condense in a magnetic field along k_z. (Ref. 34).

where k_z is the component of the electron wavevector parallel to $\vec{H}$, $m_{||}$ is an effective mass and ω_i is the cyclotron frequency.

In the free electron case, as discussed by Cowley,[31] and by Sham,[32] there are two distinct kinds of effects depending upon whether the phonon propagation vector, is parallel or perpendicular to $\vec{H}$. For $\vec{q} \,||\, \vec{H}$ there are Kohn-like singularities in $\chi^0(q,\omega,H)$ whenever q equals the length, $2k_n$, of the portion of the n'th tube that lies within the Fermi surface.[33] However even for 100·KG there are $\sim 10^3$ Landau levels below the Fermi energy, so that the tubes are very closely spaced relative to the available momentum resolution of a neutron spectrometer and the strong field induced singularities are greatly smoothed out.

When $\vec{q} \perp \vec{H}$, $\chi^0(q,\omega,H)$ has a different structure[33] reflecting the fact that phonons can now scatter electrons from the n'th to the (n + p)'th tube, subject to the conditions
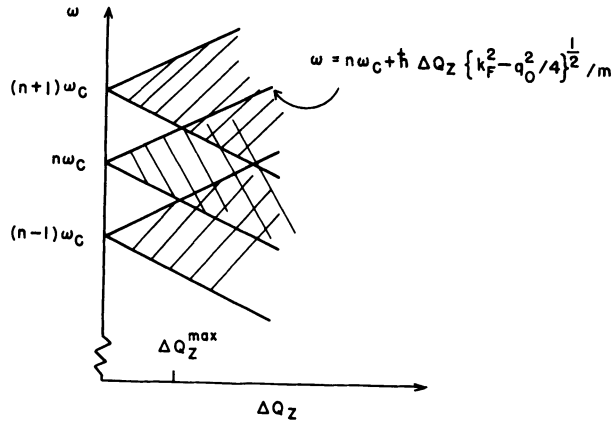
Fig. 7   Im $\chi(Q,\omega)$ is finite in the shaded area with a magnetic field perpendicular to the phonon propagation. (Ref. 34).

$$\varepsilon_{n+p}(k_z) - \varepsilon_n(k_z) \equiv p\hbar\omega_c = \hbar\omega_q \qquad (7a)$$

and

$$k_{n+p} - k_n = q \qquad (7b)$$

where ω_q and q are the frequency and wavevector of the phonon and k_n is the component of the electron wavevector $\perp H$ for the n'th tube. This is just the cyclotron resonance condition, and we consequently expect the electron-phonon interaction to contribute to the lifetimes of only those phonons whose frequencies are integral multiples of the cyclotron frequency.

A more detailed consideration of the possibility of observing the effect of a transverse magnetic field on phonon lifetimes by conventional neutron spectroscopy has been given by Pynn and Axe.[34] Figure 7 shows the effect of a small component of phonon wavevector, ΔQ_z, parallel to $\vec{H}$ on the energy quantization of electrons. $\omega_c = (eH/mc) \sim 1$ meV for $H = 100$ kG, which is well within the capability of a neutron spectrometer to resolve. The major difficulty that occurs is that typical spectrometer momentum resolution extends well beyond the value ΔQ_z^{max} in this Figure, at least in the

case of free electrons. No anomalous effects can then be observed as the smeared value of Im $\chi^0(q,\omega)$ is the same with and without the applied field.

Pynn and Axe suggested that only if there were flat sections of Fermi surface which could be aligned parallel to $\vec{H}$ could the momentum resolution be sufficiently relaxed to make a neutron scattering experiment feasible. They tested these ideas by measuring the effect of a 50 kG field on phonons near the Λ_1 Kohn anomaly in Nb.[25] Instead of measuring the width of the phonons directly, they monitored the peak intensity as a function of $\vec{H}$ and found a small oscillatory component with a period consistent with the cyclotron mass deduced from deHaas-van Alphen measurements.

It is clear that neutrons are potentially very useful to investigate Fermi surfaces, both through Kohn anomalies and cyclotron resonance effects. A distinct advantage, in principle, is that these studies could be extended to impure metals and alloys, which are difficult to study by conventional methods. Similar remarks pertain to the potential of neutron spectroscopy of superconductors. It is fair to conclude, however, that substantial technical improvements will be necessary to make these techniques broadly useful. Order of magnitude increases in reactor fluxes might go a long way toward affecting the necessary resolution, but this is not a likely short term prospect. Unconventional high resolution spectrometers exist,[35,36] but have not as yet been adapted to phonon spectroscopy. It is sobering to recognize that we will often require simultaneous improvements in energy and momentum resolution.

V.   CHARGE DENSITY WAVE INSTABILITIES

The charge density wave (CDW) state occurs as the result of a Fermi surface instability, which in the absence of electron phonon coupling would be manifested in a divergent susceptibility, $\chi^0(q_{crit}) \to \infty$, at some critical wavevector. The actual instability is a coupled mode which causes a simultaneous modulation of the electron density as well as a distortion of the lattice, i.e. a structural phase transformation. The neutrons couple to the nuclear distortions only. As might be supposed, simple theories predict that CDW phase transformations are accompanied by a soft phonon mode whose frequency is driven to zero by a "giant" Kohn anomaly.[37] The possibility of such an instability is greatly enhanced in lower dimensional systems because of the possibilities for favorable Fermi surface nesting.
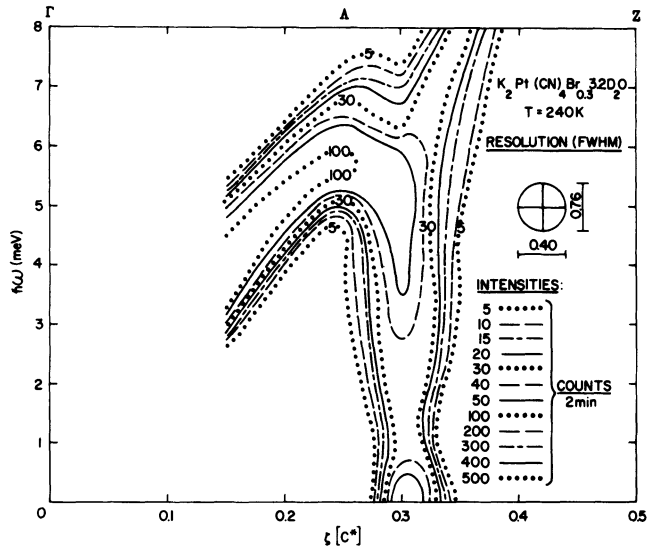
Fig. 8. Inelastic scattering intensity. Contours for KCP showing sharp Kohn anomaly in the acoustic branch near $\zeta \approx 0.3c^*$ (from Ref. 11).

In the past few years very spectacular examples of giant Kohn anomalies have been studied with neutrons in the quasi one-dimensional conductors KCP[38-40] and TTF-TCNQ.[41-42] As is demonstrated in Figure 8 the anomaly in KCP is extremely sharp. It occurs whenever $q_{||}$, the component of the phonon wavevector along the one-dimensional axis, equals $2k_F$. The strength of the anomaly is nearly independent of components of momentum perpendicular to the one-dimensional axis. There is a large quasi-elastic central peak revealing the presence of long lived short ranged correlations over a wide range of temperatures, but no actual transition temperature can be defined. It is possible that impurity pinning rather than the effect of one-dimensional fluctuations is responsible for the lack of long range order.[43]

The layered d^1-metal compounds NbX_2 and TaX_2 (X = S, Se, or Te) show a variety of structural transformations which are ralated to Fermi surface instabilities and CDW formation. Inelastic neutron scattering studies of $2H$-$NbSe_2$ and $TaSe_2$ show large Kohn-like anomalies in the LA phonons at wavevectors for which Bragg sattelite peaks occur at the onset of the CDW state.[44,45] However, the softening of the phonon is incomplete near T_o, the divergent behavior occuring instead in a quasi-elastic central peak as $T \rightarrow T_o$. The Fermi surface geometry is rather complex in these materials and alternative models of Fermi surface nesting have been proposed.
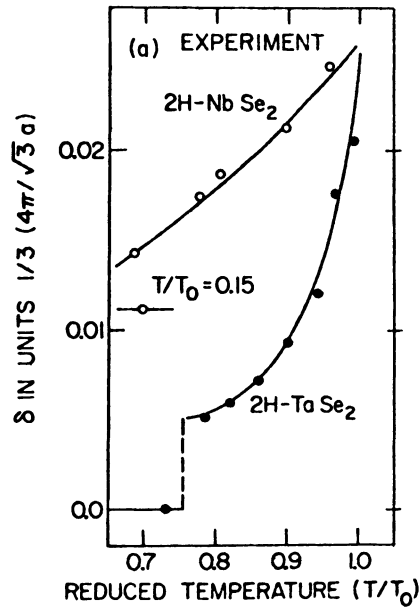
Fig. 9 Temperature dependence of the incommensurate wavevector $q_0 = (1-\delta)a^*/3$ in TaSe$_2$ and NbSe$_2$. A "lock-in" transformation (to $\zeta = 0$) occurs in TaSe$_2$ but not NbSe$_2$.

These systems have been extensively reviewed by Wilson et al.[46]

     One curious feature of CDW transformations is that the wavevector of the modulation, q_{crit}, is in general not an integral submultiple of a reciprocal lattice vector of the undistorted parent structure. The resulting structures are termed "incommensurate", and since they lack translational periodicity, they are not strictly speaking crystalline phases. However, the periodic potential of the underlying lattice causes non-sinusoidal distortions of the condensed planewave displacements and may lead to subsequent transformations which "lock-in" the period of the displacements with that of the lattice. These effects show up clearly in the neutron scattering results[45] on the layered chalcogenides shown in Figure 9. The most striking feature is the abrupt change of the satellite wavevector from $(1-\delta)a_1^*/3$ to the commensurate value $a_1^*/3$ which occurs at T $\sim$ 0.76 T$_0$. NbSe$_2$ does not achieve the commensurate state even at the lowest attainable temperatures, but as in TaSe$_2$ the satellite wavevector shows a pronounced temperature dependence, whose origin is closely related to the lock-in phenomenon itself. Moncton et. al.,[45] using a phenomenological Landau theory, showed

that this behavior could be understood by allowing additional secondary distortions with wavevectors chosen to take advantage of the periodic lattice potential. They were also able to directly verify the non-sinusoidal nature of the incommensurate state by observing secondary Bragg satellites at the postulated wavevectors. McMillan[47] and Bak and Emery[48] have recently given more detailed discussions of the nature of the incommensurate ground state.

References

1. A.D.B. Woods, B.N. Brockhouse, R.H. March, A.T. Stewart and R. Bowers, Phys. Tev. 128, 1112 (1962).
2. B.N. Brockhouse, T. Arase, G. Caglioti, K.R. Rao and A.D.B. Woods, Phys. Rev. 128, 1099 (1962).
3. S.H. Koenig, Phys. Rev. 135A, 1693 (1964).
4. See, for example, W. Cochran and R. Cowley, Handbuch der Physik, Vol XXV/2a, Springer (1967) p. 83 f.f. More generally $D(q)$ is not diagonal in G, but in simple metals the off-diagonal terms are thought to be small. (L. Sham, Proc. Roy. Soc. A283, 33 (1965)). For simplicity of notation we consider only one atom/cell.
5. W. Cochran, Proc. Roy. Soc. A276, 308 (1963).
6. T. Toya, J. Res. Inst. Catalysis, 6, 161 (1958).
7. See, for example, articles by Heine et al. in "Solid State Physics", Vol. 24, Academic Press (1970).
8. A useful review of the lattice dynamics of metals has been given by S.K. Joshi and A.K. Rajagopal in "Solid State Physics", Vol. 22, Academic Press (1968) p. 159-312.
9. A complete bibliography of neutron scattering results is contained in "Bibliography for thermal Neutron Scattering", 5'th ed., M. Sakamoto, J. Chihara, Y. Nakahara, H. Kadotani, T. Sekiya and Y. Gotah, Japanese Atomic Research Institute, Tokai-mura, Japan.
10. W. Kohn, Phys. Rev. Letters 2, 393 (1959).
11. Perhaps the simplest but by no means only way to arrive at eq. (3) is by pseudopotential methods (see Ref. 8).
12. See L.M. Roth, H.J. Zeiger and T.A. Kaplan, Phys. Rev. 149, 519 (1966).
13. B.N. Brockhouse, T. Arase, G. Caglioti, K.R. Rao and A.D.B. Woods, Phys. Rev. 128, 1099 (1962).
14. J.W. Weymouth and R. Stedman, Phys. Rev. B2, 4743 (1970).
15. G. Nilsson, "Neutron Inelastic Scattering" (International Atomic Energy Agency, Vienna, 1968) p. 187.
16. R. Stedman, L. Almquist, G. Nilsson and G. Raunio, Phys. Rev. 163, 567 (1967).

17. S.C. Ng and B.N. Brockhouse, "Neutron Inelastic Scattering" (International Atomic Energy Agency, Vienna, 1968) p. 253.
18. T.M. Rice and B.I. Halperin, Phys. Rev. B1, 509 (1970).
19. M.W. Shaw and L.D. Muhlstein, Phys. Rev. B4, 969 (1971); L.D. Muhlstein, E. Gurmen and R.M. Cunningham, "Inelastic Neutron Scattering" (International Atomic Energy Agency, Vienna, 1972) p. 53.
20. S.H. Chen and B.N. Brockhouse, Solid State Commun. 2, 73 (1964). S.H. Chen, Ph.D. Thesis, McMaster Univ. 1964 (unpublished).
21. B.M. Powell, P. Martel and A.D.B. Woods, Phys. Rev. 171, 727 (1968); C.B. Walker and P.A. Egelstaff, ibid 177, 1111 (1969).
22. R.I. Sharpe, J. Phys. C 2, 432 (1969).
23. H.G. Smith, N. Wakabayashi and M. Mostoller in "Superconductivity in d- and f-band metals", D.H. Douglass, ed., Plenum, New York 1976, p. 223.
24. H.G. Smith and W. Gläser, Phys. Rev. Lett. 25, 1611 (1970).
25. S.K. Sinha and B.N. Harmon, Phys. Rev. Lett. 15, 1515 (1975).
26. J.D. Axe and G. Shirane, Phys. Rev. Lett. 30, 214 (1973); Phys. Rev. B8, 1965 (1973).
27. G. Shirane, J.D. Axe and S.M. Shapiro, Solid State Comm. 13, 1893 (1973); S.M. Shapiro, G. Shirane and J.D. Axe, Phys. Rev. B12, 4899 (1975).
28. A. Privorotskii, Sov. Phys. - JETP 16, 945 (1963); V.M. Bobetic, Phys. Rev. A1535 (1964).
29. H.G. Schuster, Solid State Comm. 13, 1559 (1973).
30. P.B. Allen, Phys. Rev. B6, 2577 (1972).
31. R. Cowley, "Neutron Inelastic Scattering" (International Atomic Energy Agency, Vienna, 1968) p. 141.
32. L. Sham, "Modern Solid State Physics", Vol. 2, R.H. Enns and R.R. Haering, ed., Gordon and Breach, New York, 1969, p. 143.
33. A. Ya Blank and E.A. Kaner, Sov. Phys. - JETP 23, 673 (1966).
34. R. Pynn and J.D. Axe, J. Phys. F. 4, 1898 (1974).
35. M. Birr, A. Heidemann and B. Alefield, Nucl. Inst. Methods 95, 435 (1971).
36. F. Mezei, Z. Physik 225, 146 (1972).
37. S.K. Chan and V. Heine, J. Phys. F 3, 795 (1973).
38. B. Renker, H. Rietsch, L. Pintschovius, W. Gläser, P. Brüesch, D. Kuse and M.J. Rice, Phys. Rev. Letters 30, 1144 (1973).
39. K. Carneiro, G. Shirane, S.A. Werner and S. Kaiser, Phys. Rev. B13, 4258 (1976).
40. R. Comes, B. Renker, L. Pintschovius, R. Currat, W. Gläser and G. Schreiber, phys. stat. solidi b71, 171 (1975).
41. H.A. Mook and C.R. Watson, Jr., Phys. Rev. Lett. 36, 801 (1976).
42. G. Shirane, S.M. Shapiro, R. Comes, A.F. Garito and A.J. Heeger, Phys. Rev. B14, 2325 (1976).
43. L.J. Sham and B.R. Patton, "One-Dimensional Conductors", H.G. Schuster, ed., Springer-Verlag, New York, 1975.

44. N. Wakabayashi, H.G. Smith and R. Shanks, Phys. Lett. <u>50A</u>, 367 (1974).

45. D.E. Moncton, J.D. Axe and F.J. DiSalvo, Phys. Rev. Lett. 34, 734 (1975).

46. J.A. Wilson, F.J. DiSalvo and S. Mahajan, Adv. in Phys. <u>24</u>, 117 (1975).

47. W.L. McMillan, Physical Review <u>B14</u>, 1496 (1976).

48. P. Bak and V.J. Emery, Phys. Rev. Lett. <u>36</u>, 978 (1976).

PHASE TRANSITIONS IN QUASI ONE-DIMENSIONAL METALS (TTF-TCNQ AND KCP)

Per Bak

NORDITA, Blegdamsvej 17, Copenhagen, Denmark

1. INTRODUCTION

Quasi one-dimensional conductors are characterized by their very anisotropic conductivity which takes place almost entirely along one particular direction. Most of these systems are organic chain systems. The best one-dimensional organic conductor known is tetrathiafulvalene-tetracyanoquinodimenthane (TTF-TCNQ). The present activity in this field started by the observation of Coleman, Cohen, Sandman, Yamagishi, Garito and Heeger[1] that samples of TTF-TCNQ exhibit an anomalous peak in conductivity at $T \simeq 60K$ but at lower temperatures the conductivity drops sharply and the material becomes an insulator. Although it was widely believed that this behaviour was related to a phase transition it took rather long time before such a transition was actually observed.

Of particular interest in this respect is the coupling between the electron system and the lattice which may lead to at least two different types of phase transformations: either into a supercon-ducting state or into a Peierls state[2] characterized by a static charge density wave (CDW) and an accompanying periodic lattice distortion. Careful theoretical estimates, however, indicate that for an almost one-dimensional system the dielectric Peierls transition will occur before the superconducting phase transition may take place. The physical mechanism behind the Peierls transition is the decay of phonons into electron-hole pair. Because of energy and momentum conservation the phonon wavevector must connect two points on the Fermi surface. The interaction creates a dip in the phonon energy – the Kohn anomaly. For this process to be important, there should be a large density of states at points on the Fermi surface separated by the phonon wavevector. Clearly this condition

is fulfilled for one-dimensional, or nearly one-dimensional systems
where the entire Fermi surface is two planes separated by $2k_F$. At
lower temperatures it may become energetically favourable to have
static phonons at this wavevector – the Peierls transition takes
place. Energy gaps are formed at the Fermi surface, and the con-
ductivity decreases.

For the theorist, one-dimensional systems are of interest in
themselves, since they may exhibit many characteristic and unusual
properties, and because one-dimensional models are more amenable
to exact theoretical calculations than the three-dimensional coun-
terparts. The most important property of purely one-dimensional
systems is that fluctuations prevent them from undergoing phase
transitions at all. This leads to an apparant paradox since we
have just argued that one-dimensionality is required for a Peierls
distortion to take place. Clearly, three dimensional effects,
however weak, are bound to be of crucial importance when dealing
with "one-dimensional systems". The phase transformation in a
real physical 3-d system takes place as a consequence of a subtle
interplay between large one-dimensional fluctuations and weak
interchain coupling. The transition will set in at a temperature
which is significantly lower than the mean field transition tempe-
rature

$$T_0 = \epsilon_F \, \exp \left(- \frac{\pi v}{g^2} \right) \quad , \qquad\qquad 1.1)$$

where v and ϵ_F are the velocity and energy at the Fermi surface
and g is the electron phonon coupling. It is this transition which
destroys the possibility of having a very high conductivity in
TTF-TCNQ at temperatures below 50K. The Kohn anomaly and the
Peierls distortion may be seen by x-ray and neutron scattering ex-
periments which provide the most direct evidence of the phase
transition.

In addition to allowing the phase transition to take place,
the three dimensional coupling has another important effect. If
one ignores the periodic potential from the underlying atomic lat-
tice ("Umklapp terms") the phase of the CDW is free to move along
the 1-d direction. However, in the presence of interchain coupling
the _relative_ phases on different chains, as specified by $q_\perp$, the
component of $\vec{q}$ perpendicular to the chain, are fixed. The value of
$q_\perp$ is mainly determined by the Coulomb interaction which attracts
regions of opposite excess charge. We shall see that in TTF-TCNQ
$q_\perp$ varies with temperature to accomodate different ordering of
the two types of chain. If there is coupling to the underlying
lattice, the overall phase χ may be "pinned". This coupling can
cause $q_\perp$ to lock at a commensurate value to take advantage of the
extra free energy. This appears to happen in TTF-TCNQ[3]. If $\vec{q}$ has a
component which is almost commensurate –either along or perpendicu-
lar to the chain– the CDW state may consist of large commensurate

regions with constant χ separated by comparatively narrow regions
-"solitons"- where χ changes rapidly.

As the temperature is lowered below T_0, the electrons in-
teract over longer and longer distances, and the effective interac-
tion between chains is enhanced. Ultimately, this brings out the
true three dimensional phase transition. In section 2 the effects
of weak interchain coupling are calculated by means of a systematic
perturbation theory developed in ref. 5. The zeroth order term is
not the mean field solution of the system as a whole, but an "exact"
solution of the one-dimensional system. The expansion parameter is
$\frac{1}{T}$ or, equivalently, $\frac{1}{Z}$ where Z is an effective number of interact-
ing chains. In section 3 the Bak-Emery theory[3] of the phase trans-
formations in TTF-TCNQ will be reviewed. An important feature is
that the theory does not depend upon any microscopic model of the
system, but makes use of the space group symmetries of the crystal
above T_c and the observed symmetry of the ordered state below T_c.
The perturbation theory presented in section 2 will provide a pre-
scription of how actually to estimate the numerical coefficients
entering the Landau-Ginzburg theory, in addition to providing phy-
sical insight into the nature of the phase-transition. We emphasize,
however, that the theory of TTF-TCNQ is based upon an expansion of
the free energy around the true phase transition, and not the tran-
sition temperature as given by any approximative theory. No attempt
will be made to actually identifying the details of the microscopic
mechanisms involved. The most striking consequence of the theory is
the prediction of a new phase transition. This transition has now
been confirmed by several experimental groups, and was found to
occur at $T \simeq 48K$. This is one of the very rare cases that the existence
of a phase transition has actually been predicted before it was ob-
served.

Recently, charge density waves[6,7] and Kohn anomalies[8] with
wavevector components $4k_F$ along the chains have been observed, and
theoretical explanations have been proposed[9-12]. The possibility to
form these waves can be included in the Landau expansion[3]. This
does not give rise to additional phase transitions since the sym-
metry is not lowered further. In section 3.4 an alternative mecha-
nism for the $4k_F$ modes will be suggested, and in section 3.5 the
critical properties near the phase transitions are studied from a
theoretical point of view.

No one-dimensional system is ideal. Three dimensional coupling
is of crucial importance, but also imperfections or impurities are
always present. In particular, random impurities are almost neces-
sarily of importance in non-stoichiometric systems such as KCP
(K_2 Pt $(CN)_4$ $Br_{0.3}$, $3H_2O$) where there is a non-integer average
amount of Br atoms in the unit cell. The Br atoms are probably ful-
ly ionized and may act as a random potential on the CDW and in turn
induce large fluctuations of the phase and possibly destroy long
range order. It has been suggested that impurities are responsible
for the absense of a CDW transition in KCP[13,14,5].

In section 4 the theory of Bak and Brazovsky[5] on the effects of impurities on quasi-one dimensional systems will be described. The field is assumed to interact linearly with the <u>derivative</u> of the phase of the CDW and not with the phase itself. In the case of a purely one-dimensional system the dynamical structure factor (which can be measured in a neutron scattering experiment) includes a <u>central peak</u> in addition to the phason branches which are also present for the pure system. When the interchain coupling is included, the actual phase transition is determined by an interplay between impurity effects which tend to destroy correlations and <u>prevent</u> long range order and 3-d effects which tend to enhance the susceptibility. It turns out that if the impurity correlation length becomes less than a certain threshold value, then the correlation length is finite at any temperature and no dielectric phase transition can take place. This may explain the saturation of the transverse correlation length in KCP at $T \simeq 100K$[13]. Of course there is the possibility that some other kind of ordering may occur. We suggest that there is a "spin-glass" like ordering where the phases of CDW's on different chains freeze in a random way relative to each other.

2. INTERCHAIN COUPLING

In this section we shall study the effects of weak interchain coupling following closely the systematic perturbation theory derived in ref. 5. A static CDW can be described by the periodic function

$$n(x) = \rho \cos(2k_F x + \chi) \qquad \qquad 2.1)$$

where ρ and χ are order parameters. For a one dimensional system the average value of $n(x)$, $<n(x)>$, is zero, but its <u>amplitude</u> is sharply peaked around its "mean field" value. At temperatures in the region

$$T \ll T_0 \qquad \qquad 2.2)$$

only long wavelength fluctuations are essential. The fluctuations of the whole system are <u>phase fluctuations (phasons)</u>. To include the effects of these excitations we shall allow χ to be a space and time dependent function, $\chi(x,t)$. To second order in the derivatives of χ, the phase fluctuations are described by the Lagrangian

$$L_0 = \frac{v}{8\pi} \iint dx d\tau \left(\frac{\dot{\chi}^2}{u^2} + \chi'^2 \right) \qquad \qquad 2.3)$$

where τ is the Matsubara time ($0 < \tau < \beta$). This Lagrangian does not include terms dependent upon χ itself since the system is invariant to a uniform shift of χ. u is the <u>phason velocity</u>. Brazovsky

and Dzyaloshinskij have calculated the dynamic structure factor $S(q,\omega)$ corresponding to L_0 [16,33]. If we are interested in the static integrated correlation function, $S(q)$, only we may restrict ourselves to considering time independent phase fluctuations, with energies

$$F = \frac{v}{8\pi} \int dx\ \chi'^2 \qquad\qquad 2.4)$$

Before introducing the interchain coupling, let us show how the phasons destroy long-range order in a one dimensional system. The static charge-charge correlation function, or structure factor, is

$$S(x) = \langle n(0)n(x)\rangle$$

$$= \rho^2 \langle \exp i\ \{\chi(0) - \chi(x)\}\rangle \cos 2k_F x \qquad\qquad 2.5)$$

It is essentially this function which is measured in any diffraction experiment. In this paper we shall drop the trivial factor $\cos 2k_F x$, i.e. all momenta will be measured relative to $2k_F$. The correlation function can be calculated using Feynman integral approach:

$$S(x) = \frac{\int D\chi\ \exp i\ \{\chi(0) - \chi(x)\}\ \exp(-\beta F_0)}{\int D\chi\ \exp(-\beta F_0)} \qquad\qquad 2.6)$$

where $\int D\chi$ is the functional integral over all possible phase fluctuations. By introducing Fourier transforms χ_q we find

$$S(x) = \frac{\int D\chi_q\ \exp \frac{1}{2\pi} \int dq\{(1-\exp iqx)i\chi_q - \frac{v\ q^2\chi_q^2}{8\pi T}\}}{\int D\chi_q\ \exp -\frac{1}{2\pi} \int dq\ \frac{v\ q^2\chi_q^2}{8\pi T}} \qquad 2.7)$$

$$= \exp\ -\int dq\ \frac{2T\ (1 - \cos(qx))}{v\ q^2}$$

$$= \exp\left(-\frac{|x|}{R}\right)\ ,\ R = \frac{v}{2\pi T} = \frac{1}{\gamma}$$

We have used a standard formula for Gaussian functional integrals. Hence the correlation length is finite at any finite temperature and no long range order exists.

The three dimensional coupling will be taken to be of the form

$$F_1 = -\sum_{ij} \int dx\ K_{ij} \cos\ (\chi_i(x) - \chi_j(x)) \qquad\qquad 2.8)$$

The summation is over interacting chains. This term may represent
the Coulomb interaction[17]. The interaction is <u>local</u>, i.e. the
phase at position x at chain i interacts with the other chains at
the same position only. The thermodynamic average of any quantity,
O, is given by the functional integral

$$<O> = \frac{\int D\chi \; O \; (\chi) \; \exp \; -\beta(F_0+F_1)}{\int D\chi \; \exp \; - \; (F_0+F_i)} \qquad 2.9)$$

The exponentials in both the denominator and the nominator are now
expanded in β:

$$<O> = <O>_0 \; -\beta(<OF_1>_0 \; - \; <O>_0 \; <F_1>_0) \qquad 2.10)$$

$$+ \; \frac{\beta^2}{2} \; (<OF_1^2>_0 \; - \; <O>_0 <F_1^2>_0) \; + \; \ldots$$

where $< >_0$ denotes the average with respect to F_0. These averages
are all Gaussian functional integrals which can be evaluated. To
calculate the structure factor we insert $O = \exp i \{\chi_1(0) -\chi_i(x)\}$:

$$S_{11}(x) = <\exp i \{\chi_1(0) - \chi_1(x)\}>_0 \qquad 2.11)$$

$$+ \; \beta^2 \sum_i K_{1i}^2 \iint dx'dx''<\exp i \{\chi_1(0)-\chi_1(x)+\chi_1(x')-\chi_1(x'')\}>_0$$

$$\times \; <\exp i \{\chi_i(x'')-\chi_i(x') \}>_0$$

$$- \; \beta^2 \sum_i K_{1i}^2 \iint dx'dx''<\exp i \{\chi_1(0)-\chi_1(x)\}>_0$$

$$\times \; <\exp i \{\chi_1(x')-\chi_1(x'')\}>_0$$

The averages are evaluated using the formula

$$<\exp i \sum_\nu n_\nu \chi(x_\nu) >|_{\sum_\nu n_\nu = 0} = \exp \tfrac{1}{2} \sum_{\nu\mu} n_\mu n_\nu \; D_0(x_\nu - x_\mu) \qquad 2.12)$$

where n_ν = + or - and $D_0(x) = \frac{|x|}{R}$.

Introducing $K_{1i}^2 = \frac{1}{Z}(\sum_{ij} K_{ij})^2 = \frac{1}{Z}K(0)^2$ and performing the integrations we obtain

$$S_{11}(x) = \exp\left(-\frac{|x|}{R}\right)$$

$$+ \beta^2 \frac{R^2 K(0)^2}{Z} \left[\frac{1}{16} \exp(-\frac{5|x|}{R}) - \exp(\frac{-|x|}{R}) \right. \qquad 2.13)$$

$$\left. +(\frac{|x|}{4R} + \frac{(x)^2}{2R^2}) \exp(-\frac{|x|}{R})\right] \ .$$

Z is an effective number of interacting neighbours. The correlation between chains can be calculated in a similar way. The Fourier transform of the correlation function is

$$S(q) = \frac{2\gamma}{\gamma^2+q^2} - \frac{K(0)}{T} \times (\frac{2\gamma}{\gamma^2+q^2})^2 + \frac{K^2(0)}{T^2} \times (\frac{2\gamma}{\gamma^2+q^2})^3$$

$$- \frac{K(0)^2}{ZT^2} \left[(\frac{2\gamma}{\gamma^2+q^2})^3 - \frac{R^2}{16} (\frac{10\gamma}{25\gamma^2+q^2} - \frac{2\gamma}{\gamma^2+q^2}) \right. \qquad 2.14)$$

$$\left. \frac{(2\gamma^2-12q^2)\gamma}{(\gamma^2+q^2)3} + \frac{\gamma^2-q^2}{2(\gamma^2+q^2)2\gamma} \right] \ .$$

where q is the wavevector component along the chain.

To first order in $\beta(=\frac{1}{T})$ this result is equivalent to the mean-field approximation. To second order in β the corrections to the mean-field theory are given by the last term of eq. 2.14). To find the transition temperature, let us find the temperature where the correlation function diverges, i.e. 1/S(o) vanishes:

$$\frac{1}{S(0)} \simeq \frac{\gamma}{2} (1 - \frac{2K(0)R}{T} + \frac{K(0)^2 R^2}{ZT^2} \times \frac{14}{5}) \qquad 2.15)$$

To first order in $\frac{1}{T}$,

$$T_c = 2K(0)R = \frac{K(0)v}{\pi T_c} \qquad 2.16)$$

$$\text{or} \quad T_c^2 = \frac{K(0)v}{\pi} \qquad 2.17)$$

This is in agreement with the result of Scalapino, Imry and Pincus[18], but in distinct disagreement with a theory of Lee, Rice and

Anderson[19] which in fact _ignores_ phase fluctuations and leads to a T_c which is only weakly dependent upon K(o). To second order,

$$T_c{}^2 = \frac{K(o)v}{2\pi} \left[\sqrt{1 - \frac{14}{5Z}} + 1 \right] \qquad 2.18)$$

Hence, as could be expected the transition temperature is lowered relative to the "mean-field" theory. The T_c and the susceptibility $\chi_q = 1/T \; S(q)$ as calculated here give an indication of the parameters entering phenomenological calculations, as for example the Bak-Emery theory of TTF-TCNQ[3] which is described in the next section.

3. LANDAU-GINZBURG THEORY OF STRUCTURAL PHASE TRANSFORMATIONS AND CHARGE DENSITY WAVES IN TTF-TCNQ

Since the discovery of the anomalous peak in the resistivity of TTF-TCNQ[1], there has been much speculation about the possibility of a structural "Peierls" transition. However, bulk measurements gave no definite information on this question, and it took surprisingly long time before this very fundamental question was solved by means of obvious diffraction techniques. The first _direct_ evidence of a phase transition in TTF-TCNQ was X-ray diffraction photographs taken at Orsay[20], but recent neutron scattering experiments at Brookhaven have provided a much more detailed picture of the low temperature transitions[21,22]. In these experiments it appeared that there were two transitions, one at 38K, the other at 54K. At low temperatures there is a $4\vec{a} \times 3.4\vec{b} \times \vec{c}$ modulation of the lattice. As the temperature was raised above 38K the modulation period along $\vec{a}$ changes, abruptly at first, then more gradually until it reaches 2a near 51K. These experiments have been explained by Bak and Emery[3] in terms of a Ginzburg-Landau theory. The most striking consequence of this theory is that there should in fact be a _third transition_ between those already observed. The proof of the new transition is based upon _symmetry considerations only_, whereas the nature of the underlying physical mechanisms plays no role at all for this purpose. The phase transition has now been observed by several experimental groups[23-25] and seems to take place at T≈48.5K.

In this section the theory for the three phase transformations will be reviewed, and we shall also study the critical properties at the transitions. In addition, a new mechanism for the $2k_F$ anomaly recently observed will be proposed. Figure 1 indicates schematically the CDW's at the different phases.

3.1 The 54K Transition

The space group of TTF-TCNQ is the monoclinic group P 2_1/c with the b axis as the unique axis[26]. The structure consists of chains of TTF molecules and chains of TCNQ molecules arranged in

sheets in the bc plane. The x-ray and neutron scattering experiments have shown a <u>second order</u> structural phase transformation at 54K. The ordered phase at this temperature is described by an incommensurate wavevector $\vec{q}_1 = (q_a, q_b, q_c) = (a^*/2, 0.295b^*, 0)$ where a^*, b^* and c are reciprocal lattice constants. Phrased in terms of a Peierls transition, the b^* component is twice the Fermi wavevector, $2k_F$.

According to the theory of Landau and Lifshitz[27] the order parameter describing a second order phase transition should transform as a basis of an irreducible representation of the high symmetry (high temperature) space group of the crystal. The representations are labelled by the <u>wavevector</u> describing the ordered unit cell and by the representation of the group of this wavevector. The wavevector is known from the neutron scattering experiments. The group of $\vec{q}_1$ consists simply of the two-fold axis, which has only two representations described by basis functions which transform into themselves or into minus themselves, respectively. When the order parameter is subject to such a screw axis transformation $(x, y, z) \rightarrow (-x, \frac{1}{2}+y, \frac{1}{2}-z)$ it should therefore transform either as

$$\psi_{\vec{q}_1} \rightarrow \exp(i\pi 2k_F)\psi_{\vec{q}_1} \qquad\qquad 3.1a)$$

$$\text{or} \quad \psi_{\vec{q}_1} \rightarrow -\exp(i\pi 2k_F)\psi_{\vec{q}_1} \qquad\qquad 3.1b)$$

We note that the symmetry considerations tells us <u>nothing</u> about which intra-molecular modes are involved. For a detailed discussion of the possible order parameters, see ref. 3. An important point is that it is possible to use optical CDW's on the two chain systems as order parameters. The charge distributions associated with these modes are

$$\rho^i(\vec{r}) = \pm \psi_{\vec{q}_1}^i \exp(i\vec{q}_1 \cdot \vec{r}), \ i = 1,2 \qquad\qquad 3.2)$$

where the $+$ sign applies to one sublattice of type i molecules and the $-$ sign to the other sublattice of type i molecules. Since Coulomb forces tend to favour opposite excess charges on neighbouring chains it is very likely that the optical modes are dominant. In general, however, we are of course free to use <u>any</u> order parameter (as for example the accompanying lattice distortion) which has the correct symmetry properties. The optical CDW's on the two chain systems transform as 3.1a) and 3.1b), respectively. Since the order parameter should transform as <u>one</u> of these basis functions, we may conclude that <u>only one chain system developes an optical CDW at the 54K transition</u>. It is in principle possible that there is an acoustic CDW on the other chain system which transform according to the same representation.

To find the temperature dependence of the order parameters, we expand the free energy close to the phase transitions in terms of the complex order parameters $\psi_{\vec{q}_1}^1$ and $\psi_{\vec{q}_1}^2$. This free energy should be real and invariant under translations, inversion and the two-fold screw-axis transformation, which are the symmetry elements of the high temperature phase. Since the two order parameters transform like two different representations, there are no cross terms of second order.

$$F = r_1 |\psi_{\vec{q}_1}^1|^2 + b_1 |\psi_{\vec{q}_1}^1|^4 + \ldots \qquad\qquad 3.3)$$

$$+ r_2 |\psi_{\vec{q}_1}^2|^2 + b_2 |\psi_{\vec{q}_1}^2|^4 + \ldots$$

r_1 and r_2 are effective inverse susceptibilities $1/\chi_{\vec{q}_1}^1$ and $1/\chi_{\vec{q}_1}^2$ of the two chain systems, respectively. These quantities may be estimated using the theory of section 2. We found that each set is expected to order at a finite temperature. The phase transition occur when the smallest of the parameters r_1 and r_2 passes through zero. Let us assume that it is r_1, linearize around $T_1 = 54K$, and minimize F for T not too far from T_1.

$$|\psi_{\vec{q}_1}^1|^2 = \frac{a_1}{2b_1} (T_1 - T), \qquad T < T_1 \qquad\qquad 3.4)$$
$$0 , \qquad T > T_1$$

and $|\psi_{\vec{q}_1}^2|^2$ remains zero at this transition. Here $r_1 = a_1(T - T_1)$. This describes the first phase transition in TTF-TCNQ. Experiments seem to indicate that it is mainly the TCNQ molecules that order[28,24].

3.2 The 47K Transition

Let us investigate the question as to when an optical transition is driven on the second type of chain, following closely the derivation of ref. 3. Since the single chain susceptibility diverges at T=0 on both types of chains, we expect this to happen at finite temperature. It will be shown that this transition is in fact related to the observed shift of the a^* component of the wavevector describing the distortions. To study the possibility of forming a charge density wave with $q_a \neq a^*/2$ we expand the free energy in both ψ_q^1 and ψ_q^2. Of course, any possible state with periodicity described by $\vec{q}$ can be formed from linear combinations of these modes. To simplify the notation we introduce $\psi_q^i = \psi^i(a^*/2+q, 2k_F, 0)$. We shall keep ψ_q^1 exactly since it may not remain small over the whole region of interest. To second order in ψ_q^2 we have

$$F (\psi_q^{\ 1}, \psi_q^{\ 2}, q) = f (|\psi_q^{\ 1}|^2, q)$$

$$+ A (|\psi_q^{\ 1}|^2, q)(\psi_q^{\ 2}\psi_q^{\ 1*} + \psi_q^{\ 1}\psi_q^{\ 2*}) \qquad 3.5)$$

$$+ B (|\psi_q^{\ 1}|^2, q) |\psi_q^{\ 2}|^2$$

When the twofold screw axis is applied to the order parameter, $\psi_q^{\ 2}\psi_q^{\ 1} \rightarrow -\psi_{-q}^{\ 2}\psi_{-q}^{\ 1}$ and $|\psi_{-q}^{\ i}|^2 \rightarrow |\psi_{-q}^{\ i}|^2$. Therefore, f and B are even in q and A is odd in q.

We now expand F in powers of q in the neighbourhood of q = 0; and minimize with respect to $|\psi_q^2|$. We find

$$F (\psi_q^{\ 2}, q) = aq|\psi_q^{\ 2}| + b|\psi_q^{\ 2}|^2 + cq^2 + \dots \qquad 3.6)$$

In principle the coefficient c could vanish at some temperature below 54K indicating a q-deviation within the 1-system only. However, since there is always some coupling between the two systems, a phase transition involving the 2-system would already have taken place before then. Moreover, there is no obvious physical reason for a temperature dependence of c. Near T_1, the coefficients b and c are positive, otherwise the type 2 chains would already have ordered, contrary to assumption, or q = 0 would not be a minimum contrary to experiment. Now, F is minimized with respect to q

$$q = -(a/2c) |\psi_q^{\ 2}| + o|\psi_q^{\ 2}|^3 \qquad 3.7)$$

and, when this is substituted into 3.6) F becomes

$$F = (b - a^2/4c)|\psi_q^{\ 2}|^2 + D|\psi_q^{\ 2}|^4 \qquad 3.8)$$

to fourth order in $|\psi_q^{\ 2}|$. Equation 3.7) shows how the moving wavevector is associated with the development of order in type 2 chains. When D > 0, there is a second-order transition at the temperature T_2 for which $b - \frac{a^2}{c}$ vanishes. This is <u>higher</u> than the temperature at which b = 0, because c > 0. Thus the coupling helps to drive the transition of $\psi_q^{\ 2}$. Minimizing F in eq. 3.8) with respect to $\psi_q^{\ 2}$ gives

$$|\psi_q^{\ 2}|^2 = -(b - \frac{a^2}{4c})/2D = \alpha(T_2 - T), \quad T < T_2 \qquad 3.9)$$

after expanding about T_2. From Eqs. 3.7) and 3.9) the variation of q is given by

$$q^2 = \begin{cases} 0 & , \quad T_1 < T < T_2 \\ a^2\alpha/4x^2(T_2-T), & T \quad T_2 \end{cases}$$

Hence, q_a stays at $a^*/2$ in a finite temperature interval below T_1, and the deviation of q_a away from this value should occur at a separate phase transition, the "47K transition". Since we first reported our result, several experiments have shown unequivocally the existence of the predicted transition. In a recent neutron scattering experiment, Ellenson et.al.[23] found the transition to occur at $T \simeq 48.5K$ (Fig. 2). Knight shift measurements seem to indicate that the transition is indeed associated with the TTF chains[24]. Specific heat measurements[25] show a clear anomaly at 48K. In the discussion of the 47K transition the existence of the underlying lattice has been ignored. In reality, the CDW is subject to a periodic potential from this lattice. Since $2k_F$ is not close to any simple rational value the effect of such "Umklapp" terms is probably small.

3.3 The 38K Transition

It now remains to understand the transition at 38K and the reason that q_a locks to a value of $a^*/4$ at low temperature. We suggest that this "pinning" is due to extra terms in the free energy, which are allowed only when $q_a = \pm a^*/4$[3]. The simplest possible Umklapp terms are of the form

$$\delta F = K(\psi_{a^*/4} \ \psi_{a^*/4} \ \psi_{-a^*/4} \ \psi_{-a^*/4} + CC) \qquad 3.10)$$

as suggested by Bak[29] and by Bjelis and Barisic[30]. δF is dependent upon the phases θ and θ' of $\psi_{a^*/4}$ and $\psi_{-a^*/4}$, respectively

$$\delta F = 2K|\psi_{a^*/4}|^2 \ |\psi_{-a^*/4}|^2 \ \cos(2\theta-2\theta') \qquad 3.11)$$

It is always possible to make this term negative by adjusting the phases. If $|K|$ is large enough, then it becomes favourable for the system to jump to the "symmetric" state consisting of equal amounts of $|\psi_{a^*/4}|$ and $|\psi_{-a^*/4}|$, when the q_a value minimizing the remaining free energy gets close enough to $a^*/4$. This is what happens at the 38K transition[3]. (See fig. 1.) An interesting point can be made here. In principle Umklapp terms may exist at any rational value of the wavevector[31]. This opens a possibility of having phase locking at different wavevectors in the temperature range 38K < T < 47K. In an experiment, it may be difficult to distinguish such behaviour from a continuous T dependence of q_a.
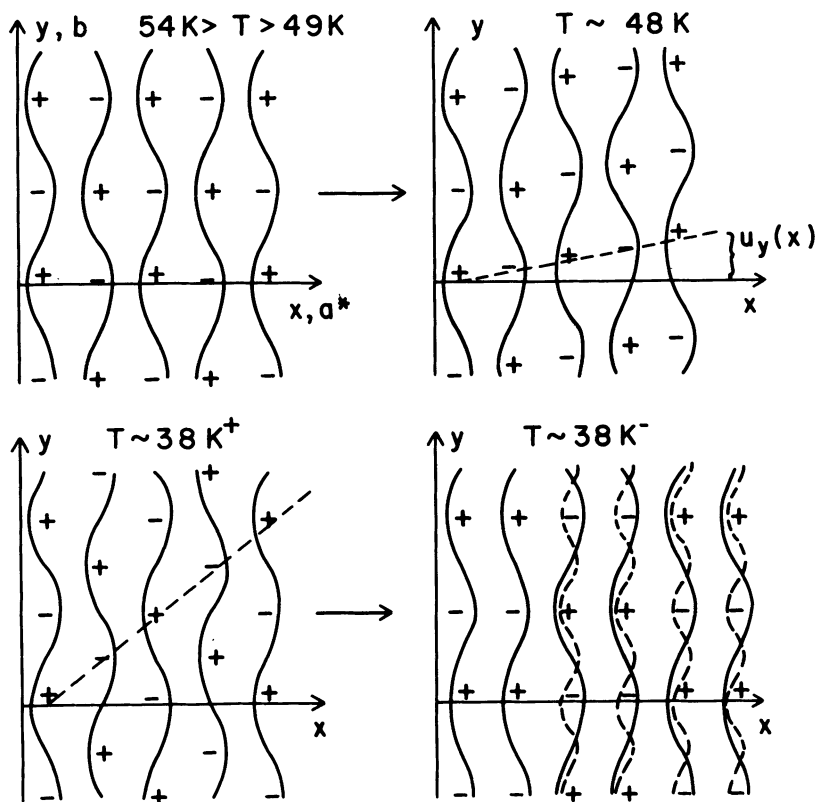
Fig. 1 Schematic diagram of phase transitions in TTF-TCNQ. The
full curves indicate the $2k_F$ modulation along the chains. The
dotted curves indicate $4k_F$ modulation below 38K. The overall sym-
metry is <u>monoclinic</u> except for the intermediate phase (48K > T >38K)
where the symmetry is <u>triclinic</u> (ref. 29).
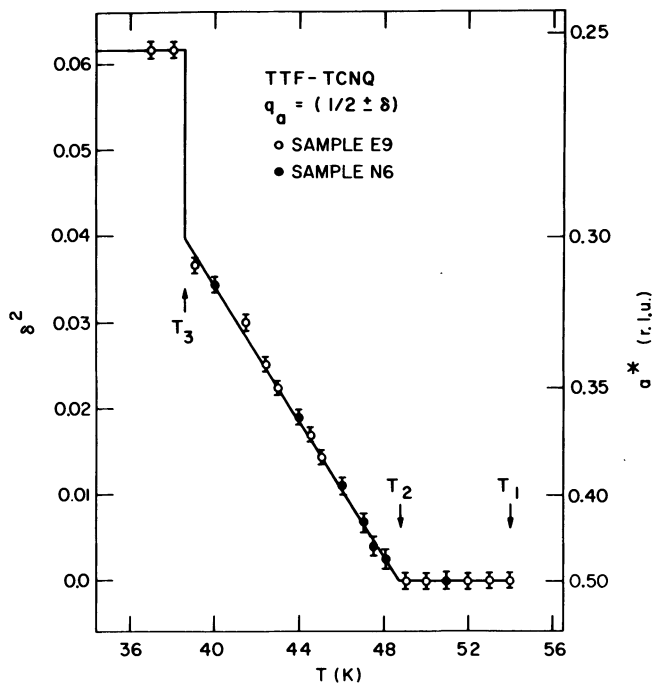
Fig. 2 Plot of observed peak positions $\delta^2 (= q^2)$ versus temperature. The three transition temperatures are also indicated (Ellenson et.al., ref. 23).
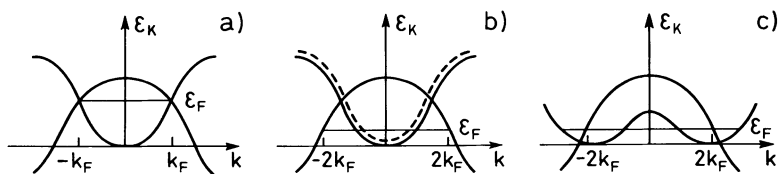
Fig. 3 a) Overlapping valence and conduction bands giving rise to $2k_F$ Peierls distortions. b),c) Band structures which allow both $2k_F$ abd $4k_F$ Kohn anomalies and distortions.

3.4 The $4k_F$ Anomaly

Recently a "Kohn" anomaly[6,8] and charge density waves[7] with wavevector component $4k_F$ along the chain direction have been observed in TTF-TCNQ. The $4k_F$ anomaly is present at room temperatures whereas there is nothing to be seen at $2k_F$ until 150K[6]. This seems to indicate that the $4k_F$ anomaly is not a simple anharmonic effect but is indeed generated by a separate mechanism. Torrance[12] attribute the "$2k_F$" scattering to spinwaves, the "$4k_F$" scattering to the usual Kohn anomaly. Emery[9] explains the $4k_F$ anomaly within the Luttinger model by assuming a large and positive intra molecular Coulomb repulsion, U, Sham proposes that anharmonic phonons are responsible[11], and Weger and Friedel guess that it is simply due to higher order diffraction from libration modes for which the "$2k_F$" scattering (approximately) vanishes[12].

Even if all these explanations are in principle possible, I shall now use this opportunity to confuse the situation further. The usual charge transfer mechanism can be understood by means of figure 3a. A valence (TTF) band and a conduction (TCNQ) band are overlapping, and because of one dimensionality and charge conservation the Fermi level is at the intersection between these bands. This picture is based upon an assumption that there is only one available orbital on each molecule. However, let us assume that there are two (almost) degenerate orbitals on one type of molecule. These orbitals could be associated with the nitrogen atoms situated at each end of the TCNQ molecule. The situation is then described by figure 3b: a charge transfer of $4k_F \times 2/b^*$ electrons from the TTF molecule will fill the two TCNQ bands up to $2k_F$ only. Clearly, the usual Peierls mechanism might then give rise to Kohn anomalies and lattice distortions with wavevector $2k_F$ on the TCNQ chains and $4k_F$ on the TTF chains. Another possibility is that there exist a conduction (valence) band with minimum (maximum) at $q_b = 0, \frac{b^*}{2}$. Then, because of inversion symmetry, there should exist another extremum at $-q_b$, as shown in figure 3c. Again, the bands corresponding to one type of molecules would be filled only up to half the Fermi wavevector of the other type of molecules. Clearly, more theoretical and experimental work on the band structure of TTF-TCNQ is required. The possibility of forming $4k_F$ modes can be included in the Landau Ginzburg theory[3]. Al all temperatures there should exist waves with periodicity given by the wavevector $2\vec{q} = (2q_a, 4k_F, 0)$. Above 47K this mode is acoustic, and below 38K it is associated with one chain system only in analogy with the $2k_F$ mode above 47K. An interesting consequence of our theory of the 38K transition[3] is that there should also exist a CDW with wave vector $(0, 4k_F, 0)$ below 38K. This mode is induced by terms like

$$\delta F = \psi_{(a^*/4, \ 2k_F, \ 0)} \ \psi_{(-a^*/4, \ 2k_F, \ 0)} \ \psi_{(0, \ -4k_F, \ 0)}$$

in the expansion of the free energy. We predict that this mode
should be _acoustic_. According to symmetry this mode is _forbidden_
when measuring around (0,2n+1,0) reflections.   This is in agree-
ment with the experiment by Kagoshima et.al.[7]: the "$4k_F$" peak at
$\vec{S}$ = (0,3-0.59,0)=(0,2+0.41,0) _vanishes_ at temperatures bolow 38K
whereas the peak at $\vec{S}$ = (0,3-0.59,1) is very sharp. We find that
there is no obvious reason that this behaviour is due to an acci-
dental polarization of the mode. The allowed $4k_F$ peaks disappear
abruptly at 38K as it should.

3.5 Critical Behaviour

Because of universality, the critical behaviour is believed to
depend upon very few properties of the system, namely the dimensio-
nality of the order parameter and the space group of the crystal.
For TTF-TCNQ the star of the wave vector associated with the 54K
transition consists of the two vectors $\pm\vec{q}_1$. Since the order para-
meter transforms as a one dimensional representation of the group
of q_1, the dimensionality of the order parameter is _two_, correspon-
ding for example to the amplitude and phase degrees of freedom, and
one should expect _three dimensional_ XY(n=2) exponents. Close to
the transition, the temperature dependence $\psi_{q_1}^{1}$ therefore should be

$$|\psi_q^1|^2 \simeq (T_1-T)^{2\beta}, \ \beta \simeq 0.33 \qquad 3.12)$$

In the case where the phase transition takes place at a non-symme-
tric $\vec{q}$ value with $q_a \neq \frac{1}{2}$, the star of $\vec{q}$ would consist of four vec-
tors, $\pm(q_a,q_b,0)$ and $\pm(-q_a,q_b,0)$, and one would expect n=4 critical
behaviour. At the 47K transition the "CDW lattice" distorts so
that the twofold axis is destroyed, as shown in figure 1. It is
this distortion that manifest itself as a shift of the $\vec{q}$ vector in
a diffraction experiment. A possible order parameter is a _homoge-
neous strain_ of the CDW:

$$\varepsilon_4' = \frac{d \ u_y(x)}{dx}$$

where $u_y(x)$ is the displacement of the CDW in the b-direction at
position $\vec{r}$. The symmetry of this transition is exactly the same as
that of a homogeneous q=0 structural phase transition in a mono-
clinic atomic lattice, where the order parameter is an ε_4 (ε_6) strain.
Hence the critical behaviour for these two systems should also be
the same. Just as the phase transition in an atomic crystal is
triggered by a _soft phonon mode_ the 47K phase transition is trigge-
red by a _soft transverse phason mode_[29]. Recently, Cowley[32] found
that the critical behaviour for the monoclinic system is classical
so no corrections to the mean field exponents are expected. Since
ε_4 and ε_4' have the same symmetry, a spontaneous ε_4 strain should
develope at the phase transition. Again it should be stressed that

Umklapp terms, i.e. the periodic potential from the underlying
lattice, has been ignored and could change the critical behaviour
at the 47K transition.

4. IMPURITIES

In real physical systems there are always some imperfections
or random impurities. In KCP the non-integer amount of Br-ions
in the formula unit may act like an external Coulomb potential on
the CDW. To investigate the effects of impurities, both in the
strictly one-dimensional system and in the quasi three-dimensional
case, we shall extend the Feynman integral method of section two,
following closely the work by Bak and Brazovsky[5]. The most impor-
tant contribution to the Coulomb interaction on a CDW is due to
backward scattering of electrons and may be written

$$U_i = - \frac{1}{2\pi} \int dx \; V(x) \; \chi'(x) \qquad\qquad 4.1)$$

where $V(x) \sim \sum_i u_i(x-l_i) - c \; \bar{u}_i$.

Here $u_i(x-l_i)$ is the Coulomb potential from an impurity ion at
site l_i. These ions are randomly distributed with concentration
c. $\bar{u}_i$ is the "average" potential of one impurity. Note that the
random field acts linearly with the <u>derivative</u> of the order para-
meter and not with the phase itself as in the model studies by
Sham and Patton[15,35].

4.1 One Dimensional Random Systems

We consider a one dimensional conductor with random impuri-
ties described by the Lagrangian

$$L = \frac{v}{8\pi} \iint dx d\tau \; (\; \dot{\chi}^2/u^2 + \chi'^2 - \frac{4V}{v} \chi' \;) \qquad\qquad 4.2)$$

It turns out to be convenient to transform the phason field χ to a
new unconstrained field ψ through the relation

$$\chi(x) = \bar{\chi}(x) + \psi(x) \qquad\qquad 4.3)$$

where $\qquad \bar{\chi}(x) = \int_{-\infty}^{x} \frac{2V(x')}{v} \; dx'.$

The Lagrangian becomes

$$L(\psi) = \frac{v}{8\pi} \iint dx d\tau \; (\; \dot{\psi}^2/u^2 + \psi'^2 \;) \qquad\qquad 4.4)$$

plus a constant term which does not affect thermodynamic averages.
To calculate an observable quantity one should <u>first</u> calculate it
for any possible impurity configuration and <u>then</u> average over the

impurity distribution function. For the structure factor we find, using 4.3):

$$S(x) = \ll <\exp i\{\chi(0,0) - \chi(x,t)\} > \gg = S_i(x)S_p(x) \qquad 4.5)$$

$$= <\exp i \{\psi(0,0) - \psi(x,t)\} > \times \ll \exp i\{ \bar{\chi}(0) - \bar{\chi}(x)\} \gg$$

where the double brackets denote averages over impurity configuration. The averages can thus be performed independently. In the small concentration, small potential limit it can be shown that

$$S_i(x) = \ll \exp i\{ \bar{\chi}(0) - \bar{\chi}(x)\} \gg = \exp(- \frac{|x|}{\xi_i}) \qquad 4.6)$$

or in Fourier space,

$$S_i(q) \quad = \frac{2\gamma_i}{q^2 + \gamma_i^2}$$

where $\xi_i = 1/\gamma_i$ is the impurity correlation length. For KCP, ξ_i is probably comparable to the correlation length $R_p = 1/\gamma_p$ for the pure system. The first factor in 4.5) has been calculated by Brazovsky[33]. In (q,ω) space

$$S_p(q,\omega) = A \frac{2\gamma_p}{\{(\omega+qu)^2 + (u\gamma_p)^2\} + \{(\omega-qu)^2 + (u\gamma_p)^2\}} \qquad 4.7)$$

The dynamical structure factor is obtained as a convolution of the Fourier transform of the pure structure factor with the impurity correlation function 4.6):

$$S(q,\omega) = \frac{1}{2\pi} \int_k S_i(k) \ S_p(q-k,\omega)dk$$

$$= A \times \left[\frac{\gamma_i}{(\omega^2 + \gamma_p^2 u^2)(q^2 + \gamma_i^2)u^2} \right. \qquad 4.8)$$

$$+ \left. \frac{2q^2(\gamma_p + \gamma_i) - \gamma_i\{\omega^2/u^2 + (\gamma_p + \gamma_i)^2 q^2\}}{\{(\omega+uq)^2 + (\gamma_p + \gamma_i)^2 u^2\} \ \{(\omega-uq)^2 + (\gamma_p + \gamma_i)^2 u^2\} \ (q^2 + \gamma_i^2)} \right]$$

The second term gives the contribution from phason modes at $\omega = \pm uq$. The first term describes a central peak not present in the pure systems, and the q-width is the inverse impurity correlation length. A very accurate neutron diffraction is required to resolve the spectrum since there is considerable overlap between the various terms. The expression should be valid for KCP at temperatures far above the "three dimensional" phase transition at $T \simeq 100K$[13].

4.2 Combined Effects of Random Impurities and Interchain coupling[5]

The model that we shall investigate is the combination of the random 1-d model and the three dimensional model studied in section 2. The random potentials are assumed to act within each chain and not affect the coupling between chains. The corresponding free energy functional is then

$$F = \int dx \sum_i \{\frac{V}{8\pi}(\chi_i' - \frac{2V_i(x)}{v})^2 - \sum_j K_{ij}\cos(\chi_i - \chi_j)\} \qquad 4.9)$$

Applying the transformation 4.3) we get a new effective free energy

$$F(\psi) = \int dx (\sum_i \frac{v}{8\pi}\psi_i'^2 - \sum_{ij} K_{ij} \cos(\bar{\chi}_i(x) - \bar{\chi}_j(x) + \psi_i(x) - \psi_j(x))) \qquad 4.10)$$

We note that F is not independent of $\bar{\chi}(x)$, as it was in the case of the one dimensional system, and the averages $< >$ and $<< >>$ do not commute any more. Hence, first the thermodynamic average $< >$ should be performed for any possible impurity configuration, and then averaged over the impurity distribution function.

The expansion 2.10), therefore, should be modified in the following way

$$<< <O> >> = << <O>_0 >> \qquad 4.11)$$
$$- \beta (<< <OF_1>_0 >> - << <O>_0 <F_1>_0 >>)$$
$$+ \frac{\beta^2}{2}(<< <OF_1^2>_0 >> - << <O>_0 <F_1^2>_0 >>) + \dots$$

where F_1 is the interacting part of 4.10).

To calculate the structure factor we insert

$$O = \exp i\{\chi_i(0) - \chi_j(x)\} \qquad 4.12)$$
$$= \exp i\{\bar{\chi}_i(0) - \bar{\chi}_i(x)\} \exp i\{\psi_i(0) - \psi_i(x)\}$$

The bookkeeping of the various terms can be performed in a diagrammatic way[5]. Each term in the expansion for the pure system is replaced by a product of this term and an impurity term. The Fourier transform of 4.11) has been evaluated. To estimate the transition temperature the inverse correlation function is expanded in $\frac{1}{T}$. To second order

$$\frac{1}{S(0)} = \frac{\gamma}{2} \times \{1 - \frac{2K(0)R}{T} + \frac{K^2(0)R^2}{ZT^2} \times \frac{14}{5} + \frac{K(0)^2R^2}{2ZT^2} f(\frac{\xi_i}{R_P})\}. \qquad 4.13)$$

where the function f is dependent upon temperature through R_p. For example, $F(\infty)=0$, $f(1)=0.375$, $f(0.1)=1.74$.

Again, to first order in $\frac{1}{T}$ we find the mean field result

$$\frac{T_c}{R} = 2K(0) \quad , \quad \frac{1}{R} = \frac{2\pi T_c}{v} + \frac{1}{\xi_i} \qquad 4.14)$$

T_c is lowered by the impurities but remains finite. To second order

$$\frac{T_c}{R} = K(0) \left(1+ \sqrt{1- \frac{1}{Z}(\frac{14}{5} + \frac{f}{2})} \; \right) \qquad 4.15)$$

For small Z, therefore, a large impurity concentration will tend to suppress the phase transition.

At low temperatures the high temperature expansion will break down. In this region, the structure factor can be calculated using a continuum representation in the transverse direction too[5]. For not too large concentrations of impurities the dynamical structure factor will consist of three different features: 1) A Bragg peak which indicates that long range order exists. 2) An elastic impurity induced peak with finite width in momentum space and 3) two phason branches originating from phase fluctuations. However, when the impurity concentration exceeds a certain limit, the continuum representation breaks down, indicating that no long range order can exist due to a "melting" of the CDW lattice. This seems to be the case for KCP. As the temperature is lowered below 100K, the transverse correlation length increases rapidly but saturates rather abrubtly around 100K. This relative sharp saturation indicates that some other ordering may occur. We suggest that there develops a "spin glass"-like ordering, where the CDW's at distant positions freeze in a random way relative to each other, but where near neighbours are correlated. In fact, our model of KCP is very similar to the three dimensional rotator considered by Edwards and Anderson[34], (which is believed to exhibit spin-glass ordering) since both models are formally three dimensional random xy-models.

5. REFERENCES

1. L.B. Coleman, M.J. Cohen, D.J. Sandman, F.G. Yamagishi, A.F. Garito, and A.J. Heeger, Sol.St.Comm. 12, 1125 (1973).
2. R.E. Peierls, Quantum theory of solids, Oxford University Press, p. 108.
3. P. Bak and V.J. Emery, Phys.Rev.Lett. 36, 978(1976), and to be published.
4. W.L. McMillan, Phys.Rev. B14, 1496(1976).

5. P. Bak and S.A. Brazovsky, to be published.
    See also A.J. Larkin and V.I. Melnikov, preprint,
    Z. Zavadovski, ZhETF 54, 1429(1968).
6. J.P. Pouget, S.K. Khanna, F. Denoyer, R. Comès, A.F. Garito
    and A.J. Heeger, Phys.Rev.Lett. 37, 437(1976).
7. S. Kagoshima, T. Ishiguro and H. Anzai, J.Phys.Soc. Japan,
    41, 2061(1976).
8. H.A. Mook and C.R. Watson, Phys.Rev.Lett. 36, 801(1976).
9. V.J. Emery, Phys.Rev.Lett. 37, 107(1976).
10. L.J. Sham, Sol.St.Comm. 20, 623(1977).
11. M. Weger and J. Friedel, Journal de Physique 38, 241(1977).
12. J.B. Torrance, H.A. Mook and C.R. Watson, Preprint.
13. J.W. Lynn, M. Iizumi, G. Shirane, S.A. Werner and R.B. Saillant,
    Phys.Rev. B12, 1154(1975).
14. K. Carneiro, G. Shirane, S.A. Werner and S. Kaiser, Phys.Rev.
    13, 4258(1976).
15. L.J. Sham and B.R. Patton, Phys.Rev. B13, 315(1976), Phys.Rev.
    Lett. 36, 733(1976).
16. S. Brazovsky and I. Dzyaloshinsky, ZhETF 71, 2338(1976) and
    ZhETF 72(1977), (to be published).
17. K. Saub, S. Barisic and J. Friedel, Phys.Lett. A56, 302(1976).
18. D.J. Scalapino, Y. Imry and P. Pincus, Phys.Rev. B11, 2042
    (1975).
19. P.A. Lee, T.M. Rice and P.W. Anderson, Phys.Rev.Lett. 31 462
    (1973).
20. F. Denoyer, R. Comès, A.F. Garito and A.J. Heeger, Phys.Rev.
    Lett. 35, 445(1975).
21. R. Comès, S.M. Shapiro , G. Shirane, A.F. Garito and A.J. Heeger,
    Phys.Rev.Lett. 35, 1518(1975).
22. R. Comès, G. Shirane, S.M. Shapiro, A.F. Garito and A.J. Heeger,
    Phys.Rev. B14, 2376(1976).
23. W.D. Ellenson, R. Comès, S.M. Shapiro, G. Shirane, A.F. Garito
    and A.J. Heeger, Sol.St.Comm. 20, 53(1976).
24. E.F. Rybaczewski, L.S. Smith, A.F. Garito, A.J. Heeger and
    B.G. Silbernagel, Phys.Rev. B14, 2746(1976).
25. K. Franulović, S. Tomic, M. Prester, D. Djurek, L. Girel and
    J.M. Fabre, Preprint.
26. B.T. Kistenmacher, T.E. Phillips and D.O. Cowan, Acta
    Crystallogr. B30, 763(1974).
27. L.D. Landau and M.E. Lifshitz, Statistical Physics, 2nd ed.
    (Pergamon, New York, 1968) Chap. XIV.
28. S. Etemad, Phys.Rev. B13, 2254(1976).
29. P. Bak, Phys.Rev.Lett. 37, 1071(1976).
30. A. Bjelis and S. Barisic, Phys.Rev.Lett. 37, 1517(1976).
31. S.A. Brazovsky and I. Dzyaloshinsky, Proceedings of the 14th
    international conference on low temperature physics, 5, 337
    (1975).
32. R.A. Cowley, Phys.Rev. B13, 4877(1976).
33. S.A. Brazovsky, NORDITA-preprint.
34. S.F. Edwards and P.W. Anderson, J.Phys. F6, 1927(1976).

35. The term 4.1) may represent <u>forward</u> scattering of conduction electrons by the impurity potential, whereas the coupling considered by Sham and Patton may represent <u>backward</u> scattering across the Fermi surface. We expect this latter coupling to be comparatively weak since it involves the $2k_F$ component of a long range Coulomb potential.

SOLITONS AND CHARGE DENSITY WAVES

Alan Luther

NORDITA
Blegdamsvej 17, 2100
Copenhagen Ø, Denmark

1. Abstract

The microscopic physics underlying the sine-Gordon equation
in quasi-one-dimensional conductors and two dimensional layered
structures is explored.

An interesting parallel between these two systems is discussed,
and the quantum nature of the former, involving the time variable,
is found to be equivalent to the second space dimension of the lat-
ter. The soliton spectrum of both are studied and the implications
of these discrete states for real physical systems, with three-di-
mensional couplings, are developed.

2. Introduction

The study of charge density waves in lower dimensional systems
has been advanced beyond the stage of speculation due to experi-
ments in both quasi-one [1] and quasi-two [2] dimensional systems.
While it is by no means clear that the special properties of one
and two dimensional models can explain these phenomena, it seems
appropriate to understand the predictions of these models, keeping
in mind a healthy skepticism about the ultimate outcome.

There appears to be much in common between the quasi-one-di-
mensional and some of the quasi-two-dimensional charge density
structures. In the former, time appears as an important dynamical
variable. Obviously, renaming this variable a second space var-
iable, one arrives at a classical two dimensional problem. To the
extent that quantum fluctuations are unimportant in the layered

structures, the two are equivalent.

An interesting consequence of this equivalence concerns the existence of soliton states [3]. Propagating wave-type solutions along a one dimensional chain have a direct correspondence to stationary domain-like excitations in the classical two dimensional system. These domain structures, in turn, have consequences for the thermodynamics and static correlation functions. This paper is intended to explore the types of soliton states which can be of interest, and to deduce some observable consequences of these states, if they exist.

If the reader has sensed skepticism about solitons solving all problems of lower dimensional systems, it is not unfounded. There can be no doubt about the importance of these states in the purely one or two dimensional case. But when interactions are turned on between the strings, or between the layers, the effects of these must be included in the original soliton solution. At present, a good understanding of the destruction of solitons, or perhaps only slight damping of solitons due to these interactions, is lacking.

On a heuristic level, the problem could be phrased in terms of energy scales. If the energies of interaction within, say, the string, are much stronger than the interactions between the strings, it is a good approximation to apply the solutions to the string problem, and treat the interactions between them as a perturbation. This will be a good approximation for temperatures larger than the mean interaction between strings, which is roughly the mean field transition temperature for the strings. The same words obviously apply in the layered case as well.

3. Change Density Waves and the Sine-Gordon Equation

With these introductory hedges in mind, let us turn to a study of charge density waves in lower dimensions. Not surprisingly, the close relation between charge density waves and the solitons is one of the first points to be encountered. The mathematics literature is filled with various equations which exhibit non-linear wave propagation [4]. Of these, the sine-Gordon equation [5] is the most relevant for the physical applications of interest here. Before discussing this equation, it is important to understand where it came from, what assumptions went into it, and why it might be of interest.

An example from the one dimensional conductor problem consists of a filled Fermi sea of electrons moving in a potential capable of causing transitions from one side of the Fermi line, at momentum plus k_F, to minus k_F, the usual charge density wave instability. To analyze this situation, we focus attention on those

states at the Fermi energy. These are described by the free par-
ticle Hamiltonian,

$$H_0 = v_F \sum_k (k-k_F) \, a_{1k}^+ \, a_{1k} - (k+k_F) \, a_{2k}^+ \, a_{2k} \tag{1}$$

where v_F is the Fermi velocity, a_{1k} (a_{2k}) describes the elec-
trons moving to the right (left). To this, is added the mixing
with the charge density wave potential,

$$H_{CDW} = V_0 \sum_k a_{1k}^+ \, a_{2k+k_F} + a_{2k}^+ \, a_{1k-2k_F} \tag{2}$$

where V_0 is the strength of the interaction. In a more realistic
model, the electron-electron interactions should be included, as
well as a description of the phonon degrees of freedom. The present
model, however oversimplified, does contain the essential physics,
and can be generalized to the more complicated situations without
undue hardship.

One of the fundamental simplifications of the one dimensional
electron gas starts with the recognition [6] that Eq. (1) can be
transformed into a simple harmonic oscillator, or one dimensional
phonon problem. While much of our intuition about metals is based
on electron Hamiltonians, results for soliton problems are based
on phonon-type fields, or fields describing a phase variable. The
flexibility to view the problem from either vantage point is ex-
ceedingly insightful.

The equivalent phonon problem is given by the Hamiltonian,

$$H_0 = \frac{2\pi v_F}{L} \sum_k [\rho_1(k)\rho_1(-k) + \rho_2(-k)\rho_2(k)] \tag{3}$$

where L is the length of the string of electrons, and the phonon
operators satisfy the commutation relations

$$[\rho_1(-k), \rho_1(k')] = [\rho_2(k'), \rho_2(-k) = \delta_{k,k'} \, kL \, (2\pi)^{-1}$$

$$[\rho_1, \rho_2] = 0 \tag{4}$$

In terms of the electron operators, the phonon operators are given
by

$$\rho_1(k) = \sum_p a^+_{1k+p} \, a_{1p}$$

$$\rho_2(k) = \sum_p a^+_{2k+p} \, a_{2p} \tag{5}$$

The key to understanding the soliton-charge density wave equivalence is contained in the H_{CDW} written in terms of the phonon variables. It is here necessary to make use of the so-called phase representation [7] of electron operators, given by

$$\sum_k a_{1k} \, e^{ikx} = (L/2\pi s)^{\frac{1}{2}} \, e^{ik_F x + \phi_1(x)}$$

and

$$\sum_k a_{2k} \, e^{ikx} = (L/2\pi s)^{\frac{1}{2}} \, e^{-ik_F x + \phi_2(x)} \tag{6}$$

where s is a cut-off length, equal to a lattice constant, and the phase variables $\phi_1(x)$ and $\phi_2(x)$ are, in turn, related to the phonon operators through

$$\phi_1(x) = 2\pi i \int^x dy \, \rho_1(y)$$

$$\phi_2(x) = -2\pi i \int^x dy \, \rho_2(y) \tag{7}$$

when substituting these into Eq. (2), one obtains the simple answer,

$$H_{CDW} = \frac{V_0 L}{2\pi s} \int dx \, \cos \Phi(x) \tag{8}$$

where the total phase $\Phi(x) = i(4\pi)^{\frac{1}{2}} (\phi_1(x) + \phi_2(x))$ has been introduced. Now it is possible to write Eq. (3) in a slightly more familiar form, if we use the additional operators, $\Phi(x)$ and $\pi(x) = i [\Phi(x), H_0]$, where

$$\Phi(x) = i \sum_p \frac{1}{\sqrt{\pi V_F}} \Big[\rho_1(p) + \rho_2(p) \Big] \frac{e^{-ipx}}{pL}$$

$$\pi(x) = i \sum_p \frac{-1}{\sqrt{\pi V_F}} \Big[\rho_1(p) - \rho_2(p) \Big] \frac{e^{-ipx}}{L}$$

(9)

with the simple result that the charge density wave problem can be written in the form

$$H = \int dx \, \frac{1}{2} \Big[\pi^2(x) + V_F^2 (\nabla\varphi)^2 \Big] + \frac{V_0}{2\pi s} \cos \sqrt{4\pi} \; \varphi$$

(10)

which is recognized as the quantum mechanical sine-Gordon equation, and, at the same time, from Eqs. (1) and (2), is the equation for an electron moving in the potential of a $2 k_F$ density wave.

The essential ingredient leading to this result is the phase representation of the charge density wave, which lead to Eq. (8). Any interaction which permits such a representation will lead to the same equation. It is interesting to note the many seemingly complicated interactions which can be written in this form. Including electron-electron interactions leads to two modifications. The first is trivial, a renormalization of the Fermi velocity. The second is a replacement of the $(4\pi)^{\frac{1}{2}}$ by another constant, β. This constant determines the nature of the soliton state solutions, and is itself determined by the strength of the electron-electron interaction. If U represents this interaction strength, then $\beta = \sqrt{4\pi} \, (1-U\rho)^{\frac{1}{2}} \, (1+U\rho)^{-\frac{1}{2}}$. (We might imagine U to be a screened Coulomb interaction, which can be comparable to the reciprocal bandwidth ρ.) These solutions will be discussed below.

It is worth a brief mention of other interactions which reduce to this sine-Gordon form. Obviously, the phase variable was constructed from two electron states - moving in opposite directions in the above example. But any combination of two phases will lead to an identical result. We might imagine a phase associated with the up spin electrons, and another associated with the down. This creates a phase field for the spin density, and we would expect a sine-Gordon equation for these degrees of freedom [8]. A further - but more complicated situation - concerns the electron-phonon interaction. When the temperature is very low, and the electron-phonon system is strongly coupled, the phase of the displacement becomes a good variable [9], and the motion of a charge density wave is governed by the free phonon part of Eq. (10). If there is an impurity present, the interaction with the charge density wave is given by

$$H = \frac{1}{2} \int dx \left[\pi^2 + c^2 (\nabla\varphi)^2 \right] + \lambda \sum_i \cos \beta\varphi(x_i) \qquad (11)$$

where c is a phonon velocity, λ the interaction strength, and
the sum runs over the impurity sites, x_i . It is this, modified
slightly from Eq. (10), which is the sliding conductivity problem.
Except for the free particle case, $\beta = \sqrt{4\pi}$, little is known
about Eq. (11). This problem will be studied below.

4. Solitons and Charge Density Waves

From a mathematical viewpoint, the problem is now well-posed -
namely, what are the eigenvalues and eigenfunctions of the
Hamiltonian Eq. (10), for general values of β ? But the physics
is not so simple. Even with this complete (but nonexistent) in-
formation, the questions of transport, impurity scattering, etc.
would remain. These are well beyond the scope of this paper.

Rather, a simple physical picture of these states is the goal
of this paper, and it is hoped that the mathematical details can be
kept to a minimum. It is possible for the reader interested in
such questions as rigor and completeness to satisfy herself as to
the current state of the art in the relevant literature.

There is substantial information about the eigenvalue spec-
trum [4,10] of the sine-Gordon equation, but little else. There are
several limiting cases which are quite helpful in understanding
the additional questions, such as matrix elements, selection rules
and the like, but here the situation is far from satisfactory.

The trivial limiting case is one good example to keep in mind.
Consider $\beta^2 = 4\pi$. From Eq. (1), Eq. (2), and Eq. (10), it is
clear that this case is a one-electron problem, which is immediate-
ly solved. The eigenvalue spectrum is

$$E = V_F K_F \pm V_F \left[(K-K_F)^2 + \left(\frac{V_0}{2\pi s} \right)^2 \right]^{\frac{1}{2}} \qquad (12)$$

and the new feature of the problem is the appearance of a gap at
the Fermi energy, a gap required to create a particle-hole pair
excitation. From the equivalence to the sine-Gordon equation,
there comes the identification of the single electron states with
a propagating solition. That is, through the miracles of modern
science, the highly complicated non-linear equation involving the
phase variables becomes a simple free electron problem when viewed
from another vantage point.

Another interesting limiting case concerns the region
$\beta^2 \to 0$. In this situation, it is permissable to expand the co-
sine, and retain the lowest order correction. The resulting equa-
tion is

$$H \to \int \frac{dx}{2} \left[(\nabla\varphi)^2 \, v_F^2 + \pi^2 + \frac{V_0}{2\pi s} \, \beta^2 \, \varphi^2 \right] \qquad (13)$$

which is very similar to the one dimensional optical phonon prob-
lem, with the eigenvalue spectrum given by:

$$E_K = v_F \left[K^2 + \frac{V_0 \, \beta^2}{2\pi s \, v_F^2} \right]^{\frac{1}{2}} \qquad (14)$$

As found above, the characteristic feature is the gap in the spec-
trum, of magnitude:

$$E_0 = \beta \left[\frac{V_0}{2\pi s} \right]^{\frac{1}{2}} \qquad (15)$$

but the reader should recognize the rather profound difference be-
tween the two cases. The former was explicitly a fermion-type
gap, while the latter is a boson gap! In a peculiar manner, the
Hamiltonian changes continuously from a free fermion problem to a
free boson problem, with complications in between.

It is possible to offer a plausible interpretation of this
gap, regardless of its fermi-bose schizophrenia. If a static cor-
relation function is calculated, such as the phase-phase correla-
tion function at large distance between the phase measurement
points, there will be an exponential fall-off, while at shorter
distances the effects of the gap will be negligible. When divided
by the Fermi velocity, the gap thus determines a wave number scale
of local ordering.

The complicated behaviour of the spectrum has been studied by
the WKB approximation [4] and by the device of finding another
equivalence to a solved model in statistical mechanics [10]. The
results of these investigations have found

$$E_K^2 = \Delta_n^2 + V_F^2 K^2$$

$$\Delta_n^2 = \Delta \sin\left(\frac{n\gamma'}{16}\right) \tag{16}$$

$$\Delta = \left(\frac{V_0}{2\pi s}\right)^{\nu}$$

where $\gamma' = \beta^2 (1 - \beta^2/8\pi)^{-1}$, $2\nu = (1 - \frac{\beta^2}{8\pi})^{-1}$, $n = 0,1,2,\cdots$
and n is a new quantum number, which has an interpretation as
labelling bound solitons. Again, a heuristic interpretation of
these states is possible, and it compares them to excitons forming
within the gap of a semiconductor. Since $\beta^2 < 4\pi$, the interac-
tion implied by the result under Eq. (10), is particle-hole attrac-
tive when bound solitons appear.

A few words about the rigor of this solution one in order.
The WKB results have been demonstrated to be exact for the eigen-
value spectrum, by studying the relationship to the spin $\frac{1}{2}$ x-y-z
spin chain in one dimension [10]. This relationship was used not
only to study the eigenvalue spectrum, but to provide an intuitive
picture for the soliton states. Without an overwhelming mass of
mathematics, the full justification of this relationship is not
possible - but some observations are of interest.

The x-y-z model is given by the Hamiltonian

$$H_s = -\sum_i J_\alpha S_i^\alpha S_{i+1}^\alpha \tag{17}$$

where $\alpha = x, y$, or z, S_i^α is a spin $\frac{1}{2}$ operator at site i, and
the sum is over N sites of a chain. Again, the study of a few
limiting cases helps establish the physics of Eq. (17). When all
J_α are equal, the Heisenberg ferromagnetic case, we know that Eq.
(17) should have spin waves. Comparison to Eq. (15), for $\beta^2 = 0$,
shows the similar behaviour. Now for the case $\beta^2 = 4\pi$. It has
been known that the x-y model, with $J_z = 0$, can be transformed
into a free electron problem, and indeed, the equivalence between
these two cases has been rigorously established.

But more has been established. In the entire region with
$J_x = J_y$, and $|J_z| < J_x$, it is intuitively clear that the rota-
tional degeneracy about the z-axis, within the x-y plane can be
described by a phase variable. A spin wave, corresponding to pre-
cession about the z-axis, corresponds to the phonon propagation of
Eq. (3), corresponds to a potential tending to "orient" the phase
in the x-y plane, along a particular direction, analogous to ori-
entation of the spin along the x axis, if J_x is larger than
J_y. In this view, a soliton is a spin wave propagating along the
chain. Bound solitons are spin wave bound states.

In addition to this simple physical picture, some new results can be derived from this equivalence. A peculiar instability in the sine-Gordon equation, at the value $\beta^2 \geq 8\pi$, has led to confusion about the meaning of charge density waves in these circumstances.

It is easy to recognize $\beta^2 = 8\pi$ as a special point, from the result states in Eq. (16). The exponent ν , in the relation between the observed gap and the applied field, goes to infinity at this point, then becomes negative. Has something gone wrong in the solution? It is instructive to consider this question from the spin chain viewpoint.

Recall that $\beta^2 = 0$ corresponds to the Heisenberg ferromagnet, $J_z = J_x = J_y$, and the phase of the sine-Gordon equation, in general, has the interpretation as a phase variable of a basal plane spin. As J_z is decreased to zero, and then downward to $J_z = -J_x = -J_y$, the Heisenberg antiferromagnetic point is reached. For more negative J_z , the spin no longer lies in the basal plane. Indeed this marks the crossover to a spin problem of Ising symmetry, and the phase variable cannot be defined as before.

This spin equivalence suggests that a new type of gap appears when $\beta^2 > 8\pi$, a gap analogous to the appearance of an Ising gap as the J_z exchange becomes large in magnitude. Obviously, in the spin problem, the equilibrium direction of the spin simply rotates to accommodate the new ground state symmetry. Once the spin operators are rotated to recognize the new equilibrium direction, we may again view the soliton as a spin wave. The $\beta^2 \geq 8\pi$ problem is simply the requirement that the phase variable must be defined about the new equilibrium direction.

To state this resolution more precisely, the sine-Gordon equation assumes that the parameters β^2 and V_0 have been defined such that, in the corresponding spin problem, $|J_z|$ is the smallest interaction. If this is not the case, the spins must be rotated to new axes, such that the new variables, denoted by a prime, do have $|J_z'|$ the smallest. If this prescription is followed, $\beta^2 < 8\pi$ is always satisfied.

Collecting these results leads to the following simple picture of charge density waves in the one-dimensional conductor. For $0 < \beta^2 < 8\pi$, that is $-1 < Up < 1/2$, there is a gap in the excitation spectrum caused by the appearance of $2k_F$ charge density waves, and for $-1 < Up < 0$, there are bound soliton states, representative of charge bunching, which may propagate. For Up outside this region, it is necessary to recognize the equivalence to an Ising-like spin problem, with a preferential orientation. Solitons, in this case, are analogous to the Ising-like spin flip excitations of the chain.

5. Solitons in Disordered Systems

A question of recurring interest, both in the quantum one-dimensional systems, and in the classical two-dimensional system, concerns the role of impurities. One hears repeatedly the common view, that since all electron states are localized in a random potential in one dimension, localization dominates the problem. It is helpful to analyze this situation from a slightly broader viewpoint, which recognizes the random potential as simply another type of interaction, in addition to the many others which are present.

This attitude is well-known from studies of phase transitions in disordered compounds. The random variable, for example a local transition temperature which varies randomly throughout a ferromagnetic alloy, can be considered as a new type of "interaction" which competes with the usual exchange, to give new physics, such as a spin glass. But the question about which phase dominates, spin glass or ferromagnetism, can only be answered if both random and exchange fields are considered simultaneously. Statements about localized states in the one-dimensional electron gas have been based on non-interacting electrons, and the question about the relevance of localization for the interacting system, is both interesting and important.

There emerges an interesting picture for this phenomena when considered from the soliton viewpoint, and the problem can be posed in the language of localized versus uniform solitons. Consider first the situation of a one-dimensional electron gas with a single impurity present. If we include an electron-electron interaction, the problem is described by Eq. (11), but for a single impurity only.

Perhaps it is worth emphasizing that, in this view, the impurity is trying to induce a local gap at $2K_F$, while in the original electron variables, the impurity is simply scattering the electron from $+K_F$ to $-K_F$. The equivalence of these two pictures follows from the fermion-boson duality. While it may seem arbitrary to choose either viewpoint, it is possible to use the soliton picture to derive a relation of this problem to another, namely, the Kondo problem of a magnetic impurity in a metal. This problem has been understood, and it is this understanding which can be applied to solve the localization problem.

It might seem surprising at first glance that these two problems are equivalent. But there is a simple plausibility argument that, while not rigorous, is convincing. The rigorous equivalence will be given later. The Kondo problem involves a spin $\frac{1}{2}$ impurity which scatters electrons with a matrix element that depends on the electron spin, in the form:

$$H_{KONDO} = H_e - \bar{J}_z \, S^z \, \sigma^z(0) - \bar{J}_\perp (S^+ \, \sigma^-(0) + h.c.) \qquad (18)$$

where $\vec{S}$ is the impurity spin operator and $\vec{\sigma}(0)$ is the spin density of the electrons at the impurity site, the origin $x = 0$, H_e the free electron Hamiltonian, and $\bar{J}_z$ and $\bar{J}_\perp$ refer to the longitudinal (spin non-flip) and transverse (spin flip) processes. But why is this relevant here?

First of all, the Kondo model is also one-dimensional, because we need work with only one partial wave, the s-wave, which depends on a one-dimensional wave vector $|k|$. There are, in fact, two types of one-dimensional electrons in this problem, spin up or spin down. These correspond to the two types of electrons in the one-dimensional conductor problem (remember that these are "spinless" electrons), namely, moving to the right, a "1" state, or moving to the left, a "2" state.

From this basis, we see that a spin flip at the impurity in the Kondo model is the same as a reflection of an electron from a static impurity in the one-dimensional conductor problem. Both drive an electron from one type to the other, do it locally, and repeatedly. There are a few subtle points which complicate the picture, such as the equivalence of the longitudinal part of the Kondo interaction, $\bar{J}_z$, to the forward scattering part of the one dimensional conductor system, which serves only to complicate matters, but can be included satisfactorily.

The important parameters in this problem, are λ of Eq. (11) and the spin-flip amplitude, $\bar{J}_\perp$, in the Kondo problem. The parameter β, arising from electron-electron interactions in Eq. (11), is related to the longitudinal coupling, $\bar{J}_z$. The relations are

$$\lambda = \bar{J}_\perp$$

$$\beta^2 = 2\pi \, (2-\epsilon)$$

Here ϵ is the scattering phase shift for $\bar{J}_z$ as in [11]. From the solution of the Kondo impurity problem, it is possible to "solve" this one as well.

The current understanding of the Kondo problem revolves around the issue whether the ground state is a singlet, with a constant magnetic susceptibility as the temperature goes to zero, or a triplet with a Curie law [11]. The former implies a gap of sorts, namely a gap between the singlet and triplet excited states. The latter has degeneracy. The scaling law arguments [11] indicate that the ground state is a singlet when $|\bar{J}_\perp| > -\bar{J}_z$, and a triplet for

$\bar{J}_\perp \leq -\bar{J}_z$. The latter case is viewed as being adequately de-
scribed by ordinary perturbation theory, while the former involves
a complicated many body ground state, which is treated by sophis-
ticated renormalization group methods.

Application of the analogy to the one-dimensional conductor
says that, for attractive interactions which satisfy
$\beta^2 \leq 4\pi(1-\lambda/2)$ (for small λ) , there is no interesting local cor-
relations or behaviour. The scattering is adequately described by
perturbation theory in that the scattering rate goes to zero, that
is an infinite conductivity, as in the Kondo problem for ferro-
magnetic coupling.

For the other sign of the inequality, which includes the
case of no electron-electron interactions, the situation is more
interesting. There the analogy suggests the build-up of a local-
ized highly correlated state which corresponds to a resonance in
the scattering. This resonance develops for the temperature less
than a characteristic "Kondo" temperature, T_c , which can be de-
termined for the special case $\beta^2 = 2\pi(2-\rho)$ to be $T_c \sim E_F \sqrt{\lambda} \, e^{-1/\lambda}$,
a special case which corresponds to the isotropic Kondo problem.
For other values of λ and β^2 the estimates of T_c are compli-
cated and will not be discussed here.

The build-up of this localized correlation, corresponding to
a local $2K_F$ gap, can be extended to the case of many impurities,
the case normally considered. If the separation between impurities
is much larger than the correlation length implied by T_c , namely
$V_F \, (T_c)^{-1}$ at $T = 0$, the properties will be determined by single
impurity characteristics and the analogy here is applicable. In
the other limit, the high concentration limit, no conclusion can be
drawn, although it is plausibly related to the "Kondo necklace"
model [13] studied for high concentrations of Kondo spins in metals.

We complete the discussion by deriving the equivalence be-
tween the Kondo impurity model and the one-dimensional conductor
problem. It is easy to show the equivalence of the free energy
for the system described by a single impurity described by Eq. (11),
and the formula for the Kondo problem,

$$e^{-\frac{F}{T}} = \sum_n \left(\frac{\bar{J}_\perp}{2\pi s}\right)^{2n} \int_0^{T^{-1}} dt_1 \ldots \int^{t_{2n-1}} dt_{2n} \; e^{\sum_{i<j}^{2n} (-)^{i-j}(2-\varepsilon)\ell n\left(\frac{t_i-t_j}{s}\right)} \tag{20}$$

where T is the temperature in the Kondo problem, ε is related
to a scattering phase shift, and for small J_z is $\varepsilon = 2J_z \rho$, F
the change in free energy due to the presence of an impurity, and
s is a cutoff parameter, introduced according to the prescrip-
tions [7] of the Luttinger-Tomanaga models. The same method used to

to derive Eq. (20), applied to the single impurity version of Eq. (11) leads to

$$
e^{-\frac{F}{T}} = \sum_n \left(\frac{\lambda}{2\pi s}\right)^{2n} \int_0^{T^{-1}} dt_1 \ldots \int_0^{t_{2n-1}} dt_{2n} \; e^{\sum_{i<j}^{2n} (-)^{i-j}\left(\frac{\beta^2}{2\pi}\right)\ell n\left(\frac{t_i - t_j}{s}\right)}
\tag{21}
$$

where s is the same cutoff parameter. Obviously the identifications $\lambda = J_\perp$ and $\beta^2 = 2\pi$ $(2-\epsilon)$ follow immediately.

6. Classical Solitons in Two Dimension

One of the recurring problems in the theory of charge density waves for the two dimensional layered structures involves the classical solution to the sine-Gordon free energy. It arises whenever a local phase variable can describe the relevant degrees of freedom, and in addition, an interaction with a lattice seeks to impose a particular phase relationship on these variables. While a microscopic derivation of this free energy expression is not intended here, it is helpful to consider a phenomenological motivation for it.

Suppose a charge density wave exists and can be described by a Ginzburg-Landau free energy expression, which fixes its amplitude according to the usual mean field theory. The phase is still left undetermined, and inversion symmetry would require a contribution to the free energy of the form

$$
F_0 = C \int d^2x \; (\nabla\phi - 1)^2
\tag{22}
$$

where C is a microscopic parameter characterizing the energy required to cause a phase distortion, and the period of the CDW is taken equal to unity.

If a periodic potential generated by the lattice is included, the CDW would prefer to arrange its phase field to be commensurate with the lattice to minimize this additional interaction, and there results a contribution of the form:

$$
F_{CDW} = \int d^2x \quad \alpha(\cos \beta\phi - 1)
\tag{23}
$$

where β is an integer, and α is another microscopic parameter characterizing the underlying lattice interaction, typically an Umklapp process. Obviously F_{CDW} prefers a phase multiple of $2\pi/\beta$, while F_0 prefers a phase increase proportional to distance.

In a rough physical sense, the solution might be expected to have phase jumps between the allowed multiples, in such a way as to maintain a stair step approximation to the straight line in- crease. From another viewpoint the phase increases linearly with distance with the F_{CDW} basically introducing harmonics. As the contributions from F_{CDW} become dominant, there ceases to be a linear increase of the phase with distance, and a type of transi- tion, the commensurate-incommensurate transition occurs. It is believed this transition is continuous, a conclusion based on numerical studies. It is interesting to consider this problem in light of the known solutions to the quantum sine-Gordon equation.

The beginning of our analysis is the total free energy given by Eq. (22) and Eq. (23). But the phase variables which appear in these expressions are just that: variables. They must be integrated out in order to find the observable free energy. The situation here is perfectly analogous to the familiar Ginzburg- Landau free energy applied to the theory of a second order phase transition. In that case, one has an order parameter variable, and two possible interpretations of the meaning of that variable. The first, and historically first as well, simply minimizes the free energy expression to solve for the mean field version of the transition. After Wilson, it became clear that the second, which treated the order parameter as a thermodynamic variable, was cor- rect. In the same manner, by the same arguments, the phase vari- able of the sine-Gordon free energy must be integrated.

With this understanding about the meaning of the phase variable, the expression for the partition function is:

$$Z = \int \delta\phi \ e^{-\beta F\{\phi\}}$$

(24)

where the $\delta\phi$ stands for the density of states available to the system which is

$$\int \delta\phi = \prod_k \int_{-\infty}^{\infty} d\phi_K$$

(25)

and the product is over all wave numbers in the Fourier transform of the phase field. The object in the partition is conventionally called the free energy functional which simply gives the energy of a particular configuration specified by $\phi(x)$. The density of states then insures that all functions are included in the parti- tion function. The observable, or thermodynamic, free energy is then $F = -K_B T \ln Z$, as usual.

The solution of the sine-Gordon classical phase problem is constructed directly from the solution to the corresponding

quantum problem. The principles underlying this equivalence have been discussed previously [14], but it is helpful to recall them briefly here again. Consider first the calculation of the angle correlation function for the special case $\alpha = 0$. This correlation function is given by:

$$C(\vec{x}) = <e^{i\phi(\vec{x})} e^{-i\phi}> \tag{26}$$

where the slanted brackets denote an average in the weighting functional of Eq. (24). Since the integrals are just Gaussian, and the result is simply:

$$C(\vec{x}) = Z^{-1} \int \delta\phi \ e^{-\beta F\{\phi\} + i\phi(\vec{x}) - i\phi}$$

$$= e^{<\phi(\vec{x})\phi - \phi^2>} \tag{27}$$

The phase correlation function is given by

$$<\phi(\vec{x})\phi> = \frac{1}{L^2} \sum_{k,k'} e^{i \ \vec{K}\cdot\vec{x}} <\phi_K \ \phi_{K'}> \tag{28}$$

where L^2 is the area of the layer. This leads to

$$<\phi(\vec{x})\phi-\phi^2> = \frac{K_B TC}{4\pi^2} \int \frac{d^2K}{K^2} (e^{i \ \vec{K}\cdot\vec{x}} - 1)$$

$$= \frac{K_B TC}{8\pi^2} \ln \left(\frac{x^2+y^2}{iS}\right) \tag{29}$$

where S is the same type of cut-off as in Eq. (7). Finally, the angle correlation function is given by

$$C(\vec{x}) = \left(\frac{S^2}{x^2+y^2}\right)^{\frac{K_B TC}{8\pi^2}} \tag{30}$$

This result, long known in the literature of the planar model, not only illustrates the meaning of the free energy functional, but provides the clue to use the quantum result if we calculate the quantum phase-phase correlation function using Eq. (10), the answer is essentially the same, with the exception that $t \to iy$, that is, the time variable becomes the other space dimension, and the temperature in this classical problem becomes related to the

coupling constant β in the quantum problem.

The corresponding angle correlation function in the quantum problem is calculated by precisely the same methods, for the corresponding case $V = 0$, giving the result:

$$\langle e^{i\phi(x,t)} e^{-i\phi} \rangle = \left(\frac{s^2}{x^2-t^2}\right)^{\frac{\beta^2}{4\pi}} \tag{31}$$

Such an equivalence between the angle correlation functions alone would not be very helpful. But this equivalence holds for all correlation functions, which can be built up from products of operations $e^{i\phi}$ at arbitrary space-time points. In particular, the correlation functions involving an arbitrary product of $\cos\phi$, are identical in the quantum and classical theories. Consequently, we can conclude that all matrix elements of the interaction, H_{CDW} or F_{CDW}, are identical. Therefore the two problems are the same.

This means the solution to the quantum sine-Gordon equation provides the solution to the classical problem, in the sense that the ground state energy of the quantum problem is the thermodynamic free energy in the classical one. Correlation functions are also equivalent, after $t \to iy$.

What features of the quantum solution are interesting here? The first qualitative feature is the gap in the excitation spectrum for the region $0 < \beta^2 < 8\pi$. A gap in the excitation spectrum implies a correlation length in the classical problem, corresponding to this gap. The behaviour of the gap, as a function of coupling constant, describes the behaviour of the correlation length as a function of temperature.

Some of the features of the quantum solution are, unfortunately, not sufficiently clear at present to resolve the obviously interesting question about a "phase transition" at $\beta^2 = 8\pi$, that is $K_B CT_c = 16\pi^2$. At this value, the gap vanishes, but the precise manner in which it vanishes as $\beta^2 \to 8\pi$ has not been elucidated yet. There is a scaling argument that this gap, Δ, vanishes as

$$\Delta \sim \sqrt{t}\, e^{-\frac{1}{t}} \tag{32}$$

where t is the temperature in reduced units, $1 - \frac{T}{T_c}$. This is a continuous transition, and it is characterized by an infinite length, as $t \to 0$.

The construction of this argument is roundabout, but it is perhaps of sufficient interest to state the general features. It relies, first of all, on the equivalence of the backward scattering model of 1-d fermions to the sine-Gordon equation. The renormalization group has been applied to the fermion problem, and through that equivalence, it implies the exponential dependence of gap on coupling constant. There is, as yet, no equivalent calculation for the ground state energy in the region $\beta^2 \to 8\pi$, that is $t \to 0$, but it is probably logarithmic, which would imply logarithmic temperature dependences in the specific heat.

Of particular interest, and some puzzlement, is the role played by the soliton bound states, which can occur for small β^2, that is well away from T_c. Presumeably, these correspond to phase jumps, and their juxtaposition must correspond to an excited state. It is tempting to identify these with the discommensuration of McMillan [15], for these appear as excited states of the free energy functional, and a correspondingly more rapid decay of correlations in space.

7. Three Dimensional Ordering

The obvious physics underlying much of the discussion here, is that it does make sense to consider the purely one and two dimensional systems independently of the three dimensional aspects of the problem. There is a limit when this view point makes physical sense, and a few remarks concerning the nature of this limit might help to put this question in perspective.

The characteristic energies of the one (or two) dimensional system in comparison with the interactions between these lower dimensional subunits is the determining consideration. In some circumstances, it is rather obvious which energies determine this ratio, but in those of interest in the real lower dimensional systems, it is not obvious.

Some qualitative remarks are of interest. Consider the problem from the mean field viewpoint. There are several ways to define what we mean by mean field. The obvious one, treating all interactions on an equal footing, predicts an ordering temperature determined by the divergence of a three dimensional susceptibility. For the CDW state, this is given by

$$\chi(\vec{Q}) = \frac{\chi(\vec{Q})}{1 - V_Q \, \chi(\vec{Q})} \tag{33}$$

where χ_0 is a 3-dim, non-interacting susceptibility, and V_Q is a 3-d screened Coulomb interaction. Compare this with the

equivalent problem viewed from a layered mean field theory view-
point, given by

$$\chi(\vec{Q}) = \frac{\chi_{2D}(\hat{Q})}{1 - V \cos(Q_z S) \chi_{2D}(\hat{Q})}$$

(34)

where $\vec{Q} = (\hat{Q}, Q_z)$ has been used. Here V is the interaction
between layers, and all complications non-essential to the com-
parison between the two types of mean field theory have been
neglected.

In the former result, the ordering is determined by a non-
interacting susceptibility. In the latter, it is the interacting
susceptibility in the lower dimensional subdivision which appears.
Obviously, the latter approach makes physical sense when the corre-
lation length within a layer becomes much longer than the correla-
tion length perpendicular to it. The correlation lengths play an
important role in this approach. One length involves essentially
one (or two) dimensional considerations. An estimate of this
length is easy to obtain, it is just the soliton or charge density
correlation length, ξ .

This length is to be compared with the perpendicular correla-
tion length. Phenomenologically, we might suppose the susceptibili-
ty for the charge density wave is

$$\chi_d(Q) = \frac{\chi_0}{1 + \hat{Q}^2 \xi^2}$$

where χ_0 is the static susceptibility. Expanding the $\cos Q_z S$
gives rise to the determination of the correlation length ratio to
be $(V \chi_0)^{\frac{1}{2}} S/\xi$. To the extent that $\chi_0 \propto \xi^2$, this ratio is un-
affected by the specific nature of excitations.

However, the ordering temperature, determined by equating the
perpendicular length with the layer separation, is most sensitive
to the nature of the excitations. With the expectation that χ_0^{-1}
is proportional to the gap in the soliton spectrum, the greater the
gap, the lower the ordering temperature. Strong interactions with-
in a layer can therefore lead to a lower temperature than would be
expected within a more conventional approximation, since χ_0 is
typically divergent at low temperatures when interactions are ig-
nored.

References

1. J. P. Pouget, S. K. Khanna, F. Denoyer, R. Comes, A. F.
    Garito, and A. J. Heeger, Phys. Rev. Lett. $\underline{37}$, 437 (1976).
    S. Kagoshima, T. Ishiguro, and H. Anzai (to be published in
    J. Phys. Soc. Japan)

2. D. E. Moncton, J. D. Axe, and F. J. Di Salvo, Phys. Rev. Lett.
    $\underline{34}$, 734 (1975)

3. A. Luther, Phys. Rev. $\underline{B15}$, 403 (1977)

4. R. Bullough, to be published in Topics in Modern Physics
    (Springer). L. D. Fadeev, JETP Letters $\underline{21}$, 64 (1975).
    R. Dashen, B. Hasslacher, and A. Neveu, Phys. Rev. $\underline{D11}$, 3424
    (1975)

5. S. Coleman, Phys. Rev. $\underline{D11}$, 2088 (1975)

6. D. C. Mattis and E. H. Lieb, J. Math. Phys. $\underline{6}$, 304 (1965)

7. A. Luther and I. Peschel, Phys. Rev. $\underline{B9}$, 2911 (1974)

8. A. Luther and V. J. Emery, Phys. Rev. Lett. $\underline{33}$, 589 (1975)

9. S. Brazovsky and I. Dzyaloshinsky, Zh EFT $\underline{71}$, 2338 (1976)
    to be published

10. A. Luther, Phys. Rev. $\underline{B14}$, 2153 (1976)

11. G. Yuval and P. W. Anderson, Phys. Rev. $\underline{B1}$, 1522 (1970).
    Here the parameter $\varepsilon = 2J_z\rho$ for small J_z is found.

12. V. J. Emery and A. Luther, Phys. Rev. $\underline{B9}$, 215 (1974)

13. S. Doniach (to be published)

14. V. L. Berezinskii, Sov. Phys. JETP $\underline{32}$, 493 (1971)
    Ibid. $\underline{34}$, 610 (1972). This connection is reviewed by J. Jose
    (to be published)

15. W. L. McMillan, Phys. Rev. $\underline{B14}$, 1496 (1976)

CHARGE DENSITY WAVES IN LAYERED COMPOUNDS

F. J. Di Salvo

Bell Laboratories

Murray Hill, New Jersey 07974 USA

The work I will describe was performed in collaboration
with many others including J. D. Axe, S. Mahajan, D. E. Moncton,
J. A. Wilson and J. V. Waszczak. While it is impossible to
cover all the interesting phenomena observed in layered compounds,
I will reference these phenomena where appropriate.

Let me outline what we will talk about. We'll start by
studying the structure of those layered compounds which are
expected to be metallic conductors. The physical properties,
such as electrical transport, show clear anomalies that I will
assert are associated with charge density wave (CDW) formation
and/or changes in the CDW structure. At this point I will
describe what a CDW is and how it comes about using a simple
model, thus introducing the parameters that characterize the
CDW. Next we'll come back to the layered compounds to get a
feel for the magnitude and temperature dependence of the CDW
parameters. Then we will discuss some of the effects of
impurities on the CDW. We'll see, by comparison to experiments
and band calculations, that the simple model first presented
for CDW formation is not adequate to explain all the data. While
more complicated models have been proposed, detailed microscopic
theories are still lacking. A number of review articles have
been written concerning the CDW properties of these compounds,[1,2,3]
including one similar to this given at the 1976 NATO conference
on one dimensional conductors.[4]

1. STRUCTURE AND PROPERTIES

The layered transition metal dichalcogenides [5] have the
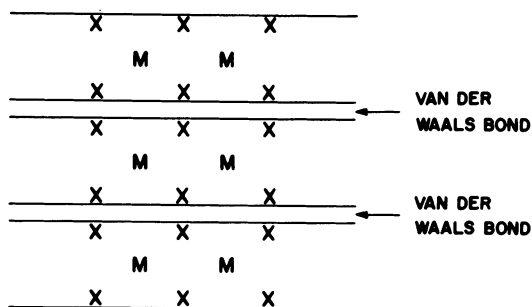chemical formula MX_2, where X = S, Se, or Te and M can be any

Figure 1. A schematic of the structure of MX_2 layered compounds shows the three atom thick sandwiches held together by relatively weak forces between adjacent sheets of X atoms.

one of a large number of metals from the periodic table. Here we will discuss primarily M = V, Nb, Ta (group Vb) and Ti (from group IVb). Since the anions are divalent, the electron configuration of the group Vb metals is d^1 and of IVb is d^0. The structure of the compounds, schematically illustrated in Fig. 1, is formed from 3 atom thick sandwiches. The top and bottom sheet of the sandwich is comprised of close packed chalcogenide (X) atoms, while the middle sheet is comprised of metal atoms. The bonding within a sandwich is strong (covalent or ionic), but between sandwiches (between adjacent X sheets) it is weak – usually labeled van der Waal's bonding. Consequently the physical properties of these compounds are anisotropic or "quasi-two dimensional". For example, these materials cleave easily, parallel to the sandwiches (or layers) much like graphite or mica. Many of the compounds are polymorphic, for two reasons: (a) The M atoms in a given sandwich are either all octahedrally coordinated (O) by X atoms or all trigonal prismatically coordinated (TP) (b) the layers can be stacked on top of one another in several different ways due to the weak interlayer forces. The unit cells, however, can all be described in the hexagonal system with the a-axis equal to the intralayer M-M distance and the c axis some multiple of the layer thickness. We will concern ourselves primarily with the two simplest polytypes: 1T – in which all the M atoms are O coordinated, and 2H – in which all M atoms are TP coordinated.

Other metals and many organic molecules (Lewis bases) can be inserted between the layers, i.e. intercalated.[6-10] Partly because of the weak interlayer bonding, intercalation usually proceeds rapidly at or near room temperature. The driving force

for intercalation appears to be electron donation to the
conduction band of the layers. Those layered compounds that
form the most intercalation compounds have the largest electron
affinity (i.e. work function), while the more active guest
species are stronger electron donors. While these general
principles of intercalation chemistry are empirically true, an
adequate microscopic picture of how organic molecules bind
to the layers is not available. Later we will talk about possible
interactions between the CDW and the intercalated species.

Since the group Vb compounds are d^1, we expect them to be
metallic because of the moderately close M-M distance (a $\sim$ 3.3A)
and the largely covalent nature of the bonds. More sophisticated
theory, such as the APW band calculations of L. F. Mattheiss (11),
leads to the same conclusion. The uppermost filled bands are
primarily based on M d states, the density of states at the Fermi
level for the group Vb compounds being 5 to 20 times that of Cu,
for 1T and 2H polytypes respectively. Consequently, we expect
these materials to be metallic conductors with conductivities
that are approximately one order of magnitude smaller than that
of Cu metal.

Some of the group Vb layered compounds are superconductors.
2H-NbSe$_2$ has the highest transition temperature (12) (7.2 K),
while for most others T_c is below 1.0°K (2H-TaS$_2$ T_c = 0.8°K (13),
2H-TaSe$_2$ T_c = 0.2 K (13)). The transition temperature is
changed by intercalation. For example, the T_c of 2H-TaS$_2$ can
be increased to $\sim$ 5 K. (6,7) The occurrence of superconductivity
leads one to expect that reasonably large electron phonon
coupling occurs in these systems. The McMillan λ obtained from
the T_c and other physical properties of 2H-NbSe$_2$ is 1.0. (14)
The large oscillator strengths of the optically active lattice
modes observed by infrared reflectivity in the group IVb
compounds also lead one to expect a large electron-phonon
coupling (15).

The resistivities (current parallel to the layers) of the
1T and 2H polymorphs of TaS$_2$ and TaSe$_2$ are shown in Fig. 2. The
original investigators of the transport properties are given in
the references: 1T-TaS$_2$ (16), 1T-TaSe$_2$ (17), 2H-TaS$_2$ (18), and
2H-TaSe$_2$ (19). While the resistivity (ρ) of the 2H-polytypes has
a metallic like slope, there is a sharp decrease at low
temperatures. The resistivity of the 1T polytypes, however, does
not look like that of a simple metal, and there are sharp dis-
continuities at first order transitions.

The anomalous properties of these chalcogenide compounds
were first noted in a magnetic susceptibility study by Quinn
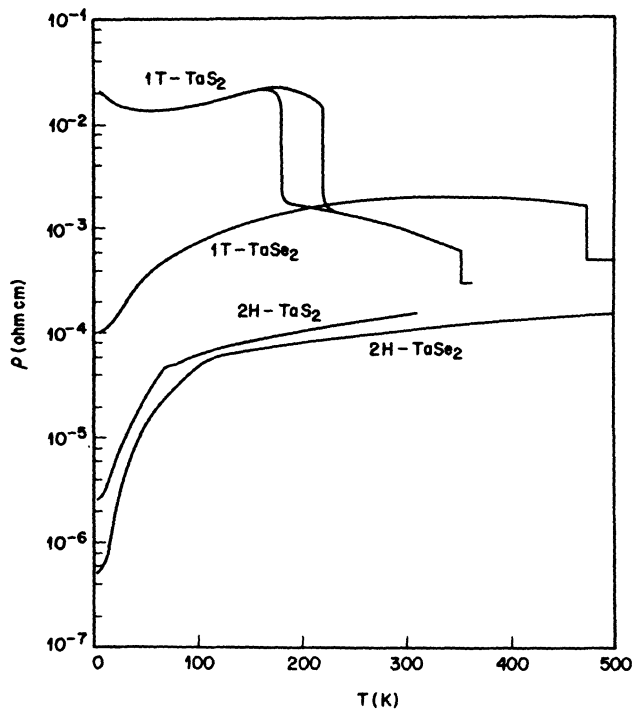et al.(20) As might be expected, the anomalies seen in Fig. 2

Figure 2. The electrical resistivity parallel to the layers of
several layered compounds from 4.2K to 500K.

are observed in almost any other physical property; such as,
magnetic susceptibility,[1] Young's modulus,[21] heat capacity,[22]
and in microscopic measurements such as NMR[23,24,25] or in some
cases XPS.[26,27]

At this point let me just assert that these anomalies in the
physical properties (Fig. 2) are due to CDW formation and proceed
to discuss what a CDW is and how it occurs, before attempting to
explain these measurements.

Charge Density Wave instabilities were theoretically proposed
by A. W. Overhauser in 1968[28], where he placed an emphasis on the
correlation energy as the source of the instability. The source

of the instability in these compounds appears to be somewhat dif-
ferent as outlined below.

    A CDW is a static, coupled, periodic distortion of both the
conduction electron density and the lattice. One is not the
consequence of the other, but they are intimately tied together.
We can see why, using a simple one dimensional model of a metal
(Fig. 3). We consider a row of uniformly spaced positive ions
and a uniform conduction electron density to preserve overall
charge neutrality. If a sinusoidal perturbation of the conduction
electrons occurs, the net charge, including the ions, oscillates
from negative to positive at maxima and minima in the wave. The
Coulomb energy of such a state is large. In fact, such an
excitation is a plasmon, one quantum of which, in normal metals,
costs on the order of 10 eV. However, if the positive ions move
toward the maxima and away from the minima, the Coulomb energy
can be greatly reduced and such a coupled distortion may become
the stable ground state of the system. Consequently, a CDW is
more likely to occur in systems with large electron-phonon
(electron-lattice) coupling. Below the onset temperature of the
CDW, T_O, the charge density and atomic displacements would be
given by (for this simple model)

$$\rho(r) = \rho_0(r)[1+\phi \cos \vec{q} \cdot \vec{r}] \qquad (1)$$
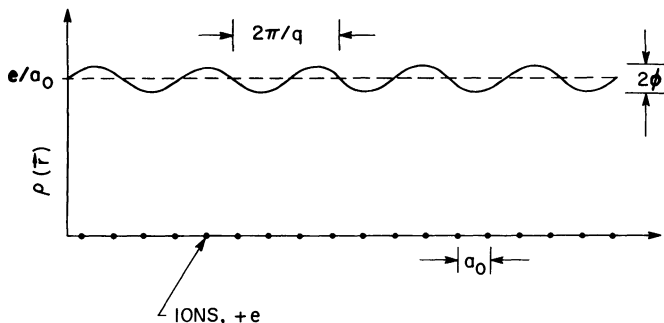

Figure 3. One dimensional model of a metal – used to show why
electron phonon coupling is important and the CDW is a coupled
distortion of the lattice and the conduction electron density.

$$\vec{\Delta x} = \vec{A} \sin \vec{q} \cdot \vec{r} \qquad (2)$$

where ϕ and $\vec{A}$ are the amplitude in charge density and atomic displacement respectively.

We further expect that lattice waves with this wave vector $\vec{q}$ and displacements parallel to $\vec{q}$ (longitudinal phonon) will be lowered in energy <u>above</u> T_O, becuase of the effective screening of the ionic charge by the electrons. Thus a dip, called a Kohn anomaly, will appear in the phonon dispersion curve (phonon energy vs. wave vector). Simple one dimensional models for this effect are published (29); some examples for the layered compounds will be given below.

Beside a large – electron phonon coupling, the shape of the Fermi surface (F.S.) is also important. In particular the F.S. determines the $\vec{q}$ of the distortions, and whether the CDW can be the ground state of the system. We can see what kind of F.S. is needed by considering a simple linear response model of the conduction electrons to a static perturbation of wave vector $\vec{q}$. First, we consider free electrons; later we will include inter-actions. In order to determine if an instability occurs, we use the following principle: If the response $\Delta\rho(\vec{q})$ to an infinitesimally small perturbation $V(\vec{q})$, becomes macroscopic, the system will spontaneously move to a distorted state. That is, if $\Delta\rho(\vec{q}) = \chi^O(\vec{q}) V(\vec{q})$, a static distortion will spontaneously occur if $\chi^O(\vec{q}) \to \infty$.

For free electrons $\chi^O(\vec{q})$ is calculated in second order perturbation theory to be: (neglecting the matrix element $|\langle \vec{k}|e^{i\vec{q}\cdot\vec{r}}|\vec{k+q}\rangle|^2$)

$$\chi^O(\vec{q}) \, \alpha \, \sum_{\vec{k}} \frac{f_{\vec{k}} (1-f_{\vec{k+q}})}{\varepsilon_{\vec{k+q}} - \varepsilon_{\vec{k}}} \qquad (3)$$

where

$\varepsilon_{\vec{k}}$ = energy of state with wave vector $\vec{k}$

$f_{\vec{k}}$ = Fermi occupation factor

We can see that $\chi^o(\vec{q})$ will become large for a given $\vec{q}$, which connects many filled states to empty states of the same energy. This can only occur if the two states are on the F.S. Figure 4 shows $\chi^o(\vec{q})$ for several situations.[30] F.S. with plane parallel sections, or equivalently, nesting electron and hole surfaces, will produce a $\chi^o(\vec{q})$ that diverges as $\ln (E_F/kT)$ when $\vec{q}$ spans (or connects) the F.S. Other cases, such as saddle points in the band structure at the Fermi level, will also lead to a similar divergence in $\chi^o(\vec{q})$.[31] We see, then, that a free electron gas can be unstable only a T = 0.

If electron – phonon and electron – electron interactions are included, instabilities may occur at finite temperatures. When interactions are included, we consider the generalized suscepti-bility, $\chi(q)$. In the simplest approximation (the random phase approximation) we have

$$\chi(\vec{q}) = \chi^o(\vec{q})/(1 - X(\vec{q})\,\chi^o(\vec{q})), \qquad (4)$$

where $X(\vec{q})$ represents all the physics – i.e., the interactions.[32] Now we see that an instability will occur at the $\vec{q}$ where $X(\vec{q})\chi^o(\vec{q}) = 1$. (Note that the RPA expression is only valid where the denominator is close to 1, we take some license here in letting it decrease to zero in order to obtain some feel for the true physics). Consequently if the F.S. has parallel (or nearly so) sections, $\chi^o(q)$ will increase as T decreases, so that at some temperature, T_o, the denominator equals zero and the system becomes unstable. It is also true that $X(\vec{q})$ will have some structure, possibly <u>also</u> peaking when $\vec{q}$ spans the F.S. We will see later some calculations of $\chi^o(q)$ for some of the layered compounds.

Overhauser's original suggestion was that a CDW might occur when $\chi^o(q)$ had no peaks or was essentially free electron like (3 DIM-Fig. 4a). In that case, using Eq. 4 as a model, the divergence comes from $X(\vec{q})$. Indeed, Overhauser showed that the correlation energy for unscreened Coulomb potentials in a Hartree-Fock calculation diverges at q = $2k_F$.[33] We return later to some discussion of the role of $X(\vec{q})$ and $\chi^o(\vec{q})$ in determining the instability. Note, however, that whichever term dominates in these models, the divergence in $\chi(\vec{q})$ will occur at a F.S. spanning vector.
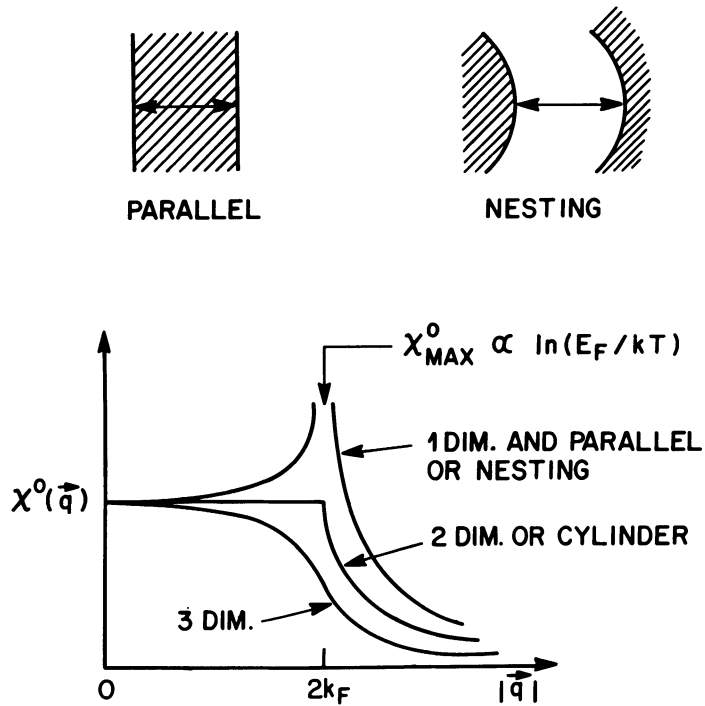
Figure 4. $\chi^0(\vec{q})$ for a number of free electron Fermi surfaces is shown vs. $|\vec{q}|$. 1, 2, and 3 DIM. refer to electrons with no periodic potential from the lattice in the given dimension. For real solids, some species of the band structure may have one dimensional dispersion. Two examples are shown: parallel and nesting pieces of Fermi surface, where the filled states are shaded.

Within the spirit of eq. 4, CDW instability occurs if the electron-phonon coupling dominates $X(\vec{q})$,[32] as suggested by the simple one dimensional model of Fig. 3. If $X(\vec{q})$ is dominated instead by the exhange, a spin density wave (SDW) will result[32], as in the metal Chromium[34].

Since $\vec{q}$ is determined by the F.S., the wavelength of the CDW, $2\pi/|\vec{q}|$, will usually be incommensurate with the lattice; that is, the wavelength will not equal a lattice translation. However, in many layered compounds, a first order transition to the commensurate state (CCDW) occurs at $T_d < T_o$. It is the incommensurate CDW (ICDW) that is the mark of a F.S. driven instability, at least in a metal where magnetic moments or permanent electric dipoles do not occur. In cases where only a commensurate distortion exists below T_o, it is more difficult to assess the role of the F.S. in "driving" the transition.

What happens below T_o? The instability produces a lattice distortion of wave vector $\vec{q}$, and a new lattice potential. This potential connects the states at the F.S. at $\vec{k}$ and $\vec{k}+\vec{q}$ in first order perturbation, splitting the states away from the Fermi level. That is, gap is produced at the F.S., just over those regions spanned by $\vec{q}$. Consequently these states contribute to χ^o with the gap energy Δ as a denominator, not zero as above T_o. Consequently, χ^o decreases in magnitude below T_o. Within simple models, the gap is expected to increase with decreasing temperature in exactly the same way as the BCS superconducting gap (29).

While this theoretical description of a CDW may be lacking, our purpose was mainly to introduce the parameters T_o, T_d, $\vec{q}$, ϕ, $\vec{A}$, and Δ; the last four of which are expected to be temperature dependent. We now return to the layered compounds and consider some of these parameters in more detail.

The CDW state below T_o can best be observed by diffraction techniques. Elastic scattering will occur at points in reciprocal space given by $\vec{k} = \vec{G} \pm n\vec{q}$ where $\vec{G}$ is any one of the reciprocal lattic vectors of the undistorted lattice that exists above T_o and n is any integer.(35,36) Thus, each main Bragg peak will have a series of satellite peaks about it with an intensity given from simple kinematic scattering theory by $I_n \sim (\vec{k}\cdot\vec{A})^{2n}/n!$ (Eq. (5)) for $\vec{k}\cdot\vec{A} \ll 1$. In fact, in the layered compounds, $\vec{A}$ is usually quite small, and the satellite peaks have only 10^{-3} or less of the intensity of the strongest main Bragg peak. This made the CDW's very difficult to find by simple power X-ray diffraction techniques. They were first discovered by electron diffraction, since the intensity of the satellite peaks can be greatly enhanced over that expected from the kinematic formula by dynamical scattering. (37) While the position of the satellite peaks is easy to obtain by electron diffraction (thus obtaining $\vec{q}$), the intensity cannot be easily used to obtain lattice displacements. The latter are obtained from X-ray or neutron diffraction measurements.

Table I lists a number of layered compounds with the CDW
onset temperature, T_o, the lock-in temperature, T_d, and CDW wave-
length in multiples of the a-axis. In all cases the CDW consists
of a superposition of three CDW's with q vectors that are related
by a 120° rotation about the c-axis (the normal to the layers).
No ditellurides are listed in Table I. These compounds frequently[5]
show strong distortions at room temperature, and there is some
indication of phase transitions at high temperatures.[38] However,
the ditellurides have a wide range of nonstoichiometry and are
difficult to prepare at the exact MX_2 composition. This intro-
duces another "parameter" in the problem, and we have not yet
undertaken detailed study of these compounds.

A large variation of T_o is seen both with a change in poly-
type and between different compounds. A CDW has not been
detected in $2H-NbS_2$, but this particular compound is difficult
to prepare, usually $Nb_{1+x}S_2$ is obtained. We will later see that
this non-stoichiometry frequently lowers or eliminates T_o. Note
also that the CDW wavelength is short - between 3 and 4 lattice
parameters (or only 10 to 14 Å.)

<div align="center">Table I</div>

Material	T_o(K)	T_d(K)	λ_{CDW}	Ref.
$1T-TaSe_2$	≈600	473	∿3.5a	1, 17
$2H-TaSe_2$	122	∿95	∿3.0a	1, 39
$1T-TaS_2$	≈600	≈200	∿3.5a	1, 2, 40
$2H-TaS_2$	∿80	?	∿3.0a	1, 41
$2H-NbSe_2$	32	no	∿3.0a	39
$1T-VSe_2$	112	∿80	∿4.0a	2, 42

$2H-NbSe_2$ has the lowest T_o and the CDW remains
incommensurate down to 4.2K. The CDW wavevector
$\vec{q} = (1-\delta)\vec{a}^*/3$, where $\vec{a}^*$ is a reciprocal lattice vector in the
plane and δ decreases smoothly from 0.02 at 32K to approximately
0.01 at 4.2K. The intensity of a first order satellite peak
(n=1) in $2H-NbSe_2$ as measured by neutron diffraction is shown in
Fig. 5 vs. temperature (39). The transition at T_o is seen to be
second order, since the intensity smoothly drops to zero. The
atomic displacements at 4.2K calculated from this data are
approximately 0.05 Å for Nb (parallel to the layers) and half that
for the Se atoms (some component perpendicular to the layers.)
The amplitude in charge density ϕ at 4.2K is estimated from NMR
measurements to be 5% to 10% of the conduction electron density

(19, 20). Measurements of the specific heat[18] and Young's
modulus[17] near T_o show that the density of states at the Fermi
level is not significantly lowered by the presence of the CDW
(i.e. the F.S. area is not significantly reduced by the presence
of the CDW).

Next we consider the CDW transition in 2H-TaSe$_2$. The
results of neutron scattering measurements[32] are shown in
Fig. 6. The inset in the upper left shows the scattering peaks
in the (HKO) plane. The open circles are the main Bragg peaks
and the dark circles are the satellite peaks. If we look in the
main part of the figure about the position labeled 4 (position 4
is at $4\vec{a}^*/3$), we see just below $T_o = 122K$ that $\vec{q} = (1-\delta)a^*/3$ and
$\delta \sim 0.02$. As T decreases, δ decreases until it discontinuously
goes to zero at $T_d \sim 95K$. Note also that a weak secondary peak
appears on the other side of $4\vec{a}^*/3$ by 2δ. This peak occurs at the
same <u>position</u> as the second order satellite coming from the Bragg
peak at 6 (i.e. $2\vec{a}^* - 2\vec{q} = \frac{a^*}{3}(4+2\delta)$). However, the intensity
calculated from Eq. (5) is much too small to be the source of
this peak. Consequently, this is due to a <u>second</u> periodic
distortion $\vec{q}_2 \delta = (1+2\delta)\ \vec{a}^*/3$. A Landau free energy model has been
developed by D. E. Moncton et al. (32) that shows how this
secondary distortion occurs and its role in "pulling" $\vec{q}$ toward
the commensurate value of $a^*/3$. W. L. McMillan has also developed
more complicated Landau models to explain this behavior and other
related phenomena, [43,44] which he will discuss at this meeting.
The main point of these measurements and models is that the CDW
lattice distortions are <u>not</u> purely sinusoidal, but include higher
harmonics that are mixed in by anharmonic terms in the free
energy. The displacement grows to $\mathring{A} \sim 0.1\ \mathring{A}$ for Ta and $\sim 0.05\ \mathring{A}$
for Se at 4.2K. If we scale by the ratio of atomic displacements
from the 2H-NbSe$_2$ data, we estimate ϕ (4.2K) $\sim$ 0.2 (e/a).

At present, the most data concerning CDW properties has been
obtained with 2H-TaSe$_2$. Figure 7 shows the Kohn anomaly seen
in the longtitudinal acoustic phonon at 300K.[39] The softening
occurs over a wide region of this branch, and the minimum near
q_o decreases with decreasing temperature as shown in Fig. 8.[45]
The simpler models predict a soft mode with $\omega(q_o) = 0$ at T_o.[29]
Instead a central peak develops as T approaches T_0. Below T_0 new
modes appear, one of which is the "stiffening" phonon seen in
Fig. 8. This and other modes have been observed by Raman scattering
below T_0[47,48], and will be discussed at this meeting by
E. Steigmeyer. Infrared reflectivity measurements below T_0 show
weak gap-like features with Δ (4.2K) $\sim$ 25kT_0.[46] This number is
much too large, since the BCS like theories give $\Delta \sim$ 4kT_0[29].
McMillan has shown that these difficulties can be resolved by
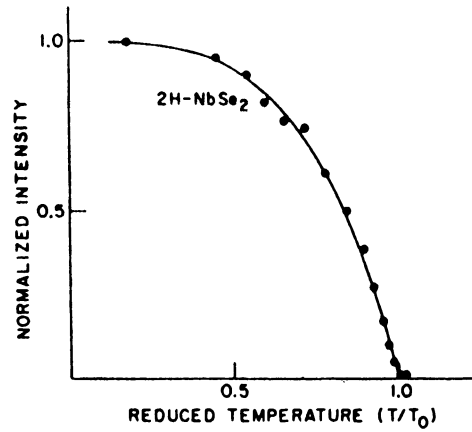including the phonon entropy (this conference).

Figure 5. The satellite intensity vs. temperature for 2H-NbSe$_2$
below T$_O$ = 32K. The intensity is proportional to the lattice dis-
placement squared. The lattice displacement may be used as an
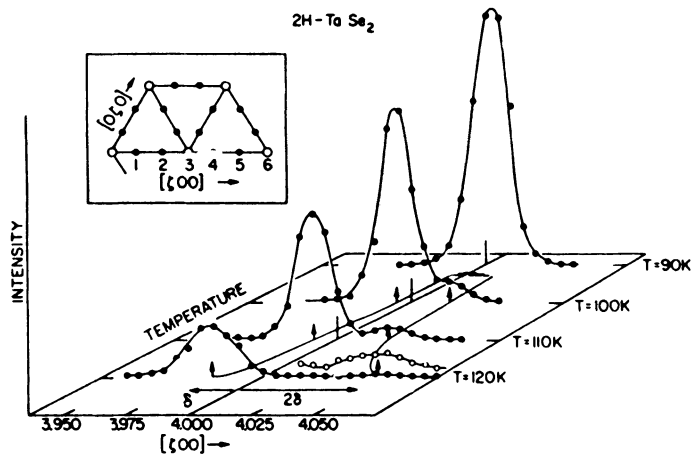order parameter in a Landau theory.

Figure 6. Elastic neutron scattering measurements of the
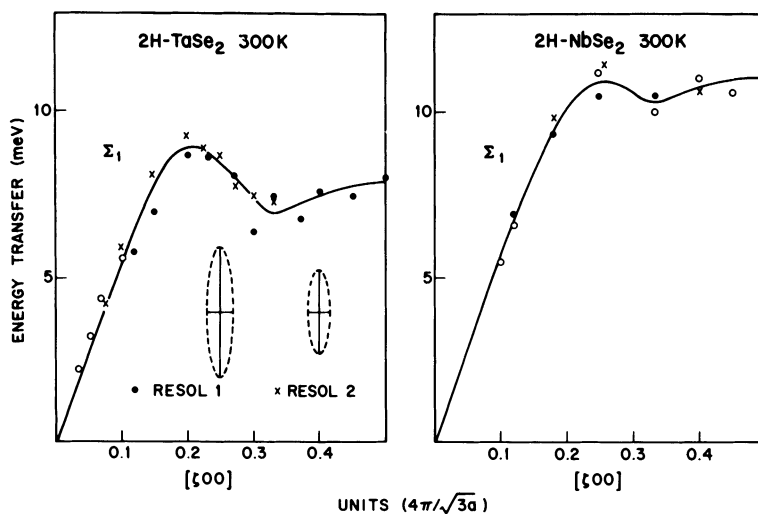satellite peak intensity and position in 2H-TaSe$_2$ vs. temperature.

Figure 7. The longtitudinal acoustic phonon dispersion curves for 2H-TaSe$_2$ and 2H-NbSe$_2$ show pronounced but very broad dips near $q_0 = 0.33$ a*. The curves are obtained by the constant Q method, the resolution functions shown are swept up parallel to the energy axis to obtain this data.

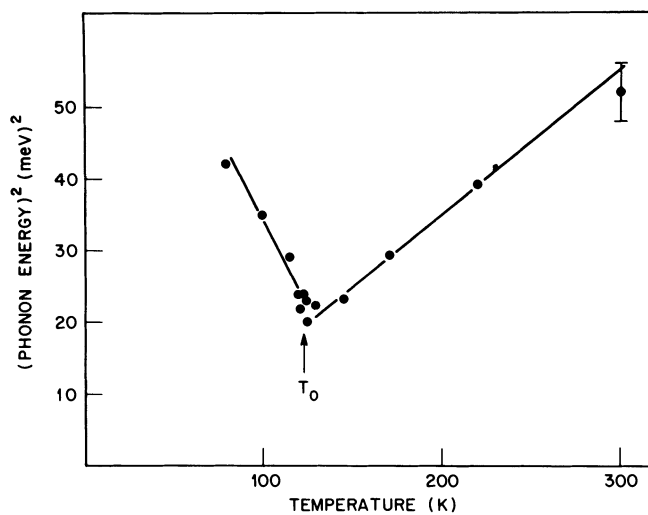Figure 8. The energy of the longtitudinal acoustic phonon (squared) at $q_0 = 0.33$ a* in 2H-TaSe$_2$ decreases as T_0 is approached from above or below. However, this energy does not decrease to zero and T_0, as simple models would suggest.

The CDW behavior of the 1T polytypes of the Ta dicholcogenides
is quite different from that of the 2H. In 1T-TaSe$_2$ electron
diffraction patterns of the (HKO) plane show a commensurate super-
lattice at room temperature (Fig. 9a) and an incommensurate CDW
(Fig. 9b) above the first order transition apparent in the resis-
tivity (Fig. 2) at T_d = 473K. In the incommensurate state $\vec{q}$=0.285$\vec{a}^*$
(i.e. q is parallel to the line joining main Bragg peaks). Also,
strong diffuse scattering, in the form of circular rings is seen
above T_d. This scattering is most likely due to CDW excitations
involving the transverse displacement of $\vec{q}$. We expect that
excitations of this sort will be soft, since at T_d q rotates by
$13°54'$ and shrinks slightly ($\sim 2\%$) to produce the 3×1 superlattice
apparent in Fig. 8a. This transition then involves primarily a
rotation of $\vec{q}$. At room temperature and below, the atomic dis-
placements are quite large, ~ 0.25 Å for Ta. Further, the amplitude
ϕ is about 1 e/a! This might be expected if we scale ϕ
from 2H-NbSe$_2$ by the ratio of the onset temperatures. With such
a large charge oscillation, the binding of the Ta core electrons
shifts enough to be observable in ESCA (26,27,49). Splittings in
the 4f binding energies of ~ 0.5 eV are clearly observed at room
temperature. This means that at room temperature and below, the
CDW is not a weak perturbation of the F.S. Rather the commensurate
phase may be thought of as a valence disproportionation of Ta^{4+}
into Ta^{5+}, Ta^{4+}, Ta^{3+}. Summarizing the behavior of 1T-TaSe$_2$, we
see that as the temperature is reduced from above T_o, the material
passes through a number of states: a normal undistorted metal,
then a second order transition to an incommensurate CDW state
where, at least close to T_o, the amplitude ϕ or $\vec{A}$ is small, and
finally, this state evolves through the transition at T_d to a
valence disproportionation. As yet there are no adequate
theories to explain the overall behavior of 1T-TaSe$_2$, although
Landau models are able to qualitatively predict the sequence of
transitions (43).

1T-TaS$_2$ is even more complicated than 1T-TaSe$_2$, as is
apparent from the two first order transitions seen in the resis-
tivity (Fig. 2). Below 200K the CDW shows the same commensurate
state as 1T-TaSe$_2$ (2). Above the transition at T_d' = 350K, the
CDW is incommensurate with $\vec{q}$ = 0.288$\vec{a}^*$ and strong diffuse
scattering is seen, very much as that shown for 1T-TaSe$_2$ in
Fig. 9b (1,40). At 350K, $\vec{q}$ rotates by $\sim 12°$ but stops 2° short
of becoming commensurate! $\vec{q}$ continues to rotate with decreasing
temperature, until at ~ 200K it jumps the last fraction of a degree
to become commensurate. This intermediate state between 200K and
352K (quasi commensurate state as we call it) appears to be
stabilized by the presence of secondary distortions.(50) The
physics of this situation is similar to that of 2H-TaSe$_2$ where
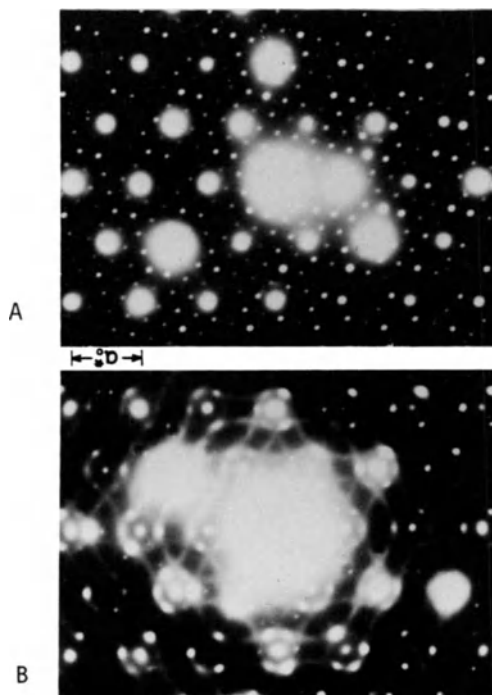secondary distortions appear immediately below T_o. In

Figure 9. (a) The basal plane diffraction pattern of the CCDW in
1T-TaSe$_2$ shows the $\sqrt{13}$ a superlattice. Many of the main Bragg
peaks appear very bright, or overexposed; the remainder of these
peaks are easily found by "extending" the hexgonal pattern of
these spots.

1T-TaSe$_2$, however, the amplitude of the CDW must be larger than
some minimum value for the secondary distortions to occur. Again
it is clear from ESCA and X-ray diffraction that the CDW amplitude
at low temperatures is as large in 1T-TaS$_2$ as in 1T-TaSe$_2$.

We have talked about transitions to the CCDW, but have not
tried to indicate why they occur. A hint to their origin can be
obtained from a correlation between T_d and the crystallographic
c/a ratio discovered by A. H. Thompson (51). Figure 10 shows the
almost linear relation between T_d and c/a for 12 different com-
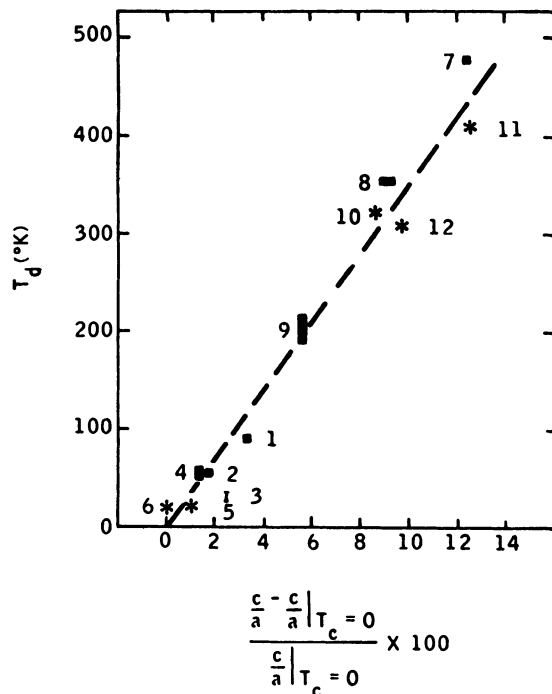pounds (or polytypes) that I will not bother to identify in detail.

Figure 10. T_d is plotted vs. the crystallographic (normalized to a specific value) from Thompson (24). Each point represents a different layered compound or a different polymorph.

Previously, F. R. Gamble had shown that the c/a ratio in these compounds was related to the ionicity difference between the cation and anion (52). Consequently, we see that T_d is related to an ionicity difference. This result suggests that the driving force toward the commensurate state involves local ionic Coulomb or covalent bonding forces. One might see how these forces arise by considering a simple case. Suppose an incommensurate CDW exists in a two dimensional hexagonal packed sheet of metal atoms. Since the CDW is incommensurate, in general the charge will be increased at some nonsymmetrical position. Ionic or covalent energies will be maximized by placing this charge at a center of symmetry; such as, (a) on a metal atom, (b) half-way between two atoms to maximize the bonding charge, (c) at a geometrical center,

like the center of a triangular set of three atoms, to make a
bonded metal cluster, (d) etc. In the real compounds we must
also consider the metal-nonmetal bonds, but this simple model
gives the qualitative idea. Note that these bonding interactions
can be expressed in terms of large electron phonon interactions.
Consequently it is somewhat artificial to separate the driving
forces for the ICDW and the CCDW, as pointed out by Thompson.[3]
Rather in these materials a proper description of the conduction
electrons is between the traditional covalent bond and metallic
bond models, as pointed out by McMillan.[43] Apparently in
these systems at small CDW amplitude the F.S. determines the
nature of the distortions, while at larger amplitudes the
bonding energies dominate.

So far we have talked about the CDW as a single layer
phenomena. The CDW's interact from one layer to the next producing
a given stacking sequence. This sequence is consistent with that
obtained by minimizing interlayer Coulomb interactions (1,53).
For example, if we consider the simplest CDW $\Delta\rho = \frac{\phi}{3} \times \sum_{i=1}^{3} \cos \vec{q}_i \cdot \vec{r}$, the contours of $\Delta\rho$ have hexagonal symmetry as shown
in Fig. 11a. The maxima (or minima, depending upon the sign of ϕ)
are at the cell edges, with minima at the center of each triangle.
Using hexagonal notation, we label the maxima A and the two minima
B and C as shown. In the incommensurate phase, the origin of the
CDW can be placed arbitrarily at any point in the layer. If we
choose point A in the first layer, then the Coulomb interaction
is minimized with the next layer by placing its charge maxima over
point B in the first layer. The third layer minimizes its
Coulomb energy with both the first and second layer by putting its
maxima over point C. This stacking sequence leads to a three
layer repeat for the CDW as is found in the 1T polytypes. The
interaction energy in the 2H polytypes is modified by the screw
symmetry between adjacent layers and the CDW repeat appears to be
two layers. In the commensurate phase, the origin of the CDW
cannot be arbitrarily chosen. Rather, it appears that the CDW
cell origin lies at a Ta site. Figure 11b shows that the CDW in
the second layer can minimize its interaction energy with the
first by translating the CDW origin by $2\vec{a}$. By continuing this
sequence, the overall interaction energy is minimized. The origin
of the CDW repeats itself every 13 layers. However, the true
unit cell is triclinic with $a = \sqrt{13}a$, $b = \sqrt{13}a$ and $c = |\vec{c}+2\vec{a}|$ (3).
In order to have long range stacking order both near neighbor and
next-near-neighbor layer interactions must be included. In
1T-Ta$_{1-x}$Zr$_x$Se$_2$ the random impurity potential of Zr can dominate
the next near neighbor interactions in the CCDW state,[53] pro-
ducing a random stacking of near neighbor layers on the three
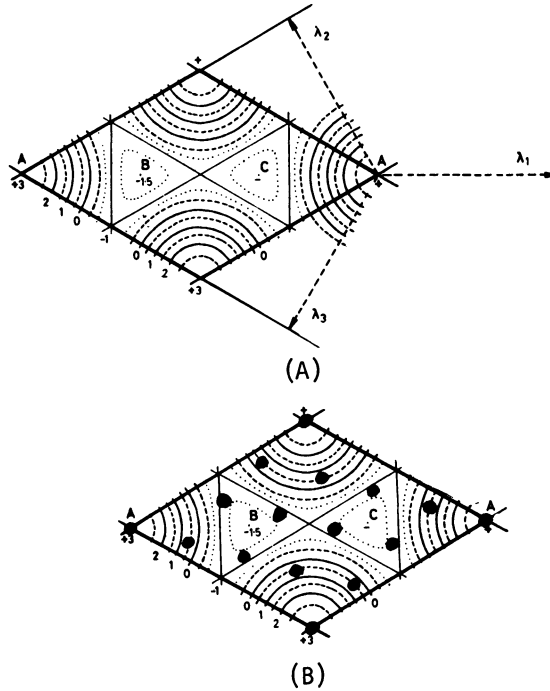sites near the B position shown in Fig. 11b.

(A)

(B)

Figure 11. (a) The CDW pattern created by $\rho = \sum_{i=1}^{3} \cos \vec{q}_i \vec{r}$ with the 3 CDW wavelengths $\lambda_i = 2\pi/q_u$ shown. (b) The CDW pattern and metal atom positions expected for the CCDW in $1T\text{-}TaS_2/Se_2$.

Having discussed in some detail the magnitude of the CDW parameters of some layered compounds, we briefly consider the resistivity. It is apparent from Fig. 2 that below the onset of the CDW the 1T polytypes become <u>more</u> resistive and the 2H polytypes <u>less</u> resistive. The simple picture introduced in discussing the driving force of the CDW leads one to expect the behavior observed for $1T\text{-}TaSe_2$; that is, below T_o the resistivity should increase (compared to the normal metal) as T decreases due to the formation of gaps at the F.S. At T_d the gaps increase discontinuously, further increasing the resistivity. Finally at low temperatures we expect metallic-like conductivity from those portions of the F.S. not destroyed by CDW gaps.

The resistivity of the 2H polytypes of TaX_2 rises slightly then decreases rapidly below T_o. A plausible model for this behavior is to assume that the sections of the F.S. eliminated by the CDW gaps are characterized by large effective masses. Above T_o, these carriers do not contribute much to the conductivity because of their large mass, but they do act as effective scattering sinks for lighter electrons on the F.S. Below T_o then, with the large mass states removed, the scattering rate can decrease leading to a decrease in resistivity even when some carriers are lost. This model is consistent with the nesting model of the CDW or the saddle point model [31] and the complex shape of the two sheeted F.S., [1,11] but definite proof of its validity does not exist.

Finally we come to $1T-TaS_2$. At each transition toward the commensurate state we expect the gaps to increase in size and the resistivity to increase. However, in the commensurate state the resistivity is very high and not at all metallic-like. Recent data show that the low temperature increase in resistivity (below 40K) is extrinsic. [54] The resistivity below 2K is described by variable range hopping and fits $\rho = \rho_o \exp (T_o/T)^{1/3}$. This form is due to Anderson localization by random impurities or defects. [55] Just why $1T-TaS_2$ should be so sensitive to these impurities, and not $1T-TaSe_2$, is not clear; but the high resistivity of $1T-TaS_2$ just below 200K indicates that the remaining carriers have a very low mobility. Suggestions of Mott localization [56] and polaron formation [1] have been made, but these are untested hypotheses.

Also note from Fig. 1 that the resistivity of all of these compounds above T_o is on the order of 10^{-4} Ω/cm. This leads to an effective scattering time for the carriers of $\sim 2 \times 10^{-15}$ sec. We expect the average Fermi velocity to be less than that of (Cu), for example, so $V_F < 1.6 \times 10^8$ cm/sec. Consequently, the mean free path, is less than 30 Å. These small numbers indicate that the treatment of scattering by the usual Boltzman equation is questionable. A similar observation has been made for other transition metal compounds, in particular, the high superconducting transition temperature $\beta-W$ compounds. [54] These difficulties are probably related to the large electron phonon interactions and the CDW instability of the layered compounds.

Next, we consider the effects of impurities. In particular, we consider the random substitution of the cation by other transition metals and the effect of this substitution on the transport properties and on CDW formation. This substitution causes randomness in the lattice potential and may also change the average conduction electron density, z. Each of these effects is related in different ways to changes in the CDW behavior.
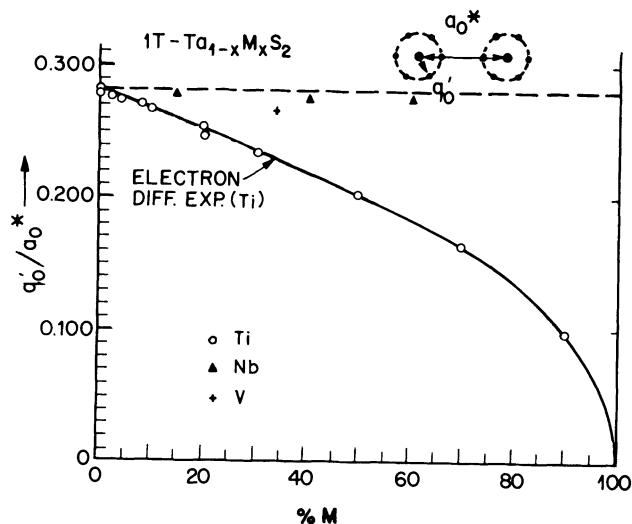
Figure 12.   q/a*, the wavelength of the CDW in the ICDW state
divided by the reciprocal lattice vector, is shown vs. x for
$1T-Ta_{1-x}M_xS_2$ where M = Ti, Nb, or V.

First, consider the effect of changing z : The calculated F.S.
for the undistorted 1T polytypes has the shape of an ellipsoid in
the plane of the layer with near perpendicular walls along c*.[1,11]
This F.S. then has sections that are near to parallel, leading to
the CDW instability. If Ti is substituted for Ta, z decreases,
and in the rigid band approximation the F.S. will shrink but
remain an ellipsoidal cylinder. Consequently, in the ICDW phase
we expect that q/a* will decrease with increasing x in $1T-Ta_{1-x}$
Ti_xS_2. The results of such measurements are shown in Fig. 12
(1,58). The solid line is a fit to the data which is close to that
expected from the rigid band approximation. Also in Fig. 10 q/a*
is shown for $1T-Ta_{1-x}Nb_xS_2$ and $1T-Ta_{1-x}V_xS_2$. In these two cases
q/a* is close to constant, as expected, since Nb and V are
isoelectric with Ta and z is constant. In the 1T polytypes, the
effect of changing z is to smoothly change the F.S. and con-
sequently q/a*. The data shown in Fig. 12 are obtained at or
above room temperature. Consequently T_o remains greater than
300K even for x $\gtrsim$ 0.7. It appears from magnetic susceptibility
that T_o is reduced, but slowly, with increasing x. This is an
expected effect of disorder (43) and occurs with Ti, Nb or V
substitution (or indeed any cation disorder).

The disorder reduces T_o, but more rapidly suppresses the
commensurate state. This can be seen in the resistivity of
$1T-Ta_{1-x}Ti_xSe_2$ (Fig. 13). With increasing x, both the transition
temperature from the incommensurate to the commensurate state, T_d,
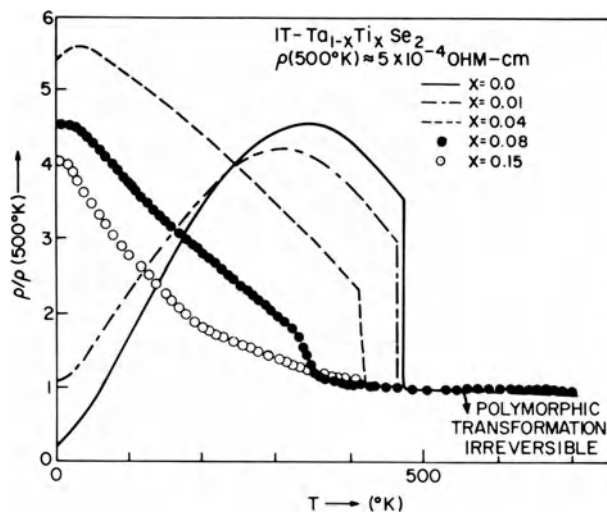and the magnitude of the resistive anomaly at T_d decrease. This

Figure 13. The electrical resistivity of $1T\text{-}Ta_{1-x}Ti_xSe_2$ shows the decrease in T_d with increasing x.

data, combined with measurements of the enthalpy of transition (58), show that for $x > x_c \simeq 0.10$ the CCDW does not occur. We can see why this occurs with a simple chemical model. Consider a one dimensional string of atoms A and B that are randomly placed on lattice sites. We wish to compare the free energy of the CCDW and ICDW. Let us consider B to be the dilute species and assume that B is more electronegative than A. (We could assume it is more electropositive, but will obtain the same result). Because the B atoms are more electronegative, the free energy will be a minimum when the CDW charge maxima lie at B sites. If there is a CCDW and the alloy is random, many of the B atoms will not lie at maxima and we must pay some free energy proportional to the ionicity difference $(X_B - X_A)^2$. If there is an ICDW, the CDW can change its phase (or equivalently its local wavevector q) so that each B atom lies at charge maxima. In this case, we must pay some elastic energy to distort the CDW - but this turns out to be small. (The elastic energy to change the wave vector q from its commensurate to incommensurate value, must be relatively small for the CCDW to even exist in the pure material.) Consequently, we expect the increase in free energy with cation substitution to be larger in the CCDW than the ICDW, and thus the ICDW becomes stable (i.e.

T_d is suppressed and for $x \gtrsim x_c$ the CCDW does not exist.)
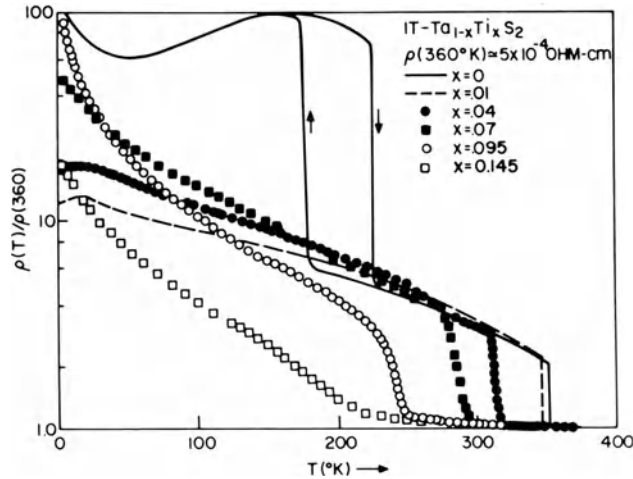McMillian's free energy model reaches the same conclusions (43).

Figure 14. The electrical resistivity of $1T-Ta_{1-x}Ti_xS_2$ shows that
both first order transitions toward the CCDW state are suppressed
with increasing x, but the commensurate state is suppressed for
$x \gtrsim 0.002$.

Similar effects are seen in $1T-Ta_{1-x}Ti_xS_2$ (Fig. 14). The
transition at 200K to the commensurate state is suppressed for
$x \gtrsim 0.002$, while the transition at T_d' (into the "quasi-commensu-
rate" state) is slowly suppressed and is finally lost when
$x \gtrsim 0.15$.

Fewer doping studies have been made for the 2H polytypes,
because most cation substitution favors growth and retention of the
1T prototype. Rather, studies of the effects of anion mixing, as in
$2H-TaSe_{2-x}S_x$, and of intercalation on the CDW are more common.(9)
These studies show that disorder and intercalation (which at least
in some cases causes both disorder and a change in the conduction
electrodensity) reduce the CDW amplitude and/or T_o. Further,
since the onset temperature is lower in these 2H polymorphs than in
the 1T polymorphs, lower concentrations of "dopants" are
necessary to suppress T_d or T_o. Such is also the case for the 1T
polytypes, say in comparing $1T-VSe_2$ (T_o = 112K)(42) and $1T-TaSe_2$
($T_o \approx$ 600K).(58)

We have discussed in some detail the magnitude and temperature dependence of the CDW in several layered compounds. Other studies of the properties of layered compounds will be mentioned shortly, but first we discuss the applicability of the simple model we will introduce to present the CDW parameters.

We focus on two aspects of the model: the bare susceptibility, and the spatial range of the interactions. Several calculations of $\chi^0(\vec{q})$ for 1T-TaS$_2$/Se$_2$ and 2H-NbSe$_2$ have been reported[59,60] and the results are reproduced in Fig. 15. These results are obtained from nonrelativistic, nonselfconsistent band calculations using muffin tin potentials, and therefore the $\chi^0(\vec{q})$ obtained should be taken as suggestive rather than definitive. First, consider 1T-TaSe$_2$, where a peak is seen in $\chi^0(\vec{q})$ at the same wave vector as observed in the ICDW state. This peak is only 3 times the value that would be obtained from a three dimensional free electron gas of the same density at $q = 2k_F$. However, even in the three dimensional electron gas $\chi^0(q)$ is large compared to, Cu, for example because the electron density is lower than in an elemental metal. The calculated temperature dependence of this peak is small. This would suggest, in the language of Eq. 4, that the interaction term X(q) has some temperature dependence in it and that T$_0$ is not primarily determined by the temperature dependence of the bare susceptibility $\chi^0(q)$. Unfortunately no microscopic calculations of X(q) of these compounds exists; we do not know, for example, if X(q) also has a peak at the same place as $\chi^0(q)$. The extreme limit of this possibility, namely that $\chi^0(q)$ is free electron like, has been considered in explaining the phonon anomalies in Nb, NbC and NbN (ref. 61 & J. Hafner in this conference). These theories conclude that X(q) is entirely responsible for the phonon anomalies, but these materials are not known to show CDW formation.

$\chi^0(q)$ for 1T-TaS$_2$ shows two weak humps at wavevectors larger than the observed wavevector of the ICDW. It is not clear if this is an artifact of the calculation or represents the "true" $\chi^0(\vec{q})$. Again $\chi^0(q)$ does not have logarithmic like peaks and little temperature dependence is calculated.

The situation for the 2H polymorphs is even less clear. Here the obtained band structure is more sensitive to calculational details, since the conduction band is only about 1 volt wide and the F.S. is two sheeted. In any case, a calculated $\chi^0(q)$ shows only a broad maximum near $\vec{q} = 0.33\vec{a}^*$,[60] whose value is about 10 times that of a free electron gas of the same density. As in the 1T polymorphys the calculated $\chi^0(q)$ shows little temperature dependence. While Ricco et al.[60] argue that the electron
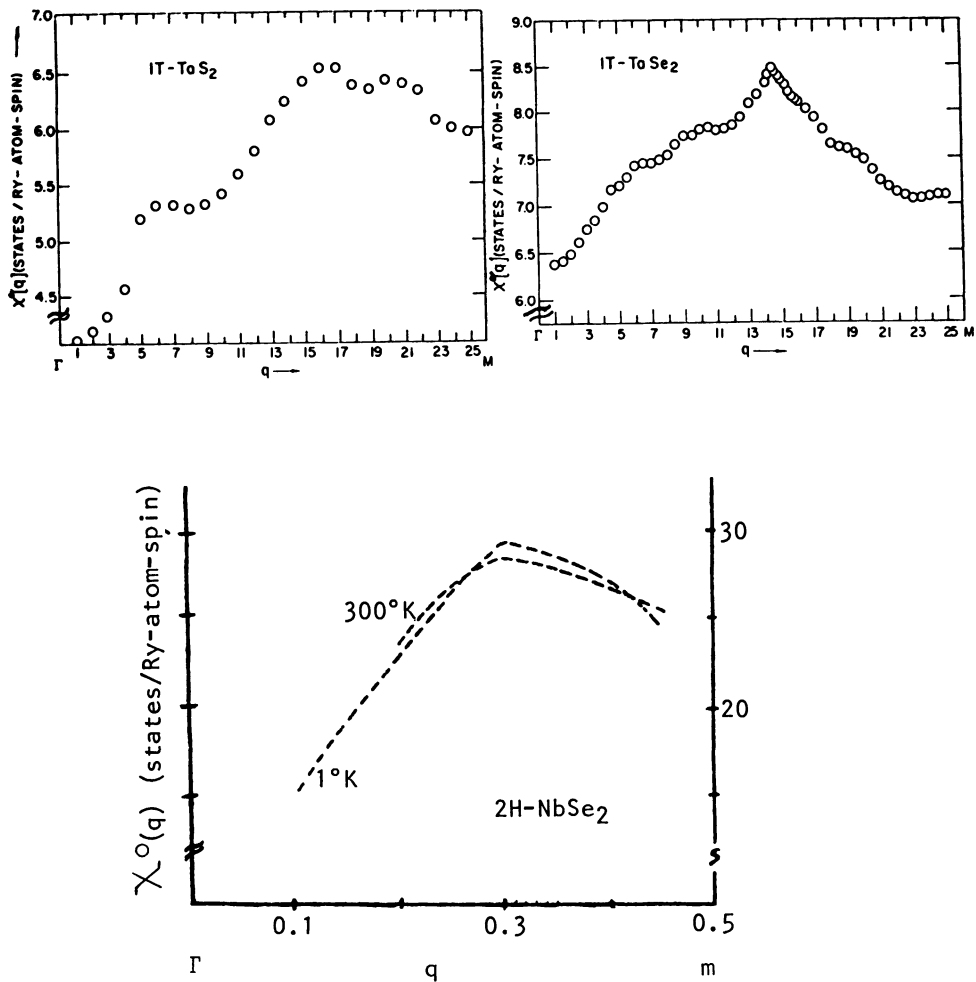
Figure 15. (top right) - The calculated $\chi^0(q)$ for 1T-TaSe2 with
q along the ΓM direction shows a weak peak at the observed ICDW
wavevector.

(top left) - The calculated $\chi^0(q)$ for 1T-TaS2 with q along the
ΓM direction shows even weaker peaks, but these do not occur
at the ICDW wavevector.

(bottom) - The calculated $\chi^0(q)$ for 2H-NbSe2 along the ΓM
direction shows a broad maximum near q_o. The calculated
temperature dependence is very small.

These three figures suggest that while $\chi^0(q)$ is relatively
large, prominent features expected from the simple model
embodied in eq. 4 are not visible.

phonon interaction along with the large value of $\chi^0(2k_F)$ is sufficient to explain the instability, they do not explain what determines the CDW onset temperature T_0.

These calculations of $\chi^0(q)$ suggest that the interactions, $X(\vec{q})$, are more important than the simple model implies in determining the appearance of the CDW. At present our understanding of the magnitude and of the energy and wave vector dependence of these interactions is limited. A more serious difficulty with the simple theory has been pointed out by McMillan (Conference proceedings). McMillan has developed a model for the 2H-TaSe$_2$ CDW that takes into account the phonon entropy. Significant contributions to the entropy due to phonon softening is expected since such a large region of phonon states in the LA acoustic phonon branch are temperature dependent. (see Fig. 7). The inclusion of this term markedly modifies the instability condition (to determine T_0), and consequently a discussion of the instability in terms of eq. 4 may be misleading. This model, when compared with experimental data, leads to the prediction of a short coherence length for the CDW of about 10 Å, a value close to the mean free path above T_0 and to the super lattice wavelength. This length is somewhat larger than found in antiferromagnetic transitions or in superfluid liquid He, but is much shorter than found in superconductors, where a mean field treatment of the thermodynamics is adequate.

These calculations of $\chi^0(q)$ and of the coherence length make the role of the F.S. less apparent than in the simple model. Yet is seems clear that the F.S. plays a role in determining the wave vector of the ICDW, but the microscopic details are still lacking. It is also clear, particularly for 1T-TaS$_2$ and TaSe$_2$, that weak coupling models of the CDW will be inadequate to describe the large amplitude of the CCDW. As has been emphasized by Thompson,[37] the general occurence of the CDW phenomena in these compounds makes it seem unlikely that the CDW is based on a subtle property of the band structure. It seems reasonable that the occurrance of the CDW is based on more general features, such as the large values of $\chi^0(q)$ and of the electron phonon interaction.[3,58]

Before closing this article, I would like to point out that I have only discussed a few of the layered compounds. I would like to briefly mention other phenomena that are connected with CDW formation or other phenomena that are of interest, at least to me. (1) 4Hb polymorphs, in which the layers alternate between octahedral and trigonal prismatic coordination, show separate uncoupled CDW transitions in the different symmetry layers[62] (2) the 2H polymorphs of group Vb are superconductors.

Several papers show that T_c increases as the CDW amplitude and/or T_0 is suppressed[9,24,63] (3) the semi metal $TiSe_2$ has a phase transition near 200K in which the hexagonal a and c axis double[54,65] (4) cation substitution in 1T-TaS_2 and 1T-$TaSe_2$ by Fe, Co, or Ni produces electron localization by the random impurity potential, even when the CCDW state is eliminated[66]. In the case of Fe a low spin to high spin conversion occurs as the temperature is increased[67] (5) TiS_2 shows an unusual T^2 resistivity from 10K to 400K[68]. At least two models have been proposed to explain this behavior[69,70]. (6) There may be technological use of layered and related compounds in rechargeable battery systems[71,72,73].

In conclusion, there now exists a large, but not exhaustive, body of empericial knowledge about CDW's in layered compounds. Largely through Landau models the data is at least qualitatively and some cases quantitatively connected. However, our understanding of this phenemona, particularly at the microscopic level is less well developed.

Finally, I wish to point out that this was not intended to be an exhaustive review of work on layered compounds. In particular, I have chosen to mainly emphasize points from my own work, and therefore the references used may not adequately give credit to many others who have contributed to this field.

References

1. J. A. Wilson, F. J. DiSalvo, and S. Mahajan, Adv. in Phys. 24, 117 (1975).

2. P. M. Williams, "Crystallography and Crystal Chemistry of Materials with Layered Structures" Vol. 2, ed. F. Levy Reidel Pub. (1976).

3. A. H. Thompson, Comments in Solid State Physics 7 125 (1976).

4. F. J. DiSalvo, 1976 NATO Conf. on Idim. conductors, Bolzano, Italy.

5. J. A. Wilson and A. D. Yoffe, Adv. in Phys. 18, 193 (1969).

6. F. R. Gamble, J. H. Osiecki and F. J. DiSalvo, J. Chem. Phys. 55, 3525 (1971).

7. F. R. Gamble, J. H. Osiecki, M. Cais, R. Pisharody,
    F. J. DiSalvo and T. H. Geballe, Science 174, 493 (1971).

8. F. J. DiSalvo, G. W. Hull, Jr., L. H. Schwartz, J. M.
    Voorhoeve and J. V. Waszczak, J. Chem. Phys. 59, 1922 (1973).

9. D. W. Murphy, F. J. DiSalvo, G. W. Hull, Jr., J. V. Waszczak,
    S. F. Meyer, G. R. Stewart, S. Early, J. V. Acrivos, and
    T. H. Geballe, J. Chem. Phys. 62, 967 (1975).

10. J. Rouxel, J. S. S. Chem. 17, 223 (1976).

11. L. F. Mattheiss, Phys. Rev. B8, 3719 (1973).

12. The first reports of super conductivity in these compounds
    are: M. H. Van Maaren and G. M. Schaeffer, Phys. Letts. 20,
    131 (1966); 24A, 645 (1967).

13. F. R. Gamble, F. J. DiSalvo, R. A. Klemm, T. H. Geballe
    Science 168, 568 (1970).

14. R. E. Schwall, G. R. Stewart and T. H. Geballe, J. Low Temp.
    Phys. 22, 557 (1976); R. E. Schwall Ph.D. Thesis Stanford
    Univ. (1973).

15. G. Lucovsky, W. Y. Liang, R. M. White, K. R. Pischarody
    S. S. Comm. 19, 303 (1976).

16. A. H. Thompson, F. R. Gamble and J. F. Revelli
    S. S. Comm. 9, 981 (1971).

17. F. J. DiSalvo, R. G. Maines, J. V. Waszezak and
    R. E. Schwall S. S. Comm. 14, 497 (1974).

18. A. H. Thompson, F. R. Gamble and R. F. Koehler, Phys. Rev.
    B5, 2811 (1972).

19. H. N. S. Lee, M. Garcia, H. McKinzie and A. Wold, J.S.S.
    Chem. 1, 190 (1970).

20. R. K. Quinn, R. Summons, and J. J. Banewicz, J. Phys. Chem.
    70 230 (1966).

21. M. Barmatz, L. R. Testardi and F. J. DiSalvo, Phys. Rev.
    B12, 4367 (1975).

22. J. M. E. Harper, T. H. Geballe and F. J. DiSalvo, Phys.
    Rev. B15, 2943 (1977).

23. E. Eherenfreund, A. C. Gossard and F. R. Gamble, Phys. Rev.
     B5, 1708 (1972).

24. C. Berthier, D. Jerome, P. Molinie, and J. Rouxel
     S. S. Comm. 19, 131 (1976).

25. J. A. R. Stiles and D. L. Williams, J. Phys. C. 9, 3941
     (1976).

26. G. K. Wertheim, F. J. DiSalvo, and S. Chiang, Phys. Rev.
     B13, 5476 (1976).

27. H. B. Hughes and R. A. Pollak, Comm. Phys. 1, 61 (1976).

28. A. W. Overhauser, Phys. Rev. 167 (1968).

29. M. J. Rice and S. Strassler, S.S. Comm. 13 125 (1973).

30. L. M. Roth, H. J. Zeigler and T. A. Kaplan, Phys. Rev. 149,
     519 (1966).

31. T. M. Rice and G. K. Scott, Phys. Rev. Letts. 35, 120 (1975).

32. S. K. Chan and V. Heine, J. Phys. F3, 795 (1973).

33. A. W. Overhauser, Phys. Rev. 128, 1437 (1962).

34. W. M. Lomer, Proc. Phys. Soc. (London) 80, 489 (1962).

35. A. W. Overhauser, Phys. Rev. B3, 3173 (1971).

36. A. Guinier "X-ray diffraction in Crystals, Imperfect Crystals
     and Amorphous Bodies. Pub. W. H. Freeman 1963.

37. J. G. Allpress, 5th N.B.S. Symp. Mat. Res. Pub. 364, pg. 727
     (1972).

38. J. Van Landuyt, J. Van Tendeloo, S. Amelinckx, Phys. Stat.
     Sol. A29, K11 (1975).

39. D. E. Moncton, J. D. Axe, and F. J. DiSalvo, Phys. Rev. Letts.
     34, 734 (1975).

40. C. B. Scruby, P. M. Williams, and G. S. Parry, Phil. Mag.
     31, 225 (1975).

41. J. P. Tidman, O. Singh, A. E. Curzon and R. F. Frindt,
     Phil. Mag. 30, 1191 (1974).

42. F. J. DiSalvo and J. V. Waszczak Journal de Physique Supplement C4, 37 157 (1976).

43. W. L. McMillan Phys. Rev. B12, 1187 (1975); Phys. Rev. B14 1496 (1976); and this conference.

44. S. A. Jackson, P. A. Lee and T. M. Rice Bull. Am. Phys. Soc. 22, 280 (1977).

45. D. E. Moncton, J. D. Axe and F. J. DiSalvo to be pub. in Phys. Rev. B15 (June 15, 1977).

46. A. S. Barker, Jr., J. A. Ditzenberger and F. J. DiSalvo Phys. Rev. B12, 2049 (1975).

47. E. F. Steigmeyer, G. Harbecke, H. Auderset, and F. J. DiSalvo, S.S. Comm. 20, 667 (1976).

48. J. A. Holy, M. V. Klein, W. L. McMillan, and S. F. Meyer Phys. Rev. Letts. 37, 1145 (1976).

49. G. K. Wertheim, F. J. DiSalvo, and S. Chiang, Phys. Letts. 54A 304 (1975).

50. Y. Yamada and H. Takatera, S.S. Comm. 21, 41 (1977).

51. A. H. Thompson, Phys. Rev. Letts. 34, 520 (1975).

52. F. R. Gamble, J.S.S. Chem. 9, 358 (1974).

53. D. E. Moncton, F. J. DiSalvo, J. D. Axe, L. J. Sham and B. R. Patton, Phys. Rev. B14, 3432 (1976).

54. F. J. DiSalvo and J. E. Graebner, to be published in S.S. Comm.

55. N. F. Mott, M. Pepper, S. Pollett, R. H. Wallis and C. J. Adkins, Proc. Roy. Soc. London A345, 169 (1975).

56. P. Fazekas and E. Tosatti, Proc. of XIII International Conf. on Physics of Semiconductors Rome 1976.

57. P. B. Allen, Phys. Rev. Letts. 37, 1638 (1976).

58. F. J. DiSalvo, J. A. Wilson, B. G. Bagley, and J. V. Waszczak, Phys Rev. B12, 2220 (1975).

59. H. W. Myron, J. Rath and A. J. Freeman, Phys. Rev. $\underline{B15}$, 885 (1977).

60. B. Ricco, V. Heine, M. Schneiber, D. T. Henington and G. Wexler, to be published.

61. S. K. Sinha and B. N. Harmon, 2nd Rochester Conf. on Superconductivity in d and f band Metals (May 1976) ed D. H. Dougles (AlP, New York).

62. F. J. DiSalvo, D. E. Moncton, J. A. Wilson and S. Mahajan, Phys. Rev. $\underline{B14}$ 1543 (1976).

63. F. J. DiSalvo, Conf. on Low Lying Lattice Modes and their Relationship to Ferroelectricity and Superconductivity (Dec. 1975) Univ. of Puerto Rico.

64. J. A. Wilson and S. Mahajan, Comm. on Physics $\underline{2}$, 23 (1977).

65. F. J. DiSalvo, D. E. Moncton and J. V. Waszczak, Phys. Rev. $\underline{B14}$, 4321 (1976).

66. F. J. DiSalvo, J. A. Wilson and J. V. Waszczak, Phys. Rev. Letts. $\underline{36}$, 885 (1976).

67. M. Eibschutz and F. J. DiSalvo, Phys. Rev. Letts. $\underline{36}$, 104 (1976).

68. A. H. Thompson, Phys. Rev. Letts. $\underline{35}$, 1786 (1975).

69. C. A. Kukhonen and P. F. Maldague, Phys. Rev. Letts. $\underline{37}$, 782 (1976).

70. J. A. Wilson, S.S. Comm. $\underline{22}$, 551 (1977).

71. M. S. Whittingham, J. Electrochem. Soc. $\underline{123}$, 315 (1976).

72. D. W. Murphy, F. A. Trumbore and J. N. Carides J. Electrochemical Society $\underline{124}$, 325 (1977).

73. J. N. Carides and D. W. Murphy, to be published in J. Electrochem. Soc.

LANDAU THEORY OF CHARGE DENSITY WAVES

W. L. McMillan

Dept. of Physics and Materials Research Lab

University of Illinois, Urbana, Ill. 61801   USA

A.   THE LANDAU FREE ENERGY

The two theoretical methods which have proved so fruitful in the study of superconductivity have been applied to the charge density wave (CDW) phase transitions in the transition metal dichalcogenides. I will discuss the (Ginzburg-) Landau theory in this lecture and microscopic mean field theory in the next lecture. The Landau theory is due to Dave Moncton and myself.[2,3] The Landau theory approach is especially powerful in the discussion of position-dependent or time-dependent properties. We don't have an adequate dynamical theory yet and I will discuss only the static Landau theory.

In order to write down a Landau theory one must choose the proper order parameter and write down an expansion of the free energy in powers of the order parameter and the gradient of the order parameter. In the CDW phase one has a static periodic lattice distortion, a band gap in the electronic band structure, and an electronic charge density wave present simultaneously. Near the onset transition the three quantities are proportional to each other and we can choose any one as the order parameter. We choose the electronic charge density and since there are three CDW's present (thinking now of our canonical material, $2H-TaSe_2$) we write

$$\rho(\vec{r}) = \rho_o(\vec{r}) \left[1 + \alpha(\vec{r})\right] \tag{1}$$

where

$$\alpha(\vec{r}) = \text{Re}[\psi_1(\vec{r}) + \psi_2(\vec{r}) + \psi_3(\vec{r})] \tag{2}$$

and the $\psi_i(\vec{r})$ are three complex order parameters, one for each CDW. For the energy of one layer we write an expansion in powers of the order parameters, keeping all terms allowed by symmetry.

$$F_1 = \int d^2r \lceil a(\vec{r})\alpha^2 - b(\vec{r})\alpha^3 + c(\vec{r})\alpha^4$$

$$+ d(\vec{r})(|\psi_1\psi_2|^2 + |\psi_2\psi_3|^2 + |\psi_3\psi_1|^2)\rceil \tag{3}$$

where $a(\vec{r})$, $b(\vec{r})$, $c(\vec{r})$ and $d(\vec{r})$ exhibit the periodicity of the crystal lattice. We will write, for example,

$$c(\vec{r}) = c_o + c_1 \sum_i e^{i\vec{K}_i \cdot \vec{r}} \tag{4}$$

where the six $\vec{K}_i$ are the six shortest reciprocal lattice vectors. We next include a random potential $U(r)$, due to impurities

$$F_2 = \int d^2r \, U(\vec{r})\rho_o(\vec{r})\alpha(\vec{r}) \ . \tag{5}$$

The gradient terms are chosen so that the free energy of the three CDW's is minimum when they lie in the right directions and have the right wavelengths; any distortion from this optimal condition costs free energy.

$$F_3 = \int d^2r \left[e(\vec{r}) \sum_i |(\vec{q}_i \cdot \vec{\nabla} - iq_i^2)\psi_i|^2 \right.$$

$$\left. + f(\vec{r}) \sum_i |\vec{q}_i \times \vec{\nabla} \, \psi_i|^2 \right] \tag{6}$$

where $|q_i| = 2\pi/\lambda$, λ is the wavelength of the incommensurate CDW, and the three $\vec{q}_i$ vectors lie in the ΓM directions 120° apart. The total free energy of one layer is the sum of these three terms

$$F = F_1 + F_2 + F_3 \ . \tag{7}$$

We could also include the coulomb interaction of CDW's in different layers. We assume that a_o changes sign at the onset transition

$$a_o = a'(T - T_{IN}) \tag{8}$$

and that the other parameters are constant. The Landau theory is a phenomenological theory and the parameters are to be determined from experiment.

B.   PHASE TRANSITIONS

The simplest thing to discuss is the state of lowest free energy. One assumes that the order parameters are plane waves with definite amplitudes, phases and wave vectors, and one varies these quantities to minimize F. For $T > T_{IN}$ the amplitudes vanish and one has the normal metal phase. For T somewhat less than T_{IN} the quadratic term is negative and one finds a finite amplitude of all three CDW's and wave vectors determined by minimizing the distortion energy F_3. The wave vectors are incommensurate with the lattice and only the uniform terms in the free energy (i.e., a_0, b_0, c_0, and d_0) contribute. The lock-in energy

$$\sum_i \text{Re}\left[\frac{c_1}{8} \int d^2 r \;\; \psi_i^3 e^{iK_i \cdot r}\right] \tag{9}$$

averages to zero. One can take advantage of the lockin energy to lower the free energy by setting the CDW wave vector equal to $\vec{K}_i/3$. This costs elastic energy and the transition temperature to the commensurate phase is governed by this energy balance. As we will see later on this treatment of the commensurate-incommensurate transition using uniform plane waves is oversimplified.

C.   FLUCTUATION MODES

Small phase and amplitude distortions of the order parameters are the collective modes of the system. Since the periodic lattice distortion is proportional to the order parameter these modes appear in the lattice dynamic structure factor and can be measured by neutron scattering. For $2H-TaSe_2$ there are three amplitude and three phase modes and these have been observed by Raman scattering.[4] The static Landau theory predicts the energy versus amplitude of these modes (but not the frequencies); one simply expands the free energy about the minimum for small distortions. Long wavelength phase distortions correspond locally to a translation of the CDW which costs very little energy in the incommensurate phase; the energy of the "phason" is proportional to k^2 where $\vec{K}$ is the phason wavenumber. In the commensurate phase the lock-in energy opposes translation of the CDW and the phason energy is proportional to a constant plus k^2. For the amplitude modes the energy is proportional to a constant plus k^2 with the constant proportional to $|T - T_{IN}|$ (within mean field theory). Thus one expects soft mode behavior near the onset phase transition with the amplitude modes stiffening in the incommensurate phase and the phase modes stiffening in the commensurate phase. Qualitatively this does happen; however the detailed behavior of the soft modes and the central peak near the phase transition are not well understood.

D. IMPURITY EFFECTS

Impurity effects may be calculated simply within Landau
theory. In the normal phase a charged impurity attracts elec-
tronic charge and the system responds by dressing an impurity
with a CDW cloud. The size of this cloud grows larger as the
phase transition is approached and the correlation length of the
CDW increases. A second impurity feels the potential of the CDW
and there is an impurity-impurity interaction which tends to space
impurities apart by one CDW wavelength. Since the impurities
drive the CDW order parameter the incommensurate-normal metal
phase transition is not sharp. In the incommensurate phase a
phase distortion of the CDW is not costly and the CDW can lower
its energy by distorting to place charge density peaks near
impurities. This effectively pins the CDW to the impurities. In
the commensurate phase the CDW is locked in to the lattice and
cannot easily distort to take advantage of the impurity potential.
Thus the incommensurate phase is favored energetically in the
presence of impurities and the incommensurate-commensurate tran-
sition temperature is strongly depressed.

E. CDW DISLOCATIONS

In the incommensurate phase the cubic term in the free energy
(proportional to c_o) fixes the relative phase of the three CDW's.
The sign of this term is such that positively charged regions of
the 3 CDW's add up on lattice sites of a hexagonal "lattice".
The lattice spacing of this CDW "lattice" is approximately three
times the crystal lattice spacing. The phason modes are just the
phonon modes of the CDW "lattice". Vacancies or interstitials in
the CDW "lattice" are not possible because the units making up the
lattice are not discrete. However a CDW dislocation is possible
and is closely analogous to the vortex line in superconductors or
superfluid helium. We emphasize that the host crystal is assumed
to be perfectly uniform and that only the CDW is distorted into a
"dislocation". In order to introduce a dislocation we insert a
vortex solution into two of the three CDW order parameters, with
the phase of the order parameter changing by 2π as one encircles
the dislocation. If one then examines the charge density map one
row of charge peaks has been removed leaving a "lattice" dis-
location.

F. DISCOMMENSURATIONS

The last concept I want to discuss is the discommensuration.
For simplicity consider a single incommensurate CDW whose wave-
length is 2% greater than three times the lattice spacing. If we
take a uniform plane wave for our CDW then for 25 lattice spacings

the CDW will be in phase with the lattice and the lock-in energy
will be negative; then for the next 25 lattice spacings the CDW
will be out of phase with the lattice and the lock-in energy will
be repulsive. The spatial average of the lock-in energy will be
zero. However, we can distort the CDW in two ways to take ad-
vantage of the lock-in energy. We can amplitude modulate the CDW
making it larger in the in-phase region and smaller in the out-of-
phase region. Or we can phase modulate the CDW making the in-
phase region larger and the out-of-phase region smaller. Both
distortions buy lock-in energy at the expense of distortion energy,
with phase-modulation costing less distortion energy. If one
considers phase modulation only (the weak coupling limit) the
nonlinear problem is simple enough to solve exactly. Far from the
lock-in phase transition one finds a weak phase modulation with
the in-phase region slightly larger than the out-of-phase region.
As one moves toward the phase transition the in-phase region
expands and the average wavelength of the CDW shifts toward
commensurability. Finally, very near the phase transition one has
large in-phase regions which are locked in to the lattice and
narrow out-of-phase regions which appear to be defects called
discommensurations. The phase of the CDW relative to the crystal
changes by $2\pi/3$ as one crosses the discommensuration. As one
continues to lower the temperature the number of discommensurations
decreases and vanishes in a continuous way at the commensurate-
incommensurate phase transition. One interprets the transition as
a defect melting transition in contrast to the more common order
parameter type of continuous phase transition. Experimentally,
the lock-in phase transition in 2H-TaSe$_2$ exhibits hysteresis and
is first order; however the transition is very sensitive to
impurities and super pure crystals are not available yet.
Additional Bragg scattering from the distortion was predicted and
observed by Moncton et. al.[1]

REFERENCES

1) D. E. Moncton, J. D. Axe, and F. J. DiSalvo, Phys. Rev. Lett.
   34, 734 (1975).

2) W. L. McMillan, Phys. Rev. B12, 1187 (1975).

3) W. L. McMillan, Phys. Rev. B14, 1496 (1976).

4) J. A. Holy, M. V. Klein, W. L. McMillan, and S. F. Meyer,
   Phys. Rev. Lett. 37, 1145 (1976).

MICROSCOPIC MODEL OF CHARGE DENSITY WAVES IN 2H-TaSe$_2$

W. L. McMillan

Dept. of Physics and Materials Research Lab

University of Illinois, Urbana, Ill. 61801   USA

The ultimate goal of the theoretician in studying a particular phenomenon is to produce a quantitative microscopic theory from which one can calculate anything. That goal has been pretty well achieved in superconductivity. We are still struggling with the theory of charge density waves. The way that one progresses in solid state physics is to compute the properties of a theoretical model, compare the predictions with experiment, and modify the model when it fails. I want to discuss one iteration of this process today.

Our present understanding of CDW's in metals follows the early work of Peierls,[1] Fröhlich,[2] Overhauser,[3] and Chan and Heine[4] and is based on the following physical picture: one starts with a normal metal and introduces a periodic lattice distortion (a static phonon distortion of finite amplitude and wavevector $\vec{q}$). The new periodicity introduces a new Brillouin zone boundary and creates a band gap in the one-electron band structure near the zone boundary. If the zone boundary is near the Fermi surface (that is, if $\vec{q}$ spans nested portions of Fermi surface) the energy of many occupied electronic states will decrease and the total electronic energy will decrease. If the gain in electronic energy more than offsets the increase in elastic energy the distorted state will be the ground state. The occupied electronic states are nonuniform and there is a charge density wave with wavevector $\vec{q}$ which screens the lattice potential. Thus the three physical properties go together, the periodic lattice distortion, the energy gap in the band structure, and the charge density wave. I believe that this physical picture is correct for the layered compounds. However in order to calculate the properties of the CDW state at finite temperature the conventional approach is to include the entropy of electrons

excited across the energy gap and to minimize the free energy. This is the right thing to do if the zero temperature correlation length ξ_0 (of the CDW) is long; it turns out to be incorrect for 2H-TaSe$_2$. What one must do at finite temperature is to include the lattice entropy; the electron energy gap is quite large and the electronic entropy is negligible.

I want to discuss three simple calculations and compare them to experiment.[5] The first is a model calculation of various energies at T = 0 and a prediction of lattice dynamics in the distorted state; the lattice frequencies have been measured by Raman scattering[6] and we can determine the magnitude of various contributions to the energy by fitting the Raman data. Next we examine the electronic energy model which, with some approximations, turns out to be identical to the BCS theory of superconductivity.[7] A comparison of this model with experiment yields some large discrepancies. Finally, we treat a lattice entropy model, which assumes a short coherence length, which is in semi-quantitative agreement with experiment.

At T = 0 we begin by writing for the displacement of the ith Ta atom in the ℓth layer from its lattice site $\vec{R}_i$

$$\vec{u}_\ell(\vec{R}_i) = \text{Im} \sum_{j=1}^{3} \hat{q}_j \phi_\ell^j(\vec{R}_i) e^{i\vec{q}_j \cdot \vec{R}_i} \tag{1}$$

where $\vec{q}_j$ is the nesting vector of the jth CDW and $\phi_\ell^j(\vec{R}_i)$ is the local complex amplitude of the CDW. The three $\vec{q}_j$ form a star in the ΓM directions. We assume that the band gap $|2W|$ is proportional to the lattice distortion.

$$W_\ell^j(x) = \alpha \phi_\ell^j(x) \tag{2}$$

Only a portion of the Fermi surface is affected by the energy gap W_ℓ^j and we assume a simplified band structure for this nested portion: we assume perfect nesting with a Fermi velocity v_F and an electronic density of states (of one spin) of $N_\uparrow(0)$ (for each CDW). Then the electronic energy is

$$E_{e\ell} = \sum_{\ell j}' \int d^2x \left[-N_\uparrow(0) |W_\ell^j(x)|^2 \log \frac{E_B^2}{|W_\ell^j(x)|^2} \right.$$
$$\left. + N_\uparrow(0) \xi_0^2 |\nabla W_\ell^j(x)|^2 \right] \tag{3}$$

where E_B is the electronic band width and ξ_0 is of order $\hbar v_F/2W$. Electrons near the gap edge cannot respond to lattice vibrations

with wave vectors further than $1/\xi_0$ from the nesting vector and we assume that $\phi_\ell^j(x)$ is a slowly varying function with a momentum space cutoff of $\vec{k}_c = 1/\xi_0$. We rewrite (3) using phonon coordinates and include several other energies.

$$PE = \frac{1}{2} \sum_\ell \int \frac{d^2x}{\Omega} \left\{ \sum_j \left[A|\phi_\ell^j|^2 - C|\phi_\ell^j|^2 \log|\phi_B/\phi_\ell^j|^2 \right.\right.$$

$$+ C\xi_0^2|\nabla\phi_\ell^j|^2 - Re(B_\ell \phi_\ell^j{}^3 e^{i(3\vec{q}_j - \vec{G})\cdot\vec{x}})$$

$$+ F Re(\phi_\ell^j \phi_{\ell+1}^j) \big]$$

$$+ D(|\phi_\ell^1\phi_\ell^2|^2 + |\phi_\ell^1\phi_\ell^3|^2 + |\phi_\ell^2\phi_\ell^3|^2)$$

$$+ Re(E\phi_\ell^1\phi_\ell^2\phi_\ell^3) \right\} \tag{4}$$

where Ω is the area of the normal state unit cell in one plane. The first term is the unscreened elastic constant and the second and third terms are the electronic contributions from (3). The fourth term is the lock-in term and the fifth is the interlayer Coulomb interaction. The sixth term is a CDW interaction which arises when two CDW's compete to open an energy gap on the same portion of Fermi surface and the seventh is a weak CDW interaction permitted by symmetry.

The lattice kinetic energy is

$$KE = \frac{M^*}{4} \sum_{\ell j} \int \frac{d^2x}{\Omega} \left| \frac{\partial\phi_\ell^j(x)}{\partial t} \right|^2 \tag{5}$$

where the Se atoms are assumed to adiabatically follow the Ta atoms with the same ratio of Se displacement to Ta displacement observed at low temperature; this yields $M^* = 206$ au. Equations (4) and (5) constitute a nonlinear dynamical model for the longitudinal acoustic phonons modes near $\vec{q}_j$.

To find the equilibrium distortion at $T = 0$ in the commensurate phase we substitute

$$\phi_\ell^j(x) = \phi_0 e^{i(\theta_\ell + \Delta\vec{q}\cdot\vec{x})} \tag{6}$$

where $\vec{\Delta q} = \vec{G}_j/3 - \vec{q}_j$ and $\theta_\ell = -\frac{1}{3}$ phase (B_ℓ) and minimize PE with respect to ϕ_o^j to find ϕ_o.

In order to find the phonon frequencies we add a small phase or amplitude distortion to the static distortion.

$$\phi_\ell^j(\vec{x}) = [\phi_o + (\alpha_k + i\beta_k)\cos(k\cdot x + \frac{k_z \ell c}{2})]e^{i(\theta_\ell + i\vec{\Delta q}\cdot\vec{x})} \tag{7}$$

and expand PE to second order in α_k and β_k. The equations of motion are then harmonic and are simple to solve; for the amplitude modes we find

$$\frac{M^* \omega_k^2}{4} = 4C - 3|B|\phi_o + 8D\phi_o^2 + \bar{E}\phi_o + 2F - 2F\cos(\frac{k_z c}{2}) + C\xi_o^2 k^2 \tag{8a}$$

and

$$\frac{M^* \omega_k^2}{4} = 4C - 3|B|\phi_o - 4D\phi_o^2 - 2\bar{E}\phi_o + 2F - 2F\cos(\frac{k_z c}{2}) + C\xi_o^2 k^2 \; . \tag{8b}$$

where $\bar{E} = \text{Re}[E\exp(i3\theta_o)]$. For the phase modes we find

$$\frac{M^* \omega_k^2}{4} = 9|B|\phi_o - 3\bar{E}\phi_o + 2F - 2F\cos(\frac{k_z c}{2}) + C\xi_o^2 k^2 \tag{8c}$$

and

$$\frac{M^* \omega_k^2}{4} = 9|B|\phi_o + 2F - 2F\cos(\frac{k_z c}{2}) + C\xi_o^2 k^2 \; . \tag{8d}$$

The (8b) and (8d) modes are doubly degenerate giving six modes. These six modes are observed in Raman scattering and from the Raman data we find

$$F = .03 \text{ eV/\AA}^2; \quad |B|\phi_o = .053 \text{ eV/\AA}^2; \quad |E\phi_o| = .036 \text{ eV/\AA}^2;$$

$$C = .29 \text{ eV/\AA}^2, \quad D\phi_o^2 = .031 \text{ eV/\AA}^2; \quad A/C + \xi_o^2 \Delta q^2 - \log|\phi_B/\phi_o|^2 = -.90.$$

There are enough parameters in the theory to fit the data and there is no consistency check on the theory.

For the second calculation we include the entropy of electrons excited across the Peierls energy gap and calculate the transition temperature, heat capacity and magnetic susceptibility. If we neglect the CDW interactions the theory is equivalent to the BCS theory and we can borrow the following results from BCS. The

energy gap at T = 0 is

$$2W(T = 0) = 3.52 \ k_B T_{IN} \tag{9}$$

where T_{IN} is the incommensurate-normal metal transition temper-
ature. The heat capacity jump at T_{IN} is

$$\Delta C_V = 3 \times 9.4 \ N_\uparrow(0) k_B^2 T_{IN} \tag{10}$$

and the change in susceptibility due to the band gap is

$$\Delta\chi = 1.3*4\mu^2 N_\uparrow(0) \tag{11}$$

including an electron-electron enhancement factor of 1.3. From
DiSalvo's[8] value $\Delta\chi = 55 \cdot 10^{-6}$ emu/mole we find $N_\uparrow(0) = .33$ states/
eV/Ta atom. Using (10) the model predicts a specific heat jump of
0.8 joules/mole K. Craven[9] finds a specific heat jump of 4
joules/mole K. Including the CDW interaction increases this
discrepancy. The theory predicts a Peierls gap of $2W(0) = .037$ eV
whereas Barker et al.[10] find an energy gap of .25 eV. We conclude
that the electronic entropy model doesn't work for $2H\text{-}TaSe_2$.

For the third calculation let's do the theory in the opposite
limit, that of small correlation length. For small ξ_0 the phonon
frequencies are modified over a large region of momentum space and
the phonon entropy is large. The phonon entropy depresses the
transition temperature so that $2W(0) \gg 3.52 \ k_B T_{IN}$; then, the
electronic entropy is negligible and one can forget about the
electrons altogether. The electronic ground state energy provides
the energy surface for the motion of the atoms; the Born-Oppenheimer
or adiabatic approximation is valid. Therefore all we need to know
is the nonlinear Hamiltonian (4) and the theory is completely
specified. Unfortunately, in spite of the recent progress in
understanding critical behavior, there are no theoretical tools
which allow us to compute either the static or dynamic behavior
of (4) assuming either classical or quantum statistics for the
lattice. For the moment we will have to be satisfied with a
rather primitive mean field theory. We first transform to a
lattice model with the number of lattice sites equal to the number
of modes of the continuum model with its cutoff $k_c = 1/\xi_0$. We
take a square lattice in one layer with a lattice spacing of $\pi\xi_0$.
We define the lattice order parameter by the value of the continuum
order parameter at the lattice site

$$\phi^j_{\ell mn} = \phi^j_\ell (\vec{x}_{nm}) \tag{12}$$

Replacing the gradient term in (4) by the finite difference we
find

$$PE = \frac{1}{2} \frac{(\pi\xi_o)^2}{\Omega} \sum_{\ell mn} \{ \sum_j [A|\phi^j_{\ell mn}|^2 - C|\phi^j_{\ell mn}|^2 \log|\phi_B/\phi^j_{\ell mn}|^2$$

$$+ \frac{C}{\pi^2} (|\phi^j_{\ell mn} - \phi^j_{\ell m+1n}|^2 + |\phi^j_{\ell mn} - \phi^j_{\ell mn+1}|^2)]$$

$$+ D(|\phi^1_{\ell mn}\phi^2_{\ell mn}|^2 + |\phi^2_{\ell mn}\phi^3_{\ell mn}|^2 + |\phi^3_{\ell mn}\phi^1_{\ell mn}|^2)\} \qquad (13)$$

where we have neglected small terms in the energy.

We now make the mean field approximation in which each local mode moves in a potential due to its neighbors.

$$V_1(\phi) = \frac{1}{2} \frac{(\pi\xi_o)^2}{\Omega} [A|\phi|^2 - C|\phi|^2 \ell n |\phi_B/\phi|^2$$

$$+ \frac{4C}{\pi^2} (|\phi|^2 - 2\phi^* \langle\phi\rangle) + 2D |\phi|^2 \langle|\phi|^2\rangle] \qquad (14)$$

Near the phase transition k_BT is greater than the phonon frequencies and we can use classical statistics. The self consistency conditions for the order parameters are then

$$\langle\phi\rangle = \int d^2\phi \, \phi e^{-V_1(\phi)/T} \Big/ \int d^2\phi e^{-V_1(\phi)/T} \qquad (15)$$

and

$$\langle|\phi|^2\rangle = \int d^2\phi \, |\phi|^2 e^{-V_1(\phi)/T} \Big/ \int d^2\phi e^{-V_1(\phi)/T} \qquad (16)$$

which we can solve numerically and predict the temperature dependence of the order parameters, the thermodynamic properties and the lattice dynamics. The predicted heat capacity jump is 1.67 k_B per mode and the transition temperature is

$$T_{IN} = .296 \, C(\pi\xi_o\phi_o)^2/2\,\Omega \qquad (17)$$

From the observed heat capacity jump of .48 k_B per Ta atom and $T_{IN} = 122.°K$ we find $\pi\xi_o \approx 10$ Å and $\phi_o = .16$ Å. The length $\pi\xi_o = 10$ A is equal to the superlattice unit cell size and is the shortest correlation length which is physically reasonable. This correlation length is consistent with the extent in k-space of the Kohn anomaly in the longitudinal acoustic branch[11] and with the fluctuation heat capacity observed by Craven so that it is safe to conclude that 2H-TaSe$_2$ is the short ξ_o limit. Moncton has measured

ϕ_o directly by neutron crystallography and finds ϕ_o between .05 $\overset{\circ}{A}$ and .09 $\overset{\circ}{A}$.

With such a short correlation length the energy gap is the same order of magnitude as the Fermi energy. We can estimate the magnitude of the energy gap very crudely as follows. From Matthiess'[12] band structure the Fermi energy is .35 eV and the (isotropically averaged) basal plane band mass is about 5 electron masses. From $\xi_o \approx \hbar v_F/2W$ we estimate $2W \approx .3$ eV which is in order of magnitude agreement with the weak absorption edge (at .25 eV) observed by Barker et al.

The phonon entropy model works well in semi-quantitative comparisons with experiment. However it does not quantitatively reproduce Monctons measurement of $\langle \phi \rangle$ versus temperature and the phonon dynamics appear to be more complicated than that predicted by the mean field calculation. Both of these discrepancies may be due to the mean field approximation and we need to develop more powerful theoretical techniques to treat the nonlinear Hamiltonian.

The physical picture of the normal state is more complicated in the phonon entropy model because the order parameter fluctuations are quite large. The mean displacement $\langle \phi \rangle$ and the mean energy gap $\langle W \rangle$ vanish at the phase transition. However, the mean square local displacement $\langle |\phi|^2 \rangle$ and the mean square local energy gap $\langle |W|^2 \rangle$ are almost as large at the phase transition as at $T = 0$. The strongly fluctuating energy gap modifies one's physical picture of the normal state and the implications for resistivity, susceptibility, etc., have not been explored. Another important theoretical problem which has not been attacked yet is the derivation of the electronic energies in (4) from a realistic band structure in the distorted state.

REFERENCES

1) R. E. Peierls, _Quantum Theory of Solids_ (Clarendon, Oxford, 1955).

2) H. Fröhlich, Proc. Roy. Soc. (London) _A233_, 296 (1954).

3) A. W. Overhauser, Phys. Rev. _167_, 691 (1968); _3B_, 3173 (1971).

4) S.-K. Chan and V. Heine, J. Phys. F: Metal Phys. _3_, 795 (1973).

5) W. L. McMillan, Phys. Rev., in press.

6)   J. A. Holy, M. V. Klein, W. L. McMillan and S. F. Meyer,
     Phys. Rev. Lett. <u>37</u>, 1145 (1976).

7)   J. Bardeen, L. N. Cooper and J. R. Schrieffer, Phys. Rev. <u>108</u>,
     1175 (1957).

8)   J. A. Wilson, F. J. DiSalvo and F. Mahajan, Adv. Phys. (GB)
     <u>24</u>, 117 (1975).

9)   R. Craven, to be published.

10) A. S. Barker, Jr., J. A. Ditzenberger and F. J. DiSalvo, to
     be published.

11) D. E. Moncton, J. D. Axe and F. J. DiSalvo, Phys. Rev. Lett.
     <u>34</u>, 734 (1975); D. E. Moncton, Ph.D. thesis (MIT, 1975).

12) L. F. Mattheiss, Phys. Rev. B<u>8</u>, 3719 (1973).

LIGHT SCATTERING BY CHARGE DENSITY WAVE MODES IN KCP AND 2H-TaSe$_2$

E.F. Steigmeier, G. Harbeke and H. Auderset

Laboratories RCA Ltd., Zürich, Switzerland

Charge density waves (CDW's) are known to occur in both quasi one- and two-dimensional materials the best studied examples of which are $K_2Pt(CN)_4Br_{0.3} \cdot 3.2H_2O$ (KCP) and 2H-TaSe$_2$, respectively (1). For studying the dynamic excitations of the CDW's, called CDW modes, light scattering turns out to be a most useful technique. Its wavevector resolution is of the order of $5 \times 10^{-5} \text{Å}^{-1}$, which is 10^3 times better than inelastic neutron scattering; such a high resolution is needed for an unambiguous analysis of the eigenfrequencies because of the considerable dispersion near the distortional wavevector.

Raman measurements on KCP (2) and KCP* (deuterated KCP) (3) show a sharp line at 44 cm^{-1} and 38 cm^{-1} (4K), respectively, of A$_1$ symmetry (xx=yy = 0, zz$\neq$ 0). It is attributed to the amplitude mode of the CDW. This mode is observed at all temperatures and its frequency never tends to zero (it rather increases slightly with temperature) suggesting that KCP is distorted at all accessible temperatures. The linewidth of the mode increases strongly with increasing temperature. The light scattering results are in good agreement with inelastic neutron scattering measurements (4) if the limited wavevector resolution of the latter are taken into account.

One of the most important findings of Raman scattering in KCP is the strong isotope effect of the amplitude mode frequency (3). This evidences that the water, situated in between the Pt chains, participates considerably in the eigenvector of the CDW mode, which therefore, by no means is of purely one-dimensional character. From the behaviour of the water stretching mode with temperature, it appears that the water may be crucially involved also in the tempe-

rature dependence of the interchain correlation.

In the hexagonal layer structure material $2H\text{-}TaSe_2$ the light scattering measurements (5) show several modes clearly associated with the CDW transitions which occur at T_{inc} = 122K, from the normal to the incommensurate, and at T_{com} = 90K, from the in-commensurate to the commensurate phase. Three of these modes are observed only below T_{com}, namely the one of A_{1g} symmetry at 43 cm^{-1}, of E_{2g} at 63 cm^{-1} and of A_{1g} at 82 cm^{-1} (4K values) (Figure 1). One mode of E_{2g} symmetry at 49 cm^{-1} (4K) persists in the incommensurate phase and disappears only at T_{inc}. Based on the fact that in the incommensurate phase the phase mode can be of zero frequency while the amplitude mode cannot, we have reason to believe this E_{2g} 49 cm^{-1}
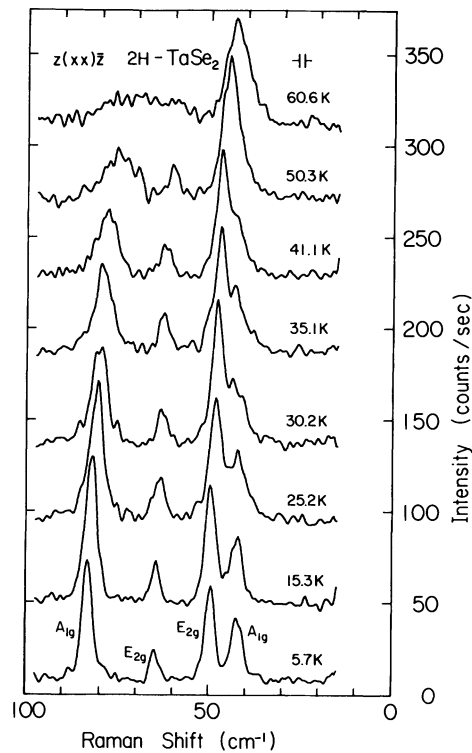

Figure 1:   Raman spectrum of $2H\text{-}TaSe_2$ at various temperatures.
            (Note that in ref. 5 overheating was less than 0.2 deg,
            while in the present figure the increased resolution
            was obtained at the cost of an overheating of about
            5-10 deg above the stated nominal temperature.)

mode to be an amplitude mode (6). All four modes soften and broaden with increasing temperature. These results represent the first observations of a softening of CDW modes in a distorted phase.

The damping constant of the E_{2g} (49 cm^{-1}) mode increases quite drastically in approaching T_{inc}, approximately as $(T_{inc}-T)^{-1}$, while the damping constants of the other three modes behave the same way in approaching T_{com}, approximately as $(T_{com}-T)^{-1}$. Increases of this extent are quite unusual.

Of particular interest is the detailed temperature dependence of the E_{2g} (49 cm^{-1}) mode frequency which varies as $(T_{inc}-T)^{1/3}$. Further, it is proportional to the order parameter, for which the coupling coefficient of the light to the CDW mode is a direct measure (7). This non-classical value of the exponent suggests that there exists quite a large region near T_{inc} where the simple meanfield theory (8), despite its qualitative success, is of limited use for describing quantitatively the thermodynamics of the CDW's.

References

(1) For introduction to this topic the reader is referred to the lectures by F.J. Di Salvo and by W.L. McMillan.

(2) E.F. Steigmeier, R. Loudon, G. Harbeke, H. Auderset and G. Scheiber, Solid State Comm. __17__, 1447 (1975).

(3) E.F. Steigmeier, D. Baeriswyl, G. Harbeke, H. Auderset and G. Scheiber, Solid State Comm. __20__, 661 (1976).

(4) K. Carneiro, G. Shirane, S.A. Werner and S. Kaiser, Phys. Rev. __B 13__, 4258 (1976).

(5) E.F. Steigmeier, G. Harbeke, H. Auderset and F.J. Di Salvo, Solid State Comm. __20__, 667 (1976).

(6) This assignment differs from the one made in the lecture of W.L. McMillan. See also J.A. Holy, M.V. Klein, W.L. McMillan and S.F. Meyer, Phys. Rev. Letters __37__, 1145 (1976).

(7) Previously such a proportionality between soft mode frequency and order parameter had been reported for the antiferro-distortive transition in $SrTiO_3$ by E.F. Steigmeier, H. Auderset and G. Harbeke in __Anharmonic Lattices, Structural Transitions and Melting__, ed. by T. Riste, NATO-ASI (Noordhoff Publishing Leiden 1974) p. 153.

(8) Lecture of W.L. McMillan.

SYMMETRY CLASSIFICATION OF MODULATED STRUCTURES

P.M. de Wolff

Technische Hogeschool Delft, Lab. v. Techn.Nat.

Lorentzweg 1, Delft (the Netherlands)

1. DEFINITION OF MODULATED STRUCTURES

In a normal crystal, symmetry is defined by a group of operations, each of these belonging to the much larger group of all proper and improper movements. The symmetry translations

$$\vec{r}' = \vec{r} + \vec{n} \tag{1}$$

where $\vec{n} = n_1\vec{a} + n_2\vec{b} + n_3\vec{c}$ (n_i = integer, i = 1,2,3) constitute an invariant subgroup of every crystal symmetry group.

We shall now try to find similar operations for modulated crystals. In an earlier paper (De Wolff, 1974, to be referred to as (I) from now), the possible point groups for such crystals have been derived from a description in four-dimensional space; the actual crystal is a section of this model, lying in the hyperplane which is constituted by the physical three-dimensional space. The same approach can very well be followed for the present purpose, viz. the derivation of symmetry operations and lattice types. We shall not do so (apart form an occasional reference) but rather emphasize the description both of the crystal and of the operations in direct three-dimensional space. The reason for choosing this alternative approach is firstly, that it is more convincing and easier to follow, the more so since the basis for the point group enumeration will be derived in passing so that (I) need not necessarily be consulted. Secondly, it is better adapted to a precise definition of the symmetry operations and of the modulated crystals themselves.

The latter are characterized by two properties: <u>a</u>) To each

153

modulated structure corresponds a <u>basic structure</u>, that is, a
"normal" crystal structure from which the modulated one can be
derived by finite modifications, which are periodically ordered.
We take displacive modulation as an example – other types of
modulation yield the same results, and the displacive case is the
more complicated one since here the modifications have vector
character. In fact they consist of a displacement $\vec{u}$ of each atom,
which depends upon:
- the kind of atom, each atom in the unit cell of the basis
structure being considered as a separate kind so that the relevant
index i runs from 1 to N, if N is the number of those atoms.
- the position of the atom in the basic structure, defined by a
vector $\vec{r}^{o}_{ip}$ where the index p symbolizes the integers p_1, p_2 and p_3
numbering the unit cell from an origin in a fixed cell. Thus if the
fractional coordinates of the i-th atom in the basic structure are
x^{o}_{ij} (j = 1,2,3), the components of $\vec{r}^{o}_{ip}$ are x^{o}_{ij} + p_j.
- a fixed vector $\vec{k}$ in reciprocal space, with components k_1, k_2 and
k_3 with respect to the reciprocal basis of the basic structure.
It is conceivable that structures exist modulated with more than
one k-vector simultaneously. Here we shall restrict ourselves to
the case of a single k-vector. The more general case is treated
e.g. by Janner & Janssen (1977).
- N periodic and continuous vector functions $\vec{u}_i(\alpha)$, each with unit
period, that is, invariant for an integer shift in α. These functions
define the displacement of the atom at position $\vec{r}^{o}_{ip}$ in the basic
structure by

$$\vec{u}(i,p) = \vec{u}_i(\vec{k}\cdot\vec{r}^{o}_{ip}) = \vec{u}_i\{\sum_1^3 k_j (x^{o}_{ij} + p_j)\} \qquad (2)$$

For convenience's sake we shall normalize the functions $\vec{u}_i$ by the
condition that the average displacement vanishes:

$$\int_0^1 \vec{u}_i(\alpha) \, d\alpha = \vec{0}, \quad i = 1\ldots N. \qquad (2a)$$

so that the x^{o}_{ij} define the average position of the i-th atom.

   <u>b</u>) At least one of the components k_1, k_2 and k_3 depends
in a continuous manner upon external parameters such as the
temperature. It can therefore be considered as an irrational number,
in contrast with the rational $\vec{k}$-components of superstructures.

   Property <u>b</u> was introduced as such in (I). Property <u>a</u> corres-
ponds to the assumed existence of a lattice of "main reflections"
in (I). The latter, however, are the diffraction image of the
average structure (smeared atoms), not of the basic structure.
Another competing structure is that of the solid phase without
modulation, usually prevailing in a higher temperature range. It
may be isostructural with the basic structure but again is not
identical to it, since the temperature difference changes both
unit cell and position parameters. Relations between these several

structures will be given in section 3.

2. SYMMETRY OPERATIONS AND -TRANSLATIONS

A symmetry operation is usually defined as a movement of the crystal, which brings it into coincidence with itself. An alternative definition leaves the crystal where it is and defines as a symmetry operation each mapping $\vec{r} \rightarrow \vec{r}'$ for which

$$\phi(\vec{r}') = \phi(\vec{r}) \quad \text{for all } \vec{r}, \tag{3}$$

ϕ being any local function, such as the electron density. For symmetry translations, the mapping is given by (1). This "mapping definition" is so obviously equivalent to the "movement definition" that the distinction is hardly ever made.

For modulated structures, however, the "movement definition" leads nowhere, but the definition (3) can readily be extended. To begin with, (2) is replaced by

$$\vec{u}(i,p) = \vec{u}_i(\vec{k} \cdot \vec{r}^{\,o}_{ip} + t). \tag{4}$$

The new parameter t is an overall phase parameter for all $\vec{u}_i$-functions simultaneously. For an infinite crystal, the introduction of t – or, more generally, a change Δt in t – is no more than an infinitesimal structural change. This fact follows from property $\underline{b}$: Indeed the change Δt is equivalent to a mere change of the origin cell by a vector $n_1\vec{a} + n_2\vec{b} + n_3\vec{c}$, provided that $\vec{k} \cdot \vec{n} = \Delta t$ (mod 1). Because of the irrationality of at least one k_j, this equation can be fulfilled to any desired degree of accuracy by a judicious choice of the integers n_j. Stated in less mathematical terms: the environment of a given atom is of course modified if t changes, but the new environment could have been found before the change for an atom elsewhere – not exactly, but with any desired degree of precision. Therefore it is plausible to extend (3) as follows: An "MS-(modulated structure-)symmetry operation" is a mapping $\vec{r} \rightarrow \vec{r}'$, $t \rightarrow t'$ such that

$$\phi(\vec{r}',t') = \phi(\vec{r},t) \quad \text{for all } \vec{r} \text{ and } t. \tag{5}$$

A mathematically exact symmetry translation can now be derived for modulated crystals, starting from (1) and adding a "compensating" change in t:

$$\vec{r}' = \vec{r} + \vec{n} \tag{6a}$$

$$t' = t - \vec{k} \cdot \vec{n}. \tag{6b}$$

$\vec{n}$ = basic structure lattice vector.

In the sense of symmetry definition (5), this operation can be interpretated most easily by looking first at (6b). Writing $\vec{u}(i,p,\tau)$ for the displacement of the atom at $\vec{r}{}^{0}_{1p}$ for $t = \tau$, we find $u(i,p,t') = \vec{u}_i(k(r^0_{1p}-n)+t) = u(i,p-n,t)$. Hence (6b) signifies that all displacements are carried over to atoms removed by a shift $\vec{n}$ from the atom to which they referred originally, the shift of course being performed on the corresponding atoms in the basic structure. Then it is obvious that (6a) indeed relates a site $\vec{r}$ before the execution of (6b), to a site at $\vec{r}{}'$ with identical ϕ after that operation, cf. fig.1. Because of the periodicity of the $\vec{u}_i$-functions, adding an integer to t is also a symmetry operation. Therefore we can now write down the complete set of <u>MS-symmetry translations</u>:

$$\vec{r}{}' = \vec{r} + \vec{n} \qquad t' = t - \vec{k}\vec{n} + s \tag{7}$$

$\vec{n}$ = basic structure lattice vector; s = integer.

Though the set (7) clearly defines a group of translations in four-dimensional $(\vec{r}, t)$-space, we shall continue to use words like "space" and "vector" in the three-dimensional sense. Moreover, we shall drop the term "pseudosymmetry" used in (I), since the approximative nature suggested by that term applies neither to translations (7) nor to the operations which will be discussed in the next sections. Instead, the term "MS-symmetry translations, MS-symmetry operations" etc. will be used for operations which include a specified mapping t → t' (even if t' should be equal to t) in order to distinguish these from normal symmetry operations.

3. PROPERTIES OF MS-SPACE GROUP OPERATIONS

Besides translations (7), a modulated crystal may have other symmetry operations. In our extended concept of symmetry, defined by (5), we shall have to specify the general nature of these operations $\vec{r} \rightarrow \vec{r}{}'$ and t → t'. Beginning with t', we observe that this parameter can depend only upon the former value t - not on $\vec{r}$, because both t and t' are defined by (4) as overall phase parameters constant in space. The actual form of this dependence has to preserve the symmetry translations consisting of integer shifts in t, hence they must be of the form $\vec{t}{}' = \varepsilon t + \delta$, where $\varepsilon = \pm 1$ and δ is a constant.
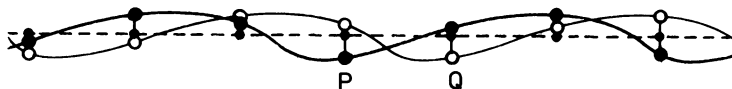

fig.1. Operation t' = t - 1 moves each displacement of the modulated chain (thick line) to the next atom, e.g. from P to Q.

The other part $\vec{r} \to \vec{r}'$ of a symmetry operation has to be a normal space group operation. As a matter of fact it belongs to the space group of the average structure. This follows if we take the average of both sides of (5) over one period of t (which according to the above is also a period of t'):

$$\phi_{av}(\vec{r}') = \phi_{av}(\vec{r}).$$

Accordingly a MS-symmetry operation has the general form

$$\vec{r}' = S\vec{r} + \vec{\rho} \tag{8}$$

$$t' = \varepsilon t - \vec{k}\vec{\rho} + \eta \tag{9}$$

where (8) is an element of the space group of the average structure. In (9) we have replaced the above constant δ by $-\vec{k}\vec{\rho} + \eta$, in analogy with (7), and in order to simplify further relations.

Finally it should be noted that (8) is also an element of the space group of the basic structure. This follows from the fact that, just as with symmetry translations (7), equation (8) connects points with identical electron density before and after the application of (9). Hence, it also connects corresponding atomic centra, which means that an atom at $\vec{r}_{ip}(t)$ is imaged by (8) in some atom at $\vec{r}_{jq}(t')$ see fig.1b.

$$\vec{r}_{jq}(t') = S\vec{r}_{ip}(t) + \vec{\rho}$$

or

$$\vec{r}^{O}_{jq} + \vec{u}(j,q,t') = S\vec{r}^{O}_{ip} + S\vec{u}(i,p,t) + \vec{\rho}. \tag{10}$$

Since by (2a) the average of $\vec{u}$, and therefore of $S\vec{u}$ as well, is zero, we obtain by averaging (10) over t and t'

$$\vec{r}^{O}_{jq} = S\vec{r}^{O}_{ip} + \vec{\rho} \tag{11}$$

which establishes the operation (8) as a normal symmetry operation of the basic structure.

Moreover, by substituting (11) in (10) we obtain

$$\vec{u}(j,q,t') = S\vec{u}(i,p,t), \tag{12}$$

an important starting point for the derivation of the relation between symmetry-equivalent $\vec{u}_i$'s which will be given in section 5.

Now that both the average and the basic structure have been shown to possess the symmetry elements (8), the question may arise what the relation is between the space group G evidently formed by

these elements, and the space groups G_{av} and G_b of the average and basic structure, respectively. Since the centre of an atom in the basic structure is the centre of gravity of the corresponding smeared atom in the average structure, each symmetry operation of the latter applies to the former as well. Combining this result with those derived above we obtain

$$G \subseteq G_{av} \subseteq G_b \tag{13}$$

In most of the structures which are known the three groups are identical.

4. REDUCED FORM OF POINT GROUP OPERATIONS

Obviously the homogeneous parts of (8) and (9) taken together form an element of a finite group K_4, which plays the same rôle as the point group of normal crystals. We shall number these elements with an index m=1...g, where g is the group order:

$$\vec{r}' = S_m \vec{r} \qquad t' = \varepsilon_m t \tag{14}$$

On the other hand, the operators S_m clearly constitute a normal point group K. The question then arises to what extent K is different from K_4. It was shown in (I) that the one-dimensional representation ε_m of K_4 is contained in S_m. Hence K and K_4 are isomorphous. Moreover the corresponding reduction of S_m to

$$S_m = \begin{pmatrix} a_m & b_m & o \\ c_m & d_m & o \\ o & o & \varepsilon_m \end{pmatrix} \tag{15}$$

occurs for a suitably chosen basis of basic structure lattice vectors. The proof of (15) will be repeated here in terms of a new approach, using the properties of the vector $\vec{k}$.

5. EQUIVALENCE AND INVARIANCE OF $\vec{k}$-VECTORS

So far, the vector $\vec{k}$ has been considered as a constant not changed by the action of a symmetry operation. However, it is clearly not a unique vector. We may guess that more or less equivalent $\vec{k}$-vectors can be derived in three ways from a given $\vec{k}$:
a) by adding a basic structure reciprocal lattice vector $\vec{n}^*$
b) by inversion, yielding $-\vec{k}$
c) by letting the point group operations S act on it.

a) The first procedure will now be shown to lead to what we shall call "t-equivalent" $\vec{k}$-vectors. Two vectors $\vec{k}$ and $\vec{k}'$ are <u>t-equivalent</u> if there exist functions u_i' such that the description

of the structure by (4), based on $\vec{k}$, can be replaced by a corresponding one based on $\vec{k}'$:

$$\vec{u}_i(\vec{k}\cdot\vec{r}^{\,0}_{ip} + t) = \vec{u}'_i(\vec{k}'\vec{r}^{\,0}_{ip} + t).\tag{16}$$

Hence the new functions $\vec{u}'_i(\alpha)$ have to obey

$$\vec{u}'_i(\alpha) = \vec{u}_i\{\alpha - (\vec{k}' - \vec{k})\vec{r}^{\,0}_{ip}\}\tag{17}$$

for all unit cells p. Since $\vec{u}_i$ is periodic with period 1, two different unit cells, lying a B.S. lattice vector $\vec{n}$ apart, can satisfy (17) only if $(\vec{k}' - \vec{k})\cdot\vec{n}$ = integer; and this has to be true for all lattice vectors $\vec{n}$. Such a Laue-type condition has the well-known consequence

$$\vec{k}' - \vec{k} = \vec{n}^*\tag{18}$$

where $\vec{n}^*$ is a reciprocal lattice vector of the basic structure. Hence, $\vec{k}'$ and $\vec{k}$ are t-equivalent only if they obey (18). Conversely, substitution of (18) in (17) yields the phase correction $-\vec{n}^*\cdot\vec{r}^{\,0}_{ip}$ to be applied to $\vec{u}_i$ in order to accomodate a shift (18), so (18) is both a sufficient and a necessary condition for t-equivalence of $\vec{k}'$ and $\vec{k}$.

b) The second of the above three procedures, inversion, never yields a t-equivalent vector, since for inversion (18) requires $2\vec{k} = \vec{n}^*$ which is impossible for the incommensurate $\vec{k}$'s considered here. This result may seem strange because $\vec{k}$ and $-\vec{k}$ are obviously equivalent vectors e.g. in the description of the diffraction image. However, t-equivalence is a mathematical concept, not a physical one. (The inversion $\vec{k}' = -\vec{k}$ can be accomodated by a condition like (16) but only with reversed sign of t on the right-hand side of that equation. Indeed t-equivalence would be physically significant if modulation were a wave phenomenon, with t proportional to the time, which would make a distinction between $\vec{k}$ and $-\vec{k}$ meaningful.)

c) Finally we investigate the kind of equivalence which arises from the action of S on $\vec{k}$. We shall show that there is t-equivalence between $\vec{k}$ and $\varepsilon_m S_m \vec{k}$ (not $S\vec{k}$!), where the index m numbers the point group operations as in (14), for m = 1...g. Starting from (12) and letting S_m act on both sides we obtain

$$\vec{u}_i(\vec{k}\cdot\vec{r}^{\,0}_{ip} + t) = S^{-1}_m\vec{u}_j(\vec{k}\cdot\vec{r}^{\,0}_{jq} + t').\tag{19}$$

The right-hand side of $\vec{u}_i$ in (19) is now brought in the form required by (16) first by substitution of (11) and (9)

$$\vec{k}\cdot\vec{r}^{\,0}_{jq} + t' = \vec{k}\cdot(S_m\vec{r}^{\,0}_{ip} + \vec{\rho}) + \varepsilon_m t - \vec{k\rho} + \eta = \vec{k}\cdot S_m\vec{r}^{\,0}_{ip} + \varepsilon_m t + \eta.$$

Since $\vec{k}(S\vec{r}) = (S^{-1}\vec{k})\cdot\vec{r}$ we obtain

$$\vec{k}\cdot\vec{r}_{jq}^{\,o} + t' = \varepsilon_m\{(\varepsilon_m S_m^{-1}\vec{k})\cdot\vec{r}_{ip}^{\,o} + t\} + \eta.$$

Substitution in (19) leads to

$$\vec{u}_i\cdot(\vec{k}\cdot\vec{r}_{ip}^{\,o} + t\ ) = S^{-1}\vec{u}_j\,\varepsilon_m\{(\varepsilon_m S_m^{-1}\vec{k})\cdot\vec{r}_{ip}^{\,o} + t\} + \eta$$

in which equation we recognize (16) with

$$\vec{k}' = (\varepsilon_m S_m)^{-1}\vec{k}, \quad \text{or} \quad \vec{k} = \varepsilon_m S_m \vec{k}' \tag{20}$$

$$\vec{u}_i'(\alpha) = S^{-1}\vec{u}_j(\varepsilon_m\alpha + \eta), \quad \text{or} \quad \vec{u}_j(\alpha) = S\vec{u}_i'\{\varepsilon_m(\alpha - \eta)\} \tag{21}$$

so any two $\vec{k}$-vectors related by (20) are indeed t-equivalent. According to (18) this means that

$$\varepsilon_m S_m \vec{k} - \vec{k} = \vec{n}^*. \tag{22}$$

We now consider the "projection operator" $\frac{1}{g}\overset{g}{\underset{1}{\Sigma}}\varepsilon_m S_m = P$. Applied to any vector $\vec{v}$, the result is a vector $P\vec{v}$ invariant under all operations $\varepsilon_m S_m$ (m = 1...g). Such vectors $P\vec{v}$ constitute a linear vector space L_t (line, plane or whole space) and P actually performs the geometric projection of $\vec{v}$ onto L_t. The one thing we do not yet know is whether L_t is not of zero dimension, that is, whether there exists a vector $\vec{v}$ so that $P\vec{v}$ is not zero. The answer is that $\vec{k}$ is such a vector. This is readily found by writing down the identity:

$$\vec{k} = P\vec{k} - (1/g)\overset{g}{\underset{1}{\Sigma}}(\varepsilon_m S_m\vec{k} - \vec{k}). \tag{23}$$

From (22) it follows that the second term is a rational vector. Hence, the first term, $P\vec{k}$, cannot be zero since that would make the left-hand side $\vec{k}$ rational as well. So $\vec{k}$ is a vector for which $P\vec{k} \neq 0$.

If $\vec{k}$ is in L_t, (20) reduces to $\vec{k}' = \vec{k}$ and (16) to $\vec{u}_i(\alpha) = \vec{u}_i'(\alpha)$. Then (21) immediately yields the important relation (de Wolff, 1977)

$$\vec{u}_j(\alpha) = S_m\vec{u}_i\{\varepsilon_m(\alpha - \eta)\} \tag{24}$$

between displacements of symmetry-related atoms.

If $\vec{k}$ is not in L_t, it can be written

$$\vec{k} = P\vec{k} + \vec{k}_0.$$

From (23) and (22) we conclude that $\vec{k}_0$ is a rational vector. It will be shown in section 8 that $\vec{k}_0$ can be disregarded – so that $\vec{k}$ becomes a vector in L_t – by introducing a new type of symmetry translations

as well as the corresponding new Bravais lattice types.

The proof that every S_m of the point group K can be written in the form (15) is obvious now: we only have to choose the $\vec{c}$ basis vector among (multiples of) the rational vectors $P\vec{n}$ left invariant by each $\varepsilon_m S_m$, that is, in L_t. If L_t is three-dimensional, (15) reduces to $\mp \mathbb{1}_3$; if not, the other basis vectors can always be chosen to obtain a form of (15) as well, because if $\vec{n}$ is a lattice vector clearly both the mutually perpendicular vectors $P\vec{n}$ and $\vec{n} - P\vec{n}$ are rational vectors.

6. POINT GROUPS

It follows from (15) that there is just one ε_m-value possible for each S_m within a given group K_4 of operators ($\mathbb{T}4$), that is, K_4 is isomorphous with K. The notation for groups K_4 can therefore be made unambiguous by using the Hermann–Mauguin symbols for the corresponding point group K, adding a prime (') to those symmetry elements which are generated by an operation for which $\varepsilon = -1$. The possible elements are enumerated below, with indices // and $\perp$ denoting their position with regard to L_t.

Generating operation has:	$\varepsilon = 1$	$\varepsilon = -1$
L_t = whole space	1	$\overline{1}'$
L_t = plane	$m_{//}$ or 1	$2'_{\perp}$ or $\overline{1}'$
L_t = line	$m_{//}, 1, 2_{//},$	$2'_{\perp}, \overline{1}', m'_{\perp}$
	$3_{//}, 4_{//}$ or $6_{//}$	$\overline{3}'_{//}, \overline{4}'_{//}$ or $\overline{6}'_{//}$

In order to enumerate the point groups K_4, one can start by looking at the possible groups K and use the isomorphism between K and K_4 to arrive at groups K_4 afterwards. Regarding the groups K we observe that any normal point group which has a reducible vector representation (that is one, which leaves at least one line invariant) may occur as a group K. As a matter of fact, if this line is inverted by an element S of such a group, then the corresponding element of K_4 will have $\varepsilon = -1$, and otherwise $\varepsilon = +1$, so that εS leaves the vectors along the line invariant and the line will serve as (part of) L_t. In this way for each of these groups, a corresponding group K_4 can be constructed.

Since all point groups except the 5 cubic groups fulfill the above condition, the group K can be any of the 27 non-cubic point groups. However a given group among these 27 can lead to more than one group K_4 if there are several inequivalent choices possible for the invariant line(s). There is no problem in the groups with 3-, 4- or 6-fold axes, which have just this axis as the invariant line, nor with the triclinic system. The orthorhombic groups have three

Table 1. Point Groups

System	Normal	Magnetic	Modulated (K_4)	Group of εS
Triclinic	1	1	1	1
	$\bar{1}$	$\bar{1}$	$\bar{1}'$	1
Monoclinic II	2	2'	2'	m
	m	m'	m	m
	2/m	2'/m'	2'/m	m
Monoclinic III	2	2	2	2
	m	m	m'	2
	2/m	2/m	2/m'	2
Orthorhombic $(L_t // c)$	222	2'2'2	2'2'2	mm2
	mm2	m'm'2	mm2	mm2
	mmm	m'm'm	mmm'	mm2
	m2m	m'2'm	m2'm'	m2m
Trigonal	3	3	3	3
	$\bar{3}$	$\bar{3}$	$\bar{3}'$	3
	32	32'	32'	3m
	3m	3m'	3m	3m
	$\bar{3}$m	$\bar{3}$m'	$\bar{3}'$m	3m
Tetragonal	4	4	4	4
	$\bar{4}$	$\bar{4}$	$\bar{4}'$	4
	4/m	4/m	4/m'	4
	422	42'2'	42'2'	4mm
	4mm	4m'm'	4mm	4mm
	$\bar{4}$2m	$\bar{4}$2'm'	$\bar{4}'$2'm	4mm
	4/mmm	4/mm'm'	4/m'mm	4mm
Hexagonal	6	6	6	6
	$\bar{6}$	$\bar{6}$	$\bar{6}'$	6
	6/m	6/m	6/m	6
	622	62'2'	62'2'	6mm
	6mm	6m'm'	6mm	6mm
	$\bar{6}$2m	$\bar{6}$2'm'	$\bar{6}'$2'm	6mm
	6/mmm	6/mm'm'	6/m'mm	6mm

invariant lines, but only for mm2 the axes are inequivalent. This leads to K_4-groups mm2 and m2'm' for L_t parallel to $\vec{c}$.

A much more fundamental distinction can be made for monoclinic groups K, depending on the choice of invariant line(s) perpendicular

to the binary axis, or parallel to that axis. There is good reason
to distinguish two systems of monoclinic groups K_4 correspondingly,
viz.

> system "monoclinic II" (L_t = plane): point groups 2', m and
> $\qquad\qquad\qquad\qquad\qquad\qquad\qquad\qquad$ 2'/m
> system "monoclinic III" (L_t = line): point groups 2, m' and
> $\qquad\qquad\qquad\qquad\qquad\qquad\qquad\qquad$ 2/m'.

The roman numerals stem from the numbers of the corresponding
four-dimensional groups, cf. (I). The reason for having two dif-
ferent monoclinic systems is that different types of lattice obtain
for each, cf. table 2. There is no such complication for the other
systems so that K_4-groups can be classified conventionally in those.
In total we find 27+1+3 = 31 groups K_4. They have been listed in
(I). These groups are in a 1-1 correspondence with the 31 "admissible
magnetic groups" (Opechowski and Guccione, 1965), consisting of
combined time- and space operations which leave a magnetic moment
vector invariant. Indeed the time inversion is formally equivalent
to our $\varepsilon = -1$, and the difference between the positions of primes
in the two lists is caused by the axial character of the magnetic
vector as compared with our polar $\vec{k}$-vector.

7. RATIONAL AND IRRATIONAL NON-ZERO COMPONENTS OF $\vec{k}$

The vector Pk, lying in L_t, has essentially more than one
non-zero coordinate in two systems, viz. two in monoclinic II, and
three in the triclinic system. In these cases it should be noted
that our definition of a moculated structure requires at least
one irrational coordinate. The remaining one(s) can be rational,
though that is not plausible from a physical point of view except
for e.g. structures with a strong layer-like character.

The component $\vec{k}_0$ of $\vec{k}$ perpendicular to L_t, if not zero, has to
be a rational vector in order to satisfy (22). It is easily deter-
mined in most systems merely by substituting for εS the generating
rotation about the unique axis, if any. The result often depends on
the kind of Bravais lattice of the structure. Firstly, since (22)
is valid for a description on a primitive base, the vector $\vec{n}^*$ in it
has to be a reciprocal lattice vector not extinguished by centring
conditions for a non-primitive base. Secondly, a solution $\vec{k}_0$ of
(22) is not significant if there exists a reciprocal lattice vector
$\vec{n}_1^*$ with the same projection along L_t. (As a matter of fact, the
equations

$$\vec{n}_1^* = P\vec{n}_1^* + \vec{k}_0 \quad \text{and} \quad \vec{k} = P\vec{k} + \vec{k}_0$$

yield $\vec{k} - \vec{n}_1^* = P(\vec{k} - \vec{n}_1^*)$ as a vector which can replace $\vec{k}$ since
according to (18) it is a t-equivalent vector, and which lies in L_t.)

This restriction invalidates many solutions for centred lattices. For instance, in system monoclinic II the solution $(0\frac{1}{2}0)$ for $\vec{k}_0$ is easily found, but when applied to a C-centred lattice, the corresponding vector (now written conventionally as (010)) coincides with (110) in the projection along L_t which in this case is the projection on $\vec{b}$. The various possibilities for all systems will now be enumerated in full, they are shown in fig.2.

For the hexagonal system one finds that (22) with $\varepsilon S = R_{\pi/3}$ already excludes any fractional vector $\vec{k}_0$. In the tetragonal system $\vec{k}_0 = (\frac{1}{2}\frac{1}{2}0)$, and in the trigonal system $(\frac{1}{3}\frac{1}{3}0)$ fulfill the condition, but they are both significant only for P-type Bravais lattices. In monoclinic III, with $\varepsilon S = R_\pi$ about the unique b-axis, $(\frac{1}{2}00)$, $(\frac{1}{2}0\frac{1}{2})$ and $(00\frac{1}{2})$ are equivalent possibilities; the latter two are valid for both P- and C-lattices. Monoclinic II, with $\varepsilon S =$ mirror with respect to the a, c-plane, yields $(0\frac{1}{2}0)$ for P-, but no significant solution for C-lattices as shown above. In the triclinic system $\vec{k}_0 = 0$ since $P\vec{k} = \vec{k}$ for any vector. Finally, with L_t along c the orthorhombic system yields $(\frac{1}{2}00)$ for P, A, C- and F-lattices, $(\frac{1}{2}\frac{1}{2}0)$ for P-lattices only and no solution for I-lattices, where it must be stressed that the coordinates refer to an orthogonal base (100), (010) of the p- or c-net of non-extinct points of the reciprocal net l=0 (for the centred lattices this differs from the convention which e.g. for a C-lattice would call this base: (200), (020)).

Both table 1 and the drawings of fig.2 are easily interpreted if one remembers that the operations εS leave a vector invariant. For each group K_4 therefore, they form one of the "pyro-electric groups", as indicated in the last column in table 1.

8. NECESSITY OF INTRODUCTION OF BRAVAIS LATTICE TYPES WITH IMPROPER TRANSLATIONS

In this section it will be shown that it is possible to assign a $\vec{k}$-vector lying in L_t to any given modulated structure notwithstanding the just-mentioned possibility of non-vanishing perpendicular components, by accounting for such components through the introduction of a new type of symmetry translations. We shall begin by showing that such a seemingly complicated procedure is necessary for the enumeration of inequivalent MS space groups.

The MS space groups are to a large extent similar to those of normal crystals. Equations (8) and (9) indicate clearly the recipe for enumeration one should follow : each generator of the basic structure's space group[*] (given by S and $\vec{\rho}$) must be completed with

[*] We use this term in a loose sense. Actually the group G is meant, which in theory may be of lower symmetry than G_b, cf.(13).
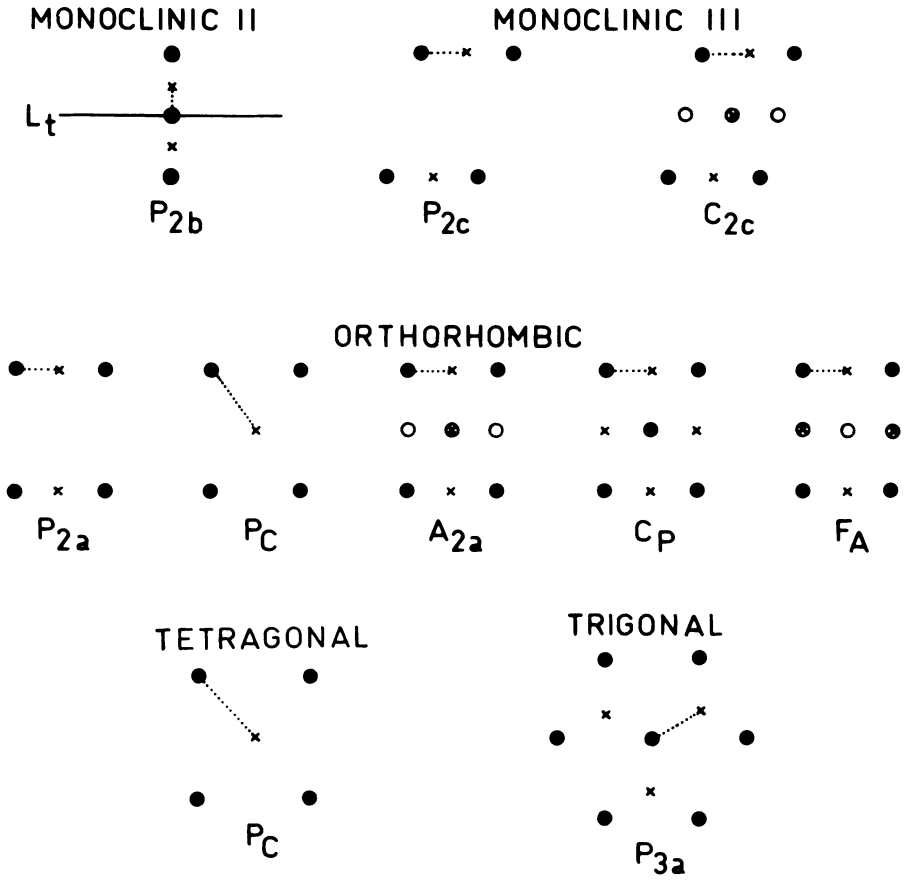
MONOCLINIC II   MONOCLINIC III

P_{2b} P_{2c} C_{2c}

ORTHORHOMBIC

P_{2a} P_C A_{2a} C_P F_A

TETRAGONAL   TRIGONAL

P_C P_{3a}

fig.2. The $\vec{k}$-vectors not in L_t, corresponding to the 10 new types of Bravais lattices in table 2. In each case L_t is normal to the paper; it is a plane for the system monoclinic II and a line other-wise. The dotted line shows the component $k_0 \perp L_t$ of the k-vector. ●,✕ basic structure reciprocal lattice points at levels 0 and ½. o,● satellites, at levels Pk and Pk+½.

some indication of the corresponding ε and η, and the lattice symbol of the basic structure must be added. For ε , the prime convention has been borrowed from magnetic groups already in (I), as an in- dication of ε = -1.

However, the results of the foregoing section show that one more distinction has to be made, namely between the possible

values of $\vec{k}_0$. This rational component of $\vec{k}$ may well influence the number of inequivalent choices for the shift η in t in the rotational generators. For instance if in the system monoclinic III the space group of the basic structure[*] is P2, the rotation over π (ε = +1) may or may not be accompanied by a shift $\eta = \frac{1}{2}$ in t, so that we obtain two MS-space groups when $\vec{k}_0 = \vec{0}$.

On the other hand, if $\vec{k}_0 = \frac{1}{2}\vec{a}^*$ the product of the same rotation with the translation $\vec{a}$ already yields such a combined operation of R_π and a shift of $\frac{1}{2}$ in t. Hence for $k_0 = \frac{1}{2}\vec{a}^*$ there is only one MS-space group, while there are two for $\vec{k}_0 = \vec{0}$. The situation is entirely comparable to normal space groups for a monoclinic structure: we have P2, P2$_1$ and C2, but C2$_1$ is equivalent with C2. Indeed it can be shown that $\vec{k}_0 = \frac{1}{2}\vec{a}^*$ corresponds to a centring in four-dimensional space.

The effect of $\vec{k}_0$ can be accounted for entirely and unambiguously by an extension of the lattice types. This is particularly simple for the non-trigonal systems. The case $k_0 = \frac{1}{2}\vec{a}^*$ for instance, signifies according to (7) that the translation $\vec{a}$ increases t by $\frac{1}{2}$. The alternative way of looking at such translations which we now propose is a) to ignore k_0, so that $\vec{k} - \vec{k}_0$ replaces $\vec{k}$; b) to account for the t-shift by allowing s in (7) to equal $\frac{1}{2}$ when n_1 is odd[**]. The t-shift is thereby incorporated in the lattice type. In itself it is an operation of order 2, and it commutes with all symmetry translations of the basic structure. Therefore it offers the same extension of lattice types as that other external binary element: time inversion, well known in magnetic symmetry.

The difference with the magnetic case is, that t-shifts of $\frac{1}{2}$ have to be considered only for the axes perpendicular to L$_t$. Nonetheless we can make full use of the existing enumeration of magnetic lattice types and their nomenclature, as given by Opechowski and Guccione (1965), cf. section 10. In the trigonal system, the case $k_0 = (\frac{1}{3}\frac{1}{3}0)$ obviously calls for a different approach. It leads to only one new type of lattice, shown in fig.7, which has a primitive hexagonal lattice of the basic structure, and a shift of $\frac{1}{3}$ in t along $\vec{a}$. In analogy with the above-mentioned nomenclature, we propose the symbol P$_{3a}$ for this lattice. The ensuing list of MS-lattice types is given in table 2, cf. section 10.

9. TWO-DIMENSIONAL EXAMPLE OF IMPROPER TRANSLATIONS

In order to elucidate the foregoing sections, we discuss the two-dimensional MS-plane groups p1m and p$_{2b}$1m illustrated in fig.3a and 3b. Both are derived from a basic structure with plane group pm.

[*] We use this term in a loose sense. Actually the group G is meant, which in theory may be of lower symmetry than G$_b$, cf.(13).
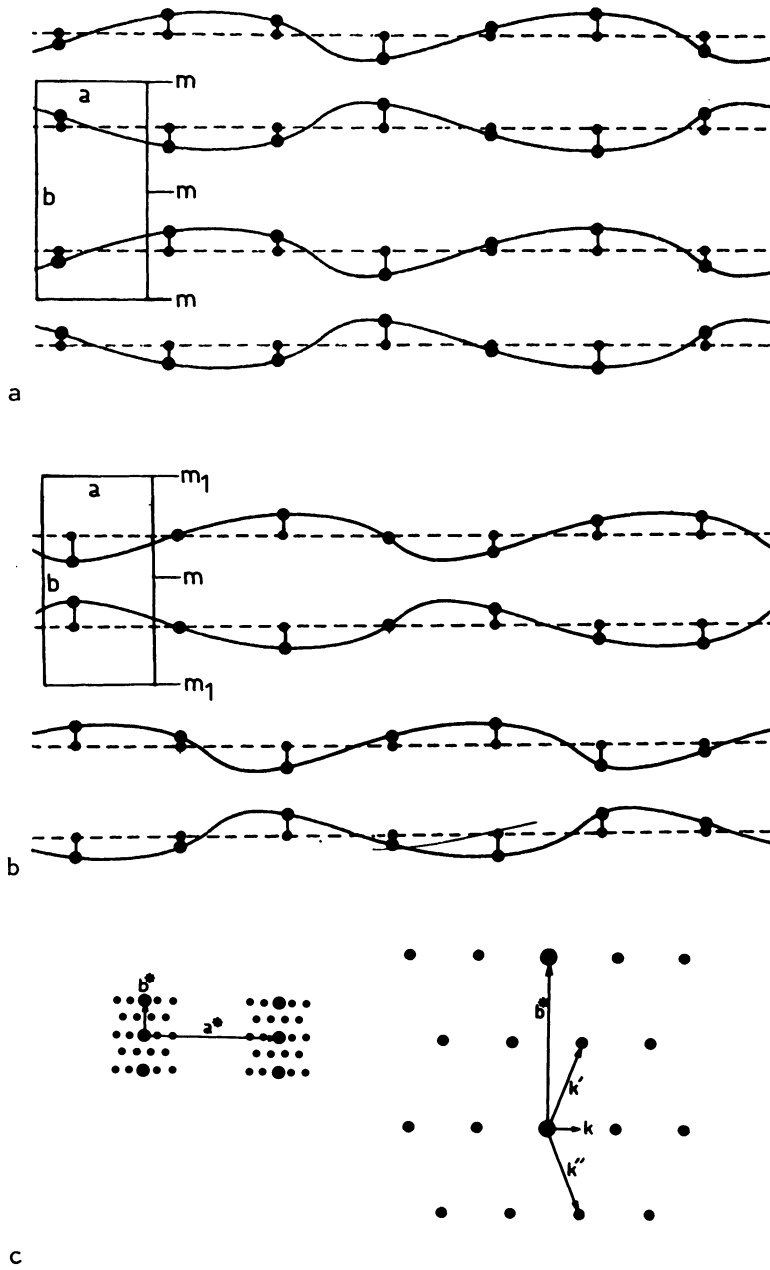[**] Such translations are termed "improper" by de Wolff (1977).

fig.3. Plane groups derived from the normal group pm. a) p1m
b) $p_{2b}1m$ c) reciprocal lattice of $p_{2b}1m$; left: overall picture,
right: enlarged portion. Large dots are main reflections.

The more elaborate notation (plm means m perpendicular to b) is not
absolutely necessary but it helps to prevent confusion. The fact
that there is no prime in either symbol means that m has ε = +1,
hence the vectors in L_t are those parallel to m. The simplest case,
therefore, is the one with $\vec{k}$ parallel to m, that is, in the direction
of $\vec{a}$: MS-plane group plm.

Just as in the three-dimensional case, the fact that L_t is the
site of a twofold symmetry element allows a second possibility for
the k-vector, called k', with a component $\vec{k}_0 = \frac{1}{2}\vec{b}^*$ normal to L_t.
This is rendered by the lattice type p_{2b}. The diffraction image
in fig.3c clearly shows that the remaining k parallel to L_t is
unique and is in agreement with the orthogonal symmetry, whereas
the original $\vec{k}'$-vector is ambiguous (its image $\vec{k}''$ with respect to
m is an equivalent choice) and clashes with the point group symmetry.
The lattice type p_{2b} eliminates these drawbacks. It does so at the
cost of an unusual extinction rule, viz. presence of m-th order
satellites for

2k + m = even

where one has to admit half-integer values of the k-index.

As explained in section 6, there is no choice if one wants to
express the influence of $\vec{k}_0$ on MS-space groups available for a
given basic structure. In this respect the situation for basic
structure space group P2 sketched there is exactly as in the present
case: apart from plm and p_{2b}lm there existst just one further
extension, viz. plm_1 (cf. fig.4; m_1 is a mirror coupled with a shift
1/2 in t), and no separate group "$p_{2b}lm_1$" (the corresponding symbols
in (I), table 2, are Pm for plm, Am for p_{2b}lm and Pc for plm_1).
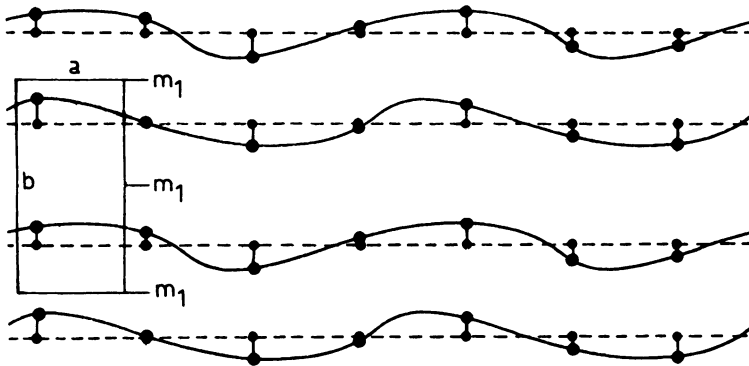
fig.4. The plane group plm_1
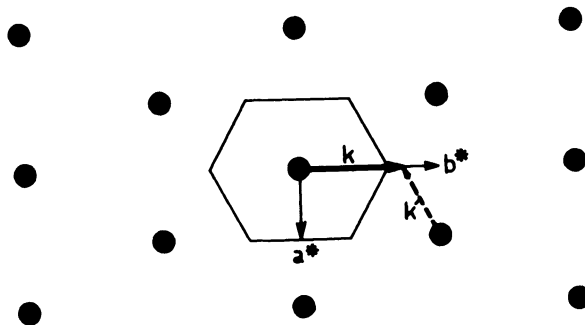
fig.5. Reciprocal centred net, L_t is parallel to $\vec{b}$. The vector $\vec{k}$, when chosen in L_t, extends beyond the first Brillouin zone shown in the figure.

10. ENUMERATION OF LATTICE TYPES

The last three sections have made it clear that among the possible criteria for normalizing $\vec{k}$, the choice of a vector belonging to L_t is by far the most prompting in order to avoid complications. It should be stressed that such a choice is by no means equivalent to a preference for the first Brillouin zone. To illustrate this, fig.5 shows a two-dimensional reciprocal net of the centred type. With orthogonal axes a > b and L_t along $\vec{b}$, one finds that $\vec{k}$ vectors lying within L_t for which
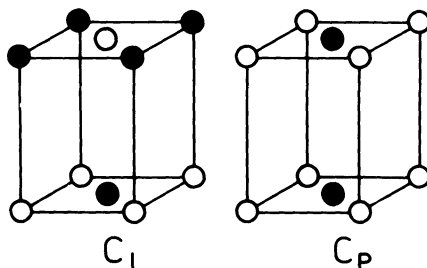
fig.6. Two magnetic Bravais lattice types which are equivalent when applied to modulated structures.

Table 2

MS-system	vectors in L_t	Lattice types		$\vec{k}$ for lattice of basic structure (irr=irrational)		
		basic structure	modulated structure	k_1	k_2	k_3
triclinic	all	P	P	irr	irr	irr
monoclinic II	b	P	P	irr	0	irr
		P	P_{2b}	irr	½	irr
		C	C_{2b}	irr	0	irr
monoclinic III	//b	P	P	0	irr	0
		P	P_{2c}	0	irr	½
		C	C_{2c}	0	irr	0
		C	C_{2c}	0	irr	½
orthorhombic	//c	P	P	0	0	irr
		P	P_{2a}	½	0	irr
		P	P^C	½	½	irr
		A	A	0	0	irr
		A	A_{2a}	½	0	irr
		C	C_{2a}	0	0	irr
		C	C^P	1	0	irr
		I	I^P	0	0	irr
		F	F	0	0	irr
		F	F^A	1	0	irr
hexagonal	//c	P	P	0	0	irr
trigonal	//c	P	P	0	0	irr
		P	P_{3a}	1/3	1/3	irr
		R	R_{3a}	0	0	irr
tetragonal	//c	P	P	0	0	irr
		P	P^C	½	½	irr
		I	I^C	0	0	irr

$$\tfrac{1}{2}\{1 + (b/a)^2\} < k_2 < 1, \quad k_1 = 0$$

fall outside the first Brillouin zône. Preference for the latter would lead to an oblique vector k' not in L_t.

Cases in which $\vec{k}_0$ is essentially non-zero (section 7) have recently been found to occur among actual modulated structures. An example is the monoclinic III-structure of TTF-TCNQ between 54K and 47K which has $\vec{k} = (\tfrac{1}{2}, 0.295, 0)$ so that it corresponds – after interchanging a and c – with the case P_{2c} in fig.2 (Bak, 1977). Hence,
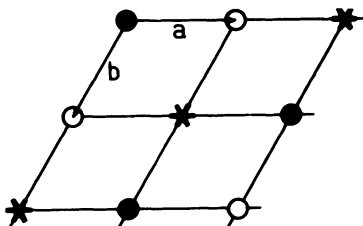
fig.7. The lattice type P_{3a}: symmetry translations perpendicular to c. The shift in t is $\frac{1}{3}$ or $\frac{2}{3}$ in going from a black dot to a circle or an asterisk, respectively.

enumeration of lattice types including all such cases is of more than   academic interest.

    The types listed in table 2 have been derived in three ways:
a) As in section 7, from the possible vectors $\vec{k}_0$, including zero.
b) for the non-trigonal systems: by studying the type or types corresponding to each magnetic lattice. Some of these lead to more than one MS-type. For instance, if L_t in an orthorhombic lattice is along c, then clearly the lattices C and A are not equivalent. On the other hand, many magnetic lattices are superfluous as an MS-type. An example is C_I, illustrated in fig.6. It has C-centring with a shift $\frac{1}{2}$ in t accompanying the centring translation as well as the c-translation. With L_t again in the $\vec{c}$-direction, however, the latter shift merely changes k_3 into $1 - k_3$. Though this may in some cases bring $\hat{k}$ within the first Brillouin zone, we prefer to disregard that criterion as we have done above, and to replace C_I by the simpler type C_P which has a t-shift for the centring trans-lation only.

REFERENCES

BAK, P. (1977) These proceedings, p. 66-87.
JANNER, A. & JANSSEN, T. (1977), Phys.Rev., 15, 643-658.
OPECHOWSKY, W. & GUCCIONE, R. (1965), "Magnetic symmetry" in Magnetism IIa, ed. Rado & Suhl. New York, Academic Press.
WOLFF, P.M. DE (1974), Acta Cryst. A30, 777-785.
WOLFF, P.M. DE (1977), Acta Cryst. A33, 493-497.

SUPERSPACE GROUPS FOR THE CLASSIFICATION OF MODULATED CRYSTALS

T. Janssen

Institute for Theoretical Physics,University of Nijmegen

Toernooiveld, Nijmegen, the Netherlands

I. Introduction

During this meeting one has heard a lot about crystals with an incommensurate phase. Characteristic for these is the absence of space group symmetry. However, as de Wolff explained already (ref.1), it is possible to extend the notion of symmetry. Our approach differs somehow from his and originates from a study of the space-time symmetry of vibrating crystals. The symmetry of a vibration mode is, in general, irrelevant, unless this mode plays a predominant role, e.g. if it is a softening mode. However, we will see that the symmetry considerations can also be applied to modulated crystals, both static and dynamic.

Consider a crystal vibrating in a single mode. For simplicity we take a one-dimensional Bravais crystal (fig. 1). The displacement of the n-th atom in the chain is given by $u_n = u \sin(qna-\omega t)$. The pattern of world lines in the x-t-plane shows invariance under a lattice of translations denoted by Σ. A basis of Σ is formed by $a_1 = (a,qa/\omega)$ and $a_2 = (0,2\pi/\omega)$. For fixed t the positions of the atoms do not have translation symmetry, but form a crystal with a displacive modulation. The difference between the structures at two different times is just an overall phase shift.
Hence, if we identify ωt with the phase ϕ, one can see the modulated crystal as a section of a periodic pattern in the xϕ-plane. In this way we have imbedded the crystal in position space (denoted by V_E) into a larger space (called superspace) which is the sum of V_E and an internal space V_I.

In the superspace V_S the reciprocal lattice Σ^* has a basis with $a_1^* = (2\pi/a,0)$ and $a_2^* = (-q,\omega)$. The projection of Σ on V_E consists of the vectors $k = n(2\pi/a) + mq$ (n,m integers). This means that the diffraction peaks of the modulated crystal belong to this projection: the points $n(2\pi/a)$ are the main reflections, the other
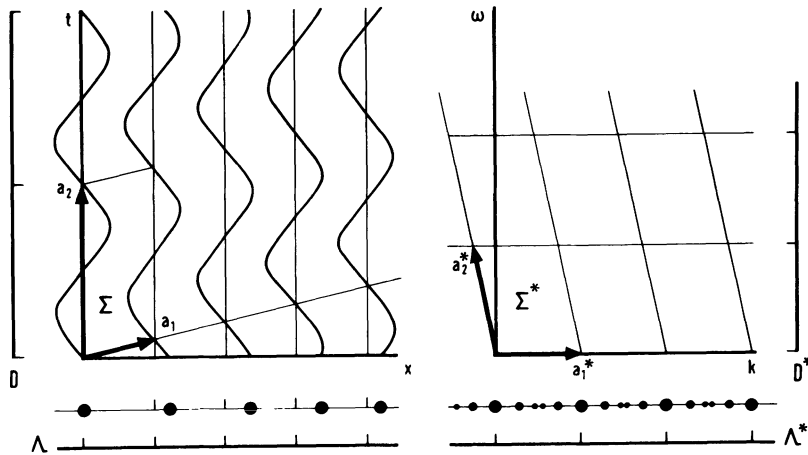
Fig. 1

ones (with $m \neq 0$) the satellites. If we denote the lattice of the undistorted crystal by Λ, the lattice in V_I spanned by $(0, 2\pi/\omega)$ by D, their reciprocal lattices by Λ^* and D^*, the projections on V_E and V_I by π_E and π_I, resp., then one has the following important properties:

$$\Sigma \cap V_I = D, \quad \Sigma^* \cap V_E = \Lambda^* , \quad \pi_E \Sigma = \Lambda , \quad \pi_I \Sigma^* = D^* \qquad (1.1)$$

Apart from the translations there is another symmetry element of the pattern in V_S: the 180° rotation which is a combination of the reflection $x \to -x$ (which is a symmetry element of the undistorted crystal) and the operation $t \to -t$ (which is a transformation in V_I). The symmetry group of the pattern is the space group p2. The elements of this group are combinations of space group elements in V_E with transformations of the internal space. This extension of the class of considered transformations is not uncommon. In the theory of non-rigid molecules, e.g., the symmetry elements are also combinations of orthogonal transformations with internal transformations. As an example, the symmetry group of C_2H_6 has 36 elements (fig.2) and is generated by i) a 120° rotation of the whole molecule, ii) a 120° rotation of the top part with respect to the bottom part (an internal transformation) and iii) a reflection followed by an internal rotation. The only Euclidean transformations are the rigid 120° rotations.

One can generalize the concepts introduced above. The displacement is not necessarily sinusoidal, but is described by a periodic function: $u_n = u(qna-\phi)$ with $u(x+2\pi) = u(x)$.
A modulated crystal with such a modulation in n dimensions (usually n=3) can be imbedded into a (n+1)-dimensional superspace. For a superposition of modulation waves the modulated crystal can be im-

bedded into (n+d)-dimensional superspace, when d is determined as
follows. The diffraction pattern of such a crystal consists of k-
vectors with

$$\underline{k} = \sum_{i=1}^{n} n_i \underline{a}_i^* + \sum_{j=1}^{d} m_j \underline{b}_j^* \qquad (1.2)$$

where $\underline{a}_i^*$ are main reflections and $\underline{b}_j^*$ basic satellites. Finally, not
only displacive modulation can be described in this way, but also
a continuous density distribution for which the spectrum is given
by eq. (1.2). The different more general cases are discussed in ref.
2.

II. Superspace groups

All the cases mentioned at the end of the first section can be
described by superspace groups, generalisations of the two-dimensio-
nal space groups, found for the simple n=1, d=1 example. The mathe-
matical definition is as follows. A superspace group G is

    a) a subgroup of $E(n) \times E(d)$ such that

    b) the translations in G form an (n+d)-dimensional lattice Σ, and

    c) the intersection of the reciprocal lattice Σ^* with V_E is an
       n-dimensional lattice Λ^*.

Condition a) means that the elements g of G are pairs (g_E, g_I) of
Euclidean transformations in, resp., n and d dimensions.
Condition b) implies that G is a space group. Condition c) gives the
space group additional structure. It implies that one can choose
standard bases for Σ and Σ^* . A standard basis for Σ is one for which
the last d basis vectors $a_{n+1}, \ldots, a_{n+d}$ belong to V_I. A standard basis
for Σ^* is one where $a_1^*, \ldots, a_n^*$ belong to V_E.
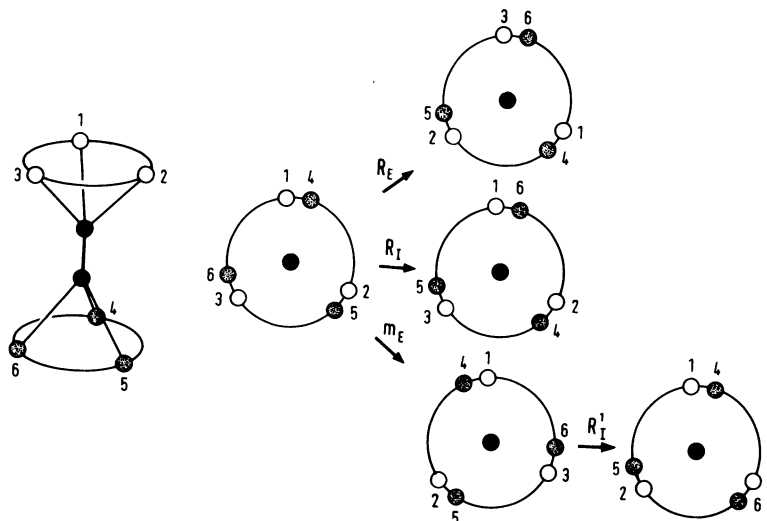
Fig.2

Because the satellites of the zero vector belong to the projection of the lattice spanned by $a^*_{n+1},\ldots,a^*_{n+d}$ on V_E, the property that the modulation is <u>incommensurate</u> can be formulated by the condition:

    d) the intersection of Σ with V_I is the zerovector.

Condition d) is not essential for the consequences and is not included in the definition. For convenience, however, we shall assume only the incommensurate case in the following.

    A superspace group is given by its lattice translations, its point group and the nonprimitive translations $v(R)$, where $R=(R_E,R_I)$ belongs to the point group K. A standard basis for Σ is given by

$$a_i = (\underline{a}_i, -\underline{\Delta a}_i) \ , \quad (i = 1,..,n), \underline{a}_i \in \Lambda \ , \ \underline{\Delta a}_i \in V_I \qquad (2.1)$$
$$a_{n+j} = (0, \underline{b}_j) \quad , \quad (j = 1,..,d), \underline{b}_j \in D$$

If $\underline{a}^*_i$ $(i=1,..,n)$ form the reciprocal basis of Λ^* and $\underline{b}^*_j$ that of D^*, the reciprocal basis of Σ^* is

$$a^*_i = (\underline{a}^*_i, 0) \quad , \quad (i = 1,..,n)$$
$$a^*_{n+j} = (\underline{\Delta b}^*_j, \underline{b}^*_j) \ , \ (j = 1,..,d), \underline{\Delta^* b}^*_j \in V_E \qquad (2.2)$$

Because D and Λ^* span V_I and V_E, resp., one can express $\underline{\Delta a}_i$ and $\underline{\Delta^* b}^*_j$ as

$$\underline{\Delta a}_i = \sum_{j=1}^{d} \sigma_{ji} \underline{b}_j$$
$$\underline{\Delta^* b}^*_j = \sum_{i=1}^{n} \sigma_{ji} \underline{a}^*_i \ . \qquad (2.3)$$

An arbitrary $k = (\underline{k}_E, \underline{k}_I)$ of Σ^* with $k = \Sigma n_i a_i$ has a projection on V_E given by

$$\underline{k}_E = \sum_{i=1}^{n} n_i \underline{a}^*_i + \sum_{j=1}^{d} n_{n+j} \underline{\Delta^* b}^*_j \qquad (2.4)$$

Comparing this with eq. (1.2), one finds that the $\underline{\Delta^* b}^*_j$ are the basic satellites. Hence the entries of the dxn matrix σ in eq. (2.3) are the coordinates of these basic satellites with respect to the basis $\underline{a}^*_1,..,\underline{a}^*_n$ of Λ^*.

    For an incommensurate modulation it is easy to show that the point group K is isomorphic to the group K_E of elements R_E. With respect to a standard basis the point group elements R are represented by matrices

$$\Gamma(R) = \begin{pmatrix} \Gamma_E(R) & 0 \\ \Gamma_M(R) & \Gamma_I(R) \end{pmatrix} , \ R \in K \qquad (2.5)$$

The matrices $\Gamma_E(R)$ form the group K_E, the matrices $\Gamma_I(R)$ the group K_I. They are n-, resp. d-, dimensional point groups. The dxn matrix $\Gamma_M(R)$ is given by

$$\Gamma_M(R) = \sigma\Gamma_E(R) - \Gamma_I(R)\sigma \, , \qquad\qquad (2.6)$$

Because $\Gamma(R)$ (hence also $\Gamma_E(R)$, $\Gamma_I(R)$ and $\Gamma_M(R)$) are integral matrices, eq. (2.6) puts strong restrictions on the possible σ's (i.e. possible modulation vectors) for given K_E and K_I. Two matrices σ can give rise to the same $\Gamma_M(R)$, i.e. to the same point group. There is a unique decomposition $\sigma = \sigma^i + \sigma^r$ such that $\sigma^i\Gamma_E(R) - \Gamma_I(R)\sigma^i = 0$, (all $R \in K$). The matrices σ^i for given $\Gamma_E(R)$ and $\Gamma_I(R)$ form a real vector space, corresponding to L_t in de Wolffs talk (ref.1). The matrices σ^r have rational coefficients.

Starting from the knowledge of the point groups in n and d dimensions, one can determine all possible σ's, i.e. all possible point groups of superspace groups. Then one can determine all superspace groups using a method discussed in ref.3.

III. Equivalence classes

In the usual crystallography one identifies isomorphic space groups. In this way one obtains 219 nonequivalent space groups. Superspace groups have an additional structure. Therefore, one defines: two superspace groups G and G' are equivalent if and only if a) they are isomorphic with an isomorphism that b) maps a standard basis for the lattice Σ of G on a standard basis for G'. Just as for usual crystallography this implies an equivalence relation for lattices: the lattices Σ and Σ' belong to the same <u>Bravais class</u> if and only if there are standard bases for both Σ and Σ' such that the holohedries (the symmetry point groups of the lattices) have the same matrices. This means that these point groups are related by $\Gamma'(R) = S^{-1}\Gamma(R)S$ (all R in K) with

$$S = \begin{pmatrix} S_E & 0 \\ S_M & S_I \end{pmatrix},$$

where S_E, S_M and S_I are integral matrices. With this equivalence relation the number of Bravais classes is finite. To give an idea, in table I is given the number of Bravais classes for n=3,d=0,1,2,3. Since the matrices $\Gamma_E(R)$ of the holohedry form an n-dimensional point group which belongs to an n-dimensional (usual) Bravais class, one can assign each Bravais class in superspace to a Bravais class in n dimensions. To this correspond the different columns in table I: Tr = triclinic, M = monoclinic, O = orthorhombic, T = tetragonal, Tg = trigonal, H = hexagonal, C = cubic.

A Bravais class is characterized by its holohedry, i.e. by the elements $\Gamma_E(R)$, $\Gamma_I(R)$ and $\Gamma_M(R)$ or equivalently by the corresponding arithmetic point groups K_E, K_I and the matrix σ^r. Since σ^r is rational a lattice can be considered as a centering (denoted by C) of a lattice with $\sigma^r = 0$ (a P lattice). For n=3, d=1 the Bravais classes with K_E in the primitive monoclinic Bravais are given in table II.

Table I: Number of Bravais classes; n=3								
d	Tr	M	0	Tg	H	T	C	total
0	1	2	34	1	1	2	3	14
1	1	7	10	2	1	3	–	24
2	1	16	39	8	4	15	–	83
3	1	26	122	18	4	30	14	215

Table II: P–monoclinic Bravais classes; n=3; d=1					
System	Bravais class	σ-matrix	centering	generators	holohedry
$2/m$ $\bar{1}\,1$	$P^{P2/m}_{\bar{1}\,1}$	$\alpha\beta 0$	–	$\begin{array}{cccc}\bar{1}&0&0&0\\0&\bar{1}&0&0\\0&0&1&0\\0&0&0&\bar{1}\end{array}$	$\begin{array}{cccc}1&0&0&0\\0&1&0&0\\0&0&\bar{1}&0\\0&0&0&1\end{array}$
	$C^{P2/m}_{\bar{1}\,1}$	$\alpha\beta\tfrac{1}{2}$	$00\tfrac{1}{2}\tfrac{1}{2}$	$\begin{array}{cccc}\bar{1}&0&0&0\\0&\bar{1}&0&0\\0&0&1&0\\0&0&1&\bar{1}\end{array}$	$\begin{array}{cccc}1&0&0&0\\0&1&0&0\\0&0&\bar{1}&0\\0&0&\bar{1}&1\end{array}$
$2/m$ $1\,\bar{1}$	$P^{P2/m}_{1\,\bar{1}}$	00γ	–	$\begin{array}{cccc}\bar{1}&0&0&0\\0&\bar{1}&0&0\\0&0&1&0\\0&0&0&1\end{array}$	$\begin{array}{cccc}1&0&0&0\\0&1&0&0\\0&0&\bar{1}&0\\0&0&0&\bar{1}\end{array}$
	$C^{P2/m}_{1\,\bar{1}}$	$\tfrac{1}{2}0\gamma$	$\tfrac{1}{2}00\tfrac{1}{2}$	$\begin{array}{cccc}\bar{1}&0&0&0\\0&\bar{1}&0&0\\0&0&1&0\\\bar{1}&0&0&1\end{array}$	$\begin{array}{cccc}1&0&0&0\\0&1&0&0\\0&0&\bar{1}&0\\1&0&0&\bar{1}\end{array}$

The symbol for an arithmetic point group (in this case a holohedry) consists of 3 parts. The topline gives the point group K_E. To each element of K_E corresponds an element of K_I. The bottom line gives K_I (for d=1 consisting of elements ± 1). In front is a symbol characterizing the centering, i.e. σ^f.

The elements g_E form, if $g = (g_E, g_I)$ belongs to a superspace group, an n-dimensional space group G_E. The symbol for a superspace group consists also of 3 parts. The top line gives G_E. In the bottom line are the corresponding elements g_I. These do not form a space group. For d=1 the possible elements are 1, -1 and s (denoting a nonprimitive translation in V_I). The superspace groups for n=3, d=1 with G_E belonging to the primitive monoclinic Bravais class are given in table III.

The superspace groups are space groups in n+d dimensions. However, because of the additional structure, the equivalence classes are different from those of ordinary space groups.

Table III: Superspace groups for the primitive monoclinic Bravais class, n=3, d=1

G_E	Bravais class			
	$P^{P2/m}_{\bar{1}\,1}$	$C^{P2/m}_{\bar{1}\,1}$	$P^{P2/m}_{1\,\bar{1}}$	$C^{P2/m}_{1\,\bar{1}}$
Pm	P^{Pm}_{1}, P^{Pm}_{s}	C^{Pm}_{1}	$P^{Pm}_{\bar{1}}$	$C^{Pm}_{\bar{1}}$
Pb	P^{Pb}_{1}	C^{Pb}_{1}	$P^{Pb}_{\bar{1}}$	$C^{Pb}_{\bar{1}}$
P2	$P^{P2}_{\bar{1}}$	$C^{P2}_{\bar{1}}$	P^{P2}_{1}, P^{P2}_{s}	C^{P2}_{1}
$P2_1$	$P^{P2_1}_{\bar{1}}$		$P^{P2_1}_{1}$	$C^{P2_1}_{1}$
P2/m	$P^{P2/m}_{\bar{1}\,1}$, $P^{P2/m}_{\bar{1}\,s}$	$C^{P2/m}_{\bar{1}\,1}$	$P^{P2/m}_{1\,\bar{1}}$, $P^{P2/m}_{s\,\bar{1}}$	$C^{P2/m}_{1\,\bar{1}}$
$P2_1$/m	$P^{P2_1/m}_{\bar{1}\,1}$, $P^{P2_1/m}_{\bar{1}\,s}$		$P^{P2_1/m}_{1\,\bar{1}}$	$C^{P2_1/m}_{1\,\bar{1}}$
P2/b	$P^{P2/b}_{\bar{1}\,1}$	$C^{P2/b}_{\bar{1}\,1}$	$P^{P2/b}_{1\,\bar{1}}$, $P^{P2/b}_{s\,\bar{1}}$	$C^{P2/b}_{1\,\bar{1}}$
$P2_1$/b	$P^{P2_1/b}_{\bar{1}\,1}$		$P^{P2_1/b}_{1\,\bar{1}}$	$C^{P2_1/b}_{1\,\bar{1}}$

This means that one can not use the knowledge of space groups in dimension 2,3 (Tables of X-ray crystallography) and 4 (as determined by Fast and myself and by Wondratschek, Neubüser and Brown). Up to now superspace groups have been determined for n=2,3 and d=1.

IV. Examples

As examples we consider two compounds discussed earlier during this conference. The structure of γ-Na_2CO_3 has been determined by de Wolff and co-workers (ref.4). One has a case n=3, d=1.

space group of basic structure: C2/m;
wave vector of modulation: $q = \alpha(a_1^* + a_2^*) + \beta a_3^*$, or $\sigma=(\alpha\alpha\beta)$,

where $\alpha \approx 0.091$ and $\beta \approx 0.318$;

superspace group $\boxed{P^{C2/m}_{\bar{1}\,s}}$

The 4-dimensional pattern is left invariant by

i) the translations $(a_1,-2\pi\alpha),(a_2,-2\pi\alpha),(a_3,-2\pi\beta),(0,2\pi)$, where $2\pi\alpha = \Delta a_1$, etc.;

ii) a two-fold rotation along the unique axis combined with inversion of the phase;

iii) the mirror in the perpendicular plane combined with a phase shift π: nonprimitive translation $\frac{1}{2}a_4$.

The data for $\underline{1}T-TaS_2$ can be found in ref.5:

space group of basic structure: $P\bar{3}m1$;
there are 3 modulation waves: $(\alpha 0 1/3),(0\alpha 1/3),(\bar{\alpha}\bar{\alpha}1/3)$ with
$\alpha \approx 0.285$; since the third is a linear combination of the first
two and $\underline{a}_3^*$, one has d=2 and

$$\sigma = \begin{pmatrix} 0 & \alpha & 1/3 \\ \alpha & 0 & 1/3 \end{pmatrix},$$

the lattice in superspace belongs to the Bravais class $C_{p6m}^{P\bar{3}m}$;

this is a centering 001/3 1/3 1/3 of $P_{p61mm}^{P6/mmm}$;

the only superspace group with G_E = $P\bar{3}m1$ belonging to this
Bravais class is $\boxed{C_{p61m}^{P\bar{3}1m}}$

This group has a 5-dimensional lattice: the translation $\underline{a}_1$ in position
space is combined with a shift-$\alpha\underline{b}_1$ in internal space, $\underline{a}_2$ with $-\alpha\underline{b}_2$,
$\underline{a}_3$ with $-(\underline{b}_1+\underline{b}_2)/3$; the modulation function as a whole can be
shifted over $\underline{b}_1$ and over $\underline{b}_2$. The roto-inversion $\bar{3}$ is combined with
a 6-fold rotation in internal space, the mirror which interchanges
$\underline{a}_1$ and $\underline{a}_2$ is to be combined with a mirror which interchanges $\underline{b}_1$ and
$\underline{b}_2$. Of course, one cannot determine the superspace group from only
the $\underline{q}$-vectors. A precise analysis must give an answer to the question
if $C_{p6/m}^{P\bar{3}/m}$ or only a subgroup is the superspace group.

V. Conclusions

Like the ordinary space groups, superspace groups can be used for
the classification of structures, for selection rules and for the
characterisation of excitations. The description of structures has
been discussed in section IV. Selection rules follow from the proper-
ties of the Fourier components of a distribution invariant under a
superspace group. If the function $\rho(r)$ in superspace is invariant
under g = {R|v(R)}, then $\hat{\rho}(Rk) = \hat{\rho}(k) \exp \{i(Rk)v(R)\}$. This has
consequences for the intensities of diffraction spots: they have
point group symmetry and $\hat{\rho}(k) = 0$ if Rk = k and $kv(R) \neq 2\pi n$.
In this way one can explain systematic extinctions in structures not
having space group symmetry.

The excitations of modulated crystals can be characterized with
irreducible representations of the superspace group. As an example,
phasons transform indeed according to such an irreducible represen-
tation. Phonons in modulated crystals should be characterized by
irreducible representations of the superspace group G, not by the
space group of the basic structure, which is no longer a symmetry
group. However, one can show that the lattice D is an invariant sub-
group of G and that G/D is isomorphic to G_E. Hence representations of
the (ordinary) space group G_E are also representations of G. More-
over since K and K_E are isomorphic, often labels corresponding to
G_E can be used. However, one has to use another k-vector labelling,
because in position space there is no Brillouin zone left.

The results presented above have been obtained in a research together with prof. A. Janner. We have profited very much from stimulating discussions with prof. P.M. de Wolff.

References

1. P.M. de Wolff: these proceedings and Acta Cryst. A30(1974)777.
2. A. Janner and T. Janssen: Phys.Rev. B15 (1977) 643.
3. T. Janssen, A. Janner, E. Ascher: Physica 42 (1969) 41.
4. W.v. Aalst, J. den Hollander, W.J.A.M. Peterse, P.M. de Wolff: Acta Cryst. B32 (1976) 47.
5. F.J. di Salvo: these proceedings; J.A. Wilson, F.J. di Salvo, S. Mahajan: Adv. Phys. 24 (1975) 117.

STRUCTURAL PHASE TRANSITIONS AND SUPERCONDUCTIVITY IN A-15 COMPOUNDS

L. R. Testardi

Bell Laboratories

Murray Hill, New Jersey   07974

I. INTRODUCTION

Ten years after the discovery by Hardy and Hulm[1] of high superconducting transition temperatures in A-15 structure materials evidence of their structural instability emerged. Shull[2] in neutron diffraction work, and Batterman and Barrett in more extensive x-ray studies found that V_3Si underwent a structural transformation at temperatures not far above the superconducting T_c ($T_c \approx$ 17K). The transition from cubic to tetragonal structure shown by the x-ray data of Fig. 1 begins at $T_m \sim$ 20.5K and progresses rapidly (though apparently continuously) on cooling down to ~17K where the onset of superconductivity arrests the progress of the transformation. The tetragonal distortions are relatively small, $(c/a-1) \approx 2.2$ x 10^{-3} and with $\Delta c/c \sim -2\Delta a/a$ so that there is little change in volume from the cubic state. Structural domains (of differing c axes orientations) occur below T_m.

Mailfert et al.[3] and Vieland et al.[4] later reported a cubic to tetragonal transformation in Nb_3Sn ($T_c \approx$ 18K) similar to that in V_3Si but with the important differences of i) $(a/c-1)$ ≈ 5.2 x 10^{-3} (opposite tetragonality though still with approximately no volume change), ii) a (first order type) discontinuity in tetragonality at T_m (but no observable latent heat), and iii) $T_m \approx$ 45K.

The (apparent) thermodynamic second order nature of the transformation in V_3Si was noted by Anderson and Blount[5] who showed that a cubic to tetragonal transformation should be first order in the absence of a new internal order parameter. A sublattice distortion has been observed in Nb_3Sn from neutron diffraction studies
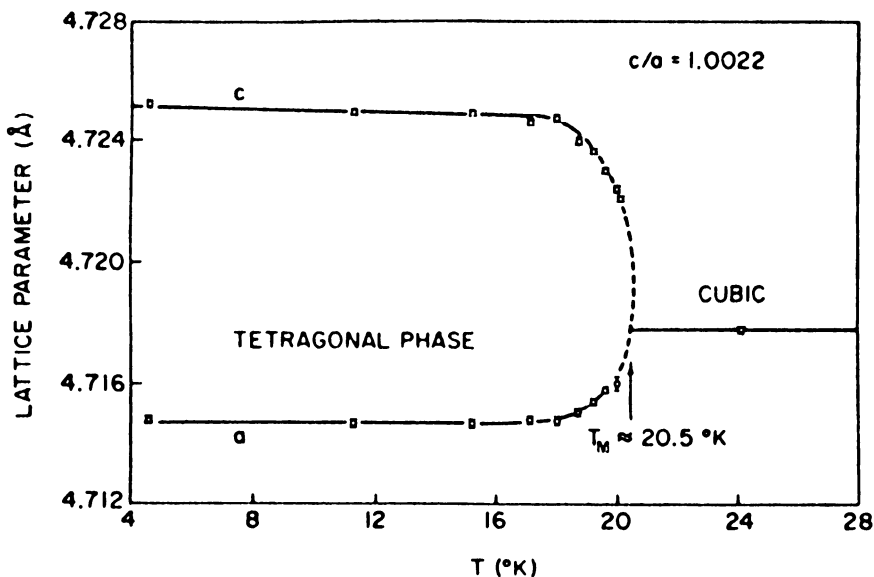
Fig. 1   The lattice parameters of V_3Si vs T showing the cubic to tetragonal transformation (after Batterman and Barrett[2]).

by Shirane and Axe.[5]   (Problem steming from V make a comparable determination in V_3Si too difficult.)   In the undistorted A-15 structure (compound formula A_3B) the transition metal atoms, A, from the orthogonal linear chains (see Fig. 2).   The sublattice distortion observed by Shirane and Axe in Nb_3Sn involves (along two of the chains) a pairing of Nb atoms in a manner similar to that expected for a Peierls distortion in a one dimensional system (see Fig. 3).

The structural transformation has now been observed in at least some samples of almost all of the high T_c ($\gtrsim$ 15K) A-15 super-conductors but has never been seen in the isostructural compounds having relatively low ($\lesssim$ 10K) T_c's.   (For further references and data see the review articles of references 6-8, herein.)   These experimental findings constitute part of the correlation and the conjectured causal relation between structural instability and high temperature superconductivity.   We present other evidence below.

II.   Instabilities and Transformation Effects on the Physical Behavior

There are numerous "anomalous" temperature dependences for the
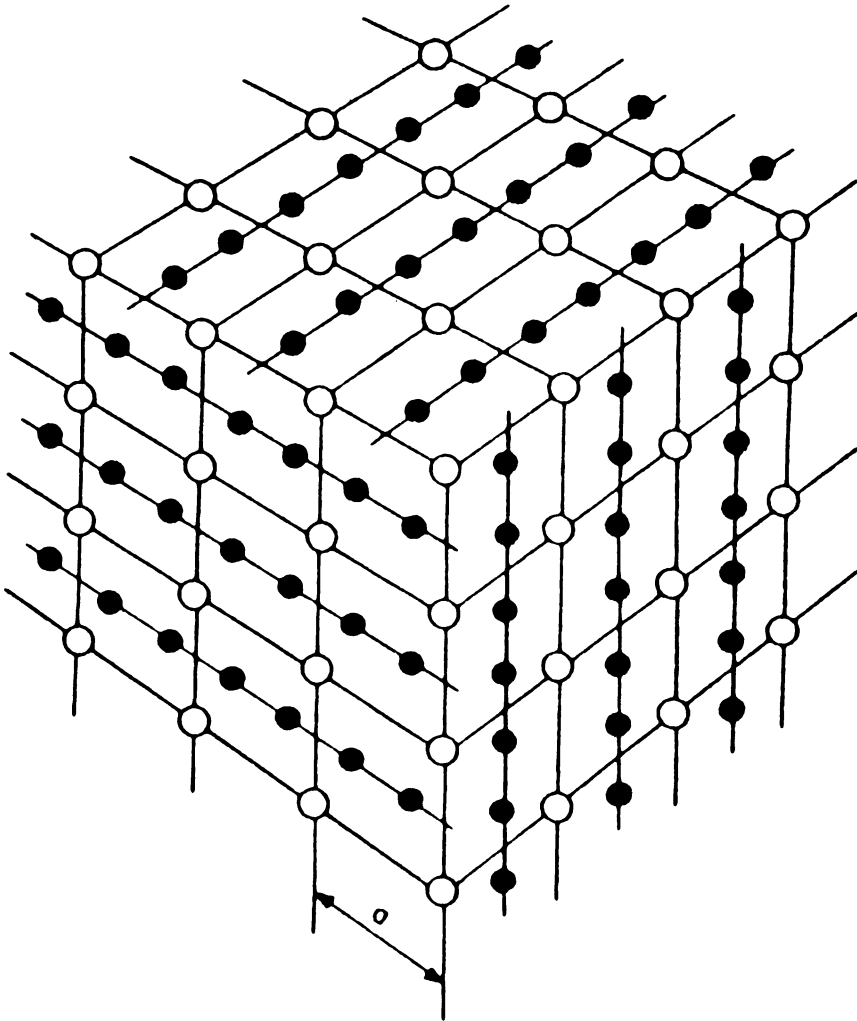
Fig. 2 The A-15 structure for compound formula A_3B. A atoms are
transition metals and form 3 linear orthogonal chains. B atoms
are usually nontransition metals (in high T_c compounds) and occur
at the bcc sites (center position not shown).

behavior of A-15 compounds, many of which are now reviewed as mani-
festations of the instability and precursors of the transformation
(see ref. 6 to 8 for futher details).

(a)   (b)
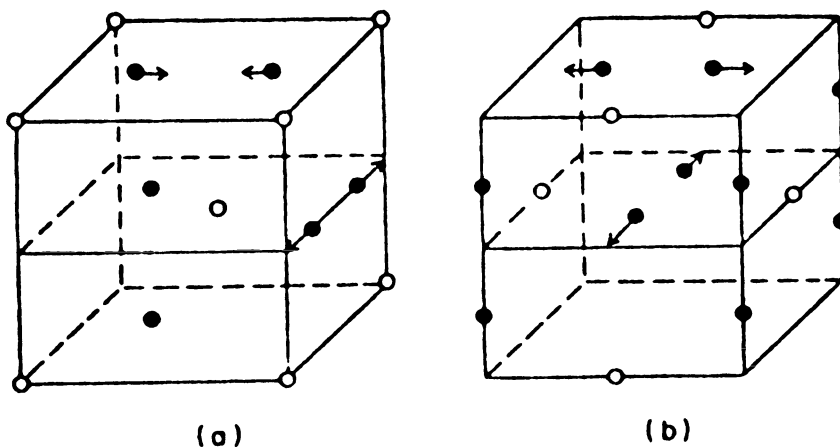
Fig. 3 The sublattice distortion due to the structural transforma-
tion in Nb_3Sn. (After Shirane and Axe[5].)

In V_3Si the elastic modulus $(c_{11}-c_{12})/2$, which defines the
shear restoring force for $[110]$ transverse waves with $[1\bar{1}0]$ polari-
zation, shows a positive temperature coefficient. This modulus
softens so greatly on cooling that it would appear (by extrapola-
tion) ready to vanish between 10K and 20K (see Fig. 4). For samples
which exhibit the Batterman-Barrett transformation the softening
is arrested at T_m but the occurrence of domains complicates the
ultrasonic experiments in which these data were obtained.

Not all samples exhibit the transformation (The metallurgical
factors are complicated but experiments show that transforming
samples have higher resistance ratios and some second phase inclu-
sions compared to nontransforming ones.). For V_3Si samples not
exhibiting the transformation it is superconductivity which arrests
the softening and, presumably, the need for the structural trans-
formation. A theoretical discussion of this observation has
recently been made by Ting and Birman.[10]

The deformation associated with soft shear modulus $(c_{11}-c_{12})/2$
is consistent with the (tetragonal) symmetry of the transformed
phase and with the lack of volume change associated with the trans-
formation. In this sense it is a specific precursor as well as a
driving force for the transformation.

The observations that superconductivity arrests the growing
structural transformation in a transforming sample, and arrests the
softening in a nontransforming sample, shows the similarity of the
interactions responsible for the structural instability and the
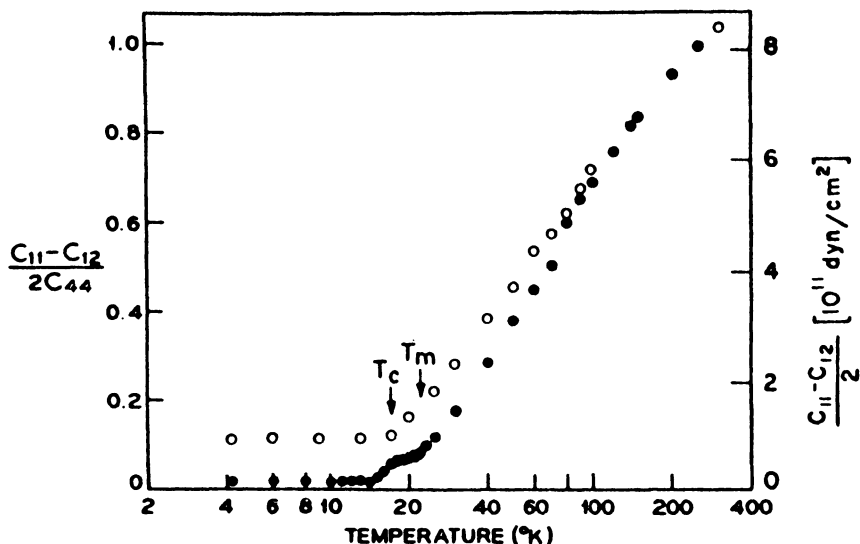
Fig. 4   Elastic modulus $(c_{11}-c_{12})/2$ vs T for transforming and non-transforming V_3Si (after Testardi et al.[9]).

high temperature superconductivity.

Keller and Hanak,[11] and Rehwald[12,13] observed a similar softening of $(c_{11}-c_{12})/2$ in Nb_3Sn. Again, several distinctive differences occurred. The modulus $(c_{11}-c_{12})/2$ was found to recover its stiffness below T_m (and above T_c) in Nb_3Sn (it does not in V_3Si where T_m and T_c differ by only $\sim 4°K$), and the modulus c_{44} shows considerably greater softening on cooling to $4°K$ in Nb_3Sn ($\Delta c/c \sim -50\%$) than in V_3Si ($\Delta c/c \sim -6\%$). The latter is not a trivial observation. Many theoretical treatments of the A-15 compounds assume noninteracting chains of transition metal atoms. Such a model will produce no anomalous temperature dependence for the c_{44} cubic face shear modulus.

Correlations of mode softening with superconductivity are observed. Shear mode softening is observed at least qualitatively (i.e. in polycrystalline samples) in all high T_c A-15 compounds (where investigated) but in none of the low T_c compounds.[9]

The occurrence of a near vanishing modulus in the ultrasonic experiments indicates that the basic instability for these compounds is macroscopic (q=0) rather than microscopic (q>0). Nevertheless our present ideas on the microscopic source of superconductivity require knowledge of the behavior of high frequency phonons to indicate some relationships of the structural instability

and the superconductivity. Shirane and Axe[5] obtained the phonon
dispersion relation for the soft (q=0) mode in Nb_3Sn shown in
Fig. 5. They find significant softening for q > 0 but considerably
less than that observed in the ultrasonic measurements. A "central
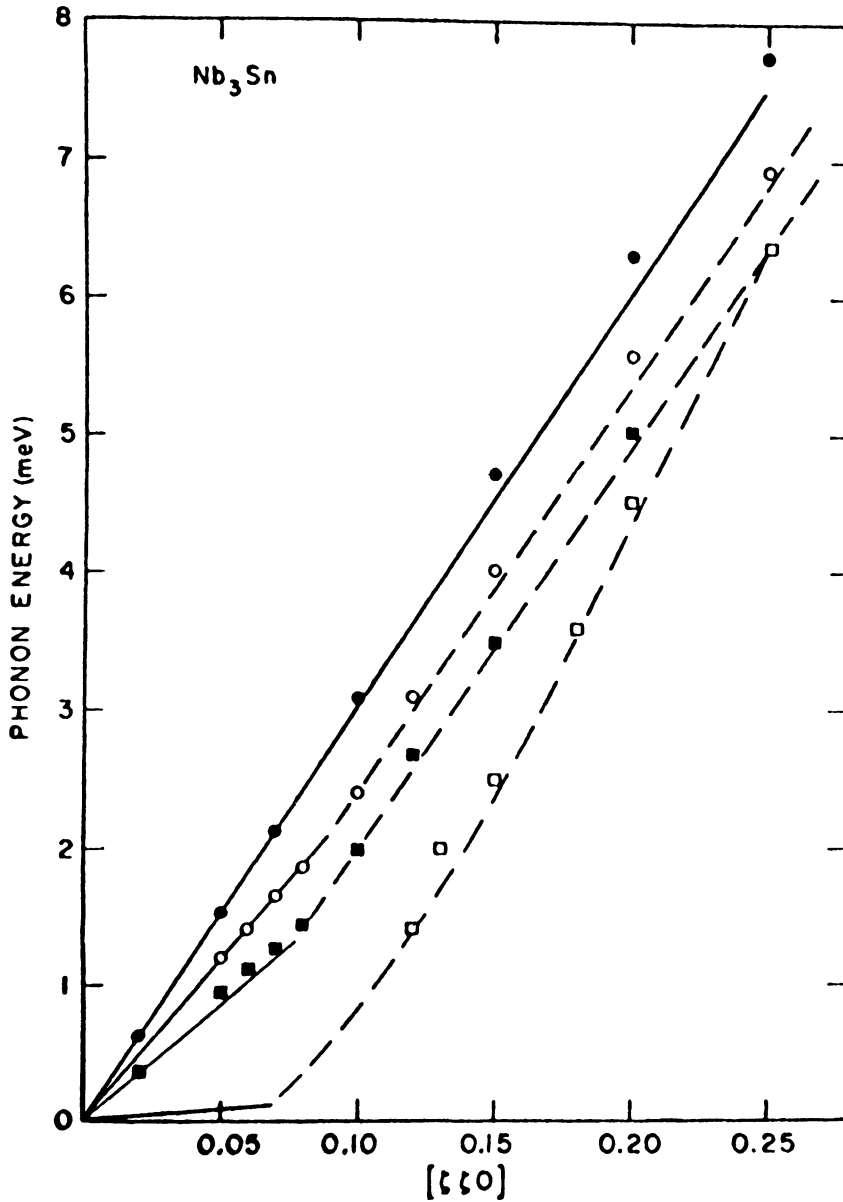
Fig. 5 Acoustic phonon dispersion curves for [110] waves with [1$\bar{1}$0]
polarization in Nb_3Sn (after Shirane and Axe[5]).

peak" is also observed on approaching the structural transforma-
tion from above.

The Karlsruhe group[14] (N. Nücker, W. Reichardt, H. Rietschel,
E. Schneider, P. Schweiss, and V. Tripadus) have obtained the total
phonon density of states F for V_3Si, V_3Ge, V_3Ga, Nb_3Al, and Nb_3Sn
at room and low temperatures. Some (but not considerable) mode
softening is found in the total density of states (7/8ths of which
is from optic modes) with evidence of optic as well as acoustic
mode softening. The results for Nb_3Sn as well as α^2F from tunneling
and α^2 (derived) are shown in Fig. 6. Note that the electron-phonon
interaction α^2 shows considerable variation with energy and is
strongest for the low frequency acoustic modes.

III. More on the Relation of Structural Instability and High
Temperature Superconductivity

It has been suggested[7,8,9] that structural instability - those
microscopic conditions which make a change in phase imminent -
promotes high temperature superconductivity. The structural trans-
formation, however, since it relieves these conditions, causes a
reduction in the T_c otherwise achievable. While a microscopic
theoretical justification in terms of soft modes and enhanced
electron-phonon interactions (α^2) is lacking, several experimental
tests support the empirical relation.

One such test is the relative variations of T_c and T_m with
chemical changes or stress. The former is more complicated and
limited results are available. Vieland and Wicklund[15] found that
$\sim 4\%$ Al added to transforming Nb_3Sn prevented the transformation and
caused T_c to increase by $\sim .5K$. Chu and Testardi[16] find that for
V_3Si hydrostatic pressure decreases T_m (while increasing T_c). In
Nb_3Sn pressure increases T_m while decreasing T_c. If instability
favors superconductivity one expects that whatever causes T_m
(always $> T_c$) to decrease/increase such that the instability is
greater/smaller at T_c will consequently cause T_c to increase/
decrease. The experimental observations are at least consistent
with this conjecture. Other data, including the pressure dependence
of the soft shear modulus and the strong anharmonic behavior of
these solids, is discussed in refs. 6 and 8.

IV. Instabilities, Unstable Phases, and Superconductivity

It is possible, then, that the structural instabilities which
occur at solid state phase transformations may be attended by con-
ditions favorable to high temperature superconductivity. If these
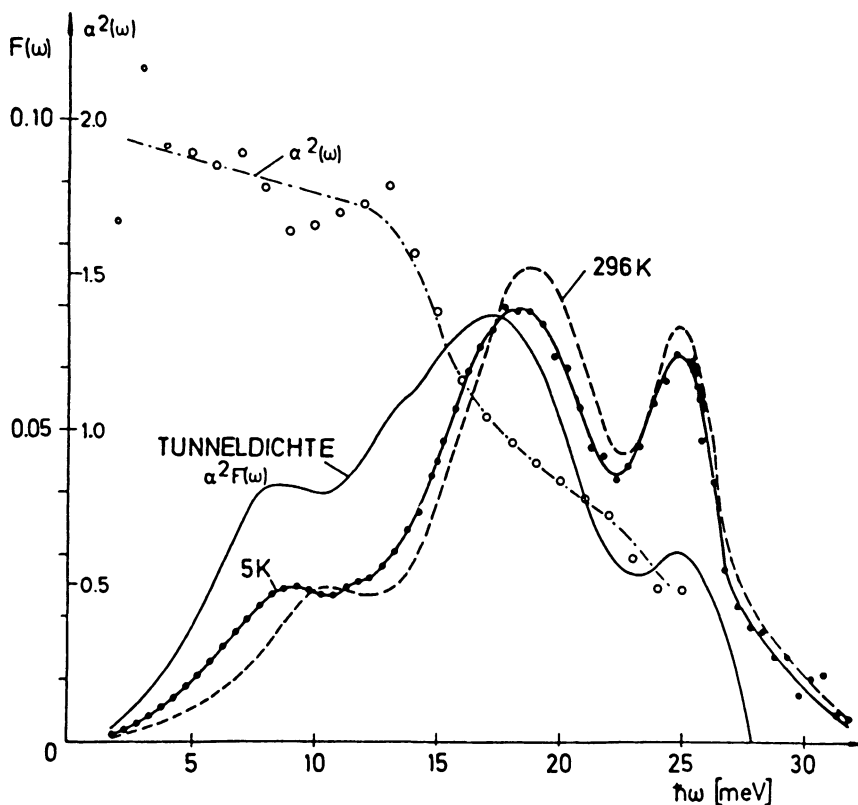
Fig. 6 Total phonon density of states, $\alpha^2 F$ (from tunneling) and α^2 (derived) for Nb_3Sn (after Karlsruhe group[14]).

conditions can be frozen in, rather than the transformation products which relieve the instability, higher T_c's may result. The first deliberate test of this was achieved[18] by sputtering (as a function of temperature) through the eutectoidal transformation temperature ($\sim 1100°C$) in a portion of the Mo-Re phase diagram (see Fig. 7). Sputtering at the eutectoidal boundary has frozen in a metastable structure with enhanced T_c. Similar though less dramatic effects have been seen in a large number of alloys.[17] Gavaler[18] was able to form metastable high T_c Nb_3Ge by hot substrate sputtering in high argon atmosphere.

V. Defects, Instabilities, and Superconductivity

The complexity of the A-15 compounds and the difficulty of
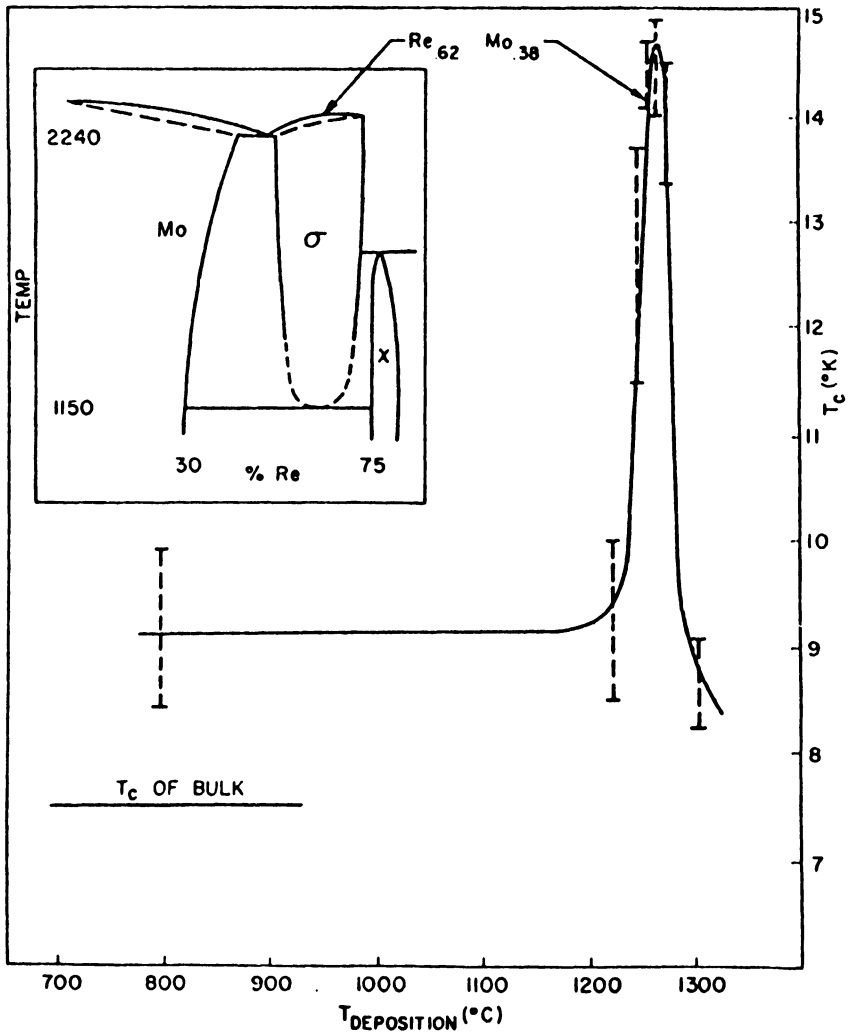
Fig. 7 T_c vs film deposition temperature for $Mo_{.38}Re_{.62}$ (after Testardi et al.[17]).

achieving near exact reproducibility in the physical properties of these materials has caused a number of investigators to consider the role of defects (see, for example, Hein,[19] and Testardi[20] for further references). "Defects" are generally described as i) non-stoichiometry, ii) antisite defects (A atoms on B sites and vice versa in the A_3B structure), iii) vacancies, interstitials, and impurities, iv) second phase inclusions, and v) strains.

Nonstoichiometry is often considered a crucial "defect" although recent work[21] indicates that, while important, these defects may not be as extremely detrimental to T_c as expected.

Blaugher et al.[22] showed from x-ray measurements that the unit cell compressibility of V_3Si at room temperature was considerably greater than that calculated from sound velocity data for pressures 0-10 kbar but was in agreement with expectations at higher pressures. The failure to agree with the ultrasonic predictions, which should apply near zero pressure, indicates that the physical process responsible for the additional mechanical compliance must require times too long to be observed at ultrasonic frequencies (20 MHz). Varma et al.[23] suggested that the result was due to a pressure dependent vacancy concentration.

A correlation between T_c (as-grown) and the electrical resistance ratio $\rho(300K)/\rho(25K)$ has been found in a number of A-15 compounds[21] (see Fig. 8 for Nb_3Ge data similar results obtain for other A-15's). This correlation, more general than that between T_c and composition, suggests that a key factor responsible for the wide range in T_c for these materials is the occurrence of a defect with universal character in A-15 compounds. Good evidence for this comes from the behavior of an initially high T_c film irradiated by 2 MeV ^{4}He particles where we find we can reproduce the as-grown correlation by varying the defect concentration only at constant chemical composition.[24] (The ^{4}He particles do not stop in the film.)

Sweedler et al.[25] have found that neutron radiation damage causes a large reduction in T_c to occur in a universally similar manner for all A-15 superconductors. They deduce from Bragg peak intensities that the effect is due to antisite defects. Similar reductions of T_c have been found with ^{4}He damage by Poate et al.[24] but it is concluded that the crucial defect lies, in part, in small bond distortions.

The defects have significant effect on the electrical resistivity and the lattice parameter as well. Increasing defect concentration causes not only a reduction in T_c and an increase in residual resistance but a reduction in the thermal part of the electrical resistivity as well.[24] Thus the defects strongly influence not only the superconducting properties but also the normal state properties which reflect the electron-phonon interaction responsible for the superconductivity.

The exact nature of the defect has not yet been established. Channelling measurements on V_3Si before and after defect formation indicate a strong tendency for bond distortions and quasi-amorphous structure. This behavior is more reminiscent of the covalently bonded group IV semiconductors rather than metallic bonding.
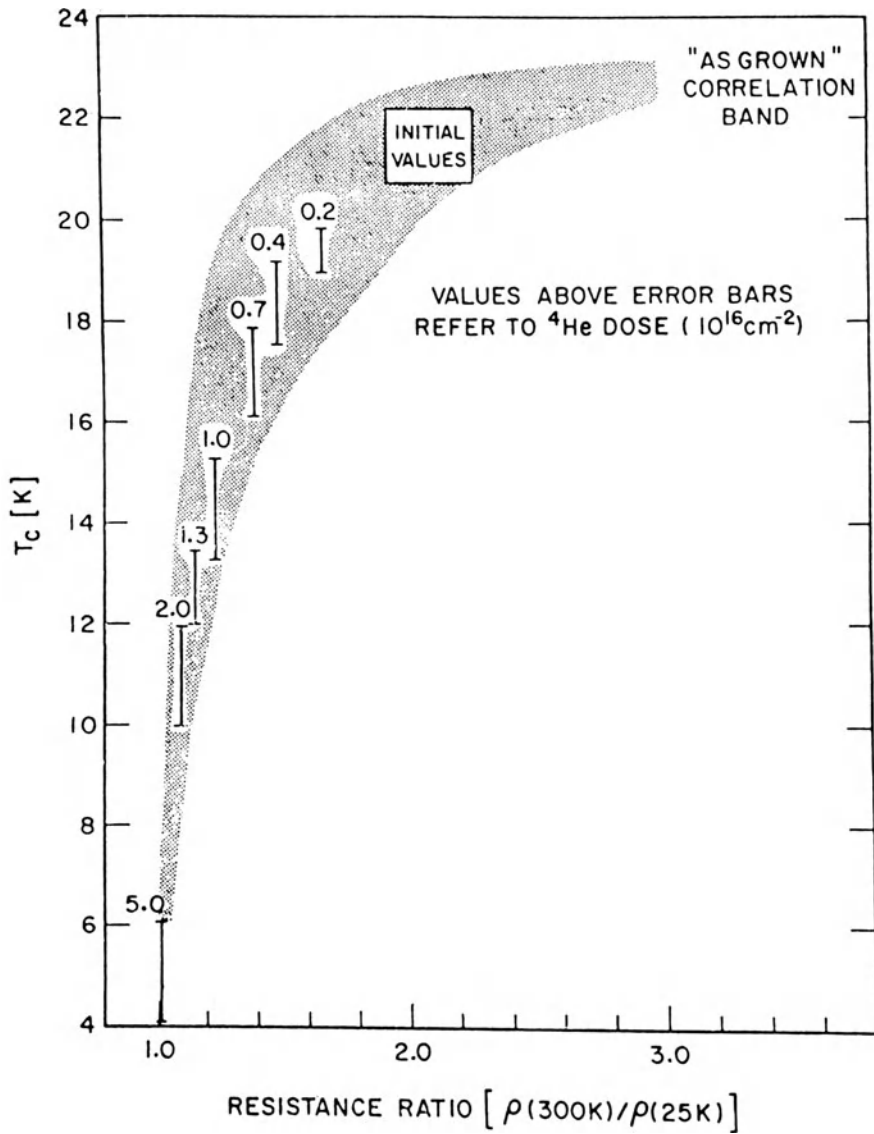
Fig. 8 T_c vs electrical resistance ratio for about 200 samples (shaded band) of V_3Si. Also shown is an initially high T_c film after various doses of 2 MeV ^4He damage (after Poate et al.[24]).

The ready tendency of the A-15 materials to form defects is another manifestation of their structural instability. The defect

problem, however, appears to be a deterrent to achieving the more unstable A-15 compounds having, perhaps, T_c's higher than any presently available.

References

1. C. G. Shull, MIT Annual Report-Research in Materials Science (1963-1964).
2. B. W. Batterman and C. S. Barrett, Phys. Rev. Lett. 13, 390 (1964); Phys. Rev. 149, 296 (1966).
3. R. Mailfert, B. W. Batterman, and J. J. Hanak, Phys. Lett. A24, 315 (1967); Phys. Status Solidi 32, K67 (1969).
4. L. J. Vieland, R. W. Cohen, and W. Rehwald, Phys. Rev. Lett. 26, 373 (1971).
5. G. Shirane, and J. D. Axe, Phys. Rev. B4, 2957 (1971); J. D. Axe and G. Shirane, Phys. Rev. B8, 1965 (1973).
6. L. R. Testardi, in "Physical Acoustics", ed. by W. P. Mason and R. N. Thurston (Academic Press, N.Y.) Vol. X, p.193 (1973) and Vol. XIII (an undate, to be published 1978).
7. M. Weger and I. B. Goldberg, in "Solid State Physics", ed. by F. Seitz and D. Turnbull (Academic Press, N.Y.) Vol. 28, p.1 (1973).
8. L. R. Testardi, Rev. Mod. Phys. 47, 637 (1975).
9. L. R. Testardi, W. A. Reed, R. B. Bateman, and V. G. Chirba, Phys. Rev. Lett. 15, 250 (1965); Phys. Rev. 154, 399 (1967); L. R. Testardi and T. B. Bateman, Phys. Rev. 154, 402 (1967).
10. C. S. Ting and J. L. Birman, Phys. Rev. B12, 1093 (1975).
11. K. R. Keller and J. J. Hanak, Phys. Lett. 31, 263 (1966); Phys. Rev. 154, 628 (1967).
12. W. Rehwald, Phys. Lett. A27, 287 (1968).
13. W. Rehwald, M. Rayl, R. W. Cohen, and G. D. Cody, Phys. Rev. B6, 363 (1972).
14. Karlsruhe group, in Progress Report KFK 2054 (1974) and KFK 2183 (1975), Gesellschaft für Kernforschung, M. B. H., Karlsruhe, Germany.
15. L. J. Vieland and A. W. Wicklund, Phys. Lett. A34, 43 (1971).
16. C. W. Chu and L. R. Testardi, Phys. Rev. Lett. 14, 766 (1974); C.W. Chu, Phys. Rev. Lett. 33, 1283 (1974).
17. L. R. Testardi, J. J. Hauser, and M. H. Read, Solid State Comm. 9, 1829 (1971); L. R. Testardi, J. H. Wernick, W. A. Royer, D. D. Bacon, and A. R. Storm, J. Appl. Phys. 45, 446 (1974).
18. J. R. Gavaler, Appl. Phys. Lett. 23, 480 (1973).
19. R. A. Hein in "The Science and Technology of Superconductivity", ed. by W. D. Gregory, W. N. Mathews, Jr., and E. A. Edelsack, (Plenum Press, N.Y.), Vol. 1, 333 (1973).
20. L. R. Testardi, to be published in "Cryogenics" (1977).
21. L. R. Testardi, R. L. Meek, J. M. Poate, W. A. Royer, A. R. Storm, and J. H. Wernick, Phys. Rev. B11, 4304 (1975); R. C. Dynes, J. M. Poate, L. R. Testardi, and R. H. Hammond, in "1976 Applied Superconductivity Conference", Stanford, to be published.

22. R. D. Blaugher, A. Taylor, and M. Ashkin, Phys. Rev. Lett. <u>33</u>, 292 (1974).

23. C. M. Varma, J. C. Phillips, and S. T. Chui, Phys. Rev. Lett. <u>33</u>, 1223 (1974).

24. J. M. Poate, L. R. Testardi, A. R. Storm, and W. M. Augustyniak, Phys. Rev. Lett. <u>35</u>, 1290 (1975).

25. A. R. Sweedler, D. G. Schweitzer, and G. W. Webb, Phys. Rev. Lett. <u>33</u>, 168 (1974).

26. L. R. Testardi, J. M. Poate, and H. J. Levinstein, Phys. Rev., to be published.

27. L. R. Testardi, J. M. Poate, W. Weber, and J. H. Barrett, to be published.

SUPERCONDUCTIVITY AND MARTENSITIC TRANSFORMATIONS IN A-15

COMPOUNDS

W. L. McMillan

Department of Physics and Materials Research Laboratory
University of Illinois at Urbana-Champaign
Urbana, IL 61801, USA

I would like to discuss the current theories of the martensitic transition in A15 compounds and our understanding of the interplay between the martensitic transition and superconductivity. Labbe and Friedel[1] proposed that the martensitic transition is driven by an electronic band Jahn-Teller effect. Gorkov[2,3] proposed an alternative model in which the martensitic transition is driven by the Peierls mechanism of an energy gap opening up near the Fermi energy. Both models are based on one-dimensional or quasi-one-dimensional energy band models which are inconsistent with APW band calculations.[4] Bhatt[5] has developed a very successful Landau theory which is based on the Gorkov model and which is, of course, free of any microscopic assumptions about the nature of the band structure. Bhatt[6] has also developed a microscopic theory using a band structure model based on the APW band structure. This model includes both the band Jahn-Teller effect and the Peierls effect and is therefore a synthesis of the Labbe-Friedel and Gorkov models. The effects on superconductivity are illustrated in a calculation by Bilbro,[7] based on the Gorkov model, in which both a Peierls energy gap and the BCS energy gap are included in the theory. I want to discuss the physical assumptions that go into the various theoretical models, without presenting much of the mathematics, and then discuss the predictions of the models and the comparison with experiment.

The most widely studied A15 compounds are Nb_3Sn and V_3Si. In Nb_3Sn there is a cubic to tetragonal structural transition at 46°K; the superconducting transition is at 18°K. In V_3Si these transitions occur at 21°K and 17°K. In the cubic phase of Nb_3Sn the Sn atoms sit on body-centered cubic lattice sites and the Nb atoms are on the cube faces at, for example, $(\frac{1}{4},\frac{1}{2},0)$ and $(3/4,\frac{1}{2},0)$ on

the xy face. The transition metal atoms form linear chains with
equally spaced atoms and with the chains running in the three ortho-
gonal directions on the three faces. This linear chain picture is
central to both the Labbe-Friedel and Gorkov models. At the mar-
tensitic transition the cubic cell distorts to a tetragonal one
with less than 1% distortion and the transition metal atoms on
two of the three sets of linear chains pair up as in a Peierls
transition. There is a drastic softening of one elastic constant
$(C_{11}-C_{12})$ as one approaches the transition from above.

      The corresponding phonon, the transverse (110) phonon with
$(1\bar{1}0)$ polarization, goes soft at long wavelengths and is the soft
mode of the transition.

      The Labbe-Friedel model is based on a one-dimensional band
structure for electrons moving along one linear chain. Consider
one atomic orbital of a particular symmetry on each atom. The
energy band for an x-direction chain is

$$E_K^x = \pm\ 2\beta_x\ \cos(k_x a/2)$$

where β_x is the x-chain transfer integral and "a" is the cubic
lattice spacing. The zone boundary is at π/a so that the two por-
tions of the band are degenerate at this point. In the cubic
phase $\beta_x = \beta_y = \beta_z$ so the band structures of the three types of
chains are identical except for a rotation of the momentum space
axes. In the tetragonal phase this degeneracy of the electronic
energy bands is broken. Suppose the unit cell dimension is de-
creased in the z direction and increased in the x and y directions
to maintain constant volume, then $\beta_z > \beta_x = \beta_y$ and the bottom of
the z-chain band is lower than the bottom of the x and y-chain
bands. If the Fermi level lies near the bottom of the bands in
the cubic phase electrons will be transferred in the tetragonal
phase from the x and y chains into the z chain and the total elec-
tronic energy will be lowered. If the electronic energy decrease
more than offsets the increased elastic energy the tetragonal phase
will be the observed phase at low temperature. Since the elec-
tronic entropy favors the cubic phase there will be a phase tran-
sition to the cubic phase at finite temperature. Thus the Labbe-
Friedel model qualitatively explains the martensitic transition in
A15 compounds although the quantitative fit to experiment is not
particularly good. Note the particular type of degeneracy which
is broken in this band Jahn-Teller effect. The degeneracy is the
equivalence of the band structure at different places in the
Brillouin zone required by cubic symmetry. Breaking the cubic
symmetry allows the bands to move and a redistribution of elec-
trons can lower the electronic energy. This effect occurs with
any band structure and is not a special property of one-dimension-
al bands. In order for this contribution to the energy to be im-
portant there must be a large density of states at the Fermi level

and the "electron phonon coupling constant" for splitting these
levels must be large enough.

The original Gorkov model assumed the one dimensional band
structure of equation (1) but concentrated on the degeneracy of
the energy bands at the zone boundary. In the tetragonal phase
the pairing of the transition metal atoms introduced a potential
with a periodicity of "a" and opened a Peierls energy gap at the
zone boundary. If the band is half full the Fermi level lies in
the Peierls gap and the electronic energy is lowered. The physics
is the same as the charge density wave models applied to the layer-
ed compounds. The degeneracy of energy levels at the zone bound-
ary (more particularly at the x point at the center of the face
of the cubic Brillouin zone) is a property of the A15 crystal
symmetry and is not a special property of the one-dimensional
bands. Gorkov[3/] has treated a band structure model including inter-
chain coupling to produce quasi-one dimensional bands. It is
necessary to assume that the bands are quite flat on the zone face
in order that the density of states affected by the Peierls gap
be large enough to explain the data.

Both the Labbe-Friedel and the Gorkov movels are electronic
models based on particular band structure assumptions. The prin-
cipal criticism of the models, it seems to me, is that the band
structure models are unrealistic. Matthiess[4/] has calculated APW
band structures for several A15 compounds and there are no bands
in Matthiess' calculation which resemble the one-dimensional or
quasi-one-dimensional bands used in the models.

One way of avoiding unrealistic band structure assumptions
while retaining the physical assumptions of the Gorkov model is to
work with a Landau theory similar to that applied to the layered
compounds. We assume that the electronic order parameters are the
amplitudes of three CDW's in the (100) directions. The CDW's are
locked in to the lattice with the wavelength equal to the cubic
lattice spacing and there are no phase fluctuations; the order
parameters are real. We write down the usual expansion of the free
energy in powers of the order parameters and gradients of the order
parameters. The theory is dynamical and we assume that the domi-
nant dissipation is electronic and arises from the redistribution
of electrons as the energy gap changes. The electronic order pa-
rameters are directly coupled to the amplitudes of the three opti-
cal phonons (at Γ) which modulate the transition metal atom separa-
tion. In the A15 structure these optical modes are bilinearly
coupled to elastic strain and we must include the three acoustic
phonon modes; we have a nonlinear dynamical problem with nine cou-
pled modes. We use the mean field approach and find the static mode
amplitudes which minimize the free energy. We then expand the free
energy around this minimum to find the mode frequencies. Since

dissipation is included the phonon modes have lifetimes and we
actually calculate the dynamical structure factor. This type of
theory can predict central peaks arising from the coupling of the
phonons to the overdamped electronic mode; however, for the A15's
no central peak is predicted.

The qualitative predictions of the theory fall into two cate-
gories. The first concerns the behavior of the soft mode. The
model predicts that the elastic constant $C_{11} - C_{22}$ goes to zero
at an extrapolated critical temperature T^* slightly below the first
order structural transformation temperature. This means that the
velocity of the long wavelength (110) transverse phonon with
polarization $(1\bar{1}0)$ goes to zero at T^*. As one moves out in momen-
tum space the phonon mode starts to recover its stiffness, and the
phonon softens dramatically only near Γ. A two-parameter fit pro-
duces quantitative agreement with the elastic constant versus
temperature and with the transverse phonon frequency versus tem-
perature and momentum. From this fit we find a correlation length
$\pi \xi_0 \approx 2a$ where a is the cubic lattice spacing.

The second group of qualitative predictions concerns the
behavior of the cubic terms in the free energy. Within the Gorkov
model the structural transition temperature is maximum if the
Fermi energy is equal to the x-point energy E_x of the relevant
energy band. Since the x-point energy is strain sensitive strain
(either compressive or tetragonal) changes the transition tempera-
ture T_m and there are cubic terms (proportional to the strain and
to the CDW amplitude squared) in the free energy which change sign
as E_F crosses E_x (say in an alloy series). The cubic terms con-
trol the sign of the tetragonality $(c/a - 1)$ but are weak enough
that they do not affect the magnitude of the tetragonality at low
temperature. Thus one expects $(c/a - 1)$ to change sign at con-
stant magnitude as E_F crosses E_x. This is observed in
$Nb_{3-x}Sb_xSn$[8] alloys. The sign of the pressure dependence of T_m is
controlled by the cubic terms and the pressure dependence of the
superconducting transition temperature is opposite to that of T_m.
These quantities should correlate with the sign of the tetra-
gonality and this correlation is observed to hold.

There are some quantitative cross checks of the Landau theory.
One uses up several experiments in determining parameters of the
theory and can only check the theory if there are more experiments
than parameters. The heat capacity jump in V_3Si is predicted to
be 0.7 joules/mole K and observed to be 0.4-0.5 joules/mole K,[9,10]
which is satisfactory.

There are problems in trying to predict Landau theory param-
eters from microscopic models. From the Gorkov or Peierls models
the electronic energy terms can be predicted from the electronic

density of states $N_\uparrow(0)$. The change in susceptibility is also pro-
portional to $N_\uparrow(0)$.[†] The values of $N_\uparrow(0)$ required to explain the
two results differ by a factor of three to five.

Now for Bhatt's microscopic calculation. Since the predict-
ions of the microscopic theory depend critically on the band
structure chosen, it is important to work with the most realistic
band structure model available. It is not possible to super-
impose the CDW calculation on the full APW calculation and one is
forced to work with simplified models. Fortunately, the density
of states near E_F in Matthiess' calculation is dominated by two
bands of $\delta_1(x^2 - y^2)$ character. These bands appear not to hy-
bridize strongly over much of the Brillouin zone. Bhatt's model
is a tight binding model with one $\delta_1(x^2 - y^2)$ orbital per transi-
tion metal atom, with nearest and next-nearest neighbor hopping
integrals which reproduce these two bands of Mattheiss' calcu-
lation. The hopping integrals are assumed to vary linearly with
interatomic spacing as the lattice distorts. Bhatt calculates the
band structure of the distorted lattice and computes the electronic
free energy which he then minimizes with respect to distortion
amplitude. There is essentially only one free parameter, the ratio
of the two hopping integrals, which he chooses to fit the ob-
served electronic density of states. The Gorkov energy term from
the Peierl's energy gap near the x-point is included in the cal-
culation; however there is insufficient phase space for this con-
tribution to be large enough to explain the phase transition.
There is, however, an electronic Jahn-Teller contribution from
non-degenerate bands far from the X-point which makes up the
deficit. Bhatt's model, therefore, includes both a Gorkov-
Peierls contribution and a Jahn-Teller contribution to the sta-
bility of the tetragonal phase. The agreement with a wide variety
of experiments on Nb_3Sn and V_3Si is nearly quantitive with dis-
crepancies typically between 25% and 50%. The correlation lengths
are large enough that the phonon entropy is not dominant but could
cause substantial corrections. In addition to providing a better
quantitative fit to experiment than the Labbe-Friedel or Gorkov
models, Bhatt's calculation contains important contributions from
both mechanisms and represents a synthesis of the earlier micro-
scopic models.

The effects of the martensitic transition on superconductivity
can be understood qualitatively very simply. As one approaches the
martensitic transition by lowering the temperature, by changing
pressure or by alloying, the lattice softens as the structure nears
the instability. This softening is most pronounced in the trans-
verse acoustic modes near Γ but it does extend over an appreciable
fraction of the Brillouin zone and the optic modes may be affected
as well. This lattice softening increases the electron-phonon
coupling constant and enhances the superconducting transition tem-
perature T_c. After passing through the martensitic transition the

lattice stiffens and T_c is reduced. I do not know how important this effect is quantitatively. The second effect is that,within the Gorkov model, there is a competition between the Peierls energy gap and the BCS energy gap. Bilbro has carried out detailed calculations for the A15 compounds. He finds that when the martensitic transition occurs at higher temperature the superconducting transition temperature is reduced (but only by 0.3 K for V_3Si) and that the martensitic transformation is arrested at T_c. Both of these effects are observed for V_3Si. The theory predicts that when the superconducting transition occurs first the martensitic transition is completely suppressed and the cubic phase is stabilized. Quantitatively the effect of the Pererls gap on T_c is small and the effect of the lattice softening is unknown. The theoretical models predict a peak in T_c near structural transitions and this behavior is observed in many systems. However, it is not clear that these effects "explain" the high T_c's of the A15 compounds. At the present time it appears to be more correct to state that the structural instability and the high T_c are both produced by the large density of states. More quantitative work on this question is highly desirable.

REFERENCES

1) J. Labbe and J. J. Friedel, J. Phys. Radium $\underline{27}$, 708 (1966).

2) L. P. Gor'kov, JETP Lett. $\underline{17}$, 379 (1973; Sov. Phys. JEPT $\underline{38}$, 830 (1974).

3) L. P. Gor'kov and O. N. Dorokhov, J. Low Temp. Phys. $\underline{22}$, 1 (1976); JETP Lett. $\underline{21}$, 310 (1975).

4) L. F. Mattheiss, Phys. Rev. $\underline{138}$, A112 (1965); Phys. Rev. B$\underline{12}$, 2161 (1975).

5) R. N. Bhatt and W. L. McMillan, Phys. Rev. B$\underline{14}$, 1007 (1976).

6) R. N. Bhatt, Ph.D. thesis, Dept. of Physics, University of Illinois at Urbana-Champaign (1976), to be published.

7) Griff Bilbro and W. L. McMillan, Phys. Rev.

8) L. J. Vieland, J. Phys. Chem. Solids $\underline{31}$, 1449 (1970).

9) J. C. F. Brock, Solid State Commun. $\underline{7}$, 1789 (1969).

10) J. P. Maita and E. Bucher, Phys. Rev. Lett. $\underline{29}$,931 (1972).

p-d HYBRIDIZATION, INCIPIENT LATTICE INSTABILITIES AND SUPERCONDUCTIVITY IN TRANSITION METAL COMPOUNDS

J. HAFNER, W. HANKE and H. BILZ

Max-Planck-Institut für Festkörperforschung

D 7 Stuttgart - 80, Germany

Neutron-scattering studies /1/ revealed the existence of anomalies in the phonon dispersion curves (Fig.1) of superconducting transition metal compounds such as the carbides and nitrides, thus establishing an empirical correlation between actual or incipient lattice instabilities and high superconducting transition temperatures. These instabilities are usually associated with a rela-
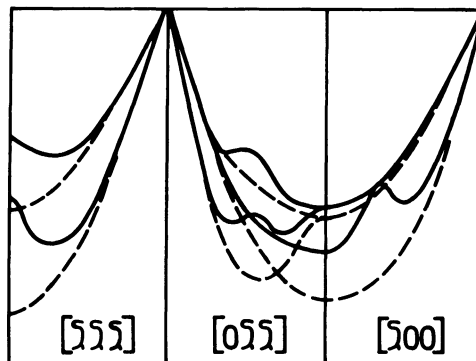
Fig.1: Acoustic phonon dispersion curves in transition metal compounds with NaCl structure. Solid lines with anomalies (NbC T_c=11°K, NbN 16.8°K, TiN 5.5°K), broken lines no anomalies (ZrC,TiC T_c <0.05°K, TiO <1°K, NbC$_{0.79}$<0.05°K).
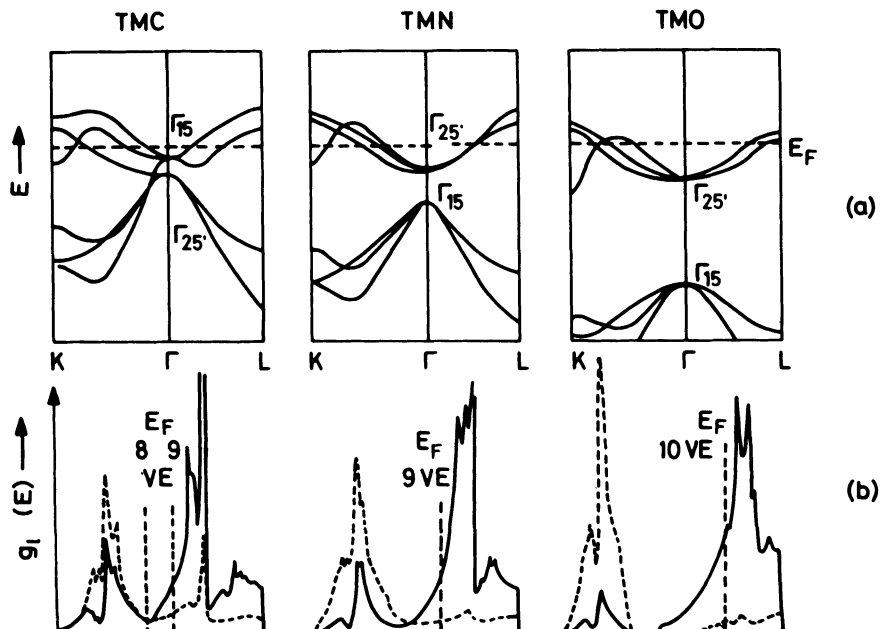
Fig.2: E($\vec{k}$) curves (a) and partial LCAO densities
of state (solid lines metal d_{xy}, broken lines
nonmetal p states) for the transition metal
carbides, nitrides and oxides (schematical,
after Neckel et al./2/). The approximate po-
sition of the Fermi level for different num-
bers of valence electrons is indicated.

tively high density of d-states at the Fermi level. How-
ever, this is in direct contradiction to the fact that
both the superconductivity and the phonon anomalies dis-
appear when we go from the carbides and nitrides to the
oxides, or introduce vacancies, whereas the d-electron
density of states further increases.

Band-structure calculations of the superconducting
carbides and nitrides of Schwarz and co-workers /2/,
which are confirmed by the X-ray emission spectra /3/,
show a strong p-d$_{xy}$ hybridization near the Fermi level
(Fig.2). The hybridization may be described as a cova-
lent-ionic bonding with the most important contributions
coming from planar (p-d)$_\pi$ interactions between nonmetal
and metal ions. The "p"- and "d"-type band complexes
(Γ_{15} and $\Gamma_{25'}$ at the center of the Brillouin zone) are

constructed of linear combinations of bonding $(d+p)_\pi$ and antibonding $(d-p)_\pi$ hybrides. For one specific transition metal the band-structure calculations show a decrease in the hybridization when we go from the carbides and nitrides to the oxides, although the total density of states increases. Similarly, in the substoichiometric carbides the empty p-states near the Fermi-level which are essential for the hybridization mechanism are no longer available /4/. If we compare the carbides of the group Vb and group IVb metals (with 9 and 8 valence electrons respectively) we see that the IVb carbides have a low density of states and very weak hybridization. Correspondingly, TiC, ZrC and HfC are non-superconducting, whereas for VC $T_c=8.7^\circ$K, for NbC $T_c=11.1^\circ$K and for TaC $T_c=10.4^\circ$K. For the nitrides of both groups, the p and d-states are strongly hybridized (TiN $T_c=5.5^\circ$K, ZrN $T_c=10.0^\circ$K, HfN $T_c=8.8^\circ$K, VN $T_c=8.5^\circ$K, NbN $T_c=16.8^\circ$K, TaC $T_c=14.3^\circ$K).

The aim of this paper is to demonstrate that in the superconducting materials the formation of covalent bonds due to the hybridization of metal-d_{xy} and nonmetal-p states leads to a resonance-like increase in the nonlocal dielectric response. The anomalous increase in the screening enhances the electron-phonon coupling, thus produces the phonon anomalies. Furthermore, it explains the high superconducting transition temperatures as resulting from a simultaneous increase of the electron-phonon coupling and a lowering of the phonon frequencies /5/.

The inverse dielectric screening matrix is the solution of the integral equation

$$\varepsilon^{-1} = 1 + v\chi\varepsilon^{-1} \tag{1}$$

where v is the electron-electron interaction. In a localized-orbital representation the polarizability χ is of a separable form /6-8/

$$\chi(\vec{q}+\vec{G}, \vec{q}+\vec{G}') = \sum_{ss'} A_s(\vec{q}+\vec{G}) \, N_{ss'}(\vec{q}) \, A_{s'}^+(\vec{q}+\vec{G}') \tag{2}$$

hence eqn.(1) is readily solved to yield

$$\varepsilon^{-1} = 1 + v A \left\{ N^{-1} - v \right\}^{-1} A^+ \tag{3}$$

The A_s may be interpreted as the form factor of a generalized charge density wave, the index $s=(\nu, \mu, e)$ standing for the set of quantum numbers of the localized orbitals ϕ_ν, ϕ_μ.

$$A_s(\vec{q}+\vec{G}) = \int \phi_\nu^*(\vec{r}) \, e^{-i(\vec{q}+\vec{G})\vec{r}} \, \phi_\mu(\vec{r}+\vec{R}_1) \, d^3r. \qquad (4)$$

N is the bare polarizability,

$$N_{ss'}(\vec{q}) = \sum_{k,n,n'} \frac{f_n(\vec{k})-f_{n'}(\vec{k}+\vec{q})}{E_n(\vec{k})-E_{n'}(\vec{k}+\vec{q})} \, e^{-i(\vec{k}+\vec{q})\cdot(\vec{R}_1-\vec{R}_{1'})}$$

$$\times \, e_\nu^*(n,\vec{k}) e_\mu^*(n',\vec{k}+\vec{q}) e_\mu(n',\vec{k}+\vec{q}) e_\nu'(n,\vec{k})$$

where $f_n(\vec{k})$ is the Fermi occupation factor, $E_n(\vec{k})$ the one-particle energies and $\vec{e}(n,\vec{k})$ is an eigenvector of the band-complex. N^{-1} may be viewed as the kinetic energy of the charge density waves, whereas V

$$V_{ss'}(\vec{q}) = \sum_{G''} A_s^*(\vec{q}+\vec{G}'') v(\vec{q}+\vec{G}'') A_{s'}(\vec{q}+\vec{G}'') \qquad (6)$$

represents their coulomb energy. Hence the screening matrix $S=(N^{-1}-V)$ coupling two charge density waves has the form of an energy denominator. In a metal it is convenient to separate out a diagonal (in G and G') part $\chi_o = -(\varepsilon_o-1)/v$ from the polarizability. The inverse dielectric matrix then becomes

$$\varepsilon^{-1} = \varepsilon_o^{-1} + v\varepsilon_o^{-1} A \left\{ N^{-1} - V \right\}^{-1} A^+ \varepsilon_o^{-1} \qquad (7)$$

Note that the interaction between the electrons in the localized states is now screened by the diagonal part ε_o^{-1}. The solution ε^{-1} provided by equ.(7) allows for an explicit inclusion of local-field effects, which are important whenever localized electrons participate in the screening. In the approximation of a local electron-ion potential the local-field correlation, i.e. the second term in equ.(7) gives the following contribution to the dynamical matrix /6-9/

$$E_{\alpha\beta}(\vec{q}) = \sum_{ss'} F_\alpha^s(\vec{q}) \left\{ N^{-1}(\vec{q}) - V(\vec{q}) \right\}_{ss'}^{-1} F_\beta^{s'}(\vec{q}) \qquad (8)$$

where $F_\alpha^s(q)$ is the component of the force in direction α experienced by an ion due to the coupling to the charge density wave.

There are two different schools of thought as to the interrelation between the dips in the phonon dispersion

curves and the structure of the screening matrix $S^{-1} =$
$(N^{-1}-V)^{-1} = N(1-VN)^{-1}$. Band-theorists have pointed out
that the intraband contribution to the bare susceptibili-
ty $N(\vec{q})$ from the bands crossing the Fermi level shows ma-
xima at the positions of the phonon anomalies, attributed
to a "nesting" of the Fermi surface /10,11/. However, the
interband contributions are larger and to some extent an-
ti-correlate with the intraband contributions. Furthermo-
re, recent work /12/ has established the importance of the
matrix-elements which again diminish the structure in the
polarizability. On the other side it has been proposed to
ascribe the phonon-dips to a resonance-like increase of
the screening matrix $(N^{-1}-V)^{-1}$ which becomes large when the
kinetic energy of the charge density waves is nearly
equal to their Coulomb energy, $N^{-1} \approx V$ /13/. The diffe-
rence between both interpretations is most easily demon-
strated by considering the schematic diagram expansion in
Fig. 3.
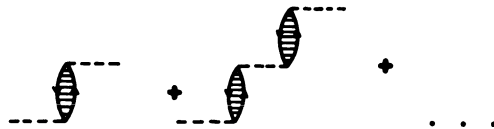
Fig. 3: Diagram expansion for the polarizability.

The band-theorists point of view corresponds to $S^{-1} \approx N$,
i.e. only the simple electron-hole loop diagram is con-
sidered. Our interpretation is a many-body theorists
standpoint: $S^{-1} = N/(1-VN)$ corresponds to a summation over
the infinite series of polarization diagrams. This is
a random-phase approximation for the local field effects,
plus local corrections for exchange and correlation,which
are incorporated in the electron-electron interaction v.
In our theory the driving mechanism for promoting the
phonon anomalies is the increase in the screening matrix.
The structure in the "bare" polarizability may be helpful,
but is not of decesive importance.

It is interesting to point out that, in a nonadia-
batic formulation, $||N^{-1}-V|| = 0$ corresponds to a plasmon
condition. This means that we can interpret the softening
mechanism as a tendency of the localized electrons to
move collectively. A coupling between a bare phonon
(screened by ε_o^{-1} only) and a plasmon mode can cause an in-
stability of the lattice. This coupling would be very
effective, provided an "acoustical" plasmon /14/ exists.
In our case, the plasmon frequency remains finite and
corresponds to the energy required to make a rigid trans-
lation of the localized electrons.

Using metal-d on-site interactions only in a para-
metrized version of the screening theory, Sinha and Har-
mon /15/ have been able to reproduce the anomalies in the
longitudinal dispersion branches. In their work the most
important role is assigned to the density of d-states at
the Fermi level - in striking disagreement with the trends
outlined in the introduction. The transverse anomalies,
which are decisive for the superconductivity and for the
lattice instabilities, cannot be reproduced by d-d inter-
actions alone /16/. In our study we consider a simple
band model based in the self-consistent band calculations
of Schwarz et al. /2/. The "p" and "d" band complexes
are described by linear combinations of bonding $(d+p)_\pi$ and
antibonding $(d-p)_\pi$ hybrids. The physical mechanism is
illustrated in Fig. 4 at the example of the anomalous lon-
gitudinal phonon at (0.5,0,0). In this direction alterna-
ting Nb and C atoms form $(pd)_\pi$ bonds (Fig.4a). The phonon
moves only the Nb atoms, the C atoms are at rest. The
covalent bonds from the C atoms to its Nb neighbours are
alternatively strengthened and weakened. Thus this dis-
placement pattern creates an electronic superstructure
(a charge density wave) which has just twice the perio-
dicity of the lattice (Fig.4c). These charge density fluc-
tuations are strongly coupled to the lattice and give ri-
se to the phonon anomalies. Of course this happens only if

C Nb C Nb C   Nb C Nb C   Nb C
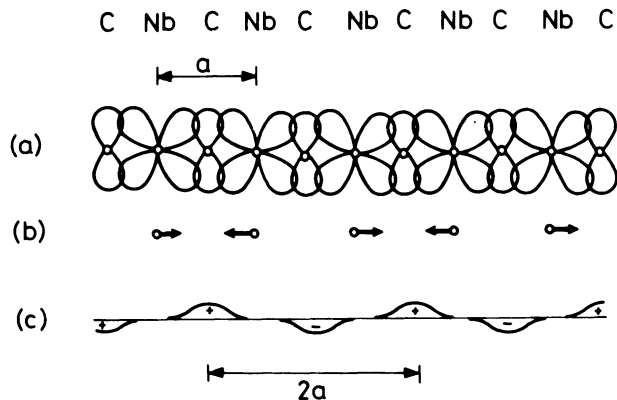
Fig. 4: (a) (p,d_{xy}) bonds along a chain of Nb and C
            atoms in the (100) direction.
        (b) Displacement pattern of a (0.5,0,0)-L
            phonon.
        (c) Charge fluctuation induced by the displacements.

the formation of this electronic superstructure is ener-
getically favourable. This is the case only if the kine-
tic and the Coulomb energies nearly cancel, i.e. when the
resonance condition $(N^{-1}-V) \simeq 0$ is satisfied. The dominant
p-d contribution to the polarizability stems from the
diagonal term $A_s N_s A_s^+$, which is proportional to the phase
factor $\sin^2(\vec{q}.\vec{R}/2)$ where $\vec{R}$ stands for the distance bet-
ween two hybrids in the plane π. The diagonal part of
the local field factor $V_{ss} \sim A_s v A_s$ has essentially the
same symmetry. Hence the resonance condition $(N^{-1}-V) \sim 0$
may be approximated very roughly by $\Delta E_{eff} - \sin^2(\vec{q}.\vec{R}/2)$
$\times |A_{pd}|^2 v \simeq 0$, where ΔE_{eff} stands for some effective ener-
gy difference between the bonding and anti-bonding hybri-
des. To satisfy this condition ΔE_{eff} must be small (i.e.
there must be bonding states just below and anti-bonding
ones just above the Fermi level) and the form factor $|A_{pd}|$
must be large enough. Because of the phase factor, the
concellation will occur at positions $q_\alpha = 0.5$ in reduced
units. The same phase factor occurs in the corresponding
contribution to the dynamical matrix (Eq.(8)), which
peaks at $q_\alpha = 0.5$. Higher overlap tends to shift the
peaks toward the zone boundary.

   The validity of our concept is illustrated by a mo-
del calculation for the acoustical vibrations in NbC.
This model is based on an LCAO-description of the p- and
d-states, nearest-neighbour hybrid overlap, an effecti-
ve-mass approximation for $N(\vec{q})$ and a local pseudopoten-
tial for the electron-ion interaction. Our model calcu-
lation, for which a quantitative agreement with experi-
ment is hardly to be expected, yields local minima in the
transverse as well as in the longitudinal dispersion
branches (Fig.5). The depth of the minima is reduced by
dehybridization and the non-locality of the (d-p) inter-
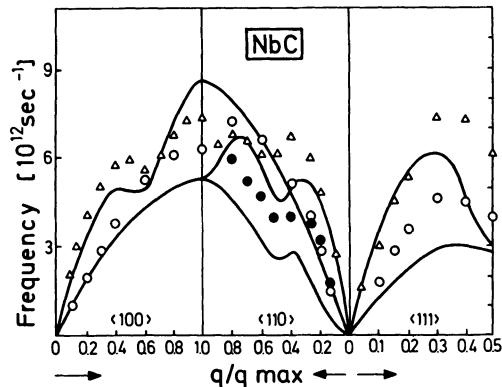
Fig.5: Dispersion curves for acoustic phonon branches in
       NbC. Circles and triangles show the exp.results/1/.

action is essential: if in the screening matrix $(N^{-1}-V)$ the local-field factor V is neglected, the phonon dips vanish at the scale of our figure.

To study the interrelation between the phonon-ano-malies and the high superconducting transition tempera-tures, we express the phonon-induced electron-electron attraction in the strong-coupling formulation by the non-local screening function. The screened electron-phonon coupling is determined by the gradient of the effective electron-ion potential, which we obtain by nonlocal screening of the bare electron-ion potential. The basic quantitiy is the electron-phonon spectral function $\alpha^2 F(\omega)$ which is given by /17/

$$\alpha^2 F(\omega) = \text{const.} \sum_{ll'} \sum_{tt'} \sum_{k,q} e^{i\vec{k}\vec{R}_l} e^{i\vec{k}+\vec{q})\vec{R}_{l'}}$$

$$\times (1-VS^{-1})_{lt} (\vec{F}^t(\vec{q})\vec{e}(q)) (\vec{F}^{t'}(\vec{q})\vec{e}(q)) (1-VS^{-1})_{t'l'}$$

$$\times \delta(E(k)-E_F) \; \delta(E(k+q)-E_F) \; \delta(\omega-\omega(q)) \qquad (9)$$

Here q stands for momentum and polarization of a phonon with frequency $\omega(q)$ and polarization vector $e(q)$, k is short for electron momentum and band index. It is imme-diately apparent that the resonance in the screening matrix leads to a selective enhancement of the spectral function: α^2 is no longer a constant or a slowly decaying function. As a first step we have calculated the electron-phonon coupling parameter $\lambda=2\int(\alpha^2 F(\omega)/\omega)d\omega$. Using our NbC model we have calculated for three different cases: (a) the local-field effects are neglected, $\lambda=0.4$, (b) they are included in evaluating the phonon frequencies, $\lambda=0.5$ and (c) they are taken into account both in the dynamical matrix and in the electron-phonon matrix-ele-ments, $\lambda=0.6$. This corresponds (via the McMillan equation with a Coulomb repulsion of $\mu^x=0.1$ and an adjusted pre-factor) to a relative change from $T_c=11.1°K$ to 6.2 K (neglecting V in the matrix elements) and further down to $T_c=2.7°K$ (neglecting V in the dynamical matrix too).Thus, the phonon anomalies are not alone responsible for the superconducting properties, the essential thing is to take the local-field effects in the spectral function in-to account.

In summary we have shown that covalent bond forma-tion due to (d-p) hybridization leads to an electronical-ly driven incipient lattice instability resulting from a resonance-like increase of the nonlocal inverse scree-ning matrix. This incipient instability produces a sof-

tening of the phonon frequencies and an increased elec-
tron-phonon coupling. Both effects together are respon-
sible for the high superconducting transition tempera-
tures.

REFERENCES

1   H.G. Smith and W. Gläser, Phys. Rev. Letters $\underline{25}$, 1611
     (1970) and $\underline{29}$,353(1972).
2   K. Schwarz, J. Phys.$\underline{C8}$,809(1975); A. Neckel, P.Rastl ,
     R. Eibler, P.Weinberger and K. Schwarz, J. Phys.$\underline{C9}$,579
     (1976).
3   L. Ramqvist,B.Ekstig, E.Källne,E.Noreland and R.Manne,
     J.Chem. Phys.Solids $\underline{32}$,149(1971)
4   K. Schwarz and N.Rösch, J. Phys. $\underline{F6}$,L433 (1976)
5   W. Hanke,J.Hafner and H.Bilz,Phys.Rev.Lett. $\underline{37}$,1560(1976
6   W. Hanke, Phys. Rev. $\underline{B8}$,4585,4591(1973)
7   L.J. Sham, Phys. Rev. $\underline{B6}$, 3581 (1972)
8   R.Pick, Phonons (Flammarion,Paris,1971),p.20.
9   S.K.Sinha,R.P.Gupta and D.L. Price,Phys. Rev. $\underline{B9}$,2564
     (1974).
10   M. Gupta and A.J.Freeman, Phys.Rev.Lett. $\underline{37}$,364(1976).
11   B.M.Klein,D.A.Papaconstantopoulos and L.L. Boyer,
     Sol. State Comm. $\underline{20}$, 937(1976)
12   R.P. Gupta and A.J.Freeman, Phys.Rev. $\underline{B13}$,4316 (1976).
13   W.Hanke and H.Bilz, In Proc. of the Int.Conf.on In-
     elastic Scattering of Neutrons (IAEA Vienna,1971).
14   H.Fröhlich,Phys.Lett. $\underline{A26}$,169(1968);B.N. Ganguly and
     R.F.Woods,Phys.Rev.Lett. $\underline{28}$,681 (1972)
15   S.K.Sinha and B.N.Harmon, Phys.Rev.Lett. $\underline{35}$,1515(1975)
16   W.Hanke,J.Hafner and H.Bilz, in Proc. of the Int.Conf.
     on Low-Lying Vibrational Modes and their Relation to
     Superconductivity and Ferroelectricity,Puerto Rico
     1975 (in print).
17   J.Bar-Sagi and W.Hanke, in Proc. of the Int.Conf. on
     Low-Lying Vibrational Modes and their Relation to
     Superconductivity and Ferroelectricity, Puerto Rico
     1975 (in print).

PSEUDO-SPIN APPROACH TO STRUCTURAL PHASE TRANSITIONS

R. B. Stinchcombe

Theoretical Physics Department
Oxford University, U.K.

ABSTRACT

Systems undergoing structural phase transitions and describable in a pseudo-spin formalism are reviewed, with particular emphasis on spin-phonon systems, Jahn-Teller systems and order-disorder and tunnelling ferroelectrics. Models for these systems are introduced, and their static and dynamical properties developed and compared to experiment. Mixed and diluted systems, and some aspects of the central peak problem and of critical behaviour are also discussed.

1. INTRODUCTION

This section begins with an extremely brief review of various types of lattice instability to put against a broader background the subset of inter-related systems to be discussed subsequently. Those systems will be ones for which a pseudo-spin description applies.

We list below examples of the various instabilities, roughly in order of decreasing applicability of the pseudo-spin description, giving for each type what drives the transition and the order parameter which develops below the transition temperature T_c.

A spin description obviously (partly) applies for linearly coupled spin-phonon systems; there the exchange of phonons can give rise to an effective spin-phonon interaction causing spontaneous ordering of the spin system for $T < T_c$ with possibly

an accompanying distortion of the lattice.   In this case the order
parameter is the thermodynamic average $<S^\alpha>$ of the component α of
spin which couples to the phonons, or the average displacement $<Q>$
of the phonon mode to which it couples.

A completely analogous situation occurs in the cooperative Jahn-
Teller transition, where the discrete levels of different ions are
coupled by phonons so that in the ordered regime the levels split
and again an appropriate phonon mode becomes macroscopically
occupied.   The order parameter is $<Q>$ for the phonon mode, or the
related electronic energy splitting, which can be written in terms
of $<\theta>$ where θ is an appropriate operator for the electronic states
of the ion, in simple cases just a (pseudo) spin operator.

Some transitions are driven by highly anharmonic phonon effects
and accompanied by an ordering of some constituents among various
positions of equilibrium.   A simple example of such order-disorder
transitions is Na NO_2 where the equilibrium positions relate to the
rotational configurations of the NO_2^- ions.   These can be
represented by a pseudo spin operator S^z in an effective Ising
Hamiltonian, with order parameter $<S^z>$.

The hydrogen-bonded ferroelectrics, typified by KDP, share
some of these characteristics: in these systems the equilibrium
positions are those of the protons in their double well.   The
pseudo-spin states $S^z = \pm 1$ then represent the two positions for
each proton, or in a more sophisticated picture (developed in §2)
they can refer to some symmetrised coordinate for all the protons
around a phosphate group.   The order parameter is $<S^z>$, or the
average of the symmetrised coordinate, or the spontaneous electric
polarisation associated with the ferroelectric transition
triggered by the proton motion.   Other hydrogen-bonded materials
like the isomorphs of KDP and also TGS and Rochelle Salt can be
described similarly.

The Peierls transition has some similarities to the Jahn-
Teller transition: the continuum of conduction band electron
states develops a gap at the fermi wave vector, for a half filled
band, as the (one dimensional) lattice doubles its unit cell.   The
order parameter is the energy gap, or the distortion coordinate, or
the occupation of the $q = 2k_F$ longitudinal acoustic phonon mode.
In the simplest (Frohlich) model for these systems, the analogue
of the pseudo-spin is the local conduction electron density.   It
would be inappropriate to represent this by a spin operator, but
some of the formal treatments of the Frohlich Hamiltonian parallel
those for pseudo-spin-phonon coupled systems.   The structural
transition in the A-15 high temperature superconducting systems
is similar in origin to the Peierls transition but differs from it
in being intrinsically three dimensional because of the role played
by the weak coupling between chains.

Anharmonic phonon effects are responsible for the properties of displacive ferroelectrics such as $K Ta O_3$, in which the order parameter is the distortion coordinate corresponding to the q = 0 soft mode; also for the behaviour of cell-multiplying structural transitions such as the cell-doubling transition in $Sr Ti O_3$ where the distortion coordinate has q = $(\frac{1}{2},\frac{1}{2},\frac{1}{2})^{\pi}/a$; and for the incommensurate transition in for example $Ba Mn F_4$. In all these cases a pseudo-spin picture is not obviously applicable.

To the extent to which the special properties of the super-ionics can be regarded as due to a sublattice melting, they are in a rather special class. The pseudo-spin picture could at best apply only in some sort of lattice-gas picture of the melting sublattice.

Despite the wide variety of these systems, and whether or not the pseudo-spin picture applies, the lattice instability is normally associated with some instability in the system to which the phonons are coupled - for example, other phonons (as in for example KDP) or conduction electrons (Peierls transition) or pseudo-spins (Jahn-Teller) and so on. And the distortion coordinate (or average of the soft mode eigenvector) is always one of the possible order parameters.

In the rest of this paper the discussion is confined to spin-phonon systems, Jahn-Teller systems and order-disorder and tunnelling ferroelectrics: these are the most strongly inter-related systems and also those describable by a pseudo-spin formalism. Occasional references will be made to parallel features of some of the other systems for which, though a different formalism may be more appropriate, some basic ideas are similar.

Reviews dealing with the systems listed above and particularly those not considered further here are: Jahn-Teller system[1,2], order-disorder and hydrogen bonded ferroelectrics[3,4], structural phase transitions[5-9], improper ferroelectrics[10], Peierls transition and A15 compounds[11-18], superionics[19]. The present volume, and reports of previous Geilo conferences[20,21] give comprehensive treatments of most of these topics.

The next section discusses models for the selected systems; it is followed by a section (§3) on general static and dynamical properties of the models; section 4 discusses mixed and dilute systems, while the final section (§5) considers some aspects of the central peak problem and critical properties, in an attempt to provide some background to current developments.

2. MODELS

(i) Spin-Phonon Systems

As an illustrative example we consider a spin $\frac{1}{2}$ system with
linear coupling of the z-component of spin S_i^z at site i to a
particular phonon branch.   Considering only that branch, the
Hamiltonian has the form

$$H = \sum_q \hbar \omega_q (a_q^+ a_q + \tfrac{1}{2}) + \sum_{iq} S_i^z A_q(i) (a_q^+ + a_{-q}) \qquad (1)$$

where $\quad A_{-q}^*(i) = A_q(i) \equiv A_q e^{i\underline{q}\cdot\underline{r}_i}$.

The last term can be written in the alternative form $\sum_{iq} S_i^z \Lambda_q(i) Q_q$,
where $\Lambda_q(i) = (2m\omega_q/\hbar)^{\frac{1}{2}} A_q(i)$, and represents a coupling of spin to
lattice displacement Q.   The exact canonical transformation

$$a_q \rightarrow \alpha_q = a_q + \sum_i A_q(i) S_i^z /\hbar\omega_q$$
$$S_i^z \rightarrow S_i^z \qquad\qquad\qquad\qquad\qquad (2)$$

which corresponds to a shift of phonon coordinates, takes the
Hamiltonian to the form

$$H = H_p + H_{SI}$$

where

$$H_p = \sum \hbar\omega_q (\alpha_q^+ \alpha_q + \tfrac{1}{2}) \qquad (3)$$

$$H_{SI} = -\tfrac{1}{2} \sum_{ij} J_{ij} S_i^z S_j^z \; , \qquad J_{ij} \equiv 2\sum_q A_q(i) A_q^*(j)/\hbar\omega_q \, , \quad (i \neq j). \quad (4)$$

This separation of the spin and phonon parts leaves the spins with
an effective Ising interaction, resulting from exchange of phonons.
The Ising model is perhaps the simplest exhibiting a phase
transition, and straightforward extensions provide descriptions of
Jahn-Teller systems (§2 (ii)) and tunnelling ferroelectrics
(§2(iii)).

The consequences of (3) and (4) are that the phonon frequencies
are unshifted, and that $\langle S^z \rangle$ becomes non zero below the Ising
transition temperature and so, since $\langle \alpha \rangle = \langle \alpha^+ \rangle = 0$,

$$\langle Q_q \rangle = - \sum_i \frac{\Lambda_q(i)}{m\omega_q^2} \langle S_i^z \rangle = - \frac{\Lambda_q}{m\omega_q^2} \langle S_q^z \rangle. \qquad (5)$$

This corresponds to a spin ordering and a lattice distortion, at
the value of q at which the Fourier transform J(q) of J_{ij}, equation
(4), has its maximum.   This is normally at q = 0, though
exceptions analogous to the antiferromagnet or spin spiral can
occur[22,23].

An important case is when the spin coupling is to strain, ε. This is usually treated separately from the phonons because of difficulties in applying boundary conditions to a strained crystal.[24,25] For uniform strain, the corresponding strain coupling term, and elastic energy terms (replacing or supplementing the phonon terms in (1)) are

$$\sum_i S_i^z \Lambda(i) \varepsilon + \tfrac{1}{2} c \varepsilon^2. \tag{6}$$

This leads to the development of a macroscopic strain below the transition. §3 will refer to approximate methods for obtaining quantities like $\langle S^z \rangle$, such as molecular field theory which is exact for strain coupling.

The above discussion actually applies more properly to pseudo-spin than to true spin systems : since the coupling to phonons is restricted by time-reversal invariance the linear coupling of a true spin operator to displacement as written in (1) could not actually occur, though coupling to the lattice momentum operator in principle could. A more interesting example of the spin-phonon system is single ion-lattice magnetostriction[26-28] where H is as above but with S_i^z typically a quadrupole operator. The coupling as written in (1) applies when S^z is a pseudo-spin operator, as it will be in all the subsequent discussions.

(ii) Jahn-Teller Systems[1,2]

The simplest situation occurs in Tm VO$_4$, and Tm As O$_4$, where (in zero field) a degenerate low lying doublet is linearly coupled to a non-degenerate phonon mode. All other electronic levels can be neglected as long as the Jahn-Teller splitting is sufficiently small. The two states $S^z = \pm \tfrac{1}{2}$ of a pseudo-spin-$\tfrac{1}{2}$ operator can be used to represent the two levels of the crystal field doublet for the ion at site i. The ion is coupled to a local lattice distortion through a Jahn-Teller energy term of the form $\sum_{iq} S_i^z \Lambda(i) Q_q$, which leads to a Hamiltonian of the same form (1) (or equivalently (3), (4)) as previously. As before, a lattice distortion $\langle Q_q \rangle$ develops below the transition at which $\langle S_i^z \rangle$ becomes non-zero.

In the molecular field approximation the Hamiltonian takes the form

$$H \approx -\sum_i \gamma_i S_i^z + \cdots$$

where the molecular field experienced by the 'spin' at site i is

$$\gamma_i = \sum_j J_{ij} \langle S_j^z \rangle. \tag{7}$$

This can be interpreted as the level splitting.

Care has to be taken with the J_{ii} term in (4) if molecular field theory is being used. Since $(S_i^z)^2 = \frac{1}{4}$, the J_{ii} term is a constant and without significance in an exact treatment. In molecular field approximation (which replaces $(S_i^z)^2$ by $2 <S_i^z> S_i^z$) it would appear as a spurious contribution unless subtracted out[24,29] and similar considerations apply if random phase approximations are used. It is therefore convenient to take J_{ii} as zero or, equivalently

$$J(q) = 2\left\{ |A_q|^2 / \hbar \omega_q - \sum_{q'} |A_{q'}|^2 / \hbar \omega_{q'} \right\}. \tag{8}$$

In Tm VO_4 and Tm As O_4, the strain terms (6) play an important role and have to be included in a straightforward generalisation of the above discussion.

Various additional generalisations of the model are required for other Jahn-Teller systems:

Coupling to a two-dimensional distortion gives rise to an interaction term of which the simplest form is $\sum \Lambda(S^z Q_1 + S^x Q_2)$, leading to an X-Y Hamiltonian in place of (4)[25,30]. This description applies to Pr $C\ell_3$[31] and Pr Eth SO_4[32]. Outside of mean field approximation, the X-Y form of the transformed Hamiltonian is only approximate (c.f. the discussion under (10), below).

Most systems have splitting in the high temperature phase, which corresponds to an additional term $- \sum_i \Gamma_i S_i^\alpha$ in the original Hamiltonian (1). If $\alpha = z$, the splitting acts like a longitudinal field in the resulting Hamiltonian (4), and no (sharp) transition occurs. This is the situation[33,34] in Ce Eth SO_4. In general the additional term prevents the transition unless $\alpha = x$. In this case, the 'transverse field' term is

$$-\sum_i \Gamma S_i^x. \tag{9}$$

This applies to Dy VO_4 which, having two Kramers doublets, is effectively a two-level system. The same term arises in Tm VO_4 if a (true) magnetic field Γ is applied since the otherwise degenerate doublet is magnetic. Spin and phonon parts cannot be exactly separated for this case, since the transformation accomplishing (2) is, for any operator A,

$$A \rightarrow e^{iS} A e^{-iS}, \qquad S = i \sum_q \frac{A_q(i)}{\hbar \omega_q} S_i^z (a_q^+ - a_{-q}). \tag{10}$$

The transverse field term (9) transforms to $- \Sigma \Gamma e^{iS} S^X e^{-iS}$, which still involves phonon terms since $[S^X, S] \neq 0$.   This can be approximately simplified[35,1], in a manner analogous to the treatment of Debye-Waller factors to yield a Ham quenched[36] effective transverse field.   In molecular field approximation these complications do not appear, and the resulting Hamiltonian involves an unperturbed (shifted) phonon part and a spin part of 'transverse Ising' form

$$H_{S2} = -\sum_i \Gamma S_i^X - \frac{1}{2}\sum_{ij} J_{ij} S_i^z S_j^z .$$

(11)

This model, which also applies for rare-earth group V compounds with the NaCℓ structure[37] and the tunnelling ferroelectrics[3,4,38], has been rather fully treated in the theoretical literature[38-43] and its properties will be discussed in §3.   The fact that the observed phonon frequencies in for example Dy VO_4 appear to be almost unaffected by the Jahn-Teller interaction[44] indicates that the molecular field approximation holds well there, implying long range effective interactions.

Other generalisations of the model are required for example for the four level system Tb VO_4, which can be represented by two pseudo-spin $\frac{1}{2}$ operators[45,44], or for triplet ground state systems[46].

The pseudo-spin method is most useful when only a limited number of low lying levels is involved.   The next subsection considers its use for ferroelectrics, particularly of the tunnelling type.

(iii) Order-disorder and Tunnelling Ferroelectrics[3-6,29,38,47]

The pseudo-spin method was first used for order-disorder ferroelectrics with well-defined positions of equilibrium (eg Na NO_2[48,49]).   A generalisation of this type is the KDP class of (hydrogen-bonded) ferroelectrics, for which the descriptions have evolved from simple pseudo-spin models to more sophisticated models[50,4] which include pseudo-spin phonon coupling and make evident the relationship to soft mode behaviour.

The crucial feature of all these models is the existence of a double well (for the coordinate of a single proton in simple models, or more generally for some coordinate related to the collective proton displacement which freezes in below T_c).

The simple spin model[3,47] is developed as follows.   With ξ_i representing the coordinate of a single proton at site i, the simplest double well potential is

$$V = -\frac{1}{2}a \xi_i^2 + \frac{1}{4}b \xi_i^4$$

(12)

with minima at $\delta = \pm (a/b)^{\frac{1}{2}}$. The two values $S_i^z = \pm \frac{1}{2}$ refer to which well the proton at i occupies. Tunnelling between the two wells causes a splitting Γ, which is accommodated by the following term in the Hamiltonian

$$-\sum_i \Gamma S_i^x .$$

(13)

Coupling between displacements of different protons, through a harmonic potential $V_{ij}(\xi_i - \xi_j)^2$ then leads to the spin inter-action term

$$-\frac{1}{2} \sum_{ij} J_{ij} S_i^z S_j^z ,$$

(14)

and we recover the transverse Ising Hamiltonian (11).

This development is inadequate in several respects. First, all but the lowest two states in the well were neglected. This approximation will fail[51] if the separation of the higher levels becomes comparable to J, Γ, where a displacive situation more correctly treated in an anharmonic phonon picture will occur.

Secondly, in the case of a specific example such as KDP, the nature of the coupling between different protons around the same PO_4 group has to be more carefully considered for two related reasons: (a) the soft mode for the system is a particular (B_2 symmetry) mode involving all the protons[52], as shown in Figure 1(a), and (b) certain configurations of the protons around a PO_4 group are energetically favoured over others[53,54]. In order of increasing energy the configurations are: the B_2 type displacement with two protons "in" (adjacent to the PO_4 group) and two "out", other displacements (E_1, E_2 symmetry) with two protons in and two out, arrangements with three in and one out or one in and three out, and least favoured of all is that (A_2 symmetry) with four in or out.

Both of these points can be overcome[29,4] by using symmetrized local normal coordinates ξ_α for the four protons, rather than a single proton coordinate, and corresponding to the B_2, A_2 and E modes shown in Figure 1(b). The $\xi_\alpha (\alpha = B_2, A_2, E_1$ or $E_2)$ are appropriate linear combinations of the four proton coordinates q_n, n = 1,...4. The effective potential of the four protons surrounding the PO_4 group in the centre of cell i can then be written as a power series in the ξ-variables. The quadratic terms are

$$\sum_\alpha A_\alpha \xi_\alpha^2(i)$$

(15)
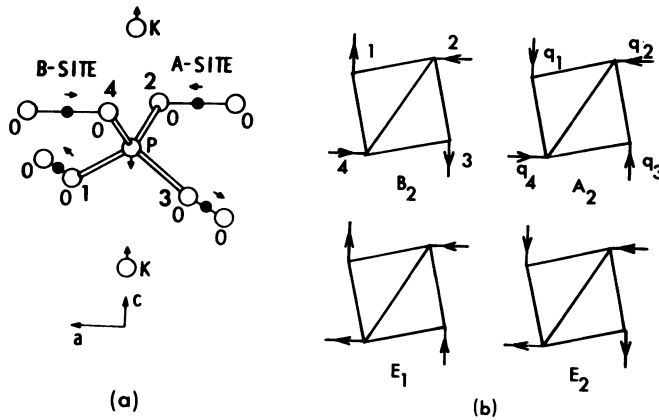
Figure 1. (a) Soft mode of KDP (after Cochran[52])
          (b) Symmetrised proton displacements in KDP.   The B_2
mode corresponds to the soft mode depicted in (a).

where $A_{E_1} = A_{E_2}$.   By putting each q_n equal to $\pm \delta$ it should be
possible to match the A_α to the energies of the Slater-Takagi
model[53,54].   This model, however, involves one more parameter
than so far appears in (15).   This can be accommodated by adding
to (15) symmetry - allowed quartic terms of the form

$$\frac{1}{2} \sum_{n=1}^{4} B q_n^4 - W \prod_{n=1}^{4} q_n .$$ (16)

Additional terms arise from considering the same types of
quadratic and quartic coupling between protons (lying in different
cells) which are adjacent to a PO_4 group at the boundary of the
unit cell.   These contributions, which involve the same para-
meters as in (15), (16) generate terms of the form ... $\xi(i) \xi(j)$,
and ...$\xi(i) \xi(j) \xi(k) \xi(\ell)$, where cells i, j, k, ℓ are all adjacent
to the same PO_4 group.

    The energies of the Slater-Takagi model make it plausible that
in the resulting combined Hamiltonian the coefficient of $\xi_{B_2}^2(i)$ is
negative, and all other $\xi_\alpha^2(i)$ terms have large positive
coefficients.

    Since (16) gives rise to a term

$$\frac{1}{8}(B - \frac{1}{2}W) \, \xi_{B_2}^4(i)$$ (17)

a double well then arises for the ξ_{B_2} coordinate provided $B > \frac{1}{2}W$, while all other ξ_α are stable and do not play an important role in the phase transition. A pseudo-spin S_i can then be associated with the ξ_{B_2} (i) of each unit cell and the tunnelling term (13) is recovered. Of the quadratic and quartic intercell terms referred to earlier, the quadratic terms in ξ_{B_2} (i) ξ_{B_2} (j) then give the usual Ising coupling (14), where i and j label adjacent cells; the quartic terms ξ_{B_2} (i)...ξ_{B_2} (ℓ) give an additional four-spin coupling proportional to

$$S_i^z S_j^z S_k^z S_\ell^z. \tag{18}$$

The above discussion depends on arguing that coupling terms between ξ_{B_2} and the other ξ_α are either small by symmetry (e.g. for low k modes) or can be accommodated as small correction terms to the coefficients by 'decouplings' of the random-phase type[4].

In addition to the near-neighbour pseudo-spin couplings arising above, longer range pair interactions arise from the dipole-dipole interactions with more distant protons.

Only proton motion was so far considered. The spontaneous polarisation arises from the resulting largely harmonic motion of other atoms in the unit cell. Their coupling to the proton soft mode will give additional terms in the Hamiltonian of the form[50,4]

$$\sum \left(S_i^z \Lambda_q^z(i) Q_q + S_i^x \Lambda_q^x(i) Q_q \right) \tag{19}$$

where the Λ^x term is small and unimportant for KDP, and will be neglected in the remainder of this discussion. In addition, strain coupling terms can arise, as in (6).

The transformation (10) can again be applied to approximately uncouple 'spin' and phonon parts, resulting in a transverse Ising model with a quartic term, coming from (18) and a quadratic term arising from three sources: (a) the ξ_{B_2} (i) ξ_{B_2} (j) terms, (b) the dipole-dipole interaction, and (c) the phonon exchange term (analogous to (8)).

(iv) Displacive Ferroelectrics[5,6,55-57]

Up to a point, the development would be similar for a displacive ferroelectric. The crucial difference occurs at the introduction of the pseudo-spin, which is appropriate provided a double well arises and that the mean square fluctuation in the soft mode local coordinate ξ_α (i) remains large even above the transition. If this is not the case, an anharmonic picture would seem more suitable. The following simple discussion[55,56] gives

the main characteristics of this picture. The lattice vibrational
energy is expanded in terms of displacements from the high
temperature configuration, using appropriate normal coordinates
(and, for simplicity, considering only fourth order anharmonic
terms):

$$H = \tfrac{1}{2} \sum \Omega \, \xi^2 + \sum W \, \xi \, \xi \, \xi \, \xi .$$

(20)

The effective Hamiltonian resulting from averaging pairs of ξ's in
the anharmonic term is

$$H_{eff} = \tfrac{1}{2} \sum \omega_q^2 \, \xi_q^2 \, ,$$

$$\omega_q^2 = \Omega_q^2 + \sum_k V(q,k) \langle \xi_k \xi_k \rangle = \Omega_q^2 + \sum_k \frac{V(q,k)}{2\omega_k} \coth \tfrac{1}{2}\beta\omega_k$$

(21)

where V is a coupling constant appropriately related to W.

If, for a particular mode and wave vector (q_c), $\Omega_{q_c}^2$ is so
negative that zero point fluctuations alone are not sufficient to
stabilize it $(\Omega_{q_c}^2 < -\tfrac{1}{2} \sum V/\omega)$, the displacive transition occurs at
$T = T_O$ such that $\omega_{q_c}^2 = 0$.

For $T > T_O$, $\omega^2 > 0$ and the reference configuration is stable.

For $T < T_O$, a non-zero $\langle \xi_{q_c} \rangle$ freezes in to stabilize a
distorted lattice having $\omega^2 > 0$, and the averaging used to obtain
H_{eff} has to be modified to include the additional non-vanishing
averages.

In not requiring spin-like behaviour for the local soft mode
coordinate, this is more general than the pseudo-spin approach
(but less easy to approximate to obtain spin-model behaviour where
it is appropriate).

(v) Hamiltonians

This section gathers together the basic Hamiltonians for the
principal pseudo-spin systems discussed above, omitting strain
terms

(a) $$H = \sum_q \hbar\omega_q \left(a_q^+ a_q + \tfrac{1}{2}\right) + \sum_q A_q \, S_q^z \left(a_q^+ + a_{-q}\right)$$

(22)

(simple spin-phonon, or simplest Jahn-Teller system: Tm VO$_4$ in
zero field).   (22) becomes, after exact canonical transformation
(10),

$$H = H_p + H_{S1} \equiv \sum_q \hbar \omega_q (\alpha_q^+ \alpha_q + \tfrac{1}{2}) - \tfrac{1}{2} \sum_{ij} J_{ij} S_i^z S_j^z \qquad (23)$$

with the Ising interaction given by (4) and (8).

(b) $$H = \sum_q \hbar \omega_q (a_q^+ a_q + \tfrac{1}{2}) - \sum_i \Gamma S_i^x + \sum_q A_q S_q^z (a_q^+ + a_{-q}) \qquad (24)$$

(cooperative Jahn-Teller systems Dy VO_4, or Tm VO_4 with applied field).   Canonical transformation (10) takes (24) approximately to the form

$$H \approx H_p + H_{S2} \equiv \sum_q \hbar \omega_q (\alpha_q^+ \alpha_q + \tfrac{1}{2}) - \sum_i \Gamma S_i^x - \tfrac{1}{2} \sum_{ij} J_{ij} S_i^z S_j^z \qquad (25)$$

which involves the Transverse Ising Hamiltonian with exchange again given by (4) and (8).

(c) $$H = \sum_q \hbar \omega_q (a_q^+ a_q + \tfrac{1}{2}) - \sum_i \Gamma S_i^x - \tfrac{1}{2} \sum_{ij} L_{ij} S_i^z S_j^z$$
$$- \sum_{ijk\ell} K_{ijk\ell} S_i^z S_j^z S_k^z S_\ell^z + \sum_q A_q S_q^z (a_q^+ + a_{-q}) \qquad (26)$$

(Hydrogen-bonded ferroelectrics.   .The Ising pair interaction L_{ij} includes the dipole-dipole part).   The canonical transformation again approximately uncouples spin and phonon terms:

$$H \approx H_p + H_{S3} \equiv \sum_q \hbar \omega_q (\alpha_q^+ \alpha_q + \tfrac{1}{2}) - \sum_i \Gamma S_i^x - \tfrac{1}{2} \sum_{ij} J_{ij} S_i^z S_j^z$$
$$- \sum_{ijk\ell} K_{ijk\ell} S_i^z S_j^z S_k^z S_\ell^z \qquad (27)$$

where

$$J_q = L_q + 2 \left\{ |A_q|^2 / \hbar \omega_q - \sum_{q'} |A_{q'}|^2 / \hbar \omega_{q'} \right\}. \qquad (28)$$

The properties of all these models are considered in the next section (see also the papers by H. Thomas, R.T. Harley, and J.K. Kjems in this volume).

3. PROPERTIES OF MODELS

The simplest model listed is (22),   applying to Tm VO_4 and $Tm_x As \ O_4$, in zero field.   From (23) and (7) the order parameter $<S^z>$ is that for an Ising model and it should show up in experiment as the splitting of the ground state electronic doublet.   For Tm VO_4 the measured splitting[58] agrees well with Ising model molecular field theory for $<S^z>$, as shown in Figure 2, and the specific heat anomaly (Figure 3) also fits extremely well to the Ising model molecular field theory curve[59].   The validity of molecular field theory is due to the dominance of the very long
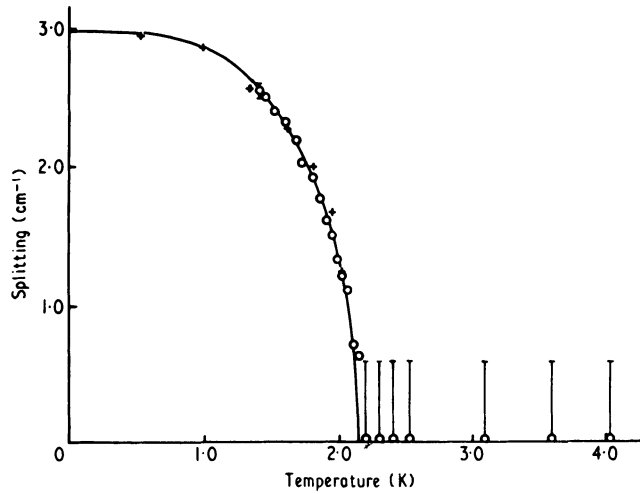
Figure 2. Ground state splitting γ in Tm VO$_4$ ($\Gamma = 0$), and a comparison with molecular field theory (solid line)[58].

range exchange interaction produced by strain coupling. No interesting dynamics is left in the Hamiltonian (23).

A related example is completely deuterated KDP. To the extent
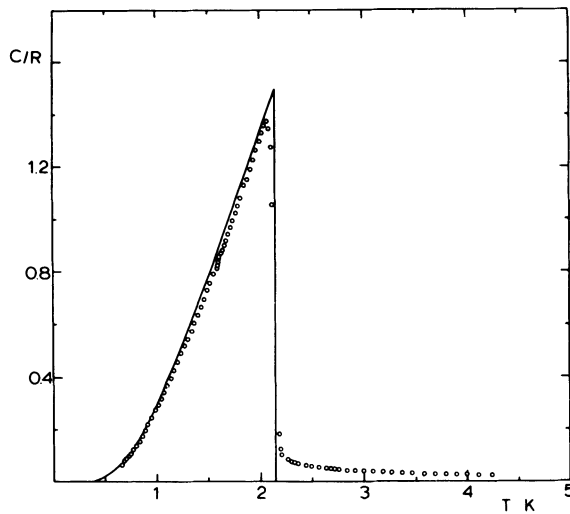
Figure 3. Experimental and mean-field (solid line) values for Specific Heat of Tm VO$_4$ ($\Gamma = 0$)[59].

to which it is described by (26), it is usual to place $\Gamma \sim 0$, since the heavier deuteron will tunnel less than a proton. The transformation to (27), without the tunnelling term, is then exact and the dynamics again become trivial. In particular[3] the pseudo-spin wave mode observed in KDP below the transition (§3 (iii)) should not be seen in deuterated KDP. The models (24), (26) with non-zero Γ have both interesting static and dynamic behaviour. The next three subsections briefly consider these aspects.

(i) Statics

The simplest approximation is molecular field theory[3,40,47]. Since molecular field theory for (24) is the same as for (25), it is sufficient to apply it to (25), concentrating on the effective spin Hamiltonian

$$H_{eff} = H_{S2} = -\sum_{i} \Gamma S_i^x - \frac{1}{2} \sum_{ij} J_{ij}\, S_i^z S_j^z \,. \tag{29}$$

Each spin experiences a mean field

$$\underline{\gamma} = \Gamma\, \underline{\hat{x}} + J(o)\langle S^z \rangle \underline{\hat{z}} \tag{30}$$

as depicted in Figure 4. The average spin vector is of magnitude $R = \frac{1}{2} \tanh \frac{1}{2} \beta\gamma$ and makes an angle θ with the z-direction. The
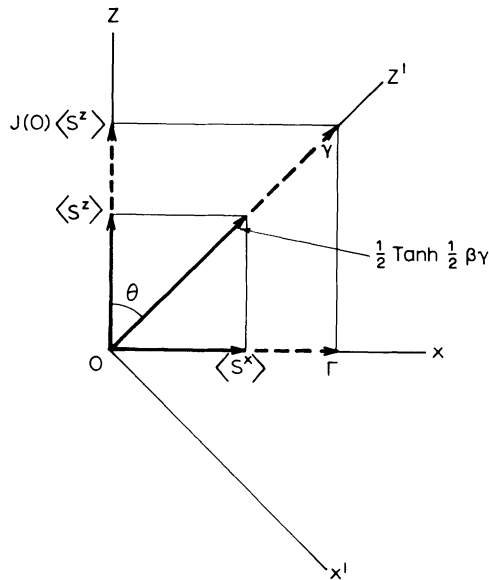
Figure 4. Molecular field and average spin for the transverse Ising model.

equation of state is therefore given by

$$\langle S^z \rangle = \tfrac{1}{2}\cos\theta\,\tanh\tfrac{1}{2}\beta\gamma = \gamma\cos\theta\,/J(o)$$

$$\sin\theta = \Gamma/\gamma\ ,\qquad \gamma^2 = \Gamma^2 + J(o)^2\langle S^z\rangle^2\ . \tag{31}$$

Provided the transverse field is sufficiently small ($\Gamma < J(0)$) the order parameter $\langle S^z \rangle$ will become non-zero at temperatures less than the transition temperature $T_c(\Gamma)$ given by

$$\Gamma/J(o) = \tfrac{1}{2}\tanh\tfrac{1}{2}\beta_c\,\Gamma . \tag{32}$$

This relationship between T_c and Γ is shown in Figure 5.   For $T < T_c$, γ (and hence $\langle S^z \rangle$) and $\langle S^x \rangle$ are given by

$$\gamma = \tfrac{1}{2}J(o)\tanh\tfrac{1}{2}\beta\gamma\ ,\qquad \langle S^x\rangle = \Gamma/J(o)\ . \tag{33}$$

For $T > T_c$

$$\langle S^z \rangle = 0\ ,\qquad \langle S^x \rangle = \tfrac{1}{2}\tanh\tfrac{1}{2}\beta\Gamma . \tag{34}$$

The molecular field specific heat[42] is of the form of a usual $\Gamma = 0$ molecular field contribution superimposed on a Schottky anomaly.   The experiments on Tm VO$_4$ and Tm As O$_4$ with no applied field ($\Gamma = 0$) agree well with the molecular field form[59,60]. Experiments[59] with an applied field ($\Gamma \neq 0$) agree satisfactorily with the relationships (33), (34) for γ and $\langle S^x \rangle$.   In addition (32) accounts well for the observed dependence[59,61] of T_c on Γ.
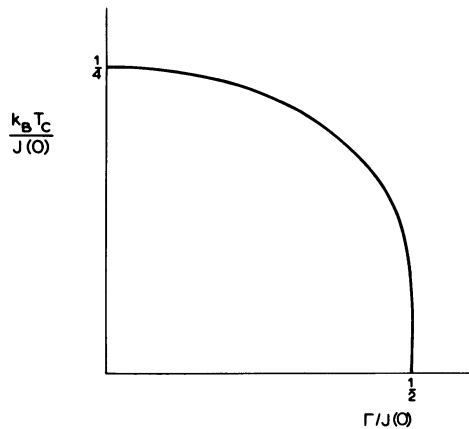
Figure 5. Mean field relationship between critical temperature and transverse field.

The decrease of T_C with Γ can also be seen in KDP, since Γ can be varied by applying pressure[62], which increases overlap and therefore the tunnelling frequency. The observed dependence of transition temperature on pressure[63] is shown in Figure 6 and has a form similar to part of the curve (Figure 5) resulting from (32). Though the coupling (28) also changes slightly with pressure (enough to cause T_C to decrease slightly with pressure for deuterated KDP, as is also shown in Figure 6), the result for KDP appears to provide strong support[64] for the tunnelling picture, and is difficult to explain in an anharmonic phonon approach.

In discussing KDP with the transverse Ising model, we have ignored the four spin coupling term in the Hamiltonian H_{S3} of (27). Its main effects, in a molecular field discussion[4], are that it yields the first order transition actually seen[65]; it also allows a satisfactory fit to the data[65] for the spontaneous polarization P_O $<S^Z>$ with roughly the same values of the parameters (e.g. P_O) as are required for the high temperature Curie-Weiss law, which supports the picture of one pseudo-spin per unit cell.

Static aspects of the transverse field Hamiltonian (29) have also been treated by series methods[66-68] or by controlled extensions[42,43,69] of molecular field theory. The series method is
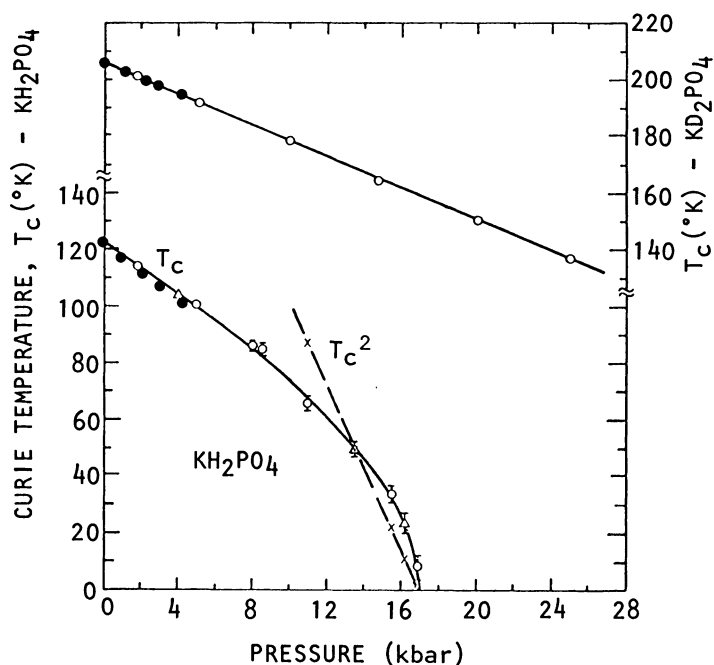
Figure 6. Relationship between critical temperature and pressure for KDP and DKDP[63].

well suited to the treatment of critical properties, which are
discussed in §5.   The other method is useful away from the critical
region.   In this approach the leading corrections can be seen to
arise from spin wave and spin fluctuation effects[42].   These include
zero point and linear spin wave effects, as well as effects arising
(in for example the low temperature specific heat) from the
temperature and field dependence of the spin wave energies (§3 (iii)).
These last effects are important near $T_c(\Gamma)$ where the spin wave
energy gap vanishes.   Similar considerations apply to the
Hamiltonian H_{S3} of (27).   It should, however, be noted that, to
the extent to which corrections to molecular field theory are being
considered, if $\Gamma \neq 0$, models (24) and (25) (or (26) and (27)) are
not equivalent.

(ii)   Formalism for Dynamics

The models are all included in the following general form

$$H = \sum \hbar \omega_q (a_q^\dagger a_q + \tfrac{1}{2}) + \sum_q A_q S_q^z (a_q^\dagger + a_{-q}) + H_S^{(0)}$$

$$\equiv \sum_q [\tfrac{1}{2m} P_q P_{-q} + \tfrac{1}{2} m \omega_q^2 Q_q Q_{-q}] + \sum_q \Lambda_q S_q^z Q_q + H_S^{(0)} \qquad (35)$$

(compare (22), (24), (26)) where the spin Hamiltonian $H_S^{(0)}$ is in the
case of Jahn-Teller systems the crystal field Hamiltonian for the
undistorted phase or, in the case of KDP, the Hamiltonian
$- \sum \Gamma S^x - \tfrac{1}{2} \sum L S^z S^z - \sum L S^z S^z S^z S^z$.   Only phonon coupling
to the z-component of pseudo-spin has been considered, but the
subsequent discussion applies to the more general Jahn-Teller case
involving coupling to a single electronic operator not represented
as pseudo-spin $\tfrac{1}{2}$, or to the Frohlich Hamiltonian for the Peierls
transition problem where S_q^z is to be replaced by the electron
density operator $\rho_q = \sum_K a_{K+q}^\dagger a_K$ and $H_S^{(0)}$ becomes the electron
Hamiltonian.

The use of

$$\omega^2 \langle\langle QQ \rangle\rangle = \tfrac{\omega}{m} \langle\langle PQ \rangle\rangle = \tfrac{\hbar}{m} + \omega_q^2 \langle\langle QQ \rangle\rangle + \tfrac{\hbar}{m} \Lambda_q \langle\langle S^z Q \rangle\rangle \quad , \qquad (36)$$

$$\omega^2 \langle\langle S^z Q \rangle\rangle = \omega^2 \langle\langle QS^z \rangle\rangle = \omega_q^2 \langle\langle QS^z \rangle\rangle + \tfrac{\hbar}{m} \Lambda_q \langle\langle S^z S^z \rangle\rangle \qquad (37)$$

leads to the following exact result[70-72] relating the phonon and
spin Green functions (momentum labels omitted, for simplicity):

$$\langle\langle QQ \rangle\rangle = \frac{\hbar/m}{\omega^2 - \omega_q^2} \left[1 + \frac{\hbar}{m} \frac{\Lambda_q^2}{\omega^2 - \omega_q^2} \langle\langle S^z S^z \rangle\rangle \right] . \qquad (38)$$

There now remains the calculation of $\ll S^Z S^Z \gg$, hereafter called $\chi(q\omega)$.

For the special case where $H_S^{(0)}$ commutes with the generator S of the canonical transformation (10) (i.e. where $\Gamma = 0$ in the ferroelectric or simple Jahn-Teller cases, or where $H_S^{(0)}$ contains only the electronic operator to which the lattice couples in more complicated Jahn-Teller cases) the transformation takes the Hamiltonian H to the form

$$H \rightarrow H_\rho + H_S \equiv H_\rho + H_S^{(o)} - \sum_q \left\{ \frac{|A_q|^2}{\hbar \omega_q} - \sum_{q'} \frac{|A_{q'}|^2}{\hbar \omega_{q'}} \right\} S_q^z S_{-q}^z . \tag{39}$$

Here, H_ρ is the free phonon form, and H_S (= H_{S1}, or H_{S2} or H_{S3},...) is an effective spin Hamiltonian containing no phonon term, as in §2(v). Since the spin operator is unchanged in the transformation, the special case has

$$\chi = \chi_S \tag{40}$$

where χ_S is $\ll S^Z S^Z \gg$ evaluated with Hamiltonian H_S. In the situation (e.g. model (22)) where this procedure is exact, χ is, however, static.

The more interesting cases, discussed for the remainder of this subsection, are where $[S, H_S^{(0)}] \neq 0$. These cases are normally dealt with by introducing approximations within Green function formalisms[71,73,44] or in diagrammatic formalisms[40,41,74,75,34].

If $\chi(q\omega)$ is represented by diagrams using $\sum_q \Lambda_q S_q^z Q_q$ as the interaction, the diagrams represent the processes of production and absorption of phonons. Some diagrams have intermediate states corresponding to the free propagation of a single phonon with wave vector and frequency having the external values, q, ω. All other diagrams constitute the "irreducible" part $\Pi(q\omega)$ of $\chi(q\omega)$. χ is given in terms of Π by the Dyson equation[8,34,74]

$$\chi = \Pi - \Pi D^o \Lambda_q^2 \chi = \frac{\Pi}{1 + \Pi D^o \Lambda_q^2} \tag{41}$$

where D^O is the free phonon propagator

$$D^o = \ll Q Q \gg_o = \frac{\hbar/m}{\omega^2 - \omega_q^2} . \tag{42}$$

The obvious approximation (of RPA type) is now to replace Π by the value corresponding to $\ll S^Z S^Z \gg$ evaluated with $H_S^{(0)}$. This,

however, is not adequate for the more delicate aspects of the dynamics[71],[76] essentially because the resulting χ does not reduce to the correct limit when $[H_S(0), S] \to 0$, where χ_S should be recovered.

Instead, a satisfactory approximation for χ can be obtained using the effective spin Hamiltonian H_S. The approximation is obtained by exploiting the contact between χ and χ_S when $[H_S(0), S] \to 0$, and the fact that χ_S can be written in a form analogous to (41): if H_S is separated into a 'tractable part' H_0, and a remainder of pair interaction form,

$$ H_S = H_0 - \tfrac{1}{2} \sum_q v(q) \, S_q^z \, S_{-q}^z \quad , \tag{43} $$

χ_S can be developed in terms of diagrams[77],[40],[41] having the same topology as the diagrams for χ, but with the phonon propagators replaced by interactions v. Thus[40],[70],[77-80]

$$ \chi_S = \frac{\Pi_S}{1 - v(q)\Pi_S} \tag{44} $$

where Π_S denotes the irreducible part of χ_S containing no $v(q)$'s with external label q. In the limit $[H_S(0), S] \to 0$ (denoted by asterisk) where χ_S becomes static and $\chi \to \chi_S$,

$$ \frac{1}{\Pi^*(q,0)} = \frac{1}{\Pi_S^*(q,0)} - v(q) + \frac{\hbar}{m}\frac{\Lambda_q^2}{\omega_q^2} \quad . \tag{45} $$

No approximations have been made so far. The approximation now introduced is that, away from the limit, the same relationship holds between the frequency-dependent irreducible parts, so that $\Pi(q, \omega)$ can be written in terms of the simpler quantity $\Pi_S(q, \omega)$. That results in[71],[76]

$$ \chi(q,\omega) = \frac{\Pi_S(q,\omega)}{1 - \left[v(q) - \dfrac{2\omega^2 A_q^2}{\omega_q(\omega^2 - \omega_q^2)} \right] \Pi_S(q,\omega)} \quad . \tag{46} $$

Π_S is evaluated using H_S. The separation indicated in (43) is obvious for the H_S arising from (22) and from (24) provided $K = 0$. Then

$$ H_0 = -\sum_i \Gamma S_i^x $$
$$ v(q) = J(q) \tag{47} $$

with J(q) given in (8), (28) respectively.   The case K ≠ 0 can be
accommodated in the scheme by approximating the four spin term by
an effective pair interaction so that in (28), L → L + 6 Σ K $<S^zS^z>$.

Quite crude approximations for $\Pi_S(q, \omega)$ are satisfactory in
some circumstances.   Among the simplest is mean field approximation.
(This will give the correct mixed modes, but will not be adequate
for subtler effects like damping, or the Peierls transition at
T = 0). Π_S is then the single site susceptibility[76,73,72], in
mean field theory for the system (43), (47).   This approximation
yields[40,72,70,78]

$$\Pi_S(q,\omega) = \frac{\Gamma <S^x>}{\gamma^2 - \omega^2} + \delta(\omega) \cos^2\theta \left(\tfrac{1}{4} - R^2\right) \tag{48}$$

with R, γ, cos θ, $<S^x>$ as in §3 (i).   The zero-frequency part of
Π_S vanishes at and above the transition but has important
consequences below.   It corresponds to longitudinal spin
fluctuations and arises because below the transition $\hat{z}$ S^z has a
component along the molecular field direction.

For more complicated situations, e.g. Jahn-Teller systems
with many levels, the corresponding approximation for Π_S is
obtained by diagonalising the full single ion Hamiltonian H_S
treating in the mean field approximation the term bilinear in the
electronic operator[76,82,81].   In cases with degenerate levels,
the zero frequency part of Π_S need not vanish at the transition if
S^z (or more generally the operator to which the distortion mode
couples) has non-zero matrix elements between the degenerate
levels, as in Tb VO_4 or in the singlet ground state system Pr_3Tl.
In such cases the zero frequency part of Π_S can cause a divergence
as the transition is approached[76,83,84], leading to a "central
peak" at discussed in Section 5.

(iii)   Dynamic Properties

In a Raman experiment in which the coupling to the light is
through the operator

$$P_1 S^z + P_2 Q \tag{49}$$

(with P_1, P_2 polarizability coefficients) the scattered intensity
is proportional to

$$I(\omega) = \frac{1}{1 - e^{-\beta\omega}} \, \text{Im} \left[P_1^2 \langle\langle S_q^z S_q^z \rangle\rangle + P_1 P_2 \{ \langle\langle S_q^z Q_q \rangle\rangle + \langle\langle Q_q S_q^z \rangle\rangle \} \right.$$
$$\left. + P_2^2 \langle\langle Q_q Q_q \rangle\rangle \right].$$

In the Raman case, q is effectively zero. Similar Green functions, but at finite q, occur for inelastic neutron scattering where in the Jahn-Teller case the corresponding P_1 is very small unless the pseudo-spins have an associated magnetic moment.

In a coupled system all these Green functions share the same poles (where the denominator of (46) vanishes) which determine the mode frequencies and Raman and neutron response. Inserting Π_S as given by (48) gives zero frequency modes below the transition (associated with order-parameter fluctuations) and also coupled spin-phonon modes[44,50,35] whose frequencies satisfy

$$(\omega^2 - \omega_q^2)[\omega^2 - (\gamma^2 - \Gamma \langle s^x \rangle J(q))] = 2\Gamma \langle s^x \rangle \omega^2 A_q^2 / \omega_q . \qquad (50)$$

If the mixing is small, one mode is phonon-like and the other mode (the 'vibron' in Jahn-Teller systems) is close to the uncoupled 'spin wave' solution

$$\omega_s(q)^2 = \gamma^2 - \Gamma \langle s^x \rangle J(q) \qquad (51)$$

(except where the modes cross). The wave-vector, and temperature-dependence of the 'spin wave' frequency[38] is shown schematically in Figure 7. The q ~ 0 vibron for Dy VO_4, Tb VO_4 has been identified in Raman scattering[44]. If only coupling to acoustic phonons is considered ω_q goes to zero at small q and the vibron solution of (50) is, for q = 0

$$\omega^2 = \gamma^2 - \lambda \Gamma \langle s^x \rangle \qquad (52)$$
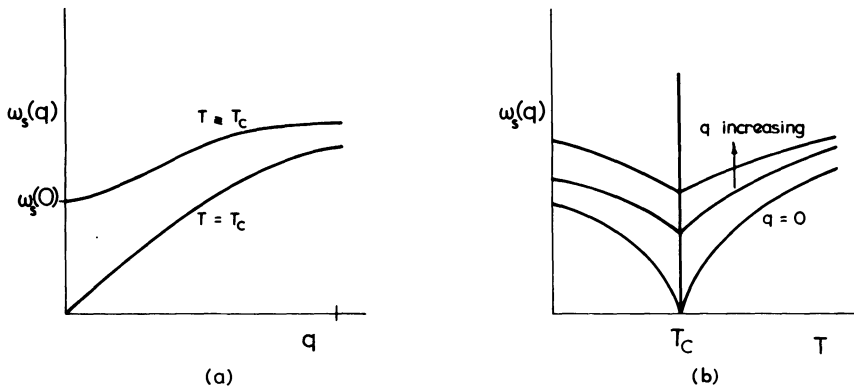
Figure 7. The (uncoupled) spin wave or tunnelling mode frequency ω_s as a function of (a) wave vector,(b) temperature.

where λ arises from the self-energy term in J(q) (the other part being cancelled by $2A_q^2/\omega_q$ from the right hand side); optic phonon contributions can also occur in λ. The temperature-dependence resulting from $<S^x>$ above the transition is seen in the experiments.

Inelastic neutron scattering[85,83,84] on Pr Aℓ O_3, Tb VO_4 and Tm VO_4 shows important characteristics of the dispersion relations given by (50), including the vibron-phonon mixing at finite q, and the acoustic mode softening near the transition, as depicted for Pr Aℓ O_3 in Figure 8.

The Raman spectra[87-92] for KDP and its isomorphs show the corresponding coupled spin-phonon modes (at q ~ 0), and the coupled spin-phonon model allows a satisfactory fit[4] to the peak positions below T_c. In deuterated KDP (Γ ~ 0), the spin (proton) mode is not seen: from (46) and (48) it can be seen that it should have zero intensity for Γ ~ 0.

The influence of pressure allows a clear identification of the spin mode in tunnelling ferroelectrics[93-97]. Since Γ increases with pressure in a roughly linear way[62], the pressure-dependence of the Raman spectra also allows a test of results such as (50). For KDP it has been shown[96,98] that the observed pressure-dependence is in rough agreement with the model (allowing also for the fact that J decreases slightly with pressure). In particular the uncoupled spin mode frequency at fixed T < T_c falls with increasing Γ (i.e. decreasing $T_c(\Gamma)$) in the way expected from (51). However, the pressure-dependence of the spin mode frequency in both phases appears to be less than is required for consistency
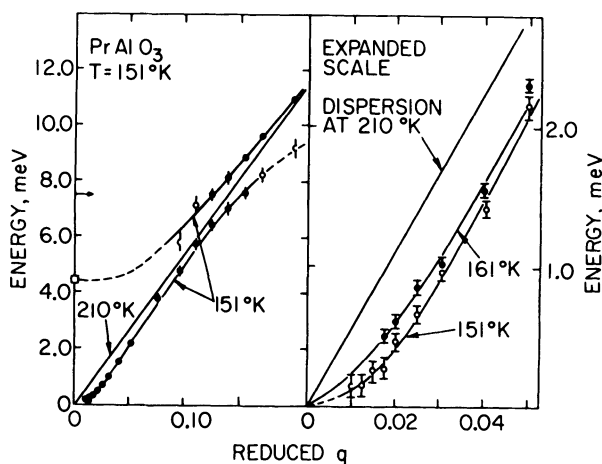
Figure 8. Inelastic neutron scattering results[85] for Pr Aℓ O_3, showing the mixed modes and the acoustic mode softening as T → T_c

with static measurements.   The temperature-dependence of the
uncoupled spin mode frequency in the paraelectric regime also
agrees with the model result (51), as can be seen from Figure 9.

An important aspect of the pressure-dependence which makes it
possible to obtain accurate spin mode frequencies in the para-
electric phase is that while the response is overdamped in the
paraelectric phase for all KDP-type crystals at atmospheric
pressure, application of moderate pressures makes the spin mode
underdamped in KDP.   Similar behaviour is seen in Rb D P[93,94] and
in KDA[99].   The reason for the reduction of damping with increased
Γ will be briefly discussed in §3 (iv).

The application of a magnetic field to Tm VO$_4$ or Tm As O$_4$
gives rise to the otherwise absent transverse field term.   The
field-dependence of the frequency and intensity of the resulting
coupled mode response (analogous to its pressure-dependence in
KDP) has been investigated by Raman and neutron methods[100,86].

One important effect of the coupling is on the elastic constants.
From (46) and (44) it is straightforward to obtain
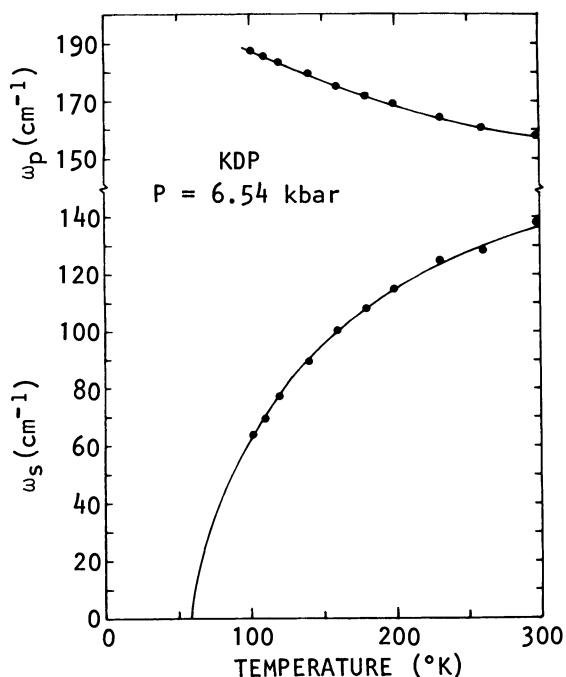
Figure 9.   Raman results[96] for the temperature-dependence of the
uncoupled mode frequencies in KDP.   The lower full line is a
fit using (51).

$$\frac{\omega^2}{\omega_q^2} = \frac{1 - v(q)\Pi_s}{1-(v(q)-\mu_q)\Pi_s} = \frac{1}{1+\mu_q \chi_s} \tag{53}$$

where $\mu_q = 2A_q^2/\omega_q$, and χ_S is the dynamic susceptibility for the effective spin system. Assuming that A_q represents coupling to an acoustic phonon such that μ is the limit of μ_q as q goes to zero, $[1 + \mu \chi_S(q,\omega)]^{-1}$ then gives the modification[101] and frequency dependence[102] of the elastic anomaly. This has been used to fit the elastic anomaly both in KDP[103,4] and in Dy VO_4 and Tb VO_4[102]. In the case of Tb VO_4 the (damped) zero-frequency part of Π_S appears to distinguish its behaviour from that of Dy VO_4, though this explanation is not supported by experiments[104] on Pr $A\ell$ O_3.

For simple considerations it is sometimes adequate to treat the dynamics starting from the approximately transformed Hamiltonians (25), (27). The excitations are then the uncoupled phonon and pseudo-spin wave modes, whose frequencies ω_q and $\omega_S(q)$ can be obtained directly from the approximate Hamiltonians or, as was used to obtain (51) above, by ignoring the right hand side of (50). The approximate Hamiltonians also give rise to the zero frequency longitudinal spin fluctuations referred to below (48).

(iv) Damping

The theoretical discussion so far given has led to undamped modes. Though some damping effects are lost in the approximation used to get (46), the more severe approximation was the use of mean field approximation for Π_S. A proper evaluation of Π_S can include all the dominant damping effects other than those that rely on resonant spin-phonon aspects. For the simpler Jahn-Teller cases, or for KDP when the four spin term is approximated by an effective pair interaction, H_S is the transverse Ising Hamiltonian. For this model, Im Π_S, which gives the damping, has been considered using the Blume-Hubbard technique[43], by diagrammatic methods[40,41,78], or within a phenomenological approach[3]. In situations where mean field theory is a suitable first approximation the leading corrections which yield damping are associated with the break up of an excitation into (i) a pseudo-spin wave and a spin fluctuation or (ii) a pair of spin waves[41,78]. Only the first process contributes to Π_S above the transition, but both contribute below because of the mixed character of the excitations.

The resulting expressions are very complicated but simplify in various regimes. For example, for $T > T_c$ and ω near the spin wave frequency $\omega_S(q)$, the Green function χ_S for the transverse Ising model (that is to say, neglecting the mixing term in A_q^2 in (46)) becomes[41]

$$\chi_s(q,\omega) \propto \left[(\omega^2 - \omega_s(q)^2)^2 + (2\omega\Delta_q)^2\right]^{-1} \tag{54}$$

where

$$\Delta_q = \frac{\pi}{4} J(q) \, \text{sech}^2 \tfrac{1}{2}\beta\Gamma \, \frac{\Gamma^2}{2\omega_s(q)^2} \sum_{q'} J(q') \delta(\omega_s(q') - \omega_s(q)). \tag{55}$$

Δ_q is a complicated function of ω for ω not near $\omega_s(q)$.

In the underdamped situation where these results apply, the ratio of damping Δ_q to frequency is, above the transition, of order $(J(o)/z\,\Gamma)\, \text{coth}\, \tfrac{1}{2}\,\beta\,\Gamma$ (with z the coordination number), so that underdamping occurs for large Γ, in agreement with the pressure dependences[87,87,92] referred to in §3 (iii). The reason is that for Γ large 'spin precession about the external field' (i.e. tunnelling) dominates the interaction processes produced by J. The increase of damping with temperature (from the coth $\tfrac{1}{2}\,\beta\,\Gamma$ factor) is due to the increase with temperature of the density of states into which the excitation can decay: that density of states is determined by the inverse of the spin wave band width, and at high temperatures the band width is proportional to $\langle S^x \rangle$, from (51).

In the more strongly damped situations which occur at higher T or lower Γ it is necessary to allow for the damping of the excitations into which the mode decays, and the self-consistent treatment of such effects[43] leads to a high temperature width typically of order $J(0)/4\, z^{\frac{1}{2}}$ when Γ and $J(0)$ are comparable. The first principles theory of overdamping in the pseudo-spin model is still at a somewhat primitive stage but it would clearly be desirable to compare a more detailed analysis with the most reliable experimental parameter $\tau^{-1} \equiv \omega^2/\Delta$.

For situations where the mode mixing has important (e.g. resonant) effects on the damping it is not possible to consider the damping within the transverse Ising model. Phenomenological discussions have been given[102,105], and also perturbation analyses[74,75,34] starting from the Hamiltonian (24). The damping for the Hamiltonian (26) has been treated with the Blume-Hubbard method[106] and also by a diagrammatic perturbation method[78], omitting the four spin term.

The above discussion applies only to damping intrinsic in the model. Damping can also arise from random strains, from domain boundaries, or from various types of substitutional disorder. We briefly discuss the first and last of these sources in the next section.

4. MIXED AND DILUTE SYSTEMS

Substitutionally disordered ferroelectrics and cooperative Jahn-Teller systems have been the subject of recent study. Consideration has been given to the effects of both dilution (partial substitution of an active component by an inactive one) and of mixing (partial substitution by another active component, with a different transverse field and interaction). Examples[107,108] of the dilute systems are $Tb_c\ Gd_{1-c}\ VO_4$, $Dy_c\ Y_{1-c}\ VO_4$, and an example[109,110] of the mixed system is $K(H_c\ D_{1-c})_2\ PO_4$ (partly deuterated KDP).

The simplest approach to such systems is the virtual crystal approximation, which is the disorder analogue of mean field theory for thermodynamics. For the transverse Ising model that allows an immediate treatment of static quantities in mean field theory (§3 (i)) by the replacements

$$(\Gamma/\gamma)^2 \longrightarrow \langle (\Gamma/\gamma)^2 \rangle_c \ , \qquad J\langle s^z \rangle \longrightarrow \langle J\langle s^z \rangle \rangle_c \qquad (56)$$

where the configurational average $\langle\ \rangle_c$ denotes the weighted mean, with probabilities c, $1-c$ of the values for pure systems composed solely of one or other of the two components. Quite simple prescriptions allow virtual crystal approximation to be extended to discuss the dynamic behaviour[108,111]. These results can be recovered within a simple scheme[72] for the transverse Ising model which automatically includes the dynamics and which can be readily generalised to deal with the coupled spin phonon system, or to allow more sophisticated treatments, such as CPA, of the disorder.

For simplicity we consider the case $T > T_c$ (deferring until the end the generalisation to $T \leqslant T_c$).

In the Hamiltonian (29) Γ is now taken to be site dependent ($\Gamma \to \Gamma_i$) and the exchange to depend in the following way on the types of spins occupying sites i, j (i.e. through μ_i, μ_j only):

$$J_{ij} \longrightarrow \mathcal{J}_{ij} \equiv \mu_i\ J_{ij}\ \mu_j . \qquad (57)$$

This replacement is exact for the dilute case, and appears to be adequate[98] for partially deuterated KDP. μ_i is like an effective dipole moment in the ferroelectric case.

The equation of motion for the Green function $\chi \equiv \ll\mu_i\ S_i^z; \mu_j\ S_j^z\gg$ can be decoupled in random phase approximation[38] above the transition to yield

$$\chi_{ij} = \phi_i\ \delta_{ij} - \phi_i \sum_k J_{ik}\ \chi_{kj} \qquad (58)$$

where

$$\phi_i = \frac{\Gamma_i \mu_i^2 \langle S_i^x \rangle}{\omega^2 - \Gamma_i^2} \quad . \tag{59}$$

This is precisely equivalent to (44), with Π_S replaced by $-\phi_i$, which is the mean field approximation (48), $T > T_C$, with the allowance of site-dependence. The disorder now occurs entirely through the site-diagonal parameter ϕ_i. The replacement of this by its mean value ϕ is virtual crystal approximation:

$$\phi_i \rightarrow \phi(\omega) = \langle \phi_i \rangle_c$$

$$= \frac{c \, \Gamma_A \mu_A^2 \, \tfrac{1}{2} \tanh \tfrac{1}{2}\beta\Gamma_A}{\omega^2 - \Gamma_A^2} + \frac{(1-c)\Gamma_B \mu_B^2 \, \tfrac{1}{2}\tanh\tfrac{1}{2}\beta\Gamma_B}{\omega^2 - \Gamma_B^2} \tag{60}$$

where c is the concentration of species A, with parameters μ_A, Γ_A and $(1 - c)$ is the concentration of species B. This gives

$$\chi \rightarrow \chi_q = \frac{\phi}{1 + \phi \, J(q)} \quad . \tag{61}$$

(i) Statics

The transition is located by the divergence of the $q = 0$ static susceptibility, that is, where[72,111-113]

$$0 = 1 + J(0)\phi(0) \tag{62}$$

with ϕ given by (60). The shape of the resulting curve of transition temperature versus concentration depends on whether ordering is possible in both or just one of the two pure systems (pure A system, pure B system)[72]. The theory gives a satisfactory fit to the concentration-dependence of the transition temperature of $Dy_c \, Y_{1-c} \, VO_4$, apart from its neglect of percolation effects, and the appropriate generalisation of the theory to the four level system appropriate to Tb VO_4 accounts well[108] for $Tb_c \, Gd_{1-c} \, VO_4$, as shown in Figure 10. In these cases $\mu_B = 0$ since the Gd and Y ions are not Jahn-Teller active.

In the corresponding description of the static behaviour of partially deuterated KDP, Γ_B can be taken as effectively zero. The theoretical results[98] for $T_c(c)$ and $C(c)$ (where C is the Curie constant) agree satisfactorily with experiment[109].
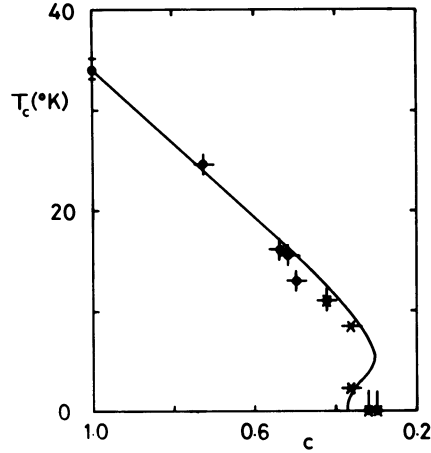
Figure 10. Measured concentration dependence of the transition temperature in $Tb_c Gd_{1-c} VO_4$. The full line is from virtual crystal theory[108].

(ii) Dynamics

Virtual crystal approximation as set out above also gives the dynamic behaviour: the excitation frequencies are given by

$$1 + \phi(\omega) J(q) = 0. \tag{63}$$

Provided none of c, (1 - c), μ_A, μ_B, Γ_A, Γ_B are zero, (63) is a quadratic equation in ω^2 with solutions $\omega_q^{(+)2}$ and $\omega_q^{(-)2}$ (with $\omega_q^{(+)} > \omega_q^{(-)}$).   In virtual crystal approximation these excitations are undamped, and Im χ is then a sum of δ- functions centred at $\pm \omega_q^{(+)}$, $\pm \omega_q^{(-)}$.   Defining the integrated intensities $I_q \pm$ of these modes to be the residues at the poles gives

$$I_q^{\pm} = \frac{\pm \pi (\Gamma_A^2 - \omega_q^{(\pm)2})(\omega_q^{(\pm)2} - \Gamma_B^2)}{2 J(q) \omega_q^{(\pm)2} (\omega_q^{(+)2} - \omega_q^{(-)2})} . \tag{64}$$

It is easy to check that in the limit c → 0 the mode frequencies become $\omega \sim \omega_B, \omega \sim \Gamma_A$ where ω_B is the pseudo-spin wave frequency for the pure B system, and that their respective intensities are O(1), O(c); analgous results apply near c = 1.

For $\Gamma_B = 0$ or $\mu_B = 0$ (as apply for deuterated KDP, or in diluted cases) only the A-like excitation occurs, and its intensity varies

roughly like c.   Related behaviour is seen in the experiments[108,110].

(iii) Generalisations

For a more complete understanding particularly of the dynamic behaviour[110] in partially deuterated KDP, the phonon coupling has to be introduced into (58) in a manner analogous to the way (46) generalises (44).   The resulting generalisation[98,111] gives a more complete understanding of the observed concentration dependences of the Raman data[110], including the combined pressure and deuteration dependences.   An example of this is shown in Figure 11 where the resulting theoretical expressions are compared to the concentration dependences of the observed logarithmic pressure derivatives of the low temperature mixed mode frequencies.

Intrinsic damping of the excitations can also be included[72], through a generalisation of $\phi_i(\omega)$ in (58), (59).

In order to treat damping caused by the disorder the CPA generalisation[72,114] of virtual crystal approximation is required. That leads to the replacement of $\phi(\omega)$ in the preceding discussion by $\tilde{\phi}(\omega)$ where

$$\tilde{\phi} = \langle \phi_i / [1 + (\phi_i - \tilde{\phi})g] \rangle_c$$

$$g(\tilde{\phi}) \equiv \frac{1}{N} \sum_q J(q) / [1 + \tilde{\phi} J(q)].$$

(65)
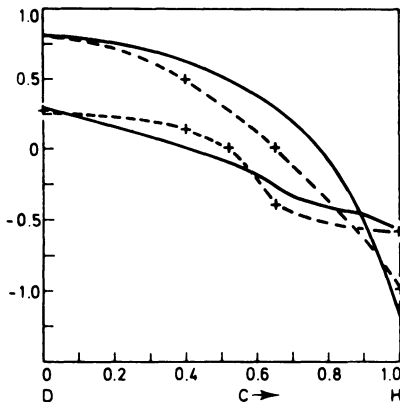
Figure 11. Experimental[110], and theoretical[98] results (full lines), for the logarithmic pressure-derivatives $\partial \ln \omega_+/\partial p$ of the frequencies of the low temperature $q = 0$ mixed modes in $K(H_c D_{1-c})_2 PO_4$.

g is small $(O(^1/z))$ in mean field-like systems, and its neglect
gives back the virtual crystal approximation (60).   Expanding $\tilde{\phi}$
to first order in g yields the leading contribution of configurational
fluctuations to the damping, through

$$\text{Im } \tilde{\phi} \sim -\langle (\phi_i - \phi)^2 \rangle_c \text{ Im } g(\phi) \qquad (66)$$

(As was noted earlier, the damping arises from Im Π, which is here
- Im ϕ).   The result (66) is proportional to the density of virtual
crystal states (whose energies $\omega^{(\pm)}$ were discussed above).   This
simple extension of the virtual crystal approximation can give a
satisfactory account of disorder damping where it is small.   In
other cases the self consistent CPA equations (65) have to be solved.

The above discussion considered the disorder resulting from
substitution.   Random strains also have similar effects, in that
they lead to a transverse field Γ varying from site to site, and a
resulting damping.   That can be treated as above, but with $< >_c$
interpreted as an averaging over the probability distribution for Γ.
In particular (66) will then yield the damping arising from this
source.

To generalise the results of this section to $T \lesssim T_c$, ϕ_i has to
be replaced by[98,115]

$$\phi_i = \Gamma_i \, \mu_i^2 \, \langle S_i^x \rangle \, / \, [\omega^2 - \Upsilon_i^2] \qquad (67)$$

where

$$\Upsilon_i^2 = \Gamma_i^2 + z_i^2 \,, \qquad z_i = \sum_j \mu_i \, J_{ij} \, \langle \mu_j S_j^z \rangle \qquad (68)$$

(compare (48)).   Virtual crystal approximation is then

$$\phi_i \rightarrow \phi = \langle \phi_i \rangle_c \,, \qquad z_i \rightarrow z = \langle z_i \rangle_c \qquad (69)$$

which is equivalent in the static case to (56).

5.   THE CENTRAL PEAK;   CRITICAL BEHAVIOUR

(i)   The Central Peak

In the discussion after (48) it was stated that when
degenerate levels contribute to Π_S, a zero frequency response can
arise;   that implies[76,81,83,84] an elastic peak in the Raman or
neutron response, or a dynamic one if the levels are weakly
broadened by residual interactions.   Such a central peak appears
to have been seen in Tb VO$_4$[83,84].

Another mechanism for the occurrence of a central component is exhibited by the zero-frequency part of (48), which is due to the z-component of spin having a longitudinal component (with respect to the mean field direction) below the transition.   Beyond molecular field theory that longitudinal component will relax and give rise to a central peak of finite width.   However, this central peak only occurs in χ below the transition.   (It could also appear in the Raman response above the transition if the operator S^x were also involved in the Raman operator (49) or in the phonon coupling in the Hamiltonian).

There remains the question how narrow such a peak would be. The pseudo-spin longitudinal mode just considered actually relaxes through decay into two pseudo-spin waves (§3 (iv)), which at low frequency and wave vector corresponds to a fluctuation in spin wave density.   This process is analogous to the origin of the relaxational mode proposed for the anharmonic phonon model by Cowley[116-118] which relies on coupling to fluctuations in phonon density and can occur in piezoelectric non-pyroelectric crystals above T_c.   In both models damping and dispersion of the decay modes (spin waves or phonons respectively) will normally give a relatively large relaxational mode damping, though this appears to be consistent with the broader peaks sometimes observed[119].

A central mode can also occur in the pseudo-spin model from non-linear fluctuations in the order parameter[3] (analogously to proposals for the anharmonic phonon model[120,121]), and indeed from most mechanisms applying in the anharmonic phonon model.   Among the most clearly established of these appears to be entropy fluctuations, which is consistent with the magnitude and wave-vector dependence of the width of some very narrow peaks[119], and appears to be responsible for the narrow but resolved central peak recently seen in KDP[122].   In addition, some types of defect structure[123,124] seem to play a role in some central peaks[119,125] (both static and dynamic) at low temperature and near T_c.

(ii) Critical Behaviour

The dependence of, for example, the order parameter $<S^z>$ on $T - T_c$ near a second order phase transition is usually described by critical indices[126] such as β in

$$\langle S^z \rangle \propto (T - T_c)^\beta. \tag{70}$$

For the transverse Ising model, the static indices are known from series expansions[127,68].   Some exact results are also known. For example, for the transverse Ising model the critical behaviour with respect to the field Γ of the thermodynamic functions at $T = 0$ in a lattice of dimensionality d, is the same as the critical

behaviour of the corresponding functions with respect to T in the $d + 1$ dimensional Ising model : this was proved[128-130] for $d = 1$, and indicated for $d = 2, 3$ by series[66,67] and subsequently confirmed[131] using standard renormalization group methods[132]. Thus for $T = 0$ the transverse Ising model has mean field exponents for $d > 3$.   In addition it can be seen that for $T \neq 0$, the transverse Ising model has the same critical indices as the Ising model with the same dimensionality[131].

The crossover near $T = 0$ is a quantum effect arising for non-commuting operators from the usual thermodynamic frequency sum becoming an integral for $T = 0$, and acting like an additional wave-vector component integral in the theory.   It would be interesting to see some aspects of the crossover behaviour exhibited experimentally.   The above discussion applies, however, only to the transverse Ising model with short range interactions, while most real transverse Ising-like systems have also long range interactions produced by strain coupling or dipole-dipole effects. This would result in mean field exponents sufficiently close to T_c[133], as appears to have been verified by observations of β for $Pr\,A\ell\,O_3$[134] and for $Tb\,VO_4$[135], though not for $Dy\,VO_4$[135].

REFERENCES

1. G.A. Gehring and K.A. Gehring, 1975, Rept. Prog.Phys. $\underline{38}$,1.
2. H. Thomas, 1974, Anharmonic Lattices, Structural Transitions and Melting, Ed. T. Riste (Noordhoff, Leiden) p. 213.
3. R. Blinc and B. Žekš, 1972, Adv.Phys. $\underline{21}$, 693
4. R.J. Elliott and A.P. Young, 1974, Ferroelectrics $\underline{7}$, 23.
5. J.F. Scott, 1974, Rev.Mod.Phys. $\underline{46}$, 83.
6. G. Shirane, 1974, Rev.Mod.Phys. $\underline{46}$, 437.
7. W. Rehwald, 1973, Adv.Phys. $\underline{22}$, 721.
8. P.A. Fleury, 1972, Comments Sol.St.Phys. $\underline{4}$, 149, 167.
9. P.A. Fleury, 1972, Proc.Int.Conf. Light Scattering in Solids, Ed. M. Balkanski, R.C.C. Leite, and S.P.S. Porto, (Flammarion, Paris) p. 747.
10. Y. Ishibashi and Y. Takagi, 1976, J. Appl.Phys. (Japan) $\underline{15}$,1621.
11. H.R. Zeller, 1973, Festkörperprobleme $\underline{13}$, 31.
12. H.R. Zeller and S. Strassler, 1975, Comments Sol.St.Phys. $\underline{7}$,17.
13. W. Dietrich, 1976, Adv.Phys. $\underline{25}$, 615.
14. L.R. Testardi, 1975, Rev.Mod.Phys. 47, 637.
15. L.R. Testardi, 1975, Comments Sol.St.Phys. $\underline{6}$, 131.
16. L.N. Bulaevskii, 1975, Sov.Phys.: Uspekhi $\underline{18}$, 131.
17. Yu.A. Izyumov and E.Z. Kurmaev, 1976, Sov.Phys.: Uspekhi $\underline{19}$, 26.
18. S.P. Ionov, G.V. Ionova, V.S. Lubimov and E.F. Makarov, 1975, Phys. Stat. Solidi $\underline{B71}$, 11.
19. B.A. Huberman, 1976, Comments Sol.St.Phys. $\underline{7}$, 75.
20. E.J. Samuelsen, E. Andersen, and J. Feder (eds.), 1971, Structural Phase Transitions and Soft Modes (Oslo, Universitetsforlaget).
21. T. Riste (ed.), 1974, Anharmonic Lattices, Structural Transitions and Melting (Noordhoff, Leiden).
22. S. Hirotsu, 1977, J. Phys. C. $\underline{10}$, 967.
23. Y. Yamada, 1977, "Electron-Phonon Interaction and Charge Ordering in Insulators" - in this volume.
24. J. Kanamori, 1960, J. Appl. Phys. $\underline{31}$, 145.
25. E. Pytte, 1971, Phys.Rev. $\underline{B3}$, 3505.
26. E. Callen and H.B. Callen, 1965, Phys.Rev. $\underline{A139}$, 455.
27. H.H. Chen and P.M. Levy, 1971, Phys.Rev.Lett. $\underline{27}$, 1383.
28. J. Sivardière and M. Blume, 1972, Phys.Rev. $\underline{B5}$, 1126.
29. R.J. Elliott, 1971, in Structural Phase Transitions and Soft Modes, ed. E.J. Samuelsen, E. Andersen and J. Feder (Oslo, Universitetsforlaget).
30. E. Pytte, 1973, Phys.Rev. $\underline{B8}$, 3954.
31. J.P. Harrison, J.P. Hessler and D.R. Taylor, 1976, Phys. Rev. $\underline{B14}$, 2979.
32. J.T. Folinsbee, J.P. Harrison, D.B. McColl and D.R. Taylor, 1977, J. Phys. $\underline{C10}$, 743.
33. J.R. Fletcher and F.W. Sheard, 1971, Solid St. Comm. $\underline{9}$, 1403.
34. N.E. Buttery, 1974, D.Phil.Thesis, Oxford.

35. R.J. Elliott, 1971, Proc.Int.Conf.Light Scattering in Solids, ed. M. Balkanski (Flammarion Press, Paris) p.354.
36. F.S. Ham, 1972, in Electron Paramagnetic Resonance, ed. S. Geschwind (Plenum Press) p. 1.
37. Y.L. Wang and B. Cooper, 1968, Phys.Rev.172, 539.
38. R. Brout, K.A. Müller and H. Thomas, 1966, Solid St.Comm. 4, 507.
39. P. Pfeuty, 1971, Ph.D. Thesis, Paris.
40. R.B. Stinchcombe, 1973, J. Phys. C6, 2459.
41. R.B. Stinchcombe, 1973, J. Phys. C6, 2484.
42. R.B. Stinchcombe, 1973, J. Phys. C6, 2507.
43. M.A. Moore and H.C.W.L. Williams, 1972, J. Phys. C5, 3168,3185.
44. R.J. Elliott, R.T. Harley, W. Hayes and S.R.P. Smith, 1972, Proc.Roy.Soc. A328, 217.
45. E. Pytte and K.W.H. Stevens, 1971, Phys.Rev. Lett. 27, 862.
46. D.K. Ray and A.P. Young, 1973, J. Phys. C6, 3353.
47. P.G. de Gennes, 1963, Solid St. Comm. 1, 132.
48. Y. Yamada and T. Yamada, 1966, J.Phys.Soc. Japan 21, 2167.
49. Y. Yamada, Y. Fujii and I. Hatta, 1968, J. Phys. Soc. Japan, 24, 1053.
50. K.K. Kobayashi, 1968, J. Phys. Soc. Japan 24, 497.
51. A.R. Bishop and J.A. Krumhansl, 1975, Phys. Rev. B12, 2824.
52. W. Cochran, 1961, Adv.Phys. 10, 401.
53. J.C. Slater, 1941, J. Chem. Phys. 9, 16.
54. Y. Takagi, 1948, J. Phys. Soc. Japan 3, 271.
55. E. Pytte, 1973, Comments Sol.St.Phys. 5, 41.
56. E. Pytte, 1973, Comments Sol.St.Phys. 5, 57.
57. E. Pytte, 1972, Phys.Rev.Lett. 28, 895.
58. P.J. Becker, M.J.M. Leask and R.N. Tyte, 1972, J.Phys. C5, 2027.
59. A.H. Cooke, S.J. Swithenby and M.R. Wells, 1972, Solid St. Comm. 10, 265.
60. J.H. Colwell and B.W. Mangum, 1972, Solid St. Comm. 11, 83.
61. B.W. Mangum, J.N. Lee, and H.W. Moos, 1971, Phys.Rev.Lett. 27, 1517.
62. G.A. Samara, 1970, J.Phys.Soc. Japan 28, Suppl.,Proc. Second Int. Meeting on Ferroelectricity p. 399.
63. G.A. Samara, 1971, Phys.Rev.Lett. 27, 103.
64. R. Blinc, S. Svetina and B. Žekš, 1972, Solid St.Comm. 10, 387.
65. W.J. Benepe and W. Reese, 1971, Phys.Rev. B3, 3032.
66. R.J. Elliott and P. Pfeuty, 1971, J.Phys. C4, 2370.
67. R.J. Elliott and C. Wood, 1971, J. Phys. C4, 2359.
68. R.J. Elliott and I.D. Saville, 1974, J.Phys. C7, 4293.
69. L. Lam and A. Bunde, 1977, J.Phys. C10, 693.
70. S. Takada, I. Ohnari, H. Kurosawa, and Y. Ohmura, 1975, Prog. Theor. Phys. 53, 936.
71. A.P. Young, 1975, J.Phys. C8, 3158.
72. E.J.S. Lage and R.B. Stinchcombe, 1976, J. Phys. C9, 3295.
73. W.J.L. Buyers, T.M. Holden and A. Perreault, 1975, Phys. Rev. B11, 266.
74. F.W. Sheard and G.A. Toombs, 1971, J.Phys. C4, 315.

75. G.A. Toombs and F.W. Sheard, 1973, J.Phys. $\underline{C6}$, 1467.
76. A.P. Young, 1976, Proc. Int. Conf. Light Scattering in Solids, ed. M. Balkanski, R.C.C. Leite, and S.P.S. Porto (Flammarion, Paris) p. 817.
77. V.G. Vaks, A.I. Larkin, and S.A. Pikin, 1968, Sov.Phys. JETP $\underline{26}$, 188.
78. S. Takada, I. Ohnari, H. Kurosawa and Y. Ohmura, 1976, Prog.Theor.Phys. $\underline{55}$, 969
79. B. Žekš and F.C. de Sá Barreto, 1976, Proc.Int.Conf. Light Scattering in Solids, ed. M. Balkanski, R.C. Leite and S.P.S. Porto (Flammarion, Paris) p. 822.
80. F. Englert, 1963, Phys.Rev. $\underline{129}$, 567.
81. S.R.P. Smith, 1976, Proc. Int. Conf. Light Scattering in Solids, ed. M. Balkanski, R.C.C. Leite, and S.P.S. Porto (Flammarion, Paris) p. 329.
82. E. Pytte, 1973, Phys.Rev. $\underline{B8}$, 3954.
83. M.T. Hutchings, R. Scherm, S.H. Smith and S.R.P. Smith, 1975, J.Phys. $\underline{C8}$, L393.
84. M.T.Hutchings, R. Scherm, and S.R.P. Smith, 1975, AIP Conference Proceeding No. $\underline{29}$, 372.
85. J.K. Kjems, G. Shirane, R.J. Birgenau, and L.G. Van Uitert, 1973, Phys.Rev.Lett. $\underline{31}$, 1300.
86. J.K. Kjems, W. Hayes and S.H. Smith, 1975, Phys.Rev.Lett. $\underline{35}$, 1089.
87. C.M. Wilson and H.Z. Cummins, 1971, Proc.Int.Conf. Light Scattering in Solids, ec. M. Balkanski (Flammarion, Paris) p. 420.
88. R.S. Katiyar, J.F. Ryan, and J.F. Scott, 1971, Phys.Rev. $\underline{B4}$, 2835.
89. I.P. Kaminov, and T.C. Damen, 1968, Phys.Rev.Lett. $\underline{20}$, 1105.
90. R.A. Cowley, G.J. Coombs, R.S. Katiyar, J.F. Ryan, and J.F. Scott, 1971, J.Phys. $\underline{C4}$, L203.
91. C.Y. She, T.W. Broberg, L.S. Walland, and D.F. Edwards, 1972, Phys.Rev. $\underline{B6}$, 1847.
92. N. Lagakos, and H.Z. Cummins, 1974, Phys.Rev. $\underline{B10}$, 1063.
93. P.S. Peercy, and G.A. Samara, 1973, Phys.Rev. $\underline{B8}$, 2033.
94. P.S. Peercy, 1973, Phys.Rev.Lett. $\underline{31}$, 379.
95. P.S. Peercy, 1975, Comments Sol.St.Phys. $\underline{7}$, 37.
96. P.S. Peercy, 1975, Phys.Rev. $\underline{B12}$, 2725.
97. P.S. Peercy, 1976, Proc.Int.Conf. Light Scattering in Solids, ed. M. Balkanski, R.C.C. Leite, and S.P.S. Porto, (Flammarion, Paris) p. 782.
98. E.J.S. Lage and R.B. Stinchcombe, 1976, J.Phys. $\underline{C9}$, 3681.
99. R.C. Leung, W.B. Spillman, N.E. Tornberg, and R.P. Lowndes, 1976, Proc.Int.Conf. Light Scattering in Solids, ed. M. Balkanski, R.C.C. Leite,and S.P.S. Porto (Flammarion,Paris) p. 796.
100. R.T. Harley, W. Hayes and S.R.P. Smith, 1972, J.Phys. $\underline{C5}$,1501.
101. V. Dvorak, 1970, Czech. J. Phys. $\underline{B20}$, 1.

102. J.R. Sandercock, S.B. Palmer, R.J. Elliott, W. Hayes, S.R.P. Smith and A.P. Young, 1972, J.Phys. C5, 3126.
103. E.M. Brody, and H.Z. Cummins, 1974, Phys.Rev. B9, 179.
104. P.A. Fleury, P.D. Lazay, and L.G. Van Uitert, 1974, Phys.Rev. Lett. 33, 492.
105. J. Feder and E. Pytte, 1973, Phys.Rev. B8, 3978.
106. M.A. Moore, and H.C.W.L. Williams, 1972, J.Phys. C5, 3222.
107. R.T. Harley, W. Hayes, A.M. Perry and S.R.P. Smith, 1974, Solid St.Comm. 14, 521.
108. R.T. Harley, W. Hayes, A.M. Perry, S.R.P. Smith, R.J. Elliott, and I.D. Saville, 1974, J.Phys. C7, 3145.
109. G.A. Samara, 1973, Ferroelectrics 5, 25.
110. P.S. Peercy, 1976, Phys.Rev. B13, 3945.
111. R. Blinc, R. Pirc, and B. Žekš, 1976, Phys.Rev. B13, 2943.
112. E. Shiles, G.B. Taggart, and R.A. Tahir-Kheli, 1974, J. Phys. C7, 1515.
113. U. Schmidt, 1974, Z. Physik. 267, 277.
114. R. Pirc and P. Prelovšek, 1976, Proc.Int.Conf. Light Scattering in Solids, ed. M. Balkanski, R.C.C. Leite, and S.P.S. Porto (Flammarion, Paris) p. 829.
115. R. Pirc and P. Prelovšek, 1977, J.Phys. C10, 861
116. R.A. Cowley, 1970, J.Phys.Soc.Japan Suppl. 28, 239.
117. G.J. Coombs and R.A. Cowley, 1973, J.Phys. C6, 121.
118. R.A. Cowley and G.J. Coombs, 1973, J.Phys. C6, 143.
119. P.A. Fleury and K.B. Lyons, 1976, Phys.Rev.Lett. 37, 161, 1088.
120. J. Feder, 1974, Anharmonic Lattices, Structural Transitions and Melting, ed. T. Riste (Noordhoff, Leiden) p.113.
121. R. Silberglitt, 1972, Solid St. Comm. 11, 247.
122. M.D. Mermelstein and H.Z. Cummins, to be published.
123. B.I. Halperin and C.M. Varma, 1976, Phys.Rev. B14, 4030.
124. J.A. Krumhansl and J.R. Schrieffer, 1976, Solid St.Comm. 17, 1515.
125. R.A. Cowley, J.D. Axe and M. Iizumo, 1976, Phys.Rev.Lett. 36, 806.
126. M.E. Fisher, 1967, Rept.Prog. Phys. 30, 615.
127. C. Domb, 1974, in Phase Transitions and Critical Phenomena, ed. C. Domb and M.S. Green (Academic Press, New York) p.357.
128. P. Pfeuty, 1970, Ann. Phys. 27, 79.
129. M. Suzuki, 1971, Phys.Lett. 34A, 94.
130. P. Pfeuty, 1976, J.Phys. C9, 3993.
131. A.P. Young, 1975, J. Phys. C8, L309.
132. K.G. Wilson and J. Kogut, 1974, Physics Reports 12, 75.
133. R.A. Cowley, 1976, Phys.Rev. B13, 4877.
134. R.J. Birgenau, J.K. Kjems, G. Shirane, and L.G. Van Uitert, 1974, Phys.Rev. B10, 2512.
135. R.T. Harley and R.M. MacFarlane, 1975, J.Phys. C8, L451.

THEORY OF JAHN-TELLER TRANSITIONS

H. Thomas

Institut für Physik, Universität Basel

Klingelbergstrasse 82, CH-4056 Basel, Switzerland

1. INTRODUCTION

In crystals containing ions with orbitally degenerate ground state, the interactions of the electron orbitals with the ligand displacements have a destabilizing effect on the ionic configuration: Jahn-Teller (JT) effect. This provides a mechanism for structural phase transitions in crystals which would be stable in the absence of electron-ion interaction. We give an introduction into the theory of such JT-induced transitions, with particular emphasis on a classification of the various types of JT-coupling and their dynamic characteristics. The dynamics of the cooperative JT effect manifests itself in bands of collective vibronic modes arising from transitions between low-lying vibronic levels of the JT complexes, and an analysis of the collective dynamic behaviour requires a thorough understanding of the vibronic excitations of a single JT complex.

Surveys of experimental and theoretical work on the JT effect can be found in Refs /1-4/. As a mechanism for structural phase transitions, the JT effect was first considered by Dunitz and Orgel /5/. Transitions of this type have been found in a number of compounds containing transition-metal or rare-earth JT ions. References to earlier work, notably on spinels and perovskites containing Cu^{2+}, Ni^{2+}, Cr^{2+} and Mn^{3+} ions, are given in Refs /6,7/. As more recent examples we mention the transitions observed in the Cu^{2+}-hexanitro compounds /8-11/, in $CsCuCl_3$ /12-14/, in the rare-earth vanadates and arsenates with zircon structure /15-19/, in $PrAlO_3$ /19-21/, and in the intermetallic compound TmCd /22/. The theory of such JT transitions has been treated by various authors /6,7,16,18,23-29/.

Electron config.	d^1	d^2	d^3	d^4	d^5	d^6	d^7	d^8	d^9
Splitting of free ion term ^{2S+1}L by cubic crystal field (intermediate field)	^2D: E, T_2	^3F: A_2, T_2, T_1	^4F: T_1, T_2, A_2	^5D: T_2, E	^6S: A_1	^5D: E, T_2	^4F: A_2, T_2, T_1	^3F: T_1, T_2, A_2	^2D: T_2, E
Filling of single-electron crystal-field levels e_g, t_{2g} (strong field) — High S: upper row / Low S: lower row	e_g / t_{2g}↑ — T_2	T_1	A_2	upper: E / lower: T_1	upper: A_1 / lower: T_2	upper: T_2 / lower: A_1	upper: T_1 / lower: E	A_2	E
Examples of 3d-ions	V^{4+}, Ti^{3+}	Cr^{4+}, V^{3+}, Ti^{2+}	Mn^{4+}, Cr^{3+}, V^{2+}	Mn^{3+}, Cr^{2+}	Co^{4+}, Fe^{3+}, Mn^{2+}, Cr^{+}	Co^{3+}, Fe^{2+}, Mn^{+}	Ni^{3+}, Co^{2+}, Fe^{+}	Cu^{3+}, Ni^{2+}, Co^{+}	Cu^{2+}, Ni^{+}

Table 1: Orbital ground states of d-ions in octahedral crystal
field. The ground states in tetrahedral crystal field
can be obtained by the following procedure:
Second row: Reverse order of levels, or interchange
$d^n \leftrightarrow d^{10-n}$
Third row: Reverse order of levels, interchange
$d^n \leftrightarrow d^{10-n}$, interchange electrons $\leftrightarrow$ holes.

2.   DYNAMICS OF JT-SYSTEMS

2.1. Electronic Configuration

Our starting point is the electronic structure of a JT ion in
the crystal field of the ligands fixed in their symmetric reference
configuration. We consider specifically the case of a transition
metal ion in a crystal field of cubic symmetry with

crystal-field energy > spin-orbit coupling

(intermediate or strong crystal field). Table 1 shows the orbital
ground states for octahedral coordination. In tetrahedral crystal
field, the order of the levels is reversed, and the ground states
are related to those of the octahedral case by

$$| d^n, \text{ tetrahedral} \rangle = | d^{10-n}, \text{ octahedral} \rangle.$$

For intermediate crystal field (crystal-field energy $\lesssim$ intraatomic
Coulomb energy), the ground state is found from the splitting of
the free-ion term ^{2S+1}L by the crystal field (Table 1, second row).

Spin state	Symmetry of crystal field	E doublet	T_1 or T_2 triplet
High-Spin	Octahedral	d^4, d^9	d^1, d^2, d^6, d^7
	Tetrahedral	d^1, d^6	d^3, d^4, d^8, d^9
Low-Spin	Octahedral	d^7, d^9	d^1, d^2, d^4, d^5
	Tetrahedral	d^1, d^3	d^5, d^6, d^8, d^9

Table 2: JT configurations of d-ions in cubic crystal field
        (small spin-orbit coupling).

JT ions are expected for the configurations listed in the first
two rows of Table 2.
For strong crystal field (crystal-field energy > intraatomic Cou-
lomb energy), the crystal-field splitting of the single-electron
d level into a t_{2g} triplet and an e_g doublet has to be taken into
account before the Coulomb interaction. These levels are then fil-
led successively under observation of Hund's maximum-spin rule: For
(crystal-field energy < intraatomic exchange energy), Hund's rule
holds for the whole d shell: High-spin case (Table 1, upper part
of third row). In this case, one finds the same ground states as
for intermediate crystal field (first two rows of Table 2). For
(crystal-field energy > intraatomic exchange energy), Hund's rule
holds only within each subshell: Low-spin case (Table 1, lower
part of third row). In this case, JT-ions are expected for the
configurations listed in the last two rows of Table 2.

    In crystal fields of lower than cubic symmetry, the levels
are generally split further. Twofold orbital degeneracy still oc-
curs in tetragonal, trigonal and hexagonal symmetry. In lower sym-
metry, all orbital states are split into singlets.

    We disregard spin-orbit interaction and consequently spin de-
generacy, which is justified if (JT-coupling > spin-orbit interac-
tion). In the opposite case (JT-coupling < spin-orbit interaction),
the spin-orbit splitting of the crystal-field ground-state multi-
plet has to be taken into account before the coupling to the li-
gand motion. The situation is then qualitatively similar to the
case of weak crystal field (crystal-field energy < spin-orbit in-
teraction): For non-Kramers ions (even number of electrons) one
can apply the same considerations to the total-angular momentum
ground-state, and one finds the same types of ground-state degene-
racies as in the orbital-momentum case. For Kramers ions (odd num-
ber of electrons), on the other hand, the ground-state degeneracy
in the crystal field is usually reduced to that of a Kramers doub-
let, which shows no JT-coupling. The only exception is the case of

a $G_{3/2}$ quartet state in cubic crystal field.

2.2. Vibronic Coupling

Next, we consider the coupling of the electrons orbitals at the JT-ion with the distortions of the ligand configuration. The dynamics of the complex are described by the electron-ion Hamiltonian:

$$H = H_{e\ell} \cdot 1_{ion} + H_{ion} \cdot 1_{e\ell} + V(x,Q) \tag{2.1a}$$

$$H_{e\ell} = \sum p^2/2m + V_{e\ell}(x) \ , \qquad H_{ion} = \sum P^2/2M \ . \tag{2.1b}$$

Here, (x,p) stand for the coordinates and momenta of the electrons in unfilled shells, and (Q,P) for the ionic normal coordinates of the complex and their conjugate momenta, with effective mass M.

The electronic operators are expressed as matrices in a fixed basis consisting of states $|\psi_i>$ belonging to the reference configuration $Q = 0$:

$$<\psi_i | H_{e\ell} \cdot 1_{ion} + V(x,Q) | \psi_j> = V_{ij}(Q) \ . \tag{2.2}$$

The vibrational amplitudes $\chi_i(Q)$ of the total vibronic wave function

$$\psi(x,Q) = \sum_i \chi_i(Q) | \psi_i> \tag{2.3}$$

are approximately determined by the matrix Schrödinger equation

$$\left(H_{ion} \ 1_{e\ell} + \underline{V}(Q) \right) \cdot \underline{\chi}(Q) \equiv \underline{H}_{JT} \cdot \underline{\chi}(Q) = E \ \underline{\chi}(Q) \tag{2.4}$$

in which $\underline{V}(Q)$ serves as an effective potential-energy matrix for the ionic motion (generalized Born-Oppenheimer approximation). The electronic motion can in good approximation be restricted to the n-dimensional subspace spanned by the states $|\psi_i>$ with excitation energies $\leq kT_c$. Usually, the cubic crystal-field splitting is larger than kT_c (for d-ions typically of the order $10^4 cm^{-1}$), such that in cubic symmetry only the ground-state multiplet has to be taken into account. In crystal fields of lower than cubic symmetry, on the other hand, the further splitting of the ground state can be comparable to kT_c, especially if the distortion from cubic symmetry is small. In such cases, the lowest excited states have to be included.

We introduce a complete set of n x n matrices

$$\underline{\underline{\xi}}_0 = \underline{\mathbf{1}}_{e\ell} \; , \; \underline{\underline{\xi}}_1 \; , \; \underline{\underline{\xi}}_2 \qquad\qquad (2.5)$$

with

$$\mathrm{tr}_{e\ell}\,\underline{\underline{\xi}}_\nu = 0 \quad (\nu\neq 0) \qquad\qquad (2.6)$$

acting on the electronic states (electronic pseudospin operators), and express the electronic operators as linear combinations of the $\underline{\underline{\xi}}_\nu$,

$$\underline{\underline{V}}(Q) = \sum_\nu V_\nu(Q)\,\underline{\underline{\xi}}_\nu = V_0(Q)\,\underline{\mathbf{1}}_{e\ell} + \underline{\underline{V}}_{JT}(Q) \qquad\qquad (2.7)$$

such that

$$\mathrm{tr}_{e\ell}\,\underline{\underline{V}}_{JT}(Q) = 0 \; . \qquad\qquad (2.8)$$

We obtain thus a separation of $\underline{\underline{V}}(Q)$ into a part $V_0(Q)\underline{\mathbf{1}}_{e\ell}$ which is independent of the electronic state (vibrational part), and a part $\underline{\underline{V}}_{JT}(Q)$ which vanishes on averaging over the electronic states (JT-part).

An expansion in powers of Q gives rise to the following classification of terms:
Vibrational part $\nu = 0$:

$$V_0(Q) = V_0^{(0)} - F\cdot Q + V_{harm}(Q) + V_{anh}(Q) \; . \qquad\qquad (2.9)$$

The zeroth-order term is a constant and may be dropped. The second-order term is the harmonic part, and the higher-order terms are the anharmonic parts of the vibrational potential of the JT-complex. We further include a linear coupling to an external field F which will later be identified with the molecular field due to lattice-dynamical interactions with neighbouring complexes.

JT-parts $\nu \neq 0$:

$$\underline{\underline{V}}_{JT}(Q) = \underline{\underline{V}}_\Delta + \underline{\underline{V}}_{JT}^{(1)}(Q) + \underline{\underline{V}}_{JT}^{nonlin}(Q) \; . \qquad\qquad (2.10)$$

The zeroth-order term describes the electronic ground-state splitting; it occurs only when excited electronic states have to be taken into account, and is thus not a JT term in the strict sense. The first-order term is the linear JT effect which plays the decisive role for the transitions considered, because it favours a distorted ligand configuration. The JT theorem states that for every reference configuration with a degenerate ground state (except for linear molecules and for Kramers degeneracy), there exists a vibrational mode Q for which symmetry permits

$$\underline{\underline{V}}_{JT}^{(1)}(Q) \neq 0 \ . \tag{2.11}$$

The higher-order terms describe nonlinear JT interactions.

We introduce symmetry-adapted vibrational coordinates Q_γ^Γ transforming as the irreducible representations Γ of the symmetry group of the JT complex, and the corresponding electronic operators $\underline{\underline{\mathcal{E}}}_\gamma^\Gamma$, such that

$$V_{harm}(Q) = \sum_\Gamma \frac{1}{2} M \, \omega_\Gamma^2 \sum_\gamma (Q_\gamma^\Gamma)^2 \tag{2.12a}$$

$$\underline{\underline{V}}_{JT}^{(1)}(Q) = -\sum_\Gamma A_\Gamma \sum_\gamma Q_\gamma^\Gamma \underline{\underline{\mathcal{E}}}_\gamma^\Gamma \tag{2.12b}$$

According to the JT theorem, at least one coupling constant A_Γ is allowed by symmetry. The possible types of JT coupling which can occur in crystals are listed in Table 3. Figure 1 shows the ligand configurations corresponding to the symmetry-adapted coordinates appearing in the linear JT effect. In the following, only the JT-active modes with a nonvanishing JT coupling will be taken into account.

Site Symmetry	Electronic State	Vibrational Coordinate	Vibronic Coupling
tetragonal	2-fold: E	1-fold: β_{1g}, β_{2g}	E $\boxtimes$ $(\beta_1 + \beta_2)$
trigonal hexagonal cubic	2-fold: E	2-fold: ε_g	E $\boxtimes$ ε
cubic	3-fold: T_1 or T_2	2-fold: ε_g 3-fold: τ_{2g}	T $\boxtimes$ $(\varepsilon + \tau_2)$
cubic	4-fold: $G_{3/2}$ (spin-orbit)	2-fold: ε_g 3-fold: τ_{2g}	$G_{3/2}$ $\boxtimes$ $(\varepsilon + \tau_2)$

Table 3: The four types of linear Jahn-Teller coupling. The representations of the electronic states and of the vibrational coordinates are denoted by upper-case Roman letters and lower-case Greek letters, respectively.

The eigenvalues of $\underline{\underline{V}}(Q)$ form a potential-energy surface in Q-space consisting of n sheets, and the vibrational motion can be visualized as a motion in this surface. From the linear JT term together with the harmonic vibrational term, one obtains minima at

$$Q_{JT} \sim A/M\omega^2 \tag{2.13}$$

β - mode
tetragonal symmetry

$Q_{\beta 2}$ $Q_{\beta 1}$

ε - mode
trigonal symmetry

Q_θ Q_ε

ε - mode
cubic symmetry

Q_θ Q_ε

τ_2 - mode
cubic symmetry

Q_ξ Q_η Q_ζ
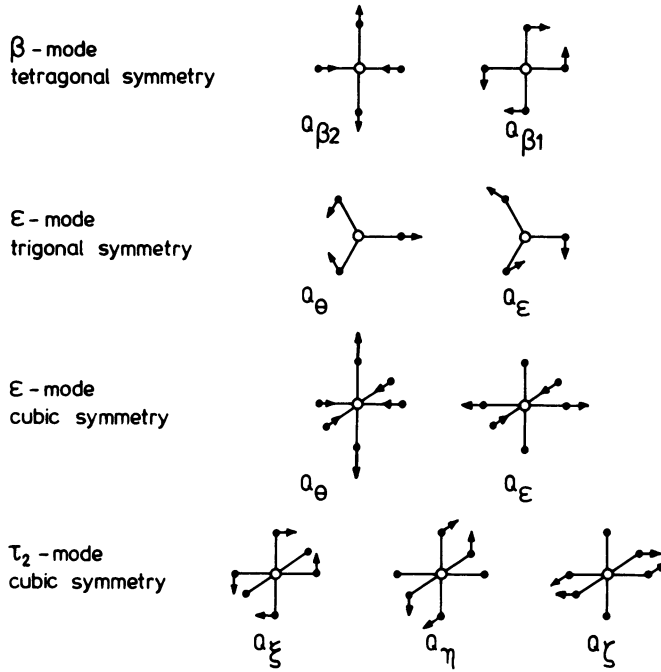
Figure 1: Ligand modes coupling to JT ions

with depth

$$E_{JT} \sim A^2/2M\,\omega^2. \qquad\qquad (2.14)$$

Thus, the JT effect favours a distorted state $Q = Q_{JT}$ over the un-distorted state $Q = 0$ by an energy E_{JT} (JT destabilization energy). We are interested here in the case of strong JT effect where the JT destabilization energy is large compared with the vibrational zero-point energy, or equivalently, where the JT distortion is large compared with the vibrational zero-point amplitude:

$$E_{JT} \gg \frac{1}{2}\hbar\omega \;;\qquad Q_{JT} \gg (2\hbar/M\omega)^{1/2}\;. \qquad (2.15)$$

In all cases, the vibronic ground state has the same degeneracy as the orbital crystal-field multiplet: The JT interaction cannot split the ground state, but can only mix electronic and vibrational motion because it has the full symmetry of the crystal field.

There exist two cases with basically different dynamic behaviour: If $\underline{\underline{V}}(Q)$ is simultaneously diagonal for all values of Q, vibrational motion leaves the electronic orbitals fixed. This occurs

for E ⊠ β and T ⊠ e coupling. If the eigenstates of $\underline{V}(Q)$ depend on Q, then vibrational motion will cause the electronic orbitals to follow, and one obtains dynamically coupled vibronic motion. This occurs for E ⊠ ε and T ⊠ τ_2 coupling.

The eigenvalues E_n of $\underline{\underline{H}}_{JT}$ determine the vibronic excitations of the JT complex. The dynamic properties are conveniently described by the dynamic susceptibility $\underset{\sim}{\chi}_s(\omega)$ to an external force $\underset{\sim}{F}$ at frequency ω,

$$\underset{\sim}{\chi}_s(\omega) = \frac{1}{Z} \sum_{mn} \frac{<m|\underset{\sim}{Q}|n><n|\underset{\sim}{Q}|m>}{E_n - E_m - \hbar\omega - i0^+} \left(e^{-\beta E_n} - e^{-\beta E_m} \right) \tag{2.16}$$

It shows with which strength the various vibronic transitions can be excited by a given force $\underset{\sim}{F}$.

2.3. Collective Behaviour, Mean-Field Approximation (MFA)

If coupling to all other modes is neglected, the crystal is described by a model Hamiltonian of the form

$$\underline{\underline{H}} = \sum_{\ell} \underline{\underline{H}}_{JT,\ell} + \underline{\underline{H}}^{int} . \tag{2.17}$$

We assume ordinary lattice-dynamical bilinear interactions between the coordinates $\underset{\sim}{Q}_\ell$ in different cells:

$$\underline{\underline{H}}^{int} = -\frac{1}{2} \sum_{\ell\ell'}' \underset{\sim}{Q}_\ell \cdot \underset{\sim}{v}_{\ell\ell'} \cdot \underset{\sim}{Q}_{\ell'} \underline{\underline{1}}_{e\ell} . \tag{2.18}$$

The matrix $\underset{\sim}{v}_{\ell\ell'}$ together with the force constants of V_{harm} of the single cell (Eq. 2.9) form that part of the dynamic matrix which describes the phonon bands constructed from the local normal coordinates Q_ℓ. If the ligands of a given JT ion belong to different lattice cells, there arise problems with the orthogonality of the Q_ℓ for different ℓ /30/. These problems have been discussed in detail in Ref. /31/; they will be disregarded in the present context. The collective response to an external field can be decomposed into the single-cell response to the molecular field and the response of the molecular field,

$$\delta \underset{\sim}{Q}_\ell = \underset{\sim}{\chi}_s(\omega) \cdot \delta \underset{\sim}{F}^{mol} , \quad \delta \underset{\sim}{F}_\ell^{mol} = \sum_{\ell'} \underset{\sim}{v}_{\ell\ell'} \cdot \delta \underset{\sim}{Q}_{\ell'} + \delta \underset{\sim}{F}_\ell^{ext} , \tag{2.19}$$

and one obtains after Fourier transformation the usual feedback result of MFA /30,32/

$$\underset{\sim}{\chi}_q(\omega) = \underset{\sim}{\chi}_s(\omega) \cdot \left(\underset{\sim}{1} - \underset{\sim}{v}_q \cdot \underset{\sim}{\chi}_s(\omega) \right)^{-1} \tag{2.20}$$

where

$$\underset{\approx}{v}_{q} = \sum_{\ell'}{}' \underset{\approx}{v}_{\ell\ell'} \exp(iq \cdot R_{\ell\ell'}) \qquad (2.21)$$

is the Fourier transform of the interaction $v_{\ell\ell'}$. The collective modes are found from the poles of $\underset{\approx}{\chi}_{q}(\omega)$, i.e. from the zeros of

$$\underset{\approx}{v}_{q} \cdot \underset{\approx}{\chi}_{s}(\omega) = \underset{\approx}{1} . \qquad (2.22)$$

Since

$$\sum_{q} \underset{\approx}{v}_{q} = \underset{\approx}{v}_{\ell\ell} = 0 , \qquad (2.23)$$

the eigenvalues of $\underset{\approx}{v}_{q}$ take on positive and negative values in the Brillouin zone. As Figure 2 illustrates, the single-cell excitations give thus rise to bands of collective modes consisting of linear superpositions of single-cell excitations with phases $\exp(iq \cdot R_{\ell})$. Of particular interest is the possibility of critical slowing down of a collective mode due to the feedback effect of the molecular field. One of the main objects of the theory is the study of the nature of the soft mode associated with the transition. This requires a thorough understanding of the underlying single-cell excitations. It is important to note that the collective modes originating from vibronic excitations of the single complex are not optical-phonon modes of the crystal, but are modes of vibronic character occurring in addition to the phonon modes in JT crystals.

The type of phase transition is determined by that mode which yields the largest feedback enhancement, i.e. by the maximum eigen-
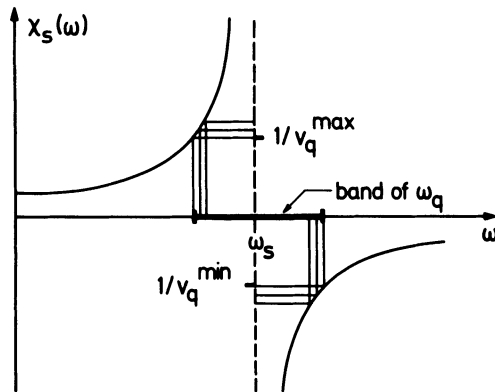
Figure 2: Single-cell excitation at frequency ω_s giving rise to band of collective excitations with frequencies ω_q.

value of v_q. If this occurs at $q = 0$, the transition will be fer-
rodistortive; for $q = \frac{1}{2} \times$ (reciprocal lattice vector), it will be
antiferrodistortive; and for other values in the Brillouin zone,
one finds transitions to more complicated commensurate or incommen-
surate phases. In the ferrodistortive case, the only candidate for
a continuous phase transition is the E $\boxtimes$ β coupling, as is easily
seen from the Landau criteria: Both the ε and the τ_2 mode have
third-order invariants, and yield therefore necessarily disconti-
nuous transitions. In the antiferrodistortive case, on the other
hand, no third-order invariants exist, and continuous transitions
are possible for all types of coupling.

In the low-symmetry phase, there exists a static molecular
field. For this reason, it is important that we study the behaviour
of the JT complex in the presence of a static field,

$$V_1^{(0)} = - \underset{\sim}{F} \cdot \underset{\sim}{Q} \tag{2.24}$$

as indicated in Eq. (2.9).

It should be noted that in MFA in its proper sense only the
correlations between coordinates in one cell and the molecular
field arising from the interactions with different cells are neg-
lected, but the vibronic correlations between the electron orbi-
tals and the ligand modes of the same complex, which play an im-
portant role in JT transitions /7,26-28,33/, are fully taken in-
to account. Neglect of these intracell correlations by a factori-
zation of correlation functions $<Q \underset{\approx}{\xi}>$ /6,24/ yields unphysical re-
sults such as a phase transition for non-interacting JT complexes
and a decreasing T_c with increasing interaction strength unless
spurious so-called "self-energy" terms are subtracted out /6,16,
25/. In the MFA as used here, no such ad hoc corrections are re-
quired.

2.4. Coupling to Elastic Strain

The model considered so far does not contain elastic deforma-
tions because the JT-active coordinates Q_ℓ leave the center of gra-
vity of each cell at rest. Coupling of the Q_ℓ to elastic strain
will however play an important role, especially in the ferrodistor-
tive case: There exist strain components of the same symmetry $\beta_{1,2}$,
ε, and τ_2 as the JT-active modes for all types of JT coupling,
which gives rise to bilinear piezodistortive coupling.

We assume a crystal structure in which the ligand modes Q_ℓ
are true intracell distortions. The elastic deformation is des-

cribed by a displacement field consisting of rigid translations $\underset{\sim}{s}_\ell$ of cells ℓ which are assumed to vary slowly with ℓ. Then, the elastic strain tensor $\underset{\sim}{\varepsilon}_\ell$ can be defined in analogy to the continuum case as the symmetrized gradient of the displacement vector, i.e.

$$\underset{\sim}{s}(\underset{\sim}{R}_\ell + \underset{\sim}{\xi}) = \underset{\sim}{A} \cdot \underset{\sim}{s}(\underset{\sim}{R}_\ell) + \underset{\sim}{\varepsilon}_\ell \cdot \underset{\sim}{\xi} \; , \tag{2.25}$$

where $\underset{\sim}{A}$ describes an infinitesimal rotation. In terms of symmetry-adapted strain components $\varepsilon^\Gamma_{\gamma,\ell}$, the elastic Hamiltonian has the form /24/

$$H^{elast} = \sum_\ell \{ \frac{1}{2} M_s \dot{s}_\ell^2 + \sum_\Gamma c_\Gamma \sum_\gamma (\varepsilon^\Gamma_{\gamma,\ell})^2 \} \tag{2.26}$$

where the c_Γ are the bare elastic constants per cell volume for strain of symmetry Γ. The strain is coupled to the distortions Q_ℓ of the JT complexes by a piezodistortive coupling term /26,28,29/

$$H' = \sum_\ell \sum_\Gamma g_\Gamma \sum_\gamma Q^\Gamma_{\gamma,\ell} \varepsilon^\Gamma_{\gamma,\ell} \tag{2.27}$$

assumed to be local. Equations (2.26) and (2.27) are reasonable descriptions in the long-wavelength limit. Since the elastic energy (2.26) together with compatibility requirements for the strain field makes short-wavelength strain components unfavourable, piezodistortive coupling is most effective for ferrodistortive and small q modes.

This coupling has important consequences even in the absence of JT coupling: It leads to an intracell distortion

$$Q^{ind}_\Gamma = \chi_\Gamma \, g_\Gamma \, \varepsilon_\Gamma \tag{2.28}$$

induced by a uniform strain ("internal strain"), and gives rise to a renormalization of elastic constants

$$c^*_\Gamma = c_\Gamma - \chi_\Gamma g^2_\Gamma \; . \tag{2.29}$$

Here, χ_Γ is the ferrodistortive static susceptibility of mode Q_Γ in the absence of piezodistortive coupling. On the other hand, a ferrodistortive distortion Q_Γ induces a uniform strain of magnitude

$$\varepsilon^{ind}_\Gamma = c^{-1}_\Gamma \, g_\Gamma \, Q_\Gamma \tag{2.30}$$

and leads to a renormalized ferrodistortive susceptibility

$$\chi^*_\Gamma = \chi_\Gamma \left(1 - c^{-1}_\Gamma \chi_\Gamma g^2 \right) \; . \tag{2.31}$$

From Equations (2.29) and (2.31) there follows the interesting relation

$$c_\Gamma^* \chi_\Gamma^* = c_\Gamma \chi_\Gamma \qquad\qquad (2.32)$$

between the renormalized and the unrenormalized quantities /29/.

For a ferrodistortive transition, Eq. (2.29) shows that there occurs an elastic instability ($c_\Gamma^*=0$) before the phase transition of the uncoupled system ($\chi_\Gamma=\infty$) is reached: Because of piezodistortive coupling, the soft vibronic Q-mode pushes the acoustic mode of the appropriate symmetry down until the sound velocity vanishes at the elastic instability $c_\Gamma^* = 0$. In the ordered phase, there exists a strain ϵ_Γ given by Eq. (2.30) proportional to the order parameter Q_Γ. Such elastic instabilities associated with a soft acoustic mode have been observed in a number of rare-earth compounds /15,17,22/, even for systems where the structural transition coincides with a magnetic transition /34,35/, as well as in nickel chromite /36/. The coupling strength g_Γ can be determined by fitting the experimental results to an equation of the form (2.29). The results show that strain coupling is very important in the rare-earth systems investigated.

By qualitative arguments it may be expected that the piezodistortive coupling in transition-metal compounds is generally smaller than in rare-earth compounds. Equation (2.28) shows that the coupling constant g_Γ measures the amount of distortion of the ligand configuration induced by a given strain. In transition-metal compounds, covalent bonding by the d-orbitals makes the ligand complex very stable, thus preventing large distortions by strain. In rare-earth compounds, on the other hand, covalent bonding by the f-orbitals in much weaker, the ligand complexes will be less stable and will therefore more readily adjust to strain.

For antiferrodistortive transitions, the piezodistortive coupling (2.27) still has important effects if the distortion has a ferrodistortive component (secondary order parameter). This is to be expected in the case of ϵ and τ_2 modes for which configurations Q and $-Q$ are not equivalent. Consequences of this coupling for antiferrodistortive E ⊠ ϵ systems are discussed in Refs. /28,29/ (see Section 3.2). In a purely antiferrodistortive structure as it may occur in the E ⊠ β case, on the other hand, bilinear coupling to uniform strain is ineffective, and one has to consider higher-order piezodistortive couplings like

$$H'' = - \sum g_{\gamma\gamma'\gamma''}^{\Gamma\Gamma'\Gamma''} Q_\gamma^\Gamma Q_{\gamma'}^{\Gamma'} \epsilon_{\gamma''}^{\Gamma'} \quad . \qquad\qquad (2.33)$$

Up to this point it was assumed that JT coupling occurs only with intracell distortions Q_Γ of the ligand configuration. In principle, there exists also a direct JT coupling to strain of the form

$$\underset{=}{V}'_{JT} = - \sum_\Gamma A'_\Gamma \sum_\gamma \epsilon^\Gamma_\gamma \underset{=}{\xi}^\Gamma_\gamma \quad , \tag{2.34}$$

as has been considered in Refs. /6,24/. This coupling is due to the crystal field at the JT ion produced by displacements of neighbouring complexes, with all ligands kept fixed in their undistorted symmetric configuration. Since this contribution to the crystal field will be much smaller than the contribution produced by the distortion of the ligand configuration, the intracell coupling (2.12b) is expected to be the dominant one if an intracell ligand distortion exists at all in the crystal structure under consideration. If, on the other hand, the distortion of the ligand configuration is the strain coordinate itself, as is the case in the perovskite structure /6/ and in the CsCℓ and NaCℓ structures /22,35/, then only the strain-JT coupling (2.34) exists, and the model of Ref. /24/ which takes only acoustic modes into account applies without modification. In the general case, it will however be difficult to distinguish experimentally a direct strain-JT coupling (2.34) from an indirect coupling via the piezodistortive effect (2.27), i.e. to distinguish A' from $A\chi g$.

3. SPECIFIC CASES

3.1. E x β Coupling

This coupling which occurs in tetragonal symmetry represents the simplest case. Disregarding anharmonic and nonlinear-JT terms, the single-cell JT Hamiltonian has the form

$$\underset{=}{H}_{JT} = \left(\frac{1}{2M} P^2 + \frac{1}{2} M \omega^2_\beta Q^2\right) \underset{=}{1}_{e\ell} - AQ \underset{\underline{=}}{\xi}_3 - FQ\underset{=}{1}_{e\ell} \tag{3.1}$$

where $\underset{\underline{=}}{\xi}_3$ is the Pauli matrix $\left(\begin{smallmatrix} 1 & 0 \\ 0 & -1 \end{smallmatrix}\right)$. The potential energy "surface" consists of two displaced parabola

$$V(Q) = \frac{1}{2} M \omega^2_\beta Q^2 - (\pm A + F) Q \tag{3.2}$$

displayed in Figure 3a. Since there is only one electronic operator, the eigenvalue problem separates into two independent harmonic oscillators ($\zeta = \pm 1$), and one finds the eigenvalues

$$E_{n,\zeta} = - E_{JT} - \frac{1}{2} F^2/M\omega^2_\beta + (n+\frac{1}{2})\hbar\omega_\beta - F Q_{JT} \zeta \tag{3.3}$$
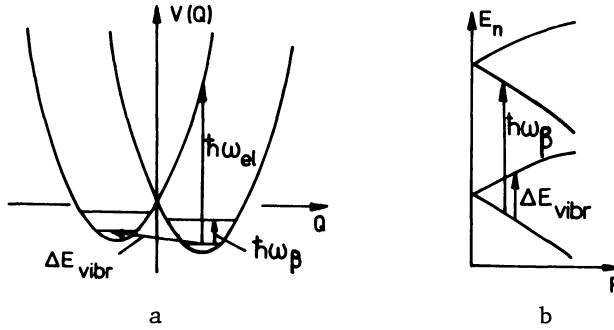
Figure 3: E ⊗ β coupling
        a: Potential energy V(Q)
        b: Shift of vibronic energy levels with field

shown in Figure 3b. Here, $Q_{JT} = A/M\omega_\beta^2$ is the JT displacement and
$E_{JT} = AQ_{JT}/2$ is the JT stabilization energy.

We now turn to the important question, by what type of experiment can the various transitions be induced, i.e. which type of coordinate will show the various excitation frequencies. Since $\underline{\underline{\xi}}_3$ commutes with P and Q, the vibrational motion does not couple at all to the motion of the electron orbital, and we find for the deviation $\delta Q = Q-Q_0$ from the minima $Q_0 = \pm Q_{JT}-F/m\omega_\beta^2$ the equation of motion

$$\ddot{\delta Q} + \omega_\beta^2\,\delta Q = 0 \qquad\qquad (3.4)$$

with unperturbed vibrational frequency ω_β: A motion of the electron orbital has no effect on the ionic motion. The low-frequency vibronic transition ΔE_{vibr} can thus certainly not be excited by a force acting on the coordinate Q. This result is due to the fact that no tunnelling occurs between the two parabola. The equations of motion for $\underline{\underline{\xi}}_\pm$, on the other hand,

$$\hbar\,\dot{\underline{\underline{\xi}}}_\pm = 2i\,A\,Q\,\underline{\underline{\xi}}_\pm \qquad\qquad (3.5)$$

couple to the vibrational coordinate Q. However, for strong JT-effect, Q fluctuates only little about the minima $Q_0^\pm$, and the main part of the motion of the electronic pseudospin $\underline{\underline{\xi}}$ consists in a precession with frequency

$$\hbar\,\omega_{e\ell} = 4\,E_{JT} \pm 2\,F\,Q_{JT} \qquad\qquad (3.6)$$

corresponding to the vertical (Franck-Condon-like) transition in Figure 3a: The ionic motion has only a small effect on the electron state, consisting in a small modulation of the precession frequency. The vibronic transition ΔE_{vibr} can thus neither be excited by a force acting on the electron orbitals. An operator associated

with the vibronic transition ΔE_{vibr} is obtained by coupling the pseudospin-flip operator $\underline{\underline{\xi}}_{\pm}$ with the vibrational translation operators ("ionic configuration-flip operators")

$$T_{\pm} = \exp \left(\pm i \, Q_{JT} \, P \right) \tag{3.7}$$

One finds indeed

$$\hbar \left(\underline{\underline{\xi}}_{\pm} T_{\pm} \right)^{\bullet} = \pm \, 2i \, F \, Q_{JT} \, \left(\underline{\underline{\xi}}_{\pm} T_{\pm} \right) \tag{3.8}$$

i.e. a precession with the vibronic frequency $\Delta E_{vibr} = 2 \, F \, Q_{JT}$.

In the cooperative system, the vibrational excitation gives rise to an optical-phonon band, which in this model is not influenced at all by the transition. The electronic excitation remains local in character, and is split by the molecular field F. The vibronic excitation will for $T < T_c$ give rise to a vibron band which becomes soft as $T \to T_c$. For $T > T_c$ the molecular field vanishes, yielding $\Delta E_{vibr} = 0$. In a realistic system, there will occur thermally activated hopping between the two degenerate states $\zeta = \pm 1$, giving rise to a vibronic relaxation band which becomes soft as $T \to T_c$. The decoupling of the phonons from the electronic motion can be formally taken into account by a transformation to displaced phonon coordinates δQ and pseudospin variables $S_{\pm} = \underline{\underline{\xi}}_{\pm} T_{\pm}$, $S_3 = \underline{\underline{\xi}}_3$ /37,38/. One then obtains an interacting Ising system completely decoupled from the optical-phonon band /38/, and the vibronic excitations become the spinwaves of this model.

In order to excite the vibronic mode, one would have to couple an external probe to the operators $\underline{\underline{\xi}}_{\pm} T_{\pm}$, i.e. the coupling would have to have matrix elements between the ground states in each of the two parabola. This appears impossible in the strong JT case considered here, where the two wave functions are spatially well separated. There will therefore probably exist no method for direct observation of this vibronic mode. But indirect methods can be found: the splitting ΔE_{vibr} has been observed in $TmVO_4$ by optical transitions from the split doublet ground state to a high-lying singlet /39/. The results displayed in Figure 4 show clearly the expected softening. Another method consists in splitting the electronic degeneracy by a static magnetic field, which changes the system into a pseudo-JT system treated in Section 3.5. Then tunnelling takes place between the two parabola, and the vibronic transition can be excited by EPR /19/.

In crystals of this type, the JT ion can couple both to the β_1 mode and the β_2 mode, and it depends on the coupling constants and the interactions which coupling determines the phase transi-
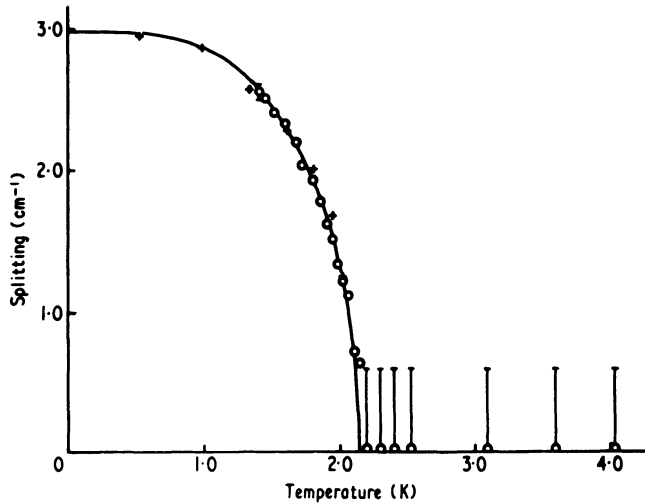
Figure 4: Ground-state splitting of $TmVO_4$ as function of tempera-
         ture. Circles from optical absorption, crosses from mag-
         netic measurements. (After /39/).

tion. In $TmVO_4$ there seems to occur an interesting competition bet-
ween these two coupling schemes /15b/.

3.2. E x ε Coupling

The linear JT coupling has the form

$$\underline{\underline{V}}_{JT}^{(1)} (Q) = -A_\varepsilon \ (Q_\theta \underline{\underline{\Sigma}}_\theta + Q_\varepsilon \underline{\underline{\Sigma}}_\varepsilon) \tag{3.9}$$

where

$$\underline{\underline{\Sigma}}_\theta = -\underline{\underline{\Sigma}}_3 = \begin{pmatrix} -1 & 0 \\ 0 & 1 \end{pmatrix}, \quad \underline{\underline{\Sigma}}_\varepsilon = \begin{pmatrix} 0 & 1 \\ 1 & 0 \end{pmatrix} \tag{3.10}$$

are electronic operators of E symmetry acting on the two-dimensio-
nal E-Hilbert space,with respect to a basis transforming as

$$\psi_\theta = |2z^2-x^2-y^2> \ ; \quad \psi_\varepsilon = |\sqrt{3}(x^2-y^2)> \ . \tag{3.11}$$

The potential energy surface of $\underline{\underline{V}}_{JT}^{(1)}(Q) + V_{harm}(Q)\underline{1}_{e\ell}$ is the well-
known Mexican hat (Figure 5a). In this case, there exists a strong
dynamic coupling between the ionic configuration Q and the elec-
tronic state: When $Q = Q \ (\cos\phi, \sin\phi)$ is turned by an angle $\Delta\phi$,
the electronic state vector in the two-dimensional Hilbert space
rotates by $-\Delta\phi/2$. Thus, by a full rotation of Q, the electronic
wave function changes sign, and so does the vibrational amplitude
$\chi(Q)$ in order to make the total vibronic wave function invariant.
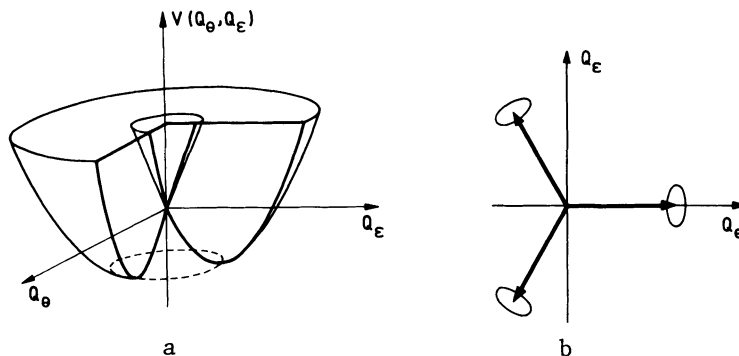
Figure 5: Potential-energy surface $V(Q_\theta, Q_\epsilon)$ for $E \otimes \epsilon$ coupling.
   a: $\underline{V}_{JT}^{(1)} + V_{harm} \underline{1}_{e\ell}$ ("Mexican hat")
   b: Warping by $\underline{V}_{JT}^{(2)} + V_{anh}^{(3)} \underline{1}_{e\ell}$ ("tricorn")
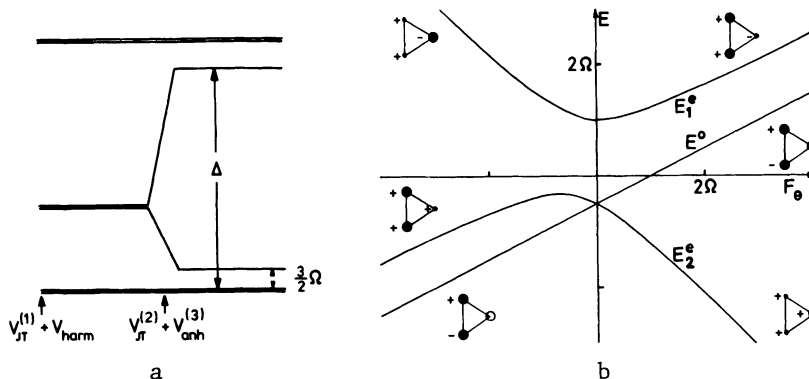
Figure 6: Vibronic energy levels for $E \otimes \epsilon$ coupling.
   a: Splitting of the rotator levels of the Mexican hat
      by $\underline{V}_{JT}^{(2)} + V_{anh}^{(3)} \underline{1}_{e\ell}$.
   b: Level shift with field in θ-direction

This "anticyclic" boundary condition $\chi(\phi + 2\pi) = -\chi(\phi)$ has important consequences for the ordering of the energy levels of $\underline{H}_{JT}$: One obtains doubly degenerate rotator eigenvalues for the motion in the brim of the hat corresponding to half-integer quantum numbers $m = \pm 1/2, \pm 3/2, \ldots /27/$.

Second-order JT coupling $\underline{V}_{JT}^{(2)}(\underline{Q})$ and third-order anharmonic terms $V_{anh}^{(3)}(\underline{Q})$ gives rise to a warping of the brim, changing the hat into a tricorn with three minima (Figure 5b). Correspondingly, the doubly degenerate rotator eigenvalues for the vibronic motion in the brim change as shown in Figure 6a into triplets correspon-

ding to states localized in these three minima, which are split in-
to doublets and singlets because of tunnelling between the minima.
Contrary to ordinary potential problems, we obtain on account of
the anticyclic boundary condition a ground-state doublet and an
excited singlet, separated by a tunnel splitting 3 $\Omega/2$.

We assume the excitation energy Δ to the next higher triplet
to be large compared to kT_c, and describe the vibronic motion in
terms of $S = 1$ pseudospin operators acting on the lowest vibronic
triplet /26/. The Hamiltonian of the JT complex takes the form

$$H_{JT} = -\frac{1}{2} \Omega \left[\sqrt{2}\ S_x - (S_x^2 - S_y^2) \right] - F_\theta Q_\theta - F_\varepsilon Q_\varepsilon \ , \qquad (3.12)$$

where the coordinates Q_θ, Q_ε are in the strong localization limit
given by

$$Q_\theta = \frac{1}{2}\ (2 - 3\ S_z^2), \qquad Q_\varepsilon = \frac{1}{2}\ \sqrt{3}\ S_z \qquad (3.13)$$

The shift of the eigenvalues with a field in the θ-direction is
shown in Figure 6b. The distribution of the vibrational amplitude
over the three valleys is schematically indicated for the different
states. In the $\Omega \rightarrow 0$ limit, this model goes over into the three-
states Potts model /29/.

In cooperative systems, the transitions between these levels
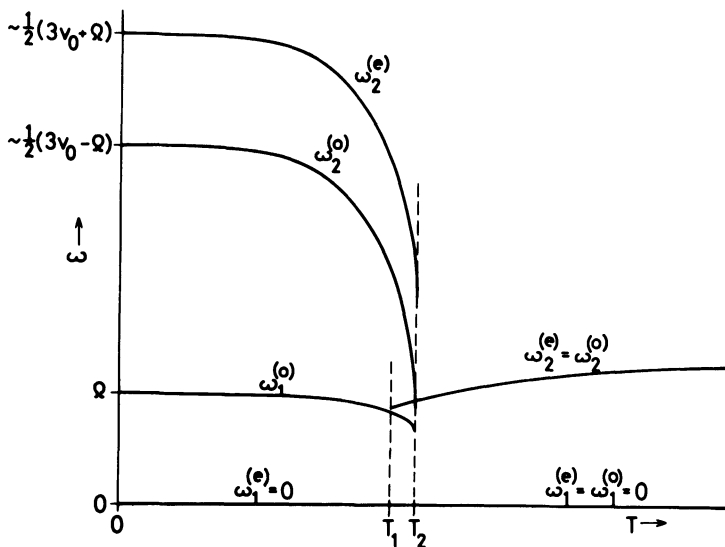
Figure 7: Collective vibronic modes for ferrodistortively coupled
          E $\otimes$ ε complexes (After /26/).

give rise to strongly temperature-dependent vibronic bands. This
behaviour was studied for the phase transitions occurring in a sy-
stem consisting of a simple cubic arrangement of JT complexes
/26-29/. Figure 7 shows the results for the case of a ferrodistor-
tive transition /26/ which is necessarily discontinuous (see Sec-
tion 2.3). The bands obtained are easily associated with transi-
tions between the levels of Figure 6b, for $T > T_c$ at $F = 0$ and for
$T < T_c$ at $F = F^{mol}(T) > 0$. An important result is the fact that
none of these finite-frequency modes is the soft mode associated
with the stability limits T_1, T_2 of the two phases. In the high-
temperature phase, it is the zero-frequency transition within the
ground state doublet which will give rise to a soft relaxational
mode. In the low-temperature phase, on the other hand, coupling to
the energy will yield a soft heat-diffusion mode, because of the
discontinuous nature of the transition /40,41/.

In the case of antiferrodistortive interactions, there exist
two competing low-temperature phases of tetragonal symmetry, the
θ-phase with the sublattice distortions in one of the three equi-
valent θ directions, and the ε phase with sublattice distortions
which close to T_c are along one of the ε directions, but cant to-
wards the two closest θ directions with decreasing T (see the in-
serts in Figure 8) /28,29/. The θ phase is favoured by tunnelling
and at $T \neq 0$ also by entropy. Therefore, in the absence of further
couplings, the θ phase is stable at all temperatures up to the
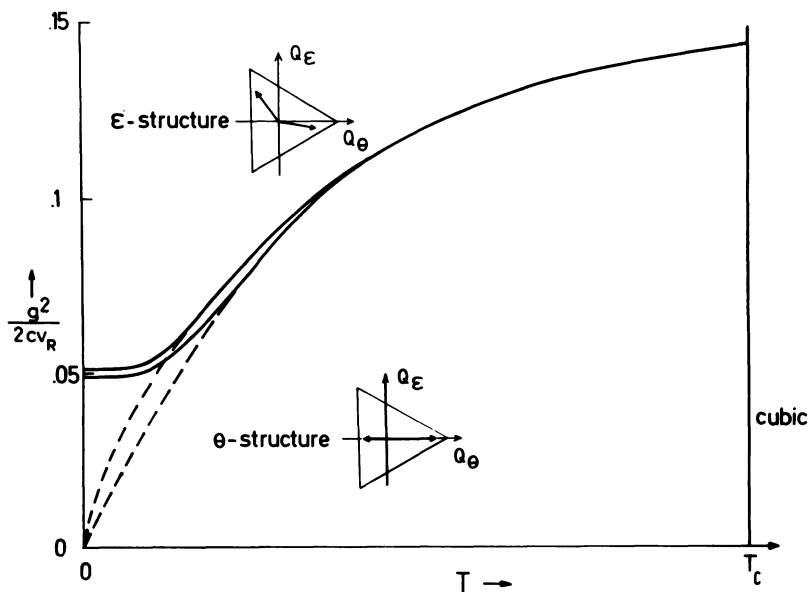
Figure 8: Phase diagram for antiferrodistortively coupled E ⊗ ε
          complexes with piezodistortive coupling. (Full line:
          $\Omega = v_R/4$, dashed line: $\Omega = 0$) (After /28,29/).

critical temperature T_C where a continuous phase transition occurs
to the cubic phase. However, both phases have a ferrodistortive
component and show therefore piezodistortive coupling (2.27) to
strain which favours the ε phase. The resulting phase diagram is
displayed in Figure 8. (Preliminary results for the $\Omega = 0$ case
reported in Ref. /27/ contain an error). One finds that the θ phase
is stable for low values, and the ε phase is stable for high va-
lues of the coupling constant g. The two phases are separated by
continuous phase transitions to an intermediate phase of ortho-
rhombic symmetry existing in a very narrow region. Thus, below a
critical value of the coupling constant, the θ structure is stable
up to T_c where it undergoes a continuous transition to the cubic
phase. In an adjacent narrow range of g, one finds the intermediate
phase at low temperatures. For larger values of g, the ε structure
is stable at low temperatures, and up to a second critical value
of g there occurs with increasing temperature first a continuous
transition to the intermediate phase and at a slightly higher tem-
perature another continuous transition to the θ phase. For still
larger values of g, the ε phase remains stable up to the conti-
nuous transition to the cubic phase at T_c.

The temperature dependence of the collective modes is shown
in Figure 9. The number of modes is now twice as large as in the
ferrodistortive case, because the two sublattices experience dif-
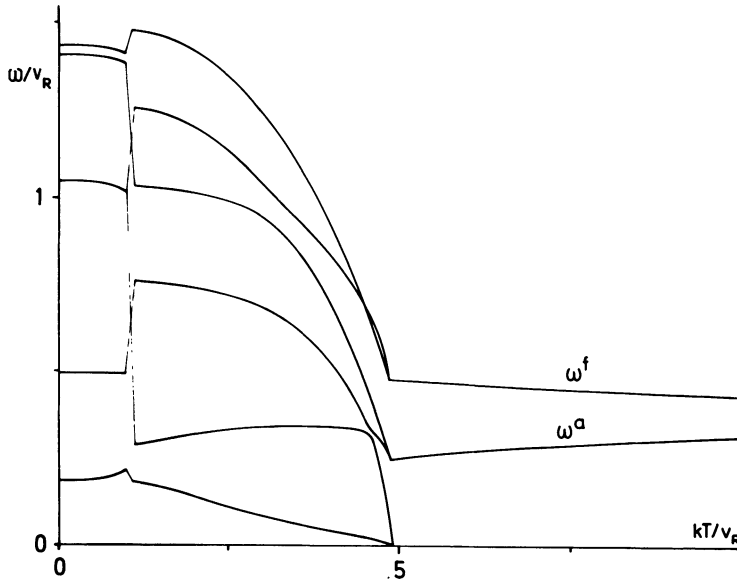
Figure 9: Collective vibronic modes for antiferrodistortively coup-
led E ⊠ ε complexes with piezodistortive coupling
($\Omega = v_R/4$, $g^2/2c = 0.075\ v_R$). (After /28/).

ferent molecular fields. For $T > T_c$, the soft mode is again a re-
laxation mode originating from the zero-frequency transition
within the ground state doublet. For $T < T_c$, we now find a dynamic
soft mode which hybridizes with other modes already at temperatu-
res close to T_c.

All modes consist of coupled vibrational and electronic mo-
tions. The temperature dependence of their oscillator strengths
and of the relative sublattice amplitudes is discussed in detail
in Ref. /28/. In addition to the vibronic excitations, there will
occur interesting elastic anomalies on account of the piezodistor-
tive coupling. Experimental investigations of the dynamics of such
E ⊠ ε systems appear highly desirable.

3.3. T ⊠ ε Coupling

In this case, the linear JT coupling has the form

$$\underline{\underline{V}}_{JT}^{(1)} = -A_\varepsilon \ (Q_\theta \underline{\underline{\Sigma}}_{T,\theta} + Q_\varepsilon \underline{\underline{\Sigma}}_{T,\varepsilon}) \tag{3.14}$$

where

$$\underline{\underline{\Sigma}}_{T,\theta} = \begin{pmatrix} -1/2 & 0 & 0 \\ 0 & -1/2 & 0 \\ 0 & 0 & 1 \end{pmatrix} \quad , \quad \underline{\underline{\Sigma}}_{T,\varepsilon} = \begin{pmatrix} \sqrt{3}/2 & 0 & 0 \\ 0 & -\sqrt{3}/2 & 0 \\ 0 & 0 & 0 \end{pmatrix} \tag{3.15}$$

are electronic operators of E symmetry acting on the threedimen-
sional T-Hilbert space. The potential energy surface consists of
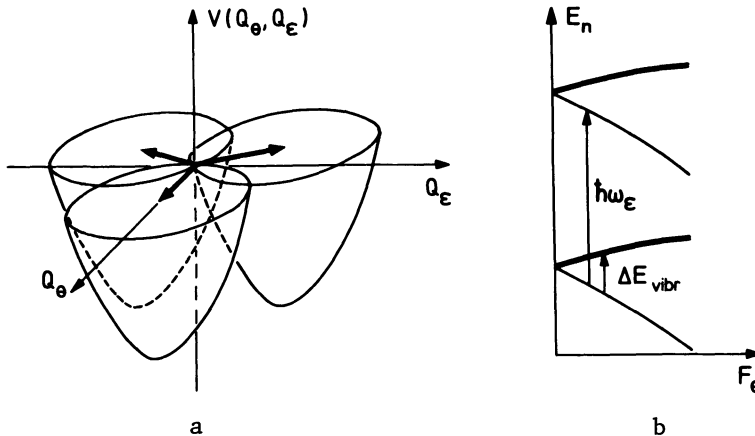
Figure 10: T ⊠ ε coupling.
        a: Potential-energy surface $V(Q_\theta, Q_\varepsilon)$
        b: Shift of vibronic energy levels with field in
           θ-direction

three shifted paraboloids, each belonging to a fixed electronic
state (Figure 10a). Since the two electronic operators commute,
the vibronic eigenvalue problem separates into three independent
harmonic oscillators (ζ = 1,2,3), with eigenvalues

$$E_n = -E_{JT} - \frac{1}{2} F^2/m\omega_\varepsilon^2 + (n+\frac{1}{2})\hbar\omega_\varepsilon - Q_{JT} \cdot \begin{cases} F_\theta \\ (-\frac{1}{2}F_\theta+\frac{1}{2}\sqrt{3}F_\varepsilon) \\ (-\frac{1}{2}F_\theta-\frac{1}{2}\sqrt{3}F_\varepsilon) \end{cases} \quad (3.16)$$

displayed in Figure 10b.

This case is thus very similar to the E ⊠ β case discussed
in Section 3.1. One finds the same types of transitions: Vibra-
tional transitions $\hbar\omega_\varepsilon$ giving rise to an optical-phonon band,
electronic Franck-Condon like transitions of local character,
and vibronic transitions ΔE_{vibr} between the ground states of the
three parabola which constitute the soft modes, and which will be
as difficult to excite directly as in the E ⊠ β case. By a trans-
formation to displaced phonon coordinates, the system can be
transformed into a three-states Potts model completely decoupled
from the optical-phonon band.

3.4. T ⊠ τ_2 Coupling

This case is described by a linear JT coupling

$$\underline{\underline{V}}^{(1)}_{JT} = -A_\tau (Q_\xi \underline{\underline{\Sigma}}_\xi + Q_\eta \underline{\underline{\Sigma}}_\eta + Q_\zeta \underline{\underline{\Sigma}}_\zeta) \quad (3.17)$$

with electronic operators
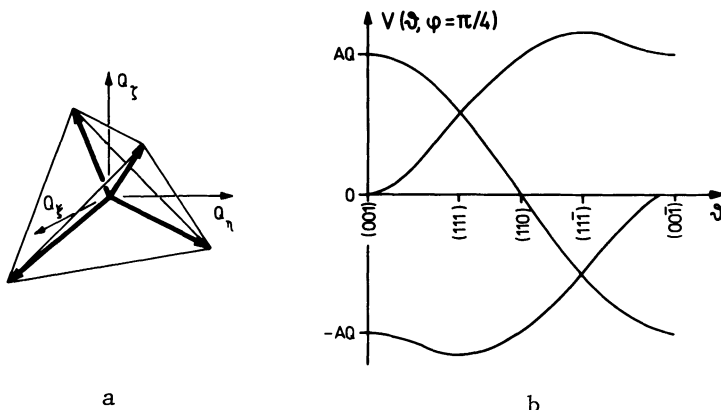
Figure 11: Potential-energy surface $V(Q_\xi,Q_\eta,Q_\zeta)$ for T ⊠ τ_2
        coupling
        a: Minima of $V(Q_\xi,Q_\eta,Q_\zeta)$
        b: The three sheets of $V(Q_\xi,Q_\eta,Q_\zeta)$ as function of ϑ
           at $\phi = \pi/4$

$$\underset{=}{\xi}_{\xi} = \begin{pmatrix} 0 & 0 & 0 \\ 0 & 0 & 1 \\ 0 & 1 & 0 \end{pmatrix} \quad , \quad \underset{=}{\xi}_{\eta} = \begin{pmatrix} 0 & 0 & 1 \\ 0 & 0 & 0 \\ 1 & 0 & 0 \end{pmatrix} \quad , \quad \underset{=}{\xi}_{\zeta} = \begin{pmatrix} 0 & 1 & 0 \\ 1 & 0 & 0 \\ 0 & 0 & 0 \end{pmatrix} \quad (3.18)$$

of T symmetry acting on the threedimensional T-Hilbert space. Because they do not commute, this case is similar to the E ⊠ ε case discussed in Section 3.2. However, the potential-energy surface is anisotropic already in the absence of higher-order coupling. It has minima for Q along (1,1,1), (1,-1,-1), (-1,1,-1), (-1,-1,1) in τ_2 configuration space (Figure 11a), which correspond to trigonal distortions of the ligand configuration. The potential-energy surface consists of three sheets, two of which penetrating each other in any of the eight (111) directions. Figure 11b shows a cross section through the surface along the meridian $\phi = \pi/4$.

This case has not been studied in much detail. The nature of the lowest vibronic modes is discussed in Ref. /42/. If the minima of V(Q) are sufficiently deep, one expects a ground state quartet corresponding to wave functions localized in the four minima, which is split into a low-lying triplet and an excited singlet due to tunnelling between the minima, in a manner analogous to the E ⊠ ε case (Figure 6a). If all other states have excitation energies > kT_c, one may construct an S = 3/2 pseudospin model for the vibronic motion. In the cooperative system, the transitions within this quartet will again give rise to bands of strongly temperature dependent collective modes. In the limit of zero tunnel splitting, the model goes over into a four-states Potts model.

In a T-type JT crystal, the JT ions can couple both to the ε mode and the τ_2 mode, and it depends on the coupling parameters and the interactions which of the two coupling schemes determines the transition. For suitable values of the parameters, there may occur an interesting competition between these two cases.

3.5. (A+B) ⊠ β Pseudo-JT Coupling

One may visualize the two electronic states as the components of an E doublet split by a small distortion of the crystal field from higher symmetry. The single-cell pseudo-JT Hamiltonian

$$\underset{=}{H}_{JT} = \left(\frac{1}{2M} P^2 + \frac{1}{2} M\omega_\beta^2 Q^2\right) \underset{=}{1}_{el} - \Delta \cdot \underset{=}{\xi}_1 - AQ \underset{=}{\xi}_3 - FQ \underset{=}{1}_{el} \quad (3.19)$$

then contains a term $\underset{=}{V}_\Delta = -\Delta \underset{=}{\xi}_1$ describing this electronic ground-state splitting 2Δ, in addition to the linear JT term $\underset{=}{V}_{JT}^{(1)} = -AQ \underset{=}{\xi}_3$. The potential energy "surface" is shown in Figure 12a. Now, there occurs tunnelling between the two minima, and the vibronic states are split already in zero field (Figure 12b). If all higher exci-
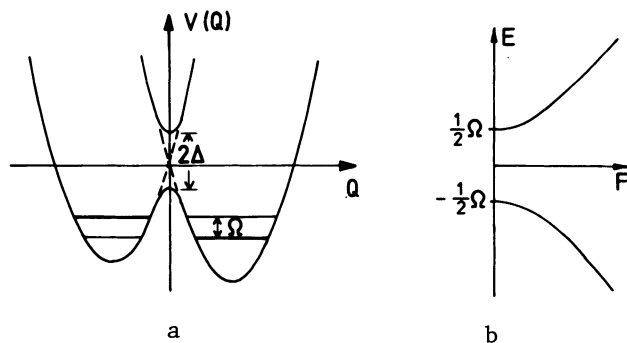
Figure 12: (A+B) ⊠ β coupling (Pseudo-JT effect)
         a: Potential energy V(Q)
         b: Shift of vibronic energy levels with field
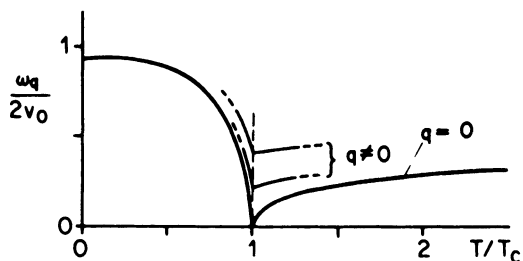
Figure 13: Collective vibronic modes for (A+B) ⊠ β pseudo-JT
         effect

ted states have excitation energies > kT_c, the vibronic motion can
be described in terms of $S = 1/2$ pseudospin operators acting on the
vibronic ground state doublet with tunnel splitting Ω. The pseudo-
JT Hamiltonian then takes the form

$$H_{JT} = -\Omega\, S_x - 2F\, Q_0\, S_z \qquad\qquad (3.20)$$

which is the same as that used for hydrogen-bonded ferroelectrics
/43/ and for magnetic singlet-singlet crystal-field transitions
/44/.

   For the cooperative system, this model becomes the Ising mo-
del with a transverse field, which shows a continuous phase tran-
sition. The tunnelling excitations give rise to a band of collec-
tive tunnelling modes (pseudospin waves) which become soft at the
transition (Figure 13).

REFERENCES

/1/ M.D. Sturge, Solid State Phys. 20, 95 (1967)
/2/ W. Gebhardt, Der Jahn-Teller Effekt. In: Festkörperprobleme
    IX, edited by O. Madelung, p. 99. Pergamon Vieweg 1969
/3/ F.S. Ham, Jahn-Teller Effects in Electron Paramagnetic Reso-
    nance Spectra, Plenum Press (1971)
/4/ R. Englman, The Jahn-Teller Effect in Molecules and Crystals,
    Wiley-Interscience (1972)
/5/ J.D. Dunitz, L.E. Orgel, J. Phys. Chem. Solids 3, 20 (1957)
/6/ J. Kanamori, J. Appl. Phys. 31, 14S (1960)
/7/ R. Englman, B. Halperin, Phys. Rev. B2, 75 (1970)
    B. Halperin, R. Englman, Phys. Rev. B3, 1698 (1971)
/8/ D. Reinen, C. Friebel, K.P. Reetz, J. Solid State Chem. 4,
    103 (1972)
/9/ C. Friebel, Z. anorg. allg. Chemie 417, 197 (1975)
/10/ D. Reinen, C. Friebel, to be published
/11/ Y. Yamada, this volume
/12/ C.J. Kroese, W.J.A. Maaskant, Chem. Phys. 5, 224 (1974)
/13/ J. Fernandez et al., Mater. Res. Bulletin 11, 1161 (1976)
/14/ S. Hirotsu, J. Phys. C10, 967 (1977)
/15a/ R.L. Melcher, B.A. Scott, Phys. Rev. Letters 28, 607 (1972)
/15b/ R.L. Melcher, E. Pytte, B.A. Scott, Phys. Rev. Letters 31,
    307 (1973)
/16/ R.J. Elliott, R.T. Harley, W. Hayes, S.R.P. Smith, Proc. R.
    Soc. A328, 217 (1972)
/17/ J.R. Sandercock et al., J. Phys. C5, 3126 (1972)
/18/ G.A. Gehring, K.A. Gehring, Rep. Prog. Phys. 38, 1 (1975)
/19/ R.T. Harley, this volume
/20/ R.T. Harley et al., J. Phys. C6, 2382 (1973)
/21/ R.J. Birgeneau et al., Phys. Rev. B10, 2512 (1974)
/22/ B. Lüthi et al., Phys. Rev. B8, 2639 (1973)
/23/ P.J. Wojtowicz, Phys. Rev. 116, 32 (1959)
/24/ E. Pytte, Phys. Rev. B3, 3503 (1971)
/25/ E. Pytte, Phys. Rev. B8, 3954 (1973)
/26/ H. Thomas, K.A. Müller, Phys. Rev. Letters 28, 820 (1972)
/27/ H. Thomas, The Jahn-Teller Effect as a Mechanism for Structu-
    ral Phase Transitions, In: Anharmonic Lattices, Structural
    Transitions and Melting, edited by T. Riste, p. 213, Leiden:
    Noordhoff (1974)
/28/ G. Schröder, H. Thomas, Z. Phys. B25, 369 (1976)
/29/ K.-H. Höck, G. Schröder, H. Thomas, to be published
/30/ H. Thomas, In: Structural Phase Transitions and Soft Modes,
    edited by E.J. Samuelsen, E. Andersen and J. Feder, p.15.
    Oslo: Universitetsforlaget (1971)
/31/ J.C.M. Tindemans-van Eijndhoven, C.J. Kroese, J. Phys. C8,
    3963 (1975)

/32/ H. Thomas, Mean Field Theory of Phase Transitions. In: Local
      Properties at Phase Transitions, Proceedings of the Interna-
      tional School of Physics "Enrico Fermi", Course LIX, edited
      by K.A. Müller and A. Rigamonti, p. 3, Bologna: Società Ita-
      liana di Fisica (1976)
/33/ B. Halperin, Phys. Rev. B7, 897 (1972)
/34/ M.E. Mullen et al., Phys. Rev. B10, 186 (1974)
/35/ P. Morin et al., Phys. Rev. B14, 2972 (1976)
/36/ Y. Kino et al., Solid State Comm. 12, 275 (1973)
/37/ J. Feder, E. Pytte, Phys. Rev. B8, 3978 (1973)
/38/ R.B. Stinchcombe, this volume
/39/ P.J. Becker, M.J.M. Leask, R.N. Tyte, J. Phys. C5, 2027 (1972)
/40/ E. Pytte, H. Thomas, Solid State Comm. 11, 161 (1972)
/41/ H. Thomas, Soft Modes at First- and Second-Order Phase Tran-
      sitions. In: Anharmonic Lattices, Structural Phase Transitions
      and Melting, edited by T. Riste, p. 231. Leiden: Noordhoff
      (1974)
/42/ M.J. Shultz, R. Silbey, J. Chem. Phys. 65, 4375 (1976)
      M.J. Shultz, this volume
/43/ R. Brout, K.A. Müller, H. Thomas, Solid State Comm. 4, 507
      (1966)
/44/ P. Fulde, I. Peschel, Adv. Phys. 21, 1 (1972)

LOCAL JAHN-TELLER EFFECT AT A STRUCTURAL PHASE TRANSITION

K.-H. Höck and H. Thomas

Institut für Physik, Universität Basel

Klingelbergstrasse 82, CH-4056 Basel, Switzerland

ABSTRACT

We consider a Jahn-Teller (JT) impurity ion with a doublet electronic ground state of E_g-symmetry at a lattice site of cubic symmetry and investigate the critical enhancement of the local JT-effect caused by the vibronic coupling to the soft mode of a structural phase transition of the host crystal. Furthermore, we study the temperature-dependence of the strain field around the JT-centre induced by the local JT-effect.

1. INTRODUCTION

Commonly, the JT-effect of JT-impurities in crystals is described in terms of a phenomenological cluster model /1/, which takes into account only the coupling of the electronic state of the JT ion to the vibrational modes of the cluster consisting of its ligands, but disregards lattice-dynamical interactions with the rest of the crystal. Recently, progress has been made by treating the more realistic problem of coupling to the continuum of phonon modes of the host crystal (multimode JT-effect) /2,3/. It was shown, that the properties of the JT-impurity become modified due to the vibronic coupling to such a continuous phonon spectrum of the host crystal as compared with the coupling to the single mode of the simplified quasi-molecular description of the cluster model. Within the framework of harmonic lattice theory these effects are expected to be ordinarily rather small, because the induced JT-distortion extends only over a few lattice distances. However, if the JT-distortion couples to the soft mode of a struc-

tural phase transition of the host crystal, the range of distortion increases as the critical temperature T_c is approached, and one obtains a strong, temperature-dependent enhancement of the local JT-effect. We show that due to this enhancement an initially weak JT-effect changes into a strong JT-effect close to the transition temperature. This behaviour is reflected in a characteristic temperature-dependence of the reduction factors p and q of the Ham-effect /1/, which measure the influence of the JT-effect on the EPR-spectrum.

2. MULTIMODE JT-EFFECT

In order to study these effects, we consider a cubic crystal composed of separate octahedral ionic complexes, the distortions of which are described in terms of local normal coordinates Q_ℓ transforming according to the irreducible representations of the cubic point group associated with the lattice-sites $\underset{\sim}{\ell}$. In the centre of the octahedron at $\ell = 0$, we assume the JT-impurity with a doublet electronic ground state ($\psi_{\ell=0,\theta}$, $\psi_{\ell=0,\epsilon}$) of E_g-symmetry, which is linearly coupled to the local normal coordinates ($Q_{\ell=0,\theta}$, $Q_{\ell=0,\epsilon}$) of the octahedron at lattice site $\ell = 0$ only. $Q_{\ell=0,\theta}$ and $Q_{\ell=0,\epsilon}$ which transform in the same way as the electronic wave functions, on the other hand, interact lattice-dynamically with local normal coordinates of neighbouring octahedra, so that the localized electronic state is indirectly coupled to the whole lattice. In the following, we assume that the host crystal undergoes a displacive structural phase transition with a soft optical phonon branch composed of local normal coordinates of type $\underset{\sim}{Q}_\ell = (Q_{\ell,\theta}, Q_{\ell,\epsilon})$ at every lattice site. We take only the soft phonon branch into account, and restrict the discussion to the high temperature phase $T > T_c$. In the basis spanned by the electronic wave functions, the Hamiltonian we then consider reads,

$$H = \frac{1}{2} \sum_\ell \{\underset{\sim}{P}_\ell^2 + \Omega_s^2(T)\underset{\sim}{Q}_\ell^2 - \sum_\alpha v\underset{\sim}{Q}_\ell \cdot \underset{\sim}{Q}_{\ell+\xi\alpha}\}\underset{\sim}{1} + V\underset{\sim}{Q}_{\ell=0} \cdot \underset{\sim}{\sigma} . \qquad (1)$$

$\underset{\sim}{P}_\ell = (P_{\ell,\theta}, P_{\ell,\epsilon})$ are the momenta conjugate to the coordinates $\underset{\sim}{Q}_\ell$, and $\underset{\sim}{\sigma} = (\sigma_\theta, \sigma_\epsilon)$ are the Pauli spin matrices with

$$\sigma_\theta = \begin{pmatrix} -1 & 0 \\ 0 & 1 \end{pmatrix} \qquad \sigma_\epsilon = \begin{pmatrix} 0 & 1 \\ 1 & 0 \end{pmatrix} .$$

Here, we have described the host crystal by an effective harmonic Hamiltonian with a temperature-dependent effective single-particle Einstein frequency $\Omega_s(T)$, an approximation usually applied in the theory of displacive structural phase transition /4/ and well justified for the study of the local JT-effect in the high-temperature phase. v and V are, respectively, the interaction coefficient of a bilinear, isotropic nearest-neighbour interaction and the local

JT-coupling constant. Due to the local JT-interaction, the translational symmetry of the system is broken and the Hamiltonian (1) cannot be diagonalized directly with the help of a Fourier transformation to phonon coordinates. The only symmetry operations which leave the system invariant are those belonging to the cubic point group at the JT-impurity site. In order to take account of the reduced symmetry, we introduce so-called symmetry-adapted coordinates /5,6/ which are irreducible E_g-linear combinations of the degenerate local normal coordinates $(Q_{\ell,\theta}, Q_{\ell,\epsilon})$ belonging to the star of a lattice vector ℓ. One finds that in general the star of a lattice vector ℓ is associated with four pairs of degenerate symmetry-adapted coordinates. In the case of isotropic nearest-neighbour interaction, however, only one pair plays a rôle in the study of the local JT-coupling. This pair is given by the totally symmetric linear combination of local normal coordinates of type $Q_{\ell,\theta}$ and $Q_{\ell,\epsilon}$, respectively, at each member of the star. Performing a final Fourier transformation to symmetry-adapted phonon coordinates q_q associated with the star of the wave vector q, the vibronic Hamiltonian (1) is then transformed into the so-called multimode JT-Hamiltonian, where the localized electronic doublet is coupled to the continuum of the q_q,

$$H = \sum_q \hbar\omega_q(T)\{\tfrac{1}{2}(p_q^2 + q_q^2)\cdot\underset{\sim}{1} + K_q(T)q_q\cdot\underset{\sim}{\sigma}\}$$

$$K_q^2(T) = (N^{-1}V^2)/(\hbar\omega_q^3)$$

(2)

We consider a ferrodistortive transition and assume a Debye dispersion

$$\omega_q^2(T) = \omega_0^2(T) + \alpha q^2$$

for the soft optical phonon branch with a MFA-type temperature dependence

$$\omega_0^2(T) \propto T - T_c \quad .$$

3. CRITICAL ENHANCEMENT

To treat the multimode JT-problem (2), we apply the method described by Englman and Halperin /3/. The Hamiltonian (2) is separated by an orthogonal transformation $\hat{q}_{q',\kappa} = \Sigma_q A_{q'q} q_{q,\kappa}$ into three parts: An effective-single-frequency JT-Hamiltonian H^{JT}, an uncoupled harmonic part H_{harm}, and a part H' which for a proper choice of the transformation $\underset{\approx}{A}$ is coupled only weakly to the electronic states,

$$H = \hbar\Omega_{eff}(T)\{\tfrac{1}{2}(\hat{p}_1^2 + \hat{q}_1^2)\cdot 1 + K_{eff}(T)\hat{q}_1 \cdot \sigma\} + H_{harm} + H' \ . \qquad (3)$$

The transformed mode $\hat{q}_1 = \Sigma_q A_{1q} q_q$, represents some kind of inter-
action mode strongly affected by the JT-coupling. Its spacial ex-
tension is no longer restricted to the immediate nearest neighbours
of the JT-impurity ion as in the simple cluster description. The
effective frequency and the effective JT-coupling constant, asso-
ciated with the interaction mode are given by

$$\Omega_{eff} = \sum_q \omega_q A_{1q}^2 \ , \qquad K_{eff} = \Omega_{eff}^{-1} \sum_q \omega_q K_q A_{1q}$$

The transformation $\underset{\sim}{A}$ is determined by minimizing the free energy
calculated with a density matrix $\rho = Z^{-1}\exp\{-\beta(\hat{H}^{JT} + H_{harm})\}$. It is
further assumed that the first excited state of $\hat{H}^{JT}$ has excitation
energy $\gg kT$. Then, the coefficients A_{1q} are found by minimizing
the ground state energy $\varepsilon_{JT}(\Omega_{eff}, K_{eff})$ of $\hat{H}^{JT}$. Working out the va-
riational calculation, we obtain the following result /Fig. 1/.
For high temperatures, we assume a weak JT-effect: the minimum of
the harmonic potential energy is only slightly lowered by the JT-
interaction, and the gain in JT-stabilization energy E_{JT} is smaller
then the zero-point energy $\tfrac{1}{2}\hbar\omega_{eff}$. As the temperature is lowered,
the JT-energy increases while the zero-point energy of oscillation
decreases, and below a certain temperature T_1 the gain in JT-stabi-
lization energy will become larger than the zero-point energy of
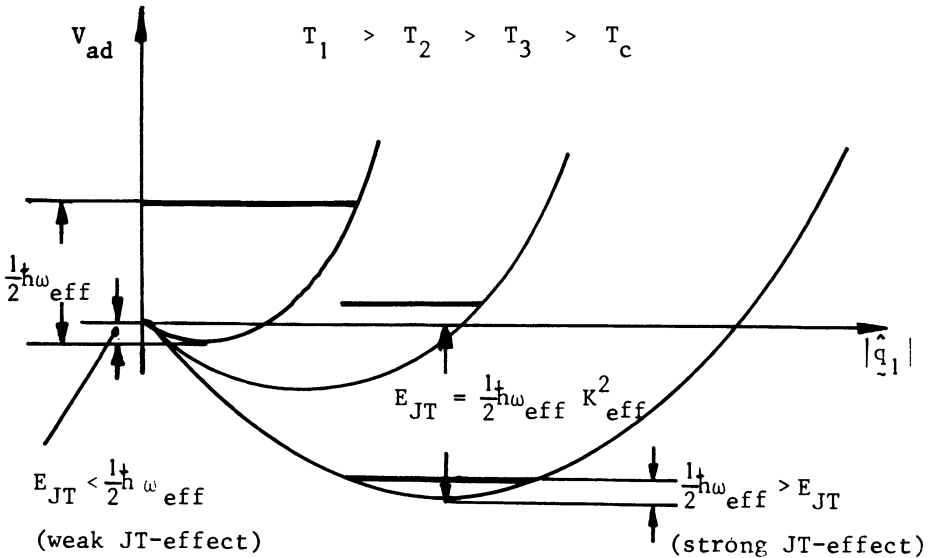
Fig. 1: Critical enhancement of the local JT-effect

oscillation, i.e. the weak JT-effect turns into a strong JT-effect. It turns out that this change occurs for a temperature close to T_c,

$$T_1-T_c \propto \exp\{-2\hbar\Delta^3/3V^2\} \qquad \Delta^2 = \omega^2_{max} - \omega^2_0$$

Fig. 2 depicts the temperature dependence of the effective JT-coupling constant $K_{eff}(T)$.

The variation from an initially weak JT-effect to a strong JT-effect as the temperature approaches T_c is reflected in a characteristic temperature dependence of the reduction factors p and q of the Ham effect /1/ (Fig. 3). For the weak JT-effect, at high temperatures, p and q are approximately equal to one. As the temperature is lowered the JT-effect increases and p and q decrease. For $T = T_c$, we finally end up with a strong JT effect, and p and q take on the limit values $q = 1/2$ and $p = 0$.

We have furthermore calculated the spatial extension of the JT-induced distortion given by the effective interaction mode $\hat{q}_1$ around the local JT-centre. We find that for $T \neq T_c$, it falls off with an Ornstein-Zernicke law $<Q_\theta(\ell)> \propto (1/\ell)\exp(-\ell/\xi)$, where ξ is the correlation length of the lattice distortions associated with the soft optical phonon branch of the host crystal. It is the divergence of ξ at T_c which gives rise to the enhancement of the local JT-effect described above. At $T = T_c$, on the other hand, the spatial dependence is governed by a power law depending on the effective JT-coupling constant $K_{eff}(T=T_c)$. It should be noted that
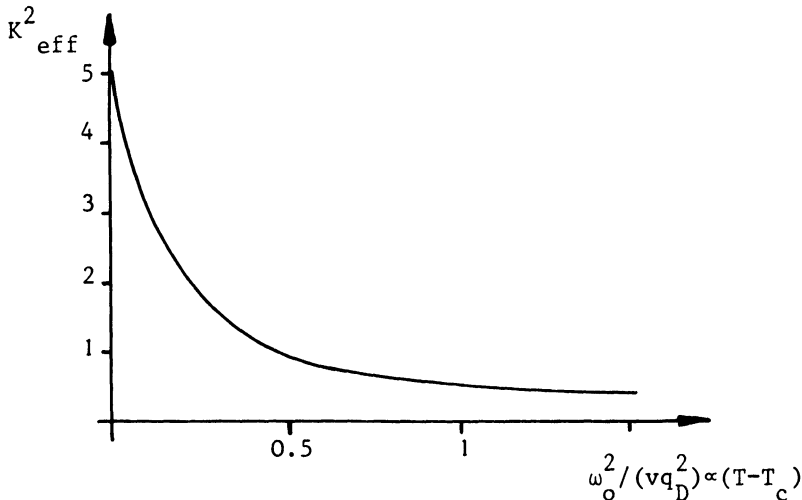
Fig. 2: Effective JT-coupling constant $K_{eff}(T)$
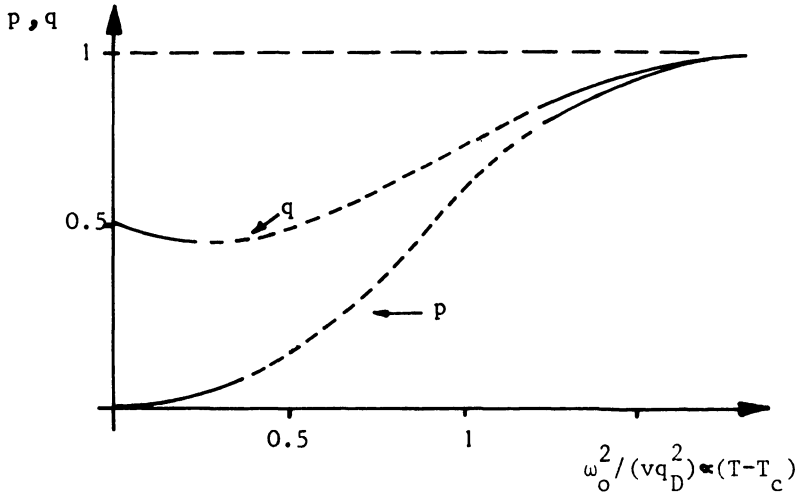
Fig. 3: Temperature variation of the reduction factors p and q.

this is the distortion field associated with the optical phonon co-
ordinates only. Because of the lattice-dynamical coupling to the
acoustical phonon coordinates there will occur in addition an ela-
stic strain field falling off with a power law already for $T \neq T_c$.
This contribution is, however, not expected to show a critical be-
haviour in our model of a soft optical phonon.

REFERENCES

/1/ F.S. Ham, in Electron Paramagnetic Resonance, ed. by S. Gschwind
    (Plenum, New York, 1972)
/2/ M.C.M. O'Brien, 1972, J. Phys. C: Solid State Phys. 5, 2045
/3/ R. Englman, B. Halperin, 1973, J. Phys. C: Solid State Phys. 6,
    L219
/4/ H. Thomas, in "Structural Phase Transitions and Soft Modes",
    ed. by E.J. Samuelsen, E.J. Andersen, J. Feder (Universitets-
    forlaget, Oslo, 1971)
/5/ K.-H. Höck, H. Thomas, to be published
/6/ K.W.H. Stevens, 1969, J. Phys. C: Solid State Phys. 2, 1934.

OPTICAL STUDIES OF JAHN-TELLER TRANSITIONS

R. T. Harley

Clarendon Laboratory, Parks Road, Oxford, England

1. INTRODUCTION

In this chapter we shall consider examples from three areas; firstly isolated 3-d transition metal ions which show localised Jahn-Teller (JT) effects; secondly, rare-earth crystals showing simple cooperative Jahn-Teller (CJT) phase transitions; and finally, examples of more complicated cooperative effects. For each of these systems the low lying electronic and vibrational excitations interact strongly and the coupled modes are of fundamental importance. They can be investigated directly by infra-red absorption and by scattering of light or neutrons and indirectly as splittings in optical absorption and fluorescence spectra. We shall describe results of optical experiments.

2. 3d-TRANSITION METAL IONS

According to the Jahn-Teller theorem (see refs. 1 to 4 and Chapter by H. Thomas in this volume) a symmetrical configuration of a molecule or ionic complex in a solid with orbitally degenerate electronic ground state is unstable because a distortion to lower symmetry must exist capable of producing a linear splitting. The system will therefore distort until reduction in energy of the lowest level (E_{JT}) is just balanced by increased elastic energy, as indicated by Q_0 in Fig. 1a. In principle the distortion will fluctuate thermally between energetically equivalent configurations (e.g. $\pm Q_0$ in Fig. 1a) so that the ground state degeneracy is unchanged. However the fluctuations may be sufficiently slow that a static distortion is observed experimentally.
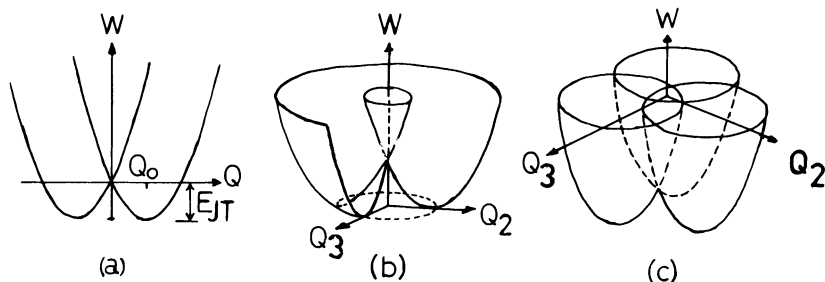
Fig. 1. Electronic energies (W) as a function of distortion co-
ordinate for (a) coupling of one-dimensional distortion (Q) to an
electronic doublet (Exβ) and for coupling of two-dimensional dis-
tortion (Q₂,Q₃) to (b) a doublet (Exε) and (c) a triplet (Txε).

     JT interactions may be classified according to the degeneracy
of the electronic state and dimensionality of distortion involved.
Figure 1 illustrates schematically three possibilities denoted Exβ,
Exε and Exτ, where Roman and Greek letters indicate respectively
the electronic and distortional degeneracies. We consider below
experiments on 3d ions with Exε and Exτ couplings and in later
sections rare-earths coupled to one-dimensional distortions.

     The d-orbitals of a 3d-ion in a cubic crystal are split by
crystal field and Coulomb effects into singlets (A) which can show
no JT effect and into doublets (E) and triplets (T) which can.
These orbital states may have spin degeneracy. Strong JT effects
occur for E states in octahedral and T states in tetrahedral
environments (1) and in general coupling to two-dimensional
distortions is predominant.

     The low lying excitations of such a complex are determined by
the combined effects of JT coupling and spin-orbit interaction;
extra splittings may also occur if the crystal field is other than
cubic. In general this leads to considerable complication but we
shall consider here two simple illustrative examples.

<h2 style="text-align:center">Cu^{2+}:CaO</h2>
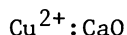
     In CaO, Cu^{2+} occupies an octahedral site and has a ^2E ground
state. There is a strong Jahn-Teller coupling to two-dimensional
modes of distortion (Exε) and since the spin-orbit interaction
cannot split an orbital doublet in first order it can be neglected.
If the nuclear motion is harmonic, then the electronic levels as a
function of displacements may be represented by the surface in

Fig. 1b where Q_2 and Q_3 represent the two components of ε mode dis-
tortion. This is simply the surface formed by revolving the dia-
gram for a one dimensional distortion (Fig. 1a) about the vertical
axis. The excitations are found by including the nuclear kinetic
energy in the calculation and they correspond to rotational energy
levels in (Q_2,Q_3) space, each of which is doubly degenerate (see
ref. 1). The nuclear and electronic motions are dynamically
coupled to give vibronic excitations (see discussion by H. Thomas
in this volume).

Anharmonicity and higher order JT couplings cause local minima
at $120°$ intervals in the circular trough of Fig. 1b corresponding
to compression or extension of the complex along the cube axes and
lead to splittings of the rotational levels. The results of a
calculation for various values of anharmonicity assuming E_{JT} large
are shown in Fig. 2a and the Raman spectrum of $CaO:Cu^{2+}$ together
with the transition assignments in Fig. 2b (5). Analysis of the
spectra gave values of anharmonic barrier height $(2\beta) = 43$ cm^{-1},
$E_{JT} = 6000$ cm^{-1}, and effective vibrational frequency $\hbar\omega \sim 350$ cm^{-1}.
Similar measurements for $Ni^{3+}:Al_2O_3$ gave $2\beta = 120$ cm^{-1},
$E_{JT} = 1100$ cm^{-1} and $\hbar\omega \sim 465$ cm^{-1} (6).
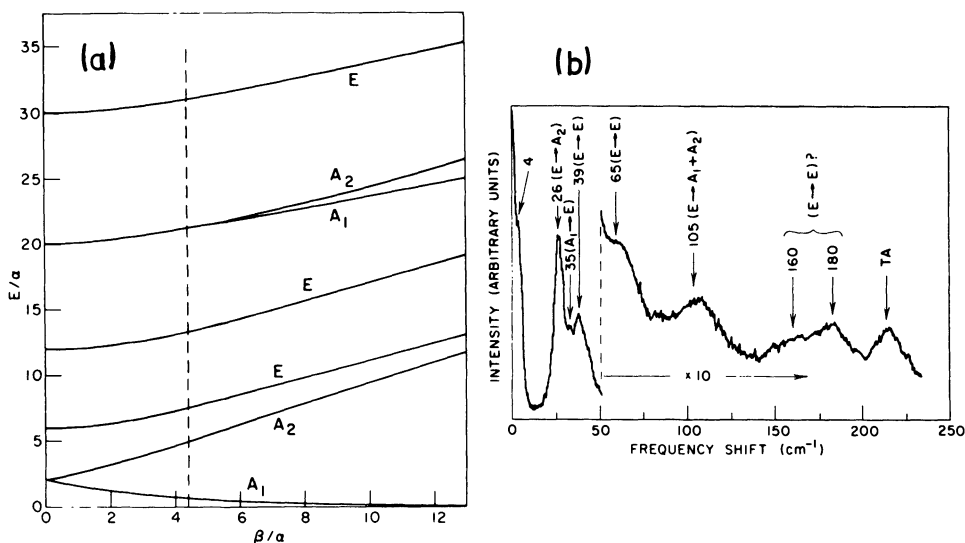
Fig. 2. (a) Calculated quasi-rotational energy levels above the
doublet (E) ground state for (Exε) coupling as a function of
anharmonicity (β). (b) Raman spectrum of $CaO:Cu^{2+}$ at 4.2 K with
lines assigned to transitions in (a); the measured frequencies
indicate $\beta \simeq 4.3\alpha$ and $\alpha = 5.2$ cm^{-1} (Ref. 5).

If the anharmonicity is large (Fig. 2a) the ground state becomes triply degenerate. This corresponds to the case of very deep potential minima in the trough of Fig. 1b with the complex confined to one of them. For smaller values of anharmonicity a splitting develops due to tunneling between minima. For $CaO:Cu^{2+}$ this tunneling splitting is ~ 4 cm^{-1} (see Fig. 2b) and for $Ni^{3+}:Al_2O_3$ ~ 60 cm^{-1}.

$$Ti^{3+}:Al_2O_3$$

Our second example is Ti^{3+} in Al_2O_3 which shows $T\times\varepsilon$ coupling. The site symmetry is predominantly octahedral with a small trigonal component and Ti^{3+} has a $^2T_2$ ground state showing weak JT coupling (see ref. 1). The triplet may couple to both two and three-dimensional distortions, but in practice the latter may be neglected. Figure 1(c) shows the splitting of an electronic triplet as a function of two-dimensional distortions (Q_2,Q_3); there are three disconnected minima at 120° intervals corresponding to distortions along the cubic axes. The system will be confined to one of these and its low lying excitations are pure vibrations about the displaced equilibrium configuration which may be represented crudely by a series of harmonic oscillator levels with spacing $\hbar\omega$ (see chapter by H. Thomas). Small perturbations due to spin-orbit coupling and anharmonicity may mix the electronic and vibrational motions and allow tunneling between minima comparable to the case of $Cu^{2+}:CaO$ discussed above. For Ti^{3+} however the JT coupling is weak compared with spin-orbit and trigonal crystal field effects and the Raman spectrum (Fig. 3a) (7) shows little resemblance to that of Cu^{2+} (Fig. 2b). Fig. 3(b) summarises the situation (8); from the right hand side (columns 7-5) it shows the sequence of calculated splittings of the free ion state omitting the JT (vibronic) coupling and from the left (columns 1-4) including it. The observed splittings which have energies δ_1 and δ_2 are a compromise between the splittings calculated for zero JT coupling (column 5) and strong JT coupling (column 3). In the latter case the ground state is a triplet corresponding to the three independent distorted configurations of Fig. 1(c). This reduction of spin-orbit and trigonal field splittings due to the vibronic character of the states favoured by JT coupling is an example of the Ham effect (1,2). The excitations of Ti^{3+} and V^{4+} in Al_2O_3 have also been observed using infra-red techniques (9).

Few experiments of the type illustrated in Figs. 2 and 3 in which the excitations of isolated JT ions are observed directly have been performed so far and there is likely to be increasing interest in them. There is a wide variety of ions and host crystals to investigate. At high concentrations interaction between the
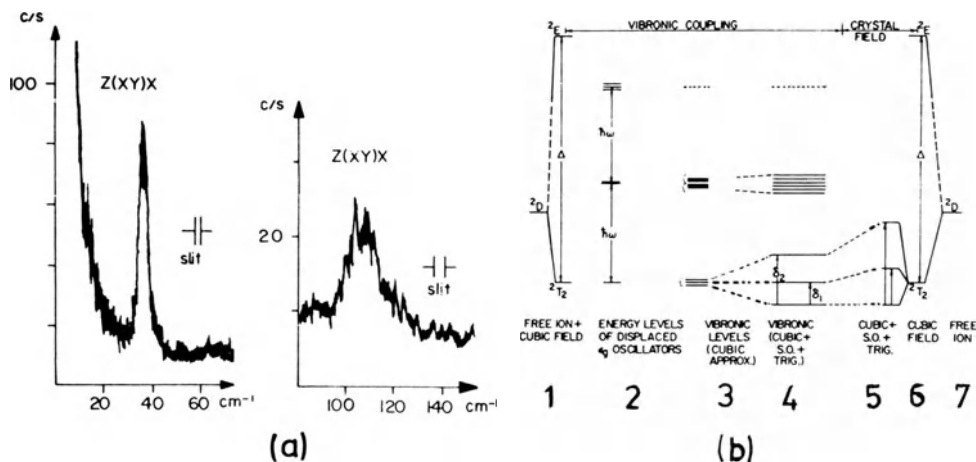
Fig. 3.   (a) Raman spectrum of $Ti^{3+}:Al_2O_3$ at 10 K (Ref. 7).
(b) Illustration of the origin of the observed transitions δ_1 and
δ_2 discussed in text (Ref. 8).

individual JT complexes can occur and measurements as a function of
both temperature and concentration will be interesting.   Theoretical
treatments of cooperative systems of 3d transition metal ions often
consider only a ground triplet split by tunneling (see ref. 10 and
chapter by H. Thomas in this volume); it is clear from figure 2
that this may not be adequate if the transition temperature is
greater than ~ 20 K.

3. COOPERATIVE JAHN-TELLER EFFECTS IN RARE-EARTH CRYSTALS

The second order structural phase transitions in rare-earth
vanadates and arsenates ($ReVO_4$ and $ReAsO_4$ where Re is Tm^{3+}, Dy^{3+} or
Tb^{3+}) are particularly clear examples of cooperative Jahn-Teller
(CJT) effects (4).   JT distortions associated with individual rare-
earth ions interact because they share ligands and this results in
a cooperative instability of the entire crystal.   The excitations
of the system consist of coupled electronic and phonon modes
(which have been called 'vibrons' (4)) and the phase transition is
accompanied by strong temperature dependence of these modes.
Optical methods of investigating these modes are illustrated in
Fig. 4.   Raman and infra-red transitions (A) give energies near
k = 0.   A Brillouin-zone-average of the vibron energy may be
obtained from the separation of optical absorption lines due to
transitions C and B to a highly excited electronic state, assumed
to have no dispersion.   This average is expected to be very close
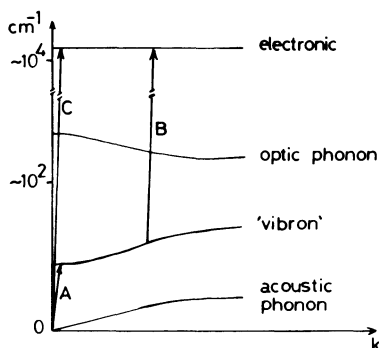
Fig. 4.   Schematic diagram of dispersion curves in a CJT system.
A is a Raman or infra-red transition; C is an optical transition
from the ground state; B is an optical transition from a low-lying
'vibron' mode.

to the uncoupled electronic transition energy (11,4). These cry-
stals are tetragonal (D_{4h}) at high temperatures and below the
transition temperature (T_D) orthorhombic (D_{2h}) with two molecules
per unit cell in both phases. The distortion is one-dimensional;
B_{1g} $(B_2$ at the rare earth site) for Dy^{3+} or B_{2g} (B_1) for Tb^{3+}
and Tm^{3+} (12).

     Fig. 5 shows the temperature dependence of the lower elect-
ronic states observed as splittings in optical absorption spectra

(a) $TmVO_4$ **(b)** $DyVO_4$ **(c)** $TbVO_4$
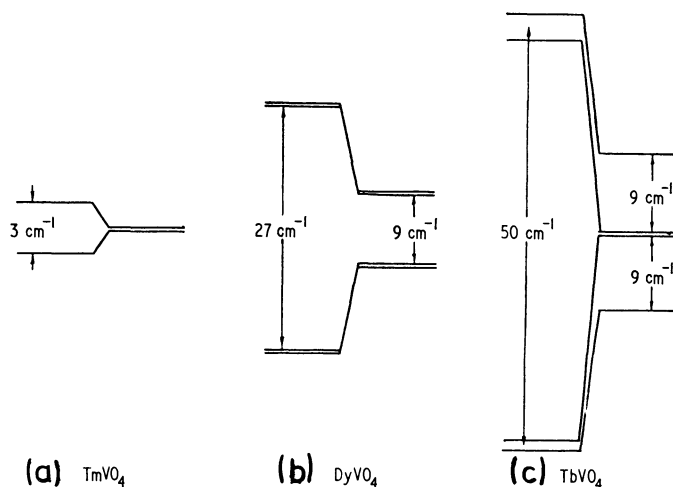
Fig. 5.   Low-lying electronic levels of rare-earth ions in $ReVO_4$
crystals above (right) and below T_D (left). The levels for $ReAsO_4$
are similar.

Table 1.   Transition Temperatures in $ReVO_4$ and $ReAsO_4$

	Tm		Dy		Tb	
	VO_4	AsO_4	VO_4	AsO_4	VO_4	AsO_4
T_D (measured)	2.14(14)	6.04(15)	14.0(12)	11.2(16)	33.5(17)	25.5(18)
T_D (calc.)*	2.14	6.35	19.1	~17	34.5	28
T_N (measured)	-	-	3.05	2.44	0.51	1.35

*Calculated from electronic level splittings using molecular field theory.

(4); Tm^{3+} and Tb^{3+} are non-Kramers ions whereas Dy^{3+} is a Kramers ion. Molecular field theory may be used to calculate values of T_D from the observed splittings for $T \to 0$ (12). These are compared with experimental values of T_D in Table 1; the correlation of calculated and measured values of T_D shows that electronic energy drives the transitions. However a close look at Table 1 shows that Tm and Tb compounds obey molecular field theory much better than Dy. This and other evidence (13) shows that the dominant site-site interaction is virtually infinite range for Tm and Tb but nearest neighbour only for Dy. (Dy and Tb compounds order antiferromagnetically at very low temperatures (see Table 1).)

Optic phonon modes of B_{1g} or B_{2g} symmetry at $k \simeq 0$ observed by Raman scattering have very little temperature dependence, although the phase transitions involve lattice distortions of these symmetries (12). To a first approximation the JT interaction causes a shift of the origin of vibration without changing the frequency. The process is analogous to that for the isolated complex of Fig. 1a in which the JT effect shifts the origin of the parabolic potential without altering its shape.

The doubly degenerate (E_g) optic phonons of the tetragonal phase show small splittings below T_D which are proportional to the orthorhombic distortion and are due to anharmonic effects (Fig. 6(a)). They can be used to monitor the distortion and hence the order parameter of the transitions; solid curves in Fig. 6(a) are derived from molecular field theory (12). Measurement of optical birefringence is a more precise method for monitoring the distortion very close to T_D. Fig. 6(b) shows results for $TbVO_4$ and
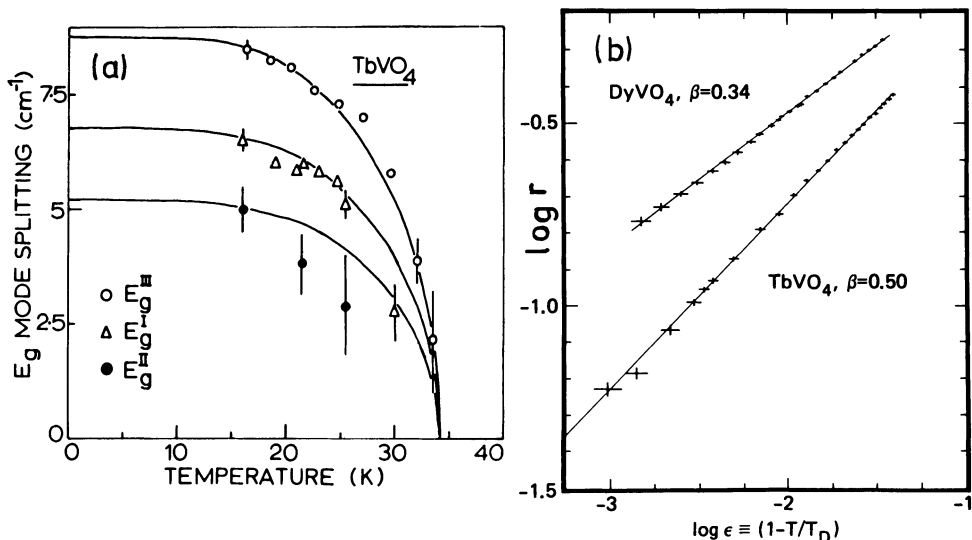
Fig. 6. (a) Measured splitting (points) of E_g optic phonon modes of TbVO$_4$ due to CJT distortion compared with molecular field theory (curves) (Ref. 12). (b) Log-log plot of temperature dependent birefringence (r) of TbVO$_4$ and DyVO$_4$ (Ref. 13).

DyVO$_4$ which have exponents of 0.50 ± .03 and 0.34 ± .03 respectively (13). These values are consistent with long-range interactions in TbVO$_4$ and short-range in DyVO$_4$. The reason for the dominance of short-range interactions in DyVO$_4$ is not known. As discussed by J. K. Kjems in this volume, renormalization group theory predicts (44) a classical value of exponent asymptotically close to T_D so it appears that the measurements (Fig. 6(b)) have not reached this region.

Low lying coupled electronic-phonon modes or vibrons can be observed by both infra-red absorption and Raman scattering. TbVO$_4$ is a good illustrative example; Fig. 7(a) shows typical Raman spectra (12) and Fig. 7(b) the temperature dependence of both Raman and infra-red (17) vibron frequencies. The upper Raman line (open circles) which is that displayed in Fig. 7(a) originates from uncoupled electronic transitions indicated by a circle in the inset. The infra-red line (solid circles) is also thought (17) to be associated with this transition; there is a 17 cm^{-1} Davydov splitting between the Raman and infra-red vibron frequencies because the even parity (Raman) mode is linearly coupled to both optic and acoustic modes near k = 0 whereas the odd parity (infra-red) mode is coupled to optic modes only (17). The solid curves in Fig. 7(b) are the results of calculations based on molecular field and random phase approximations (12).
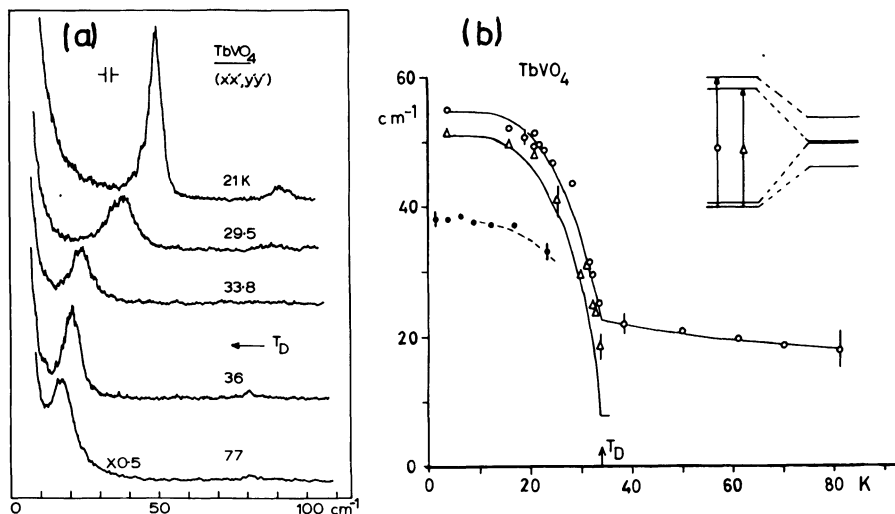
Fig. 7. (a) Raman spectra of TbVO$_4$ at various temperatures.
(b) Temperature dependence of Raman (open symbols) and infra-red
(solid circles) spectra of TbVO$_4$. Electronic transitions involved
are indicated in insert. Solid curves are molecular field and
R.P.A. theory (Refs. 12 and 17).

Interaction between the even parity vibrons and acoustic modes
near k = 0 causes dramatic changes in the acoustic slopes associated
with the transition (19,20) (Fig. 8). For DyVO$_4$ (Fig. 8(a)) the
elastic constants at ultrasonic and Brillouin scattering frequencies
are the same but there is a marked difference for TbVO$_4$ (Fig. 8(b)).
A static elastic constant is the ultimate soft mode ($\frac{1}{2}(C_{11}-C_{12})$ for
Dy and C_{66} for Tm and Tb compounds), and measurements at ultrasonic
frequencies (~10 MHz) are in the static regime. The difference
between ultrasonic and Brillouin measurements in TbVO$_4$ is caused by
coupling of the acoustic mode to electronic transitions between the
doublet levels of Tb^{3+} (Fig. 5(c)). Above T$_D$ the electronic tran-
sition is centred at zero frequency and it will have a width $\Delta\omega$.
Measurements made at low frequencies ($\omega \ll \Delta\omega$) see the full acoustic
softening at T$_D$, whereas at higher frequencies ($\omega > \Delta\omega$) there will
be only a partial softening caused by coupling to transitions
between the singlet levels (Fig. 5(c)) which give rise to the
'vibron' at ~ 20 cm^{-1} (Fig. 7(b)). The frequency of Brillouin
measurements is apparently comparable to $\Delta\omega$ because the experi-
mental curve (Fig. 8(b)) lies between the fully softened ultrasonic
curve and the value C$_I$ computed for $\omega > \Delta\omega$; a value of 8.4 GHz has
been deduced for the 'single ion' value of $\Delta\omega$ and this will be
expected to show critical narrowing at T$_D$ due to cooperative
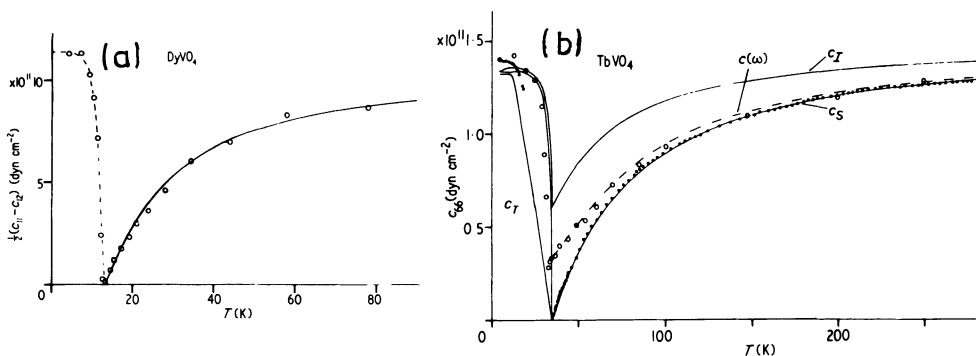
Fig. 8. Elastic constants measured using Brillouin scattering
(open circles) and ultrasonics (solid circles) for (a) DyVO$_4$,
(b) TbVO$_4$. Curves in (b) are molecular field and R.P.A. theory
for $\omega > \Delta\omega$ (C$_I$), $\omega \sim \Delta\omega$ (C(ω)) and $\omega \ll \Delta\omega$ (C$_S$) (Ref. 20).

effects (20). A zero frequency mode which shows some of the
expected features has been observed by neutron scattering in TbVO$_4$
(ref. 21 and seminar by S. R. P. Smith in this volume) and study
of Fig. 5a shows that in Tm compounds there should be a similar
zero frequency mode above T$_D$ which would give rise to frequency
dependent elastic constants.

Applied magnetic fields may help or inhibit CJT distortions.
In TmVO$_4$ and TmAsO$_4$ the ground doublet (Fig. 5a) may be split by a
magnetic field parallel to the c-axis or by crystallographic JT
distortion; these two perturbations have different symmetry and
are mutually exclusive. As a field is applied below T$_D$ the JT
distortion is reduced and eventually becomes zero when the
magnetic energy (gβH where g $\sim$ 10) just cancels the energy
associated with the CJT distortion (11). The splitting of elect-
ronic levels (Fig. 9(a)) is constant at low fields and shows a
normal linear increase at high fields (22). Fig. 9(b) shows the
behaviour of the JT distortion monitored by splitting of an E$_g$
optic phonon mode. The quenching of the field dependence of the
levels at low fields by the JT coupling (Fig. 9(a)) may be regarded
as a rather unusual example of the Ham effect (section 2).

Dy and Tb compounds have large g-values in the ab plane which
lead to enhancement of JT distortions by applied fields. Figure
10 shows measurements of E$_g$ phonon splittings (proportional to
orthorhombic distortion) for DyVO$_4$ up to 13 T; substantial dis-
tortions can be induced well above T$_D$ (23). At temperatures above
T$_D$ the two Kramers doublets of Dy (Fig. 5(b)) have equal g-values
($\sim$10) but as T $\to$ 0, due to JT admixture of the wavefunctions below
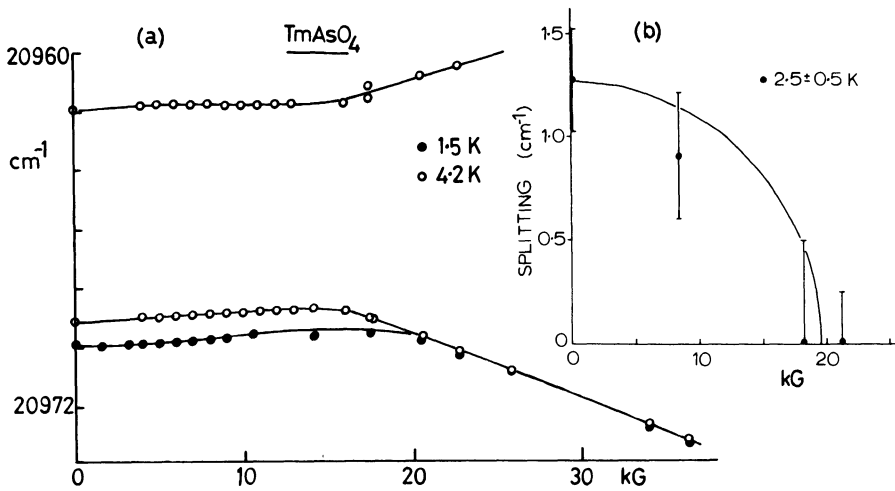
Fig. 9. Magnetic field dependence in TmAsO$_4$ of (a) electronic levels observed by optical absorption (Ref. 22) and (b) splitting of an E$_g$ phonon mode due to CJT distortion observed by Raman scattering (Ref. 11).
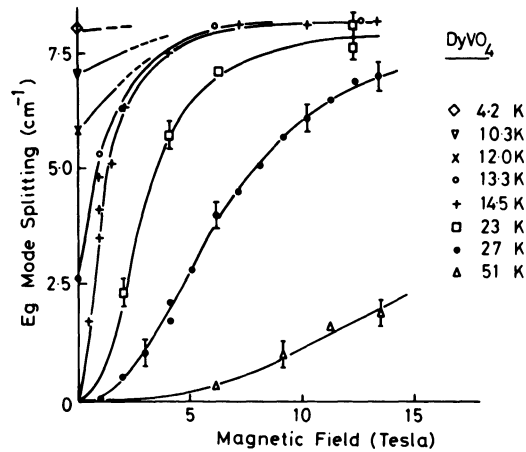
Fig. 10. Magnetic field dependence of E$_g$ phonon splitting in DyVO$_4$ (Ref. 23).

T_D, the g-value of the lower state becomes ~20 and that of the
upper state ~0 (12,24). Thus at finite temperatures the system
can gain energy, when a field is applied, by undergoing a dis-
tortion which increases the g-value of the lower doublet and so
decreases the ground state energy. A similar argument can be
applied to Tb (25). A mechanism of this type may be responsible
for the magnetic field induced splittings observed in optic phonon
modes of other rare-earth crystals notably CeF_3 (26). Although no
cooperative transition occurs a JT interaction may nevertheless be
present.

Interesting phenomena are observed when the JT ions are
diluted with inactive ions. Fig. 11 shows measurements of tran-
sition temperatures for mixed crystals $Dy_pY_{1-p}VO_4$ and $Tb_pGd_{1-p}VO_4$
compared with molecular field theory in which the molecular field
parameter is scaled linearly with concentration of JT active ions
(27). This gives a good description of $Tb/GdVO_4$ for which site-
site interactions are long range (solid curve Fig. 11b) but not
for Dy/YVO_4 (Fig. 11a) which has short-range interactions. The
results for $Tb/GdVO_4$ (Fig. 11b) show that over a narrow range of
composition near p = .35 the crystal undergoes two transitions.
The energy level scheme of Tb^{3+} in the undistorted phase (Fig. 5c)
has a singlet lowest with a doublet at ~ 9 cm^{-1} and the strength
of the CJT coupling or equivalently Tb concentration (p) in the
mixed crystal must exceed a threshold before a distortion will
occur at T = 0. However just before this threshold is reached
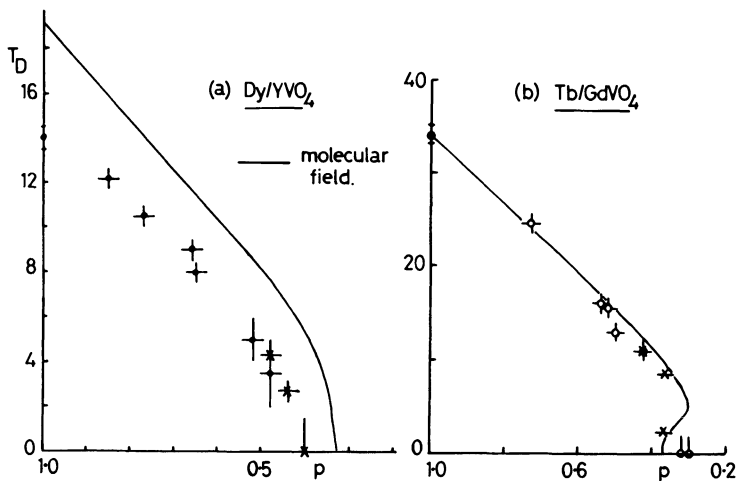
Fig. 11. Dependence of T_D on concentration of JT ions (p) in
(a) $Dy_pY_{1-p}VO_4$ and (b) $Tb_pGd_{1-p}VO_4$. Solid curves are scaled
molecular field theory (Ref. 27).
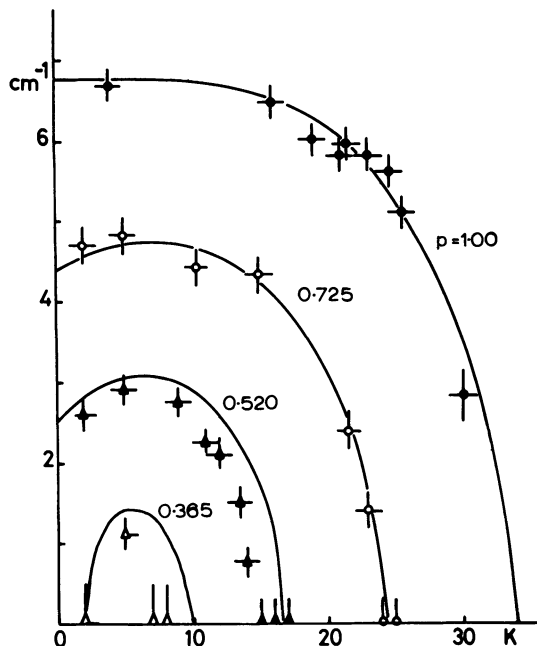
Fig. 12. Variation of E_g phonon splitting (proportional to orthor-
hombic distortion) in $Tb_pGd_{1-p}VO_4$ (Ref. 27).

distortion is energetically favoured at a non-zero temperature which
populates the 9 cm^{-1} doublet; at higher temperatures populations of
all the levels increase and the distortion is suppressed. Variation
of the distortion with composition and temperature is shown in
Figure 12. Measurements of one of the Raman active vibron modes in
$Tb/GdVO_4$ crystals are shown in Fig. 13 (cf. Fig. 7b) and compared
with calculations in the scaled molecular field and random phase
approximations.

4. OPTICAL STUDIES OF COMPLICATED JAHN-TELLER TRANSITIONS

(a) UO_2 has cubic fluorite structure at high temperature and
undergoes simultaneous cooperative Jahn-Teller distortion and
magnetic ordering at T_N = 30.8 K resulting from the triplet ground-
state of U^{4+} (28). Recent experiments (29) have shown that the
CJT distortion involves a zone-boundary mode and therefore the
existing microscopic theory of the transition (28) must be modified.
The atomic displacements below T_N (see Fig. 14) correspond to an
X_5^+ optic phonon mode which is observed at 233 cm^{-1} by Raman (30)
and neutron scattering (31) and generates a T_{2g} symmetry distortion
at the U^{4+} site. This mode shows little temperature dependence.
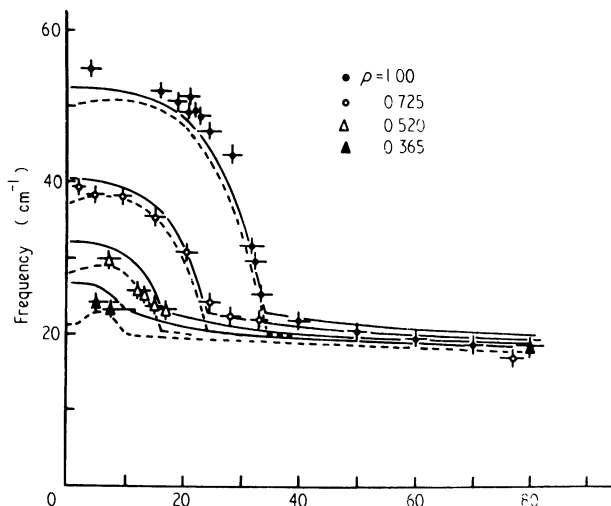
Fig. 13. Measured frequencies of the vibron in $Tb_pGd_{1-p}VO_4$ due to transitions indicated by the circle in the insert to Fig. 7(b). Solid and dashed curves are molecular field and R.P.A. theory for two different choices of parameters (Ref. 27).
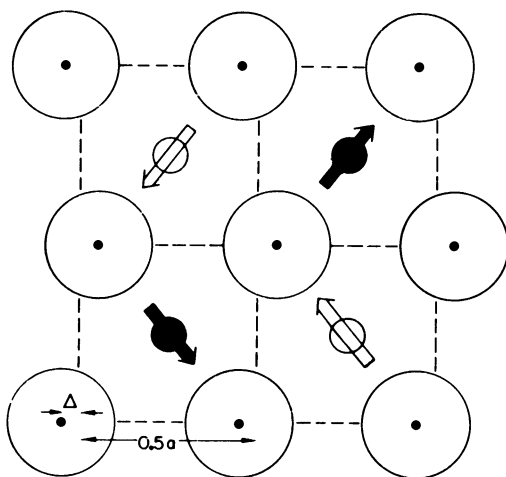
Fig. 14. <001> projection of low temperature structure of UO_2. Oxygen atoms (large circles) are in the plane and uranium atoms a/4 above (small solid circles) and below (small open circles). The values of Δ is 0.014 Å. Arrows indicate a possible arrangement of U^{4+} magnetic moments (Ref. 29).
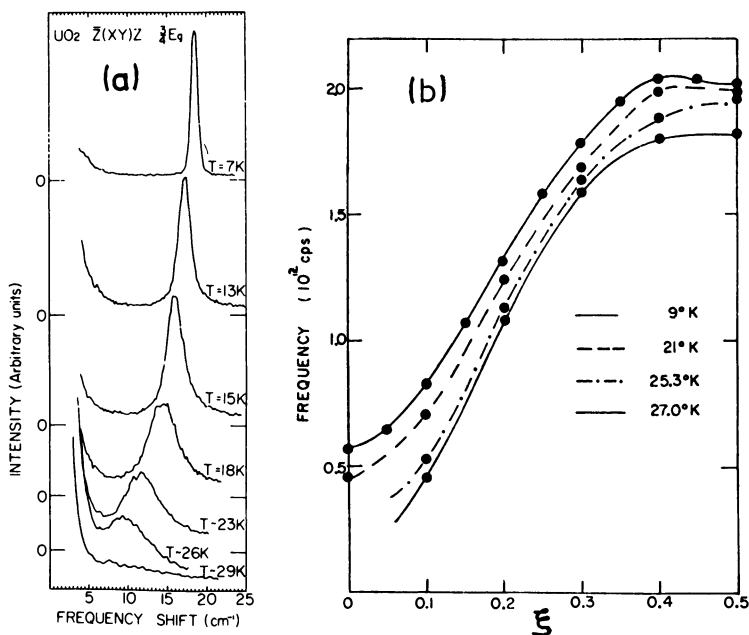
Fig. 15. Temperature dependence of electronic excitations in UO_2 in (a) Raman spectra (Ref. 30), and (b) neutron scattering in the $[\xi,\xi,1-\xi]$ direction (Ref. 32).

Phonon and electronic (spin-wave) excitations have been measured using neutron scattering (31,32), infra-red (28) and Raman scattering (30). The strongest feature in the Raman spectra (Fig. 15a) softens below T_N and corresponding behaviour is observed for a spin-wave at the X-point of the high temperature cell in the neutron spectrum (origin in Fig. 15b). This temperature dependence is compared with that of magnetic Bragg intensity in Fig. 16. The elastic constant C_{44} measured by ultrasonics softens by 24% between 240 K and T_N (34).

The new results for UO_2 suggest that the transition is more nearly second order than was previously believed and that the magnetic order may be of the four-sublattice type. Above T_N the strongest electron-phonon interaction must occur on the zone-boundary but there must also be substantial coupling to acoustic modes at the zone-centre which gives rise to the anomaly in C_{44} at T_N.

(b) $PrAlO_3$ has a distorted perovskite structure and undergoes phase transitions at 210 K and 151 K caused by interaction of Pr^{3+}
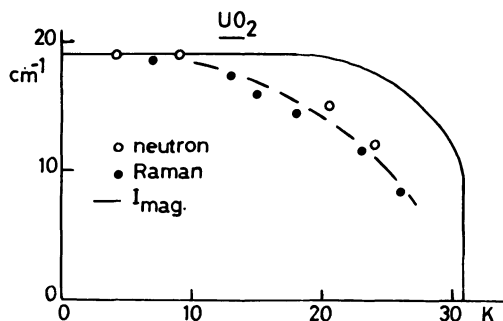
Fig. 16.   Temperature dependence of X-point electronic mode of UO_2 observed by Raman and neutron scattering and of the intensity of a magnetic Bragg reflection (Refs. 32,33).

electronic states with small staggered rotations of the AlO_6 units and accompanying lattice strains (35,36). A third transition at 118.5 K (37) probably involves similar interactions (see below). Splittings of the $3H_4$ ground multiplet observed by optical fluorescence can be accounted for quite accurately by calculations (38) (Fig. 17) in which the crystalline electric field at the Pr^{3+} site is modified by including effects of AlO_6 rotations and lattice strains measured directly by neutron diffraction (36) and e.s.r. (39). The resultant AlO_6 rotation (~9°) is almost independent of temperature; above 210 K its axis is along $[111]$, between 210 K and 151 K along $[101]$ and below 151 K it swings continuously towards $[001]$ approaching this direction asymptotically as T → 0.

The temperature dependence of excitations observed by Raman scattering is shown in Fig. 18 (40). Brillouin scattering measurements (37.41) show that the transitions at 151 K and 118.5 K are accompanied by soft acoustic modes which may be linearly coupled to the Raman mode which lies lowest at each temperature.

The splitting of the lowest two Pr^{3+} levels (B_1 and A_1 in Fig. 17) associated with the 151 K transition is analagous to the behaviour of the levels in $DyVO_4$ (Fig. 5b) and the temperature dependences of the Raman excitations (40) (B_1 in Fig. 18) and the elastic constant (41,36) are quite well accounted for by the theory developed for $DyVO_4$ (12, see chapter by K. J. Kjems in this volume). Transitions between the electronic levels (B_1 and A_1 Fig. 17) couple linearly to an optic phonon of B_1 symmetry resulting in two vibron modes (B_1 in Fig. 18). The lower branch is coupled to the acoustic mode which is the soft mode at 151 K. At 118.5 K the lowest Raman mode (Fig. 18) is a pure phonon with eigenvector ϕ_y (staggered rotation of AlO_6 about $[010]$) (40) which may couple linearly to strain e_{yz} (42). This will cause a renormalisation of
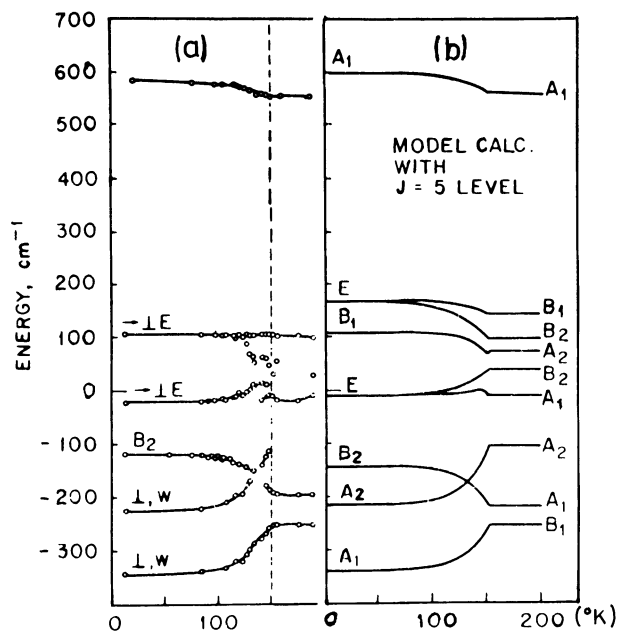
Fig. 17. Electronic energy levels of $^3H_4$ multiplet of Pr^{3+} in PrAlO$_3$ (a) measured using optical fluorescence (Ref. 35) and Raman scattering (Ref. 38), and (b) calculated as described in the text (Ref. 38).
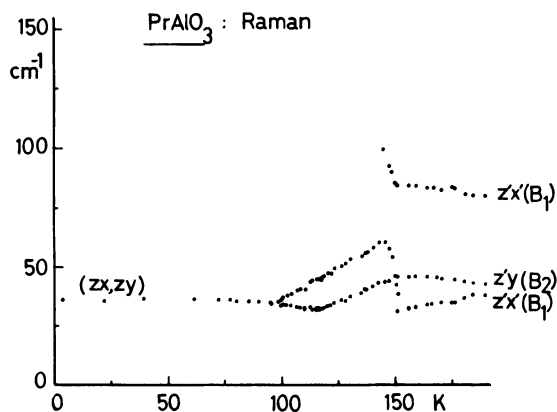
Fig. 18. Frequency of low-lying modes in the Raman spectrum of PrAlO$_3$. x, y and z refer to the cube axes and z' and x' are at $45°$ to the cube axes in the $[010]$ plane. Modes marked B$_1$ are coupled electron-phonon modes and B$_2$ is a pure phonon mode (Ref. 40).

the elastic constant C_{44} given by

$$C_{44} = C_{44}^{c} - \text{Const.} \; \Phi_z^2 \omega^{-2} \tag{1}$$

where ω is the frequency of the lowest Raman mode (Fig. 18) and Φ_z is the static component of AlO_6 rotation along $[001]$. This expression with the constant chosen to make C_{44} zero at 118.5 K, is compared with the Brillouin measurements in Fig. 19 (43). The very asymmetric shape is caused by the temperature dependence of Φ_z which increases continuously below 151 K (see above). The measured elastic constant is actually $\frac{1}{2}(C_{44}+C_{55})$ whereas the calculation is for C_{44}; a more detailed calculation would probably remove this discrepancy.

5. CONCLUSION

Optical and infra-red techniques are extremely useful for the study of excitations in Jahn-Teller systems. Crystals containing rare-earth ions for which the electron-phonon interaction involves one dimensional distortions and is relatively weak have received most attention and can be described by quite simple theoretical models. Further measurements of the odd-parity vibron modes in rare-earth systems and their contributions to dielectric behaviour (see Seminar by D. R. Taylor in this volume) and of effects of J.T. couplings involving two-dimensional distortions would be interesting. By contrast 3d-ions which have much stronger interactions have not been investigated extensively; the excitations of isolated 3d complexes and effects of cooperative interactions will probably be subjects of increasing interest in the future.
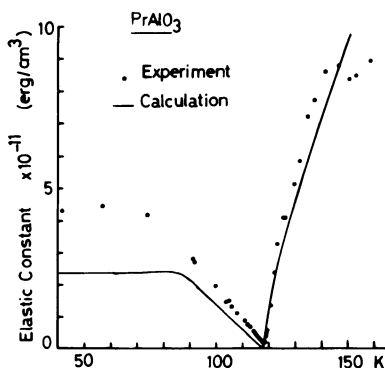
Fig. 19. Brillouin scattering measurements of $\frac{1}{2}(C_{44}+C_{55})$ for $PrAlO_3$ (points, Ref. 37) compared with calculation of C_{44} (curve) using eq. 1 (Ref. 43).

REFERENCES

Reviews: (1)   M. D. Sturge, Solid State Physics, 20 91 Ed. F. Seitz,
                D. Turnbull and H. Ehrenreich (New York, Academic
                Press, 1967).
          (2)   F. S. Ham in "Electron Paramagnetic Resonance" p.1
                Ed. S. Geschwind (New York, Plenum, 1972).
          (3)   R. Englman "The Jahn-Teller effect in molecules and
                crystals" (London, Wiley, 1972).
          (4)   G. A. Gehring and K. A. Gehring, Rep. Prog. Phys. 38
                1 (1975).

(5)   S. Guha and L. L. Chase, Phys. Rev. B12 1658 (1975).
(6)   L. L. Chase and C. H. Hao, Phys. Rev. B12 5990 (1975).
(7)   B. F. Gächter and J. A. Koningstein, Solid State Commun. 14
      361 (1974).
(8)   R. M. Macfarlane, J. Y. Wong and M. D. Sturge, Phys. Rev.
      166 250 (1968).
(9)   R. R. Joyce and P. L. Richards, Phys. Rev. 179 375 (1969).
(10) H. Thomas and K. A. Müller, Phys. Rev. Letts. 28 820 (1972).
(11) R. T. Harley, W. Hayes and S. R. P. Smith, J. Phys. C5 1501
      (1972).
(12) R. J. Elliott, R. T. Harley, W. Hayes and S. R. P. Smith,
      Proc. Roy. Soc. A328 217 (1972).
(13) R. T. Harley and R. M. Macfarlane, J. Phys. C8 L530 (1975).
(14) P. J. Becker, M. J. M. Leask and R. N. Tyte, J. Phys. C5 2027
      (1972).
(15) J. E. Battison, A. Kasten, M. J. M. Leask, J. B. Lowry and
      K. J. Maxwell, J. Phys. C9 1345 (1976).
(16) H. G. Kahle, L. Klein, G. Müller-Vogt and H. C. Schopper, Phys.
      Stat. Sol. (b) 44 619 (1971).
(17) H. B. Ergun, K. A. Gehring and G. A. Gehring, J. Phys. C9 1101
      (1976).
(18) L. Klein, W. Wüchner, H. G. Kahle and H. C. Schopper, Phys.
      Stat. Sol. (b) 48 K139 (1971).
(19) R. L. Melcher and B. A. Scott, Phys. Rev. Letts. 28 607 (1972).
(20) J. R. Sandercock, S. B. Palmer, R. J. Elliott, W. Hayes,
      S. R. P. Smith and A. P. Young, J. Phys. C5 3126 (1972).
(21) M. T. Hutchings, R. Scherm and S. R. P. Smith, AIP Conference
      Proceedings 29 372 (1975).
(22) B. W. Mangum, J. N. Lee and H. W. Moos, Phys. Rev. Letts. 27
      1517 (1971).
(23) R. T. Harley, C. H. Perry and W. Richter, J. Phys. C (in press).
(24) E. Pytte, Phys. Rev. B8 3954 (1973).
(25) J. W. McPherson and Y. L. Wang, J. Phys. Chem. Sols. 36 493
      (1975).
(26) G. Schaak, Solid State Commun. 17 505 (1975).
(27) R. T. Harley, W. Hayes, A. M. Perry, S. R. P. Smith, R. J.
      Elliott and I. D. Saville, J. Phys. C7 3145 (1974).

(28) S. J. Allen, Phys. Rev. 166 530 (1968) and 167 492 (1968).

(29) J. Faber and G. H. Lander, Phys. Rev. B14 1151 (1976).

(30) P. J. Colwell, L. A. Rahn and C. T. Walker "Light Scattering
        in Solids" Ed. M. Balkanski, R. C. C. Leite and
        S. P. S. Porto, p.239 (Paris, Flamarion, 1976).

(31) G. Dolling, R. A. Cowley and A. D. B. Woods, Canadian J.
        Physics 43 1397 (1965).

(32) R. A. Cowley and G. Dolling, Phys. Rev. 167 464 (1968).

(33) B. C. Frazer, G. Shirane, D. E. Cox and C. E. Olsen, Phys.
        Rev. 140 A1448 (1965).

(34) O. G. Brandt and C. T. Walker, Phys. Rev. Letts. 18 11 (1967).

(35) R. T. Harley, W. Hayes, A. M. Perry and S. R. P. Smith,
        J. Phys. C6 2382 (1973).

(36) R. J. Birgeneau, J. K. Kjems, G. Shirane and L. G. Van Uitert,
        Phys. Rev. B10 2512 (1974).

(37) P. A. Fleury, P. D. Lazay and L. G. Van Uitert, Phys. Rev.
        Lett. 33 492 (1974).

(38) K. B. Lyons, R. J. Birgeneau, E. I. Blount and L. G. Van
        Uitert, Phys. Rev. B11 891 (1975).

(39) M. D. Sturge, E. Cohen, L. G. Van Uitert and R. P. van Stapele,
        Phys. Rev. B11 4768 (1975).

(40) R. T. Harley, W. Hayes, A. M. Perry and S. R. P. Smith,
        J. Phys. C8 L123 (1975).

(41) P. A. Fleury "Light Scattering in Solids" ed. M. Balkanski,
        R. C. C. Leite and S. P. S. Porto, p.747 (Paris,
        Flamarion, 1976).

(42) J. C. Slonczewski and H. Thomas, Phys. Rev. B1 3599 (1970).

(43) R. T. Harley, J. Phys. C (in press).

(44) R. A. Cowley. Phys. Rev. B13 4877 (1976).

ELECTRIC SUSCEPTIBILITY STUDIES OF COOPERATIVE JAHN-TELLER ORDERING IN RARE-EARTH CRYSTALS

D. R. Taylor

Clarendon Laboratory Oxford University, U.K. and

Queen's Univ., Kingston, Canada (permanent address)

The study of dielectric anomalies at structural phase transitions, for many years a standard technique, has only recently been applied to Jahn-Teller (JT) phase transitions. A number of interesting results have already been obtained, some of which will be described below. They include the identification of novel JT behaviour in $PrCl_3$ and some of its isomorphs[1-3], and the observation of interesting dielectric anomalies in previously studied JT systems such as $DyVO_4$[4] and CeES[5] (ES = ethyl sulphate). For convenience only rare-earth insulating JT systems will be discussed. Many of their properties have been reviewed in lectures by Harley, by Kjems, and by Stinchcombe at this conference, and in an article by Gehring and Gehring[6].

Consider first the conditions under which a significant electric dipole moment (EDM) can occur at the site of a rare-earth ion. The point symmetry must of course be non-centric, but if the low-temperature ordering of the crystal is to be affected the ion must also have degenerate or approximately degenerate electronic levels. The latter case does not further restrict the symmetry, but for exact degeneracy the symmetry cannot be too low. For the important case of non-Kramers doublet levels Müller[7] showed that an EDM occurs for only seven point groups: C_3, C_{3v}, C_{3h}, D_3, D_{3h}, D_{2d}, S_4. The existence of an EDM implies a linear splitting of the electronic levels in an applied electric field. In addition it should be clear that ions satisfying the above conditions are JT active, although the converse is not true.

PrCl_3. $PrCl_3$ is representative of a number of compounds containing Pr ions in threefold symmetry in which electric dipole splittings were first investigated[8,9]. The ground state is a non-

Kramers doublet transforming as the E' representation of the C_{3h} point group. The symmetric product $[E' \times E'] = A' + E'$. The doublet can therefore be split by a magnetic field H_z parallel to the threefold axis, which transforms like A', and electric field components E_x, E_y which transform like E'. It is convenient to describe these splittings by an effective spin $S = \frac{1}{2}$ Hamiltonian[8,9]:

$$\mathcal{H} = g_z \beta H_z S_z + \gamma (E_x S_x + E_y S_y) \tag{1}$$

where γ is the "uncorrected" EDM (if E_x, E_y are laboratory fields). Eqn. (1) shows the formal similarity of electric and magnetic dipole moments in these systems, but leaves unanswered questions about the physical origin and typical magnitude of γ. The major contribution to γ can be visualized as follows: E_x or E_y distort the rare earth site by displacing anions and cations in opposite directions. This removes the threefold symmetry and consequently splits the electronic doublet in proportion to the field. The magnitude of γ will depend on the electronic wave functions but is typically comparable to, and sometimes much greater than, the magnetic dipole moment[10].

In $PrCl_3$ the Pr ground doublets will also be split by dis-tortins of E' symmetry. These distortions will be coupled by the lattice and this can be described in terms of an effective spin-spin interaction[6] by transforming the electron-phonon Hamiltonian as described in the lecture by Stinchcombe. Since the distortion mode is an E' doublet the interaction takes the XY form[11]

$$\mathcal{H}_{ij} = J_{ij}(S_x^i S_x^j + S_y^i S_y^j) \tag{2}$$

Such an interaction has been directly confirmed by EPR measure-ments[12] on diluted $PrCl_3$, which also established the magnitude $J_{ij} \approx 2$ cm^{-1} for nearest neighbours. Each Pr has two nearest neighbours along the threefold axis and it is clear that more distant interactions are small since the low-temperature properties show marked one-dimensional behaviour. For example the specific heat shows a broad maximum which is fit quite well by the XY chain specific heat[1,12], followed by a narrow spike indicating long-range ordering at only 0.4 K. Since E_x and E_y couple to the E' dis-tortions as described above the E' distortions carry an EDM. The JT ordering is therefore expected to be antiferroelectric, and this was confirmed by electric susceptibility measurements[1] as shown in fig. 1. Above the broad maximum due to short-range ordering the data are fitted to the high-temperature series for the 1-D XY sus-ceptibility, yielding $J = 2.0$ cm^{-1} in agreement with other experi-ments. The data also determine the EDM γ ($\gamma = 6.6 \times 10^{-31}$ C.m[1,2]), and it turns out that the nearest-neighbour interaction agrees in magnitude with the point electric dipole-dipole interaction: $J \sim \gamma^2/4\pi\varepsilon_o R^3$. As yet the symmetry of the low temperature phase has not been determined, but the distortion is expected to be E_{2g}
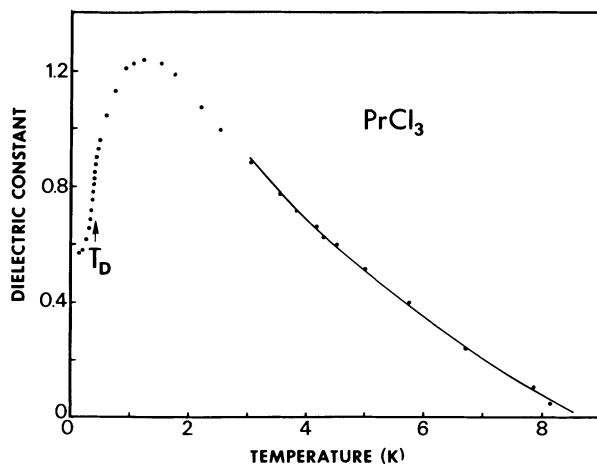
Fig. 1. Electric susceptibility of $PrCl_3$

or E_{1u} with the unit cell doubled along the threefold axis. In summary $PrCl_3$ has some unique properties compared to JT systems previously studied, in particular the quasi 1-D antiferroelectric ordering. On the other hand the low ordering temperature is inconvenient for structural studies. Similar behaviour has been observed in $PrES$[2], which shows the same 1-D ordering but no long-range order down to ~0.06 K, and in $PrBr$[3], which has a phase transition at 0.37 K.

$DyVO_4$. One of the most extensively-studied JT systems, $DyVO_4$ differs in many ways from $PrCl_3$. The Dy ions are at D_{2d} sites, and their lowest energy levels are two nearly degenerate Kramers doublets. At the 14 K phase transition a B_{1g} lattice distortion occurs, corresponding to a B_2 distortion at Dy sites. Because the distortion mode is a singlet the effective spin-spin interactions are Ising rather than XY. There is reason to expect a dielectric anomaly in this system because D_{2d} symmetry allows an EDM parallel to the tetragonal axis, and this EDM belongs to the B_2 representation. Hence the B_2 distortion carries an EDM which is therefore an order parameter. Recently the electric susceptibility of $DyVO_4$ was measured[4,13] with results as shown in fig. 2. This curve resembles the typical "parallel" magnetic susceptibility in a 3-D antiferromagnet and was interpreted[4] in terms of improper antiferroelectric ordering; that is the EDM's of the two Dy ions in each unit cell order antiparallel but the unit cell is not doubled. This conclusion is reinforced by the relatively large Dy EDM in this crystal. The high-temperature data of fig. 2 indicate $\gamma \sim 10^{-30}$ Cm[13], which, together with the lattice structure suggests strong antiparallel
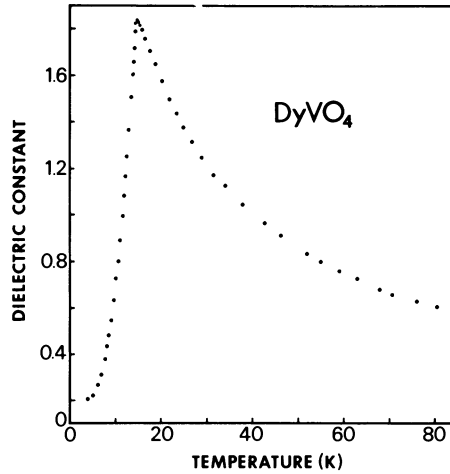
Fig. 2. Electric susceptibility of DyVO$_4$

nearest-neighbour electric dipole interactions. There is consider-
able experimental evidence, as discussed by Harley and Kjems in
their lectures, that the spin-spin interactions in DyVO4 are very
short-range, in contrast to other JT systems, such as TmVO4 which
undergoes a different distortion and which clearly has long range
interactions. It is interesting that in both DyVO4 and PrCl3 where
electric dipole ordering occurs the effective spin-spin interactions
are short-range.

     CeES. The Ce electronic levels in CeES resemble those in
DyVO4: two Kramers doublets separated by only a few cm^{-1}. The JT
behaviour of CeES is entirely different however because the Ce
levels couple most strongly to a uniform (A') lattice distortion.
This behaviour[14], originally proposed to explain the specific heat
anomaly, is only possible in systems with accidental degeneracy
because separation of the levels can be increased, and hence the
total energy lowered, by a change in unit cell parameters without
lowering the symmetry. The effective spin-spin coupling in this
case is that of an Ising interaction in a longitudinal field[5]. No
phase transition occurs: the doublet separation and the lattice
strain increase monotonically from high- to low-temperature limits[14].
Although in this case no electric dipole ordering occurs, electric
susceptibility is a useful probe because an electric field perpen-
dicular to the hexagonal axis couples the two non-Kramers doublets
and hence allows their separation to be monitored. Using mean
field theory[5] the electric susceptibility is given by

$$\chi_E = (N\gamma^2/2\Delta) \, \tanh(\Delta/2kT) \tag{3}$$

where Δ is the separation between the doublets. Δ varies with temperature according to[14]

$$\Delta - \Delta_{\infty} = (\Delta_0 - \Delta_{\infty}) \tanh(\Delta/2kT) \qquad (4)$$

where Δ_{∞} and Δ_0 are the high- and low-temperature limits. This gives χ_E a "sharper" temperature dependence than if Δ is constant (no JT coupling) just as the specific heat peak is sharper than a simple Schottky peak[14]. Electric susceptibility measurements[5] confirm this interpretation and give reasonable quantitative agreement with the specific heat results[14].

In summary, in JT systems where the crystal symmetry allows electric dipole coupling between degenerate or nearly degenerate crystal field levels the electric susceptibility technique is a very effective probe of JT distortions.

REFERENCES

1.   J.P. Harrison, J.P. Hessler, D.R. Taylor, Phys. Rev. B14, 2979 (1976).
2.   J.T. Folinsbee, J.P. Harrison, D.B. McColl, D.R. Taylor, J. Phys. C 10, 743 (1977).
3.   D.R. Taylor, J.P. Harrison, D.B. McColl, Physica 86-88B, 1164 (1977).
4.   H. Unoki, T. Sakudo, Phys. Rev. Letters 38, 137 (1977).
5.   D.R. Taylor et al (to be published).
6.   G.A. Gehring, K.A. Gehring, Rep. Prog. Phys. 38, 1 (1975).
7.   K.A. Müller, Phys. Rev. 171, 350 (1968).
8.   F.I.B. Williams, Proc. Phys. Soc. 91, 111 (1967).
9.   J.W. Culvahouse, D.P. Schinke, D.L. Foster, Phys. Rev. Letters 18, 117 (1967).
10.   J.W. Culvahouse, L. Pfortmiller, D.P. Schinke, J. Appl. Phys. 39, 690 (1968).
11.   E. Pytte, Phys. Rev. B8, 3954 (1973).
12.   J.W. Culvahouse, L. Pfortmiller, Bull. Am. Phys. Soc. 15, 394 (1970).
13.   R.T. Harley, D.R. Taylor (to be published).
14.   J.R. Fletcher, F.W. Sheard, Solid St. Commun. 9, 1403 (1971).

NEUTRON SCATTERING STUDIES OF THE COOPERATIVE

JAHN-TELLER EFFECT

J.K. Kjems

Research Establishment Risø

DK-4000 Roskilde, Denmark

ABSTRACT

The results of neutron scattering studies of the Jahn-Teller transitions in $PrAlO_3$, $TbVO_4$, $TmVO_4$, $TmAsO_4$, and $PrCu_2$ are summarized. It is found that RPA theory gives an excellent description of both the static and dynamic behaviour of these systems. Within this theory the momentum dependences of the effective electron-phonon coupling parameters have been derived from the measurements on $PrAlO_3$ and $TmVO_4$, and in the latter case an excellent agreement is found with the results of a similar analysis of ultrasonic and Brillouin scattering experiments. The soft phonon response in both $PrAlO_3$ and $TbVO_4$ contains a diverging quasielastic component which only in the case of $TbVO_4$ can be accounted for by the RPA theory adapted by Smith for this problem.

1. INTRODUCTION

The cooperative Jahn-Teller Effect (CJTE) has many
fascinating aspects and the efforts that have been de-
voted to this subject have often had quite different
motivations. One may view the CJTE as a basic mechanism
for structural phase transitions belonging to the class
of pseudo-spin-phonon coupled systems which also in-
duces the hydrogen bonded ferroelectrics[1] and molecular
crystal systems[2] where the pseudo-spin relates to the
proton positions and the molecular orientations, re-
spectively. In the CJTE-systems the driving force for
the phase transition can be readily identified. The
free energy of the electronic system with a degenerate
or near degenerate ground state is reduced by lowering
of the local symmetry around the Jahn-Teller active
ions. The electronic energy gain is linear in the dis-
tortions whereas the balancing elastic energy has a
quadratic dependence so at low enough temperatures the
total free energy will be minimized by a finite distor-
tion. The coupling between the lattice deformations and
the electronic degrees of freedom can be pictured as an
effective quadrupole-quadropole interaction mediated by
the phonons[3] in analogy to the usual Rudermann-Kittel
exchange interaction in metals where the electrons play
the roles of the go-betweens. As in the magnetic case
it is a useful first approximation to neglect the micro-
scopic origin of the interactions and to work with model
Hamiltonians which then describe the thermodynamics of
the phase transitions quite well on the basis of effec-
tive ion-ion interaction parameters. Regarded in this
manner the simplest Jahn-Teller systems are realizations
of the 3-dimensional Ising model with or without a
transverse field.

The CJTE systems differ from the usual magnetic
systems in the sense that the energy bands of the inter-
action mediators, the phonons, overlap with the energies
of the localized electronic excitations and this gives
rise to strong mode mixing[3] which in turn enables accu-
rate measurements of the electron-phonon coupling matrix
elements including their q-dependence[4].

A variety of experimental methods have been applied
in the study of the CJTE. They range from bulk methods
like specific heat, susceptibility and thermal expansion

measurements to the use of microscopic probes like x-ray, neutron and light scattering as well as resonance and ultrasonic methods. These notes focus on the results that have been obtained by the use of neutron scattering to characterize both the static and the dynamic properties of systems that display the CJTE. The theoretical background is to a large extent covered in the lectures by Stinchcombe at this school and also in the recent review articles by Gehring and Gehring[5] and by Fulde[6]. Thus the theoretical discussions in this paper will be limited to what is needed in order to comprehend the analysis of the data that are presented.

The systems that so far have been studied in various degrees of detail by neutron scattering all contain rare earth ions and they are the insulators $PrAlO_3$ (T_D = 151 K), $TbVO_4$[7] (T_D = 33 K), $TmVO_4$[8] (T_D = 2.1 K), and $TmAsO_4$ (T_D = 6.0 K) and the metallic compound $PrCu_2$ (T_D = 8.0 K). The experimental results for these systems are reviewed with the following organization of these notes. First the properties of the neutron as a spectroscopic tool is summarized followed by a short description of the zoology of the crystal structures and symmetries of the systems involved. Then follows a short theoretical discussion aimed at the fixing of the nomenclature. The experiments are then summarized beginning with the static and critical properties followed by the results for the normal modes and the mode mixing. Finally some conclusions are drawn together with some guesses at what may result from the continued studies.

2. THE NEUTRON PROBE

All the known Jahn-Teller transitions involve zone centre modes and so neutron scattering is only one of many tools that can be applied. The first spectroscopic studies were made using Raman and Brillouin scattering and ultrasonic methods[5]. The power of the neutron probe lies partly in the fact that excitations can be followed throughout the Brillouin zone and partly in the versatility of neutron spectrometry which allows you to study both the structural changes through Bragg diffraction and the excitation spectrum with the same set-up. The neutron couples both to the translational degrees of freedom of the atoms in the crystal and to the electronic degrees of freedom of the Jahn-Teller ions. The

deformations of the unit cell that result from a CJT-
transition give rise to shifts in the positions of Bragg
peaks and the internal displacements of atoms within the
unit cell can in principle be detected through intensity
changes. An alternative method to determine the internal
displacements that result from a CJTE-transition is im-
purity ESR by which one can monitor the orientation of
the electric field gradient tensor at the impurity site.
This method has been very successful in the study of
the 151 K transition in $PrAlO_3$ as will be discussed
later.

The change in the electronic energy levels can in
some cases be observed directly via magnetic dipole
transitions which couple to the neutron moment. The
cross section for such processes is given in the non
interacting limit by the "crystal field" formulae[9]

$$\frac{\partial^2 \sigma}{\partial\Omega\partial\omega} = N(\frac{1.91\ e^2}{2mc^2}\ g_J)^2\ f^2(\vec{\kappa})\ \frac{k_f}{k_i} \sum_{n,m} \rho_n |<n|\vec{J}_\perp|m>|^2$$

$$e^{-2W}\delta(E_n - E_m + \hbar\omega)$$

$$(1)$$

where g_J is the Landé factor, f the form factor, $\vec{\kappa} = \vec{k}_i - \vec{k}_f$
the momentum transfer, and ρ_n the occupation probability
for the $<n|$ electronic state in the J manifold with the
energy E_n. The energy transfer is $\hbar\omega = \frac{\hbar^2}{2M_n}(k_i^2 - k_f^2)$. M_n

is the neutron mass and m the electron mass. $J_\perp$ is the
component of the total angular momentum operator <u>perpen-
dicular</u> to the momentum transfer $\vec{\kappa}$. It should be stress-
ed that the polarization information is given in the
negative sense that the component <u>parallel</u> to the momen-
tum transfer <u>does not</u> contribute to the scattering. The
cross section for crystal field transitions changes if
there is noticeable dispersion due to ion-ion inter-
actions and as an example we quote the result for a J^z
transition[11] with a dipole matrix element α and energy
splitting 2Δ

$$\frac{\partial^2 \sigma}{\partial\Omega\partial\omega} = (\frac{1.91\ e^2}{2mc^2}\ g_J)^2\ \frac{k_f}{k_i}\ f^2(\vec{\kappa})\sin^2\psi\alpha^2\ \frac{2\Delta}{E_{\vec{\kappa}}}\ \rho_0(T)\ e^{-2W}\ (2)$$

where ψ is the angle between the z-axis and $\vec{\kappa}$. E is the
dispersed energy of the mode given by the RPA formulae

$$E_{\vec{\kappa}} = 4\Delta(\Delta - \alpha^2 J(\vec{\kappa})) \tag{3}$$

where $J(\vec{\kappa})$ is the Fourier transform of the ion-ion interaction. More general expressions for a many level system with interactions have been worked out by Fulde and Peschel,[12] Young[13] and by Buyers.[14]

The phonon cross section has some characteristic differences compared to the magnetic cross section. The one phonon creation cross section[9] is given by

$$\frac{\partial^2 \sigma}{\partial\Omega\partial\omega} = \frac{(2\pi)^3}{2v_o} \frac{k_f}{k_i} \frac{1}{\omega} \left| \sum_j a_j \, e^{+i\vec{\kappa}\cdot\vec{r}_j} \frac{\vec{\kappa}\cdot\vec{u}_j(\vec{\kappa})}{\sqrt{M_j}} \right|^2$$

$$\frac{1}{1-e^{-\hbar\omega\beta}} \, e^{-2W} \tag{4}$$

with $u_j(\vec{\kappa})$ being the eigenvector for the jth atom for the mode in question. It is important to note that in general the phonon scattering increases with the square of the momentum transfer whereas the magnetic cross sections decrease with the form factor. This can be used together with the different temperature dependences to identify the origin of the observed scattering.

As we shall see later the CJTE leads to mixed crystal field-phonon modes and in principle this could give rise to interesting interference effects. However, in most cases only one of the modes has an appreciable cross section and when the modes mix they "share" this scattering power and may both become observable in certain regions of the Brillouin zone.

3.SYMMETRIES AND CRYSTAL FIELDS

One of the keys to the understanding of the CJTE is the way in which the symmetry of the crystalline electric field at the active ion sites determines the electronic levels, the crystal field splittings. For a number of years this has been an active field of research on its own and a large number of materials have been characterized.[15] In cases of high local symmetry only few parameters are needed to define the crystal field Hamil-

tonian

$$H_{CEF} = \sum_{\substack{n=2,4,6 \\ m=-n,n}} B_n^m \chi_n \hat{O}_n^m (J) \tag{5}$$

where B_n^m are the crystal field parameters, χ_n the re-[16]
duced matrix elements tabulated by Elliot and Stevens,
and $\hat{O}_n^m(J)$ are the angular momentum operator equivalents.
The actual number of parameters needed in the different
crystallographic phases one for example encounters in a
system like $PrAlO_3$ are the following[4]:

$O_h, 2; \quad D_3, 6; \quad C_{2v}, 9; \quad C_s, 15; \quad$ and $D_{2d}, 5.$
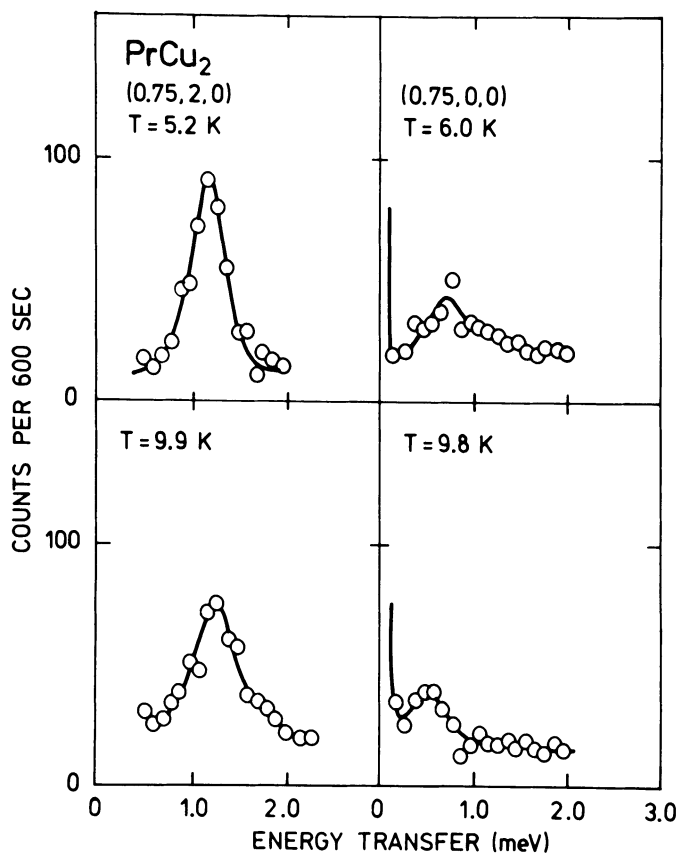
Fig. 1.   Left hand side: Constant Q scans at (0.75,2,0)
          at 5.2 K and 9.9 K in $PrCu_2$.
          Right hand side: Constant Q scan at (0.75,0,0)
          at 5.6 K and 9.8 K in $PrCu_2$.
          The Jahn-Teller transition occurs at T_D = 8 K.

Hence it is often necessary to make some simplifying as-
sumptions in order to arrive at a qualitative description
as it was done for $PrAlO_3$ by Lyons et al.[17]

As an example we discuss the crystal field level
diagram for Pr^{+3} $^3H_4$ in orthorhombic, C_{2v}, symmetry.
This pertains both to $PrAlO_3$ and to $PrCu_2$ above T_D. In
the low C_{2v} symmetry, which contains two mirrorplanes
and a two-fold axis, the ninefold multiplet is split
into 9 singlets, namely $3A_1 + 2A_2 + 2B_1 + 2B_2$. As an
example of an observed transition Fig. 1 shows some re-
cent inelastic neutron constant Q-scans obtained with
a single crystal of $PrCu_2$ which was oriented with the
a-b plane in the scattering plane of the spectrometer.
The scans refer to the same point (0.75,0,0) in the
reduced Brillouin zone with different polarizations.
The strong transition at 1.3 meV in Fig. 1.a disappears
when $\vec{K}$ is directed along the a* axis, Fig. 1.b. Hence
one concludes that this transition is induced by the
J^x component of the total angular momentum operator.
One then deduces that the two levels connected must be
either A_1-B_2 or A_2-B_1. Unfortunately, this piece of
information is clearly insufficient to make level as-
signments, but hopefully with enough data collected
one can make some realistic attempts. Fig. 1 also
shows that the phase transition   at 8 K essentially
leaves the strong J^x transition unaffected whereas the
much weaker J^y or J^z transitions in Fig. 1.b are shifted
appreciably in energy. Tentatively, the present results
are interpreted to give a crystal field level scheme
for the lowest 4 levels in $PrCu_2$ as indicated in Fig. 2
together with the much more firmly established results
for the other CJTE-systems.

In $PrAlO_3$ a combination of fluorescence, neutron
and Raman spectroscopy paired with model calculations
have resulted in a detailed understanding of the full
level scheme   (see figure 17 in the proceeding paper
by Harley). At T_D = 151 K only the B_1 transition between
the lowest two that couples to the lattice and drives
the phase transitions.
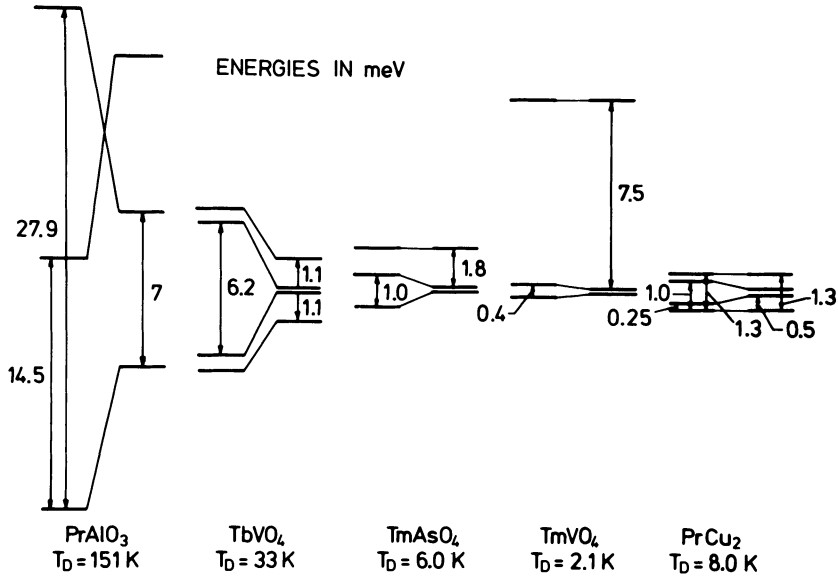
Fig. 2.   Schematic representation of the change in the
          lowest electronic energy levels for the CJTE
          systems that so far have been investigated by
          neutron scattering.

4.THEORY

The theory developed by Elliott et al.[1] for a two
level system with a splitting, 2Δ, is briefly summarized.
The interaction with the lattice is expressed as a lin-
ear coupling between electric quadrupole operators, often
in a pseudospin representation, and the normal modes of
the lattice of compatible symmetry.

$$H = \sum_{n,\vec{k},p} \xi_p(\vec{k})e^{i\vec{k}\cdot\vec{R}_n} S_n^z(a_{p,\vec{k}} + a_{p,\vec{k}}^+)$$

$$+ \sum_{\vec{k},p} \hbar \omega_p(\vec{k})(a_{p,\vec{k}}^+ a_{p,\vec{k}} + \tfrac{1}{2}) \qquad (6)$$

$$+ \Delta\sum_n S_n^x$$

where S_n^z and S_n^x are the pseudospin operators represent-
ing two electronic states at the energies $\pm\Delta$, $a_{p,\vec{k}}^+$ is
the operator for a phonon of wavevector $\vec{k}$, band p and

frequency $\omega_p(\vec{k})$ and $\xi_p(\vec{k})$ denotes the corresponding Jahn-Teller coupling. The detailed solutions of this Hamiltonian are discussed in the paper by Stinchcombe. The first step is a displaced oscillator transformation which gives

$$H = \sum_{\vec{k}} \hbar \, \omega_p(\vec{k})(\gamma^+_{p,\vec{k}}\gamma_{p,\vec{k}} + \tfrac{1}{2}) - \sum_{\vec{k}} J(k) \, \vec{S}_{\vec{k}}\vec{S}_{-\vec{k}} + \Delta N^{\frac{1}{2}} \, S^x_o$$

where

$$\gamma_{p,\vec{k}} = a_{p,\vec{k}} + \frac{\xi_p(\vec{k})}{\hbar \, \omega_p(\vec{k})} \, S^z_{\vec{k}} \tag{7}$$

and

$$K_p(\vec{k}) = \frac{|\xi_p(\vec{k})|^2}{\hbar \, \omega_p(\vec{k})} \quad , \quad J(\vec{k}) = \sum_p K_p(\vec{k}) - N^{-1} \sum_{p,\vec{k}} K_p(\vec{k})$$

This shows that the linear Jahn-Teller coupling gives rise to an effective quadrupole-quadrupole interaction, $J(\vec{k})$, which here includes the static strain contributions. As a first approximation for the static properties one ignores the non-commutation of the displaced oscillator and the transverse field parts of Eq. 6 and simply treats the Ising model in a transverse field via molecular field theory. The essential results are the following[1,5]

(a) T_D is defined by

$$\frac{\Delta}{J(0)} = \tanh(\frac{\Delta}{kT_D}) \tag{8}$$

(b) Below T_D the order parameter $<S^z>$ is given by

$$<S^z> = \frac{J(0) <S^z>}{W} \tanh(\frac{W}{kT}) \tag{9}$$

where

$$W^2 = J^2(0)<S^z> + \Delta^2 \text{ and } <S^x> = \frac{\Delta}{W} \tanh(\frac{W}{kT})$$

(c) If the elastic strain energy is taken as $\frac{1}{4}NV_o Ce^2$ then the equilibrium strain is

$$<e> = 4 \, K_a(0)<S^z>/V_o C \tag{10}$$

and similarly for the optic mode displacements

$$<Q_0> = - K_0(0)<S^Z>/M\omega^2(0) \qquad\qquad (11)$$

The results for the dynamics are quoted later under the discussion of the mixed modes.

5. STATIC AND CRITICAL PROPERTIES

The temperature dependence of the order parameter below T_D has been thoroughly studied in $PrAlO_3$. The static strain has been determined from the twinning patterns that evolves due to domain formation[4] below T_D. The optic phonon order parameter[10] has been deduced from measurements of the electric field gradient tensor around a Gd^{+3} impurity as sensed by ESR and the electronic order parameter, as manifested in the splitting, 2W, has been measured by fluorescence[10,17,20] relative to the $^3P_0$ state of the Pr^{+3} ion. Fig. 3 summarizes all these results on normalized scales together with the simplest mean field calculation[4]. The internal consistency between these different measurements of the temperature dependence of $<S^Z>$ offers strong support to the basic
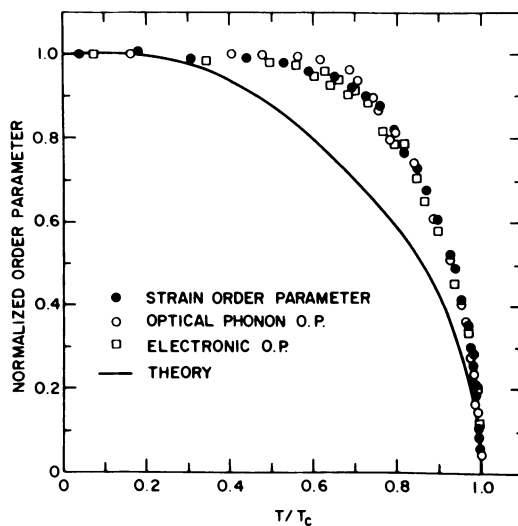
Fig. 3. The experimentally determined order parameters in $PrAlO_3$ displayed on normalized scales. The full line illustrates the results of the simplest mean field calculation for a two level system.

physical assumptions in the theory of the CJTE. The discrepancy between the mean field calculation and the experimental results for $PrAlO_3$ is probably due to oversimplifications in the description of this rather complicated system. For the simpler $TmVO_4$ system Segmüller et al.[21] find complete agreement between the mean field calculation of the strain order parameter and the results of an X-ray experiment.

The critical exponent, β, for the order parameter has been determined for $PrAlO_3^4$, $TbVO_4^{22}$, $TmAsO_4$ and $TmVO_4^{21}$ and in all cases one finds $\beta \cong 0.50$. The only CJTE system that does not conform to this picture is $DyVO_4^{22}$ where Harley found $\beta = 0.34$ using birefringence as a probe. The fact that all but one CJTE-systems display the classical exponent $\beta = 0.5$ has often been ascribed to the long range nature of the strain mediated interactions. However, as pointed out by Cowley[23] and by Als-Nielsen and Birgeneau[24] this may be too naive. More rigorous arguments can be made on basis of renormalization group theory paired with the Ginzburg[25] criterion and the concept of marginal dimensionality, d^*. In order to obtain a self-consistent picture within mean field theory Ginzburg stated that below the transition temperature the fluctuations in the order parameter, $\delta\sigma$, averaged over a suitable region, Ω, should be small compared to the averaged order parameter, σ_Ω.

$$(\delta\sigma)^2_\Omega \ll \sigma^2_\Omega$$

The suitable region is the one spanned by the correlation length, ξ, and it is the real space counterpart of the volume in reciprocal space determined by the half value of the critical susceptibility, κ_q. The key point is that the volume of the correlated regions in real space may diverge more rapidly than ξ^d in cases where the interactions are anisotropic.

$$\Omega_\xi \propto \xi^{d+m} \qquad m > 0$$

The marginal dimensionality is defined by

$$d^* = (\gamma' + 2\beta)/\nu' - m$$

$$d^* = (1 + 2 \cdot \tfrac{1}{2})/\tfrac{1}{2} - m = 4 - m \quad \text{(mean field exponents)}$$

where γ', β, and ν' are the usual critical indices for susceptibility, order parameter, and correlation
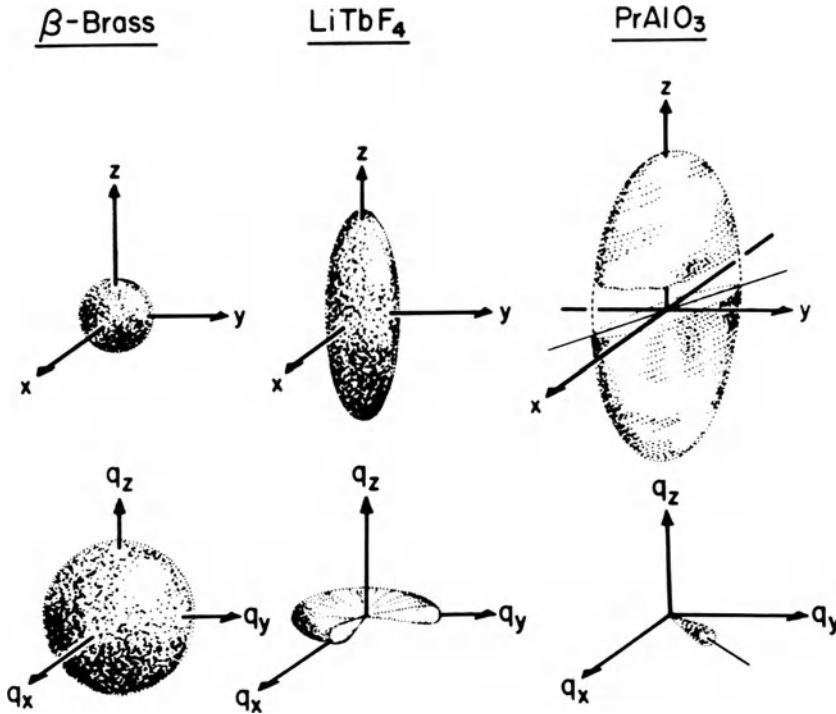
Fig. 4. Examples[24] of the shapes of the half height contours of the susceptibility in reciprocal space and the corresponding correlated regions in real space for 3 model systems with marginal dimensionalities d* = 4 (β-brass), d* = 3 ($LiTbF_4$) and d* = 2 ($PrAlO_3$ and other Jahn-Teller systems).

length, respectively. The Ginzburg criterion can then be expressed as follows. The molecular field theory is self-consistent if d > d* and not for d < d*. For d = d* there are logarithmic corrections to the mean field results. Examples of the shape of κ_q and the corresponding correlated regions in real space are shown in Fig. 4 for 3 model systems. The first is β-brass a d = 3 Ising system with isotropic interactions. Here m = 0 and d* = 4 so mean field theory fails. The second example is $LiTbF_4$, a dipolar coupled Ising ferromagnet where m = 1 d* = d = 3, and experiments have shown very beautifully that the exact renormalization group theory

applies. The third example shown in Fig. 4 is $PrAlO_3$ which represents the class of transition of interest in the present context. Here the fluctuations are confined to the lines in reciprocal space along which the acoustic anomalies occur. In real space the correlated volumes have "pan-cake" shape, and their volume diverges as ξ^{d+2} i.e. m = 2. ξ measures the thickness of the "pan-cake". Hence d* = 2 and mean field theory is expected to be exact. Indeed one finds that the all Jahn-Teller system discussed here displays classical exponent with the notable exception of $DyVO_4$. The non-classical result for $DyVO_4$ is quite puzzling, and we intend to check it using diffraction methods.

6. NORMAL AND MIXED MODES

The coupling of the electronic mode often called the vibron or the quadrupole exciton to the lattice modes have been observed directly in $PrAlO_3$[4], $TbVO_4$[7] and in $TmVO_4$[8]. The RPA solution for the unperturbed quadrupole mode is given by Eq. 5 and in the simplest picture the frequency of this mode at $\vec{k} = 0$ tends to zero as T_D is approached. However, the two first terms in the Hamiltonian, Eq. 9, do not commute and this gives rise to mode mixing and anticrossing between the lattice modes and the electronic mode. Ultimately it is the acoustic mode that becomes the soft mode at the transition. This was first demonstrated experimentally for $DyVO_4$[26] by Melcher and Scott who also studied $TmVO_4$[27]. The acoustic anomalies in $TbVO_4$[28] have been studied by Sandercock et al. using ultrasonics and Brillouin scattering and the same probes have been applied to $PrCu_2$[19] and $PrAlO_3$[29], respectively. The first neutron scattering study of the acoustic dispersion in a CJTE-system was the measurement of the Σ_3-branch in $PrAlO_3$[4] which is shown in Fig. 5.

The RPA solution for the mixed mode frequencies, $\omega(\vec{k})$, was derived by Elliott et al. and for $> T_D$ the result is contained in the equation

$$\hbar\omega(\vec{k})(\omega^2(\vec{k})-\omega_v^2(\vec{k})) = \sum_p \frac{4\Delta<S^x>\omega^3(\vec{k})K_p(\vec{k})}{\omega^2(\vec{k})-\omega_p^2(\vec{k})} \tag{12}$$

where ω_v and ω_p refer to the unperturbed vibron and phonon frequencies, respectively. In the limit of small $|\vec{k}|$ the frequency of the mode with predominantly acous-

tic character is given by

$$\omega^2(\vec{k}) = \omega_a^2(\vec{k}) \; \frac{\Delta - J(\vec{k})<S^x>}{\Delta - (J(\vec{k}) - K_a(\vec{k}))<S^x>} \qquad (13)$$

This expression has been applied to $PrAlO_3$ at various temperatures and the results are shown as the broken lines labelled 2, 3 and 4 in Fig. 5 where the lines marked 1 and 210 K served to establish the parameter values.
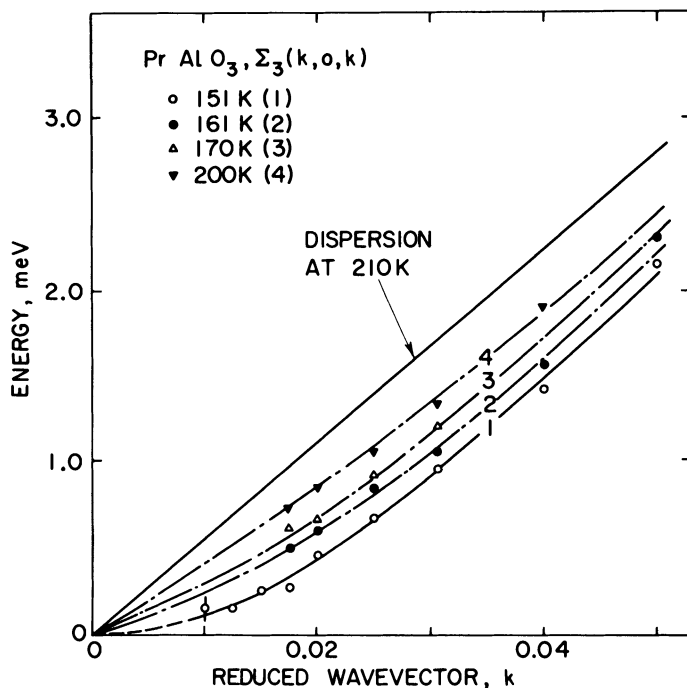
Fig. 5.   The observed dispersion of the B_1 acoustic mode in the orthorhombic phase of $PrAlO_3$ at different temperatures. There is an abrupt structural change to a rhombohedral structure at 205 K and the CJTE transition is at 151 K. The unit of the reduced wavevector is $2\pi/3.76$ Å^{-1}.
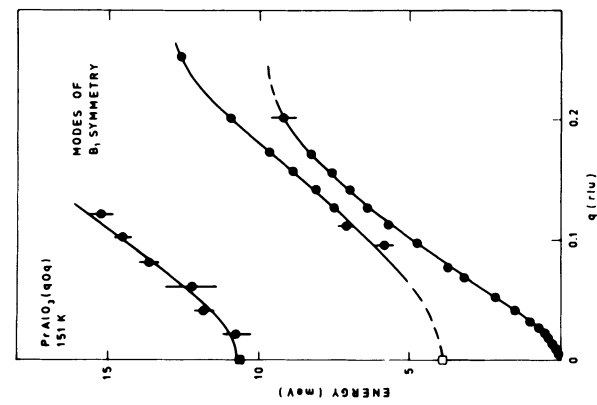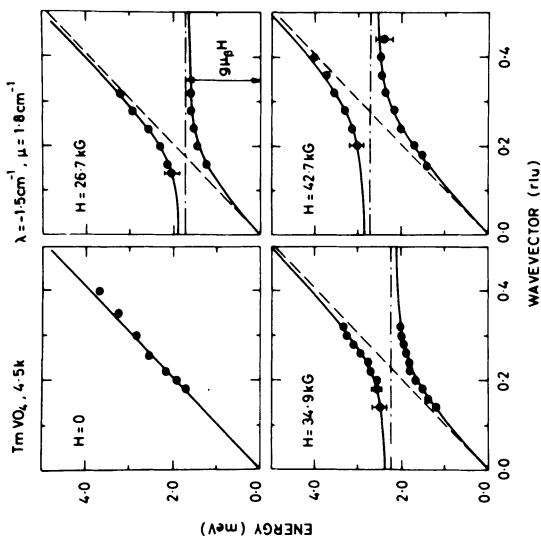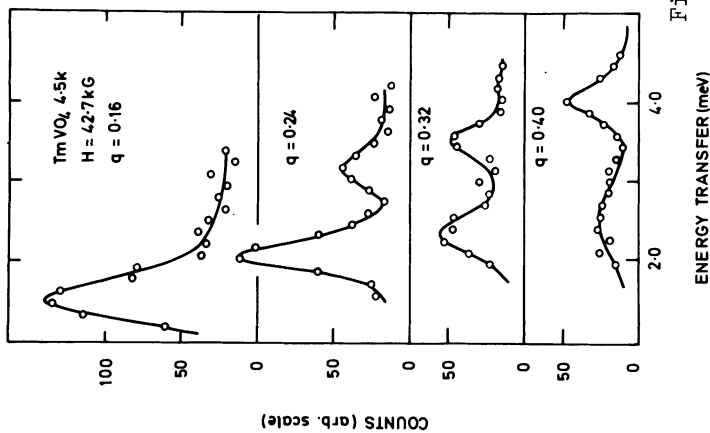
Figure 8.

Figure 7.

Figure 6.

Fig. 6. Observed spectra for the B_1 acoustic phonon in $TmVO_4$ propagation along (100) and polarized along (010). The zone boundary is at $q = 1.0$. The phonon anticrosses the Zeeman split doublet ground state at $2D = g\mu H = 2.7$ meV.

Fig. 7. The mixed mode dispersion in $TmVO_4$ at 4.5 K for external field along c with the strengths indicated on the figure. The full circles correspond to the peak positions in the inelastic scans. The full lines correspond to calculations with $g = 10.6$, $C_{66} = 1.90 \times 10^{11}$ erg/cm^2, $\rho = 6.80$ g/cm^3, $K_a(0) = 1.8$ cm^{-1} and $J(0) = +0.3$ cm^{-1}. The broken lines illustrate the unperturbed phonon disper-sion and the Zeeman splitting, respectively.

Fig. 8. Dispersion of the mixed modes of B_1 symmetry in $PrAlO_3$ at $T = T_D = 151$ K.

The anticrossing of the acoustic mode and the quadrupole exciton in $TmVO_4$[8] was observed with an applied field along the tetragonal axis, c^*. This resulted in a finite splitting $2\Delta = g\mu_B H$ of the ground doublet. Fig. 6 shows the typical shifts in the intensities from the lower to the upper branch one observes with increasing wavevector. Fig. 7 shows the observed dispersion curves together with the calculated ones based on Eq. 15 using the parameters derived from the acoustic anomaly. The corresponding results for $PrAlO_3$ showing all three modes involved are shown in Fig. 8.

In the measurements on $TbVO_4$ Hutchings[7] et al. found a strong feature in their spectra at zero energy transfer, which diverged as $T \rightarrow T_D$ and $|\vec{q}| \rightarrow 0$. They ascribed this scattering to transitions within the excited doublet (see Fig. 2) and the following formulae was derived for the wavevector dependence of the central peak intensity

$$I(k) \alpha \frac{2K_a(\vec{k})g_2}{\beta\omega_a(\vec{k})(1-J(\vec{k})g_1)(1-J(\vec{k})(g_1+g_2))} \qquad (14)$$

Here they used a Green's function formalism akin to the one used by Buyers in his description of singlet ground state dynamics.

$$g_1 = \frac{\tanh(\beta\Delta)}{\Delta} \frac{\cosh\beta\Delta}{1+\cosh\beta\Delta}$$

and

$$g_2 = \frac{\beta}{1+\cosh\beta\Delta}$$

are single ion susceptibilities arising from the assumed equal strength transitions between the singlets at 0 and 2D and within the doublet at D.

   Both the anticrossing dispersion curves and the central peak scattering can in principle be used to derive experimentally determined effective interaction parameters $K_a(\vec{k})$ and Fig. 9 shows the results of such analysis for $TmVO_4$. This $|q|$-independent result, which is consistent with the parameter that was derived in the ultrasonic experiment[17], confirms that the coupling to the acoustic mode is proportional to the strain produced by the phonon mode as given by the Debye-model.
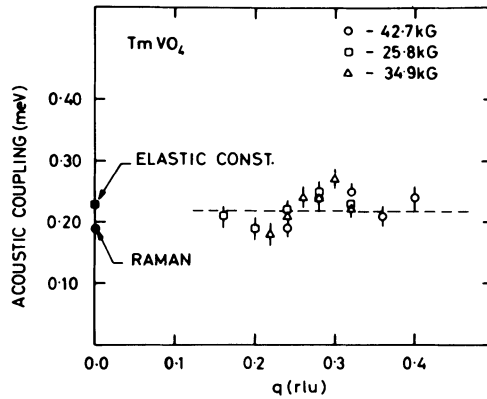
Fig. 9.   Wavevector dependence of the CJTE-coupling
           parameters for $TmVO_4$ as determined from the
           experimental data shown in Fig. 7 and the
           use of Eq. 15.

7. DISCUSSION

   The overall agreement between the simple mean field and RPA theories and the experimental observations including the temperature dependences is remarkably good. For instance one finds for the prototype

CJTE-system $TmVO_4$ that only two, now well known, parameters are needed to describe all the details of the field and temperature dependences of such varied quantities as the order parameter[20,21] $\Delta(T,H)$, the elastic constant[27] $C_{66}(H,T)$, the susceptibility[30] $\chi(T)$, the specific heat[30] $C_v(T)$ and the mixed-mode frequencies[8] $\omega(k,H,T)$ in the field and temperature ranges where the ground doublet can be regarded as isolated. This is probably a consequence of the limited role played by the fluctuations in these systems which also makes Landau theory correct for critical exponents. However, there are manifestations of some fluctuations, namely the central peak scattering as observed in $TbVO_4$[8] and less pronounced in $PrAlO_3$[4]. The theoretical description by Hutchings et al. does[3] not apply to $PrAlO_3$ since there are no degenerate electronic levels above T_D. Surprisingly, one does not find similar central peak scattering near T_D in neither $TmVO_4$ not in $TmAsO_4$. Based on Eq. 17 one would expect to observe scattering with intensity $\sim 1/k$ as $T \to T_D$ in $TmAsO_4$. The actual observed scattering falls off much more rapidly and it is confined to the q_y direction within the instrumental resolution of $q_x = \pm 0.01$ rlu. This could indicate that the scattering in $TmAsO_4$ originates in· changes in the mosaic distribution as T_D is approached. The paper presented by Møllenbach at this ASI lends support to this interpretation.

Another aspect of the analysis of the CJTE-systems is the understanding of the interaction parameters and their underlying microscopic mechanisms. Dohm[31] has pointed out that second order strain effects may be important for these systems and Fulde[6] has suggested that in the metallic systems the interaction with the conduction electrons also gives rise to quadrupole couplings. In this context a system like $PrCu_2$ may hold some essential clues to be unravelled by skilled searchers although the complexity of the level scheme may prevent any definite conclusions.

Further detailed studies of the soft phonon response in these systems may also be warranted since they could shed light upon the related magnetic problem of ordering in singlet ground state systems where a similar insufficient understanding persists for the relative roles of soft mode and central peak contributions

to the generalized susceptibility. As an amusing final point we note that the CJTE-systems that order magnetically presumably are the simplest examples of singlet ground state systems so they may hold the key to the solutions of this problem in more than one sense.

REFERENCES

1. R.J. Elliott in "Structural Phase Transitions and Soft Modes", Edited by E.J. Samuelsen, E. Andersen and J. Feder. Universitetsforlaget, Oslo 1971.

2. Y. Yamada, Y. Noda, J.D. Axe and G. Shirane, Phys. Rev. B9, 4429 (1974).

3. R.J. Elliott, R.T. Harley, W. Hayes, and S.R.P. Smith, Proc. R. Soc. A328, 217 (1972).

4. R.J. Birgeneau, J.K. Kjems, G. Shirane, and L.G. Van Uitert, Phys. Rev. B10, 2512 (1974).

5. G.A. Gehring and K.A. Gehring, Rep. Prog. Phys. 38, 1 (1975).

6. Peter Fulde in "Handbook on the Physics and Chemistry of the Rare Earths", Editors K.A. Gschneidner and Le Roy Eyring, to be published.

7. M.T. Hutchings, R. Scherm, and S.R.P. Smith, AIP Conference Proceeding No. 29, p. 372 (1975).

8. J.K. Kjems, W. Hayes, and S.H. Smith, Phys. Rev. Letters 35, 1089 (1975).

9. See for example W. Marshall and S.W. Lovesey "Theory of Thermal Neutron Scattering", Clarendon, Oxford (1971).

10. M.D. Sturge, E. Cohen, L.G. Van Uitert and R.P. van Stapele, Phys. Rev. B11, 4768 (1975).

11. R.J. Birgeneau, AIP Conf. Proc. 10, 1664 (1973).

12. P. Fulde and I. Peschel, Z. Phys. 241, 82 (1971) and Adv. Phys. 21, 1 (1972).

13. A.P. Young, J. Phys. C: Solid State Phys. 8, 3158 (1975).

14. W.J.L. Buyers, AIP Conf. Proc. 24, 27 (1975).

15. For recent reviews see Proceedings of the Second International Conference on "Crystal Field Effects in Metals and Alloys". Edited by A. Furrer, Plenum Press, New York (1977).

16. R.J. Elliott and K.W.H. Stevens, Proc. R. Soc. A218, 553 (1953).

17. K.B. Lyons, R.J. Birgeneau, E.I. Blount, and L.G. van Uitert, Phys. Rev. B11, 891 (1975).

18. M. Wun and N.E. Philips, Phys. Letters 50A, 195 (1974).

19. K. Andres et al., AIP Conf. Proc. 34, 222 (1976).

20. R.T. Harley, W. Hayes, A.M. Perry, and S.R.P. Smith, J. Phys. C6, 2382 (1973).

21. A. Segmüller, R.L. Melcher, H. Kind, Solid St. Comm. (1974).

22. R.T. Harley and R.M. Macfarlane, J. Phys. C8, L53? (1975).

23. R.A. Cowley, Phys. Rev. B13, 4877 (1976).

24. J. Als-Nielsen and R.J. Birgeneau, to be published in Am. Journ. of Phys.

25. V.L. Ginzburg, Soviet Phys. Sol. Stat. 2, 1824 (1960).

26. R.L. Melcher and B.A. Scott, Phys. Rev. Lett. 28, 607 (1972).

27. R.L. Melcher, E. Pytte, and B.A. Scott, Phys. Rev. Letters 31, 307 (1973).

28. J.R. Sandercock et al., J. Phys. C5, 3126 (1972).

29. P.A. Fleury, P.D. Lazay, and L.G. Van Uitert, Phys. Rev. Letters 33, 492 (1974).

30. A.H. Cooke, S.J. Swithenby, and M.R. Wells, Solid State Comm. 10, 265 (1972).

31. Volker Dohm, Z. Phys. B23, 153 (1976).

GAMMA-RAY DIFFRACTION STUDIES OF THE MOSAIC DISTRIBUTION IN TmAsO$_4$ NEAR THE COOPERATIVE JAHN-TELLER TRANSITION AT 6 K

K. Møllenbach and J.K. Kjems

Risø National Laboratory
DK-4000 Roskilde, Denmark

S. H. Smith

Clarendon Laboratory
Oxford University, England

ABSTRACT

The structural cooperative Jahn-Teller phase transformation in TmAsO$_4$ has been studied using gamma-ray diffraction. Precise measurements of the critical exponent, β, confirms the earlier reported classical value $\beta = 0.50 \pm .03$. Precurser effects in the mosaic structure of the sample are observed as T_D is approached from above.

The static and dynamic properties of the cooperative Jahn-Teller effect have been well characterized by the application of a variety of experimental methods to the rare earth insulators[1,2]. Recently a new high resolution gamma-diffraction technique has been developed[3] which allows for very accurate determination of the mosaic distribution of single crystals. In structural phase transitions where strain is an order-parameter one often finds twinning patterns which can be directly related to the magnitude of the strain and hence an accurate measurement of these patterns near T_D can yield the critical behaviour of the order-parameter. Here we report on

a study of the cooperative phase-transition in $TmAsO_4$
at T_D = 6 K using this technique. We find that the order-
parameter has a classical index β = 0.50 and maybe more
interestingly that there are clear precurser effects
observable in the mosaic distribution as T_D is ap-
proached from above.

   The experiment was done using a gamma-ray diffrac-
tometer similar to the one described by Schneider[3].
412 keV gamma-radiation from a 125 Ci Au-foil is colli-
mated in a single slit beam-defining system. The lower
limit to the angular width of the primary beam is 15
sec of arc. The instrument takes advantages of the typi-
cal small-angle scattering resolution function[4]: A re-
latively poor resolution along the momentum transfer
vector, κ, and an extreme narrow resolution perpendicu-
lar to κ. The high energy of the gamma-rays makes the
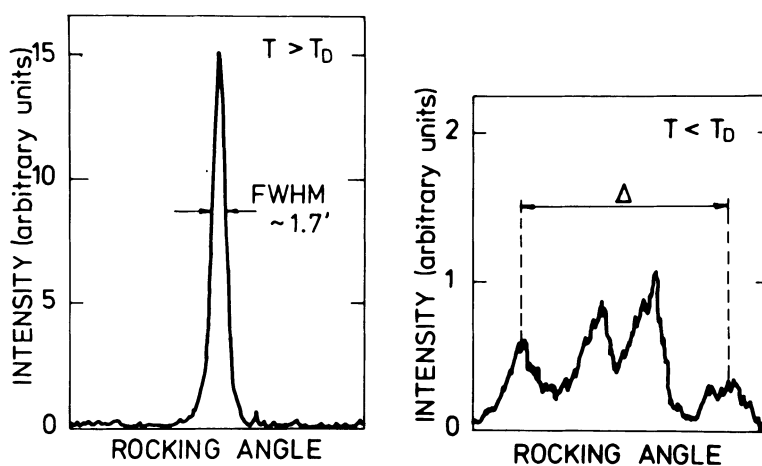
Fig. 1.
Examples of mosaic distributions of the (200) reflection
in $TmAsO_4$ above and below T_D. In the right hand side
figure T = 5.92 and Δ = .26°.

scattering probability per unit path length in the crys-
tal small giving a negligible secondary extinction and
a very small primary extinction. These characteristics
make this instrument well suited for a study of the
Jahn-Teller phase-transition. The $TmAsO_4$ sample in this
experiment had the size $1.5 \times 1.5 \times 10$ mm^3, and was
grown in the Clarendon Laboratory.

The phase-transition in $TmAsO_4$ is driven by the
coupling of the electronic E-doublet of the tetragonal
phase to the B_{2g} strain. As the orthorhombic distor-
tion proceeds a twinning pattern evolves which gives
rise to a splitting of the mosaic distribution of the
(200)-Bragg reflection. The splitting is proportional to
the B_{2g} strain[5]. Examples of mosaic distributions are
shown in fig. 1. In the right-hand-side picture the
method of measurement of the twinning angle is indicated.
The ideal twinning pattern consists of three equally
spaced peaks. The outer ones originate from domains with
(020) twinning planes and the centre peak from (200)
twinning planes. In our measurements the centre peak was
also split, probably due to external strains. In figure
2 we show the twinning angle as a function of tempera-
ture. These data together with neutron measurements show
that for $10^{-1} > 1-T/T_D > 5 \cdot 10^{-4}$ the twinning angle
follows the simple power law

$$\Delta \sim (1-T/T_D)^{0.50 \pm 0.03} , \quad T_D = 6.130 \text{ K}.$$

Changes in the crystal mosaic structure can be ob-
served above T_D both on cooling and heating of the
sample. One finds both a broadening of the rocking-
curve and a decrease in the peak intensity on approach-
ing T_D from above. This is shown in the right-hand-side
of figure 2. This phenomenon is consistent with neutron
scattering observations. The present measurements can-
not distinguish between the possible origins of the ob-
served changes in the mosaic structure above T_D. As T_D
is approached the elastic constant C_{44} tends to zero
and if the crystal has internal stresses it may relax in
the observed fashion. In a more speculative interpreta-
tion one could relate the relaxation to the fluctuations
of the quadrupole moments although at present we have no
evidence for any dynamical effects.
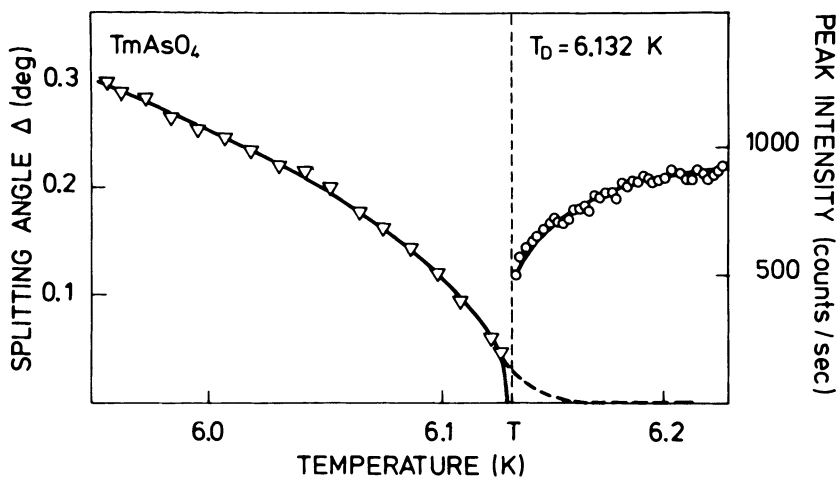
Fig. 2.
Left-hand-side: The splitting angle of the (200) mosaic
distribution as a function of temperature (∇). Right-
hand-side: The peak intensity of the (200) reflection
above T_D (O). The dashed line at the bottom indicates
the precurser changes in the observed width.

REFERENCES

1.   Kjems, J.K.: Lecture at this NATO ASI.
2.   Harley, R.T.: Lecture at this NATO ASI.
3.   Schneider, J., J. Appl. Cryst. 7, 541 (1974).
4.   can be deduced from:
     Bjerrum Møller, H. and Nielsen, M., Acta Cryst. A25,
     547 (1969).
5.   Birgeneau, R.J., Kjems, J.K., Shirane, G., and Van
     Uitert, L.G., Phys. Rev. B10, 2512 (1974).

THE CENTRAL PEAK IN TbVO$_4$

S.R.P. Smith* and M.T. Hutchings†

*Department of Physics, University of Essex
Colchester, Essex, U.K.
†Materials Physics Division
Harwell Didcot, Oxon., U.K.

A central peak (i.e. a low frequency anomaly) has been observed in neutron scattering experiments on TbVO$_4$ above the Jahn-Teller phase transition at T_D = 33 K (1). The measurements provide what is probably at present the most clearly understood example of a central peak occurring in a structural phase transition, though the frequency width has still to be measured directly.

The lowest levels of Tb^{3+} consist of two singlets separated by a splitting 2ε = .49 THz, with a degenerate doublet midway between them (2). The mode of distortion at the phase transition (B_{2g} at $\underline{q}$ = 0) has roughly equal matrix elements between the singlet levels and within the levels of the doublet. Thus, one expects an anomalous response near zero frequency in measurements which involve a coupling to the electronic doublet, and because this coupling is directly involved in the phase transition, one also expects to observe critical effects near T_D in such measurements. The central peak in the neutron scattering measurements is therefore an illustration of the anomalous low frequency response of the doublet, and this condition is similarly illustrated by elastic constant measurements of C_{66} (3), which show that at ultrasonic (10 MHz) frequencies, the elastic constant falls to zero at T_D, but remains finite in the Brillouin scattering ($\sim$ 10 GHz) measurements (2).

Fig. 1(a) shows how the central peak grows as T falls towards T_D, and also shows the softening of the acoustic phonon along $[010]$ and transversely polarized along $[100]$; more detailed scans of the central peak are given in Fig. 1(b). The width of the peak is determined by the instrumental resolution. The variation with temperature of the central peak intensity vs. q_y is shown in

Fig. 2(a) and at $T = T_D$ in Fig. 2(b). The measurements are restricted by Bragg contamination at low q_y, but demonstrate the type of divergence expected in the intensity as $T \to T_D$ and $\underline{q} \to 0$. The peak is strongly localised along the $[010]$ axis, with a width perpendicular to the axis of $\Delta q_x \sim .015$ r.l.u. at $T = T_D$, $\underline{Q} = (0, 1.95, 0)$.

The measurements have been analysed using the theoretical techniques of linear response function theory, as discussed by Stinchcombe (4). In the mean field approximation, one can write the single site susceptibility for Tb^{3+} (for $T > T_D$) as

$$\pi_s(\omega) = 4\varepsilon^2 g_1 / (4\varepsilon^2 - \omega^2) + \Gamma_2 g_2 / (\Gamma_2 - i\omega)$$

where g_1 and g_2 are the static susceptibilities of the singlets and the doublet respectively, and Γ_2 is the frequency width of the doublet response (~ 10 GHz). From this (using, for example, eqs. (38) and (46) of Stinchcombe's paper), one can write the coupled acoustic phonon response near the central peak $(\omega \ll \omega_q, \varepsilon)$ as

$$G_{aa}(\underline{q},\omega) = <<c_q^+ + c_{-q} ; c_q^+ + c_{-q} >> = \frac{2}{\omega_q} \frac{\Gamma_2 \left[1 - \mathcal{J}(\underline{q})(g_1 + g_2)\right] - i\omega \left[1 - \mathcal{J}(\underline{q}) g_1\right]}{\Gamma_2 \left[1 - J(\underline{q})(g_1 + g_2)\right] - i\omega \left[1 - J(\underline{q}) g_1\right]}$$

where $J(\underline{q})$ is the total Jahn-Teller coupling, and $\mathcal{J}(q) = J(\underline{q}) - K_a(\underline{q})$, where $K_a(\underline{q})$ is the coupling to the acoustic phonon branch. This result shows that the central peak has a width

$$\Gamma(\underline{q}) = \Gamma_2 \left[1 - J(\underline{q})(g_1 + g_2)\right] / \left[1 - J(\underline{q}) g_1\right]$$

which tends to zero as $q \to 0$ and $T \to T_D$, when $1 - J(0)(g_1 + g_2) = 0$. Unfortunately, the critical narrowing of the linewidth cannot be resolved because of the frequency resolution of the spectrometers (.012 THz for IN2 and .022 THz for IN3 at ILL, Grenoble), but the validity of the analysis has been checked by convoluting the theoretical expressions for the central peak response with the instrumental response, as shown by the solid curves in Fig.1(b), assuming that $J(q)$ has the form $J(\underline{q}) \sim J(0)(1 - \alpha q^2)$ for $\underline{q}$ along $[010]$. Further comparisons are given in ref. (1). The agreement between theory and experiment is satisfactory at each temperature; the details of the temperature dependence are qualitatively correct, though there are difficulties in obtaining quantitative agreement which may be partly due to the problems associated with the convolution procedure.

One concludes from this work that the mechanism for and description of the central peak in $TbVO_4$ are satisfactorily understood. One can expect this type of central peak in any phase transition in which the mode of distortion (the "soft mode") couples to a
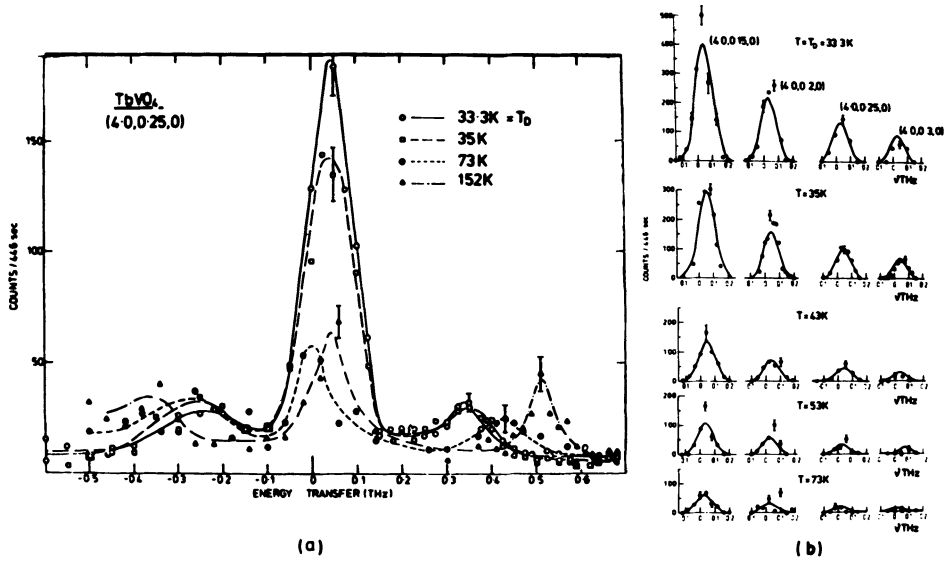
Fig. 1. (a) Neutron groups observed on IN3 scanning energy
            transfer at $\underline{Q}$ = (4.0, 0.25, 0).
        (b) Central peak scans (with background subtracted) at four
            values of $\underline{Q}$ and five temperatures. The solid lines are
            the results of convoluting the theoretical response
            with the instrumental resolution function (IN3).
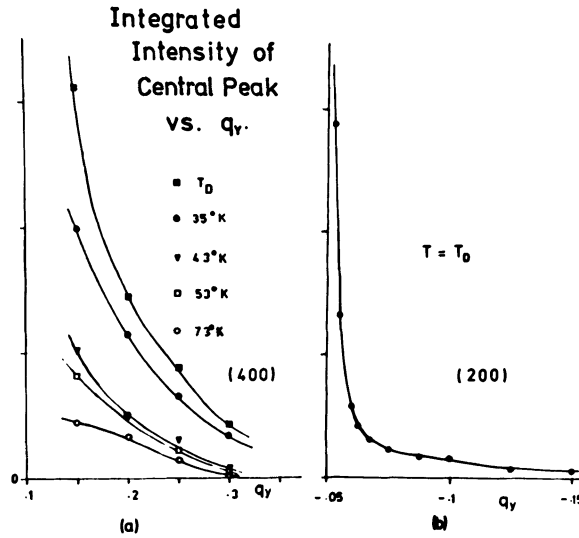
Fig. 2. (a) Central peak intensity vs. wavevector (4.0, q$_y$, 0) at
            various temperatures (IN3).
        (b) Central peak intensity vs. wavevector (2.0, q$_y$, 0) at
            T = T$_D$ at higher resolution (IN2).

degenerate electronic doublet (as is often illustrated, of course, in magnetic phase transitions). It is also significant that the localisation of the central peak response along <010> axes indicates that the effective exchange coupling J_{ii} is long range in {010} planes, which is consistent with the success of classical mean field theory in describing the behaviour of $TbVO_4$ (2).

References

1.   M.T. Hutchings, R. Scherm and S.R.P. Smith, "Magnetism and Magnetic Materials - 1975", ed. J.J. Becker, G.H.Lauder and J.J. Rhyne (A.I.P. Conf. Proc. No. 29; 1975) pp.372-8.

2.   See the article by R.T. Harley.

3.   J.R. Sandercock, S.B. Palmer, R.J. Elliott, W. Hayes, S.R.P. Smith and A.P. Young, J.Phys.C. <u>5</u>, 3126-46 (1972).

4.   See the article by R.B. Stinchcombe.

THE NATURE OF THE EIGENFUNCTIONS IN A STRONGLY COUPLED JAHN-TELLER

PROBLEM

Mary Jane Shultz

DEAP/Pierce Hall, Harvard University

Cambridge, Massachusetts 02138 U.S.A.

I. INTRODUCTION

In the lectures of Stinchcombe, Harley, Thomas, and Kjems we have heard about the role of the cooperative Jahn-Teller effect in driving a phase transition. These lectures have dealt primarily with doubly degenerate electronic states coupled to either nondegenerate or double degenerate vibrational modes. (For an introduction to the Jahn-Teller effect, see the lecture of Professor Thomas in this volume.) In this seminar we are interested in the nature of the wavefunctions for a single Jahn-Teller complex which exhibits strong coupling between a triply degenerate electronic state and a triply degenerate vibrational mode ($T \times \tau$). The nature of these wavefunctions is of interest because, as Professor Thomas said, "The excitations of the single Jahn-Teller complexes give rise to bands of collective modes, and an analysis of the collective modes requires a thorough understanding of the excitations of a single complex."

The purpose of this seminar is to give a physical understanding of what the eigenfunctions and distorted configurations look like, rather than to present a detailed calculation. Those readers who are interested in the details are referred to a recent paper by Shultz and Silbey[1]. The organization of this seminar is as follows. The next section describes the physical setting for the $T \times \tau$ Jahn-Teller problem; the third section describes the Hamiltonian and details the effect of the electron-phonon coupling on the electronic state; the fourth section describes the spectral calculation; and the last section presents the summary and conclusions.

331

II. THE PHYSICAL SETTING

We are interested in calculating the absorption spectrum for an S→P transition in octahedral symmetry. An example of this transition occurs in the alkali halide phosphors. These are simple cubic crystals like NaCl with a few of the Na^+ ions replaced by heavy metal impurities such as In^+ or Tl^+. Since the electron associated with these impurities is fairly well localized on the impurity center, we will employ the quasimolecular approximation. That is, we will assume that the electronic state is only affected by motion of the impurity and its six nearest halide neighbors. Due to the localization mentioned above, this is a fairly good approximation.

Since the P excited state is triply degenerate in octahedral symmetry, it will have a linear Jahn-Teller interaction with the vibrational modes of the ligands giving structure to the absorption spectrum. From group theory it is known[2] that the triply degenerate excited state will couple to the α_{1g}, ε_g, and τ_{2g} vibrational modes. However, since coupling to the α_{1g} and ε_g modes is trivial, we will treat coupling to the τ_{2g} vibrational modes only. These modes are shown in Fig.1a-c. Note particularly the combination mode $Q_4 + Q_5 + Q_6$. This combination corresponds to motion of the six halide ligands toward one of the cubic diagonals as shown in Fig.1d. In this configuration one expects that the electronic state $p_x + p_y + p_z$ will have a lower energy than the two orthogonal states, because an electron in this orbital will spend more time near the three halide ligands. In fact, it is a balance between this electronic energy lowering and the halide-halide repulsion which determines the minimum point of the adiabatic potential surface.

The details of the adiabatic potential surface are in fact fairly complicated[3,4]. However, the important features are the four minimum points in configuration space which are displaced from the origin in the directions I=(1,1,1), II=(-1,-1,1), III=(-1,1,-1) and IV=(1,-1,-1). These configurations correspond to distortions of the octahedron along one of the four cubic diagonals and are the four trigonal distortions referred to by Professor Thomas in his lecture. We shall refer to this surface again later when generating approximate eigenfunctions for the strong coupling case. First, however, we will present the Hamiltonian for the excited P state and indicate how the electron-phonon coupling affects the electronic state.

(a)   (b)   (c)   (d)
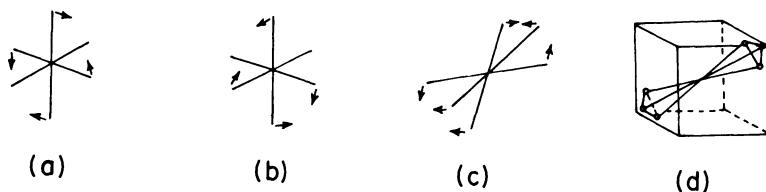
Fig. 1a-c: The τ_{2g} Normal Modes.   (a) Q_4 (b) Q_5 (c) $Q_4 + Q_5 + Q_6$.
Fig. 1d: Distorted Configuration for Large Finite k.

III. THE HAMILTONIAN

The Hamiltonian for the $T^{\times}\tau$ Jahn-Teller interaction has been derived using group theory by earlier authors[3] and is given in second quantized notation as $H = H_o + V$ where

$$H_o = (b_4^{\dagger}b_4 + b_5^{\dagger}b_5 + b_6^{\dagger}b_6 + 3/2)\underset{\approx}{1} \tag{1}$$

$$V = (k\omega/\sqrt{2})[(b_4 + b_4^{\dagger})\underset{\approx}{\tau}_1 + (b_5 + b_5^{\dagger})\underset{\approx}{\tau}_2 + (b_6 + b_6^{\dagger})\underset{\approx}{\tau}_3]$$

where

$$\underset{\approx}{1} = \begin{bmatrix} 1 & 0 & 0 \\ 0 & 1 & 0 \\ 0 & 0 & 1 \end{bmatrix}, \quad \underset{\approx}{\tau}_1 = \begin{bmatrix} 0 & 0 & 0 \\ 0 & 0 & 1 \\ 0 & 1 & 0 \end{bmatrix}, \quad \underset{\approx}{\tau}_2 = \begin{bmatrix} 0 & 0 & 1 \\ 0 & 0 & 0 \\ 1 & 0 & 0 \end{bmatrix}, \quad \underset{\approx}{\tau}_3 = \begin{bmatrix} 0 & 1 & 0 \\ 1 & 0 & 0 \\ 0 & 0 & 0 \end{bmatrix}.$$

In this notation, the operator b_j ($b_j^{\dagger}$) destroys (creates) a quantum of vibrational excitation in mode Q_j, k is a unitless coupling constant which represents the relative energy of interaction between the electronic and vibrational modes, and the matrices are written with respect to the electronic orbitals p_x, p_y, p_z. Since the matrices $\underset{\approx}{\tau}_1$, $\underset{\approx}{\tau}_2$, $\underset{\approx}{\tau}_3$ do not commute, this Hamiltonian entails a non-trivial coupling between the electronic and vibrational modes.

To appreciate the effect of this electron phonon coupling on the electronic state, it is useful to think in the terms of scattering theory. That is, if we put an electron in the p_x orbital at time zero and let the interaction V act repeatedly, what happens to the electron? The answer is shown schematically below

$$
\begin{array}{c}
\text{(2)}
\end{array}
$$

When V acts a single time, the electron is scattered from the p_x orbital into the p_y and p_z orbitals with a coefficient that depends on the value of the Q_5 and Q_6 vibrational modes. Similarly, when V acts again, the electron is scattered out of the orbital that it was in and into the remaining two. This coupling makes the problem difficult to solve when k is large, because then the eigenfunctions of H_o are not very close to eigenfunctions of H.

In the next section we will develop a canonical transformation which will generate a basis of approximate eigenfunctions. We will then use these eigenfunctions to calculate the absorption spectrum.

IV. ABSORPTION SPECTRUM

The absorption spectrum for a dipole allowed transition can be written in terms of the electronic autocorrelation function as [5]

$$I(\Omega) = 2 \text{ Re} \int_0^\infty dt \, \exp(i\Omega t) \sum_{i=1}^3 <C_i(t)C_i^\dagger> \qquad (3)$$

where $C_i(C_i^\dagger)$ destroys (creates) an electron in orbital i. Thus, we need to know the time evolution of the electronic operator C_i, or equivalently the time evolution of the electronic state. But remember that the time evolution is given by

$$C_i(t) = \exp(iHt) \, C_i \, \exp(-iHt). \qquad (4)$$

Thus, if the electronic orbitals were eigenfunctions of H, we would be finished. However, the electronic orbitals are not eigenfunctions of H. In fact, for the strongly coupled case, they are not even close. (This is a direct result of the breakdown of the Born Oppenheimer Approximation.) The idea for calculating the absorption spectrum, then, is to find a set of wavefunctions such that $H\Psi \simeq E\Psi$. These wavefunctions are then related to the electronic wavefunctions and the spectrum is calculated.

The approximate wavefunctions are generated by looking at the adiabatic potential surface. The important feature of the potential surface is that it has four minimum points which are displaced from the origin by an amount proportional to k and which are separated by barriers of height proportional to k^2. Thus, for infinite k, the molecule cannot get from one configuration to another. Therefore, we first solve for the wavefunction in each well independently.

We calculate the separate well wavefunctions in two steps. Firstly, we displace the origin of the vibrational coordinant system with a canonical transformation which is analogous to a phonon shift operator. Secondly, we make a transformation which accounts for the difference in potential felt by an electron localized between the halides and one localized in the perpendicular directions. The resulting first order wavefunctions localized in well I are

$$\psi_I^{inm\ell} = \exp(S)(\alpha_1)^n(\alpha_2)^m(\alpha_3)^\ell \bar{C}_i^\dagger |0>/(n!m!\ell!)^{\frac{1}{2}} \qquad (5)$$

where

$$S = -k\{(2/3)^{\frac{1}{2}}(\alpha_3 - \alpha_3^\dagger)\underset{\approx}{1} + (1/6)^{\frac{1}{2}}(\bar{C}_2^\dagger\bar{C}_2 + \bar{C}_3^\dagger\bar{C}_3)(\alpha_3 - \alpha_3^\dagger)$$

$$-(2)^{\frac{1}{2}}(\bar{C}_2^\dagger\bar{C}_2 - \bar{C}_3^\dagger\bar{C}_3)(\alpha_1 - \alpha_1^\dagger)\}$$

$$\bar{C}_1 = (3)^{-\frac{1}{2}}(C_1 + C_2 + C_3), \quad \bar{C}_2 = (2)^{-\frac{1}{2}}(C_1 - C_3),$$

$$\bar{C}_3 = (6)^{-\frac{1}{2}}(C_1 - 2C_2 + C_3), \quad \alpha_1 = (6)^{-\frac{1}{2}}(-b_4 + 2b_5 - b_6),$$

$$\alpha_2 = (2)^{-\frac{1}{2}}(-b_4 + b_5), \quad \alpha_3 = (3)^{-\frac{1}{2}}(b_4 + b_5 + b_6).$$

Here $|0\rangle$ is the electron-phonon vacuum state. Ignoring the exp(S) term, this wavefunction is merely a Born Oppenheimer product of an electronic state times a vibrational state. The exp(S) factor is the phonon dressing of the electronic state and is a direct result of the breakdown of the Born Oppenheimer Approximation.

Wavefunctions localized in the other wells are similarly calculated, and we have the following important results for the lowest energy set of wavefunctions. Firstly, the interwell overlap vanishes for large k

$$\lim_{k\to\infty} \left\langle \psi_J^{1nm\ell} | \psi_K^{1'n'm'\ell'} \right\rangle = 0 \qquad\qquad J\neq K \qquad\qquad (6)$$

Secondly, the interwell interaction energy decreases with k

$$\left\langle \psi_J^{1nm\ell} | H | \psi_K^{1'n'm'\ell'} \right\rangle \Big/ \left\langle \psi_J^{1nm\ell} | \psi_K^{1'n'm'\ell'} \right\rangle \propto k^2 \exp(-8k^2/9) \quad J\neq K \quad (7)$$

Finally, the second order wavefunctions are nearly eigenfunctions for large k

$$\lim_{k\to\infty} \left\langle \psi_J^{1nm\ell} | H - E_{exact} | \psi_J^{1nm\ell} \right\rangle \Big/ \left\langle \psi_J^{1nm\ell} | \psi_J^{1nm\ell} \right\rangle << \omega \ . \qquad (8)$$

where E_{exact} is the known asymptotic energy. These results indicate that in the limit of strong electron phonon coupling, our separated well model is a good one.

The final step is to recover the full octahedral symmetry of the original problem by forming appropriate (un-normalized) functions which transform as irreducible representations of the octahedral group by combining states of the four wells. For example, for the lowest A_2 and T_1 states, we have

$$\Phi_{T_1} = \frac{1}{2} \begin{Bmatrix} \psi_I + \psi_{II} - \psi_{III} - \psi_{IV} \\ \psi_I - \psi_{II} + \psi_{III} - \psi_{IV} \\ \psi_I - \psi_{II} - \psi_{III} + \psi_{IV} \end{Bmatrix}$$

$$\Phi_{A_2} = \frac{1}{2} (\psi_I + \psi_{II} + \psi_{III} + \psi_{IV}) \qquad\qquad (9)$$

Using these wavefunctions, we calculate the matrix elements of the total Hamiltonian to second order and find a singlet triplet splitting of [6]

$$E_{A_2} - E_{T_1} = (272/243) \ k^2 \ \omega \ \exp(-8k^2/9) \qquad\qquad (10)$$

Note that due to the octahedral symmetry of the original problem, the lowest state remains a triplet independent of k. The above result (valid asymptotically for $k\to\infty$) is in good agreement with the result $0.8 \ k^2\omega \ \exp(-0.8k^2)$ given by Caner and Englman [7] as a reasonable fit of their numerical data for $k\simeq 2.5$.
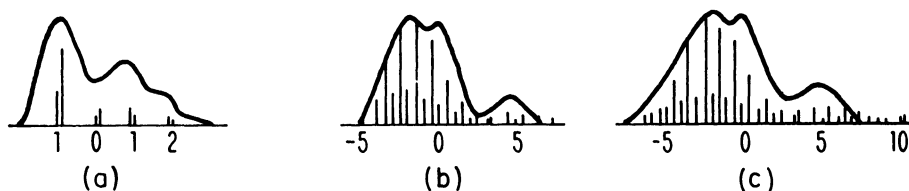
Fig. 2: Absorption Spectra. Solid lines are numerical results of Englman et al.[8], bar spectra are this calculation. Energy is in units of ω. (a) k=1, $k_B T$=0; (b) k=2.3, $k_B T$=0; (c) k=2.3, $k_B T$=0.5.

Finally, we use the above wavefunctions to calculate the absorbtion spectrum and find the spectra shown in Fig.2. (For details of the spectral calculation, see[1].) Fig.2 compares our spectra with the exact numerical spectra of Englman et al.[8] and we find good agreement even for fairly small k. Further, the analytical formula has the advantage of being valid for larger values of k.

V.   SUMMARY AND CONCLUSIONS

In this work we have used a canonical transformation technique to generate approximate eigenfunctions for a strong coupling problem. This transformation can be viewed as replacing the description of the motion of the strongly coupled individual electrons and nuclei by a description in terms of weakly interacting collective modes. After transformation, the interaction parameter is $k^2 \exp(-k^2)$; therefore, even for large k, the perturbation is small.

Using the transformed Hamiltonian, we have derived analytic expressions for the asymptotic eigenvalues and for the spectral density. In both cases we find good agreement with earlier numerical results [7,8].

REFERENCES

1. Shultz, M.J. and Silbey, R. (1976). *J. Chem. Phys.* <u>65</u>, 4382.
2. Toyozawa, Y. and Inoue, M. (1966). *J. Phys. Soc. Japan* <u>21</u>, 1663.
3. Van Vleck, J.H. (1939). *J. Chem. Phys.* <u>7</u>, 72.
4. Opik, U. and Pryce, M.H.L. (1957). *Proc. Roy. Soc. London* <u>238A</u>, 425.
5. See eg. Gordon, R.G. (1967). In *Advances in Magnetic Resonance*, Vol. 3 (ed. Waugh, J.S.).
6. Shultz, M.J. and Silbey, R. (1974). *J. Phys. C* <u>7</u>, L325.
7. Caner, M. and Englman, R. (1966). *J. Chem. Phys.* <u>44</u>, 4054.
8. Englman, R.; Caner, M.; and Toaff, S. (1970). *J. Phys. Soc. Japan* <u>29</u>, 306.

COOPERATIVE PSEUDO JAHN TELLER MODEL OF THE SEQUENCE OF FERRO-

ELASTIC TRANSITIONS IN BARIUM SODIUM NIOBATE

D. Paquet

Centre National d'Etudes des Télécommunications

196 rue de Paris, 92220 Bagneux (France)

Barium sodium niobate ($Ba_2NaNb_5O_{15}$ or BSN) has recently been shown (1) to posses four phases, whose labelling, temperature stability range and most probable space symmetries are listed in Table I. In this paper we will point attention only on the three lower temperature polar phases. The room temperature one is a ferroelastic orthorhombic mm2 phase sandwiched between two tetragonal phases of same point symmetry 4mm which, moreover, are expected to belong to the same space symmetry.

Fig. 1 shows the temperature behaviour of the birefringence Δn_{ab} and the spontaneous strain e_6 obtained from the work of Schneck et al. (1). The two phase transitions display first order (hysteresis) and diffused characters. The diffuseness has been attributed (2) to the local disorder of the cations in the structure.

The high temperature phase transition has been studied by Brillouin scattering (3). The difference between elastic constants $(C_{11}-C_{22})$ associated to the onset of the spontaneous strain e_6 does not go monotonically to zero on heating the crystal to the transition temperature (Fig. 2). Tolédano (4) has shown that this anomalous behaviour is due to the fact that the phase transition is of the improper type : the order parameter is not the spontaneous strain, but a physical quantity transforming as an irreducible representation of the paraelastic space group situated at the Z point of the Brillouin zone boundary of the P4bm space group. The phase transition is thus associated to a breakdown of the translational symmetry corresponding to a doubling of the unit cell along the polar c-axis. This prediction has been checked using X-ray diffraction (5) : the intensity of the superstructure line vanishes

Phase labelling	Temperature range	Space group
I	T > 858 K	P4/mbm
II	858 K > T > 573 K	P4bm
III	573 K > T > 105 K	Ccm2$_1$
IV	T < 105 K	P4bm

Table I - Different stable phases of BSN
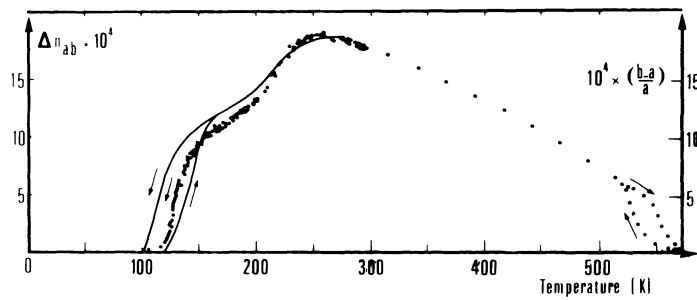
Fig. 1 - Temperature dependence of the birefringence Δn_{ab} in the (001) plane (dotted line) and of the spontaneous strain (b-a)/a (solid line). (From Ref. 1).
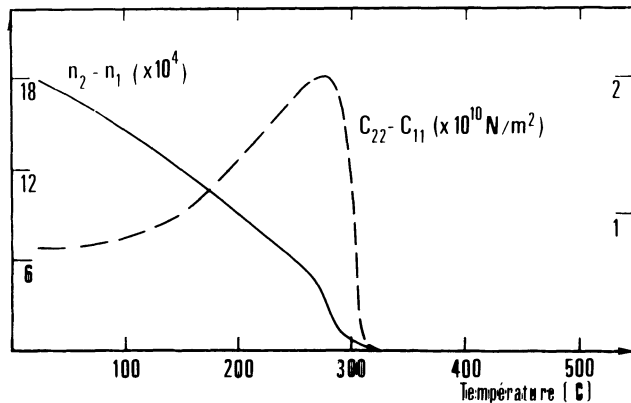
Fig. 2 - Compared variations of the optical and elastic anisotropies in the (001) plane. Both should decrease in a proper ferroelastic. They show opposite variations in the improper ferroelastic transition of BSN . (From Ref. 2).

at 573 K, and exhibits also a spread of the transition temperature.

The low temperature ferroelastic phase transition has been recently discovered by Schneck et al.(1). Birefringence and pyroelectric measurements show that below 105 K the crystal recovers a tetragonal symmetry and remains polar. X-ray print indicates that it belongs to the 4/mmm Laue class. Its point symmetry is thus 4mm, as confirmed by nonlinear optics experiments. Assuming that Landau theory can be used to describe this phase transition, the space group of the low temperature phase must be a supergroup of the ferroelastic phase one. Every supergroup of $Ccm2_1$ corresponding to the 4mm point symmetry is associated to an increase of the translational symmetry, and among those satisfying the Landau-Lifschitz criteria, the only one compatible with a continuous change in the positions of the various atoms is P4bm. The two ferroelastic phase transitions thus appear as completely symmetrical, the two extreme phases (II and IV) being identical.

This sequence of two inverse ferroelastic phase transitions is puzzling because, while entropy is expected to be an increasing function of temperature, the "configurational" entropy decreases with increasing temperature at the low temperature phase transition. Hence in phase IV, an "internal" degree of freedom, different from atomic vibrations, should order to compensate the excess of configurational entropy. We assume that this internal degree of freedom is of electronic nature. A careful analysis of the tungsten bronze structure of BSN (6) (Fig. 3) actually shows that the onset of the spontaneous strain corresponds to tilts of the oxygen octahedra surrounding the niobium atoms. Though all the octahedra in the tetragonal unit cell are non equivalent, they all undergo the same distortion (a Γ_4^+ rotation and a Γ_5^+ shear), and the cooperative onset of these octahedral distortions builds up a bidimensional crystal normal mode possessing the same symmetry properties as the abstract order parameter deduced from the phenomenological theory. We thus believe that the ferroelastic transitions are driven by the cooperative tilt of the oxygen octahedra induced by a Jahn-Teller interaction between the octahedral vibrations and some d-electrons localized on the niobium ions (7).

If one accepts that BSN is a pure ionic compound, then one finds that the d states of the Nb^{5+} ion are empty. However several experimental and theoretical data show that, in oxygen octahedra ferroelectrics, the effective charge of the transition metal ion is substantially reduced from its formal value. Infrared absorption in $LiNbO_3$ (8), where the oxygen octahedra have exactly the same dimensions as in BSN, leads to an effective charge of +3.2. Some $SrTiO_3$ (9) band calculations assume highly correlated electrons in the same octahedral unit. We thus built up an effective hamiltonian for the
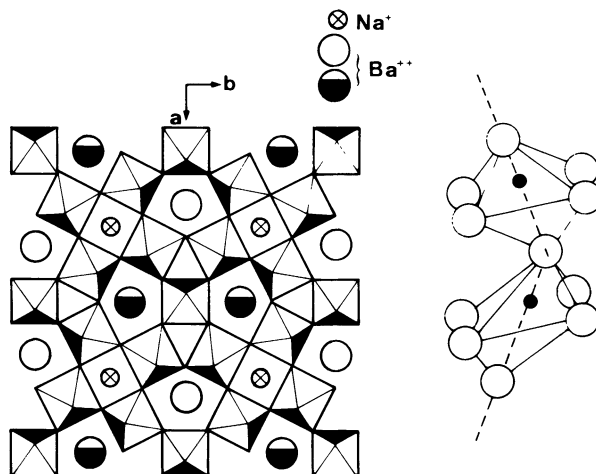
Fig. 3 - Schematic representation of the distorted tungsten bronze structure of BSN at room temperature. Left : half unit cell. In the consecutive half cell along |001|, the tilt of the octahedra and the positions os the shaded barium atoms are inverted. Right : two consecutive octahedra along the |001| axis. The c-parameter corresponds to two octahedra heights.
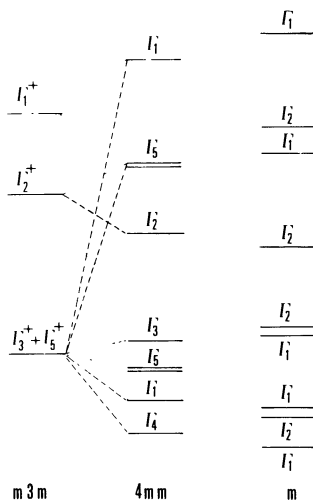
Fig. 4 - Splitting of the electronic energy levels of the Nb^{3+} ion in phases I (site symmetry m3m), II and IV (site symmetry 4mm) and III (site symmetry m).

octahedral units whose levels exhibit the same symmetry properties
as those of two correlated d electrons in the crystal field at the
niobium site. We found a nine-dimension manyfold, as sketched in
Fig. 4, described by the local hamiltonian :

$$H = \zeta \, h_{so} + d \, h_p + a \, (\sigma_1 \, q_1 + \sigma_2 \, q_2)$$

where h_{so}, h_p, σ_1, σ_2 are electronic operators corresponding respec-
tively to the spin orbit interaction, the tetragonal part of the
crystal field induced by the spontaneous polarization of the crystal,
and the coupling to the bidimensional (q_1, q_2) octahedral distortion.
ζ, d and a are constants measuring the strength of these interac-
tions. It must be outlined that, in the paraelastic phases, where
the Nb site symmetry is 4mm, the ground state is a singlet, due to
the tetragonal components of the crystal field induced by the
spontaneous polarization.

The hamiltonian of the whole crystal becomes :

$$H = \sum_{j=1,2} \{ \frac{1}{2M} \, P_j(\vec{k}) \, P_j^*(\vec{k}) + \frac{M\omega^2}{2} \, Q_j(\vec{k}) \, Q_j^*(\vec{k}) \}$$

$$+ \frac{1}{2} \, V \, C_{66} \, e_6^2$$

$$+ g \, e_6 \{ Q_1(\vec{k}) \, Q_1^*(\vec{k}) - Q_2(\vec{k}) \, Q_2^*(\vec{k}) \}$$

$$+ \sum_{\ell,\alpha} \{ \zeta \, h_{so}(\ell,\alpha) + d \, h_p(\ell,\alpha) + a \sum_{j=1,2} \sigma_j(\ell,\alpha) \, q_j(\ell,\alpha) \}$$

The first term corresponds to the energy of the bidimensional crys-
tal normal mode, the second one to the elastic energy associated
with the spontaneous strain e_6, the third one to the coupling
between the spontaneous strain and the normal mode, the last one to
the sum over each individual octahedral unit (ℓ,α) of the local
hamiltonians. This total hamiltonian, though more complicated, is
very similar to the one discussed by Stinchcomb in his lecture.
Using the same technics (displaced operators, neglect of the self
energy and of the non commutation of the σ_j with h_{so} and h_p, mean
field approximation), we obtain the single site hamiltonian :

$$h_m = \zeta \, h_{so} + d \, h_p - b_o < \sigma > \sigma$$

with $b_o = n_o a / M\omega^2$, n_o being the number of Jahn Teller active ions
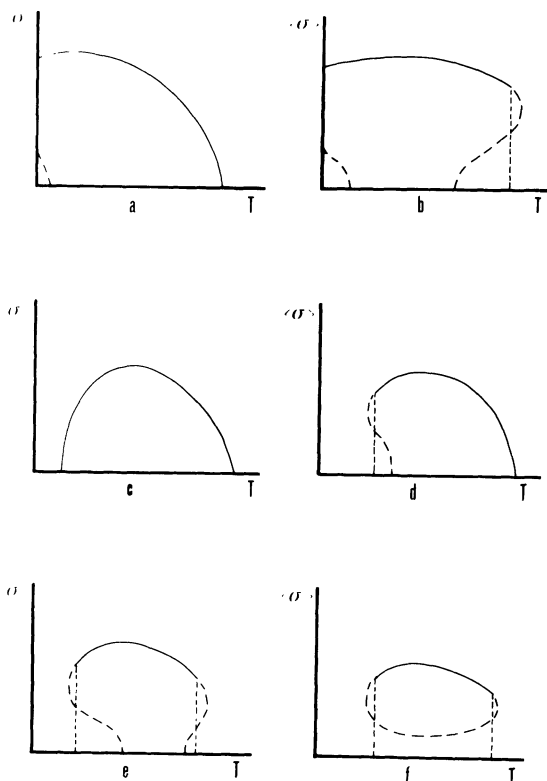
Fig. 5 - Different behaviours of the order parameter < σ > versus
temperature, depending on the relative values of ζ, d, b_o. The
experimental behaviour of BSN corresponds to case e.

in the tetragonal unit cell. The individual octahedral distortions
and the spontaneous strain are then given by :

$$q(\ell,\alpha) = -\frac{b_o}{a} < \sigma > \cos (\vec{k}.\vec{h}_\ell)$$

$$e_6 = \frac{3gb_o}{C_{66} \, v \, M\omega^2} < \sigma >^2$$

The mean field self consistency equation has been solved in a com-
puter, and a phase diagram has been drawn. Six different behaviours
have been found (Fig. 5) depending on the relative values of ζ , d,
b_o : zero, one, or two phase transitions, of first or second order

type. The three coefficients have been fitted, with physical mean-
ingful values, to describe the two first order ferroelastic phase
transitions occuring in BSN.

   The model predicts that an electric field applied along the
polar axis would change the strength of the tetragonal component
of the crystal field (d) and thus change the transition temperatu-
res (Fig. 6). A similar effect, due to the change of the b_0 coef-
ficient by substitution of the Nb atoms by non Jahn-Teller active
ions, must occur (Fig. 7). These experiments will be performed to
test the model.

   As a conclusion we shall emphasize that the occurence of the
low temperature phase transition strongly depends on the polarity
of the crystal : the tetragonal crystal field splits the five fold
degenerate cubic ground state ; the latter becomes a singlet. The
electron-vibration coupling thus occurs through pseudo Jahn-Teller
effect. At very low temperature the ground state alone is occupied
which does not induce any distorsion. However, as this state is a
singlet, the electronic entropy vanishes, and the system "stores"
the order. At higher temperatures, higher states are occupied, and
the cooperative onset of the octahedral distortions occurs through
pseudo Jahn-Teller coupling. Then at much higher temperatures, the
increase of the electronic entropy overcomes the decrease in ener-
gy, which leads to a minimum of the free energy for zero distor-
tion. This process is quite similar to the one discussed by R.T.
Harley for $Tb_p Gd_{1-p} VO_4$ in his lecture.
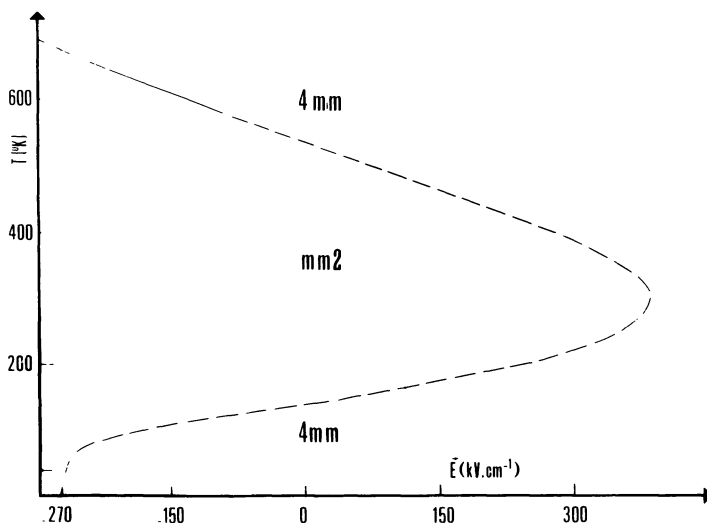
Fig. 6 - Ferroelastic transition temperatures vs applied electric
field along |001|. Dashed line : first order phase transition ;
solid line : second order phase transition.
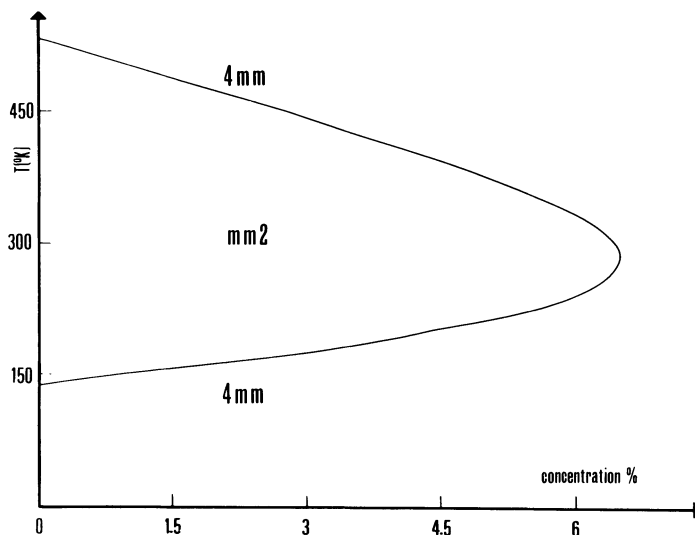
Fig. 7 - Ferroelastic transition temperatures vs concentration of Jahn-Teller inactive impurities substituted to the niobium atoms.

References

1. J. Schneck, J. Primot, R. Von der Mühl, and J. Ravez, Sol. State Commun. 21, 57 (1977)
2. J.C. Tolédano and J. Schneck, Sol. State Commun. 16, 1101 (1975)
3. J.C. Tolédano, M. Busch and J. Schneck, Ferroelectrics 13, 328 (1976)
4. J.C. Tolédano, Phys. Rev. B12, 943 (1975)
5. J. Burgeat and J.C. Tolédano, Sol. State Commun., 20, 281 (1976
6. P.B. Jamieson, S.C. Abrahams, and J.L. Bernstein, J. Chem. Phys. 50, 4352 (1969)
7. D. Paquet, J. Chem. Phys., 66, 886 (1977)
8. F. Gervais, Sol. State Commun. 18, 191 (1976)
9. T.F. Soules, E.J. Kelly, D.M. Vaught, J.W. Richardson, Phys. Rev. B6, 1519 (1972)

SINGLE ION AND COOPERATIVE JAHN-TELLER EFFECT

FOR A NEARLY DEGENERATE E DOUBLET

L.F. Feiner

Philips Research Laboratories

Eindhoven, The Netherlands

ABSTRACT

Single ion behaviour in $Fe:CoCr_2S_4$ and cooperative behaviour in $FeCr_2S_4$ of Fe^{2+} are treated within a model where this Jahn-Teller (JT) ion interacts with local displacements and which takes full account of the spin-orbit splitting of the electronic ground doublet. Calculated static properties are compared with experiment. The discussion includes qualitative effects due to the splitting of the ground doublet and the problem as to what extent the strengths of spin-orbit coupling, single ion JT coupling, and interaction between JT complexes can be estimated separately.

1. PHYSICAL SYSTEM AND MODEL

Experimental information is available on two very similar compounds, one $(Fe:CoCr_2S_4)$ where Fe^{2+} acts as an isolated Jahn Teller (JT) impurity, and the other one $(FeCr_2S_4)$ where the Fe^{2+} ions interact and take part in a cooperative JT effect [1]. I wish to investigate whether it is possible to describe both single ion and cooperative behaviour with one coherent model.

Both materials have the normal spinel structure with Fe^{2+} at the purely cubic tetrahedral site, at the center of a tetrahedron of S^{2-} ions. We notice that each S^{2-} is ligand to at most one Fe^{2+}, and that in $FeCr_2S_4$ the Fe^{2+} ions build up a diamond lattice, which consists of two interlacing Bravais lattices. Below 175 K the compounds are magnetically ordered and each Fe^{2+} experiences a magnetic exchange field H_{ex} from the Cr^{3+} ions, which is directed along one of the cubic axes. Consequently [2], the cubic crystal

field splits the ^5D free ion groundstate of Fe^{2+} into a higher $^5T_2$ and a lower ^5E multiplet, separated by about 3500 K, while the spin degeneracy is removed by H_{ex}, which splits the magnetic sub-levels by about 300 K. Second order spin-orbit interaction between E and T_2 states finally separates the components of the electronic grounddoublet by 2 δ_{LS}, which is about 50 K.

The experimental information consists of (i) ^{57}Fe Mössbauer measurements, which, when analyzed on the basis of the usual spin Hamiltonian, yield the magnetic hyperfine field H_{hf} and the com-ponents of the electric field gradient (EFG) V_{xx}, V_{yy} and V_{zz} at the Fe nucleus [1], (ii) specific heat measurements on $FeCr_2S_4$ [3].

To describe the local static properties of the Fe^{2+} ion at low temperatures I assume (i) that it is sufficient to take into account only the JT active nearly degenerate E grounddoublet, and (ii) that the (cubic invariant) interaction of the JT ion is only with the E-type vibrations of the ion's own S^{2-} tetrahedron. This gives the following Hamiltonian for a <u>single Fe^{2+} ion</u> in $Fe:CoCr_2S_4$:

$$\mathcal{H}_{single} = \hbar\omega \left[\tfrac{1}{2}\left(p_\theta^2 + p_\varepsilon^2 + q_\theta^2 + q_\varepsilon^2\right) \right.$$
$$\left. + k\left(q_\theta\,\sigma_\theta + q_\varepsilon\,\sigma_\varepsilon\right) - \delta\,\sigma_\theta \right], \qquad (1)$$

where σ_θ and σ_ε are the usual pseudo spin operators, i.e. Pauli matrices $-\sigma^z$ and σ^x acting on the electronic states E_θ and E_ε [4], $\hbar\omega$ is the vibrational energy quantum, and k and $\delta = \delta_{LS}/\hbar\omega$ are dimen-sionless parameters characterizing the strength of the JT coupling and the spin-orbit splitting, respectively. In the present case of E states in tetrahedral coordination where the JT coupling is only weak or intermediate, it is important to include the spin-orbit splitting right from the beginning.

To treat the <u>interacting Fe^{2+} ions</u> in $FeCr_2S_4$ I assume that the $[Fe^{2+}S^{2-}_4]$ complexes (i) are described each by the same Hamiltonian as in the single ion case, and (ii) are now coupled by lattice dynamical forces between the displacements of S^{2-} ions in complexes that are nearest neighbour to each other. In order to have cubic invariance (apart from the spin-orbit term) the total Hamiltonian is then

$$\mathcal{H} = \sum_i \left(\mathcal{H}_{single}\right)_i + \tfrac{1}{2}\hbar\omega \sum_{n.n.} \lambda \left(q_{\theta i}\,q_{\theta j} + q_{\varepsilon i}\,q_{\varepsilon j}\right) , \qquad (2)$$

where λ is a dimensionless force constant characterizing the strength of the interaction between complexes.

Crystal field theory [5] yields $H_{hf} = A - B\langle\sigma_\theta\rangle$, $V_{zz} = C\langle\sigma_\theta\rangle$, $\left(V_{xx} - V_{yy}\right)/\sqrt{3} = C\langle\sigma_\varepsilon\rangle$, where A, B and C are constants. Therefore the task is to calculate the thermal averages of the electronic pseudo spin operators.

2. CALCULATIONS, RESULTS AND DISCUSSION

For the <u>single ion</u> case I have performed numerical diagonalizations of Hamiltonian (1) using the familiar basis of electronic-vibrational product states [4]. For $k \lesssim 1.5$ and $\delta \lesssim 0.3$ inclusion of states with up to 7 vibrational quanta was sufficient to obtain an accuracy better than 0.5% in the thermal averages.

The low temperature behaviour can be understood qualitatively by looking at the lowest two levels. Consider the JT interaction first. It changes the exactly degenerate electronic states E_θ and E_ε into degenerate vibronic states Ψ_θ and Ψ_ε, thereby reducing the magnitude of the pseudo spin operators by the Ham factor q. Secondly, the spin-orbit splitting splits the states but also changes their wavefunctions by mixing the vibronic state Ψ_θ (Ψ_ε) with higher lying states of A_1 (A_2) symmetry. It thereby shifts the values of σ_θ in the two states by the same amount, b. For $k_B T/\hbar\omega \lesssim 0.3$ we find, with an accuracy of a few percent,

$$\langle \sigma_\theta \rangle = b + q \tanh \left(\Delta/k_B T \right), \qquad (3)$$

where $\Delta/\hbar\omega \simeq q \cdot \delta$ is half the splitting, and $b \approx b_1(k) \cdot \delta$, while $\langle \sigma_\varepsilon \rangle = 0$ by symmetry. The result (3) is, due to the constant b, qualitatively different from the result of static crystal field theory. Quantitatively, b can become about one third of q for $k \lesssim 1$ and $\delta \lesssim 0.2$.

For the case of <u>interacting ions</u> I have performed a molecular field calculation assuming (i) that the coupling is antiferrodistortive, i.e. $\lambda > 0$, and (ii) that ordering takes place in two sublattices. For a JT complex, say in sublattice 1, feeling the average displacements of its neighbours in sublattice 2, one gets a molecular field Hamiltonian

$$\mathcal{H}_1^{mf} = \hbar\omega \left[\tfrac{1}{2} \left(p_{\theta 1}^2 + p_{\varepsilon 1}^2 + \hat{q}_{\theta 1}^2 + \hat{q}_{\varepsilon 1}^2 \right) \right.$$
$$+ k \left(\hat{q}_{\theta 1} \sigma_{\theta 1} + \hat{q}_{\varepsilon 1} \sigma_{\varepsilon 1} \right) - \delta \sigma_{\theta 1}$$
$$+ g \left(\langle \sigma_{\theta 2} \rangle \sigma_{\theta 1} + \langle \sigma_{\varepsilon 2} \rangle \sigma_{\varepsilon 1} \right)$$
$$\left. - z\lambda g \left(\langle \sigma_{\theta 1} \rangle \sigma_{\theta 1} + \langle \sigma_{\varepsilon 1} \rangle \sigma_{\varepsilon 1} \right), \qquad (4) \right.$$

where $g = z\lambda k^2/(1-(z\lambda)^2)$, z (=4) is the number of nearest neighbours, and the carets indicate displaced coordinates. The fourth term in Eq. (4) represents antiferrodistortive coupling of the XY type between the pseudo spins on the two sublattices, the fifth term additional ferrodistortive intrasublattice coupling, while the spin-orbit splitting acts as an external field in the XY plane. In contrast with the usual treatment [6] involving displaced phonons and retaining only the resulting coupling between the pseudo spins, I have taken the JT

interaction into account, in the same way as in the single ion case. This inclusion of local dynamics makes the details of the temperature dependence different from those of the analogous magnetic system. The qualitative features, though, are the same. At high temperatures, we have a paradistortive phase where the averaged sublattice pseudo spin vectors $\langle\vec{\sigma}\rangle_{1,2}$ are equal and along the θ direction preferred by the field δ. Upon lowering the temperature $\langle\sigma_\theta\rangle$ increases until at a temperature T_D it reaches the value $\delta/2g$. Here a second order phase transition occurs after which $\langle\sigma_\theta\rangle$ remains constant, while ε components of $\langle\vec{\sigma}\rangle_i$ now develop, of equal magnitude but opposite direction on the two sublattices.

The accuracy of the experimental data is not sufficient to determine the parameters uniquely. A typical example of a fit is given in Fig. 1 for the electric field gradient and in Fig. 2 for the hyperfine field. Here, first the model parameters k, δ and $\hbar\omega$ and the constant C have been chosen such as to reproduce the single ion EFG data, and then the parameter $z\lambda$ has been determined from the value of
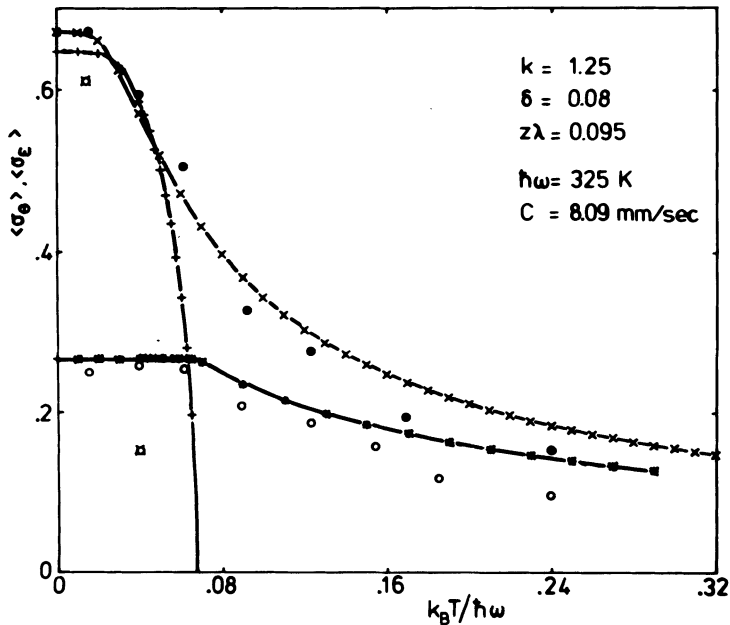
Fig. 1: Calculated (curves) thermal averages of the pseudo spin operators and measured (dots, circles) electric field gradient as a function of temperature. Single ion: $\langle\sigma_\theta\rangle\equiv$ —x—, $\bullet$ (Fe:CoCr$_2$S$_4$); interacting ions: $\langle\sigma_\theta\rangle\equiv$ —*—, $\circ$(FeCr$_2$S$_4$); $\langle\sigma_\varepsilon\rangle\equiv$ —+— , $\square$(FeCr$_2$S$_4$).

V_{zz} in $FeCr_2S_4$ at T = 0. The constants A and B have been fixed from the T = 0 values of H_{hf} in the two compounds. The data allow the range $0.75 \leqslant k \leqslant 1.25$, $0.06 \leqslant \delta \leqslant 0.10$. The corresponding value for $\hbar\omega$ varies between 225 K and 450 K, but δ_{LS} is always between 22 K and 28 K. Both results can be compared with experiments for similar compounds: from optical absorption measurements [7] $\delta_{LS} \simeq 28$ K, from an analysis of Raman and infrared data [8] $\hbar\omega$ is estimated to be of the order of 300 K. In addition, the values obtained for A (258 kG), B (280 kG) and C (8.09 mm/s) are in satisfactory agreement with crystal field calculations [5] without the need to invoke strong covalency.

The calculated temperature dependence of $\langle\sigma_\theta\rangle$ and $\langle\sigma_\epsilon\rangle$ shows qualitative agreement with the EFG data on $FeCr_2S_4$. The lower values and weaker temperature dependence of V_{zz} in $FeCr_2S_4$ compared with $Fe:CoCr_2S_4$ are explained as consequences of the cooperative effect. The calculated value of $V_{xx} - V_{yy}$ at 4 K agrees quantitatively. In fact the model explains, why at low T the EFG has axial symmetry in $Fe:CoCr_2S_4$ and not in $FeCr_2S_4$. It also explains that at low T the hyperfine field decreases strongly in $Fe:CoCr_2S_4$ (where the agreement is quantitative), but not in $FeCr_2S_4$.
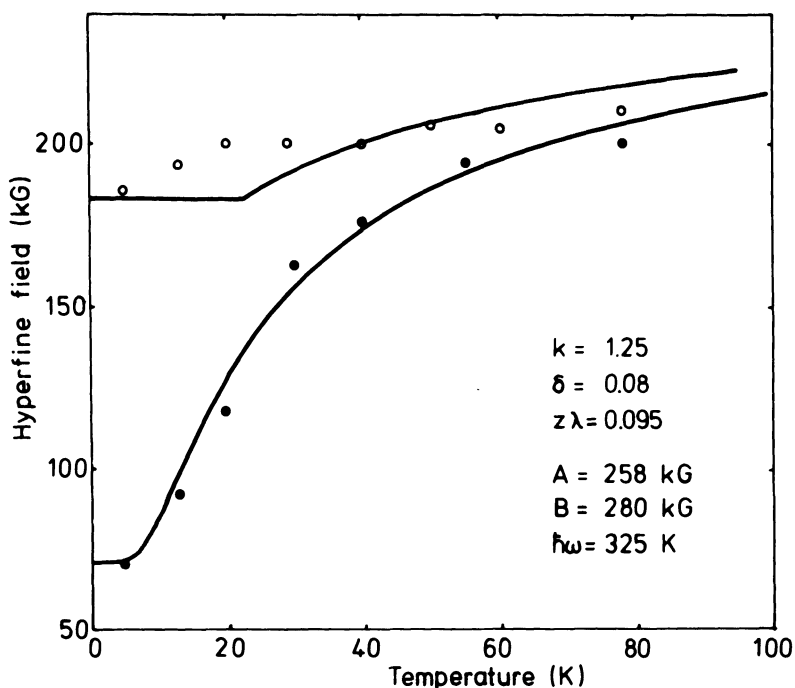
Fig. 2: Calculated (curves) and measured (dots, circles) hyperfine field as a function of temperature; $\bullet \equiv Fe:CoCr_2S_4$, $\circ \equiv FeCr_2S_4$.

On the other hand, the calculated transition temperature is much higher than the experimental value 9.25 K, obtained in specific heat measurements [3]. For the parameters used in the figures one calculates 22 K, and this is the main cause for the quantitative disagreement in the EFG above the transition. The discrepancy is partly due to the use of the molecular field approximation in a situation where the interaction is assumed to be of short range. But even multiplication with a correction factor appropriate for an XY model with four neighbours yields 13.5 K.

3. CONCLUSIONS

The local dynamics associated with a purely electronic splitting in a JT system can have a qualitative effect even on static properties. If one tries to get quantitative information about the parameters describing such a system, it may be dangerous to neglect this dynamics.

The single JT ion system $Fe:CoCr_2S_4$ and the interacting JT ions system $FeCr_2S_4$ can be reasonably well described within one model with quite satisfactory values of the parameters. However, as to the determination of these parameters separately, the spin-orbit splitting is well determined, whereas the other parameters have a rather large range of possible values.

REFERENCES

1. A.M. van Diepen and R.P. van Stapele, Solid State Comm. 13, 1651 (1973).
2. B. Hoekstra, R.P. van Stapele, and A.B. Voermans, Phys. Rev. B6, 2762 (1972).
3. F.K. Lotgering, A.M. van Diepen and J.F. Olijhoek, Solid State Comm. 17, 1149 (1975).
4. R. Englman, 'The Jahn-Teller Effect in Molecules and Crystals' (Wiley, London, 1972).
5. A.M. van Diepen and R.P. van Stapele, Phys. Rev. B5, 2462 (1972).
6. G.A. Gehring and K.A. Gehring, Rep. Progr. Phys. 38, 1 (1975).
7. S. Wittekoek, R.P. van Stapele, and A.W.J. Wijma, Phys. Rev. B7, 1667 (1973).
8. P. Brüesch and F. d'Ambrogio, Phys. Stat. Sol. (b) 50, 513 (1972).

STUDY OF THE MOTT TRANSITION IN n.TYPE CdS BY SPIN FLIP RAMAN

SCATTERING AND FARADAY ROTATION

R. Romestain

Laboratoire de Spectrométrie Physique

Boîte Postale 53, 38041 Grenoble-Cédex

I. Introduction

The importance of correlations between electrons in a metal has been pointed out 40 years ago. Though band calculations which treat the interaction of electrons through a self consistent potential provides a good description of most atoms and solids, they are unable to explain why a theoretical crystalline array of monovalent atoms would either be a good conductor or an insulator depending on the distance d between atoms. First treatment of this effect was proposed in 1949 by N.F. Mott[1]. He showed that one gets an insulator until the density of electrons is such that they screen the Coulomb interaction ; there should be a critical density when the screening is large enough so that electrons are no more bound to the positive ions, this in turn would improve the effectiveness of the screening. One thus expects a quite sharp transition which can be estimated at a density N such that

$$N^{1/3} a_o = 0.2$$

where a_o is the Bohr radius of localized electrons. Another approach was put forward by Hubbard[2]. He introduces a Hamiltonian which takes into account the repulsion U between two electrons on the same site, and the transfer energy T which represents the overlap between orbitals on different sites and thus the ability of electrons to hop from one site to the next. The larger T/U, the easier one forms a conduction band. A crystalline array with adjustable interatomic spacing has not been studied yet. Nature provides us with solids which do demonstrate a metal-non metal transition but they also show a simultaneous structural transition due to electron-vibration

interaction ; they are too much coupled to differentiate the ef-
fects and causes of each. On the other hand there exists a class
of materials which undergo a purely electronic transition : the
doped semiconductors. The radius of electron orbital is so large
(around 20 Å) that the transition occurs at a very small density
(around 10^{17} cm^{-3}), one does not expect the lattice to be sensitive
to a concentration of impurity of 10^{-5}. A lot of work has been do-
ne on Si doped with P donors. The transition happens where expec-
ted, and it has been studied by a variety of experiments (see ref.
3 and following papers). There is a conduction which does not re-
quire any activation energy, so that even at low temperature Si:P
has most of the properties of a metal.

However it still does not correspond to the theoretical model :
donors are introduced in a random way and distance between sites
can only be determined statiscally. Near critical concentration
electron may hop between close-by sites but may find regions where
the distance is too large to jump and thus conduction might not
occur through a macroscopic crystal. Coexistence of two phases (a
conducting and a non conducting one) in the same crystal is contro-
versial. Magnetic susceptibility measurements[4] can be interpreted
as showing such a coexistence but it was demonstrated[5] that taking
correlations into proper account, could lead to similar results.

The experiments we are going to describe shed some light on
this problem. CdS has the simplifying feature that being a direct
gap semiconductor wave functions of electrons are simple to descri-
be when Si conduction band minimum is on the edge of Brillouin zone.

We will first review the basic properties of CdS before going
into the detail of the calculation of spin flip Raman Scattering
(SFRS). Emphasis will be given on SFRS linewidth since it gives a
direct estimate of the diffusion of electrons in the vicinity of
the Mott transition. Results obtained by Faraday rotation will al-
so be presented.

II. Basic properties of Cadmium Sulfide

CdS is a hexagonal crystal (wurtzite structure). Optical pro-
perties of "pure" CdS have been extensively studied[6] so that a great
deal is known about the detailed structure of the conduction and
valence band together with the excitonic levels.

Band structure

The CdS crystal has some covalent character but for simplicity
let us assume that it is ionic so that orbitals for electron can be
thought of being localized either on cation Cd^{++} or anion S^{--}. Then
the highest occupied levels are the 3 p electrons of the S^{--} ion.
The next level is a 5 s orbital on the Cd^{++}. From these levels one
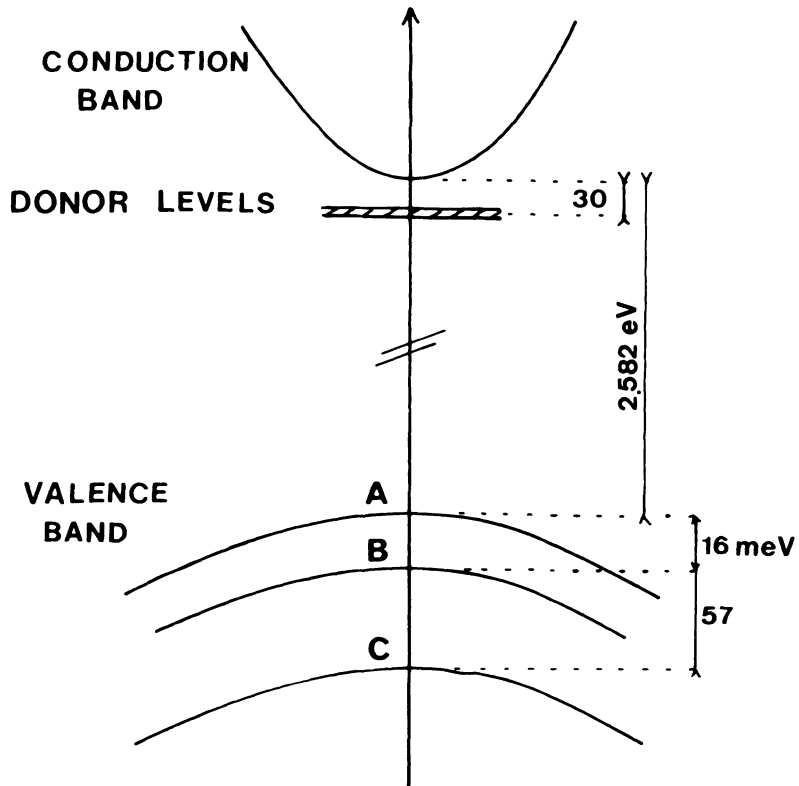
Fig. 1 : Band structure of Cadmium Sulfide

builds up bands shown in fig. 1 the 3 p level is actually split by the combined action of spin orbit interaction leaving a J = 3/2 highest and J = 1/2 lowest and the crystal field of hexagonal symmetry : this leaves 3 doublets Γ_9 (or A) Γ_7 (or B) Γ_7 (or C) respectively 16 and 57 meV from each other. The A valence band is thus made up of electrons whose orbital momentum and spin are parallel to the C-axis of the crystal. The maximum of each band is obtained at the center of the Brillouin zone i.e. $\vec{k}$ = 0. The effective mass is roughly equal to m_0, mass of the electron.

The conduction band, made up from the 5 s orbital has its minimum at $\vec{k}$ = 0. It lies at E_g = 2.58 eV above the A valence band maximum. The effective mass m^* is much lighter, almost isotropic with m^* = 0.19 m. Detailed calculations show that there is a mixing of valence band and conduction band (this is often carried out through the so called k.p approximation), this results in a orbital magnetic moment which appears as a modification of the g factor of the conduction electron from its g = 2 expected value. In small gap materials this can be huge (g = 50 for In Sb). For CdS the g-shift is much smaller and it was found that $g_{//}$ = 1.79 while $g_\perp$ = 1.77.

Impurity levels

If an impurity enters the crystal substitutionnally, it should have the same electric charge that the ion it substitutes for. However it usually has a tendency to keep a closed shells electronic structure. For instance when In substitutes for Cd^{++}, it first looses 3 electrons to become In^{+++}. This would leave the equivalent of one positive charge which will attract a conduction electron if any is available. If the dielectric constant of the lattice is large the Coulomb force will be very attenuated and the lowest bound state will actually be very loosely bound (30 meV for CdS). The radius is a_0 = 28 Å, so that the electron spend so little time on the impurity itself that it is almost insensitive to its chemical nature : the difference, the central cell correction, between different donors accounts for no more than a few percent in the binding energy. Radius a_0 and binding energy E_D are estimated directly from the values of the effective mass m^* and the dielectric constant ε, in the same way as for the hydrogen atom, so that the ground state is similar to a 1 s hydrogenic wavefunction and

$$a_o = \varepsilon \frac{\hbar^2}{m^* e^2} \qquad\qquad E_D = \frac{m^*}{\varepsilon^2} \frac{e^4}{2h^2}$$

Free exciton

Excitation of an electron from the top of valence band to the bottom of conduction band results in a very strong absorption of light as soon as $\hbar\omega > E_g$: this is the fundamental absorption. But the electron can be attracted to the hole left in the valence band

forming bound states with hydrogenic behaviour. The binding energy being 28 meV, recombination of electron and hole will generally lead to the emission of light at E_g - 28 meV ; similarly there is absorption at this frequency.

Bound exciton

The free exciton is neutral, still it can be attracted to a neutral donor in the same way two hydrogen atoms link together to form a hydrogen molecule. The corresponding excited state is rough-ly 8 meV below the free exciton (2.547 eV) : this can be conside-red as one excited state of the neutral donor. Depending on the valence band A or B which the hole belongs to, there can be two such excited levels corresponding to emission lines called I_2 and I_{2B} respectively. Excitation consists in taking one electron from a valence band, putting it next to the electron of the donor, so that they will have spins antiparallel.The symmetry properties of the complex so formed are thus primarily the ones displayed by the va-lence band the hole belongs to. For Spin Flip Raman Scattering, these excited states will be the virtual states which will allow matrix elements of electric dipole operator to be taken. Their value has been evaluated either from direct absorption measurement[7] correlated to concentration of donors or from the lifetime of the exciton[8] : it happens to be extremely large since it corresponds to an oscillator strength f = 10 or 6. It is to be remembered that the sum of all oscillator strengths of a n electron system is equal to n. The huge value of f is connected to the fact that during op-tical excitation not only the electron promoted from the valence band but also the closed shells electrons which are responsible for the dielectric constant, are involved.

III. Spin Flip Scattering

Spin Flip Raman Scattering was detected by Thomas and Hopfield in CdS[7] in a dilute sample. First linewidth studies were performed by Scott, Damen and Fleury[9]. The ground state of the donor has a spin equal to 1/2 and upon application of a magnetic field H it splits into two sublevels which we will call $|a>$ and $|b>$ separated by a Zeeman energy

$$\hbar\omega_Z = g\mu_B H.$$

Since g = 1.8, a 10 kG field yields a 25 GHz splitting.

If a spin is in the $|a>$ state it can scatter a incident pho-ton at frequency ω_L and wavevector $\vec{k}_L$; a photon is emitted at fre-quency $\omega_L - \omega_Z$ while the spin goes to state $|b>$. Two lines are indeed detected Stokes at $\omega_L - \omega_Z$ and Anti Stokes at $\omega_L + \omega_Z$. They are propor-tionnal respectively to the population of each state, their ratio is the Boltzmann factor exp $\hbar\omega_Z/kT$ which is typically 1.5 at 2 K and
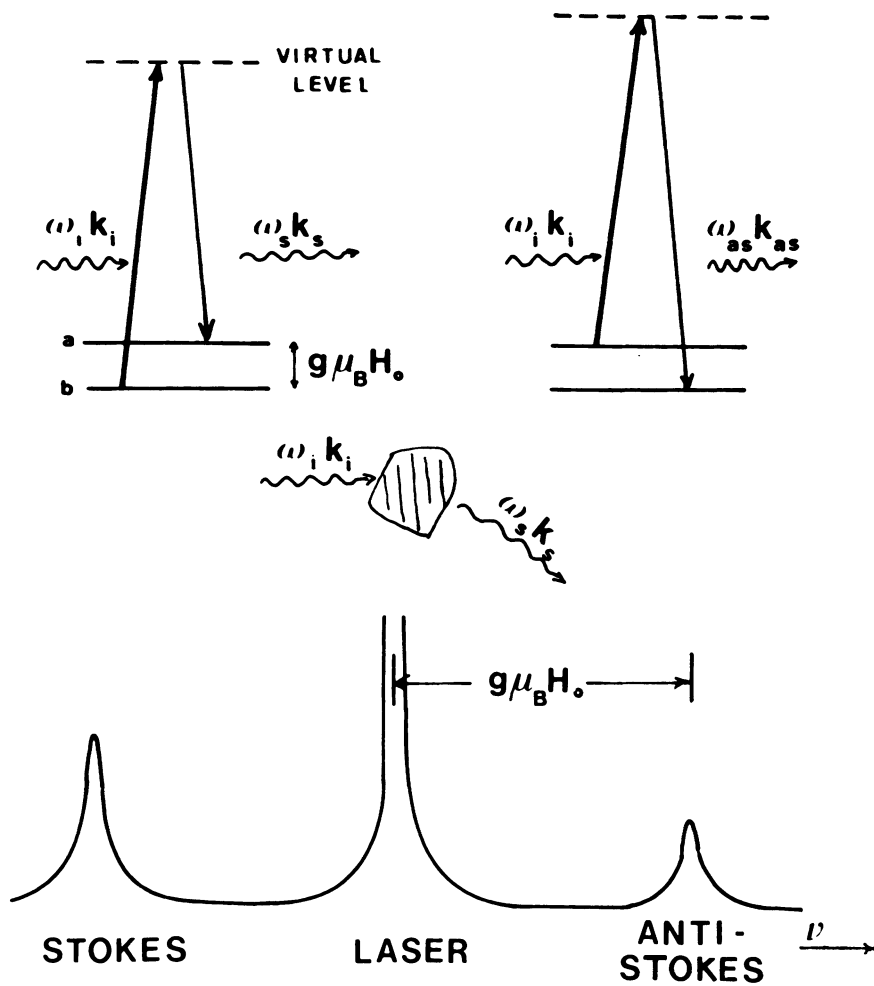
Fig. 2 : Schematic of spin flip Raman Scattering

10 kGauss.

For the experiment the CdS crystal is cooled at low tempera-
ture and laser light is focussed on to it. Scattered light at an
angle θ from the incident beam is collected by a lens, passed
through a Fabry Perot, and then frequency analyzed with the help
of a small pinhole. Optimum resolution can be 30 MHz. Signal to
noise ratio is improved, when needed, by photon counting and mul-
tichannel analyser. The index of the crystal being very large
n ≠ 3, the viewing angle corresponds closely to the perpendicular
to the exit face, so that bevels had to be cut in the crystals
to allow large variations of θ.

To determine the magnitude of the scattering we will use a
semi classical treatment[10]. The electric field of the incident
beam $\vec{E}_L \cos \omega_L t$ admixes some excited states $|n\rangle$ in the ground
state wavefunctions $|a\rangle$ and $|b\rangle$ with energy $\hbar\omega_a$ and $\hbar\omega_b$, which
become :

$$(1) \quad |\psi_a\rangle = e^{-i\omega_a t + \phi}\{|a\rangle - \frac{1}{2} \sum_n |n\rangle \frac{\langle n|\vec{E}_L \cdot \vec{er}|a\rangle}{E_n - E_a - \hbar\omega_L} e^{-i\omega_L t}\}$$

where ϕ is a random phase constant.

Though no electric dipole could appear between states $|a\rangle$ and
$|b\rangle$ because they have the same parity, the modified ψ_a and ψ_b dis-
play matrix elements of $\vec{er}$, for instance

$$(2) \quad \langle\psi_a|\vec{er}|\psi_b\rangle = \sum_n \frac{\langle a|\vec{E}_L \cdot \vec{er}|n\rangle\langle n|\vec{er}|b\rangle}{E_n - E_a - \hbar\omega_L} e^{-i(\omega_L \omega_b + \omega_a) t + i\phi}$$
$$+ \text{ a similar term with } e^{+i(\omega_L + \omega_b - \omega_a)t + i\phi}$$

In the classical treatment of spontaneous emission of radia-
tion one also calculates a dipole matrix element between an exci-
ted and a ground state : the existence of such an oscillating
dipole gives rise to emission of light at its frequency during
the transition between the two states. The same applies here but
light will be emitted at frequency $\omega_L + \omega_{ba}$ while the system goes
from state $|a\rangle$ to state $|b\rangle$. The random phase factor ϕ represents
the fact that oscillating dipoles are incoherent, thus one will
add emitted power by each spin instead of emitted electric field.
One can then define a cross section for spontaneous Raman Scatte-
ring so that intensity of scattered radiation per unit solid an-
gle in a direction Ω is given as a function of incident intensi-
ty I_L and length l of the region of the crystal under study :

$$I_S = N.l. \frac{d\sigma}{d\Omega} I_L$$

where N is the concentration of scattering centers, that is neu-
tral donors.

One can get a simplifying view of the problem by introducing a so-called Raman dipole D^2 which operates in the 2-dimensional manifold of the unperturbed states $a(t) = |a> e^{-i\omega_a t - i\phi}$ and $b(t) = |b> e^{-i\omega_b t}$ such that for instance

$$(3) \quad <\psi_b(t)|\vec{er}|\psi_a(t)> = <b(t)|\vec{D}^{(2)}|a(t)>$$

In most general fashion the components of any such operator may be expressed in terms of Pauli $\vec{\sigma}$ matrices for a spin $S = 1/2$

$$(4) \quad D_k^{(2)} = \sum_{ij} \alpha_{ijk} E_{Li} \sigma_j e^{-i\omega_L t} + \beta_{ik} E_{Lj} \tilde{I} e^{-i\omega_L t} + C.C.$$

For cubic symmetry this expression simplifies greatly, giving

$$(5) \quad \vec{D}^{(2)} = \vec{\sigma} \times \vec{E}_L (\alpha e^{-i\omega_L t} + C.C.) + (\beta \vec{E}_L \tilde{I} e^{-i\omega_L t} + C.C.)$$

where

$$(6) \quad \alpha = \sum_n \frac{i}{2} \frac{<a|ex|n><n|ez|b>}{E_n - E_a - \hbar\omega_L}$$

In equ. (5), β represents the usual polarizability which gives rise to the index of the crystal as well as Rayleigh scattering. Radiation of the dipole D can be calculated classically and yield a Raman electric field $\vec{E}_R$ polarized parallel to $\vec{D}$, the intensity being given by

$$(7) \quad \frac{d\sigma}{d\Omega} = 4 |\alpha|^2 \frac{\omega^4}{c^4}$$

Though expression (5) is valid only for cubic symmetry, and is a little more complicated for hexagonal symmetry as for CdS, it gives the salient features observed in this case. Due to the vector product $\vec{\sigma} \times \vec{E}_L$ Raman Scattering will be polarized perpendicular to the laser polarisation; a typical configuration would then be for instance $\vec{E}_L // \vec{u}_z // \vec{H}$, $\vec{E}_R // \vec{u}_x \perp \vec{H}$ so that σ_y will have matrix element between $|a>$ and $|b>$. At this point nothing has been said upon the wavevector of light, though obviously it cannot be parallel to the electric field.

An important point to stress is the energy denominator : if the frequency of the laser is such that $\hbar\omega_L$ almost matches the difference in energy between the ground state and one excited state $|n>$ the value of $d\sigma/d\Omega$ is enhanced. This happens to be case when the 4880 Å line of an Ar ion laser is used since the excited state corresponding to the I_2 line lies at 4867 Å. The cross section is so large that real forward scattering has in some cases been detected though the exciting beam actually goes through the detection system. The so-called Rayleigh scattering is often smaller than the Raman Scattering. A typical values of $d\sigma/d\Omega$ is 2.10^{-18} cm^2. Now we are in position to understand how the light can flip a spin though there is no direct interaction between an electric field and a spin.

This occurs because the excited state |n> carries the orbital momentum of the p.like valence band for which there is a strong spin orbit interaction. The state |n> is a superposition of spin up and spin down wave functions and thus can be connected to both |a> and |b> through electric dipole, giving a non-zero value of α. If all spin orbit states |n> were degenerate (no spin orbit interaction) all the contributions of different |n> would cancel out.

IV. Study of the SFRS linewidth

If the donor electron is localized, then the SFRS linewidth should simply reflect the EPR linewidth, be it due to inhomogeneous broadening (strains or local fields) or homogeneous broadening (relaxation time T_2 or T_1). This has been verified for a sample with concentration 10^{+17} where the linewidth of 0.003 cm^{-1} is independent of scattering angle and also equal to the measured EPR linewidth.

On the other hand if the electron moves with velocity $\vec{v}$, then the Raman line will have an additional Doppler shift : it experiences a laser frequency Doppler shifted by $\vec{k}_L.\vec{v}$ and radiates at an angle θ a Raman frequency which will be shifted by $-\vec{k}_S.\vec{v}$, so that $\Delta\omega_{Dop} = \vec{q}.\vec{v}$ if $\vec{q}$ is the scattering vector $\vec{q} = \vec{k}_L - \vec{k}_S$. For electron velocities of $v \sim 10^7$ cm s^{-1} corresponding to Fermi velocities for the concentrations used $\Delta\nu_{Dop} \sim 10^{12}$ Hz. On the other hand, the electrons undergo collisions at a rate τ_c approaching 10^{14} s^{-1} so that Doppler shift is collisionally narrowed giving rise to a diffusionnal line whose effective linewidth is given by

(9) $\Delta\nu_{eff} = 4\pi(\Delta\nu_{Dop})^2 \tau_c$

A uniform repartition of the velocities on the Fermi surface yields an angular average

(10) $(\Delta\nu_{Dop})^2 = \dfrac{V_F^2}{3} (2 \sin \dfrac{\theta}{2})^2 k^2$ and

(11) $\Delta\nu_{eff} = \dfrac{16\pi}{3} \dfrac{V_F^2}{\lambda^2} \sin^2 \dfrac{\theta}{2} \tau_c$

Alternate description of the SFRS linewidth[11]

We have derived a formula giving what we called Raman dipole $\vec{D}^2$, this dipole interacts with the radiation field at its frequency giving rise to emission as we have seen. This interaction can be expressed by the Hamiltonian

(12) $\mathcal{H}_{SF} = \vec{D}^{(2)} \vec{F}_R e^{+i\omega_R t} = (\vec{\sigma} \times \vec{E}_L).\vec{E}_R e^{+i\omega_R t} (\alpha e^{-i\omega_L t} + C.C.)$

if we introduce the spatial dependence of the radiation field one will obtain terms of the form :

(13) $\mathcal{H}_{SF} = \vec{\sigma} \, (\vec{E}_L \times \vec{E}_R) \, e^{-i(\omega_L - \omega_R) + i \, \vec{q} \, \vec{r}} = \vec{\sigma} \, \vec{H}^+$

where again $\vec{q} = \vec{k}_L - \vec{k}_R$.

The effect of the radiation will then be the same as a magnetic field interacting with the spins. When the field is constant the effect of the interaction depends on the static susceptibility χ_o, for an oscillating magnetic field $H_1 \cos \omega_1 t$ like the one used for magnetic resonance one would need define a susceptibility at $\omega_1 \neq 0$. Here we introduce a susceptibility $\chi(\omega, q)$ as a response to a field with time and space dependence $H^+ = H \, e^{-i(\omega t + \vec{q} \, \vec{r})}$.

Still the q value corresponding to the wavelength of light 0.5 μ is large compared to the average inter electron spacing or to the Bohr radius of a donor. Under such conditions one expects that the spin transverse magnetization M^+ can be described by a modified Bloch equation of the form :

(14) $\dfrac{dM^+}{dt} + i \, \omega_s \, M^+ + \dfrac{M^+ - \chi_o H^+}{T_2} - D_s \, \nabla^2 \, M^+ = \dfrac{i\mu g}{\hbar} \, M_o \, H^+$

where $\omega_s = \omega_a - \omega_b$ is the precession induced by the static field while $\mu g/\hbar \, H^+$ is the one induced by the oscillating H^+, T_2 is a transverse spin-relaxation time. D_s is the spatial spin diffusion constant.

If H^+ is a plane wave

$H^+(r,t) = H_o^+ \, e^{-i(qr - \omega t)}$,

eq (14) has the solution

(15) $M^+ = \dfrac{(-\omega_s + \frac{i}{T_2}) \, \chi_o \, H^+}{(\omega - \omega_s) + i(\frac{1}{T_2} + D_s \, q^2)}$

from which it follows that

(16) $\chi^+(q,\omega) = \dfrac{(-\omega_s + \frac{i}{T_2}) \, \chi_o}{(\omega - \omega_s) + i(\frac{1}{T_2} + D_s q^2)}$

For magnetic resonance it is well known that imaginary part of susceptibility gives rise to absorption, that is real transitions. For the same reasons Im χ^+ will describe the actual dependence of spin flip scattering; the linewidth follows :

(17) $\gamma = \dfrac{1}{T_2} + D_s q^2$

We must emphasize the fact that D_s introduced phenomenologically

in eq (14) can represent either a real motion of electrons carrying
their spin (particle diffusion D) or pure spin diffusion as would
occur in case of localized electrons interacting via dipole dipole
coupling. In that sense eq (14) is more general than eq (11) but
the pure spin diffusion introduced appears difficult to evaluate
in a random system.

Mott transition in CdS

We have so far demonstrated the usefulness of SFRS in that it
gives direct information upon the motion of the particles scatte-
ring the light. One major advantage is its selectivity : at the
Stokes frequency only donors can participate, that would not be
true for conventional Rayleigh scattering. We will see later that
Faraday rotation has also this advantage and we will make use of
it. Before going into the results obtained by SFRS let us review
the main experiments showing unambiguously the Mott transition
in CdS.

The occurence of Mott transition is displayed very clearly by
conductivity measurements taken at Helium temperature on samples
of different concentrations[12] : this is seen in figure (3) where
over a range extending between $N = 10^{18}$ to $N = 10^{17}$ cm^{-3} the con-
ductivity drops by more than 4 orders of magnitude. Above $N = 9\ 10^{17}$
cm^{-3} the number of carriers as determined by Hall effect[13] is almost
insensitive to temperature (see fig. 4). In this regime the electrons
are definetely moving in a not completely filled band like they would
in a metal. Below $N = 5\ 10^{17}$ cm^{-3} on the other hand the number of
carriers reflects a thermal activation from bound states, behaving
like semiconductors though the dependence in temperature is more
complicated.
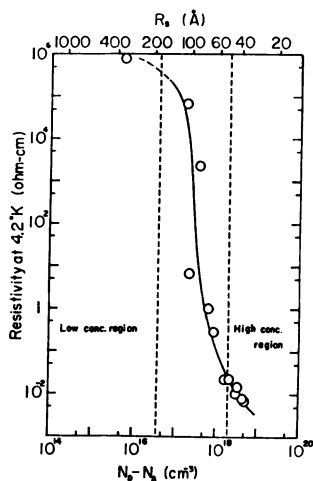
Fig. 3 : Resistivity of CdS as a function of concentration of
neutral donors at 4.2 K (from ref. 12)
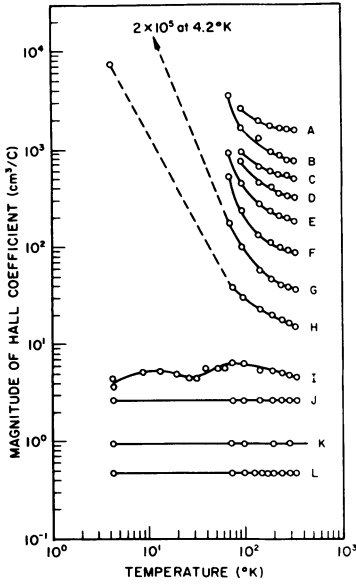
Fig. 4a
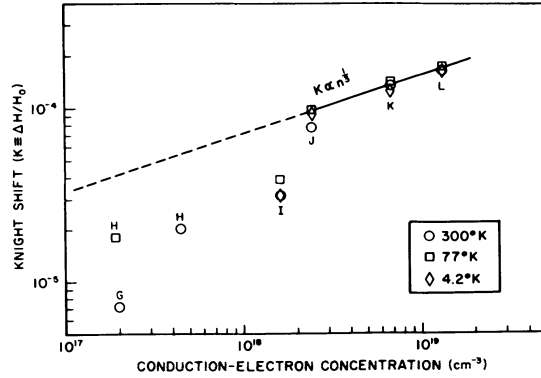
Fig. 4b

Fig. : 4a Hall coefficients of different CdS samples. The labelling
of samples is the same as in fig. 4b. Concentration is 2 10^{17}
for sample G ; H = 4.5 10^{17}, I = 1.6 10^{18}, J = 2.5 10^{18}
(from ref. 13)

Experiments performed on the NMR of the ^{113}Cd isotope[13] reveals
more precise feature of the transition on the metallic side. The
Knight Shift (fig. 4b) has an expected $N^{1/3}$ dependence on concen-
tration when N > 2 10^{18}. Then the sample has all the caracteris-
tics of a metallic sample : the impurity band formed around 9 10^{17}
cm^{-3} merges with the conduction band.

Analysis of experimental results

The diffusional scattering is already clearly present at a
concentration N = 2.4 10^{17} cm^{-3} which lies at the onset of Mott
transition and still has a semiconductor behaviour. The SFRS line-
width is shown in fig. 5 for forward scattering $\theta = O(\vec{q} = O)$ and
$\theta = 90°$. At $\theta = 90°$, $\Delta\nu = 300$ MHz whereas for $\theta = O$, $\Delta\nu = 60$ MHz
including an instrumental linewidth of 30 MHz. The q^2 dependence
of $\Delta\nu$ is illustrated in fig. 6 for a more metallic sample with
N = 1.4 10^{18} for scattering angles close to the forward direction.

$\theta = 90°$

CdS
$N_D - N_A = 2.4 \times 10^{17}$
$T = 1.6 °K$

ANTI-
STOKES   LASER   STOKES

0.01
cm⁻¹

Fig. 5a

FORWARD SCATTERING

ANTI-
STOKES

STOKES

0°

0.002
cm⁻¹
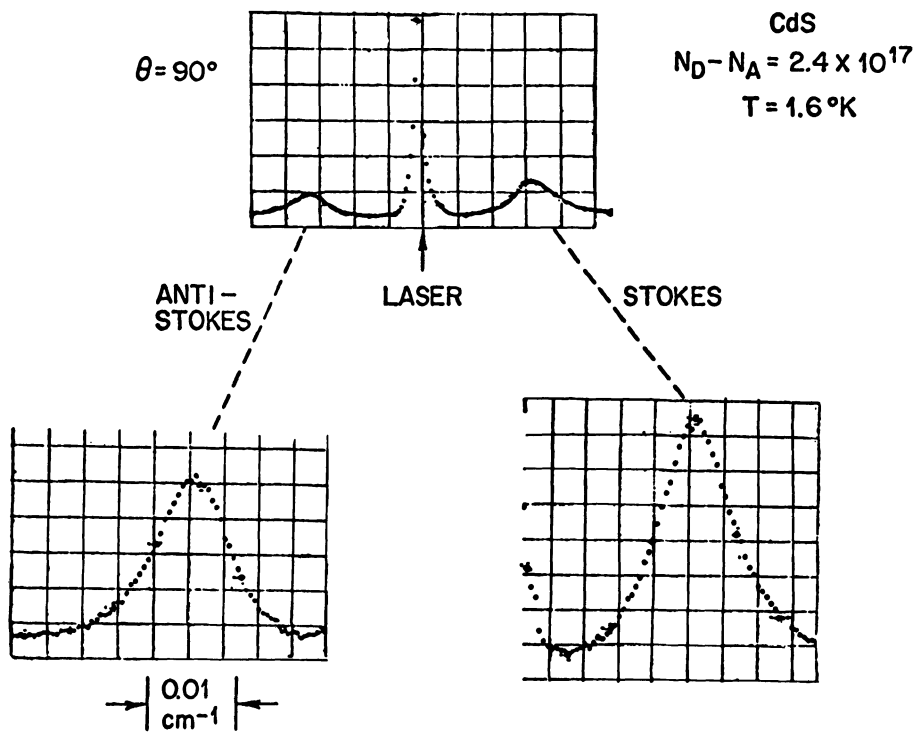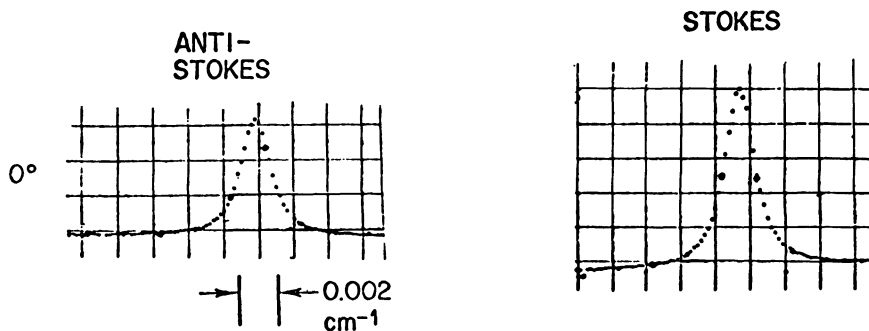
Fig. 5b

SFRS in a sample with $N = 2.4 \; 10^{17}$. The lower portion of fig. 5a shows Stokes and Anti Stokes on an expanded scale. Fig. 5a is 90° scattering, Fig. 5b is 0° scattering. Both are taken with the same resolution
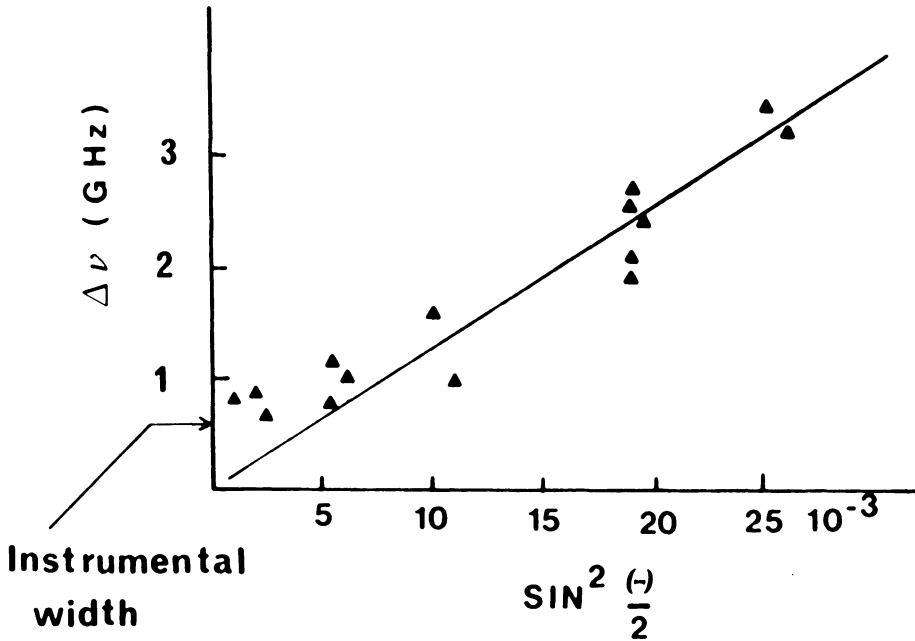
Fig. 6 : Linewidth of small angle forward scattering illustrating
the diffusional motion of carriers via the q^2 dependence
of the linewidth when N = 1.4 10^{18} and T = 1.6 K

The linewidth can be evaluated using relation (11) when the
impurity band has merged into the conduction band so that v_F can
be deduced from the electron concentration N, and effective mass
m^* :

$$(18) \quad v_F = \frac{\hbar}{m^*} (3\pi^2 N)^{1/3}$$

τ_c can in turn be deduced from resistivity measurement (12) since

$$(19) \quad \rho = \frac{m^*}{Ne^2\tau_c}$$

So equation (11) can be rewritten in that case

$$(20) \quad \Delta v = \frac{6.10^{15}}{\rho N^{1/3}} \, cm^{-1}$$

ρ is in Ω cm and N in cm^{-3}.

The increased diffusional motion with increasing N and metal-
lic character is illustrated in Table I where the results are com-
pared with Eq (20). The agreement which is reasonable down to N =
2.4 10^{17} is much better than could be hoped. Below 10^{18} one does

	n	$\rho(2K)$ ohm-cm	$\Delta\nu_{eff}(calc)$ cm^{-1}	$\Delta\nu_{meas}(cm^{-1})$ $\theta = 90°$ T = 2K
A	1.0×10^{17}	$> 10^5$	–	0.003
B	2.4×10^{17}	20.0	0.016	0.008
C	5.0×10^{17}	1	0.25	0.125
D	1.4×10^{18}	0.1	1.9	2.0
E	4.0×10^{19}	0.0014	45	14

Table I : Comparison of measured SFRS linewidths with $\Delta\nu_{eff}$
        calculated from eq (4), where ρ is in ohm-cm

not expect an effective mass formalism to be applicable since the
impurity band has certainly a more complicated shape. Besides va-
riation of linewidth by a factor of two are observed in different
regions of the same sample. This is undoubtedly due to even slight
inhomogeneities in concentration since $\Delta\nu$ varies so rapidly with
N in this regime. It should be emphasized that the SFRS technique
probes a region of the sample that in our case is of the order of
100 microns. Such variation of N are of course averaged in a typi-
cal transport measurement. Nevertheless there is clear evidence of
increasing diffusion with increasing N though more detailed theo-
retical calculations are needed to understand the Mott transition
region.

V.   Measurement of χ_0 by Faraday rotation

In addition to the off diagonal component of the dipole $\vec{D}^{(2)}$
in eq (5) which gives rise to SFRS there is a diagonal part asso-
ciated with σ_z. This corresponds to a dipole radiating at the same
frequency ω_L but rotated with respect to the incident polarization.
For instance

$$(21) \quad <a|D_y^{(2)}|a> \sim \alpha <a|\sigma_z|a> E_x \, e^{-i\omega_L t}$$

This rotated dipole gives rise to a Faraday rotation[14] per
unit length along z given by

$$(22) \quad \frac{\phi}{1} = \frac{8\pi^2}{n} N \alpha <\sigma_z>$$

Since the susceptibility is proportionnal to the derivative of the magnetization $<\sigma_z>$ with respect to H, then the specific rotation R = d/dH (ϕ/l) is proportionnal to χ.

As α can be made extremely large for the donors by choosing near resonant light excitation as described for the SFRS, one has a way of measuring very selectively the χ of the donors independent of other magnetic impurity present in the sample. In figure 7a is shown the transmission of linearly polarized light through the sample as detected through a polaroïd. The separation between peaks is plotted versus H in fig. 7b. There is a small temperature independent rotation η, due to interband transitions which is substracted to give spin Faraday rotation ϕ - η. This quantity follows a Brillouin function for S = 1/2 and g = 1.79 as expected for the donors in CdS. When R is studied as a function of temperature, a plot of 1/R versus T yields an antiferromagnetic Curie-Weiss θ of 0.3° K (the same results are found using 4965 Å excitation although the rotations are smaller). This would suggest searching for a spin glass at lower temperatures.
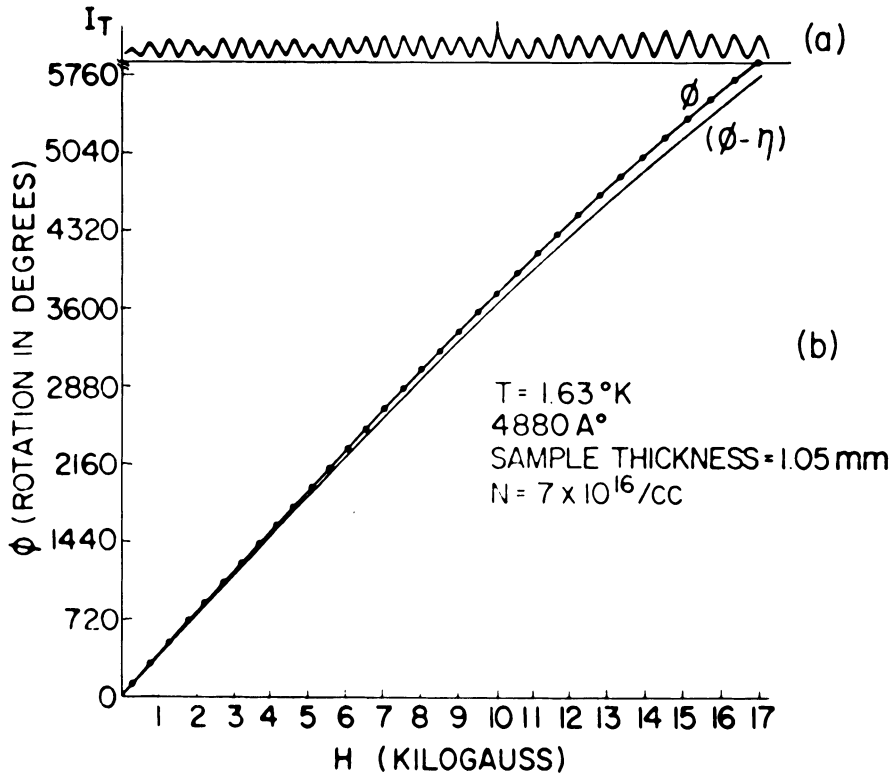
Fig. 7 : Faraday Rotation for localized centers N = 7 10^{16} cm^{-3}

In the very metallic region, for example with $N = 6 \times 10^{18}$, χ shows no saturation with H and is independent of T as one would expect from a Pauli susceptibility. However, in the metallic transition region, χ displays both temperature dependent as well as temperature independent components. This is illustrated in Fig. 8 for $N = 1.4 \times 10^{18}$. This temperature dependent component increases with decreasing concentration and is fairly dominant when $N = 2.4 \times 10^{17}$.

The variation of R with temperature, T, mirrors the variation of susceptibility with T in a given sample. To determine the absolute value of χ, however, one needs specific knowledge of the quantity α in eq (6). This may be easily calculated in the insulating limit where there is only one significant excited level corresponding to an exciton bound to the neutral donor (I_2) whose position and oscillator strength is well known[6]. Using this exciton level the calculated α agrees very well with the magnitude of the rotation observed in fig. (8). However, as one crosses to the metallic regions with increasing concentration, the bound exciton loses meaning and the question arises as to the changing spectrum of the electron-hole excitation. In the case of the very metallic samples, the lowest such excitation corresponds to the energy needed to promote an electron from the top of the valence band to the Fermi level now in the conduction band, and the oscillator strength is spread out among the unoccupied states. The most feasible way to determine α in this case would be experimentally by measuring the optical absorption spectrum. However, beyond the transition on the metallic side even up to $N \sim 2 \times 10^{18}$, it is observed that the luminescence feature corresponding to electron-hole recombination does not move and while it broadens somewhat, its width still remains small compared to the 5 meV separation from the laser line. Therefore, up to $N \sim 10^{18}$ we tentatively take α to be the same as in the dilute limit for our analysis of absolute χ in this region.

Thus if we compare the absolute magnitude of the temperature dependent component of the rotation for $N = 1.4 \times 10^{18}$ to that found per localized spin in the insulating region for $N = 7 \times 10^{16}$, we find that the temperature dependent part in fig. 8 corresponds to approximately 10^{16} electrons with free moments or 1% of the total. The same figure is arrived at by comparing the ratio of the temperature dependent and temperature independent parts assuming the latter to be Pauli like with a degeneracy temperature $T_F = 265°$ K corresponding to $N = 1.4 \times 10^{18}$. By contrast, for the $N = 2.4 \times 10^{17}$ sample which shows only a very small temperature independent susceptibility, an analysis of χ in terms $\chi_p + \chi_{c.w.}$ shows that the number of Curie-Weiss electrons is comparable to the number of Pauli like electrons. Very similar results for χ were obtained by Quirt and Marko[4] for Si : P.
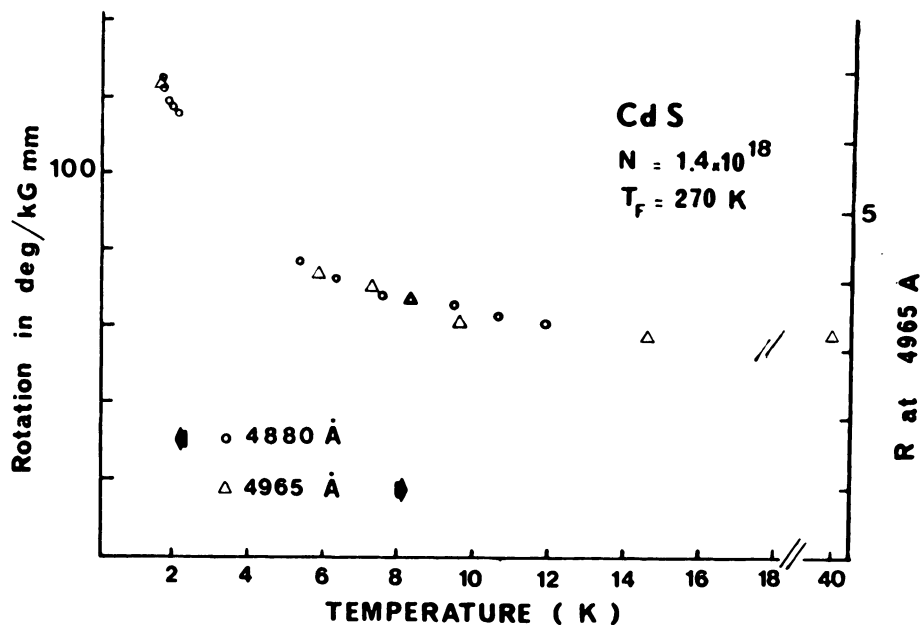
Fig. 8 : Susceptibility of donors in a concentrated sample
N = 1.4 10^{18}

VI. Discussion of results

Some may be inclined to interpret the two components χ_p and $\chi_{c.v.}$ that are observed as arising from well defined microscopic regions of metallic and insulating material with nondiffusing electrons respectively, associated with the clustering due to basic statistical randomness in donor positions. However, we will now present evidence that there are no nondiffusing spins beyond the metallic transition which seems to argue against the simultaneous coexistence of two such phases. If there were nondiffusing spins imbedded in a metallic matrix, we would certainly expect their number to be greatest close to the M-NM transition point as for example in the sample with N = 2.4 x 10^{17}. If one looked at 90°

scattering in such a sample, one would expect to see a narrow line with no angular dependence, superimposed on the broader diffusional line with q^2 dependence. However, one always sees only a single line with q^2 dependence as shown in fig. 2a and no evidence for nondiffusing carriers. This is further illustrated in fig. 6 where again the narrow line observed at $\theta = 0$ broadens continuously as q^2 with increasing angle about $\theta = 0$. We are inclined to believe that the temperature component of χ is coming from electrons in singly occupied sites of the correlated electron motion[4,5]. Because of randomness some or all of these singly occupied sites may even have fixed positions in space. However, the electrons in these singly occupied sites are still in dynamic equilibrium with the rest of the electron sea and leave this site to be filled by another carrier replacing it. Equivalently stated, the electrons on singly occupied sites are Anderson local moments or Friedel virtual bound states which while giving rise to a $\chi_{c.w.}$ still have diffusive character in the SFRS.

References

1. N.F. Mott, Proc. Phys. Soc. (London) A 62, 416 (1949)
2. J. Hubbard, Proc. Roy. Soc. A (276), 238 (1963)
3. N.F. Mott, Journal de Physique C-4, 302 (1977)
4. J.D. Quirt, J.H. Marko, Phys. Rev. 7, 3842 (1973)
5. K.A. Chao, K.F. Berggren, Phys. Rev. Lett. 31, 880 (1975)
6. D.G. Thomas, J.J. Hopfield, Phys. Rev. B, vol. 128 n° 5, p.2135 (1962)
7. D.G. Thomas, J.J. Hopfield, Phys. Rev. 175 n° 3, 1021 (1968)
8. C.H. Henry, K. Nassau, Phys. Rev. B, vol. 1 n° 4, p. 1628 (1970)
9. J.F. Scott, T.C. Damen, P.A. Fleury, Phys. Rev. vol. 6, n° 10, 3856 (1972)
10. R. Romestain, S. Geschwind, G.E. Devlin, P.A. Wolff, Phys. Rev. Lett. vol. 33 n° 1, 10 (1974)
11. P.A. Wolff, S. Yven, P. Maldague, private communication
12. S. Toyotomi, K. Morigaki, J. Phys. Soc. Jap. 25, 807 (1968)
13. F.D. Adams, D.C. Look, L.C. Brown, D.R. Locker, Phys. Rev. B vol. 4 n° 7 (1971)
14. R. Romestain, S. Geschwind, G.E. Devlin, Phys. Rev. Lett. 75, 803 (1975)

ELECTRON PHONON INTERACTIONS AND CHARGE ORDERING IN INSULATORS

Y. Yamada

College of General Education

Osaka University, Toyonaka, Osaka, 560 JAPAN

I. CHARGE ORDERING IN INSULATORS

There are various kinds of crystals which undergo structural phase transitions upon change of any external circumstances, especially of temperature. These structural transitions are understood in terms of the instability of the lattice against some particular atomic displacement field, or phonon mode. Since it is obvious that a harmonic phonon system can not become unstable by change of temperature, some sort of interaction of harmonic phonons with some physical variables would be needed to trigger the phase transition.

In this lecture, let us take up localized electron system as the variable to trigger the phase transitions through the interaction with phonons. In this case, the ordering in the distributions of local charge density takes place below the transition temperature along with the condensation of a particular phonon mode. This is certainly in contrast to the topics concerning charge density waves in metals where the charge ordering is seen in itinerant electron system.

In the case of insulators, the electron associated with the ordering is more or less localized in space. Therefore, each electron can be specified by the site number rather than the wave vector K as is done in itinerant electron case.

The charge ordering process in insulators is generally considered to be as follows: In higher symmetry phase, there is a fluctuating part $\delta\rho$ in the charge density of the localized electrons, and, due to some sort of interactions between these

fluctuating parts at different sites, a cooperative ordering of charge density will set in when the external circumstances such as temperature, pressure etc. are varied.

It would be convenient to expand the fluctuating part of the charge density localized at a site in spherical harmonics as follows:

$$\delta\rho = \sum_{\ell,m} R^m_{\ell}(r) Y^m_{\ell}(\theta,\phi) \qquad (1)$$

The coeffiants of the ℓ'th terms are associate with the tensor components of 2^ℓ multipoles:

$$q^m_\ell = \sqrt{\frac{4\pi}{2\ell+1}} \int r^\ell R^m_{\ell}(r) r^2 dr \qquad (2)$$

We may categorize the various types of charge order into "grades" by specifying the lowest order fluctuating term which 'freezes' in the low temperature phase as is shown in Table I. The most widely observed charge order is, of course, the case of 1st grade ordering, namely the dipolar ordering. Ferroelectric or antiferro-electric ordering fall into this class.

However, we can consider the case of even lower grade: the 0'th grade ordering. In this case, the total charge, integrated around each site, itself is fluctuating in the higher symmetry phase. Various kinds of mixed valence systems such as Fe_3O_4, SmS, etc. would be categorized as belonging to this class. Later, we will discuss Fe_3O_4 as an example of this class in some detail. On the other hand, we may also consider the cases of higher grades than dipolar ordering. In fact, from this stand point, various kinds of Jahn-Teller ordering is categorized as quadrapolar ordering. We will discuss this type charge ordering by taking up the case of $K_2PbCu(NO_2)_6$ as an example.

TABLE I

Classification of the charge ordering associated with local electronic state, with respect to the lowest multipoles appearing in the ordered phase.

grade	multipole	example
0th	monopole	mixed valence systems
1st	dipole	ferroelectrics, antiferroelectrics
2nd	quadrupole	Jahn-Teller systems
---	---	---

Whatever the grade of the charge order is, the most important characteristic of the ordering of localized electron, as compared with itinerant electron case, consists in that the energy eigenstates of electrons are consisted of well separated discrete levels. And the eigenstates relevant to the phase transition are restricted to the ones with excitation energies comparable to or less than kTc, Tc being the transition temperature. Usually only several eigenstates should be considered. In such the case, the pseudospin description of the electronic system is very useful.

We expand the electronic potential with respect to small atomic displacements, or more properly with respect to phonons. Then we can go through the procedure to obtain 'coupled pseudospin-phonon formalism' describing localized electron-phonon system. This procedure has been extensively discussed in the separate lectures in this seminar[1,2].

One of the advantage of introducing pseudospins to describe local electronic state is that the property of cooperative ordering of real spin system under various conditions are extensively investigated in connection with the study of magnetic materials. Hence, there are good chances that we can directly infer what will happen in our pseudospin system by making analogy with the corresponding real spin system. We will see later a good example where such analogy works well.

We concentrate ourselves to the lowest order bilinear coupling between pseudospins and phonons:

$$H_{int} = \frac{1}{\sqrt{N}} \sum_{\ell} \sum_{k,s} \xi_{k,s} \, \sigma_{\ell} \, Q_{k,s} \, e^{ik \cdot r_{\ell}} . \tag{3}$$

where the spin operator σ_{ℓ} describes the state of electron localized at ℓ'site, $Q_{k,s}$ is the amplitude of phonon mode specified by the wave vector k and the branch number s. The property of the linearly coupled spin-phonon systems is discussed extensively in the separate lecture in this seminar[1]. The exchange of phonons gives rise to an effective spin-spin interaction causing spontaneous ordering of spin system below a critical temperature T_C, accompanied by a distortion of the lattice or a condensation of phonon mode.

In the following, we discuss two typical examples of the charge ordering of 2nd grade and 0'th grade. In both cases, it is shown that the pseudospin-phonon formalism can be worked out, though the physical contents for the 'pseudospin' is not the same. Thus, we try to view these phase transitions on a more or less unified stand point.

II. SECOND GRADE ORDERING : JAHN-TELLER ORDERING IN $K_2PbCu(NO_2)_6$

II·1 Introduction

The crystal of $K_2PbCu(NO_2)_6$ belongs to the isomorphous crystal system generally expressed as $R_2MCu(NO_2)_6$, where R=K, Rb, Cs, Tl and M=Ca, Sr, Ba, Pb. These crystals contain octahedral $Cu(NO_2)_6$ complex in common. As is well known, Cu^{2+} ion in a cubic crystal field is Jahn-Teller active, whence $Cu(NO_2)_6$ group has the tendency to become slightly distorted from the regular octahedron. Not only that, the crystal lattice as a whole would become distorted due to the interactions between local distortions. In fact, some of the crystals undergo phase transitions which is considered to be associated with the cooperative Jahn-Teller effect.

In particular, the system $R_2PbCu(NO_2)_6$ is very interesting in that it exhibits successive phase transitions[3,4,5,6] $K_2PbCu(NO_2)_6$ being the typical example[3,4] In this section, we try to understand the property of this sequencial cooperative Jahn-Teller ordering, as one of the interesting example of 2nd grade ordering, on the general basis discussed in the preveous section.

II.2 Successive Phase Transitions

The undistorted 'prototype' structure[7] is depicted in Fig. 1. It belongs to cubic system (space group F3m) and $Ni(NO_2)_6$ complex sitting at the corner of the cell forms the regular octahedron. It is well known that when Ni→Cu, the local 3d electrons of Cu^{2+} ion strongly couple to local distortions with Eg symmetry, conventionally specified as the Q_2-mode and the Q_3-mode[8]. The electronic state is represented in terms of Pauli spin operators σ^x and σ^z, and the stable ground state is expressed as a 'circle' in the two-dimensional σ^x-σ^z plane. In the pseudospin description, the cubic phase corresponds to the case when the spin direction is not fixed and σ_ℓ at the ℓ'th site is fluctuating around the circle.

The crystal of $K_2PbCu(NO_2)_6$ has the undistorted cubic structure at room temperature. This crystal undergoes two phase transitions at 280°K and 273°K successively[3,4] The lower temperature phases are reported to have pseudotetragonal[9] unit cell with c/a<1. In order to understand overall feature of successive transitions, we show the precise measurement of the temperature variations of X-ray scattering angles of two fundamental reflections in Fig. 2. The intermediate phase (Phase II) is known to have tetragonal cell, while the lowest temperature phase, strictly speaking, has a lattice symmetry lower than orthothombic.

It is interesting to compare these with the temperature

K₂PbNi(NO₂)₆

● K
◎ Pb
• Ni
△ NO₂
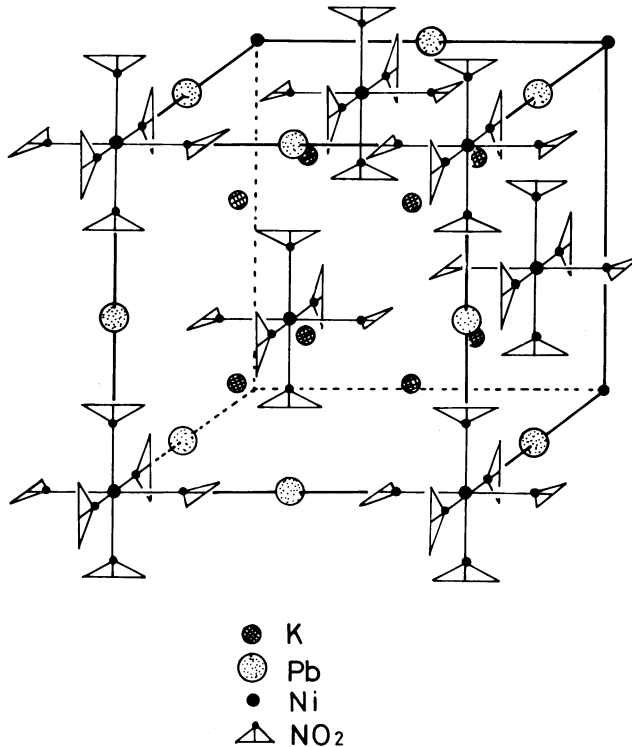
Fig. 1 The undistorted 'prototype' structure of $R_2MNi(NO_2)_6$.
When Ni→Cu, the octahedral $Cu(NO_2)_6$ complex tends to be distorted
due to Jahn-Teller effect.

dependence of ESR absorption lines of Cu^{2+} ions.[4,10] We see that
there is a fairly good correspondence between the lattice
distortion and the 3d electronic state of Cu ions, which indicates
the important role of Jahn-Teller effect in these phase transitions.

    Recently, we have carried out precise structural measurements
in Phase II and Phase III[11,12] using X-rays and neutrons, which
have revealed interesting features involved in these phase
transitions.

II·3 Phase III : Canted Pseudospin Structure, Antiferrodistortive
Phase
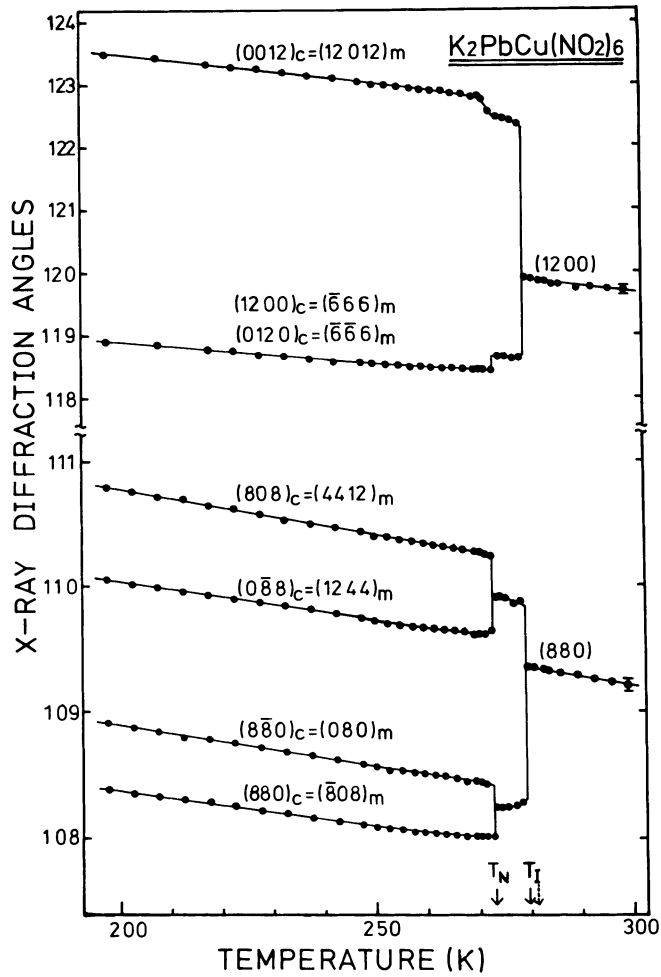
Fig. 2. Temperature dependences of the diffraction angle of the two fundamental Bragg reflections: $(1200)_c$ and $(880)_c$ in cubic indices. Phase II is indexed by a tetragonal lattice while Phase III by a monoclinic lattice.

In Phase III, we have observed the super lattice reflections at $(H\pm1/2, K\pm1/2, L\pm1/2)$ in cubic indices, namely at L-points of the Brillouin zone of fcc unit cell. This will imply that some of the L zone-boundary phonon modes condenses in Phase III. Therefore we look for the L zone-boundary modes which are compatible with the local Q_2- and the Q_3-mode. Following convensional symmetry analysis, we find that the L_3- and the L_5-mode are the possible

Jahn-Teller active phonons, whose displacement pattern are depicted
in Fig. 3. We can easily see the local Q_3-mode is compatible with
this L-mode. The structure analysis including super lattice
reflections confirmed this displacement pattern.

This is an antiferrodistortive structure, where in one sub-
lattice the a-axis is the direction of tetragonal elongation of the
octahedron formed by $Cu(NO_2)_6$ complex while in the other the b-axis
becomes the direction of elongation. In terms of the pseudospin
description of local electronic configuration, this structure may
be characterized as the 'canted spin' structure as is illustrated
in Fig. 4.

Concerning the electronic state of Phase III, there have been
very interesting debates between 2 groups based on ESR measurements.
Reinen et al[6],[13] assumes 'locally elongated' configuration implying
that the wave function $\psi_g = 2z^2 - x^2 - y^2$ should be taken as the ground
state. The uniform contraction of the lattice ($c/a<1$) is attained
by taking local unique axis along the a-axis or the b-axis alte-
natively. (antiferrodistortive state).

On the other hand, Harrowfield[4],[14] assumes 'locally contracted'
configuration as the ground state. In this case, each ionic group
contracts along the tetragonal unique axis, thus the uniform
contraction of the lattice is attained simply by the ferrodistortive
state. It is interesting that, as far as the 'averaged' property
is concerned, these two models are equally good to explain the
anisotropy of the g-tensor observed by ESR experiments. Our
structural analysis is certainly consistent with Reinen's picture.

II·4 Phase III : 'Fan' Spin Structure, Incommensurate Phase

The property of Phase II is more interesting. We have per-
formed neutron diffraction experiments in Phase II. The most
remarkable point is that, in addition to the uniform bulk
contraction, we have observed satellite reflections at (H±0.425,
K±0.425, 0)$_c$ in cubic indices. That is, Phase II is considered as
an 'incommensurate' phase. In Fig. 5, the diffraction pattern in
(001) zone is schematically shown.

The model for the static structure in this phase would be
that the local Jahn-Teller distortion is modulated along [110] with
$|k_0|=0.425$. We look for phonons on Σ-line ($k=[\xi\xi 0]$) which is
compatible with the local Q_2- and Q_3-mode. The symmetry property
of the low frequency acoustic phonons on Σ-line is summarized in
Table II. We assumed that the most probable candidate of the
phonon mode which is condensed in Phase II is TA_1-mode, propagating
along [110] and polarized along [1$\bar{1}$0]. The structure based on this
model is illustrated in Fig. 3. A preliminary structure analysis
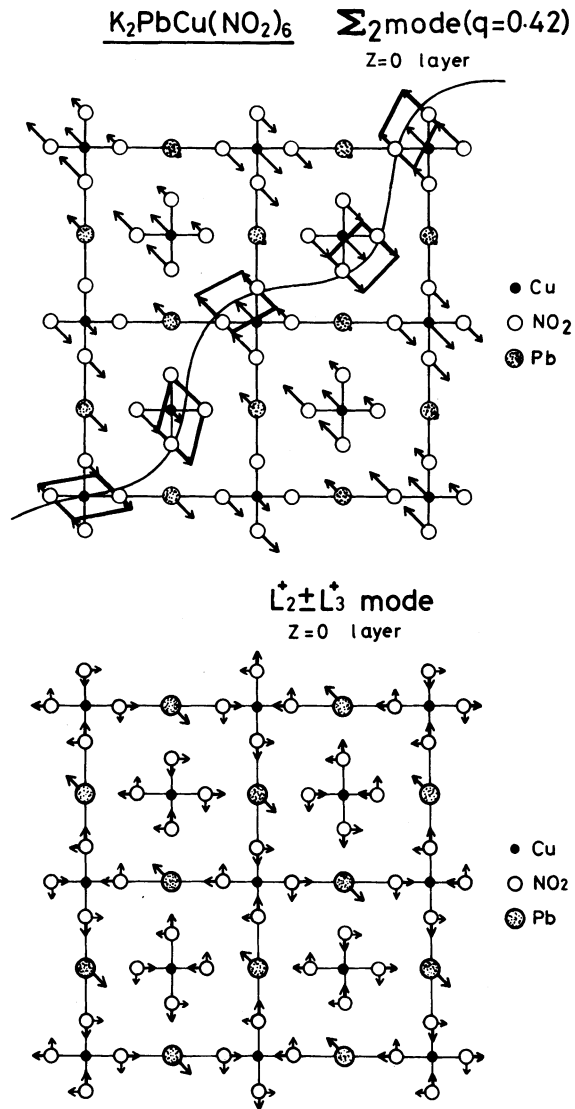
Fig. 3 Model structures in the low temperature phases.
Phase II (upper figure): Jahn-Teller active phonon mode (TA$_1$-mode)
with wave vector k_0=(0.425, 0.425, 0) is 'freezed'. This is an
incommensurate phase.
Phase III (lower figure): Jahn-Teller active zone boundary mode
(k=1/2 1/2 1/2) is 'freezed'. This is an antiferrodistortive
(commensurate) phase.

Phase II   **Phase III**

'fan spin'   'canted spin'
structure   structure
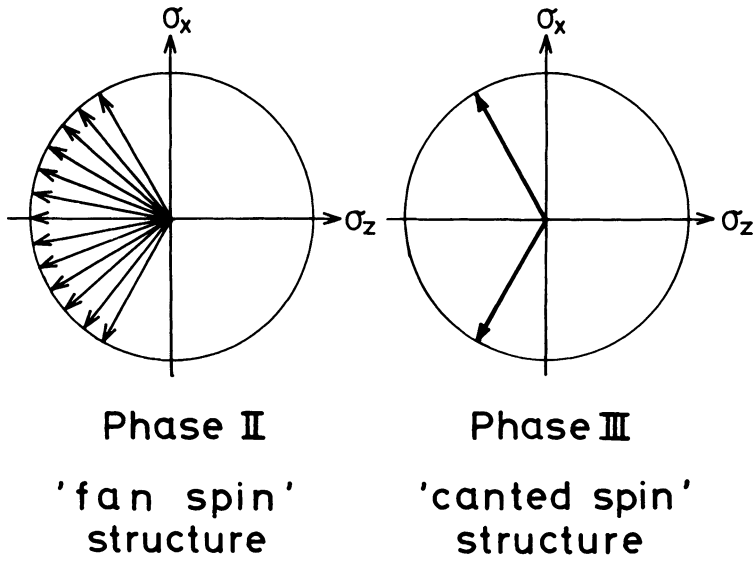
Fig. 4 Pseudospin descriptions of the low temperature phases.
Phase II : a fan spin structure. The spin direction (the
electronic state) in the σ^x-σ^z plane changes from site to site
sinusoidally leaving a tetragonal contraction ($<\sigma^z><0$) as the
average.
Phase III : a canted spin structure. In one sublattice, the
octahedron is elongated along the a-axis while in the other it is
elongated along the b-axis.

TABLE II

Symmetry property of the little group of k=$[\xi\xi 0]$ (Σ-line) of Fm3m.
The compatibility of the local Jahn-Teller mode with these
irreducible representations are also given in the third column.

$O_h^5(\Sigma)$=mm2		E	C_{2d}	m_z	m_d	local	phonon
A_1	Σ_1	1	1	1	1	Q_3	LA
A_2	Σ_3	1	1	-1	-1		
B_1	Σ_2	1	-1	1	-1	Q_2	TA_1
B_2	Σ_4	1	-1	-1	1		TA_2
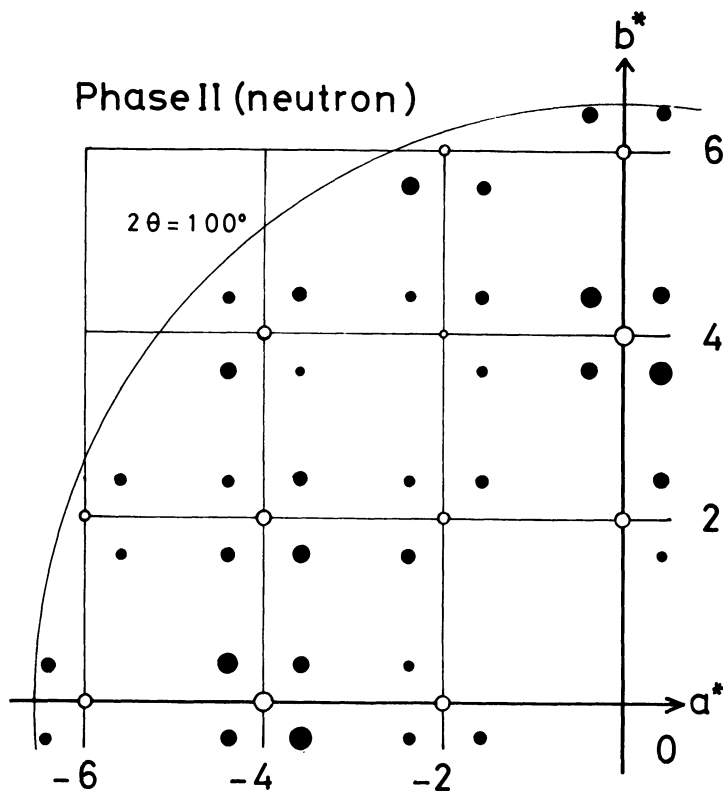
Fig. 5 The neutron diffraction pattern in (001) zone observed in Phase II. Many satellite reflections appeared around each fundamental reflections. Size of the solid circles roughly the observed intensity ratio between various satellites.

has shown that this is consistent with the observed intensity distribution of satellites.

It is worthwhile to point out that in terms of pseudospin description, this phase is expressed as a 'fan' spin structure. (See Fig. 4) In Phase II, it has the modulated local distortion of the Q_3-mode as well as the uniform distortion of the Q_2-mode. Therefore the orientation of the 'pseudospin' in the two dimensional σ^x-σ^z plane changes from site to site, which will result in the 'fan' spin structure. Such the structure has been studied in real spin system, and it is known that when a helical spin system is brought under the influence of external magnetic field perpendicular to the screw axis, this type structure is stabilized[15].
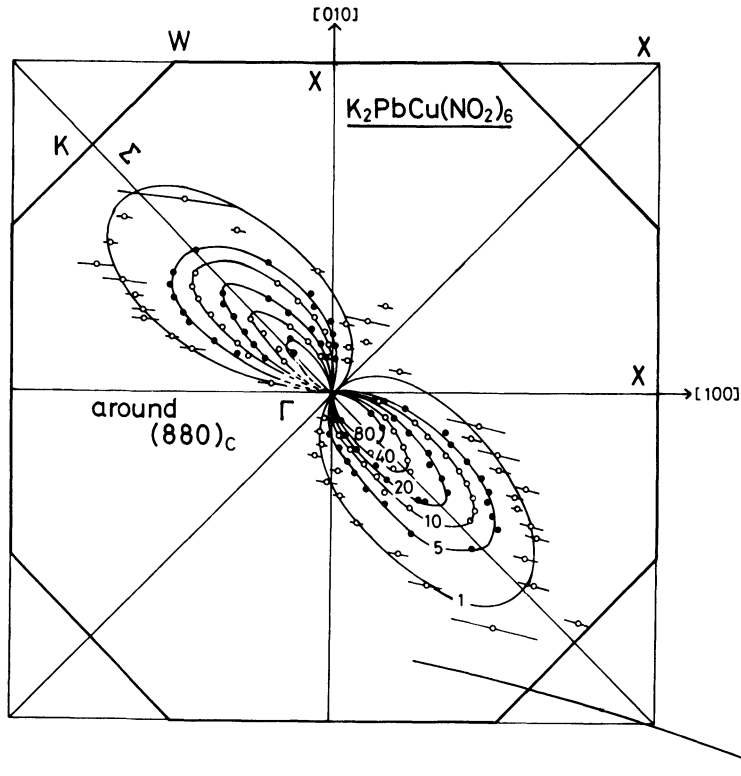
Fig. 6 Observed X-ray critical diffuse scattering around (880)$_c$
obtained in Phase I. Strong anisotropy at the Γ-point suggests
that the interaction between local distortions are of long range.

Later, we will discuss the correspondence between our 'fan
pseudospin' system and the fan structure in real spin systems.

From lattice dynamical point of view, this picture would imply
the softening of the TA$_1$ branch particularly at k≅[0.4, 0.4, 0]
avobe the transition temperature. We tried to observe softening
of TA$_1$ branch along k=[ξξ0]. However, we could not observe any
well defined TA$_1$-mode above the upper transition point. Instead,
as is often the case, strong quasielastic streaks were observed
running along the <110> directions. Fig. 6 shows the intensity
contours of observed X-ray diffuse scattering around (880)
reflection. Particularly we notice the characteristic 'pinching'
in the contour around Γ-point (the origin of the Brillouin zone).
This pattern is very similar to that observed in ferroelectric
substance such as KDP[16]. This correspondence is more than
accidental. It is known that when the interaction between local
distortions is via elastic strains, it falls off as 1/r^3, exactly

the same as electrostatic dipolar interaction. Such the long range forces, when Fouier transformed, always gives rise to the singlarity at the Γ-point. Therefore, we consider that the critical fluctuations is in fact mainly associated with the transverse acoustic mode.

II·5 Summary and Discussions

Summarizing, the successive phase transitions in $K_2PbCu(NO_2)_6$ have been studied by precise X-ray and neutron scattering measurements. The experimental results can be interpreted as sequencial cooperative Jahn-Teller phase transitions. In the intermediate phase, the local Jahn-Teller distortions are modulated with the wave vector $k_0=(0.42, 0.42, 0)$. In the lowest temperature phase, it has an antiferrodistortive phase where the axis of local tetragonal elongation alternates from site to site. From the structural view point the successive phase transitions in this crystal is characterized as normal→incommensurate→commensurate structural transitions which is accompanied by cubic→pseudo-tetragonal→pseudomonoclinic bulk distortion. On the other hand, the change of the electronic state of the Jahn-Teller active Cu^{2+} ion is characterized as para→fan→canted spin ordering.

The most conspicuous feature in the successive phase transitions of $K_2PbCu(NO_2)_6$ is the appearance of incommensurate phase where the local Jahn-Teller mode propagates with incommensurate wave vector k_0. It has been shown that in two dimensional Q_2-Q_3 plane, this structure corresponds to a 'fan structure' given in Fig. 4. It is known that in the magnetic system, this type of spin structure is realized when a helical spin system is brought into uniform magnetic field perpendicular to the screw axis. On the other hand, it is also well known that the 3d electronic state of Cu^{2+} ion in cubic crystalline field is completely described by Pauli spin operators, which is called 'pseudospins'. It would be interesting to look for formal correspondence between our 'pseudospin' system and real spin system and whence deduce the origin of stability of the 'fan pseudospin' structure by comparing with the real spins.

We begin with the well known Jahn-Teller hamiltonian,

$$H_{JT} = \sum_{\ell} g \ (\sigma_{\ell}^x Q_{2\ell} + \sigma_{\ell}^z Q_{3\ell}), \qquad (4)$$

where σ_{ℓ}^x and σ_{ℓ}^z are Pauli spin operators to describe 3d electronic state of Cu^{2+} ions at the ℓ'site. On Σ-line ($[\xi\xi 0]$ in the Brillouin zone, these local modes are compatible with phonon modes belonging to $B_1(\Sigma_3)$ and $A_1(\Sigma_1)$ irreducible representations. Therefore, these local modes are expanded with respect to phonon modes as follows:

$$H = \sum_{\ell} g_0 (\xi \sigma_{\ell}^{x} + \eta \sigma_{\ell}^{z})$$

$$+ \sum_{\ell} \sum_{k,\Sigma_3} \frac{g_{k,\Sigma_3}}{\sqrt{N}} (Q_{k,\Sigma_3} \sigma_{\ell}^{x} e^{ik \cdot r_{\ell}} + c.c.) \tag{5}$$

$$+ \sum_{\ell} \sum_{k,\Sigma_1} \frac{g_{k,\Sigma_1}}{\sqrt{N}} (Q_{k,\Sigma_1} \sigma_{\ell}^{z} e^{ik \cdot r_{\ell}} + c.c.)$$

where, we have included the coupling to uniform strains: $\xi = e_{xx} - e_{yy}$, $\eta = 2e_{zz} - e_{xx} - e_{yy}$. The importance of the role of strains has been pointed out by Kanamori[17] and Elliott et al[18]. Among these, we only retain the most important terms which become condensed in the low temperature phase to obtain

$$H = \sum_{\ell} g_0 (\sigma_0^{x} \xi + \sigma_{\ell}^{z} \eta)$$

$$+ \sum_{\ell} \frac{g_{k_0 2}}{\sqrt{N}} (Q_{k_0,TA_1} \sigma_{\ell}^{x} e^{ik_0 \cdot r_{\ell}} + c. c.) \tag{6}$$

$$+ \frac{g_{k_0 3}}{\sqrt{N}} (Q_{k_0 LA} \sigma_{\ell}^{z} e^{ik_0 r_{\ell}} + c. c.)$$

In the molecular field approximation, we may introduce the following effective 'pseudomagnetic fields'

$$H_0^{z} \equiv -g_0 \langle \eta \rangle \tag{7}$$

$$H_{k_0,\ell}^{x} \equiv -g_{k,TA_1} \langle Q_{k_0,TA_1} \rangle \cdot \cos k_0 \cdot r_{\ell} , \tag{8}$$

$$H_{k_0,\ell}^{z} \equiv -g_{k,LA} \langle Q_{k_0 LA} \rangle \cdot \sin k_0 \cdot r_{\ell} . \tag{8'}$$

H_0^{z} is a uniform 'pseudofield' while $H_{k_0 \ell}$ is a staggered pseudo-field modulated with wave vector k_0. Making use of these expressions we have

$$H_{JT} = -\sigma_{\ell}^{z} H_0^{z} - \sum_{\ell} (\sigma_{\ell}^{x} H_{k_0 \ell}^{x} + \sigma_{\ell}^{z} H_{k_0 \ell}^{z}) \tag{9}$$

which corresponds to the hamiltonian studied by Nagamiya[15] to investigate fan structure in the real spin system, where H_0^{z} and $H_{k_0 \ell}$ mean uniform external magnetic field and the staggered exchange field. The only difference is that in Eq. (9), H_0^{z} stands for the spontaneous strain, not the applied field. To make this point consistent, we should introduce a higher order anharmonic interaction :

$$H_{anh} = A \sum_{\ell} Q_{k_0 TA_1} Q_{-k_0 TA_1} \cdot \sigma_{\ell}^{z} . \tag{10}$$

By the suitable choice of parameters g_0, g_{k_0}, and A, we should be able to obtain the self consistent solution to stabilize the fan pseudospin structure.

III. ZEROTH GRADE ORDERING IN Fe_3O_4

III·1 Introduction

The 123 K phase transition of magnetite is one of the 'time honored' problems which has been the subject of extensive studies since Verwey[19] proposed the existance of 'charge ordering' below the transition in 1941. The 'charge order' means that the total charge integrated around each particular site alternates from site to site. Thus, in the framework given in §1, this falls into the case of 0'th grade ordering.

The crystal structure of Fe_3O_4 in the high temperature phase is so called 'inverse spinel' type. The tetrahedrally coordinated A-sites are solely occupied by Fe^{3+} ions, while the octahedral B-sites accomodate Fe^{2+} ions and the remaining Fe^{3+} ions at random with equal probability. Large electrical conductivity of this substance at room temperature is considered to be due to hopping of d-electrons within the disordered B-sites. It is this disorder that causes the 123 K phase transition.

The important characteristic of the 123 K phase transition is that the electrical conductivity decreases by factor of 10^{-2} at the transition.[20] Based on this fact, Verwey proposed the ordering of charges within the octahedral site below the transition temperature which eliminates the disorder of Fe^{2+} and Fe^{3+}, whence explains the drastic decrease of the conductivity. The 'frozen' charge ordering scheme proposed by Verwey is explained in Fig. 7. In this ordering, the unit cell remains unchanged.

However, recent observations on this phase transition by electron diffraction[21], neutron diffraction[22], Mössbauer effect[23,24] and magnetic resonance[24,25] have casted doubt on the validity of the Verwey type charge ordering scheme. The details of historic aspects of the experimental progress have been discussed in the seperate lecture.[26]

As is illustrated in there, the electron diffraction pattern[21] exhibits some super structure lines indicating that the unit cell in the low temperature phase is doubled along the cubic principal axes. Moreover the neutron diffraction experiments[22] have shown that the doubling of the unit cell is mainly caused by small displacements of atoms. This strongly suggests that some **internal** lattice mode is associated with this phase transition.
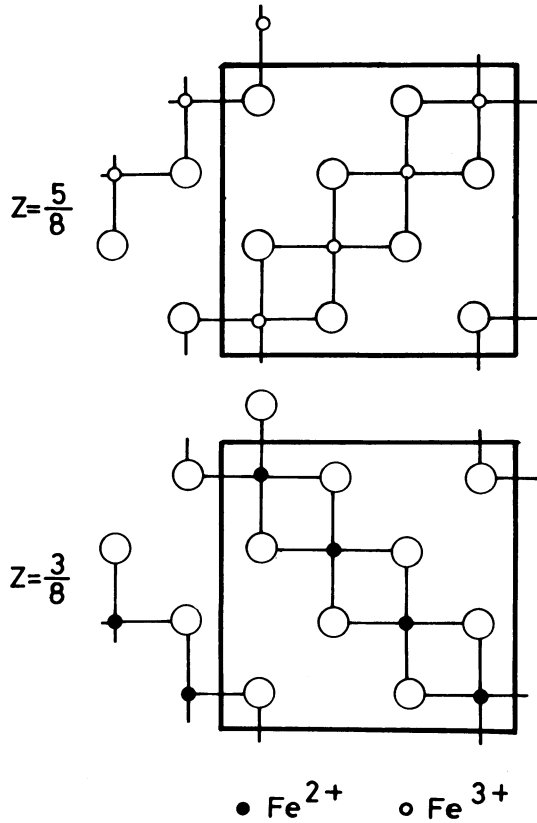
Fig. 7. The charge ordering scheme proposed by Verwey[1]. Two atomic planes occupied by Fe^{2+} and Fe^3 alternates successively along the z-direction. Cubic unit cell is not doubled in this ordering scheme.

When combined with the existence of the charge ordering below T_v, the phase transition temperature, these considerations naturally lead to the assumption that the interaction between electrons and phonons is playing the crucial role in this phase transition. The important implication of the above assumption is that the charge density fluctuation which is coupled to the unstable phonon mode is also an 'internal' mode modulated by the same wave length (twice the cubic unit cell length).

In the following, we try to understand the 123 K transition in Fe_3O_4 on the basis that this phase transition is viewed as the instability of a coupled charge density-phonon mode driven by the

coupling between local electrons and phonons?[27]

III·2 Symmetry Property of The Phonon Field and The Charge Density Field

The observed neutron critical scattering has shown strong peaks at (H, 0, L±1/2] reciprocal lattice points accompanied by ridge-like streaks running along [001] direction[28]. This suggests that the relevant phonon modes which become unstable at the phase transition have the wave vector $k=(00\xi)$ (specified as Δ-points in the reciprocal space). Especially, the mode with $k=(00\ 1/2)$ will become condensed in the low temperature phase as is confirmed by the electron diffraction and the neutron diffraction measurements. Therefore we begin with examining the symmetry property of the phonon field as well as the charge density field at Δ-points in the cubic reciprocal space.

Phonon Field

The little group of $k=(00\xi)$ of space group O_h^7 has five irreducible representations denoted by Δ_1, Δ_2, Δ_3, Δ_4, and Δ_5. Among these, Δ_5 is a two dimensional representation and the others are all one dimensional, Δ_1 being the identity representation. The 42 phonon branches are characterized by the following symmetry properties,

$$\Delta = 7\Delta_1 + 3\Delta_2 + 7\Delta_3 + 3\Delta_4 + 11\Delta_5. \tag{11}$$

Among these phonon branches, the Δ_5-modes are particularly important for the later discussions. It should be pointed out that all the singlet modes share the common feature in the pattern of displacement in that the atom pair which is related by two fold axis along [001] moves out of phase, while in the Δ_5-mode, they move in phase as is seen in Fig, 8. It should be also mentioned that for an arbitrary value of $k=(00\xi)$, the atomic displacement is modulated along [001] direction with the corresponding wave length a/ξ. Thus, for the particular case of $k=(00\ 1/2)$, the wavelength is twice the cubic unit cell dimension along the c-axis.

Charge Density Field

The electrons which are associated with the 123 K phase transition are a pair of excess 3d-electrons coming from two Fe^{2+} ions per primitive cell located at octahedral sites. Since the magnetic ordering has been attained at this temperature, the spin degeneracy is already lifted. Therefore, there are four orbitals per primitive cell to accommodate these two electrons.

As for the electronic states of these electrons above T_V, there are evidences[29,30,31] that these electrons are localized at
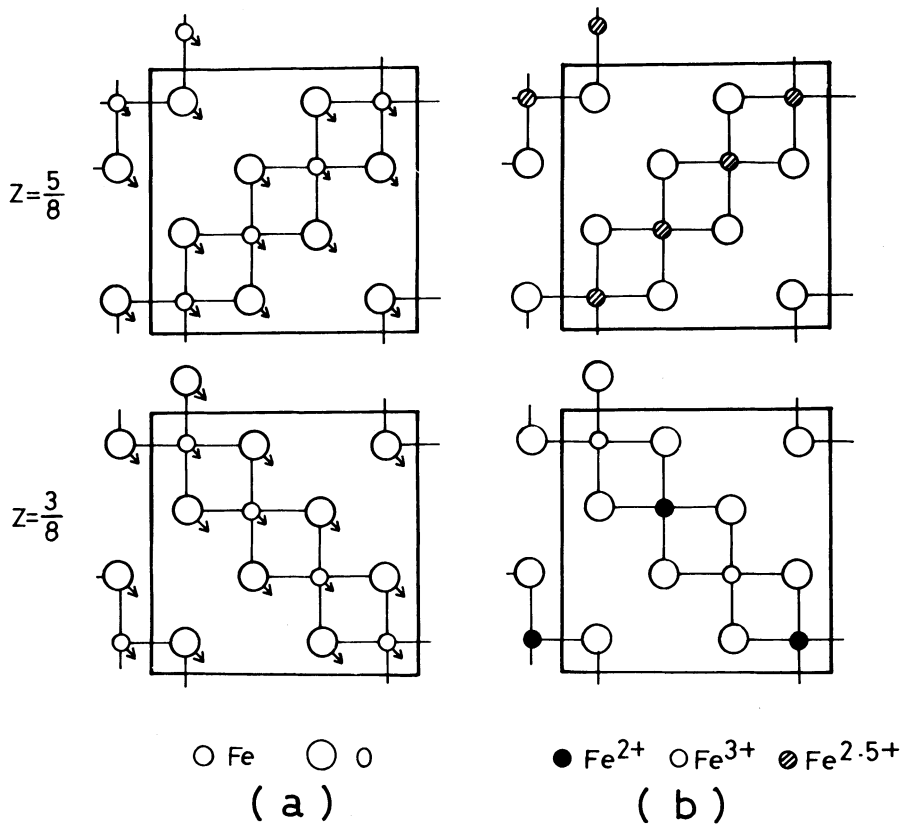
Fig. 8. Schematic discription of the displacement pattern as well
as the charge density pattern with the symmetry Δ_5^1. This pattern is
modulated along the z-axis with an arbitrary wave vector.

each site rather than forming bands, thus giving rise to a hopping disorder in charge density at the octahedral sites. We take this standpoint and consider the symmetry property of the localized charge density fluctuations. First we assume the condition of local charge neutrality within the unit cell (Anderson's condition)[32] is satisfied. We have then six configurations of two electrons in the unit cell as is given in Fig. 9. The pattern of charge density waves with an arbitrary wave vector k is obtained by multiplying the phase factor $e^{ik \cdot r_i}$. We are especially interested in the modes with k=[00ξ]. Along this particular line, the allowed charge density patterns are further limited[33] to cases (c)~(f) in Fig. 9.

We may define the charge density fluctuation operator as follows:

$$\delta\rho = c_m^+ c_m - 1/2 \qquad m = 1, 2, 3, 4 \qquad (12)$$

where $c_m^+ c_m$ is the number operator of the 3d electron localized at m'th site in the unit cell. The relevant two electron states (c)~(f) in Fig. 9, will be given by: $|1010\rangle$, $|1001\rangle$, $|0110\rangle$ and $|0101\rangle$, in terms of the eigen functions for these number operators as is illustrated in Fig. 9. We then symmetrize this charge density fluctuation field (a scaler field), so that the pattern of the charge density with wave vector k will belong to one of the irreducible representations of the same little group Δ as phonons does.

It is shown that we can construct the following symmetrized 'charge density modes'

$$\delta\rho(\Delta_1) = \delta\rho_1 + \delta\rho_2 + \delta\rho_3 + \delta\rho_4 - 2$$
$$\delta\rho(\Delta_4) = \delta\rho_1 + \delta\rho_2 - (\delta\rho_3 + \delta\rho_4)$$
$$\delta\rho(\Delta_5^1) = \delta\rho_1 - \delta\rho_2 \qquad\qquad (13)$$
$$\delta\rho(\Delta_5^2) = \delta\rho_3 - \delta\rho_4$$

Among these, only the Δ_5-modes have non-zero eigenvalues when operated on the above defined four eigenstates. By taking these four eigenfunctions as basis vectors, we have

$$\delta\rho(\Delta_5^1) = \begin{pmatrix} 1 & 0 & 0 & 0 \\ 0 & 1 & 0 & 0 \\ 0 & 0 & -1 & 0 \\ 0 & 0 & 0 & -1 \end{pmatrix} \equiv \sigma^z(\Delta_5^1) \qquad (14)$$

$$\delta\rho(\Delta_5^2) = \begin{pmatrix} 1 & 0 & 0 & 0 \\ 0 & -1 & 0 & 0 \\ 0 & 0 & 1 & 0 \\ 0 & 0 & 0 & -1 \end{pmatrix} \equiv \sigma^z(\Delta_5^2) \qquad (15)$$

Namely, we have deduced (4-dimensional) pseudospin representations
to express charge density fluctuation field.

It is worthwhile to point out that as $k \to 0$, the Δ_4-and the
Δ_5-modes become degenerate to form Γ_{25} (triplly degenerate) mode,
and the charge density pattern proposed by Verwey is exactly one
of these triplly degenerate modes. It should be also noted that in
the case of the Δ_5-mode condensation, there is a particular
complication involved. Since the Δ_5 is doublly degenerate any
linear combination of these two modes is equally stable. In order
to eliminate this ambiguity, we have to take into account the
higher order interaction.

III·3 Pseudospin-phonon Formalism and Neutron Scattering Cross
Sections

We assume that the bilinear coupling between the phonon field
and the charge density field is important to trigger the phase
transition. The interaction hamiltonian is then generally given
by

$$H_{int} = \sum_{\ell,m} \sum_{\ell'm'\alpha} g^{\alpha}_{\ell m \ell'm'} \delta\rho_{\ell m} u^{\alpha}_{\ell'm'} \; , \quad \alpha=x, y, z, \qquad (16)$$

where $u^{\alpha}_{\ell'm}$ is the α-component of the displacement vector at site
$(\ell'm')$.
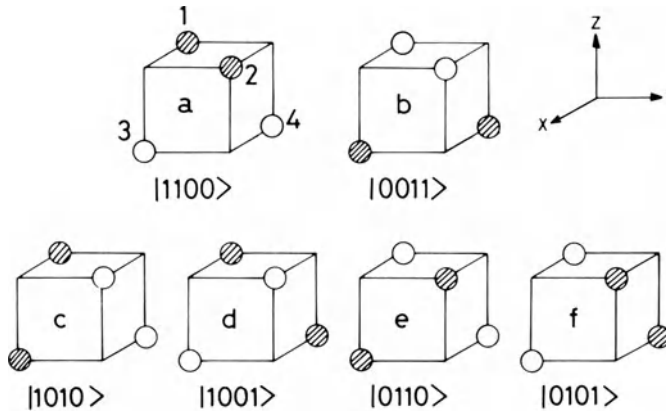
Fig. 9. Possible charge configurations satisfying the local charge
neutrality condition. The state vectors corresponding to each
configuration are given below each cubes.

Making use of the pseudospin representations of the charge density operator, we rewrite the above expression into the familiar pseudospin-phonon formalism,

$$H_{int} = \sum_k \zeta_{(k,\Delta_5)} \{\sigma^z_{(k,\Delta_5^1)} Q_{(k,\Delta_5^1)} + \sigma_{(k,\Delta_5^2)} Q_{(k,\Delta_5^2)}\} \quad (17)$$

Here,

$$\sigma^z_{(k,\Delta_5^1)} = \frac{1}{\sqrt{N}} \sum_\ell \sigma^z_{\ell(\Delta_5^1)} e^{ik\cdot r\ell} \quad . \quad (18)$$

The general property of such the coupled system has been discussed extensively elsewhere. Namely, by a suitable choice of the coupling parameter, the system undergoes the phase transition, below which the ordering of 'pseudospins' (the charge density) and the condensation of the phonon take place at the same time. It is predicted that the symmetry of both charge density mode and the phonon mode should belong Δ_5-type. In particular the pattern of the charge density below T_v should be as given in Fig. 8.

Let us consider the experiments to verify the above model. The neutron scattering cross sections at $T \lesssim T_v$ is particularly interesting from the following reason. As has been stated, the spin degeneracy is already lifted in the temperature region in question. Hence, the charge density ordering is always accompanied by the same ordering of magnetic spin density distribution. Therefore, both the atomic displacement and the charge ordering are detectable by neutrons as nuclear and magnetic scattering respectively. These scattering cross sections are expressed as

$$\frac{d^2\sigma}{d\Omega d\omega}\bigg|_{nuc} = NkT \sum |F^s_d(k)|^2 \phi^s_{QQ}(k,\omega) \quad , \quad (19)$$

$$\frac{d^2\sigma}{d\Omega d\omega}\bigg|_{mag} = N \left(\frac{e^2\gamma}{mc}\right)^2 \sum_s |F^s_m(k)|^2 \phi_{\sigma\sigma}(k,\omega) \quad . \quad (20)$$

Here, ϕ^s_{QQ} and $\phi_{\sigma\sigma}$ stand for the spectral densities of the correlation functions of phonons and pseudospins;

$$\phi^s_{QQ}(k,\omega) = \int <Q_{(k, s, o)} Q_{(k, s, t)}> e^{i\omega t} dt \quad (21)$$

$$\phi^s_{\sigma\sigma}(k,\omega) = \int <\sigma^z_{(k, s, 0)} \sigma^z_{(k, s, t)}> e^{i\omega t} dt \quad (22)$$

Below T_v, these simply give $\sum_{kn} \delta(k-k_h \pm k_0) \delta(\omega)$. $F^s_d(k)$ and $F^s_m(k)$ are the structure factors due to nuclear displacements and charge (magnetic spin) distributions belonging to the symmetry s respectively. They are explicitly given by

$$F_d^S(k) = \sum_j \frac{b_j e^{-W_j}}{\sqrt{M_j}} (k \cdot e_{k,s}^j) \ e^{ik \cdot r_j} \tag{23}$$

where b_m is the neutron scattering amplitude, M_m the mass and $e_{(k,s)}^m$ is the polarization vector of the m'th atom. And

$$F_m^S(k) = \sum_{j'} S_m^S \ f_{(k)} e^{ik \cdot r_{j'}} \tag{24}$$

where S_m^S is the magnetic moment of Fe^{2+} ion perpendicular to k, $f(k)$ is the magnetic form factor.

Therefore, in principle, we can determine, by analizing the intensity distribution of the super lattice reflections, what is the pattern of the charge ordering as well as that of the atomic displacements in the actual crystal.

III·4 Summary

(1) We have seen that in Fe_3O_4, a charge ordering and lattice distortion take place at the same time. The atomic displacement field as seen by neutron scattering is associated with the phonon mode at the middle of the Σ-line (K=00 1/2) , not the uniform (zone center) mode.

(2) Assuming electron-phonon coupling scheme similar to polaron (namely linear coupling between charge density and local atomic displacement) , the effective interaction hamiltonian is formally reduced to pseudospin-phonon coupling, whose property is extensively investigated.

(3) Starting from this hamiltonian, we have predicted a possible charge ordering pattern, the Δ_5-type ordering.

(4) It has been also pointed out that in order to investigate such the coupled charge-displacement field, neutron scattering technique is particularly powerful, because neutron wave can 'sense' atomic displacements through nuclear interaction, and charge density (magnetic spin density) through magnetic interaction.

The detailes of the experimental results recently performed on this material will be discussed by Shirane in the separate lecture[26].

References

[1] Stinchcomb, this conference
[2] H. Thomas, this conference
     The relevant references are sited in the above lectures
[3] B. V. Harrowfield and R. Weber, Phys. Lett. 38A, 27 (1972).
[4] B. V. Harrowfield, A. J. Dempster, T. E. Freeman and
    J. R. Pilbrrow, J. Phys. C. 6, 2058 (1973).
[5] D. Reinen, C. Friebel and K. P. Reetz, J. Solid State Chem. 4
    103 (1972).
[6] D. Mullen, G. Heger and D. Reinen, Solid State Comm. 17 1249.
    (1975)
[7] S. Takagi and M. D. Joesten, Acta Cryst B31, 1968 (1975) :
    The prototype structure is seen in the crystals containing
    Jahn-Teller inactive complex such as $K_2PbNi(NO_2)_6$.
[8] M. D. Sturge, Solid State Physics, 20, 91 (1967). Ed.
    F. Seitz, D. Turn bull H. Ehrenreich Academic Press, New York.
[9] S. Takagi, P. G. Lemhert and M. D. Joesten, J. Am. Chem. Soc.
    96' 21, 6606 (1974).
[10] C. Friebel, Z. anorg. allg. Chem. 417, 197 (1975).
[11] Y. Noda, M. Mori and Y. Yamada, Solid State Commun. 19, 1071
     (1976).
[12] Y. Noda, M. Mori and Y. Yamada, to be published in Solid
     State Commun.
[13] D. Reinen, Solid State Commun. 21, 137 (1977).
[14] B. V. Harrowfield, Solid State Commun. 19, 983 (1976).
[15] T. Nagamiya, Solid State Physics 20, 306 (1967)
     edited by F. Seitz, D. Turnbull and H. Ehrenreich
     Academic Press, New York
[16] J. Skalyo Jr., B. C. Frazer and G. Shirane, Phys, Rev. B1, 278
     (1970).
[17] J. Kanamori, J. appl. Phys. Suppl. 31, 14 (1960),
[18] R. J. Elliott, R. T. Harley, W. Hayes and S. R. P. Smith,
     Proc. Roy. Soc. A328, 217 (1972).
[19] E. J. W. Verwey and P. W. Haayman, Physica 8, 979 (1941).
     E. J. W. Verwey, P. W. Haayman and N. C. Romeijin,
     J. Chem. Phys. 15. 181 (1947).
[20] S. Chikazumi, AIP Proc. 29, 382 (1976).
[21] T. Yamada, K. Suzuki and S. Chikazumi, Appl. Phys. Lett. 13,
     172 (1968).
[22] J. Samuelson, E. J. Bleeker, L. Dobrzynski, and T. Riste,
     J. Appl. Phys. 39, 1114 (1968).
[23] R. S. Hargrove and W. Kundig, Solid State Commun. 8, 303 (1970)
[24] M. Rubinstein and D. W. Forester, Solid State Commun. 9, 1675
     (1971).
[25] M. Rubinstein, G. H. Strauss and F. J. Bruni, AIP. Conf. Proc.
     No.10, 1384 (1972).
[26] G. Shirane, this conference
[27] Y. Yamada, AIP. Conf. Proc. No. 24, 79 (1975).
[28] Y. Fujii, G. Shirane and Y. Yamada, Phys. Rev. B11 2036 (1975).

[29] W. Kündig and R. S. Hargrove, Solid State Commun. 7, 223
     (1969).
[30] A. A. Samokhvalov, N. M. Tutikov and G. P. Skovnyakov
     Soviet Phys, Solid State 10, 2172 (1969).
[31] D. L. Camphausen, Solid State Commun. 11, 99 (1972).
[32] P. W. Anderson, Phys. Rev. 102, 1008 (1956)
[33] T. Matsuura and A. Yoshimori, Prog. Theor. Phys. 36, 679
     (1966).

THE VERWEY TRANSITION IN MAGNETITE[*]

G. Shirane

Brookhaven National Laboratory

Upton, New York 11973 U. S. A.

We will first review the characteristics of the Verwey transition in magnetite at 123 K. An ordering takes place among Fe^{2+} and Fe^{3+} ions on the octahedral sites of the inverse spinel structure, accompanied by a sudden change of electrical resistivity. We shall discuss in some detail recent neutron scattering measurements at Brookhaven in collaboration with Chikazumi's group at the University of Tokyo.

I. INTRODUCTION

The Verwey transition in magnetite is one of the oldest problems in magnetism as well as in phase transitions.[1] We shall review a part of this complex problem from the viewpoint of electron-phonon interactions, the topic of this conference. In the first lecture, we shall survey the historical background up to 1973. The second lecture concerns recent neutron scattering experiments carried out at Brookhaven in collaboration with Professor Chikazumi's group at the University of Tokyo.

Let us start by discussing the major characteristics of this phase transition at 123 K. At higher temperatures, magnetite has the inverse spinel structure, a structure which many technically important magnetic materials possess. The unit cell contains 8 Fe_3O_4 units, 8 Fe^{3+} on the tetrahedral sites and the random distribution of 8 Fe^{2+} and 8 Fe^{3+} ions on the octahedral sites. A

very pronounced phase transition has been observed around T_V=123 K.
The most dramatic anomaly is in resistivity, as shown in the most
recent data (Fig. 1) in Chikazumi's review article.[2] It has a
high conductivity for T>T_V, but it becomes a reasonably good
insulator below T_V.

Verwey[1] proposed a model, thirty years ago, that this phase
transition is caused by an electronic charge ordering among the
Fe^{2+} and Fe^{3+} ions on the octahedral sites. This ordering scheme
is shown in Fig. 2 together with the concomitant orthorhombic sym-
metry. This is a very simple and attractive model which implies
that alternate layers (or strings) of Fe^{2+} and Fe^{3+} are stacked
along the c axis. Subsequent magnetic[3], dilatometric, and x-ray[4]
measurements all appeared to support the orthorhombic symmetry
required by the Verwey model. Then in 1958, Hamilton[5] presented
the most convincing evidence in his celebrated neutron scattering
paper.A magnetic cross section was observed at (002) below T_V
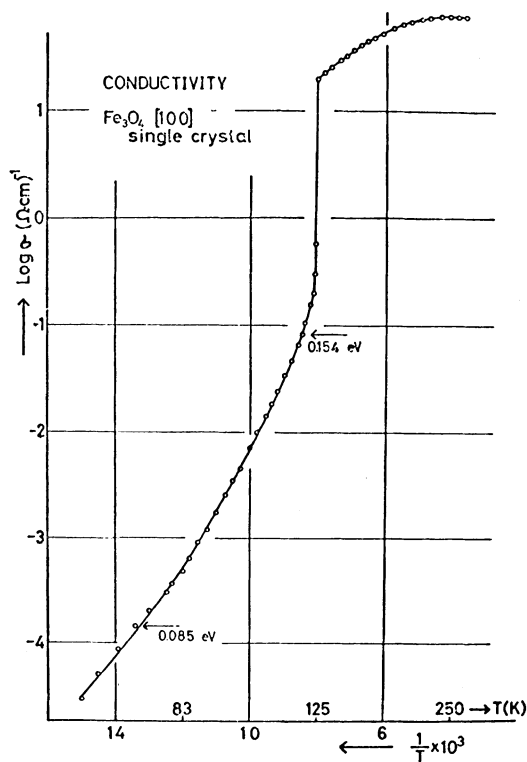
Fig. 1. Temperature dependence of conductivity for Fe_3O_4 along
the cubic [100]. (Ref. 2).
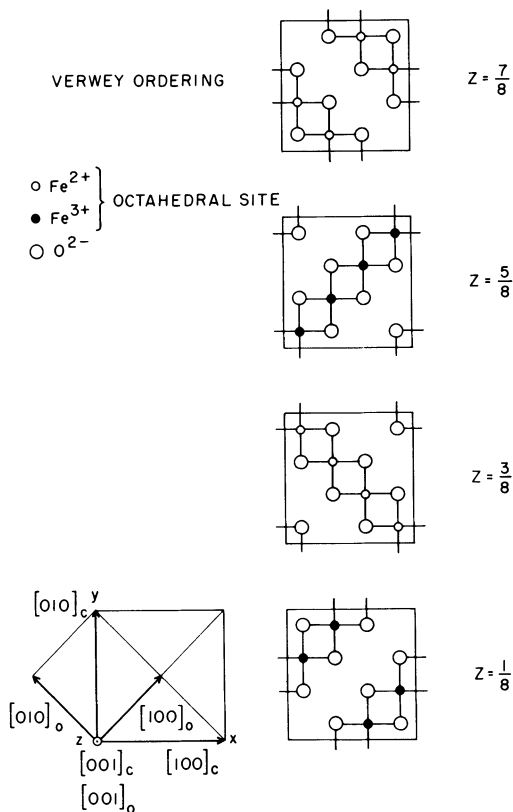
Fig. 2. The Verwey ordering scheme together with the resulting
orthorhombic symmetry.

where none is allowed above T_V. At that point, the problem appeared
to be completely solved.

Since then, many new experimental results have been reported
which indicate that some basic modification is needed to the ori-
ginal Verwey model. The most important discovery was reported
by Samuelsen et al[6] in 1968. In their neutron diffraction experi-
ment below T_V, they observed satellites at reciprocal-lattice
points with half integer such as (4 0 ½). This study, as well as
independent electron diffraction work by Yamada et al[7] both re-
ported that such satellites appear only along the orthorhombic c
axis. In particular, Samuelsen et al noted that the satellite in-
tensities are proportional to Q^2, where $\vec{Q}$ is a reciprocal lattice

vector. Based on this fact they concluded that the satellites result mainly from atomic displacements and they are not directly due to the magnetic ordering of Fe^{2+} and Fe^{3+}. Other experiments such as NMR and Mössbauer measurements showed the existence of more than two nonequivalent octahedral sites below T_V. There was other experimental evidence to indicate that the low temperature symmetry is lower than orthorhombic.

II. CRYSTAL AND SYMMETRY

Let us now examine more closely the crystallographic aspect of this problem. Figs. 3 and 4 are taken from Chikazumi's review article[2] and demonstrate the crystallographic notation used in this talk. The unit cell below T_V has a nearly rhombohedral shape as shown in Fig. 4, though the true symmetry is monoclinic or lower. We may use two types of cell description: (A) Pseudo-rhombohedral cell with [001] axis as the unique magnetic c axis and [110] axis as the monoclinic b axis. In this, $\alpha = 90° - 0.16°$. (B) Pseudomonoclinic cell with the common c axis with the rhombo-hedral cell.

There are two types of twins: i) c axis zig-zag (c* common) as shown in Fig. 3 and ii) monoclinic a and b axes rotated. One can view these domains as 4 different <111> directions of the rhombohedral cell. These twinnings have caused considerable dif-ficulty and confusion in the interpretation of experimental re-sults. A truly untwinned crystal has been obtained recently by Chikazumi's group by a combined field cooling and a squeezing operation.[2,8] It has been known for some time that the magnetic
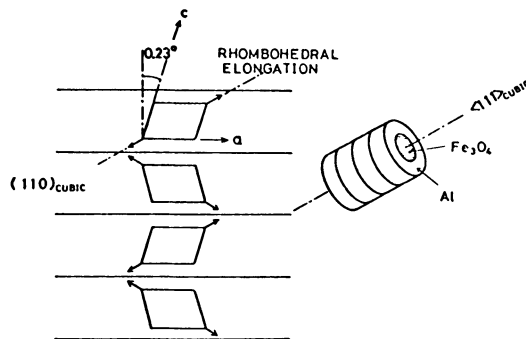
Fig. 3. Twinning of Fe_3O_4 and the squeezing technique to create an untwinned crystal. (Refs. 2 and 8).
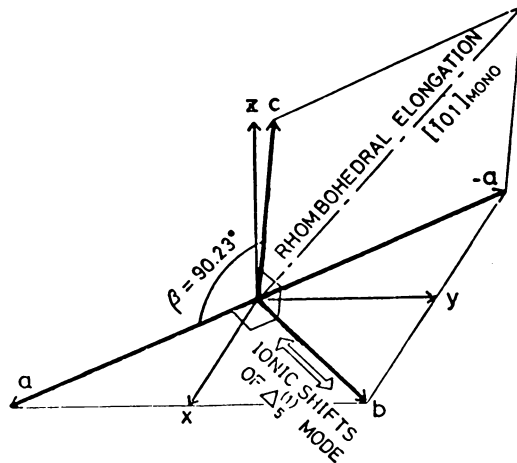
Fig. 4. Low temperature unit cell of magnetite. abc refers to
the monoclinic axes. (Ref. 2).

c axis can be aligned by an <100> magnetic field through T_V. If
one puts tight aluminum rings aroung the <111> axis, then this
particular rhombohedral elongation will be established. For neu-
tron scattering purposes, a cylindrical crystal (3mm in diameter
and 6mm in length) was successfully made into a 99% untwinned
crystal.

There is an additional advantage to these squeezed crystals.
In order to separate out magnetic components from nuclear scatter-
ing,one has to apply a magnetic field below T_V. In a field cooled
crystal (without squeezing) the c axis tends to follow the field
direction. The desired experimental condition is to reorient the
spin direction without changing the c axis. This is realized in
the squeezed monocrystal and thus we can experimentally separate
out small magnetic components.

The rhombohedral cell shape was properly identified by early
x-ray studies[9] but was disregarded in favor of the orthorhombic
assignment by the single crystal studies.[4] More recent x-ray[10]
as well as neutron diffraction studies[11,12] have now clearly es-
tablished the rhombohedral cell shape.

A series of neutron scattering experiments have been carried

out as a joint project between the University of Tokyo and Brook-
haven. In the following we shall discuss in some detail the re-
sults of these measurements.

III. CRITICAL SCATTERING

When our neutron scattering work was initiated, the c-axis
doubling was already established. We, however, assumed that the
basic magnetic ordering was already firmly established by
Hamilton's neutron experiment. It appeared that the transition
is accompanied by atomic displacements as clearly established by
Samuelsen et al.[6] The key experiment was to look for critical
scattering at both reflections, the (40½) type due to atomic dis-
placements and the magnetic (002) reflection. This could give us
a clue to the true order parameter of this complex phase tran-
sition. As we will see later, the (002) reflection has been
absent at all temperatures! But this is the story after.

One crystallographic piece of information. The space group
above T_V is Fd3m; reflections such as (200), (600), and (420) are
missing because of space group requirements. The Verwey ordering
scheme requires (002) type magnetic reflections appear as one can
easily see in Fig. 2.

Fig. 5 depicts a typical example of critical scattering re-
ported by Fujii et al.[13] The sharp increase of the (40½) type
reflection is limited to a narrow temperature range above T_V. It
shows the typical divergence toward T_c, which is a few degrees
below T_V (see Fig. 10). The critical scattering was measured at
several Brillouin zones and shown, in general, to be quite similar
to those of the satellite below T_V.

Yamada[14] proposed a model to explain this critical scatter-
ing based upon an electron phonon coupling. This model involves
the Δ_5 phonon mode as shown in Fig. 6. Ionic shifts of oxygen and
Fe ions are such that they give a larger space for Fe^{2+} ions and
a smaller space for Fe^{3+}. The most important result of the Yamada
model is the charge ordering scheme which differs from that pre-
dicted by the Verwey model. The Fe^{3+} ions are not forming chains
in c planes but both Fe^{2+} and Fe^{3+} form alternate chains as shown
in Fig. 6. Since the Yamada model modulates a charge density wave
along the c axis, it creates grey (disordered) layers as well.

There is a unique and simple prediction of the Yamada model
for the magnetic cross section due to the spin ordering below T_V.
The (002) type should be missing and the (20½) type reflection
should show the main magnetic scattering. This prediction, how-
ever, is only partially fulfilled. Before discussing the low
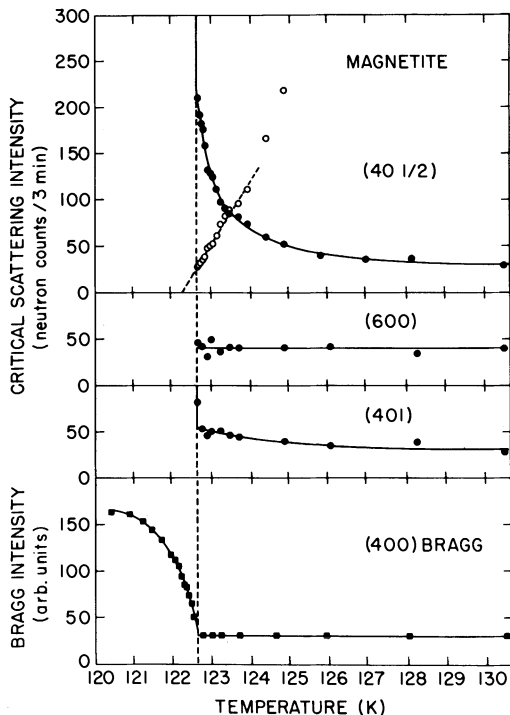
Fig. 5.   Critical scattering just above T_V.   Open circles for
$(40\frac{1}{2})$ is T/I.   (Ref. 13).

temperature study, we describe an __additional__ type of diffuse
scattering which is widely distributed in q space over a large
temperature range, as shown in Fig. 7 and 8.   This type of dif-
fuse streak was first recognized by Chiba et al[15] in their elec-
tron diffraction study.   A detailed study was carried out by
Shapiro et al[16] on a large magnetite crystal.   Somewhat surprising-
ly, this scattering showed one-dimensional nature along the <001>
direction.   It shows a gradual temperature dependence (Fig. 9)
with extrapolated divergence at 106 K.

At present, we can offer only a qualitative picture for this
diffuse scattering and its relation to the sharp critical peak
described above.   A major feature of the profile can be explained
by an elongated correlation range based upon the Yamada model.
The shape of the elliptical cross section is determined by the
shape of the 1-D "clusters."   This correlation grows with little
change of shape for wide temperature range (see Fig. 10).   Only at
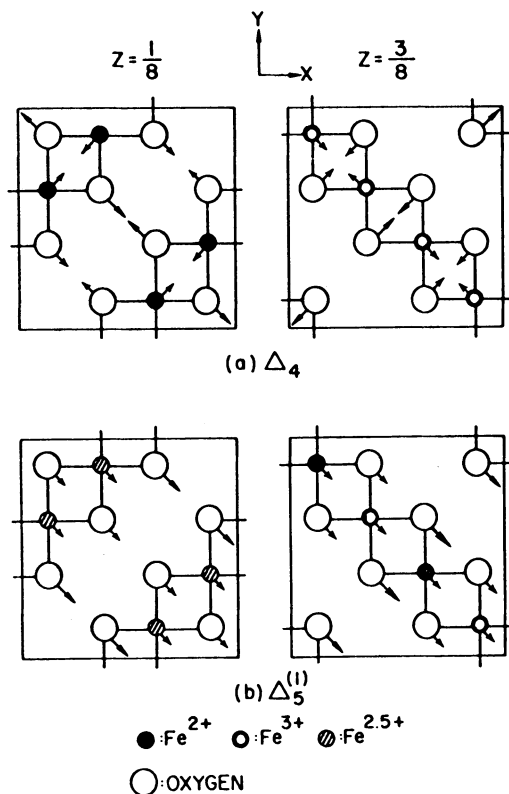
Fig. 6. The Yamada model based upon the Δ_5 phonon mode. Δ_4 corresponds to the Verwey model. (Ref. 14).

a few degrees above T_V, the 3-D critical scattering sets in, peaking at positions corresponding to low temperature satellites. The latter behavior is shown for $(40\frac{1}{2})$ by the steep broken line in Fig. 10.

IV.   STRUCTURE BELOW T_V

It is essential to have a reliable knowledge of the low temperature structure to establish the charge ordering scheme in magnetite. As it turned out, this is a difficult and complex problem. Moreover, there is one important aspect of the analysis we did not fully appreciate at the outset.[12] In ordinary magnetic structure determination, one uses the magnetic structure factor
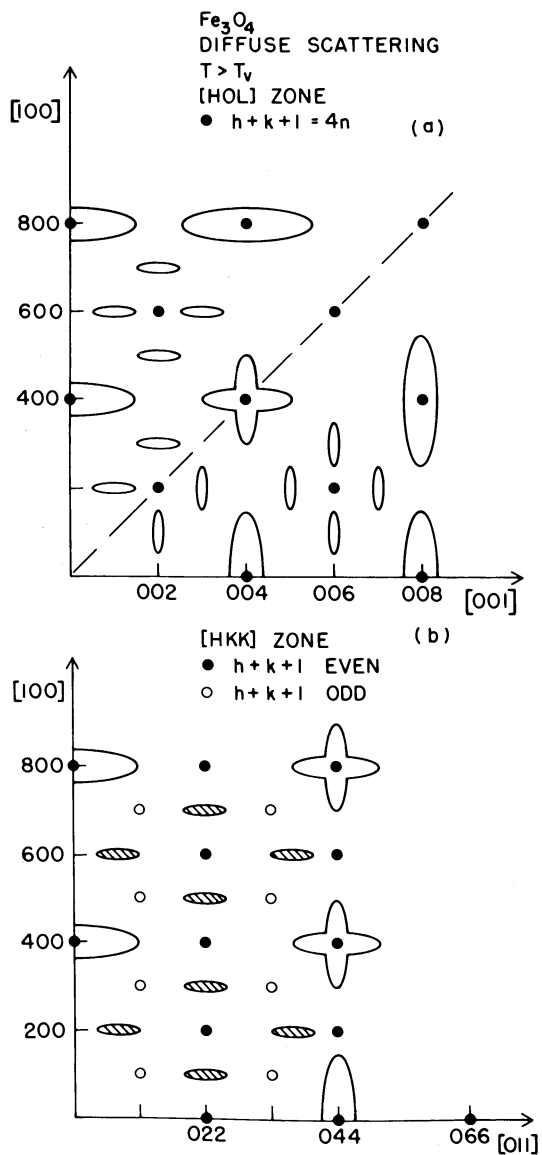
Fig. 7. Intensity distribution of diffuse scattering in two different zones. (Ref. 16).

Fig. 9. Temperature dependence of diffuse scattering in Fe$_3$O$_4$. (Ref. 16).
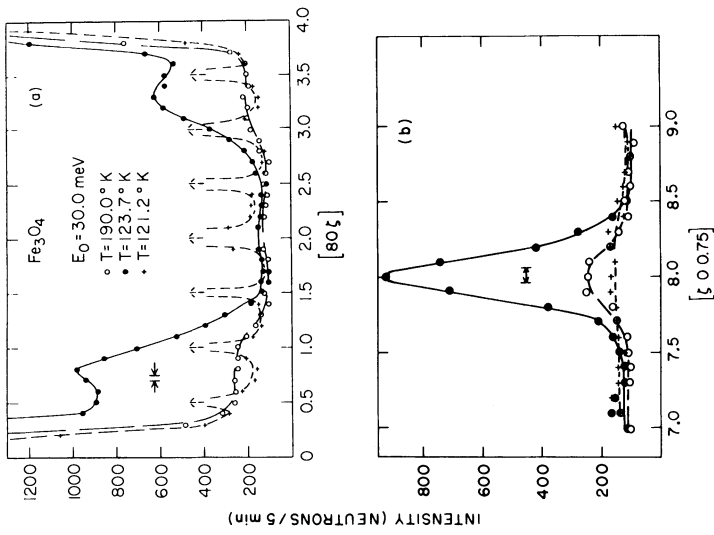
Fig. 8. Cross sections of diffuse streak shown in Fig. 7. (Ref. 16). Broad peaks around $\zeta = 0.75$ and 3.25 result from 1-D correlation.

$$F_M = \sum_j \Delta P_j \, e^{i(\vec{Q}\cdot\vec{r}_j)} \tag{1}$$

where $Q = a*h + b*k + c*\ell$, and $\vec{r}_j$ atomic position and ΔP_j is due to magnetic modulation, namely $\pm 0.5\mu_B$ for the difference between the Fe^{2+} and Fe^{3+} magnetic moments. Usually we can use the cubic parameter $\vec{r}_j$ and neglect the higher order effect of atomic shift Δ_j at T_V.

For magnetite we have to use a more complete formula. This originates from the unusual situation that the spin modulation ΔP_j is superposed on a much larger average component $\bar{P}$, corresponding to $4.5\mu_B$. Now (1) becomes

$$F_M = \sum_j (\bar{P} + \Delta P_j) \, e^{i\vec{Q}\cdot(\vec{r}_j + \vec{\Delta}_j)} \tag{2}$$

Expanding in Δ_j we obtain

$$F(Q) \cong \sum_j \bar{P} \, e^{i\vec{Q}\cdot\vec{r}_j} + \sum_j \Delta P_j \, e^{i\vec{Q}\cdot\vec{r}_j}$$

$$+ \, i \sum_j \bar{P} \, (\vec{Q}\cdot\vec{\Delta}_j) \, e^{i\vec{Q}\cdot\vec{r}_j} \tag{3}$$
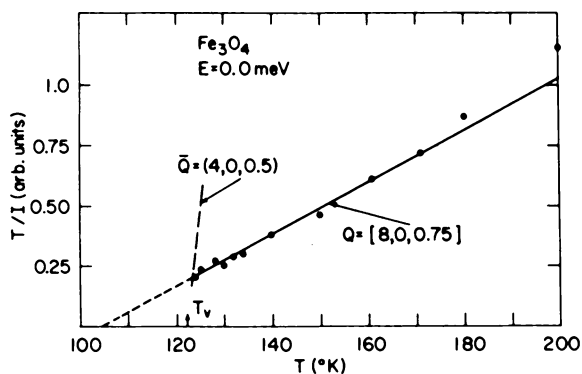
Fig. 10. Comparison of temperature dependence of 1-D diffuse peak at (8,0,0.75) and 3-D critical scattering at (40½). (Ref. 16).

The last term cannot be ignored for magnetite because $\bar{P}$ is considerably larger than ΔP_j. Thus we can establish ΔP_j only if we know Δ_j accurately enough.

Three types of neutron scattering experiments have been carried out so far for this purpose: (1) High resolution data were obtained for selected reflections, in particular (002) and (20½) to establish magnetic scattering below T_V. Measurements were carried out on a "regular" field cooled[12] as well as "squeezed" field cooled crystals.[18] (2) A polarized beam study on selected reflections from squeezed monocrystal.[17] Structure analysis at 78 K utilizing 1400 reflections.[18] Only the part (1) has been published and the other two are now in the process of final data analysis.

Table I lists some examples of the high resolution scattering experiment. The attempt here is to establish reliably a weak scattering cross section in the presence of much stronger reflections. The most crucial part of the experiment was to eliminate simultaneous reflections (see Fig. 11). Table I includes two simple charge ordering schemes, the Verwey model and the AB model. The latter is calculated for the double c axis. The Yamada model is a more general AB type modulation based upon the specific phonon mode coupling.

We have not yet established a satisfactory charge ordering scheme below T_V. We can, however, rule out some models unambiguously because of very low limits established in this experiment. First of all, the original Verwey ordering scheme is ruled out because of extremely low limits set for the magnetic cross sections for (402) and (002). The Chikazumi-Chiba model[19] is also ruled out. Previous neutron data must have been severely distorted by simultaneous reflections.

In Table I, F_M^2(cal) for AB model (Fig. 12) involves only ΔP_j terms and not $i\bar{P}(\vec{Q}\cdot\vec{\Delta}_j)$ terms. Agreement with observed is less than satisfactory and, in particular, (20½) poses the vital disagreement. In fact, we have yet to prove that any part of the magnetic cross sections is due to the spin modulation ΔP_j, and not to the magneto-distortive term $\bar{P}(\vec{Q}\cdot\vec{\Delta}_j)$. Table I demonstrates that the observed magnetic cross sections are quite weak. It is conceivable, though very unlikely, that large magnetic peaks exist outside of (h0ℓ) and (hhℓ) zones. If the actual spin modulation is less than $0.15\mu_B$, compared with full $0.5\mu_B$, then the corresponding magnetic intensity $(\sim\Delta P^2)$ would be difficult to detect.

Preliminary results of the current structure analysis[18] show several promising aspects. (1) The Δ_j's have been determined by least square analysis without any preassumed model. Yet they

Table I

Comparison of $F_M^2(obs)$ with two model calculations. These are put into absolute units of millibarns per cubic unit cell (Ref. 12). $F_M^2(cal)$ assumes full $Fe^{2+} - Fe^{3+}$ modulations of $\pm 0.5\mu_B$. Total $F^2(obs)$, nuclear plus magnetic, are given for (400) and ($40\frac{1}{2}$) for comparison.

h0ℓ	$F_M^2(obs)$	$F_M^2(cal)$	
		Verwey model	AB model
402	< 16	10,500	---
002	< 26	17,980	---
20$\frac{1}{2}$	< 72	---	3,500
201$\frac{1}{2}$	$\sim$ 300	---	3,100
202$\frac{1}{2}$	$\sim$ 400	---	2,400
	$F^2(obs)$		
400	4×10^6		
40$\frac{1}{2}$	1.3×10^4		

possess essential features of the Yamada model. (2) The magnetic cross sections based upon this structure give good agreement with the recent polarized beam experiment.[17] (3) The Fe atoms on the octahedral sites may be divided into different kinds with respect to their distances to surrounding oxygens, in accord with NMR and Mössbauer measurements.[20-22] The final step to the spin modulation is still missing.
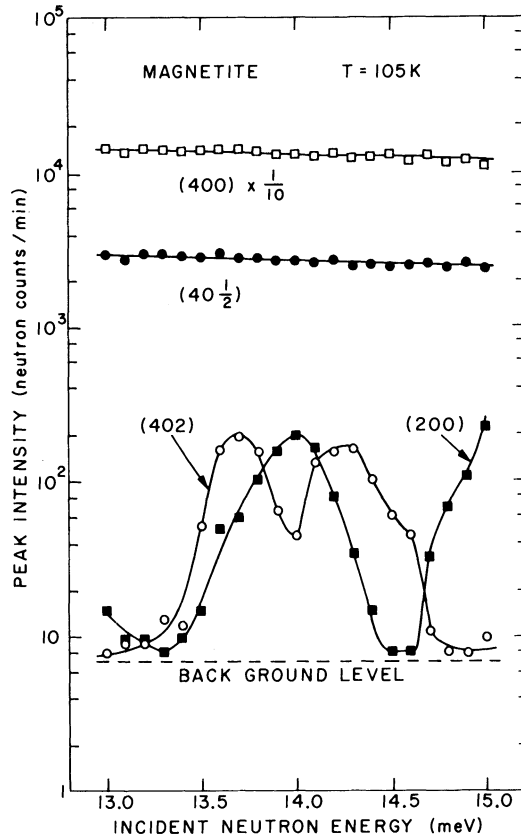
Fig. 11. Test of simultaneous reflection for selected peaks in
Fe_3O_4. (Ref. 12).
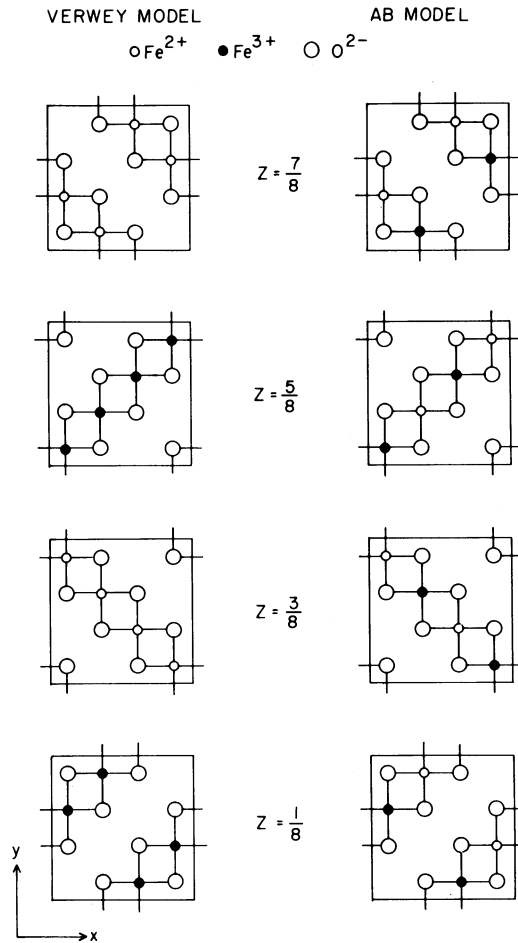
Fig. 12. Two charge ordering schemes in Fe_3O_4.

REFERENCES

1. E. J. W. Verwey and P. W. Haayman, Physica $\underline{8}$, 979 (1941); E. J. W. Verwey, P. W. Haayman, and N. C. Romeijin, J. Chem. Phys. $\underline{15}$, 181 (1947).
2. S. Chikazumi, AIP Proc. $\underline{29}$, 382 (1976).
3. B. A. Calhoun, Phys. Rev. $\underline{94}$, 1577 (1954).
4. S. C. Abrahams and B. A. Calhoun, Acta Crystallogr. $\underline{6}$, 105 (1953).
5. W. C. Hamilton, Phys. Rev. $\underline{110}$, 1050 (1958).
6. E. J. Samuelsen, E. J. Bleeker, L. Dobrzynski, and T. Riste, J. Appl. Phys. $\underline{39}$, 1114(1968); Kjeller Rept. KR-122 (1967).
7. T. Yamada, K. Suzuki, and S. Chikazumi, Appl. Phys. Lett. $\underline{13}$, 172 (1968).
8. K. Abe, Y. Yamamoto, and S. Chikazumi, J. Phys. Soc. Japan $\underline{41}$, 1894 (1976).
9. N. C. Toombs and H. P. Rooksby, Acta Crystallogr. $\underline{4}$, 474 (1951); H. P. Rooksby and B. T. M. Willis, Acta Crystallogr. $\underline{6}$, 565 (1953).
10. J. Yoshida and S. Iida, J. Phys. Soc. Japan $\underline{42}$, 230 (1977).
11. M. Iizumi and G. Shirane, Solid State Commun. $\underline{17}$,433 (1975).
12. G. Shirane, S. Chikazumi, J. Akimitsu, K. Chiba, M. Matsui, and Y. Fujii, J. Phys. Soc. Japan $\underline{39}$, 947 (1975).
13. Y. Fujii, G. Shirane, and Y. Yamada, Phys. Rev. B $\underline{11}$, 2036 (1975).
14. Y. Yamada, AIP Proc. $\underline{24}$, 79 (1975).
15. K. Chiba, K. Suzuki, and S. Chikazumi, J. Phys. Soc. Japan $\underline{39}$, 839 (1975).
16. S. M. Shapiro, M. Iizumi, and G. Shirane, Phys. Rev. $\underline{14}$, 200 (1976).
17. G. Shirane, M. Iizumi, J. Schweitzer, and S. Chikazumi, to be published.
18. M. Iizumi, T. Koetzle, G. Shirane, S. Chikazumi, M. Matsui, and S. Todo, to be published.
19. S. Chikazumi, K. Chiba, M. Matsui, J. Akimitsu, and S. Todo, Proc. Intern. Conf. Magnetism, Moscow (NAUKA, Moscow, 1974) Vol. 1-(1) 137.
20. M. Rubinstein and D. W. Forester, Solid State Commun. $\underline{9}$, 1675 (1971).
21. R. S. Hargrove and W. Kundig, Solid State Commun. $\underline{8}$, 303 (1970).
22. S. Iida, K. Mizushima, M. Mizoguchi, J. Mada, S. Umemura, K. Nakao, and J. Yoshida, AIP Proc. $\underline{29}$, 388 (1976).

PARTICIPANTS

ANDRESEN, A.F.   Institutt for Atomenergi, P.O.B. 40,
                           2007 Kjeller, Norway

AUSLOOS, M.R.   Dept. of Physics, University of Liege,
                           4000 Sart Tilman, Belgium

AXE, J.D.   Dept. of Physics, Brookhaven National
                           Lab., p.t. Risø Research Establishment,
                           4000 Roskilde, Denmark

BAK, P.   NORDITA, Blegdamsvej 17, 2100 Copenhagen,
                           Denmark

BERRE, B.   Dept. of Physics, Agricultural University
                           of Norway, 1432 Ås-NLH, Norway

BLEIF, H.J.   Hahn-Meitner Institut für Kernforschung,
                           Postfach 390128, 1 Berlin 39, Germany

DESJARDINS, S.   Dept. of Physics, University of Rhode
                           Island, Kingston, R.I. 02881, USA

DULTZ, W.   Dept. of Physics, University of Regensburg,
                           Universitätsstrasse 31, 8400 Regensburg,
                           W-Germany

EVANS, B.J.   Dept. of Chemistry, University of Michigan,
                           Ann Arbor, Michigan 48109, USA

FEDER, J.   Dept. of Physics, University of Oslo,
                           Blindern, Oslo 3, Norway

FEINER, L.F.   Philips Research Laboratorium, Eindhoven,
                           The Netherlands

FITZGERALD, W.J.   Institut Laue-Langevin, B.P. 156, Centre
                           de Tri, 38042 Grenoble-Cedex, France

FLEURY, P.A.   Bell Laboratories, 600 Mountain Ave.,
                       Murray Hill, N.J. 07974, USA

FORTUIN, C.M.   Inst. of Theoret. Physics, University of
                       Nijmegen, The Netherlands

FOSSHEIM, K.   Dept. of Physics, The Technical Univerisity
                       of Norway, 1734 Trondheim-NTH,   Norway

FRIEDEL, J.   Lab. de Physique des Solides, Université
                       Paris-Sud, Batiment 510, 91405 Orsay,
                       France

HAFNER, J.   Max-Planck-Institut für Festkörperforschung,
                       Büsnauer Strasse 171, 7000 Stuttgart 80,
                       W-Germany

HARLEY, R.T.   Clarendon Laboratory, University of Oxford,
                       Parks Road, Oxford OX1 3PU, England

HEMMER, P.C.   Dept. of Theoretical Physics, The Technical
                       University of Norway, 7034 Trondheim-NTH
                       Norway

HÖCK, K.H.   Dpet. of Physics and Astronomy, Ruhr-
                       Universität Bochum, 463 Bochum-Querenburg,
                       W-Germany

JANSSEN, T.   Inst. of Theoretical Physics, Catholic
                       University, Toernooiveld, Nijmegen,
                       The Netherlands

JØSSANG, T.   Dept. of Physics, University of Oslo,
                       Blindern, Oslo 3, Norway

KJEMS, J.K.   Dept. of Physics, Research Establishment
                       Risø, 4000 Roskilde, Denmark

LEROUX HUGON, P.   C.N.R.S. Lab. de Physique des Solides,
                       1 Place A. Briand, 92190 Meudon, France

LUTHER, A.   NORDITA, Blegdamsvej 17, 2100 Copenhagen,
                       Denmark

MAASKANT, W.J.A.   Gorlaeus Laboratoria, Rijksuniversiteit
                       Leiden, Postbus 75, Leiden, The Netherlands

McMILLAN, W.L.   Dept. of Physics, University of Illinois,
                       Urbana, Ill. 61801, USA

MØLLENBACH, K.	Dept. of Physics, Research Establishment Risø, 4000 Roskilde, Denmark
NEDELLEC, P.	Lab. de Physique des Solides, Université Paris-Sud, Batiment 510, 91405 Orsay, France
OTTINSEN, T.	Dept. of Physics, University of Oslo, Blindern, Oslo 3, Norway
PAQUET, D.	C.N.E.T., Groupt P.E.C., 196 rue de Paris, 92220 Bagneux, France
de Pater, H.	Lab. voor Technische Natuurkunde, Technische Hogeschool, Delft, The Netherlands
POPPE, U.	Inst. für Festkörperforschung der KFA, Postfach 1913, 517 Jülich 1, W-Germany
PYNN, R.	Institut Laue-Langevin, B.P. 156 Centre de Tri, 38042 Grenoble-Cedex, France
RICCA, A.M.	C.I.S.E., P.B. 3986, Milan, Italy
ROMESTAIN, R.	Université Scientifique et Médicale, Lab. de Spectrométric Physique, B.P. 53, 38041 Grenoble-Cedex, France
RYAN, J.F.	Clarendon Laboratory, University of Oxford, Parks Road, Oxford OX1 3PU, England
Di SALVO, F.J.	Bell Laboratories, 600 Mountain Avenue, Murray Hill, N.J. 07974, USA
SHIRANE, G.	Dept. of Physics, Brookhaven National Laboratory, Upton, L.I., N.Y. 11973, USA
SHULTZ, M.J.	DEAP/Pierce Hall, Harvard University, Cambridge, Mass. 02139, USA
SIEGEL, E.	Molecular Energy Research Company, 23 Bergenline Ave., Westwood, N.J. 07675, USA
SLAGSVOLD, B.J.	Dept. of Physics, The Technical University of Norway, 7034 Trondheim-NTH, Norway
SMITH, S.R.P.	Dept. of Physics, University of Essex, Wivenhoe Park, Colchester CO4 3SQ, England

STEIGMEIER, E.F.   Laboratories RCA, Badenerstrasse 569,
                         8048 Zürich, Switzerland

STEINSVOLL, O.   Institutt for atomenergi,
                         2007 Kjeller, Norway

STINCHCOMBE, R.B.   Dept. of Theoretical Physics, University
                         of Oxford, 12 Parks Road, Oxford OX1 3PQ,
                         England

TAYLOR, D.R.   Clarendon Laboratory, University of Oxford,
                         Parks Road, Oxford OX1 3PU, England

TESTARDI, L.R.   Bell Laboratories, 600 Mountain Avenue,
                         Murray Hill, N.J. 07974, USA

THOMAS, H.   Dept. of Physics, University of Basel,
                         4056 Basel, Switzerland

de WOLFF, P.M.   Lab. voor Technische Natuurkunde, Technische
                         Hogeschool, Delft, The Netherlands

YAMADA, Y.   College of General Education, Osaka
                         University, 1-1 Machikaneyama, Toyonaka-sho,
                         Osaka 560, Japan

YOUNGBLOOD, R.   Dept. of Physics, Research Establishment
                         Risø, 4000 Roskilde, Denmark

ØSTGAARD, E.   Dept. of Physics, NLHT, 7000 Trondheim,
                         Norway

ORGANIZING COMMITTEE:

ANDERSEN, E.   Institutt for atomenergi, P.O.B. 40,
JARRETT, G.   }   2007 Kjeller, Norway
RISTE, T.

413